Durability of GFRP Bars Extracted from Bridges with 15 to 20 Years of Service Life

June 1, 2019

Authors:

Benzecry, Vanessa, University of Miami

Brown, Janna, University of Miami

Al-Khafaji, Ali, Missouri University of Science and Technology

Haluza, Rudy, The Pennsylvania State University

Koch, Ryan, Owens Corning Composites

Nagarajan, Mala, Owens Corning Composites

Bakis, Charles E., The Pennsylvania State University

Myers, John J., Missouri University of Science and Technology

Nanni, Antonio, University of Miami

Review Panel:

Bradberry, Timothy E., Texas DOT

Elkaissi, Jamal, Federal Highway Administration

Gooranorimi, Omid, Walker Restoration Consultants

Nolan, Steven, Florida DOT

Shahawy, Mohsen, SDR Engineering Consultants Inc.

Sprinkel, Michael M., Virginia Transportation Research Council

DISCLAIMER

DURABILITY OF GFRP BARS EXTRACTED FROM BRIDGES WITH 15 TO 20 YEARS OF SERVICE LIFE

ABSTRACT

Glass fiber reinforced polymer (GFRP) rebars have been used in concrete structures as a substitute for steel rebars due to their non-corrosive behavior. To validate their performance in concrete structures, it is important to understand their long-term durability. A collaborative study between the University of Miami, Penn State University, Missouri University of Science and Technology (Missouri S&T) and Owens Corning Composites investigated the durability of GFRP rebars extracted from eleven bridges in service for 15 to 20 years. The bridges investigated are located in the U.S. and are exposed to wet and dry cycles, freezing-and-thawing cycles, and deicing salts, therefore making them prone to corrosion of steel reinforcement.

To investigate the durability of in-service GFRP rebars, 4 in. (102 mm)-diameter concrete cores were extracted from each bridge subjected to this investigation. A variety of tests were performed to evaluate the physico-chemical and mechanical properties of the GFRP bars and the condition of the surrounding concrete. Carbonation depth, chloride penetration and control pH tests were performed on the concrete. The extracted bars were tested for horizontal shear strength and tensile strength using cut-off strips. The cross sections of GFRP specimens were analyzed by scanning electron microscopy (SEM) imaging and energy dispersive X-ray spectroscopy (EDS) to observe any changes in their microstructure. Bars were also tested for fiber content, water absorption, moisture content and glass transition temperature (T_g). The results of these tests were compared to collected data from pristine bars at the time of installation or to current standards when pristine data was not available.

During the extraction of cores, the bridge structures were visually inspected and no signs of deterioration were detected. The SEM and EDS results showed minimal physical damage (0.05 to 0.12%) and minimal elemental distribution changes in some bridges. Most of the results from fiber content and Tg were in accordance with ASTM D7957 for quality control and certification, while the results of the horizontal shear test were inconclusive. The tensile strength test indicated a reduction in tensile stress of 2.13% over a period of 17 years in service. This study provides positive indication on the long-term durability of GFRP bars as an internal reinforcement for concrete structures.

ACKNOWLEDGMENTS

The authors are grateful to the Strategic Development Council (SDC) of the American Concrete Institute (ACI) for providing the funding that allowed the extraction of the cores and the distribution of samples to four laboratories for the performance of the tests. Similarly, the authors acknowledge the collaboration and help provided by the state and local authorities that have jurisdiction on the selected bridges for allowing this research to take place.

Several other individuals provided technical support to this endeavor. In particular, the authors thank Jason Cox of Missouri S&T, and Bryan Barragan, Doug Gremel, and Nelson Yee of Owens Corning Infrastructures Solution. Jinhoo Kim and Jeffrey Kim of Penn State University are acknowledged for their assistance with water absorption measurements and glass transition temperature measurements, respectively.

TABLE OF CONTENTS

LIST OF FIGURES

LIST OF TABLES

NOMENCLATURE

The following acronyms were used to identify the various bridges from which cores were extracted

VA and GI =	Gills Creek Bridge
CO and OF =	O’Fallon Park Bridge
OH1 and SA =	Salem Ave. Bridge
IA and BE =	Bettendorf Bridge
OH2 and CU =	Cuyahoga County Bridge
WV =	McKinleyville Bridge
IN =	Thayer Road Bridge
KY =	Roger’s Creek Bridge
TX and SI =	Sierrita de la Cruz Creek Bridge
MO1 and WA =	Walker Box Culvert Bridge
MO2 and SO =	Southview Bridge

1. Introduction

Reinforced concrete (RC) has been used widely in construction due to its availability and price. However, RC structures using traditional mild steel present many durability issues and therefore possess relatively short life expectancy. Most of the bridges built in the U.S. were designed with an intended 50-year life span. According to the ASCE 2017 Infrastructure Card (ASCE, 2017) almost 40% of the bridges in the U.S. are over 50 years old. Moreover, of the bridges that have not yet reached 50 years of service, many of them require maintenance repairs, as RC structures may present deterioration early during their service life.

The main cause of concrete deterioration in RC structures is corrosion of the steel reinforcement. Corrosion is influenced by environmental conditions. In bridges for example, corrosion can be accelerated due to deicing salts or proximity to salt water environment. Damage due to corrosion costs for highway bridges are estimated to be $13.6 billion per year, according to NACE International (Chhabra et al., 2018). With the objective of eliminating corrosion, and increasing life expectancy of bridges, glass fiber reinforced polymer (GFRP) have been used as a primary reinforcement in bridge decks. To provide confirmation that GFRP rebars provide an increase in the durability of GFRP RC structures, research studies are necessary. Most research studies have been performed under laboratory environments; however, actual performance of GFRP is better validated from monitoring existing concrete structures reinforced with GFRP.

This study provides findings on durability of GFRP and conditions of its surrounding concrete in existing structures from 11 bridges. These bridges are located in the U.S. and have between 15 to 20 years in service. This study is a collaboration between the University of Miami, Penn State University, Missouri S&T, and Owens Corning Composites. To perform the investigation of the existing bridges, concrete cores were extracted from the bridges. The extracted GFRP rebars underwent a variety of tests to determine their current physical, mechanical, and chemical properties. The GFRP tests included horizontal shear, modified tensile strength, scanning electron microscopy (SEM) imaging, energy dispersive X-ray spectroscopy (EDS), fiber content, water absorption, moisture content and differential scanning calorimetry (DSC). The surrounding concrete also underwent tests such as pH, carbonation and chloride content. The goal of this collaboration is to compare these results to data collected at the time of installation, when available, and draw conclusions on the durability of the GFRP rebar after at least 15 years. When test data from the time of installation is not available, results are compared to current standards, for reference.

2. Bridges

Eleven bridges in various locations across the U.S. were chosen for the investigation. Each of the bridges contains GFRP rebars in the deck or other location and has been in service for at least 15 years. These bridges are referred to as follows:

1. Gills Creek Bridge (VA)
2. O'Fallon Park Bridge (CO)
3. Salem Ave. Bridge (OH1)
4. Bettendorf Bridge (IA)
5. Cuyahoga County Bridge (OH2)
6. McKinleyville Bridge (WV)
7. Thayer Road Bridge (IN)
8. Roger's Creek Bridge (KY)
9. Sierrita de la Cruz Creek Bridge (TX)
10. Walker Box Culvert Bridge (MO1)
11. Southview Bridge (MO2)

A summary of each bridge is given below. When the details of the bridges were available, references are provided. Otherwise, a short explanation is included.

2.1. Gills Creek Bridge (VA)

Gills Creek Route 668 Bridge was constructed through a project between the Virginia Department of Transportation (VDOT), the Virginia Transportation Research Council (VTRC), and Virginia Tech, with funding provided through the Federal Highway Administration's (FHWA) Innovative Bridge Research and Construction (IBRC) program. The bridge was completed in 2003 and crosses over Gills Creek in Franklin County, Virginia (Phillips et al. 2005).

Gills Creek Bridge consists of three spans with a total length of 170 ft (51.8 m) and width of 30 ft (9.1 m). The bridge is made of steel girders with a concrete deck. The first span (A), adjacent to abutment, has a length of 45 ft (13.7 m) and is reinforced with GFRP as the top mat and epoxy-coated steel rebars as bottom mat. The remaining two spans have only epoxy-coated steel rebars. The bridge is shown in Fig. 1 and Fig. 2.

Fig. 1–Gills Creek Bridge

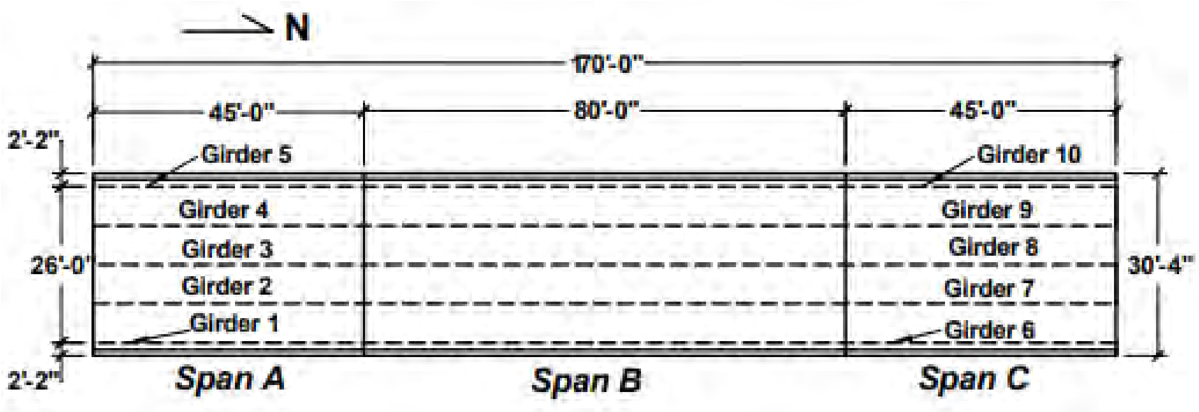

Fig. 2–Gills Creek Bridge plan view

Ten concrete cores were extracted from Gills Creek Bridge deck to be used for durability testing. The location of the extracted cores is shown in *Fig. 3*.

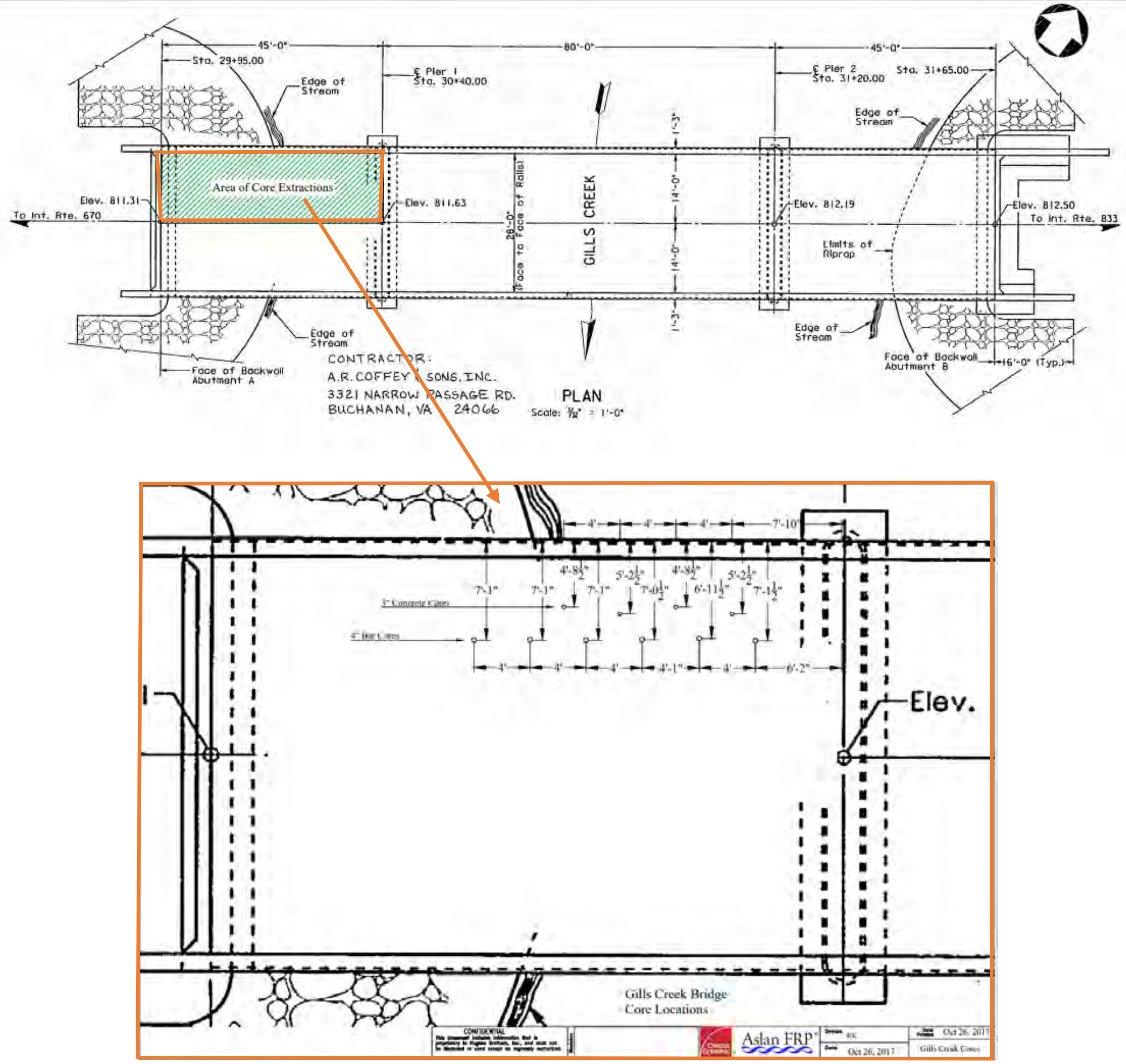

Fig. 3–Gills Creek Bridge location of extracted cores

2.2. O'Fallon Park Bridge (CO)

O'Fallon Park Bridge, located west of Denver, was built under the FHWA IBRC program, the City and County of Denver in cooperation with the Colorado Department of Transportation (CDOT) and FHWA. One of the objectives of this project was to investigate the feasibility of the use of FRP in highway bridge decks. Therefore, the bridge has a similar configuration to a highway bridge deck (Camata and Shing 2004).

The O’Fallon Park Bridge deck has a total length of 43.75 ft (13.34 m) and a width of 16.25 ft (4.95 m). The bridge deck is made of concrete reinforced with GFRP bars and is supported by five reinforced concrete risers built over an arch as shown in Fig. 4 (Camata and Shing 2004).

The bridge was designed for H-25-44 loading but is mainly used for pedestrian traffic and occasional small vehicles (Camata and Shing 2004). The bridge was completed in 2003.

The O’Fallon Park Bridge is shown in *Fig. 4* and *Fig. 5*.

Fig. 4–O'Fallon Park Bridge

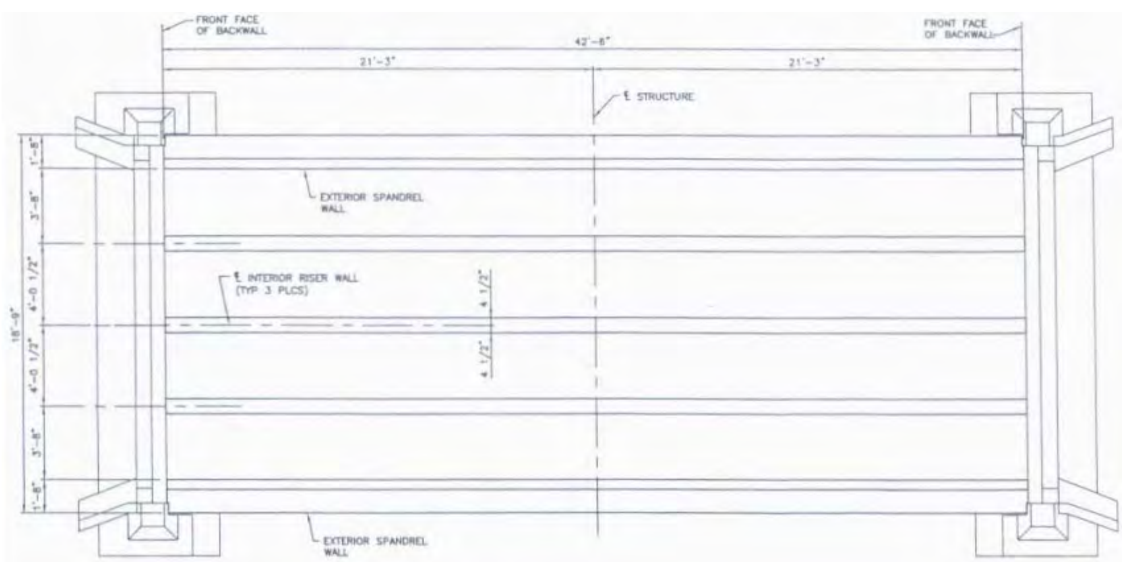

Fig. 5–O'Fallon Park Bridge plan view

Ten concrete cores were extracted from underneath the bridge deck of O'Fallon Park Bridge. The location of the extracted cores is shown in Fig. 6 and *Fig. 7*.

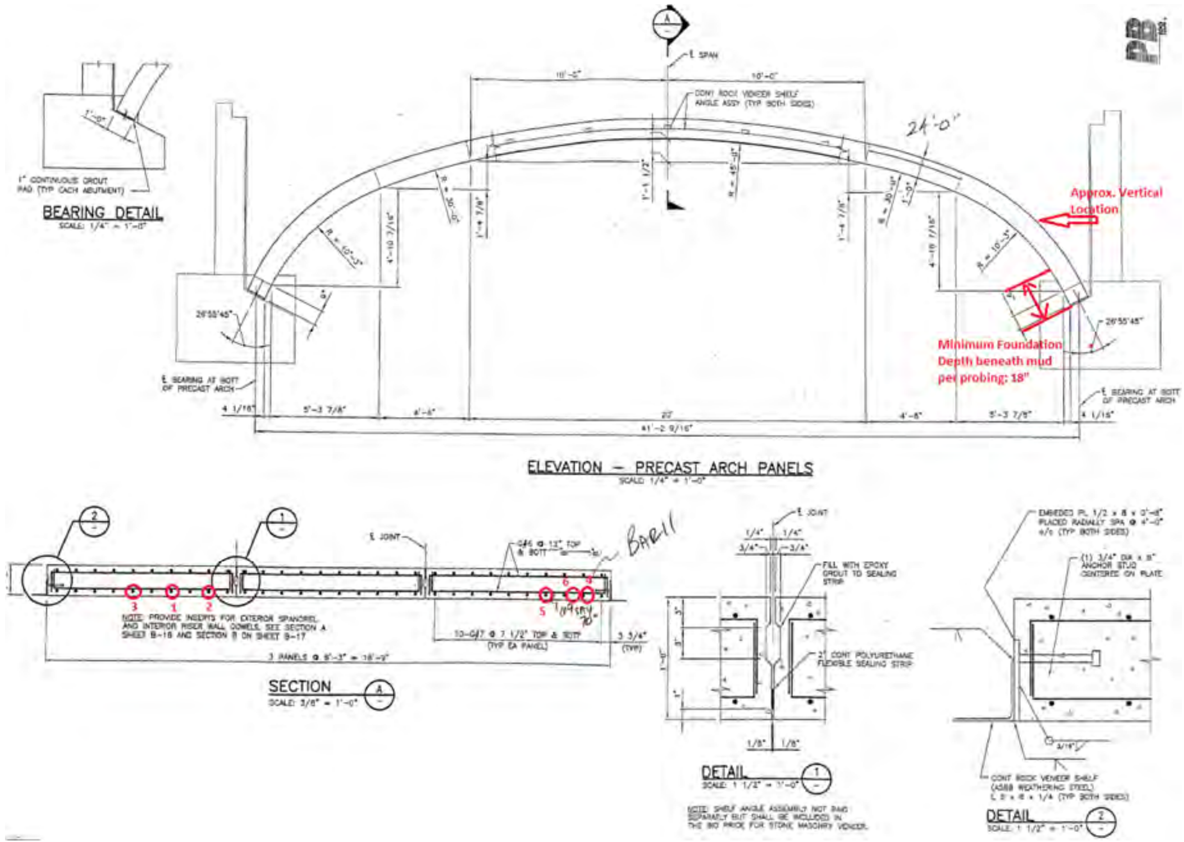

Fig. 6–O'Fallon Bridge location of extracted cores

Fig. 7–Core extraction of O'Fallon Park Bridge

2.3. Salem Ave. Bridge (OH1)

Salem Ave. Bridge is located on State Route 49 in Dayton, Ohio (*Fig. 8*). Each side is 680 ft (207.3 m) long and consists of built-up steel stringers with five spans of approximately 130 ft (39.6 m) each that crosses the Great Miami River. This project was completed in 1999. The work on one bridge consisted of a retrofit of the concrete deck with composite materials from four different manufacturers. For the other bridge, only one deck system was composed with FRP. (Reising et al. 2001).

The four systems of FRP were identified as FRP-1, FRP-2, FRP-3, and FRP-4 as shown in *Fig. 9*. The deck system FRP-1 is made of pultruded components that are bonded and interlocked in the factory to form the deck panel. FRP-2 is made of upper and lower fiberglass fabric skin faces with multiple wrapped cells that form the stiffening webs in the longitudinal and transverse directions. FRP-3 system uses a corrugated core sandwich system. FRP-4 is a hybrid system that consists of concrete deck poured over pultruded GFRP panels reinforced with GFRP tubular sections (Reising et al. 2001).

Fig. 8–Salem Ave. Bridge aerial view

Photo credit: Google maps

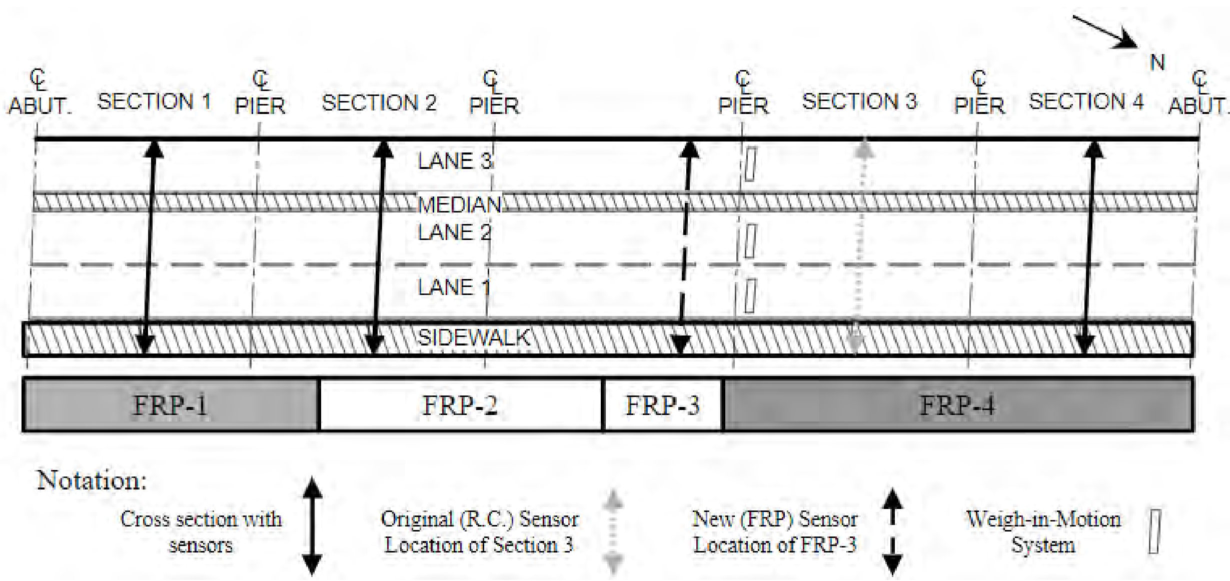

Fig. 9–Salem Ave. Bridge plan view

Five concrete cores were extracted from the Salem Ave. Bridge deck to be used for durability testing. The location of the extracted cores included the four different FRP systems and is shown in *Fig. 10*.

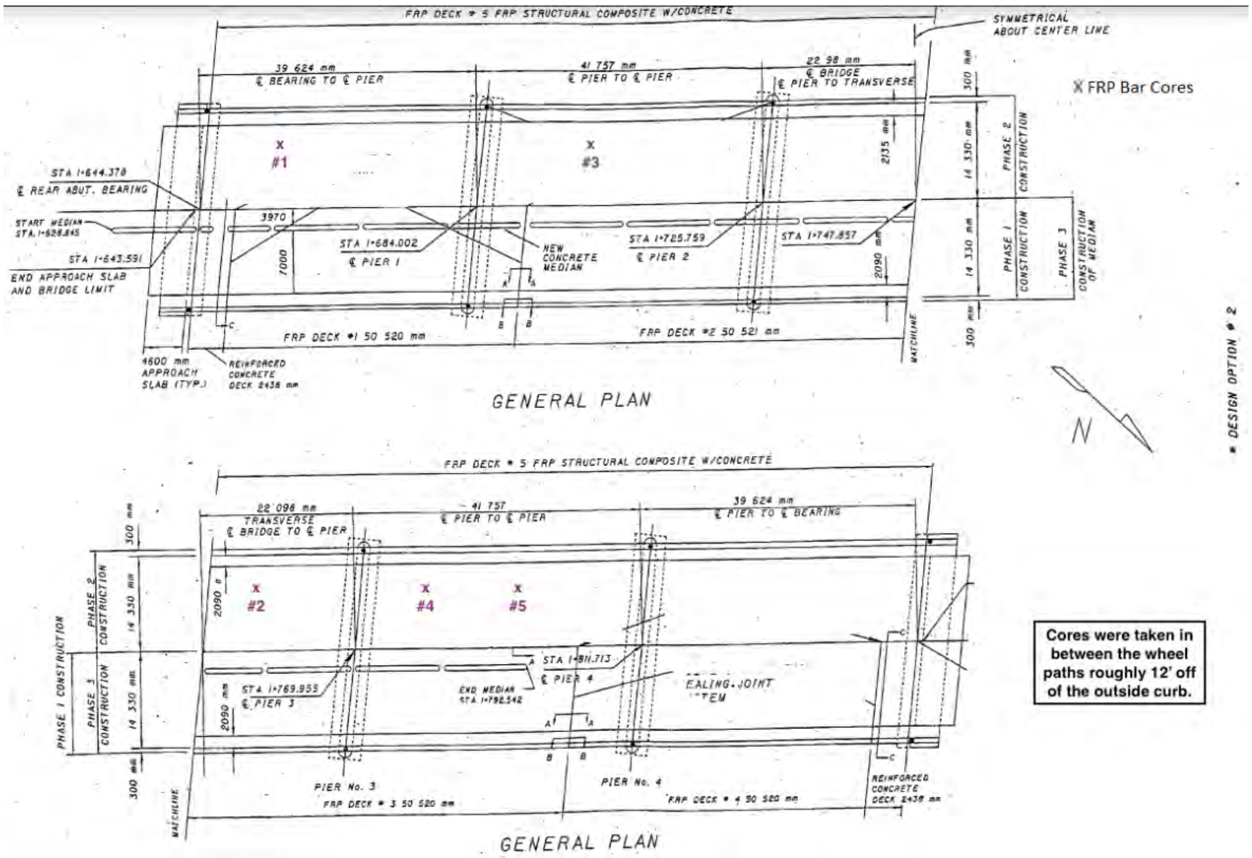

Fig. 10–Salem Bridge location of extracted cores

2.4. Bettendorf Bridge (IA)

Bettendorf Bridge is the extension of 53rd Avenue over Crow Creek in Bettendorf, Iowa. The three-span bridge was constructed in 2001 using funding provided through the FHWA IBRC program. (Wipf, 2006). The bridge is 173 ft (52.7 m) long and 98 ft (29.9 m) wide. The deck system is supported by prestressed concrete (PC) girders and is made of three different material combinations. The west and middle span decks were continuously constructed with cast-in-place concrete reinforced with epoxy coated steel and GFRP bars, respectively. The east bridge deck used pultruded FRP panels.

The bridge can be observed in Fig. 11 and Fig. 12.

Fig. 11–Bettendorf Bridge

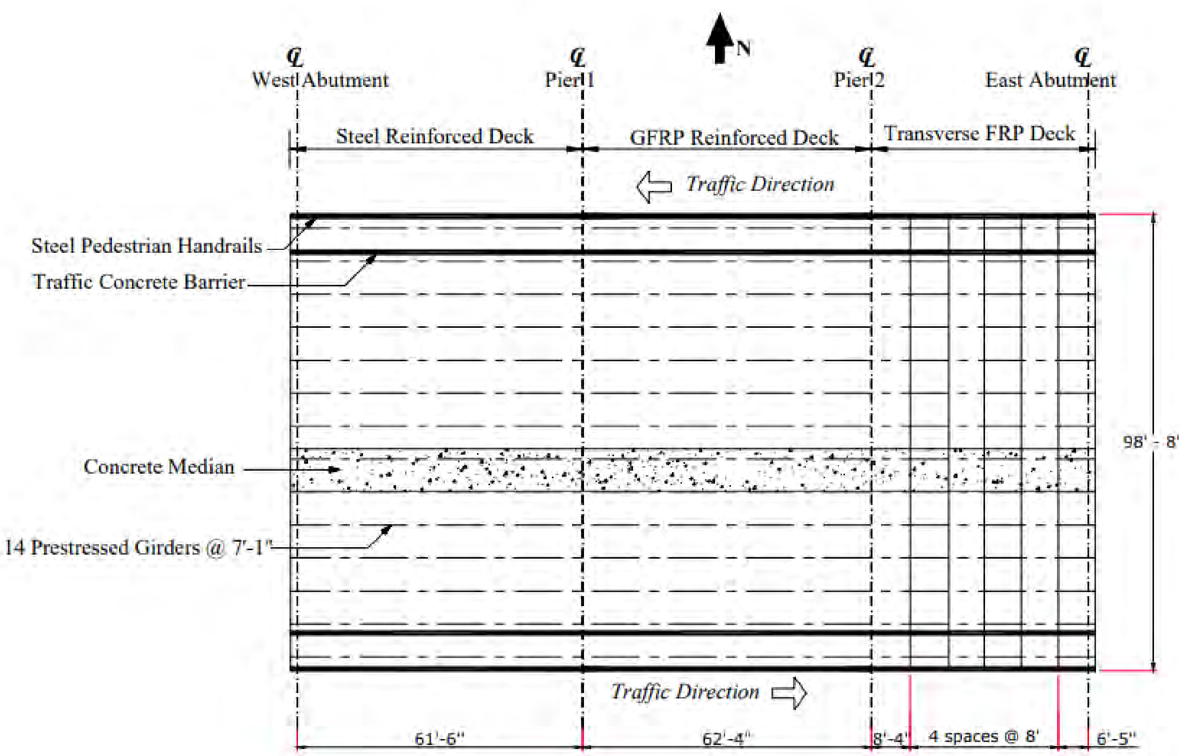

Fig. 12–Bettendorf Bridge plan view

Six concrete cores were extracted from Bettendorf Bridge deck to be used for durability testing. The location of the extracted cores is in *Fig. 13*.

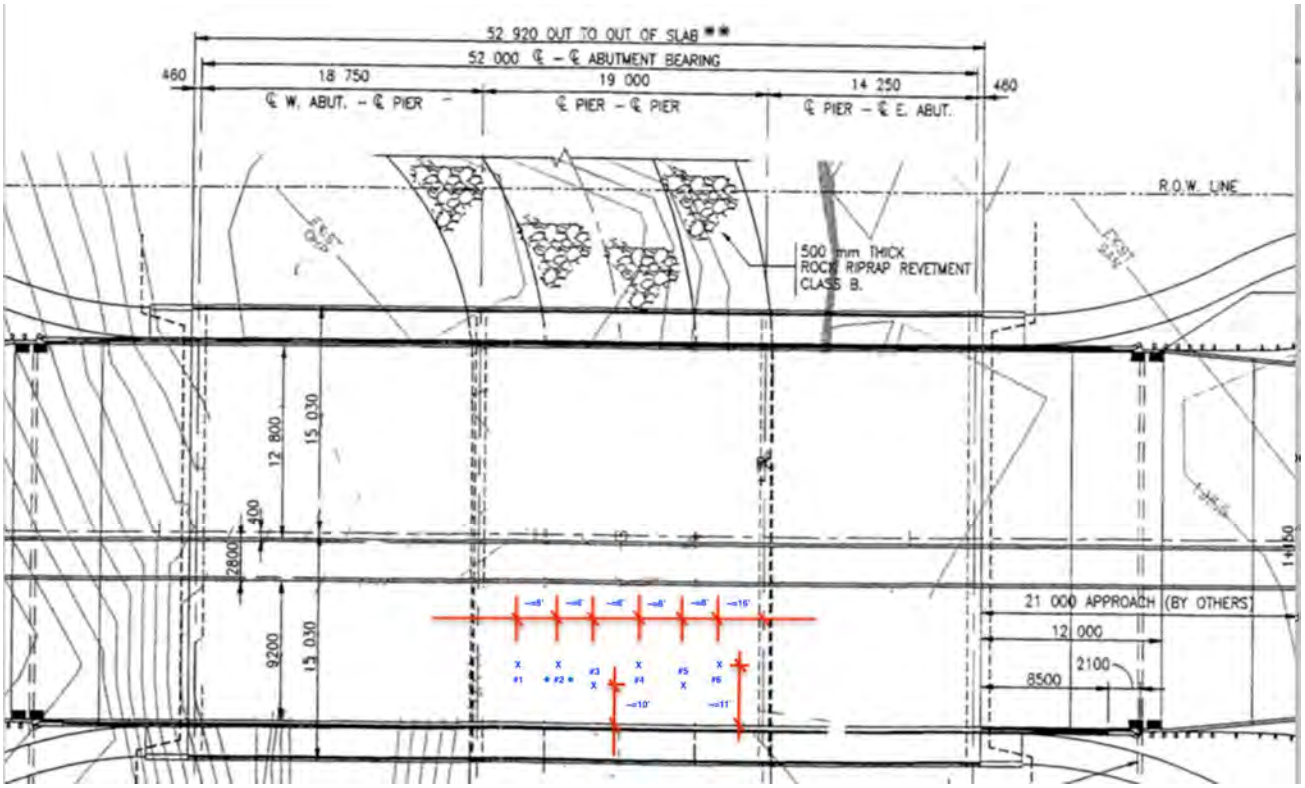

Fig. 13–Bettendorf location of extracted cores

2.5. Cuyahoga County Bridge (OH2)

Miles Road Bridge No. 178, also known as Cuyahoga County Bridge is located in the Southeastern Lake Erie Snowbelt in Ohio. This bridge consists of two spans of 45 ft (13.7 m) and 38 ft (11.6 m) wide deck. This bridge was a rehabilitation project in cooperation with the Cuyahoga County (Ohio) Engineering Department to implement a monitoring system to collect strain, temperature and deflection data. This project was built in 2002 and is the first deck on a multi-span vehicular bridge to be entirely reinforced with GFRP rebars (Eitel 2005).

The Cuyahoga County Bridge is shown in *Fig. 14*. The plan and section view are shown in *Fig. 15*.

Fig. 14–Cuyahoga County Bridge

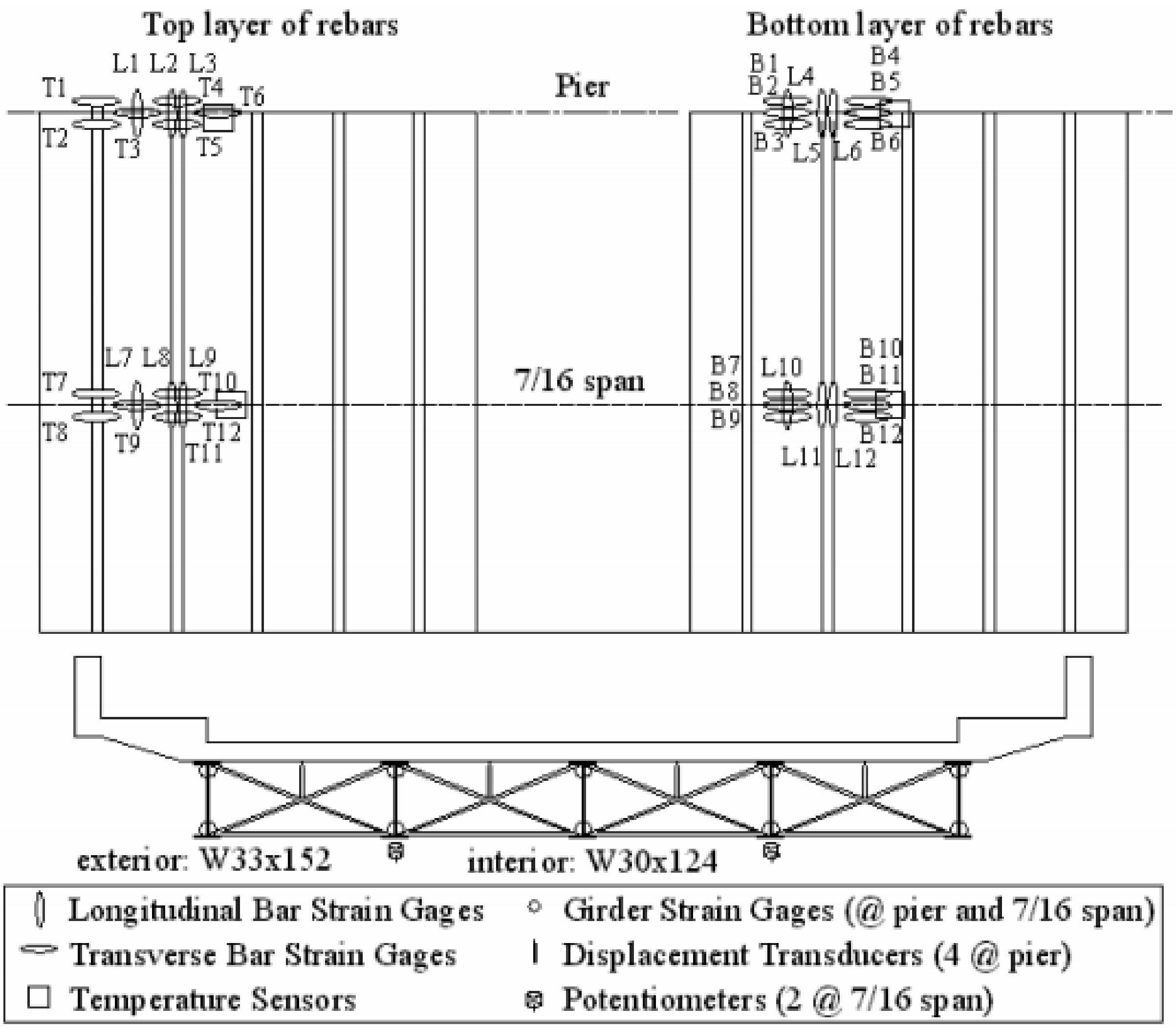

Fig. 15–Cuyahoga County Bridge plan and section view

Eight concrete cores were extracted from the Cuyahoga County Bridge deck. The locations of the extracted concrete cores are shown in Fig. 16 and Fig. 17.

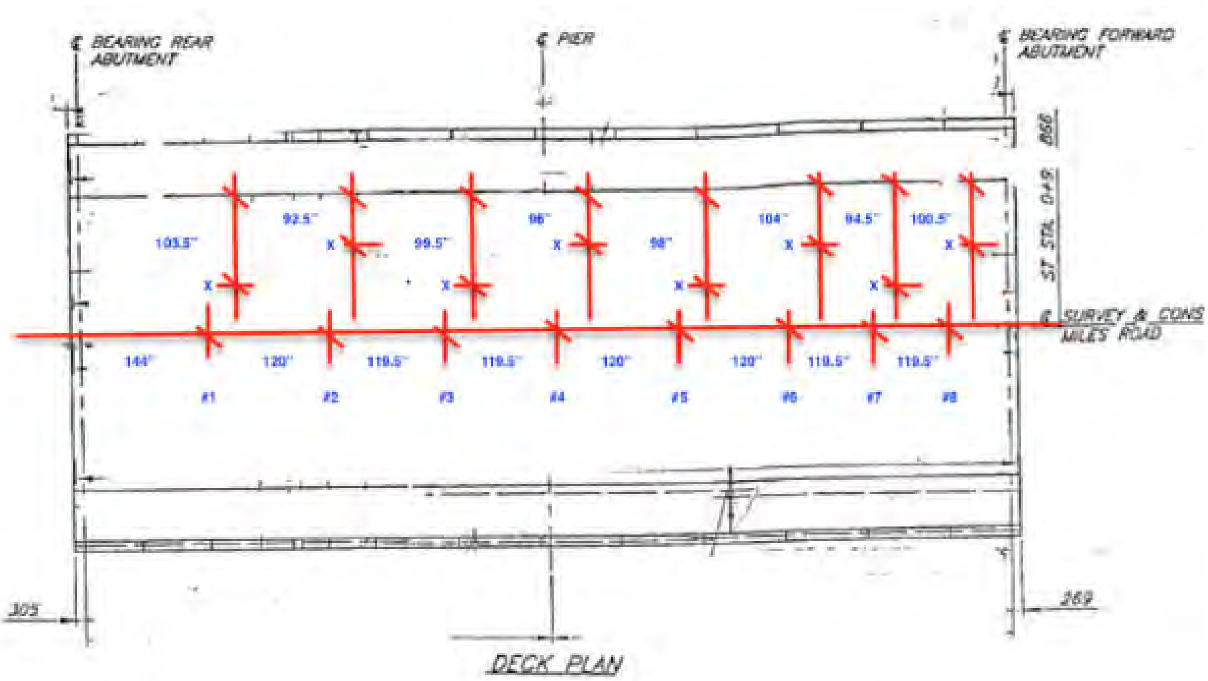

Fig. 16–Cuyahoga Bridge location of extracted cores

Fig. 17–Coring operation of Cuyahoga Bridge

2.6. McKinleyville Bridge (WV)

McKinleyville Bridge located in Brooke County (District 6), West Virginia, was built in 1996. It was the first FRP reinforced concrete vehicular bridge in the U.S. (Kumar et al., 1996). The bridge consists of three spans with a maximum span length of 73 ft (22.3 m). The bridge crosses the Buffalo Creek and has a total length of 180 ft (54.9 m) and deck width of 29.5 ft (9 m).

The bridge was designed for HS-25 loading and it is estimated that 150 vehicles cross the bridge per day over the two lanes. The bridge deck is 9 in. (229 mm) cast in place concrete with two types of GFRP rebars (Shekar et al. 2003).

The McKinleyville Bridge is shown in *Fig. 18*.

Fig. 18–McKinleyville Bridge

Five concrete cores were extracted from *McKinleyville Bridge* deck. *Fig. 19* shows the location of six extracted cores; however, only five concrete cores were received.

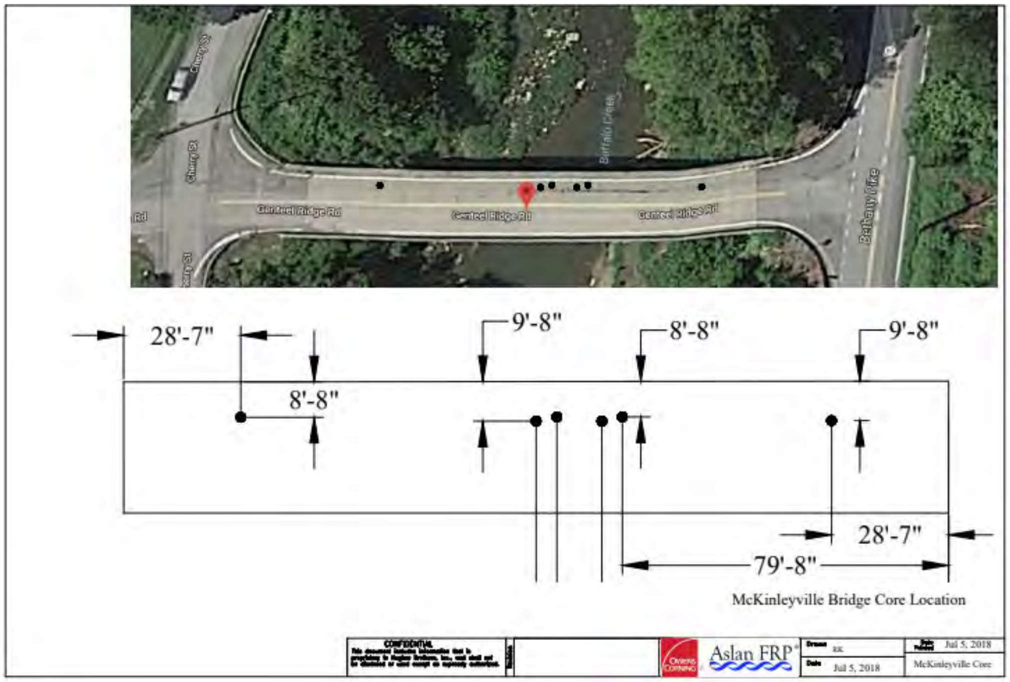

Fig. 19–McKinleyville Bridge location of extracted cores

2.7. Roger's Creek (US 460) (KY)

Roger’s Creek Bridge is the US-460 Bridge over Roger’s Creek in Bourbon County, Kentucky. The bridge was built in 1997 and is a simply supported Precast Concrete Institute (PCI) girder 36.5 ft (11.1 m) in length and 36 ft (11 m) in width. The bridge deck is partially reinforced with GFRP and steel rebars. The GFRP reinforcing bars are placed as the top mat that measures 9 ft x 15.5 ft (2.7 m x 4.7 m) and runs over three supporting beams (Harik et al. 2004).

The Roger’s Creek Bridge is shown in Fig. 20 and Fig. 21.

Fig. 20–Roger's Creek Bridge

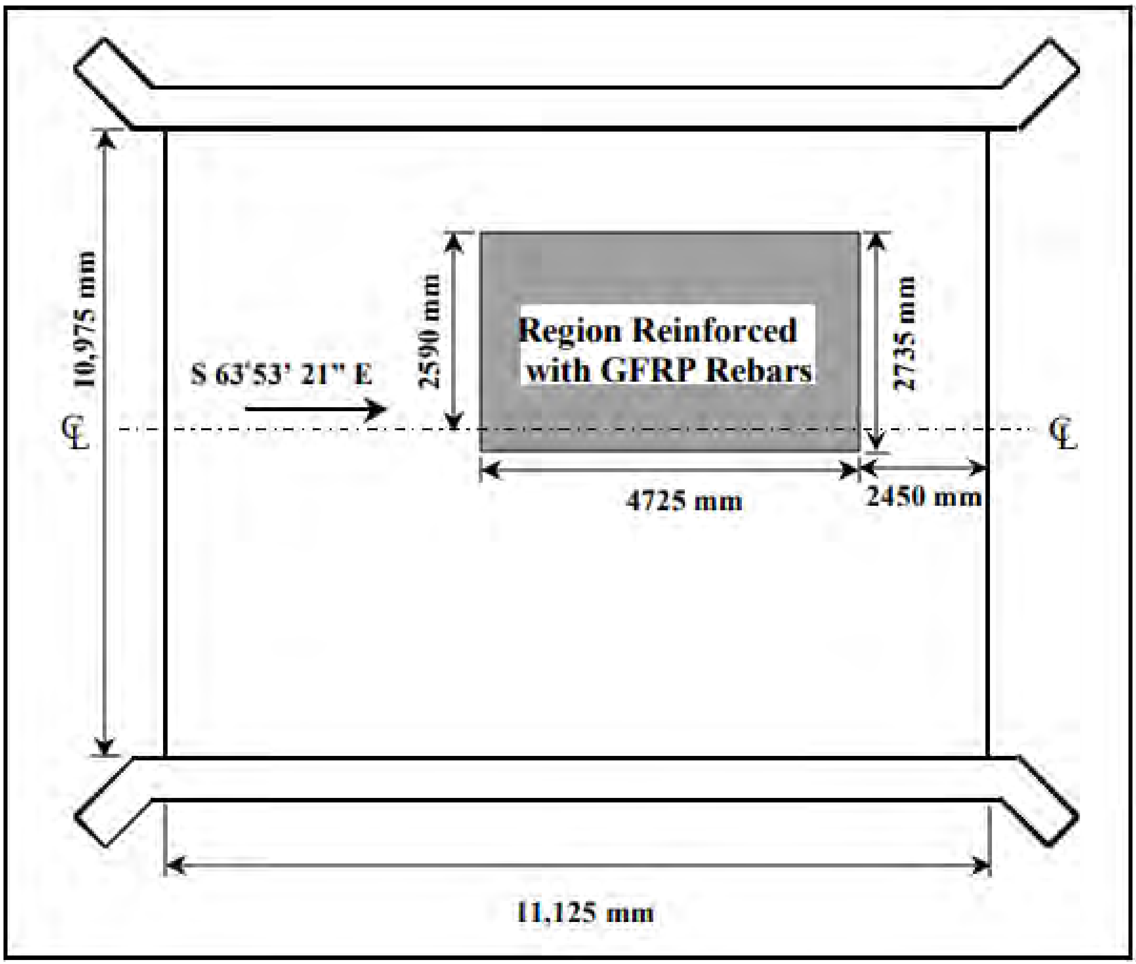

Fig. 21–Roger's Creek Bridge deck plan view

Six concrete cores from the Roger's Creek Bridge deck were extracted. The location of the extracted cores is shown in *Fig. 22*.

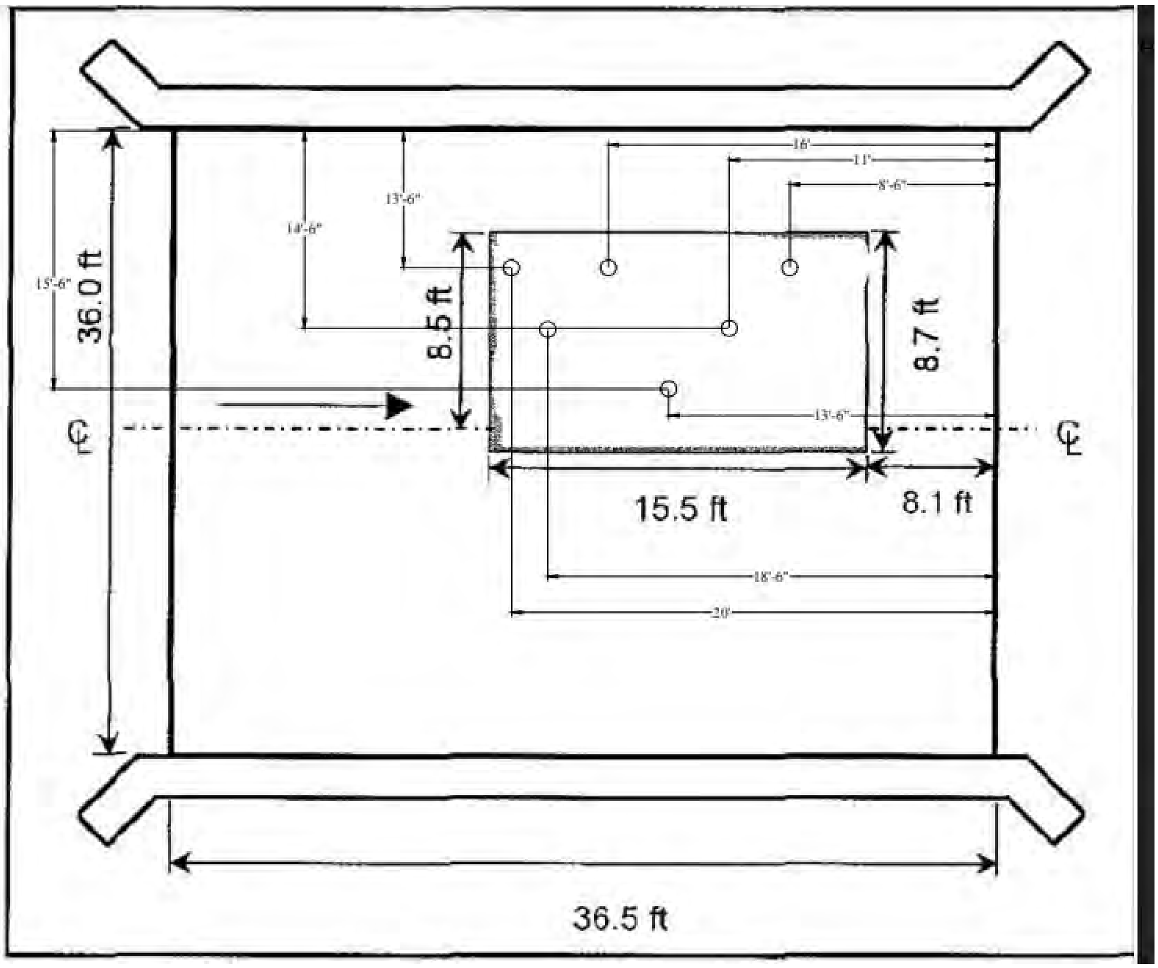

Fig. 22–Roger's Creek Bridge location of extracted cores

2.8. Thayer Road Bridge (IN)

Thayer Road Bridge, located on Thayer Road crossing I-65 Newton County, Indiana was a concrete deck replacement project performed in 2004. This project was an Indiana DOT project with support of Purdue University. The bridge has five spans of 39.8 ft (12.1 m), 63.5 ft (19.4 m), 77.8 ft (23.7 m), 63.5 ft (19.4 m), and 40 ft (12.2 m), respectively, summing up to a total length of 284 ft (86.6 m) with a 34.5 ft (10.5 m)-wide deck.

The bridge is designed for 40 mph traffic of cars and trucks. The deck is supported by seven wide flange steel girders. The replaced bridge deck uses GFRP rebar in its top mat and epoxy coated steel rebars on the bottom mat (Frosch and Pay 2006).

The Thayer Road Bridge is shown in *Fig. 23*, *Fig. 24*, and *Fig. 25*.

Fig. 23–Thayer Road Bridge

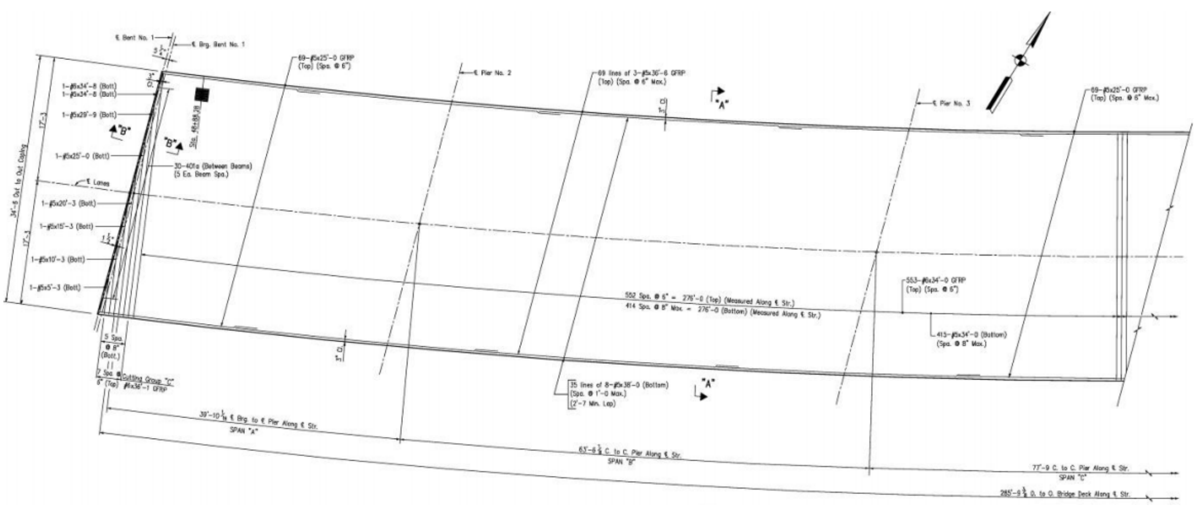

Fig. 24–Thayer Road Bridge partial plan view 1

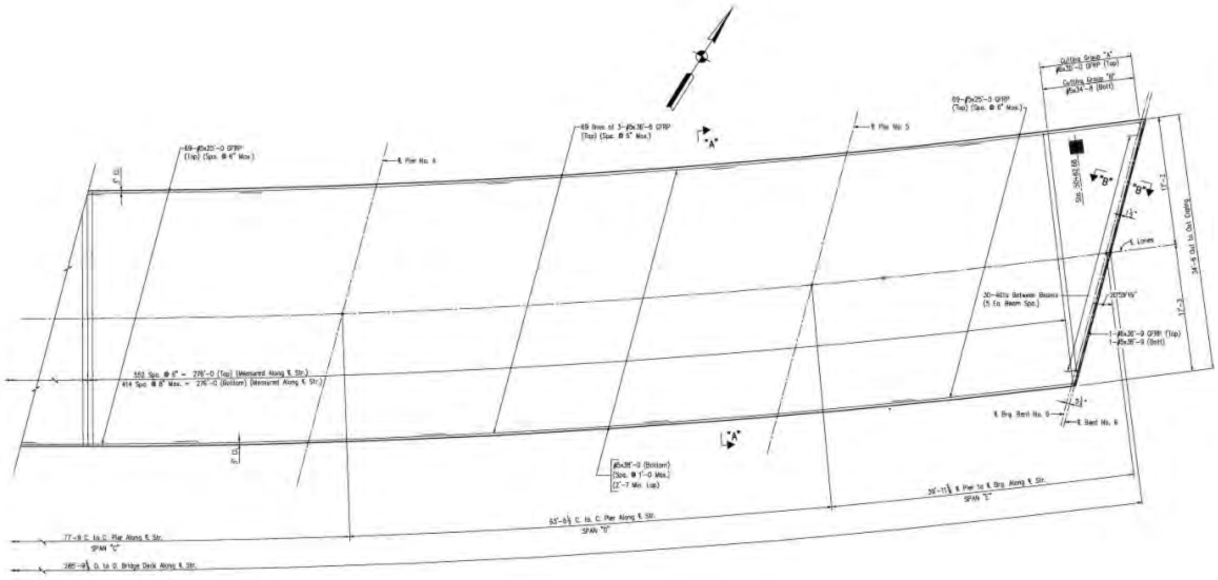

Fig. 25–Thayer Road Bridge partial plan view 2

Six concrete cores were extracted from Thayer Road Bridge deck to be used. The location of the extracted cores is shown in *Fig. 26*.

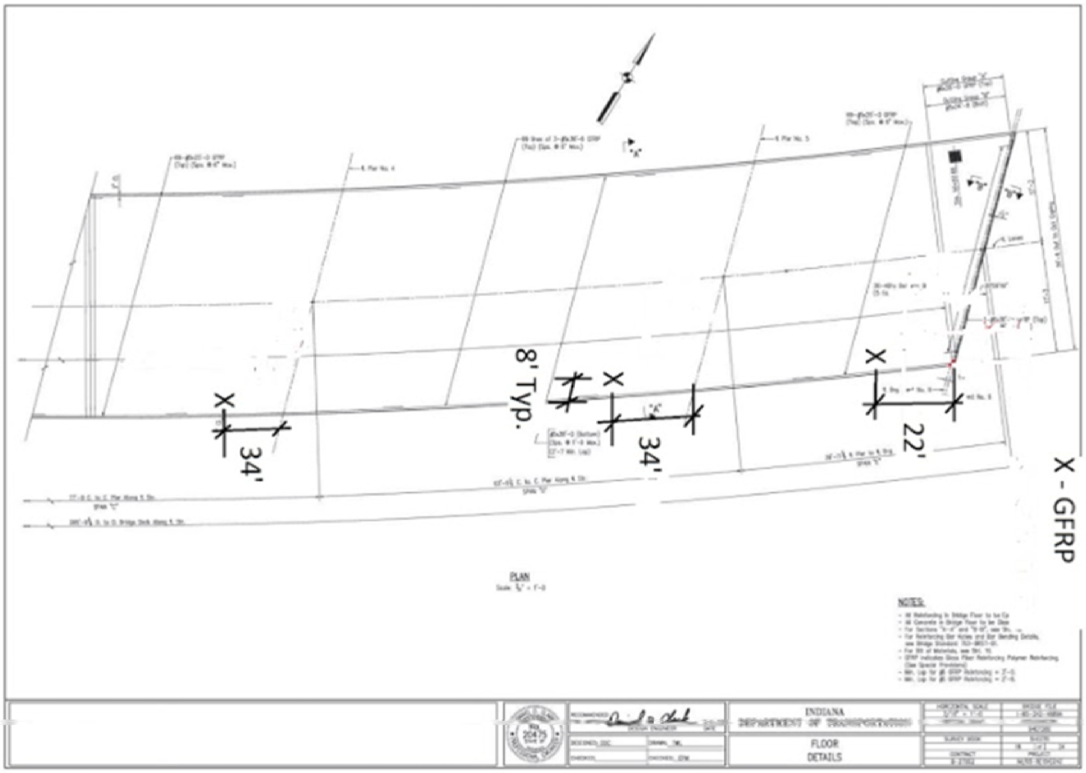

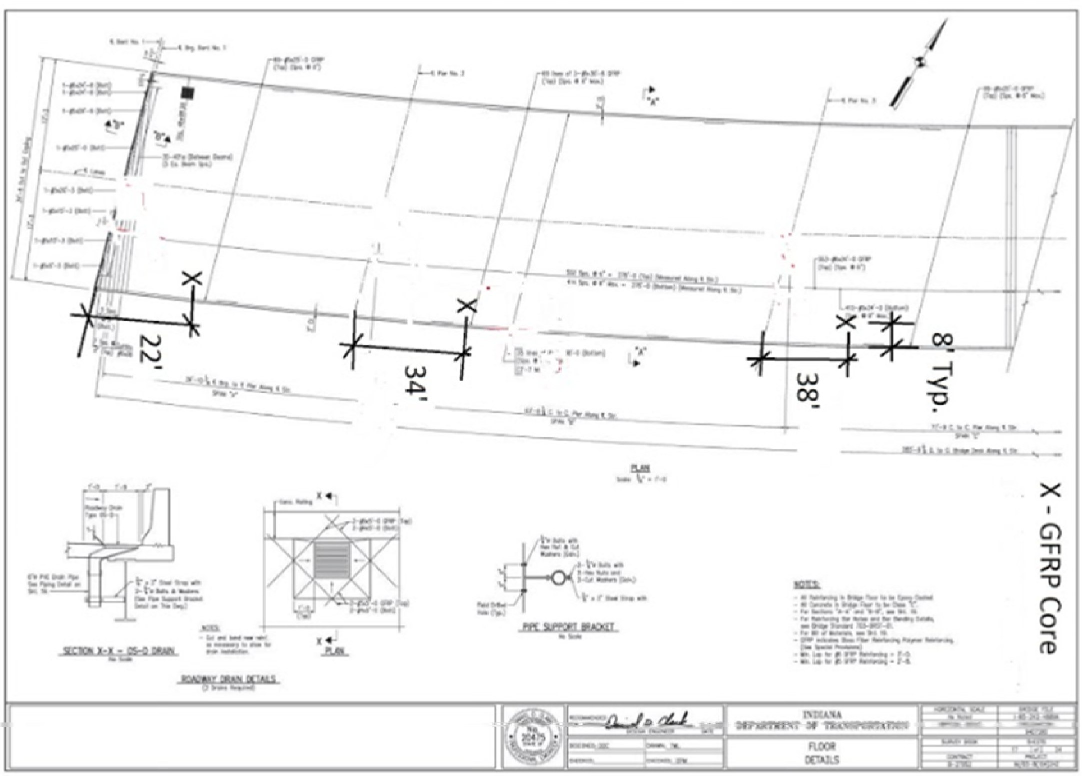

Fig. 26–Thayer Road Bridge location of extracted cores

2.9. Sierrita de la Cruz Creek Bridge (TX)

Sierrita de la Cruz Creek Bridge was built in 2000 to replace the original bridge that was structurally deficient due to corrosion (Phelan et al. 2003). The bridge is located 25 miles northwest of Amarillo, Texas and is the first bridge in Texas to implement GFRP as a concrete reinforcement.

The bridge consists of seven spans, 79 ft long (24.1 m) and 45 ft (14.3 m) wide, supported by six PC Texas type "C" concrete I-beams. The GFRP was implemented at the top mat in two spans of the concrete deck (spans 6 and 7).

The Sierrita de la Cruz Creek Bridge is shown in *Fig. 27* and *Fig. 28*.

Fig. 27–Sierrita de la Cruz Creek Bridge

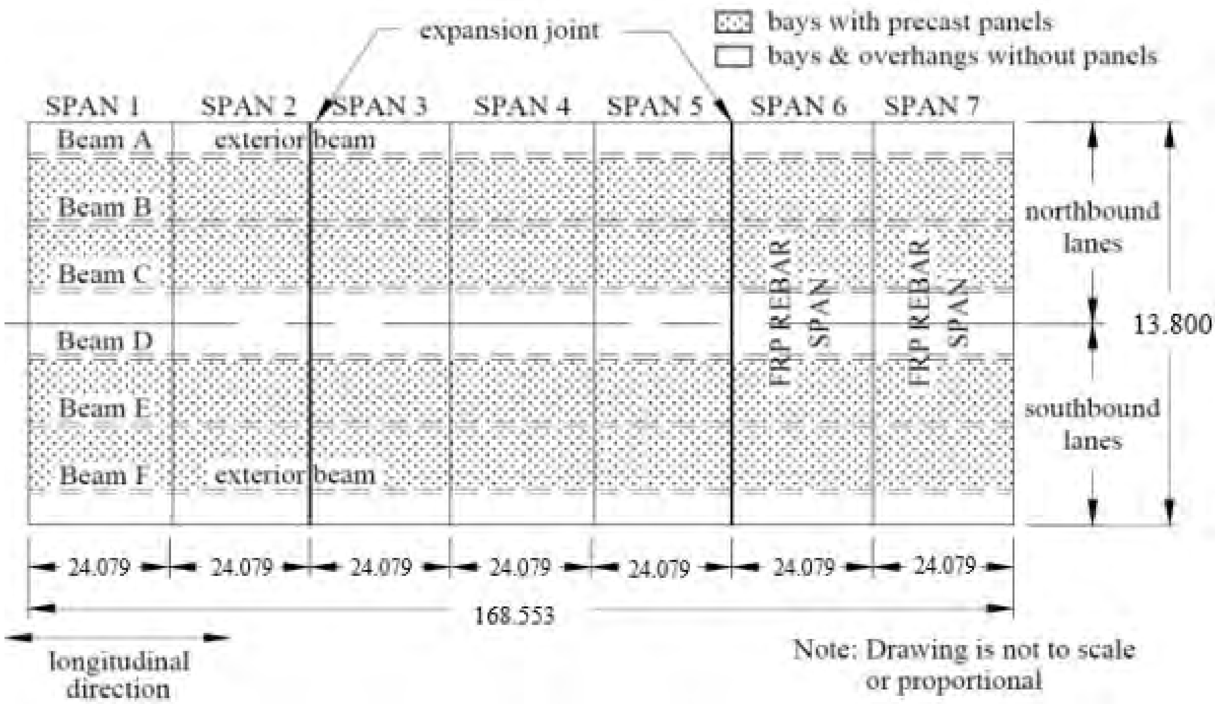

Fig. 28–Sierrita de la Cruz Creek Bridge plan view

Two concrete cores were extracted from Sierrita de la Cruz Creek Bridge deck and three bars for tensile testing. The location of the extracted cores is shown in *Fig. 29*.

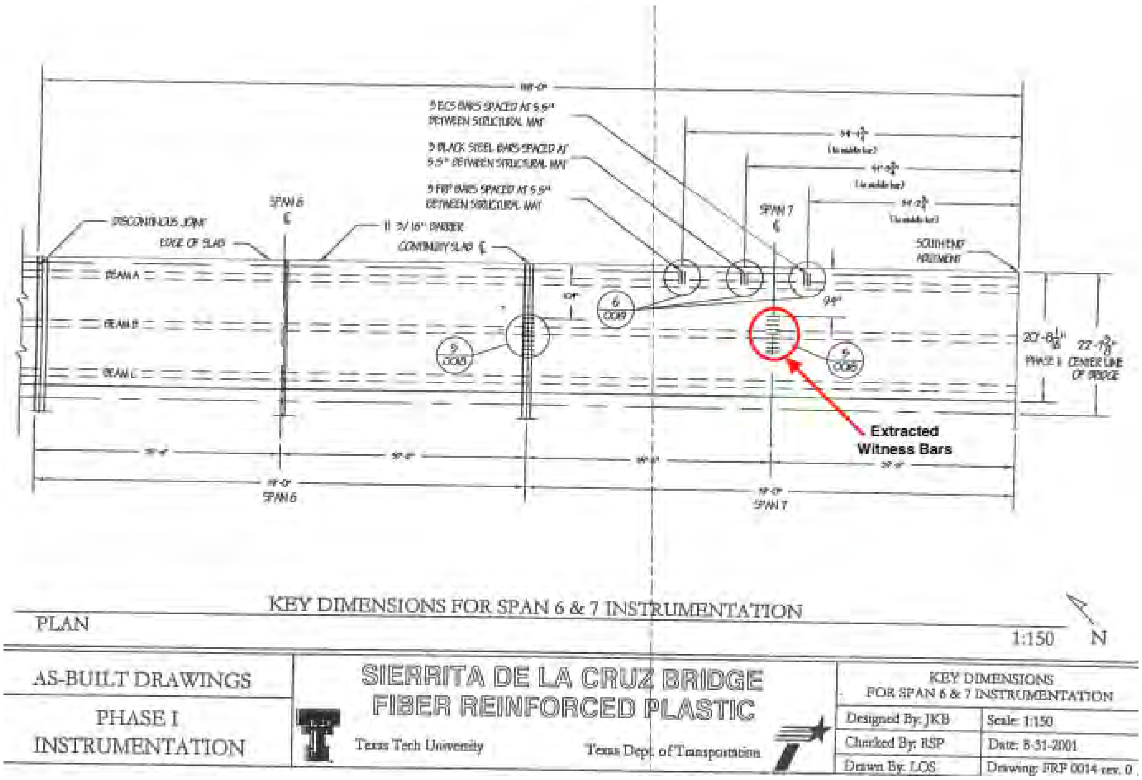

Fig. 29–Sierrita de la Cruz Creek Bridge location of extracted cores

2.10. Walker Box Culvert Bridge (MO1)

The Walker Box Culvert Bridge was constructed in 1999 on Walker Avenue in the City of Rolla, Missouri, to replace the original bridge that was made of three concrete-encased corrugated steel pipes. The original bridge became unsafe to operate due to excessive corrosion of the steel pipes. GFRP bars were implemented in the new bridge as an alternative for steel rebar to extend the service life beyond that of conventional steel-RC construction. The new bridge is 36 ft (11 m)-wide, consisting of 18 4.92 x 4.92 ft (1.50 x 1.50 m) box culverts with a thickness of 5.9 in. (150 mm). The RC boxes were entirely reinforced with No.2 GFRP bars pre-bent and cut to size by the manufacturer (Alkhrdaji and Nanni 2001).

The Walker Box Culvert Bridge is shown in Fig. 30.

Six concrete cores were extracted from Walker Box Culvert Bridge. The extracted cores were taken near cracked areas, where the concrete is most affected by environmental conditions, as shown in *Fig. 31*.

Fig. 30–Walker Box Culvert Bridge

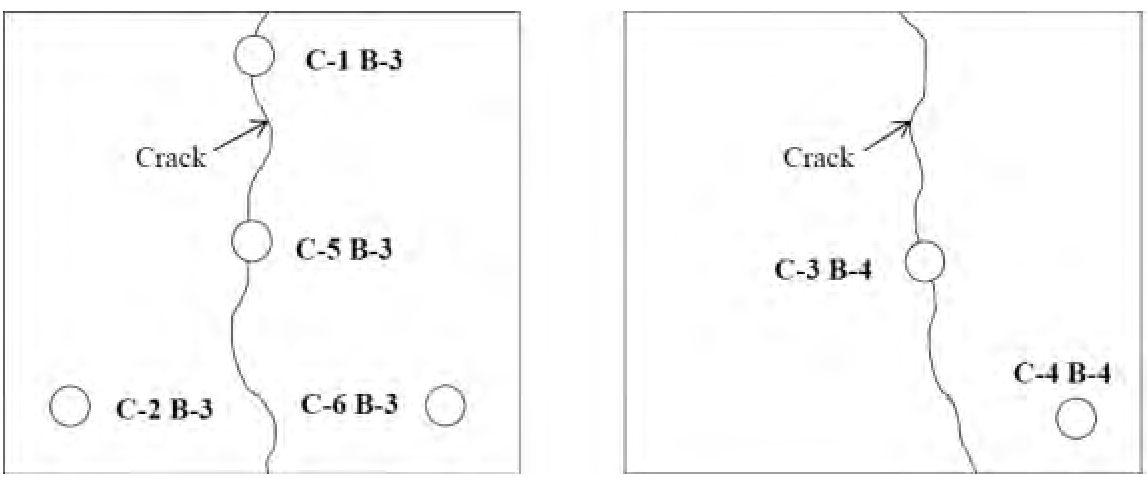

Fig. 31–Walker Box Bridge location of extracted cores. (Wang et al. 2018)

2.11. Southview Bridge (MO2)

Southview Bridge initially included four-cell steel reinforced concrete (RC) box-culverts as shown in *Fig. 32*. The 10 in. (254 mm) thick RC bridge slab went through a widening in 2004, which included the construction of an additional lane and a sidewalk (Holdener et al. 2008). The new deck was built on three conventional RC walls as for the existing structure. The concrete deck of the complementary part implemented Nos. 3, 4 and 6 GFRP bars and No. 3 prestressed CFRP tendons (Fico et al. 2006).

The construction of the FRP reinforced slab, plus a 6.6 ft (2m) wide conventional RC sidewalk on the opposite side, allowed extending the overall width of the bridge from 12.8 ft (3.9 m) to 39.0 ft (11.9 m) as shown in *Fig. 33*.

Ten concrete cores were extracted from Southview Bridge. However, only two cores used for durability testing in this study. The location of the extracted cores is shown in *Fig. 34*.

Fig. 32–Southview Bridge before extension

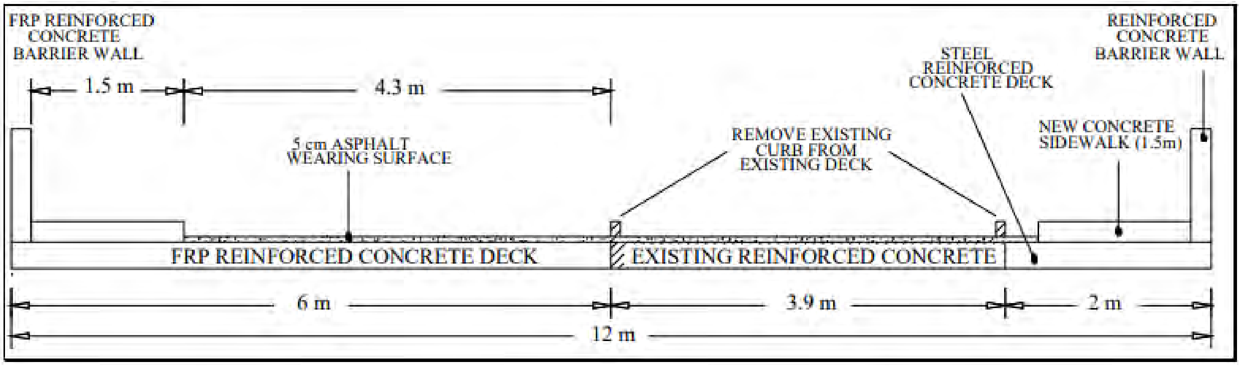

Fig. 33–Southview Bridge plan view of bridge extension

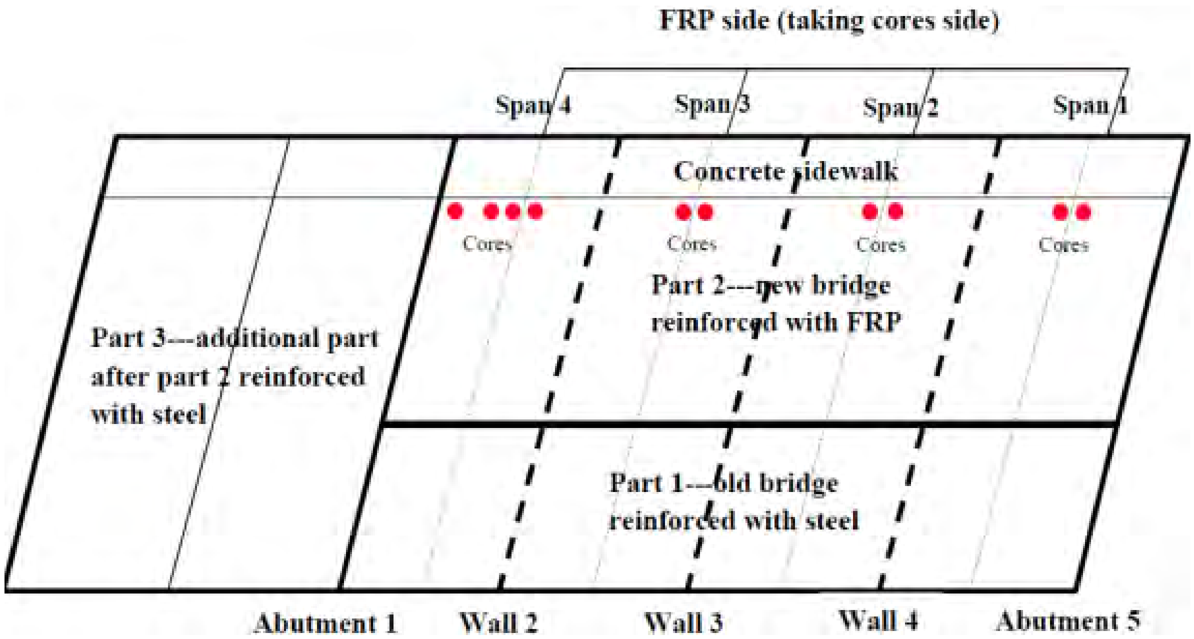

Fig. 34–Southview Bridge location of extracted cores (Wang et al. 2018)

3. Sample extraction and sample inventory

3.1. Sample extraction

Concrete core samples were extracted from the bridges using a 4 in. (102 mm) diameter concrete core barrel. The targeted location of extraction were areas with cracks and signs of environmental deterioration.

The inability to identify the exact location of the GFRP rebars hindered the extraction process. Therefore, some concrete cores had no GFRP rebars and others had GFRP samples shorter than 2 in. (51 mm). For this reason, to have a minimum of three samples per test, bars from the same bridge with the same nominal diameter were considered to be the same bar.

Moreover, samples were not sealed hermetically upon extraction from the bridges, which may have affected some concrete test results such as carbonation. All samples were shipped to the University of Miami after extraction. Samples of core extractions are shown in *Fig. 35* and *Fig. 36*. Pictures from each extracted core are included in Appendix I. Additional smaller diameter cores were taken to sample the concrete.

Fig. 35–Gills Creek Bridge core sample

Fig. 36–Cuyahoga Bridge core sample

The desired core sample had two or more full size (4 in. [102 mm]) GFRP rebars. The ideal core sample size was 4 in. (102 mm) in diameter by 6 in. (152 mm) in depth. However, the depth of the core sizes and length of rebar varied considerably.

3.2. Sample inventory

Upon reception of the cores, an inventory of all samples was compiled. Approximate GFRP rebar lengths were determined and concrete cover was measured. Concrete cores were placed in sealed plastic bags for storage until distribution to other labs. The inventory of samples, including core size, clear cover, number of GFRP rebar, and GFRP rebar length, can be found in Appendix I. The core samples are identified using a two-part identification scheme NN_Cx, where NN is the state abbreviation of the bridge's location, and Cx indicates the x-th core number. The GFRP rebar samples are identified in a three-part identification scheme, NN_Cx_Bx, where NN is the state abbreviation of the bridge's location, Cx indicates the x-th core number, and Bx indicates the x-th bar number. In cases where more than one specimen of a certain bar was tested, an extra (-x) suffix is used to identify the bar number.

Table 1 provides a summary of inventory for all bridges in the report.

Table 1. Summary of inventory for Gills Creek, O'Fallon Park, Salem Ave., Bettendorf, Cuyahoga, McKinleyille, Thayer Road, Roger's Creek, Sierrita de la Cruz, Walker Box and Southview bridges

Bridge Name	**Core Label**	**No. of GFRP Rebars**	**Rebar Length, in. (mm)**	**Core Depth, in. (mm)**
Gills Creek	VA_C1	1	1.50 (38)	4.50 (114)
	VA_C2	2	2.00 & 1.50 (51 & 38)	3.50 (89)
	VA_C3	2	2.75 & 3.25 (70 & 83)	4.00 (102)
	VA_C4	2	2.5 & 1.25 (64 & 32)	3.75 (95)
	VA_C5	0	N/A	3.00 (76)
	VA_C6	1	3.75 (95)	3.50 (89)
	VA_C7	0	N/A	4.00 (102)
	VA_C8	0	N/A	4.50 (114)
	VA_C9	0	N/A	5.00 (127)
	VA_C10	0	N/A	4.00 (102)
O'Fallon Park	CO_C1	1	3.25 (83)	1.50 (38)
	CO_C2	2	2.25 & 2.75 (57 & 70)	3.25 (83)
	CO_C3	2	3.50 & 2.00 (89 & 51)	0.50 13)
	CO_C4	1	3.25 (83)	5.00 (127)
	CO_C5	2	3.75 & 3.50 (95 & 89)	2.00 (51)
	CO_C6	0	N/A	3.00 (76)
	CO_CB	0	N/A	4.75 (121)
	CO_CC	0	N/A	6.00 (152)
	CO_CD	0	N/A	4.75 (121)
	CO_CE	0	N/A	3.00 (76)
Salem Ave.	OH1_C1	2	3.00 & 3.50 (76 &89)	5.25 (133)
	OH1_C2	2	3.50 & 2.75 (89 & 70)	5.50 (140)
	OH1_C3	1	3.25 (83)	5.00 (127)
	OH1_C4	1	2.75 (70)	5.00 (127)
	OH1_C5	1	3.50 (89)	5.00 (127)
Bettendorf	IA_C1	0	N/A	2.75 (70)
	IA_C2	0	N/A	2.00 (51)
	IA_C3	1	3.75 (95)	4.50 (114)
	IA_C4	1	3.75 (95)	4.75 (121)
	IA_C5	1	3.75 (95)	4.50 (114)
	IA_C6	1	3.75 (95)	4.50 (114)

Continued

Bridge Name	Core Label	Quantity of GFRP Rebars	Rebar Length (in)	Core Depth (in)
Cuyahoga	OH2_C1	1	2.5 (64)	4.5 (114)
	OH2_C2	1	2.5 (64)	4.5 (114)
	OH2_C3	1	3 (76)	4.5 (114)
	OH2_C4	2	3.00 & 3.25 (76 $ 83)	4.75 (121)
	OH2_C5	2	3.75 & 2.00 (95 & 51)	4.75 (121)
	OH2_C6	1	3.75 (95)	4.25 (108)
	OH2_C7	0	N/A	4.25 (108)
	OH2_C8	1	2 (51)	--
McKinleyville	WV_C1	3	2.50, 0.88 & 3.13 (64, 22 & 80)	5 (127)
	WV_C2	0	N/A	4.38 (111)
	WV_C3	3	3.13, 3.05 & 2.75 (80, 77 & 70)	4.5 (114)
	WV_C4	2	1.88 & 2.88 (48, 73)	4.63 (118)
	WV_C5	2	3.38 & 3.38 86 & 86)	2 (51)
Thayer Road	IN_C1	2	2.75 & 3.40 (70 & 86)	4.88 (124)
	IN_C2	1	2 (51)	4.75 (121)
	IN_C3	2	3.50 & 3.00 (89 & 76)	4.38 (111)
	IN_C4	2	3.50 & 3.40 (89 & 86)	3.75 (95)
	IN_C5	1	3.6 (91)	4.75 (121)
	IN_C6	1	2.13 (54)	2.87 (73)
Roger’s Creek	KY_C1	2	3.60 & 1.60 (91 & 41)	3. 88 (99)
	KY_C2	0	N/A	2.63 (67)
	KY_C3	0	N/A	3.88(99)
	KY_C4	1	3 (76)	4 (102)
	KY_C5	0	N/A	2.63 (67)
	KY_C6	1	3 (76)	4 (102)

Continued

Sierrita de la Cruz Creek	TX_C1	2 (51)	N/A	--
	TX_C2	2 (51)	N/A	--
Walker Box Culvert	MO1_C1	2 (51)	N/A	5.25 (83)
	MO1_C2	2 (51)	N/A	5.25 (83)
	MO1_C3	2 (51)	N/A	5.25 (83)
	MO1_C4	2 (51)	N/A	5.25 (83)
	MO1_C5	2 (51)	N/A	5.25 (83)
	MO1_C6	2 (51)	N/A	5.25 (83)
Southview	MO2_C1	1 (25)	N/A	6.25 (159)
	MO2_C2	2 (51)	N/A	5.25 (83)

4. Test Procedures

4.1. GFRP tests

The bars were cleaned of any adhered concrete using the edge of a spatula steel and were cut into pieces for various tests using a water-cooled diamond abrasive wheel. The collaborators determined that the GFRP rebar samples should be preconditioned before testing because of the differing conditions in each lab. To dry out the samples without further curing the rebar, the rebars were put in the oven at 104°F (40°C) for 48 hours before all tests except moisture content and modified tensile strength. These latter specimens were excluded from pre-conditioning because moisture content was intended to provide insight into the differing lab conditions and modified tensile strength was only performed at the University of Miami.

The following sections describe the various test procedures.

4.1.1. Fiber content

Burn-off is a technique that involves igniting the polymer matrix in a composite sample until only the fibers remain in order to measure the weight percentages of matrix and fibers in the sample. Fiber content of the extracted GFRP rebars was determined according to ASTM D2584 at the University of Miami, Penn State University, and Missouri S&T. An alternative procedure involving an acid wash was performed at Owens Corning on samples from Cuyahoga and Gills Creek.

4.1.1.1. Fiber content

The fiber content of the extracted GFRP rebars was determined using the procedure outlined in ASTM D2584 for at least three samples from each bridge. The samples were first cut into small samples varying from 0.5 in. (13 mm) to 1 in. (25 mm) and approximate weight of 5 g, and then pre-conditioned as described previously. Crucibles used to hold each sample were heated in a muffle furnace at 932°F (500°C) for 10 minutes to remove any combustible material from previous tests. Crucibles were then allowed to cool to room temperature in a desiccator. Specimen and crucible were weighed together, and then placed into the muffle furnace. Furnace temperature was gradually increased to 1049±82°F (565±46°C). Specimens and crucibles were removed from the furnace and cooled to room temperature in a desiccator. Once cooled, specimens and crucibles were removed from the desiccator and immediately weighed. Fibers were then removed, and crucible, sand, and helical wrap were weighed.

Calculations for the weight percentages of the fiber and resin are shown in Eq. (1) and Eq. (2), respectively, Eq. (1) Weight percentage of fibers

$$w_f = \frac{W_f}{W_f + W_m} \cdot 100\%$$

Eq. (2) Weight percentage of resin

$$w_m = \frac{W_m}{W_f + W_m} \cdot 100\%$$

where W_f is the weight of the longitudinal fibers and W_m is the weight of the matrix. The matrix weight includes all the weight lost during burn-off. The fiber weight is the difference in weight measured when removing the burned-off longitudinal fibers from the crucible, leaving the sand particles, helical wrap (if any), and filler in the crucible. This procedure for calculating fiber and matrix weight fractions follows that prescribed in ASTM D7957.

Although all university labs followed the procedure outlined in ASTM D2584, the exact procedures varied slightly. Detailed procedures at each lab are described in Appendix II.

4.1.1.2. Fiber content acid washout procedure

For three specimens from both Cuyahoga County Bridge and Gills Creek Bridge, the fiber content was determined using an alternative procedure at Owens Corning. ASTM D2584 procedure was followed and then an acid washout was used to remove filler from the specimen. This allows for a more realistic estimation of fiber content because remnant filler is removed from the fibers.

4.1.2. Water absorption

Water absorption was measured using ASTM D570 with 50°C (122°F) distilled water as the immersion medium. Specimens were cut to a length of 1 in. (25 mm) using a water-cooled diamond saw. The specimens were preconditioned at 104°F (40°C) for 48 hours. Specimen weights were recorded before and after pre-conditioning. The weight after pre-conditioning was used as the basis for additional percent weight changes during the water absorption test. A plastic container with a loose-fitting lid was used to hold the distilled water and specimens during the water absorption test (shown in *Fig. 37*). The lid of the container was closed while the container was in the oven.

Fig. 37–Moisture uptake specimens immersed in distilled water

ASTM D570 Sections 7.1 and 7.4 were then followed at 122 °F (50°C) as is requested in Table 1 of ASTM D7957. Specimens were removed from the oven, dried, and weighed after 24 hours, one week, three weeks, five weeks, and every two weeks thereafter. Measurements continued until the increase in weight per two-week period, as shown by three consecutive measurements, averages less than 1% of the total increase in weight.

Drying and measurement procedures at each lab are described in Appendix II.

4.1.3. Horizontal shear

Apparent horizontal shear strength was measured using ASTM D4475. Length of specimens varied depending upon nominal size. Because of the limited sample size, a minimum length (i.e., 4 bar diameters) was used. The length of specimens and span length depending on bar size is described in Table 2.

Table 2. Minimum span length and length of specimen

No.	Span, in. (mm)	Length, in. (mm)
3	1.12 (28)	1.50 (38)
4	1.50 (38)	2.00 (51)
5	1.87 (47)	2.50 (64)
6	2.25 (57)	3.00 (76)
7	2.62 (67)	3.50 (89)

The specimens were pre-conditioned at 104°F (40°C) for 48 hours and then placed in a desiccator to cool. Once cooled, specimens were removed from desiccator and test was performed according to ASTM D4475. The test setup used was according to ASTM D4475 as shown in Fig. 38 and Fig. 39.

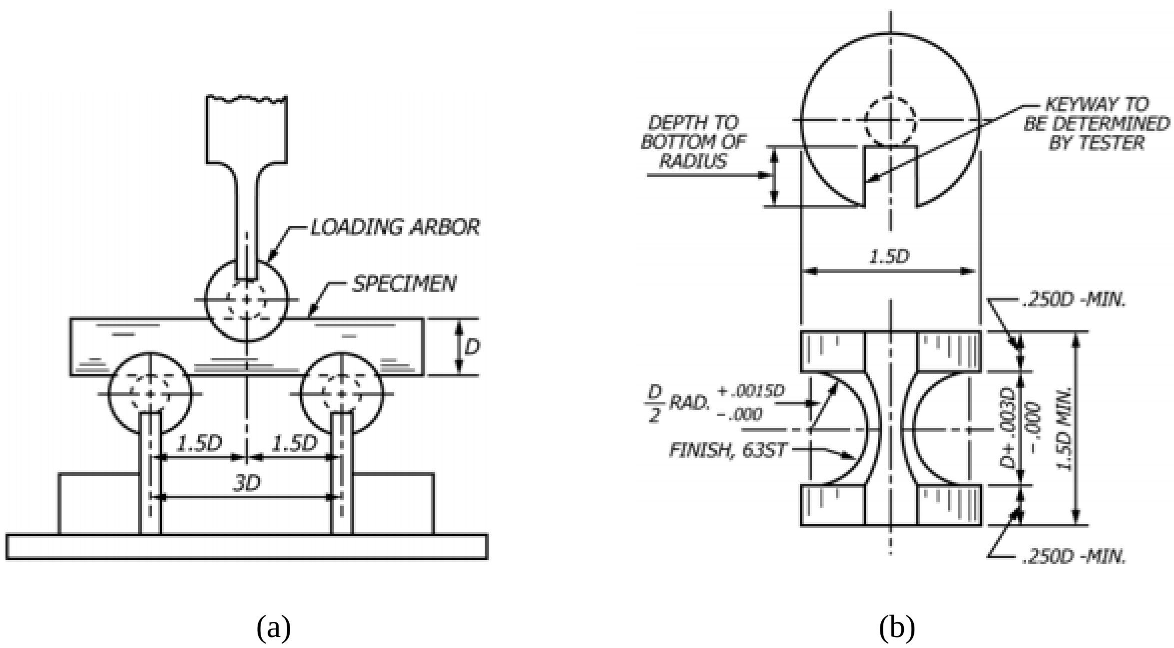

Fig. 38–Test setup for ASTM D4475. (a) Span configuration for 3D span. (b) Anvil dimensions

Due to available anvil sizes at the University of Miami, the Bettendorf Bridge horizontal shear samples were not tested using these anvils. Instead, small steel cylinders were used as the loading arbor. These were not according to ASTM D4475 as shown in *Fig. 38*.

The load rate used was 0.05 in./min. (1.27 mm/min.) and the time of the test did not exceed the allowable ASTM D4475 time limit of 20 min. The load was applied to the specimen until an interlaminar shear failure took place. The shear capacity was calculated according to ASTM D4475 using Eq. (3):

Eq. (3) Shear capacity

$$S = 0.849\, P/d^2 \; (lb;\ in)$$

$$S = 547.8P/d^2 \; (N;\ mm)$$

where S is the interlaminar shear stress, psi (MPa), P is the breaking load, lb (N), and d is the nominal diameter of the specimen, in. (mm). An image of the setup used is shown in Fig. 39.

Fig. 39–Horizontal shear test setup

4.1.4. Differential scanning calorimetry (DSC) and modulated differential scanning calorimetry (MDSC)

Differential Scanning Calorimetry (DSC) or Modulated Differential Scanning Calorimetry (MDSC) measures the heat flow into small pieces of bar in a sealed aluminum pan, relative to an empty pan, during a constant rate of temperature change from one limit to another. Modulated DSC is an extension of DSC, where a sinusoidal temperature oscillation is overlaid on the conventional linear temperature slope. Changes in the rate of heat flow into or out of the specimen can be used to assign a glass transition temperature, T_g, by any of several indications on the heat-flow-versus-temperature graph (ASTM E1356-08). The T_g was assigned by drawing three tangents to the total heat flow curve, finding the middle value of total heat flow between the two points where the tangents intersect, and identifying the temperature corresponding to the middle value of total heat flow. This measure of T_g is known as the mid-point temperature, T_m, in ASTM E1356. The exact procedures followed for DSC are described in Appendix II.

4.1.5. SEM/EDS

Scanning electron microscope (SEM) images of full cross sections of the extracted bars were taken at the University of Miami (UM), Missouri S&T, and Owens Corning. Sample preparation at the University of Miami involved cutting GFRP rebar into approximately 0.25 in. (6 mm) long specimens using a water-cooled diamond saw. These small samples were mechanically paper-sanded using different grades including: 180, 320, 800, and 1200, and polish cloths of 1 and 3 microns as shown in Table 3.

Table 3. SEM polishing procedure at UM

Surface type	Grade	Cycle time (min)
Sand disc grit	180	2
	320	2
	600	2
	1200	2
Polishing cloth	3 microns	3
	1 micron	3

After polishing, samples were subjected to a thin gold sputter-coat to allow for higher magnification microscopy without charging effects. SEM imaging focused on fibers located on the outer layer of the bar, as these fibers are more likely to be damaged. Polishing procedures at other laboratories are described in Appendix II.

In conjunction with the SEM, Energy Dispersive Spectroscopy (EDS) was also performed at the University of Miami and Missouri S&T. This process gives a chemical microanalysis of the specimen.

4.1.6. Moisture content

Moisture content of the bars was measured by drying the as-received bars (no pre-conditioning) to equilibrium in a forced-air oven set to 176°F (80°C), according to ASTM D5229 procedure D. The specimens were cut to a length of 0.5 in. (13 mm) using a water-cooled diamond saw and were dried following cutting. This drying process involved blow drying the samples with compressed nitrogen, then hand drying with a lint-free tissue paper. After drying, the specimens were weighed on a digital scale with 1 mg resolution and placed in a corrugated aluminum pan with labels for each specimen position, as shown in Fig. 40. The corrugated pan was chosen because it would allow convection underneath the specimen so that both faces were exposed to circulating air in the oven. Once the dry-out test was underway, specimens were weighed every day for 10 days and every week thereafter. For weight measurement during the dry-out process, the hot specimens were allowed to cool to room temperature in a desiccator for 30 min before weighing. Following weighing, the specimens were promptly returned to the oven. The dry-out test was terminated when the weight changes of all of the specimens were less than 0.02% for two consecutive weighing periods.

Fig. 40–Dry-out specimens in corrugated aluminum pans

4.1.7. Constituent volume contents by image analysis

Optical microscopy was used to measure the constituent volume contents of the O’Fallon bars based on the assumption that all features observed on a plane cut perpendicular to the fibers extend to infinity in the bar. This assumption is unproven, particularly for voids. 0.5 in. (13 mm) long specimens were cut from the bars using a water-cooled diamond abrasive saw and were potted in an epoxy consisting of Epon Resin 862 (Hexion Responsible Chemistry 2019) cured with Jeffamine T403 (Huntsman 2008). The pucks were cured for 48 hours at room temperature. Once cured, the pucks were mechanically paper-sanded using different grades including: 320, 800, 1200, 2400 and 4000 and polish cloths of 1 and 3 microns as shown in Table 4 and Table 5.

Table 4. Sanding procedure

Sanding Disc Grit (FEPA Standard)	Spindle Speed (rpm)	Table Speed (rpm)	Force, lb (N)	Cycle Time (min)	Number of Cycles
P320	65	120	1 (4.5)	2	3
P800	65	120	1 (4.5)	2	3
P1200	65	150	1 (4.5)	2	3
P2400	80	150	2 (9.0)	2	3
P4000	80	150	2 (9.0)	2	3

Table 5. Polishing procedure

Polishing Particle Size	Cycle Time (min)	Number of Cycles
3 μm	3	3
1 μm	3	3

1 μm = 39.37 μin

Image analysis was performed using 30 individual micrographs for each bar. The micrographs were obtained at evenly spaced intervals along a radial path emanating from the center of the bar in the case of fiber content and along the full diameter in the case of void content.

For fiber volume content, each image area was 10394 μin x 7795 μin (264 μm × 198 μm) (*Fig. 41*(a) and the total analyzed area comprised 0.018% of the bar area. Due to the similar reflected light intensity associated with the glass fibers and inorganic filler particles, fiber cross-sections had to be manually detected. Using a Matlab script, circles were fitted to each fiber as shown in *Fig. 41*(b) and their enclosed areas, minus the partial areas outside the rectangular field of view, were summed to obtain the fiber area. Fiber volume content was then obtained by dividing the fiber area by the area of the field of view and multiplying by 100%.

For void volume content, each image area was 41811 μin x 31378 μin (1062 μm × 797 μm) (*Fig. 41*(c)) and the total analyzed area comprised 0.299% of the bar area. The images were over-exposed to highlight the contrast between voids and the remaining solid surface (fibers and matrix). Using a MATLAB® script, pixels with intensity less than a judiciously selected level (for example, that for voids) were assigned a color of white and counted. The remaining pixels were assigned a color of black and counted as well (*Fig. 41*(d)). Void volume fraction was calculated by dividing the number of white pixels by the total number of pixels in the field of view and multiplying by 100%.

The matrix volume content was not measured with either of the two sets of images collected for fiber and void contents. However, an approximate value of matrix volume content was obtained by subtracting the fiber and void contents from 100%.

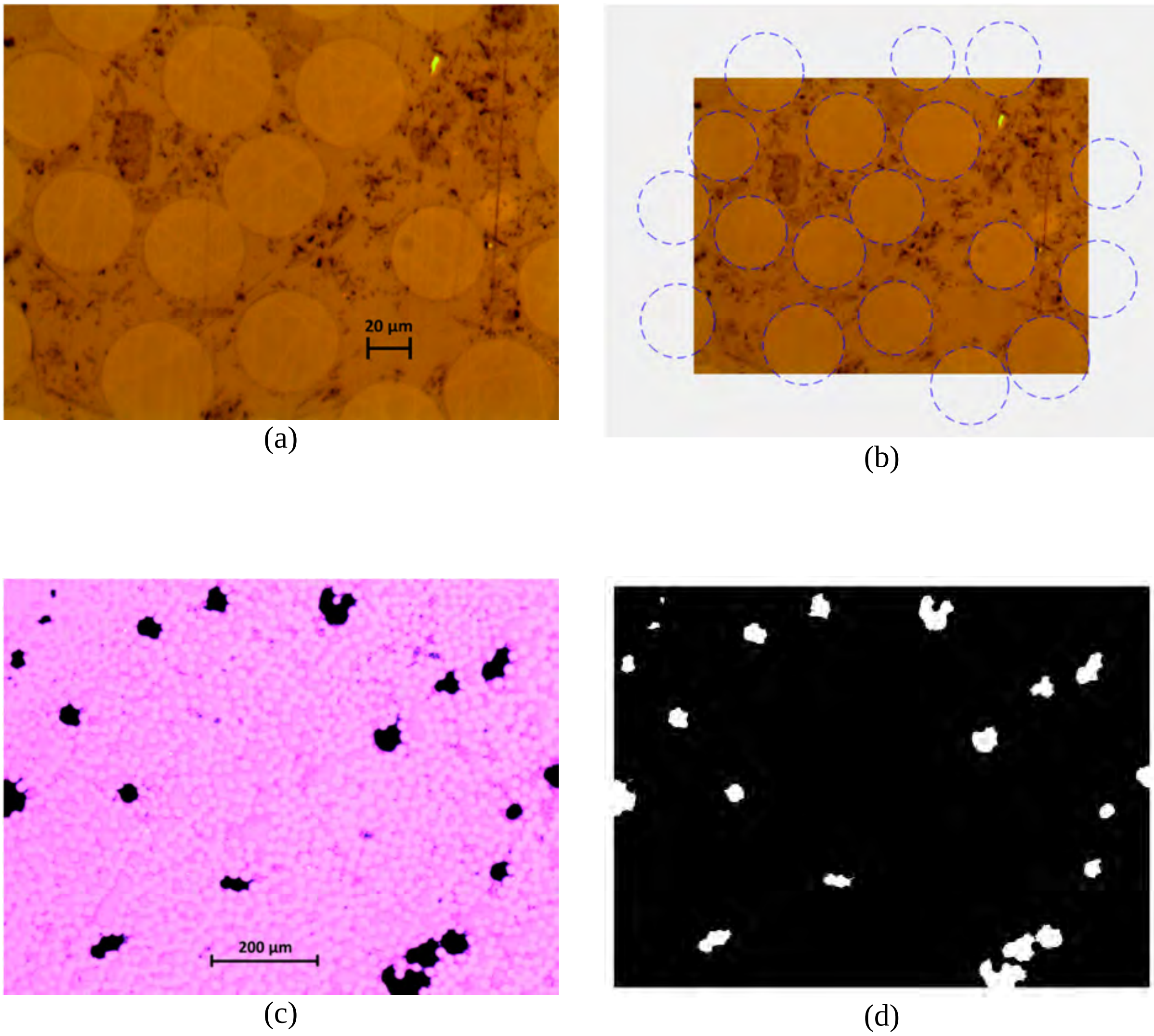

Fig. 41–Example micrographs: (a) Raw image for fiber volume content (b) Full-fitted circles around fibers for fiber volume content; (c) Raw image for void volume content; (d) Thresholded image for void volume content

4.1.8. Modified tensile strength test

Due to the size of the GFRP rebar specimens extracted from the Sierrita de la Cruz Creek Bridge, it was decided that a modified tensile strength test would be performed. Extracted rebars as well as virgin (unused) rebars were cut into coupons and tested to determine a coupon ultimate tensile strength. The coupons were approximately 0.45 x 10 x 0.1 in. (11 x 254 x 3 mm) (width x length x thickness) using a precision saw at Owens Corning. Full-size rebars of the same kind as the virgin coupons were used for a full-sized tensile strength test according to ASTM D7205. Using the results from the virgin full-size rebars and from tensile tests performed in 2000 on bars used in Sierrita de la Cruz Creek, a correlation factor was calculated between the coupon ultimate tensile strength and the full-sized ultimate tensile strength. This correlation factor was then applied to the results of the extracted tensile coupons to estimate the full-sized tensile strength of the extracted rebars.

4.1.8.1. Coupon test procedure

Both the 22 in. (559 mm) extracted rebars and the virgin rebars were cut into coupons approximately 0.45 x 10 x 0.1 in. (11 x 254 x 3 mm) (width x length x thickness) using a precision saw at Owens Corning. The coupons were labeled as left, center and right. All coupons were sliced to the same size, the left coupon is the first slice from the edge, center the second and right the third slice. See Fig. 42. Tabs of 2.25 in. (57 mm) length were attached to both ends, providing a gauge length of approximately 5.4 in. (137 mm) for testing. Specimens were then placed in sealable plastic bags and shipped to the University of Miami. A specimen with tabs attached is seen in *Fig. 43*.

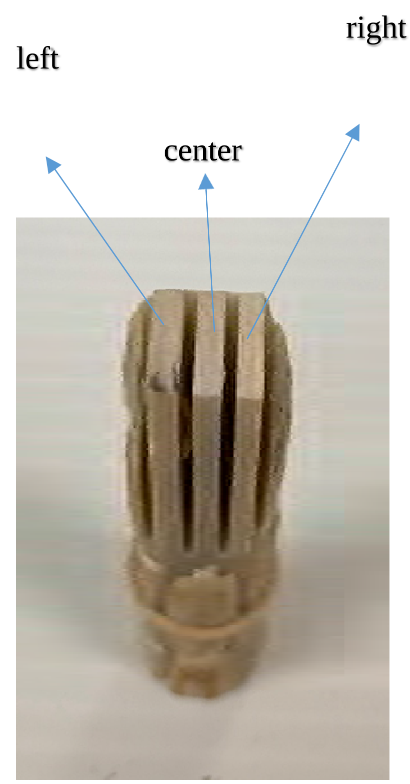

Fig. 42–Sierrita de la Cruz bar after coupon slices extraction

Fig. 43–GFRP coupon for tensile test

One 0.24 in (6 mm) strain gauge was attached longitudinally, slightly below the midpoint of the specimen. During testing, an extensometer was placed directly above the strain gauge. The extensometer was removed at a load of 4000 lb (17,793 N) during testing of the virgin samples, and varying loads for the extracted samples. Specimens were tested in a 22 kip (100 kN) load frame. Tabs were gripped at a pressure of 1500 psi (10 MPa) to avoid crushing of the tab during testing. Strain was applied at rate of 0.05 in./in. (0.05 mm/mm) until failure was reached.

4.1.8.2. Full sized test procedure

Full sized virgin rebars were tested according to ASTM 7205. Before testing, the bars were anchored at the end with steel tubes to prevent grip-induced damage. The steel tubes were cleaned to ensure adhesion with the expansive grout. The GFRP bar goes through the hole of the steel pipe and through the PVC cap and the pipe is filled with grout. The pipes with rebars were placed on a fixture to ensure the bar is held axially aligned in the tube. At least 12 hours should elapse before flipping the bar to place the anchor at the other end.

The GFRP bar was mounted in the 200 kip (890 kN) machine, an extensometer was placed on the bar and the machine was pre-loaded to about 5 kips (22 kN) to ensure proper rebar grip. The specimen was loaded monotonically in tension and the extensometer was removed prior to failure. Force, longitudinal strain, and longitudinal displacement were recorded during the test.

4.2. Concrete tests

4.2.1. Chloride penetration

Chloride penetration depth was evaluated using a 0.1M silver nitrate solution to determine the presence of chlorides at the depth of the GFRP rebar. Concrete cores were split to expose a fresh surface and compressed air was used to remove dust particles from this surface. The silver nitrate solution was sprayed onto the surface and allowed to dry. A lighter color indicates areas of chloride penetration, and a darker color indicates areas not affected by chlorides.

4.2.2. Chloride content

ASTM C1543 was used in this study to determine the chloride content level. There are mainly two techniques of chloride analyses: acid-soluble and water-soluble. In this study, water-soluble technique was used, as it can measure the chlorides free to deteriorate the passive layer of concrete (Myers et al. 2012). The test was carried out using Rapid Chloride Testing (RCT) equipment made by Germann Instruments, Inc. The procedure started by extracting some concrete powder from the concrete cores (about 23 grains (1.5-2.0 g)) and then poured into a vial that has 0.3 oz. (9 ml) of extraction liquid. Next, the mixture was shaken for 5 min. and then left for 24 hours to get a complete reaction. After that, the calibration process started by submerging an electrode into calibrating fluids of 0.005%, 0.020%, 0.050%, and 0.500% chloride concentrations. The readings from calibration were used to draw the chloride content curve on a log-scale paper. After calibration, the electrode was submerged into the specimens' vials. The readings were then taken and dropped on the line to see what equivalent chloride contents these points had. The test was conducted twice for each specimen and two specimens were used in this study. An image from the test is shown in *Fig. 44*.

Fig. 44–Chloride content test

4.2.3. Carbonation depth

Carbon dioxide that penetrates the surface of concrete can react with alkaline components in the cement paste, primarily $Ca(OH)_2$. As a result, the pH value of the pore solution will decrease. Phenolphthalein indicator solution is used to identify the depth of this reaction within concrete. This test was carried out by spraying the solution over a fresh-cut concrete surface and then monitoring the change in surface's color. Concrete cores were split to expose a fresh surface, compressed air was used to remove dust particles, and then phenolphthalein indicator solution was sprayed onto the surface and allowed to dry. Specimens turn pink when pH is above 9, and remains colorless when pH is below 9. The solution mixture has 1% phenolphthalein, 70% ethyl-alcohol and 29% distilled water per volume ratio.

4.2.4. pH

4.2.4.1. Procedure according to Grubb, Limaye and Kakade

For nine of the 11 bridges, the procedure outlined by Grubb, Limaye, and Kakade (Grubb et al. 2007) was used to determine the pH of the extracted concrete cores at various depths. Cores were split and then drilled to collect 77 grains (5 g) of concrete dust for each test. Split cores were drilled at three varying depths from 0.5 in. (13 mm) below the surface of the concrete to 0.5 in. (13 mm) above where the GFRP rebar had been located.

The concrete dust was then mixed with 0.34 oz. (10 ml) of fresh distilled water at a temperature of 73.4°F (23°C). The mixture was stirred for 30-second intervals three times over seven minutes and then filtered through No. 40 filter paper. A calibrated pH probe was then used to read the pH of the mixture.

The pH test was performed on concrete dust from one-half of the split cores, and phenolphthalein indicator solution was sprayed on the surface of the other half of the split cores. Once the phenolphthalein indicator solution dries, specimens with pH above 9 turn pink, while specimens with pH below 9 remain colorless.

4.2.4.2. Rainbow indicator

For the other three bridges, namely: McKinleyville, Roger's Creek and Thayer Bridge, a different method was used. A rainbow indicator from Germann Instruments, Inc. was sprayed on a fresh surface of concrete. Once the indicator dries, a change in color can be observed on the concrete sample. The color indicates the pH value, according to the color pallet seen in *Fig. 45*.

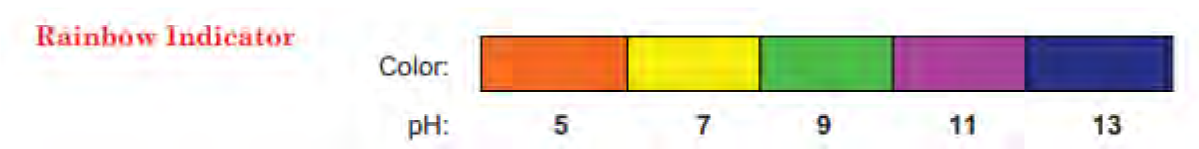

Fig. 45–Rainbow indicator color palette

5. Test Distribution

The testing of concrete and GFRP rebars was performed through a collaboration between the University of Miami, Penn State University, Missouri University of Science and Technology and Owens Corning. The distribution of samples for durability testing was divided between the collaborators based on their testing capabilities. Most concrete tests were performed at the University of Miami, while the GFRP tests were divided based on the testing capabilities of each laboratory. The GFRP testing capabilities of each collaborator are indicated with an "x" in Table 6.

Table 6. Testing capabilities of collaborators

GFRP Tests	**University/Company**			
	University of Miami (UM)	**Missouri University of Science & Technology (MS&T)**	**The Pennsylvania State University (PSU)**	**Owens Corning (OC)**
Fiber Content	x	x	x	x
Glass Transition Temperate (DSC)		x	x	x
Scanning Electron Microscopy (SEM)	x	x		x
Energy-Dispersive X-ray Spectroscopy (EDS)	x	x		x
Interlaminar Shear	x	x		
Moisture Content			x	
Water Absorption	x	x	x	
Direct Tension	x			

One challenge in testing was the relatively small sample size due to a) the limited number of cores that could be extracted; and, b) the difficulty of locating GFRP rebars during the extraction process. With the exception of the Sierrita de la Cruz Creek Bridge which had longer samples, the maximum length of the extracted GFRP rebar was 3.75 in (95 mm). This limited the collaborators to small-scale tests with few repetitions. For each bridge, each test was repeated at least three times. For some tests that required sample sizes of 1 in. (25 mm) or smaller, the bars were cut to the required dimension so that the minimum of three repetitions could be achieved with one bar. For other tests, however, to achieve a minimum of three repetitions per test method, bars of the same size from the same bridge were assumed to have had identical exposure conditions. For example, the fiber content test was conducted on OH1_C1_B1, OH1_C2_B1, and OH1_C5_B1, as shown in Appendix III.

A complete breakdown of the testing matrix, including length of bar designated for each test and laboratory conducting the test can be found in Appendix I. Table 7 shows a summary of the laboratories performing tests on each bridge.

Table 7. Test performed by bridges and laboratories

Bridge	Fiber Content	Moisture Content	Moisture Absorption	DSC	SEM/EDS	Horizontal Shear	Tension
IA	UM		UM	S&T	UM	UM*	
OH2	MST, PSU, OC	PSU	PSU	MST, PSU, OC	OC	MST	
VA	UM, OC		UM	MST, OC	OC		
CO	UM, PSU	PSU	PSU	PSU	UM	UM	
OH1	UM		UM	S&T	UM	UM	
WV	OC, PSU		PSU	PSU	OC	UM	
IN	UM, OC		PSU	PSU	OC	UM	
KY	MST, OC			MST	OC		
TX	UM			UM	UM	UM	UM
MO1	UM			UM	UM	UM	
MO2	UM			UM	UM	UM	

*Failure mode was not as expected-results invalid

6. Test Results

6.1. GFRP test results

6.1.1. Fiber content

Tests performed at the University of Miami, Missouri S&T, and Penn State University followed the burnoff procedure explained in Section 4.1.1.1, while the tests performed at Owens Corning followed the burnoff and acid wash procedures explained in Section 4.1.1.2. The fiber contents for all bars following the burnoff tests according to the ASTM D7957 GFRP bar specification, which include remnant filler attached to the fibers, are shown in Table 8. The fiber contents were above 70%—the minimum required percentage by ASTM D7957 for quality control and certification—for all bridges except Roger’s Creek. The fiber content results for the individual bars are provided in Appendix III.

Table 8. Average fiber content for each bridge

Bridge	No. of Samples	Average Fiber Content (%)	Standard Deviation (%)
Gills Creek*	6	72.1	1.78
O'Fallon Park	6	72.9	1.93
Salem Ave.	3	72.5	0.06
Bettendorf	3	73.3	1.29
Cuyahoga County*	15	76.4	2.41
McKinleyville	6	73.5	2.82
Thayer Road	3	76.5	0.078
Roger’s Creek	5	69.2	1.08
Sierrita de la Cruz Creek	9	76.4	N/A
Walker Box Culvert	4	82.8	N/A
Southview	4	73.4	N/A

*Although Owens Corning measured fiber content on some of the bars from this bridge, the fiber weights included in this table include remnant filler particles remaining on the fibers after burnoff.

The Owens Corning fiber content results following acid washing are given in Appendix III. The percent weight of fiber without remnant filler was typically about 13 percentage points less than the weight of the fiber with remnant filler.

The image analysis results indicate a fiber volume content of about 53%, a matrix content of about 46% and void content of about 1% for a small sampling of Cuyahoga and O’Fallon bars. The image analysis details for three individual bars are given in Appendix III.

6.1.2. Water absorption

Water absorption test, as described in Section 4.1.2, was performed on eight of the eleven bridges. These include Gills Creek, O'Fallon Park, Salem Ave., Bettendorf Bridge, Cuyahoga, McKinleyville, Thayer Road, and Roger's Creek.

According to ASTM D570 Sections 7.1 and 7.4, water absorption results include a value for 24-hour absorption and long-term immersion. The results of 24-hour absorption, equilibrium absorption and length of saturation results for the individual bridges are reported in Appendix III.

Table 9. Average long-term immersion

Bridge	**Number of Samples**	**Average 24hr Immersion (%)**	**Weight Change at Equilibrium (%)**	**Length of Saturation (days)**
Gills Creek	3	0.58	1.57	179
O'Fallon Park	3	0.01	0.30	110
Salem Ave.	5	0.10	0.30	85
Bettendorf	3	0.54	2.16	179
Cuyahoga	7	0.19	1.51	228
McKinleyville	6	0.10	0.23	56
Thayer Road	5	0.02	0.02	56
Roger's Creek	3	0.05	0.16	77

For Cuyahoga and O'Fallon Park bridges, long-term data of moisture uptake and weight gain at equilibrium were analyzed. Percent weight changes for the O'Fallon and Cuyahoga bars up to Dec. 15, 2018 (271 days) are shown on a log time scale in *Fig. 46*. By 259 days, all bars had met the ASTM D570 equilibrium condition of less than 5 mg (1.1×10^{-5} lb) average weight gain per two-week period over the last three bi-weekly measurement intervals. Table 10 lists the weight gains at equilibrium and at the last measurement (271 days). The average weight gain for the O'Fallon bars at saturation is 0.30%, which is much less than the 1% qualification limit established in ASTM D7957 for the same test conditions.

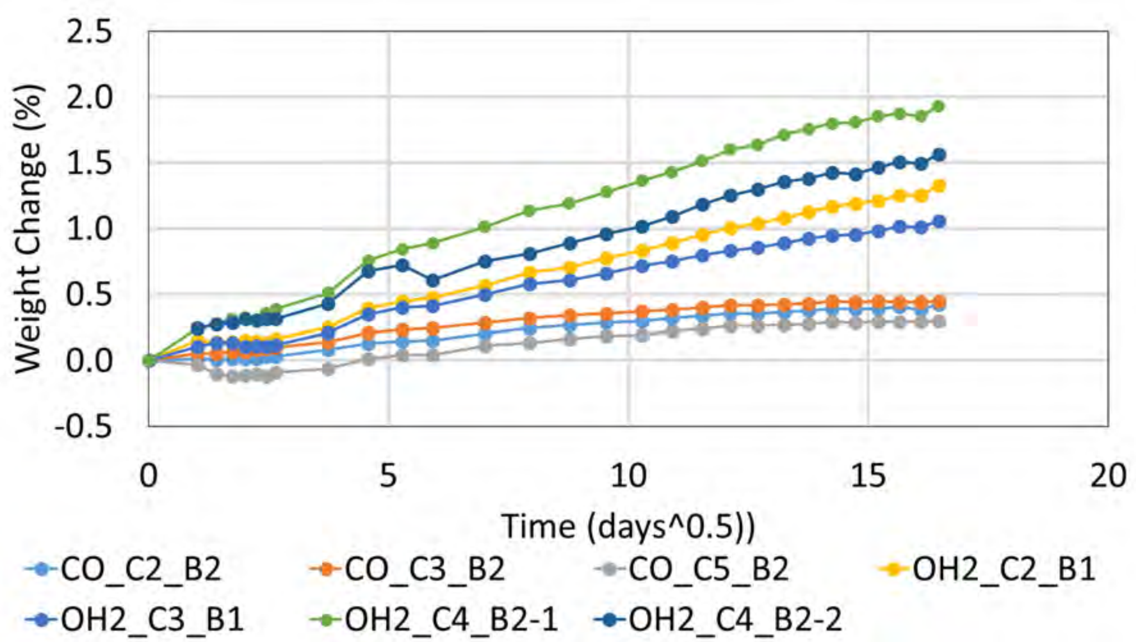

Fig. 46–Graph of Cuyahoga and O'Fallon moisture uptake versus square root of time for exposure to 122°F (50°C) distilled water

Table 10. Percent weight change of O'Fallon and Cuyahoga bars for exposure to *122°F (50°C)* distilled water

Specimen ID	**% Weight Change at D570 Equilibrium / days**	**% Weight Change at 271 Days**
CO_C2B_B2	0.322 / 119	0.421
CO_C3_B2	0.355 / 91	0.446
CO_C5_B2	0.223 / 119	0.298
OH2_C2_B1	1.254 / 259	1.325
OH2_C3_B1	0.946 / 203	1.058
OH2_C4_B2-1	1.874 / 245	1.931
OH2_C4_B2-2	1.417 / 217	1.563

6.1.3. Horizontal shear

The horizontal shear test followed the procedure described in Section 4.1.3.

Horizontal shear tests were performed in eight out of the 11 bridges. The samples from Gills Creek, Roger's Creek and Walker Box Culvert were too small to run the test.

Due to the size of the specimens of Bettendorf Bridge, the bars were not tested according to ASTM D4475. The anvils available at the University of Miami did not fit the specimens properly, and an alternative test set up was attempted (Fig. 47). The failure mode of the specimens was not acceptable for horizontal shear, and therefore the results are invalid and were not included in Table 11.

Table 11. Average apparent shear strength

Bridge	**Nominal Diameter**	**Number of Samples**	**Average Apparent Shear Strength, psi (MPa)**
O'Fallon Park	#7	2	6115 (42)
Salem Ave.	#6	3	6459 (45)
Cuyahoga	#6	3	4316 (30)
McKinleyville	#3	3	5214 (36)
Thayer Road	#5	3	6809 (47)
Sierrita de la Cruz Creek	#5	5	6047 (42)
Southview Bridge	#6	3	6340 (44)

Fig. 47–Modified horizontal shear test setup for short bars

6.1.4. DSC and modulated DSC

DSC and modulated DSC were performed on bars from eight bridges according to the procedures described in Section 4.1.4. For the remaining three bridges, the dynamic mechanical analysis (DMA) method was used. The DMA test method is briefly described in the T_g section of Appendix III, in the sub-section on the Sierrita de la Cruz Creek bridge. In Table 12, the average T_g for each bridge is given. *Fig. 48* shows an example DSC curve for O'Fallon core No. 2, bar No. 2 (OF_C2_B2). Test results for individual specimens are provided in Appendix III.

Table 12. Average T_g results for all bars

Bridge	**Average T_g (°F)**	**Average T_g (°C)**
Bettendorf	228	109
Cuyahoga	198	92
Gills Creek	202	95
O'Fallon Park	176	80
Salem Ave.	226	108
Roger’s Creek	203	95
Sierrita de la Cruz Creek*	239	115
Walker Box Culvert*	233	112
Southview*	213	101
McKinleyville**	202	95
Thayer Road**	189	87

Notes:
*T_g obtained with dynamic mechanical analysis rather than DSC.
**The lower of the two T_g values is reported.

The lowest T_g was 176°F (80°C) for O’Fallon Park Bridge and the highest was 239°F (115°C) for Sierrita de la Cruz Creek. It should be kept in mind that bars from Sierrita de la Cruz Creek were analyzed using DMA rather than DSC. According to the ASTM D7957 GFRP bar specification, the T_g is required to be equal to or greater than 212°F (100°C) as a critical parameter in load transfer capability of the resin.

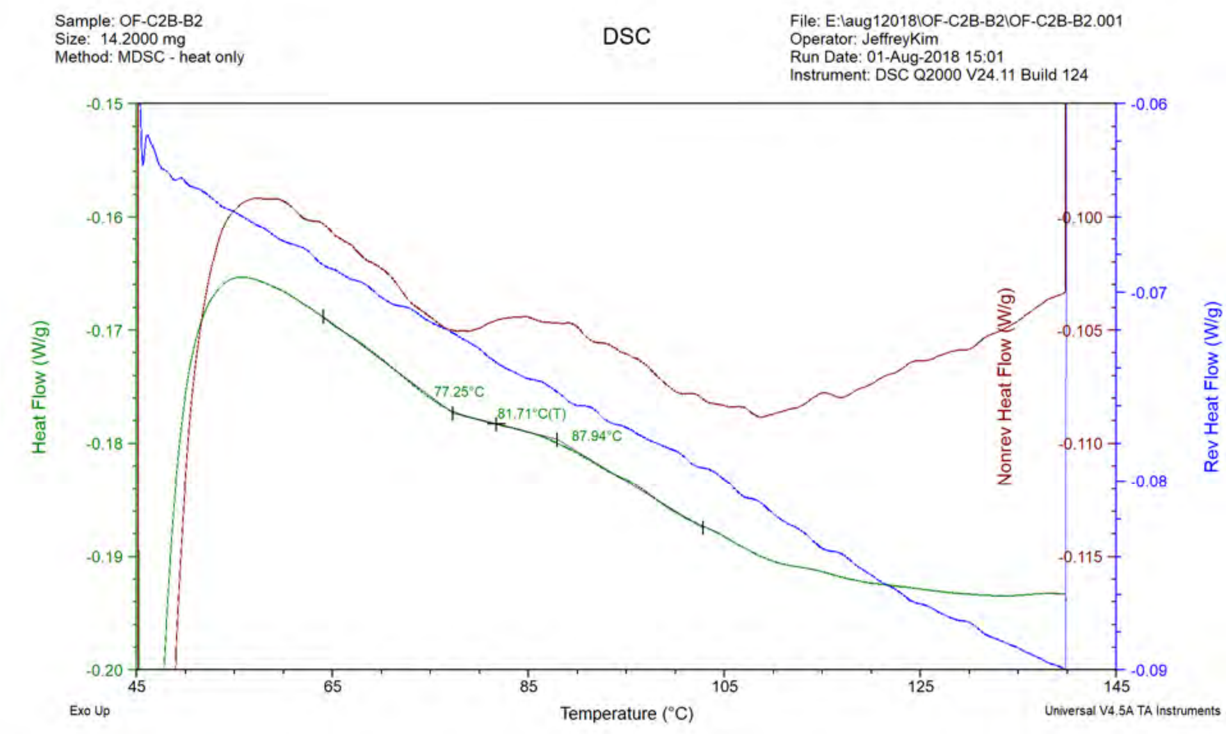

Fig. 48–Example differential scanning calorimetry curve for determining T_g on a bar from the O'Fallon bridge

6.1.5. SEM/EDS

SEM imaging and EDS analysis were performed at the University of Miami for bridges Bettendorf, O'Fallon, Salem Ave., Sierrita de la Cruz Creek, Walker Box Culvert and Southview. Samples from the remaining bridges were tested at Owens Corning. The SEM imaging and EDS followed the procedure described in Section 4.1.5.

Evidence of GFRP rebar fibers being negatively affected by concrete environment after 15 years in service is minimal--0.05 to 0.12 % of total fibers for Cuyahoga and Gills Creek bridges. The number of fibers evidently affected is about 192 out of 352,000 fibers, estimated from counting fibers with obvious signs of damage in one quadrant, multiplied by four. This is much less than predicted by accelerated test methods, and has a negligible impact on mechanical properties. See Section 1.4 and 1.5 in Appendix V.

Some bars from McKinleyville and Roger's Creek bridges presented physical damage on fibers on the outer edge of the rebar. This physical damage is likely due to the specimen preparation procedure (saw cutting and polishing). The damaged fibers were typically located near a void in the resin matrix. See section 1.6 and 1.8 in Appendix V.

In the bars from Thayer Road Bridge, the physical damage was likely from the manufacturing process as the fiber damage is isolated to perimeter fibers and appears to be a partial fiber.

The results of each bridge are presented in Appendix V. *Fig. 49* shows an SEM image without any deteriorated fibers, while *Fig. 50* shows an SEM image with fibers possibly deteriorated by concrete exposure.

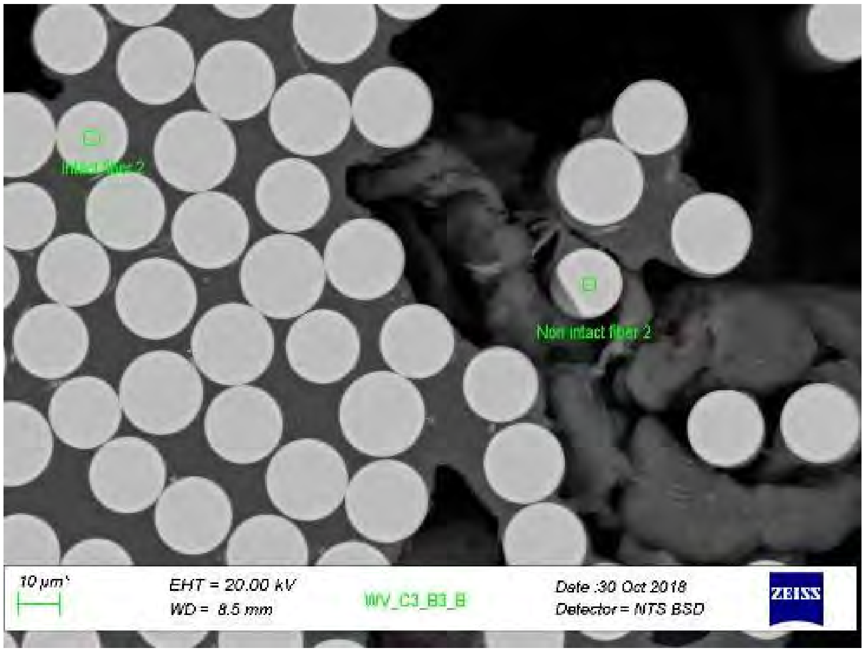

Fig. 49–Sample from McKinleyville Bridge – no fibers negatively affected by concrete

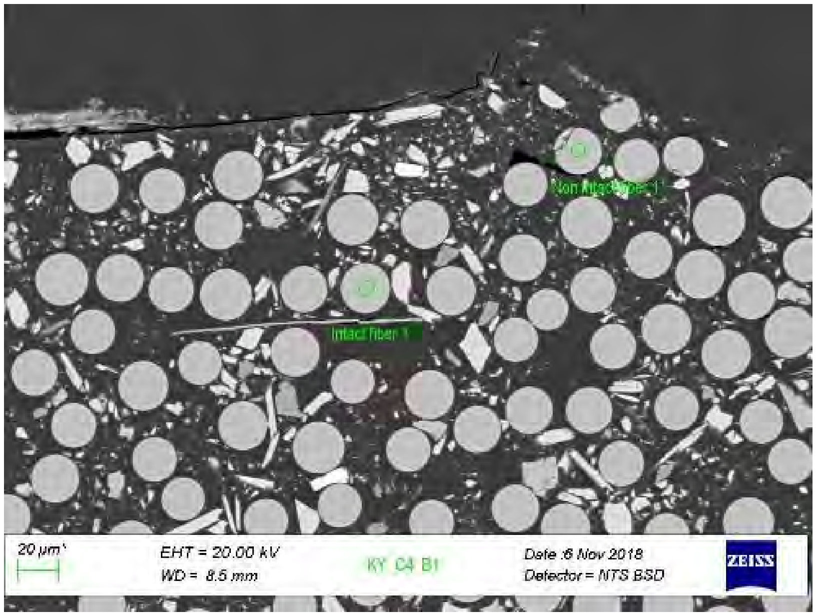

Fig. 50–Sample from Roger's Creek Bridge - few fibers may be negatively affected by concrete exposure

The results of EDS analysis showed the predominance of Si, Al, Ca (from glass fibers) and C (from the matrix) chemical elements in the extracted samples. No change in elemental distribution was found between central fibers and non-intact fibers. *Fig. 51* shows the result of EDS in samples from Walker Box Culvert Bridge.

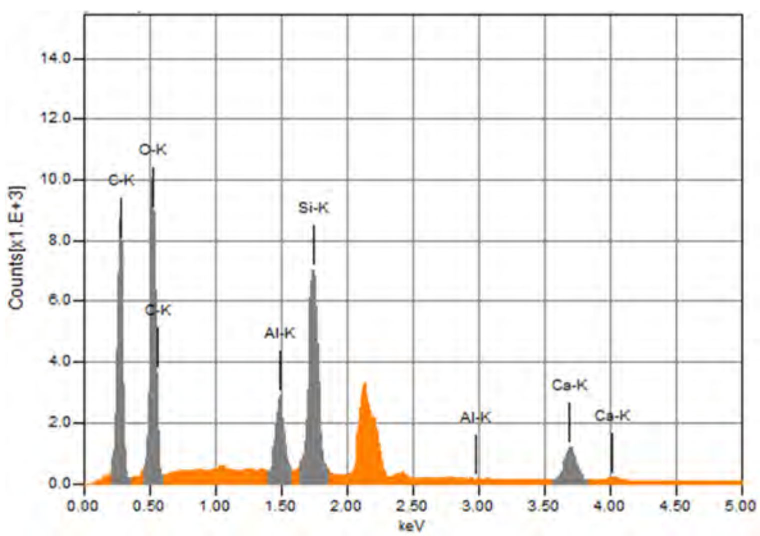

Fig. 51–Result of the EDS analysis performed on GFRP samples extracted from Walker Box Culvert Bridge

6.1.6. Moisture content

Moisture content measurement was performed in five of the 11 bridges: Gills Creek, Salem Ave., Bettendorf, O'Fallon Park and Cuyahoga. Of the ones completed to-date (Cuyahoga and O'Fallon), all dry-out specimens reached equilibrium after 56 days at 176°F (80°C). A plot of percent weight loss versus the square root of time (in days) is shown in *Fig. 52*. It can be seen that the weight loss is not monotonic. It is suspected that the deviations from monotonic weight loss are due to abnormal humidity conditions in the laboratory, while affecting the weigh measurement, although this possibility cannot be verified.

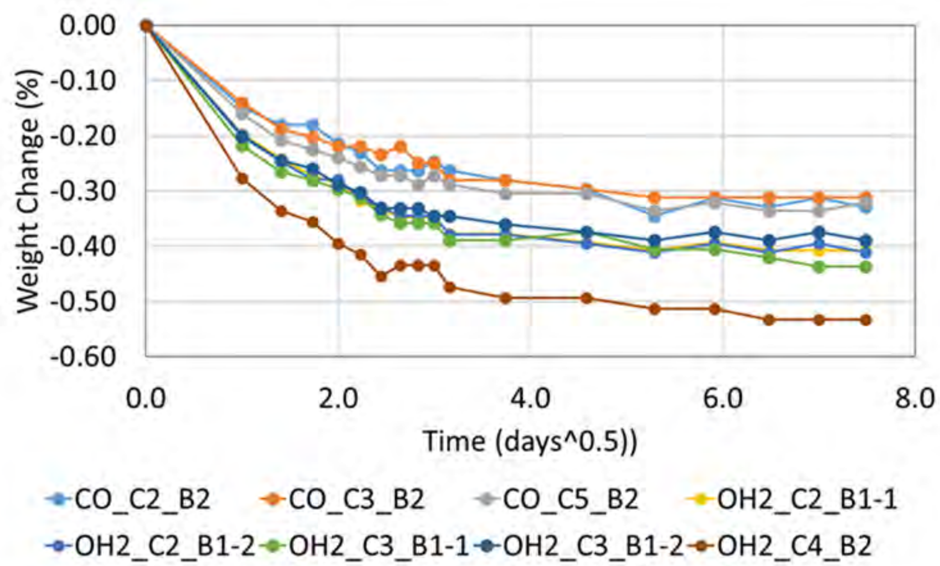

Fig. 52–Weight change versus the square root of drying time, in 176°F (80°C) circulating oven air for Cuyahoga and O'Fallon bridges

The weight changes at equilibrium, as a percent of weight before the drying procedure, are listed in Table 13. Overall, the weight losses from the dry-out procedure ranged from 0.31% to 0.53%. Upon conversion of these results to weight gains from a substantially dry initial state, the as-received moisture content of these bars due to field exposure likewise ranged from 0.31% to 0.53%. The moisture content of the bars during the several months' time between when the bars were extracted from the bridges to when they were tested could be affected by the environment in which they were stored.

Table 13. Percent weight change at equilibrium for specimens dried in 176°F (80°C) circulating oven air for Cuyahoga and O'Fallon

Specimen ID	% Weight Change
CO_C2B_B2	-0.329
CO_C3_B2	-0.312
CO_C5_B2	-0.320
OH2_C2_B1-1	-0.408
OH2_C2_B1-2	-0.411
OH2_C3_B1-1	-0.436
OH2_C3_B1-2	-0.389
OH2_C4_B2	-0.533

It is noteworthy that the OH2_C4_B2 bar with the highest as-received moisture content of all tested bars is also the only smaller diameter (5/8 in. (16 mm)) bar of all bars tested. The other bars have a larger (3/4 in. (19 mm)) diameter, which according to theory leads to less weight gain/loss for a given immersion/dry-out time because of a larger moisture permeation path in the material.

The O'Fallon bars had generally less as-received moisture (0.320%, on average) than the Cuyahoga bars (0.436%, on average). As a point of reference, ASTM D7957 requires that GFRP bars absorb no more than 1% moisture at saturation at a temperature of 122°F (50°C).

6.1.7. Constituent volume contents by image analysis

Table 14 shows the fiber, matrix, and void volume contents of O'Fallon bars based on image analysis. A summary is provided in Table 14 and the detailed results for each collected are shown in Appendix III. The fiber volume contents range between 52.3% and 53.5% while the void volume contents range from 0.5% to 0.7%.

Table 14. Bar constituent contents, in percent by volume, according to image analysis (mean +/- standard deviation)

Specimen ID	Fiber Volume Content (%)	Matrix Volume Content (%)	Void Volume Content (%)
CO_C2B_B2	53.3±6.6	46.1±6.8	0.5±0.8
CO_C3_B2	52.3±5.3	47.0±5.1	0.7±0.6
CO_C5_B2	53.5±9.6	45.9±9.7	0.6±0.9

6.1.8. Modified tensile strength

6.1.8.1. Coupon test

The coupons of approximately 0.45 x 10 x 0.1 in. (11 x 254 x 3 mm) (width x length x thickness) were tensile tested at the University of Miami as described in Section 4.1.8.1. The coupons tested were extracted from Sierrita de la Cruz Creek Bridge and from pristine bars from the same manufacturer. The coupons were from the left, center and right side of a rebar circumference. The coupons from Sierrita de la Cruz Creek Bridge were labeled according to the side (L-left, R-right and C-center); however, the coupons from the pristine bars were not labeled relative to their location on the bar cross-section. The results of the modified tensile test for each coupon is shown in Appendix VI. Table 15, Table 16 and Table 17 show the summary of the results for the coupons for Sierrita de la Cruz Creek Bridge. Table 18 shows the summary of the results for the coupons from pristine bars.

Table 15. Sierrita de la Cruz Creek extracted coupons - left side of bar

Sample #	**Area, in^2 (mm^2)**	**Peak Load, lbs (N)**	**Max Stress, psi (MPa)**
1L	0.0405 (26.13)	N/A	N/A)
2L	0.0402 (25.94)	3,653 (16,249)	90,689 (625)
3L	0.0402 (25.94)	2,992 (13,309)	74,386 (513)
average	0.0403 (26)	3,323 (14,779)	82,538 (569)
std. deviation	0.0002 (0.129)	467 (2079)	11,528 (79)

Table 16. Sierrita de la Cruz Creek extracted coupons – center of bar

Sample #	**Area, in^2 (mm^2)**	**Peak Load, lb (N)**	**Max Stress, psi (MPa)**
1C	0.0223 (14.39)	4,935 (21,952)	89,350 (616)
2C	0.0447 (28.84)	4,486 (19,955)	100,216 (691)
3C	0.0452 (29.16)	4,621 (20,555)	102,164 (704)
average	0.0374 (24.13)	4,681 (20,822)	97,243 (670)
std. deviation	0.0131 (8.45)	230 (1023)	6,904 (48)

Table 17. Sierrita de la Cruz Creek extracted coupons - right side of the bar

Sample #	**Area, in^2 (mm^2)**	**Peak Load, lb (N)**	**Max Stress, psi (MPa)**
1R	0.0526 (33.94)	5,049 (22,459)	95,747 (660)
2R	0.0528 (34.06)	4,605 (20,484)	87,131 (601)
3R	0.0533 (34.39)	4,337 (16,292)	81,194 (560)
average	0.0529 (34.13)	4,664 (20,747)	88,024 (607)
std. deviation	0.0004 (0.258)	360 (1601)	7,317 (50)

Table 18. Pristine coupons properties (same manufacturer)

Sample #	Peak Load, lb (N)	Max Stress, psi (MPa)
1F	4,929 (21,925)	95,210 (656)
2F	4,609 (20,502)	83,094 (573)
3F	4,894 (21,770)	88,488 (608)
4F	4,538 (20,186)	102,772 (709)
5F	5,321 (23,669)	114,108 (787)
6F	4,065 (18,082)	89,583 (618)
7F	4,110 (18,282)	100,585 (694)
8F	4,609 (20,502)	97,934 (675)
9F	5,207 (21,162)	99,929 (689)
10F	4,618 (20,542)	98,265 (678)
average	4,690 (20,862)	96,997 (669)
std. deviation	413 (1837)	8,654 (60)

6.1.8.2. Full-size bar test

Ten #5 pristine bars were tested for tension capacity at the University of Miami as described in Section 4.1.8.2. The test set up is shown in Fig. 53 and the results of the test is shown in Table 19. The average peak load was 36,989 lbs. (164,535 N), which is similar the manufacture's specification dated 2002. The results of the tension test for each bar is shown in Appendix VI. All bars failed as shown in Fig. 54.

Table 19. Pristine full bar properties

Sample #	Rebar Area, in^2 (mm^2)	Peak Load. lb (N)	Max Stress, psi (MPa)
1	0.31 (200)	37,312 (165,972)	120,361 (829)
2	0.31 (200)	38,008 (169,068)	122,606 (945)
3	0.31 (200)	35,608 (158,392)	114,865 (792)
4	0.31 (200)	37,259 (165,736)	120,190 (829)
5	0.31 (200)	38,186 (169,860)	123,181 (849)
6	0.31 (200)	35,264 (156,862)	113,755 (784)
7	0.31 (200)	37,488 (166,755)	120,929 (834)
8	0.31 (200)	37,212 (165,527)	120,039 (828)
9	0.31 (200)	36,756 (163,499)	117,897 (813)
10	0.31 (200)	36,972 (164,460)	119,265 (822)
Average	0.31 (200)	36,989 (164,535)	119,318 (823)
Std. Deviation		936	3,041

Fig. 53–Tensile test set up

Fig. 54–Pristine GFRP tension failure

A correlation between the extracted coupons, pristine new generation coupons, pristine new generation bars and vintage bars was established to determine the possible degradation of the bars after 17 years of exposure. It was found that the pristine new generation coupons when compared to the new generation pristine full-sized rebars showed a strength of about 18.7% lower. The extracted coupons when compared to the vintage rebars had a difference of 20.8% in their strength. Possible reasons to explain the difference in strength between full-size bars and slices are damage to fiber during saw-cutting and use of nominal area for full-size bars.

It was found that the new generation bars have 4.6% more strength than the vintage bars. This is likely the result of improved manufacturing quality over the years. By assuming the change in strength between coupons (sliced bars) and full-sized rebars is equal to 18.7%, for bars that have no degradation, it could be determined that the extracted bars had a reduction in strength of 2.13% due to long-term degradation. The 2.13% reduction in tensile strength is observed over 17 years of service and it would correspond to a drop in strength of 12.5% over a period of 100 years if the degradation rate is assumed to be linear.

Table 20 shows the properties of the pristine coupons compared to the properties of the pristine full sized bars. Table 21 shows the properties of Sierrita de la Cruz Creek extracted coupons compared to full-size vintage rebar data from 2000. Table 22 shows the long-term durability strength correlation.

Table 20. Pristine coupons compared to pristine full-sized bars

Rebar Size	Peak Load, lb (N)	Max Stress, psi (MPa)	Standard Deviation, psi (MPa)	Peak Load Average, lb (N)	Average Max Stress, psi (MPa)
1	37,312 (165,972)	120,360 (830)	3,041 (21)	37,007 (164,615)	119,318 (823)
2	38,008 (169,068)	122,608 (845)			
3	35,608 (158,392)	114,867 (792)			
4	37,259 (165,736)	120,190 (829)			
5	38,186 (169,860)	123,181 (849)			
6	35,264 (156,862)	113,756 (784)			
7	37,488 (166,755)	120,928 (834)			
8	37,212 (165,527)	120,040 (828)			
9	36,756 (163,499)	117,987 (813)			
10	36,972 (164,460)	119,265 (822)			
1F	4,929 (21,925)	95,210 (656)	8,654 (60)	4,690 (20,862)	96,997 (669)
2F	4,609 (20,502)	83,094 (573)			
3F	4,894 (21,770)	88,488 (610)			
4F	4,538 (20,186)	102,772 (709)			
5F	5,321 (23,669)	114,108 (787)			
6F	4,065 (18,082)	89,583 (618)			
7F	4,110 (18,282)	100,585 (694)			
8F	4,609 (20,502)	97,934 (675)			
9F	5,207 (23,162)	99,929 (689)			
10F	4,618 (20,542)	98,265 (678)			
% difference full-size to slice					18.71%

Table 21. Sierrita de la Cruz Creek extracted coupons compared to vintage rebar data

Sample #	Peak Load, lb (N)	Max Stress, psi (MPa)	Average Peak Load, lb (N)	Average Max Stress, psi (MPa)
1P	35,659 (158,619)	116,229 (801)	35,670 (158,668)	113,840 (785)
2O	37,519 (166,893)	122,291 (843)		
3O	32,693 (145,426)	106,561 (735)		
4O	33,833 (150,497)	110,277 (760)		
1L	N/A	N/A	4,335 (19,283)	90,110 (621)
2L	3,653 (16,249)	90,689 (625)		
3L	2,992 (13,309)	74,386 (513)		
1C	4,935 (21,952)	89,350 (616)		
2C	4,486 (19,955)	100,216 (691)		
3C	4,621 (20,555)	102,164 (704)		
1R	5,049 (22,459)	95,747 (660)		
2R	4,605 (20,484)	87,131 (601)		
3R	4,337 (19,292)	81,194 (560)		
% difference full-size to slice				20.84%

Table 22. Long-term durability strength correlation

Sample	Full size Strength, psi (MPa)	Coupon Strength, psi (MPa)	Change Between Coupon and Full-size
Pristine	119,318 (823)	96,997 (669)	18.71%
Extracted bars	113,840 (785)	90,110 (621)	20.84%
Difference due to degradation %			2.13%

6.2. Concrete test results

6.2.1. Chloride penetration

Chloride penetration test was performed in all 11 bridges. The tests consisted of applying a 0.1M silver nitrate solution in fresh broken concrete cores, as described in Section 4.2.1. The difference in the color of the concrete due to the silver nitrate was difficult to identify in some of the samples.

In some bridges, McKinleyville, Roger's Creek, Thayer Road, Southview and Walker Box, no chloride penetration was observed and in the worst case, for about 2.5 in of chloride penetration was observed.

The bridges that presented chloride penetration were Gills Creek, O'Fallon Park, Bettendorf, Salem Ave. and Cuyahoga. No visual chloride penetration was observed for the remainder of the bridges.

Fig. 55 shows the worst case scenario, where the chloride penetration was approximately 2.5 in. (64 mm) and *Fig. 56* shows the best-case scenario, where no visual chloride penetration was observed. The test results of the individual bridges are reported in Appendix IV.

Fig. 55–Cuyahoga Bridge sample with visual chloride penetration

Fig. 56–Southview Bridge sample with no visual chloride penetration

6.2.2. Chloride content

Chloride content for Cuyahoga Bridge was performed at Missouri S&T. The chloride content test was conducted using a water-soluble method that detects only the chloride content that deteriorates the oxide layer. Per Broomfield (2006), the chloride content is insignificant if the presence is less than 3%, low if it is between 3 to 6%, moderate if it is between 6-14%, and high if it is more than 14%. All the results were less than 1.2%; thus, the chloride content can be considered insignificant.

6.2.3. Carbonation depth

Carbonation depth tests were performed according to Section 4.2.3.

All 11 bridges were tested for carbonation depth. The purple zone indicated no carbonation and the white zone indicates the carbonation depth. Most samples presented some carbonation near the surface, but others presented no carbonation at all. Sierrita de la Cruz Creek Bridge, however, presented significant depth of carbonation reaching near the core of the sample. The samples from Sierrita de la Cruz Creek Bridge tested for carbonation are shown in Fig. 57. Fig. 58 shows an example where carbonation happened near the surface for the case of Cuyahoga Bridge.

The results of each individual bridge are reported in Appendix IV.

Fig. 57–Sierrita de la Cruz Creek Bridge carbonation depth

Fig. 58–Cuyahoga Bridge carbonation depth near the surface (deck)

6.2.4. pH test

The pH tests conducted at the University of Miami were performed with phenolphthalein indicator solution analysis or with the rainbow indicator as described in Section 4.2.4. The pH tests at Missouri S&T were conducted according to the extended procedure described Appendix II.

The pH of the samples varied between 9 and 13. The lowest average pH for was 10 for Roger's Creek and McKinleyville Bridge, while the highest average pH was 12.2 for Cuyahoga and Gills Creek Bridge. The average results for each bridge can be observed in Table 23. *Fig. 59* shows a sample tested with phenolphthalein indicator solution for Cuyahoga Bridge and *Fig. 60* its corresponding pH based on color range.

Table 23. Average pH

Bridge	**Average pH**	**Bridge**	**Average pH**
Bettendorf	12.1	Roger's Creek	10
Cuyahoga	12.2	Thayer Road	12
Gills Creek	12.2	Sierrita de la Cruz Creek	11.5
O'Fallon Park	12.1	Walker	11.5
Salem Ave	11.6	Southview	11.5
McKinleyville	10		

Fig. 59–Cuyahoga Core 4 pH test with phenolphthalein

Fig. 60–pH color range for Cuyahoga core 4

Fig. 61 shows a sample tested with the rainbow indicator. The test results for the individual bridge are shown in Appendix IV.

Fig. 61–McKinleyville pH range using the rainbow indicator

7. Conclusions

A variety of tests to assess physical, mechanical and chemical performance of GFRP and its surrounding concrete from 11 bridges with 15 to 20 years of service were undertaken to provide information on the durability of concrete structures reinforced with GFRP.

GFRP tests

The bars were cleaned of any adhered concrete using the edge of a steel spatula and were cut into pieces for various tests using a water-cooled diamond abrasive wheel. GFRP bar coupons were preconditioned before testing because of the differing conditions in each laboratory except those to be used for moisture content and modified tensile strength.

Bar coupons were tested for: a) fiber content (burnout and acid washout), b) constituents content by image analysis, c) water absorption, d) moisture content and e) glass transition temperature (T_g). GFRP bar cross-sections were analyzed by scanning electron microscopy (SEM) and energy dispersive X-ray spectroscopy (EDS) to observe any changes in microstructure. GFRP coupons were tested for horizontal shear strength and tensile strength for cut-off strips. Test results were compared to data collected from pristine bars at the time of bridge construction or currently manufactured bars when pristine data was not available. Finally, observations about compliance with current standards (ASTM D7957) were made. The outcomes of the tests are briefly summarized as follows:

- The results from <u>fiber content</u> measurement by weight using the ASTM D7957 modification of the ASTM D2584 burnoff test were above the 70% minimum required in ASTM D7957 for all bridges except one. For the post-burnoff specimens that were washed with an acid solution to remove remnant filler particles, the fiber content was approximately 10 to 13 percentage points less than the fiber content including remnant filler, indicating that remnant filler contributes significantly to the weight measurement.
- <u>Constituent contents</u> by volume, measured by image analysis for specimens from Cuyahoga and O'Fallon bridges, indicated a fiber volume content of about 53%, a matrix volume content of about 46% and void volume content of about 1%.
- The <u>water absorption</u> tests (ASTM D570) showed significant variability in weight gains after 24-hours and at saturation. Weight gains at equilibrium range between 0.02% and 2.16%. The current qualification limit established in ASTM D7957 is 1.0%.
- The <u>moisture content</u> tests for all bridges indicated a weight change at equilibrium less than 0.533%. It should be noted that several months passed between the time of extraction and the time of testing without the specimens being in a hermetically sealed container; thus, the measured moisture content could have been affected by the environment exposure.
- The <u>glass transition temperature</u> (T_g) measured by DSC method varied from 175°F (80°C) to 239°F (115°C). The limit currently established by ASTM D7957 requires a T_g equal to or higher than 212°F (100°C), which was achieved in bars from 5 out of 11 bridges. It should be noted that the current standards exclude the use of polyester resin that may have been used in some of the bars manufactured in the late 90's to early 2000's.

- The SEM results showed an estimated physical damage of the glass fibers in the range of 0.05 to 0.12% thus demonstrating that deterioration in the concrete environment after 15 years of service is minimal. The observed deterioration that occurs at the periphery of the bar is much less than predicted by accelerated test methods and has a negligible impact on mechanical properties. Some of the specimens showed fiber damaged that was caused by the preparation of the sample (i.e., cutting and polishing) stressing the importance of the preparation procedure that, as of today, is not standardized.
- The EDS showed no apparent sign of degradation as the chemical elements detected did not change from the distribution of those of a pristine bar.
- The results of the horizontal shear test were consistent with the values listed in current data sheets for the same manufacturers and higher than the values obtained from original bars when available. For example, the results from Sierrita de la Cruz Creek Bridge and Southview Bridge presented shear strengths 16 and 5% higher than the original bars, respectively. The post-curing of the resin over time may have been the reason for the increase in the shear strength. The difficulty of testing GFRP bar coupons in a fixture originally designed to test smooth bars remains an unresolved challenge.
- For the Sierrita de la Cruz Creek Bridge, tensile strength tests were conducted on strips saw-cut from extracted bars and strips as well as full-size bars currently produced by the same manufacturer. Additionally, tensile test data were available from pristine bars tested at the time of bridge construction. This allowed estimating the change in strength due to aging. Results indicated a reduction in tensile stress of 2.13% over a period of 17 years of service that would correspond to a drop in strength of 12.5% over a period of 100 years if the degradation rate is assumed to be linear.

Concrete tests

Concrete coupons were tested for: a) carbonation depth, b) chloride penetration and c) pH.

- The carbonation depth in most concrete cores was near the surface. An irregular carbonation depth with the maximum depth of 2.5 in. (64 mm) was observed in one of the concrete cores, indicating that carbonation may have reached some GFRP rebars.
- Chloride penetration tests were performed on samples from all bridges. In some bridges, no chloride penetration was observed and, in the worst case, about 2.5 in. (64 mm) of chloride penetration was observed. As for the carbonation depth, chloride penetration may have reached some GFRP rebars.
- Concrete pH values were recorded on samples from all bridges and found to be between 9 and 13, which met the expectation of the types of concrete and ages as used.

Overall considerations

GFRP bars from different manufacturers were used in these bridges. In terms of bar constituents, the glass fiber used was most probably E-type while the resin could have been vinyl ester or polyester.

The study provides a positive indication on the long-term durability of GFRP bars as the internal reinforcement for concrete structures. In general, GFRP bars did not show sign of significant physico-mechanical deterioration due to alkalinity and moisture of surrounding concrete.

For the samples obtained in one bridge, the estimated tensile strength reduction due to aging was 2.13% over a period of 17 years of service that would correspond to a drop in strength of 12.6% over a period of 100 years, assuming linear degradation. The strength reduction factor (C_E) currently adopted by most design guides to account for environmental degradation of GFRP bars is equal to 0.7. This value appears to be overly conservative based on the outcomes of this study.

8. References

ACI 440.6, 2008, *Specification for Carbon and Glass Fiber-Reinforced Polymer Bar Materials for Concrete Reinforcement*, American Concrete Institute, Farmington Hills, MI.

Alkhrdaji, T., and Nanni, A. 2001, "Construction and Long-Term Monitoring of a Concrete Box Culvert Bridge Reinforced with GFRP Bars," *Technical Report: #RDT01-016*, Center for Infrastructure Engineering Studies, UMR, Rolla, MO.

ASCE, 2017, "2017 Infrastructure Report Card." V. 11.

ASTM D7957/D7957M-17, 2017, *Standard Specification for Solid Round Glass Fiber Reinforced Polymer Bars for Concrete Reinforcement*, ASTM International, West Conshohocken, PA.

ASTM C1543-10a, 2010, *Standard Test Method for Determining the Penetration of Chloride Ion into Concrete by Ponding*, ASTM International, West Conshohocken, PA.

ASTM-D2584-18, 2018, "*Standard Test Method for Ignition Loss of Cured Reinforced Resins*, ASTM International, West Conshohocken, PA.

ASTM D4475-02, 2016, *Apparent Horizontal Shear Strength of Pultruded Reinforced Plastic Rods by the Short-Beam Method*, ASTM International, West Conshohocken, PA.

ASTM D5229/D5259M, 2014, *Standard Test Method for Moisture Absorption Properties and Equilibrium Conditioning of Polymer Matrix Composite Materials*, ASTM International, West Conshohocken, PA.

ASTM D570−98, 2018, *Standard Test Method for Water Absorption of Plastics* ASTM International, West Conshohocken, PA.

ASTM D7205/D7205M–06, 2011, *Standard Test Method for Tensile Properties of Fiber Reinforced Polymer Matrix Composite Bars*, ASTM International, West Conshohocken, PA.

STM E1356-08, 2014, "*Standard Test Method for Assignment of the Glass Transition Temperatures by Differential Scanning Calorimetry*, ASTM International, West Conshohocken, PA.

ASTM E1640, 2013, *Standard Test Method for Assignment of the Glass Transition Temperature by Dynamic Mechanical Analysis*, ASTM International, West Conshohocken, PA.

Broomfield, J.P. 2006, *Corrosion of Steel in Concrete*, V. 2: 1–50.

Camata, G., and Shing, P.B., 2004, "Evaluation of GFRP Deck Panel for the O'Fallon Park Bridge," *Report No. CDOT-DTD-R-2004-2*, Colorado Department of Transportation.

Camata, G. 2004, “Evaluation of GFRP Deck Panel for the O'Fallon Park Bridge,” *Report No. CDOT-DTD-R-2004-2*, Colorado Department of Transportation.

Chhabra, G.S.; Singh, V.; and Singh, M; 2018, *Corrosion Costs and Preventive Strategies in the United States*, NACE International. V. 31.

Eitel, A.K., 2005, “Performance of a GFRP Reinforced Concrete Bridge Deck,” *Thesis, 1-154*, Case Western Reserve University, Cleveland, Ohio.

Fico, R.; Galati, N.; Prota, A.; and Nanni, A.; 2006, *Southview Bridge Rehabilitation in Rolla, Missouri*.

Frosch, R.J; and Cihan, Pay, A; 2006, “Implementation of a Non-Metallic Reinforced Bridge Deck, Volume 2: Thayer Road Bridge,” *Publication FHWA/IN/JTRP-2006/15-2*. Joint Transportation Research Program, Indiana Department of Transportation and Purdue University, West Lafayette, Indiana, 2006.

Gooranorimi, O.; Myers, J.; Nanni, A.; ,2017, “GFRP Reinforcements in Box Culvert Bridge: A Case Study After Two Decades of Service,” *Concrete Pipe and Box Culverts, ASTM STP1601*, J. Meyer and J. Beakley, Eds., ASTM International, West Conshohocken, PA, pp. 75–88.

Gooranorimi, O.; Nanni, A.; 2017, “GFRP Reinforcement in Concrete after 15 Years of Service,” *Journal of Composites for Construction*, 2017.

Grubb, J.; Limaye, H.; and Kakade, A.; 2007, “Testing pH of Concrete: Need for A Standard Procedure,” *Concrete International*, Vo 29, No. 4, pp. 78-83.

Harik, I.E.; Alagusundaramoorthy, P.; Gupta, V.; Hill, C.; and Chiaw, C.C.; 2004. “Inspection and Evaluation of a Bridge Deck Partially Reinforced With GFRP Rebars,” *Report No. KTC-04-21/FRPDeck-1-97-1F*, Kentucky Transportation Center Research Report,

Hexion Responsible Chemistry, 2019, Epon Resin 862 Technical Data Sheet issued 2019, https://www.hexion.com/CustomServices/PDFDownloader.aspx?type=tds&pid=1acdf63b-5814-6fe3-ae8a-ff0300fcd525.

Holdener, D.; Myers, J.J.; and Nanni, A.; 2008, “An Overview of Composites Usage in Bridge Facilities in the State of Missouri, USA.” *Proceedings of the International Conference and Exhibition on Reinforced Plastics*.

Huntsman, 2008, “JEFFAMINE ® T-403 Polyetheramine,” https://www.ulprospector.com/en/na/Coatings/Detail/848/34455/JEFFAMINE-T-403-Polyoxypropylenetriamine.

ICC-ES, International Code Council-Evaluation Service, 2015, AC 454, *Acceptance Criteria for Fiber-Reinforced Polymers (FRP) Bars for Internal Reinforcement of Concrete Members*.

Kumar, S.V.; Thippeswamy, H.K.; and Gangarao, H.V.S; 1996, "McKinleyville Bridge: Construction of the Concrete Deck Reinforced with FRP Rebars," *Paper 6-F*,In International Composites EXPO, 97:10.

Mufti, A.A.; Banthia, N.; Benmokrane, B.; Boulfiza, M.; and Newhook, J.P.; 2007,"Durability of Durability of GFRP Composite Rods," *Concrete International*, V. 29, No. 2, pp. 37-42.

Myers, J.J.; Volz, J.S.; Sells, E.; Porterfield, K.; Looney, T.; Tucker, B.; Holman, K.; 2012, "Self-Consolidating Concrete (SCC) for Infrastructure Elements Report E – Hardened Mechanical Properties and Durability Performance," Missouri Department of Transportation, *Report TRyy1103*, Jefferson City, Mo.

Phelan, R.; Vann, W.; and Bice, J.; 2003, "FRP Reinforcement Bars in Bridge Decks: Field Instrumentation and Short-Term Monitoring," *Research Report: 9-1520-04*, Texas Department of Transportation. Lubbkock, TX.

Phillips, K.A.; M. Harlan; Roberts-Wollmann, C.L.; and Cousins, T.E.; 2005, *Performance of a Bridge Deck with Glass Fiber Reinforced Polymer Bars as the Top Mat of Reinforcement*, Virginia Center for Transportation Innovation and Research. Charlottesville, VA.

Reising, R., Shahrooz, B.; Hunt, V.; Lenett, M. ; Sotir, C.; Neumann, A.; Helmicki, A.; Miller, R.; Kondury, S.; and Morton, S.; 2001, "Performance of Five-Span Steel Bridge with Fiber-Reinforced Polymer Composite Deck Panels." Transportation Research Record: *Journal of the Transportation Research Board, No. 1770*.

Shekar., V; Petro, S.; GangaRao, H.; 2003, "Fiber-Reinforced Polymer Composite Bridges in West Virginia, *Transportation Research Record: Journal of the Transportation Research Board*.

Wang, W.; Gooranorimi, O.; Myers, J.J.; Nanni, A.; 2018, "Microstructure and mechanical Property Behavior of FRP Reinforcement Autopsied from Bridge Structures Subjected to In-situ Exposure," *16th International Congress on Polymers in Concrete 2018* (ICPIC 2018), Washington, DC, Apr. 29 – May 1, 2018.

Wipf, J.T., 2006, *Evaluation of the Bettendorf Bridge*, Iowa, Ames: Center for Transportation Research and Education. Ames, IA.

Appendix I: Sample Inventory

This appendix displays the extracted concrete cores from eleven bridges as an inventory and the GFRP test distribution by collaborator for each bridge.

The core samples are identified using a two-part identification scheme NN_Cx, where NN is the abbreviation of the bridge name or state and Cx indicates the x-th core number. This inventory presents information on the dimension of the extracted core, number of GFRP bars in the core, concrete cover of the GFRP bar and picture of each core.

The inventory and test distribution are divided by bridge name, the bridges presented here are: *Bettendorf, Cuyahoga*, *Gills Creek*, *O'Fallon Park*, *Salem Ave.*, *Sierrita de la Cruz Creek, Walker Box Culvert*, *Southview, McKinleyville*, *Thayer Road and Roger's Creek*. It must be noted that *Walker Box Culvert*, *Southview* and *Sierrita de la Cruz* are not included in the test distribution because all the GFRP tests for these bridges were performed at the University of Miami.

NOMENCLATURE

VA and GI =	Gills Creek Bridge
CO and OF =	O’Fallon Park Bridge
OH1 and SA =	Salem Ave. Bridge
IA and BE =	Bettendorf Bridge
OH2 and CU =	Cuyahoga County Bridge
WV =	McKinleyville Bridge
IN =	Thayer Road Bridge
KY =	Roger’s Creek Bridge
TX and SI =	Sierrita de la Cruz Creek Bridge
MO1 and WA =	Walker Box Culvert Bridge
MO2 and SO =	Southview Bridge

Concrete Sample Inventory
Bettendorf

Core	Height (in)	Diameter (in)	Clear cover (in)	Notes	Picture
BE_C1	2.75	3.75	--	Missing steel rebar	
BE_C2	2	3.75	--	Steel rebar, core has hole in center	
BE_C3	4.5	3.75	2.5	(1) GFRP rebar	

Core	Height (in)	Diameter (in)	Clear cover (in)	Notes	Picture
BE_C5	4.75	3.75	2.5	(1) GFRP rebar	
BE_C6	4.5	3.75	2.5	(1) GFRP rebar	
BE_C7	4.5	3.75	2.5	(1) GFRP rebar	

Cuyahoga

Core	Height (in)	Diameter (in)	Clear cover (in)	Notes	Picture
CU_C1	4.5	3.75	2.5	(1) GFRP rebar	
CU_C2	4.5	3.75	2.5	(1) GFRP rebar	
CU_C3	4.5	3.75	2.25	(1) GFRP rebar	

Core	Height (in)	Diameter (in)	Clear cover (in)	Notes	Picture
CU_C4	4.75	3.75	1.75	(2) GFRP rebar	
CU_C5	4.75	3.75	1.75	(2) GFRP rebar	
CU_C6	4.25	3.75	2.5	(1) GFRP rebar	

Core	Height (in)	Diameter (in)	Clear cover (in)	Notes	Picture
CU_C7	4.25	3.75	2.5	(1) GFRP rebar	
CU_C8	2.75	3.75	2.75	(2) GFRP rebar	

Gills Creek

Core	Height (in)	Diameter (in)	Clear cover (in)	Notes	Picture
GI_C1	4.5	3.75	2.5	(1) GFRP rebar	
GI_C2	3.5	3.75	2	(2) GFRP rebars	
GI_C3	4	3.75	2.25	(2) GFRP rebars	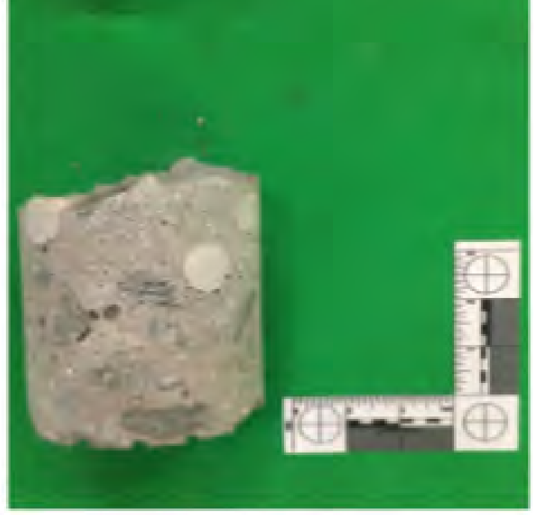

Core	Height (in)	Diameter (in)	Clear cover (in)	Notes	Picture
GI_C4	3.75	3.75	2.25	(2) GFRP rebars	
GI_C5	3	3.75	2.5	Missing '	
GI_C6	3.5	3.75	2.25	(1) GFRP rebar	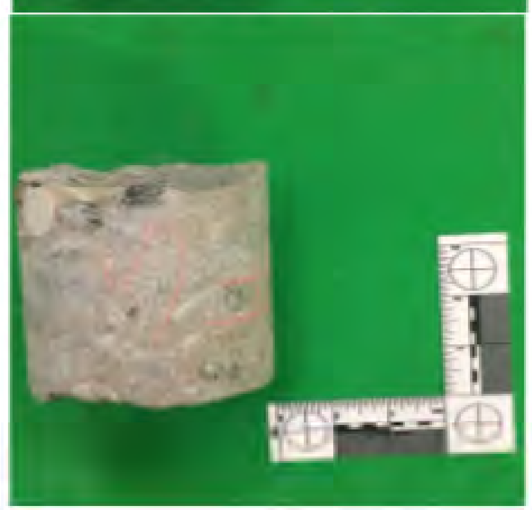

Core	Height (in)	Diameter (in)	Clear cover (in)	Notes	Picture
GI_C7	4	2.75	2.25	Concrete sample	
GI_C8	4.5	2.75	2.25	Concrete sample	
GI_C9	5	2.75	2.25	Concrete sample	

Core	Height (in)	Diameter (in)	Clear cover (in)	Notes	Picture
GI_C10	4	2.75	2.5	Concrete sample	

O'Fallon Park

Core	Height (in)	Diameter (in)	Clear cover (in)	Notes	Picture
OF_C1	1.5	3.75	1.5	(1) GFRP rebar	
OF_C2	3.25	3.75	2.5	(2) GFRP rebars	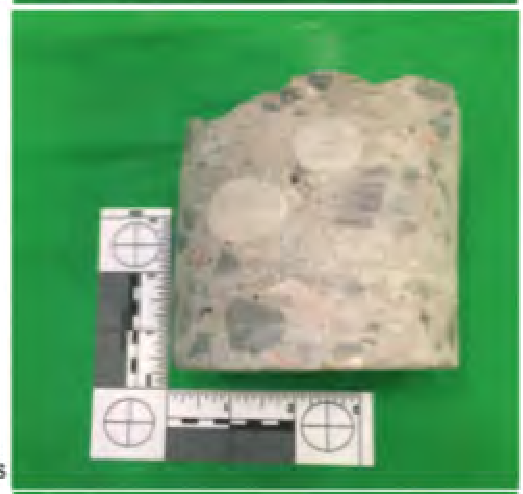
OF_C3	0.5	3.75	0.5	(2) GFRP rebars	

Core	Height (in)	Diameter (in)	Clear cover (in)	Notes	Picture
OF_C4	5	3.75	1.25		
OF_C5	2	3.75	0.75	(1) GFRP rebar	
OF_C6	3	3.75	--	Concrete sample	

Core	Height (in)	Diameter (in)	Clear cover (in)	Notes	Picture
OF_CB	4.75	3.75	1.5	(1) GFRP rebar	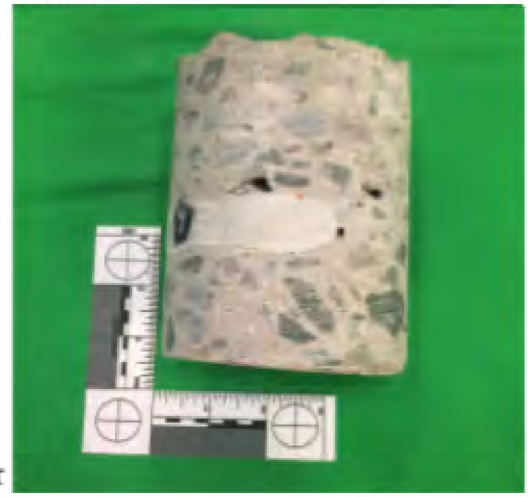
OF_CC	6	3.75	4.5	(2) Steel rebars	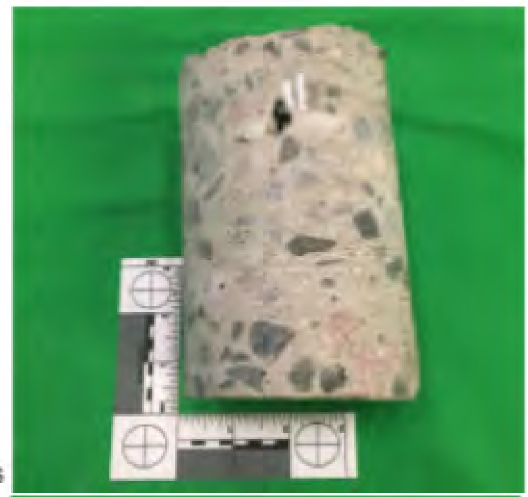
OF_CD	4.75	3.75	--	Concrete sample	

Core	Height (in)	Diameter (in)	Clear cover (in)	Notes	Picture
OF_CE	3	3.75	1.25	(2) GFRP rebars	

Salem Ave

Core	Height (in)	Diameter (in)	Clear cover (in)	Notes	Picture
SA_C1	5.25	3.5	2.5	(2) GFRP rebars	
SA_C2	5.5	3.5	2.75	(2) GFRP rebars	
SA_C3	5	3.5	1.5	(1) GFRP rebar	

Core	Height (in)	Diameter (in)	Clear cover (in)	Notes	Picture
SA_C4	5	3.5	3.75	(1) GFRP rebar	
SA_C5	5	3.5	3	(1) GFRP rebar	

Sierrita de la Cruz Creek

Core	Height (in)	Diameter (in)	Clear Cover (in)	Notes	Pictures
TX_C1		3.75		(2) GFRP Rebars	
TX_C2		3.75		(2) GFRP Rebars	

Walker Box Culvert Bridge

Core	Height (in)	Diameter (in)	Clear Cover (in)	Notes	Pictures
MO1_C1	5.25	3.75		(6) GFRP Rebars	
MO1_C2	5.25	3.75		(6) GFRP Rebars	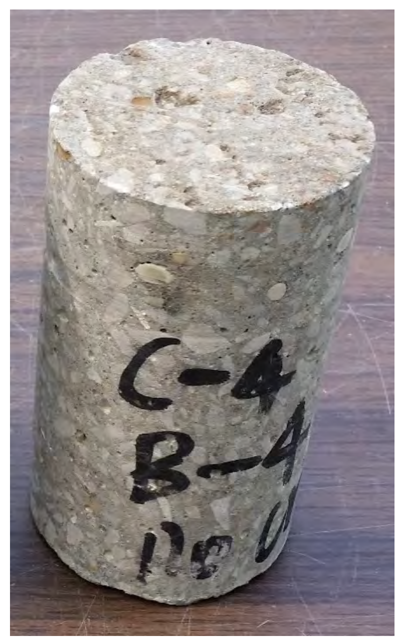

Southview Bridge

Core	Height (in)	Diameter (in)	Clear Cover (in)	Notes	Pictures
MO2_C1	6.25	3.75		(1) GFRP Rebar	
MO2_C2	5.25	3.75		(2) GFRP Rebar	

McKinleyville Bridge

Core	Height (in)	Diameter (in)	Clear Cover (in)	Notes	Pictures
WV_C1	5	3.75	1.75	(3) GFRP Rebars	
WV_C2	4.38	3.75	1.5	Untestable Rebars	

WV_C3	4.50	3.75	2.25	(3) GFRP Rebars	
WV_C4	4.63	3.75	2	(2) GFRP Rebars	
WV_C5	2	3.75	1.375	(2) GFRP Rebars	

Thayer Road Bridge

Core	Height (in)	Diameter (in)	Clear Cover (in)	Notes	Pictures
IN_C1	4.88	3.75	1.25	(2) GFRP Rebars	
IN_C2	4.75	3.75	1.50	(1) GFRP Rebar	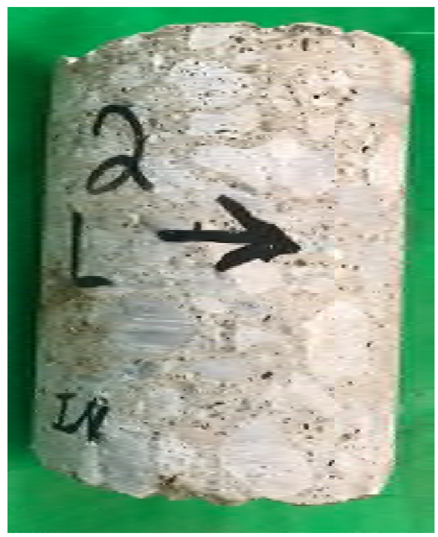
					

IN_C3	4.38	3.75	1.00	(2) GFRP Rebars	
IN_C4	3 6/8	3 6/8	3	(2) GFRP Rebars	
IN_C5	4 6/8	3 6/8	1	(1) GFRP Rebar	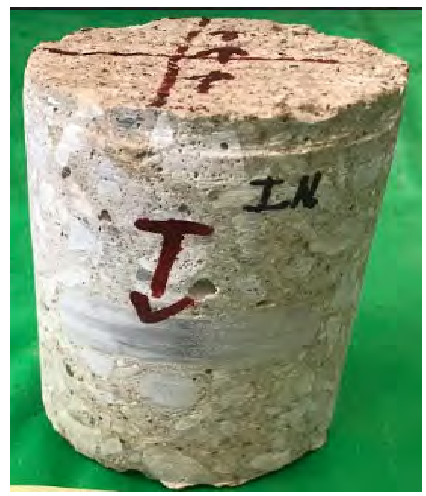
IN_C6	2 7/8	3 6/8	1 3/8	(1) GFRP Rebar	

Roger's Creek Bridge

Core	Height (in)	Diameter (in)	Clear Cover (in)	Notes	Pictures
KY_C1	3.88	3.75	2.88	(1) GFRP Rebars	
KY_C2	2.63	3.75	2.00	(1) GFRP Rebar	
KY_C3	3.88	3.75	N/A	Concrete Sample	

KY_C4	4.00	3.75	2	(1) GFRP Rebar	
KY_C5	2.63	3.75	2.75	(1) GFRP Rebar	

Test Matrix for Salem Ave. Bridge

Salem Ave					
		University of Miami	Missouri S&T	Penn State	Owens Corning
Core #	**Test**				
SA_C1_B1	Fiber Content- burn	After			
Note:	Tg				
Length: 3	SEM/EDS				
Used:	Interlaminar Shear	3			
	Moisture Content				
	Water Absorption				
SA_C1_B2	Fiber Content				
Note:	Tg- DSC		3 x 0.5		
Length: 3.5	SEM/EDS				
Used: 3.5	Interlaminar Shear				
	Moisture Content		2 x .5		
	Water Absorption	1			
SA_C2_B1	Fiber Content- burn	After			
Note:	Tg				
Length: 3.5	SEM/EDS	0.5			
Used: 3.5	Interlaminar Shear	3			
	Moisture Content				
	Water Absorption				
SA_C2_B2	Fiber Content				
Note:	Tg- DSC				
Length: 2.75	SEM/EDS				
Used: 2.5	Interlaminar Shear				
	Moisture Content	0.5			
	Water Absorption	2 x 1			
SA_C3_B1	Fiber Content				
Note:	Tg- DSC		0.5		
Length: 3.25	SEM/EDS				
Used: 3	Interlaminar Shear				
	Moisture Content		0.5		
	Water Absorption	2 x 1			
SA_C4_B1	Fiber Content				
Note:	Tg				
Length: 2.75	SEM/EDS	0.5			
Used: 2	Interlaminar Shear				
	Moisture Content	2 x 0.5			
	Water Absorption	1			
SA_C5_B1	Fiber Content- burn	After			
Note:	Tg- DSC				
Length: 3.5	SEM/EDS	0.5			
Used: 3.5	Interlaminar Shear	3			
	Moisture Content				
	Water Absorption				

Test Matrix for O'Fallon Park Bridge

O'Fallon Park					
		University of Miami	Missouri S&T	Penn State	Owens Corning
Core #	**Test**				
OF_C1A_B1	Fiber Content- burn	0.5			
Note:	Tg				
Length: 3.25	SEM/EDS	0.5			
Used: 1.5	Interlaminar Shear				
	Moisture Content	0.5			
	Water Absorption				
OF_C2B_B1	Fiber Content				
Note:	Tg				
Length: 2.25	SEM/EDS	0.5			
Used: 1.5	Interlaminar Shear				
	Moisture Content	2 x .5			
	Water Absorption				
OF_C2B_B2	Fiber Content- burn			0.5	
Note:	Tg- MDSC			0.5	
Length: 2.75	SEM/EDS				
Used: 2	Interlaminar Shear				
	Moisture Content				
	Water Absorption			1	
OF_C3_B1	Fiber Content				
Note: Bar needs	Tg				
to be machined for	SEM/EDS				
shear testing	Interlaminar Shear	3.5			
Length: 3.5	Moisture Content				
Used: 3.5	Water Absorption				
OF_C3_B2	Fiber Content- burn			0.5	
Note:	Tg- MDSC				
Length: 2	SEM/EDS				
Used: 1.5	Interlaminar Shear				
	Moisture Content				
	Water Absorption			1	
OF_C4_B1	Fiber Content				
Note: Bar needs	Tg				
to be machined for	SEM/EDS				
shear testing	Interlaminar Shear	3.25			
Length: 3.25	Moisture Content				
Used: 3.25	Water Absorption				
OF_C5_B1	Fiber Content				
Note: Bar needs	Tg				
to be machined for	SEM/EDS	0.5			
shear testing	Interlaminar Shear	3.25			
Length: 3.75	Moisture Content				
Used: 3.75	Water Absorption				
OF_C5_B2	Fiber Content- burn			0.5	
Note:	Tg- MDSC			2 x 0.5	
Length: 3.5	SEM/EDS				
Used: 2.5	Interlaminar Shear				
	Moisture Content				
	Water Absorption			1	

Test Matrix for Bettendorf Bridge

Bettendorf					
		University of Miami	Missouri S&T	Penn State	Owens Corning
Core #	**Test**				
BE_C3_B1	Fiber Content- burn	After			
Note:	Tg- DSC		0.25		
Length: 3.75	SEM/EDS	0.5			
Used: 3.75	Interlaminar Shear	3			
	Moisture Content				
	Water Absorption				
BE_C5_B1	Fiber Content- burn	After			
Note:	Tg				
Length: 3.75	SEM/EDS				
Used: 3.5	Interlaminar Shear	3			
	Moisture Content	2 x .5			
	Water Absorption				
BE_C6_B1	Fiber Content- burn	After			
Note:	Tg- DSC		0.25		
Length: 3.75	SEM/EDS	0.5			
Used: 2	Interlaminar Shear	3			
	Moisture Content				
	Water Absorption				
BE_C7_B1	Fiber Content				
Note:	Tg- DSC		0.25		
Length: 3.75	SEM/EDS				
Used: 2	Interlaminar Shear				
	Moisture Content	0.5			
	Water Absorption	3 x 1			

Test Matrix for Gills Creek Bridge

Gills Creek					
		University of Miami	**Missouri S&T**	**Penn State**	**Owens Corning**
Core #	**Test**				
GI_C1_B1	Fiber Content- acid				0.5
Note:	Tg				
Length: 1.5	SEM/EDS				0.5
Used: 1	Interlaminar Shear				
	Moisture Content				
	Water Absorption				
GI_C2_B1	Fiber Content- burn				
Note:	Tg- DSC		0.5		
Length: 2	SEM/EDS				
Used: 2	Interlaminar Shear				
	Moisture Content	0.5			
	Water Absorption	1			
GI_C2_B2	Fiber Content- acid				0.5
Note:	Tg				
Length: 1.5	SEM/EDS				0.5
Used: 1	Interlaminar Shear				
	Moisture Content				
	Water Absorption				
GI_C3_B1	Fiber Content	After			
Note: Bar needs	Tg				
to be machined for	SEM/EDS				
shear testing	Interlaminar Shear	2.75			
Length: 2.75	Moisture Content				
Used: 2.75	Water Absorption				
GI_C3_B2	Fiber Content- burn	After			
Note: Bar needs	Tg- DSC				
to be machined for	SEM/EDS				
shear testing	Interlaminar Shear	2.75			
Length: 3.25	Moisture Content	0.5			
Used: 3.25	Water Absorption				
GI_C4_B1	Fiber Content				
Note:	Tg- DSC		2 x .5		
Length: 2.5	SEM/EDS				
Used: 2.5	Interlaminar Shear				
	Moisture Content	0.5			
	Water Absorption	1			
GI_C4_B2	Fiber Content- acid				0.5
Note:	Tg				
Length: 1.25	SEM/EDS				0.5
Used: 1	Interlaminar Shear				
	Moisture Content				
	Water Absorption				
GI_C6_B1	Fiber Content	After			
Note: Bar needs	Tg- DSC				
to be machined for	SEM/EDS				
shear testing	Interlaminar Shear	2.75			
Length: 3.75	Moisture Content				
Used: 3.75	Water Absorption	1			

Test Matrix for Cuyahoga Bridge

Cuyahoga					
		University of Miami	Missouri S&T	Penn State	Owens Corning
Core #	**Test**				
CU_C1_B1	Fiber Content- acid				0.5
Note:	Tg- DSC				0.5
Length: 2.5	SEM/EDS				1
Used: 2	Interlaminar Shear				
	Moisture Content				
	Water Absorption				
CU_C2_B1	Fiber Content- burn				
Note:	Tg- MDSC			0.5	
Length: 2.5	SEM/EDS				
Used: 2.5	Interlaminar Shear				
	Moisture Content			2 x .5	
	Water Absorption			1	
CU_C3_B1	Fiber Content				
Note:	Tg- MDSC			2 x 0.5	
Length: 3	SEM/EDS				
Used: 3	Interlaminar Shear				
	Moisture Content			2 x .5	
	Water Absorption			1	
CU_C4_B1	Fiber Content		After		
Note:	Tg				
Length: 3	SEM/EDS				
Used: 3	Interlaminar Shear		2/7/2018		
	Moisture Content				
	Water Absorption		2/7/2018		
CU_C4_B2	Fiber Content				
Note:	Tg			0.5	
Length: 3.25	SEM/EDS				
Used: 3	Interlaminar Shear				
	Moisture Content			0.5	
	Water Absorption			2 x 1	
CU_C5_B1	Fiber Content		After		
Note:	Tg				
Length: 3.75	SEM/EDS				
Used: 3	Interlaminar Shear		2/7/2018		
	Moisture Content				
	Water Absorption		2/7/2018		
CU_C5_B2	Fiber Content-acid				0.5
Note:	Tg- DSC				0.5
Length: 2	SEM/EDS				0.5
Used: 1.5	Interlaminar Shear				
	Moisture Content				
	Water Absorption				
CU_C6_B1	Fiber Content- burn		After		
Note:	Tg				
Length: 3.75	SEM/EDS				
Used: 3.5	Interlaminar Shear		2/7/2018		
	Moisture Content				
	Water Absorption		2/7/2018		
CU_C8_B1	Fiber Content- acid				0.5
Note:	Tg- DSC				0.5
Length: 2	SEM/EDS				0.5
Used: 1.5	Interlaminar Shear				
	Moisture Content				
	Water Absorption				

Test Matrix for Thayer Road Bridge

Thayer Road, Indiana					
		University of Miami	Missouri S&T	Penn State	Owens Corning
Core #	**Test**				
IN_C1_B1	Fiber Content- burn	After			
Size: #5	Tg				
Length: 2.75"	SEM/EDS				
Used: 2.5"	Interlaminar Shear	1 x 2.5"			
	Moisture Content				
	Water Absorption				
IN_C1_B2	Fiber Content- acid				3 x .5"
Size: #6	Tg- MDSC				
Length: 3.4"	SEM/EDS				3 x .5"
Used: 3"	Interlaminar Shear				
	Moisture Content				
	Water Absorption				
IN_C2_B1	Fiber Content- burn				
Note: #5	Tg- MDSC			1 x .5"	
Length: 2"	SEM/EDS				
Used: 1.5"	Interlaminar Shear				
	Moisture Content				
	Water Absorption			1 x 1"	
IN_C3_B1	Fiber Content- burn	1 x 1"			
Note: #5	Tg- DSC				
Length: 3.5"	SEM/EDS				
Used: 3.5"	Interlaminar Shear	2.5"			
	Moisture Content				
	Water Absorption				
IN_C3_B2	Fiber Content				
Note: #6	Tg- DSC			1x.5"	
Length: 3"	SEM/EDS				
Used:	Interlaminar Shear				
	Moisture Content				
	Water Absorption			2x1"	
IN_C4_B1	Fiber Content- burn	1 x 1"			
Size: #5	Tg				
Length: 3.5"	SEM/EDS				
Used: 3.5"	Interlaminar Shear	2.5"			
	Moisture Content				
	Water Absorption				
IN_C4_B2	Fiber Content				
Size: #5	Tg- MDSC			2 x .5"	
Length: 3.4"	SEM/EDS				
3"	Interlaminar Shear				
	Moisture Content				
	Water Absorption			2 x 1"	
IN_C5_B1	Fiber Content- burn				3 x .5"
Size: #5	Tg				
Length: 3.6"	SEM/EDS				3 x .5"
Used: 3"	Interlaminar Shear				
	Moisture Content				
	Water Absorption				
IN_C6_B1	Fiber Content- acid				3 x .5"
Size: #5	Tg				
Length: 2.12"	SEM/EDS				1 x.5"
Used: 2"	Interlaminar Shear				
	Moisture Content				
	Water Absorption				

Test Matrix for Roger's Creek Bridge

Roger's Creek/ Bourbon County Bridge. Kentucky					
		University of Miami	**Missouri S&T**	**Penn State**	**Owens Corning**
Core #	**Test**				
KY_C1_B1	Fiber Content- burn		2 x .5"		
Size: #5	Tg- DSC		2 x .25"		
Length: 3.6"	SEM/EDS				
Used: 2.5"	Interlaminar Shear				
	Moisture Content				
	Water Absorption		1"		
KY_C1_B2	Fiber Content		2 x .5"		
Size: #5	Tg- DSC		2 x .25"		
Length: 1.6"	SEM/EDS				
Used:	Interlaminar Shear				
	Moisture Content				
	Water Absorption				
KY_C2_B2	Fiber Content				
Size: #5	Tg- DSC				
Length: 1"	SEM/EDS				2 x.5"
Used: 1"	Interlaminar Shear				
	Moisture Content				
	Water Absorption				
KY_C4_B1	Fiber Content- burn				3 x .5"
Note: #5	Tg- DSC				
Length: 3"	SEM/EDS				1 x .5"
Used:	Interlaminar Shear				
	Moisture Content				
	Water Absorption				
KY_C6_B1	Fiber Content- burn		1 x .5"		
Note: #5	Tg- DSC		1 x .25"		
Length: 3"	SEM/EDS				
Used: 2.75	Interlaminar Shear				
	Moisture Content				
	Water Absorption		2 x 1"		

Test Matrix for McKinleyville Bridge

McKinleyville Bridge, West Virginia					
		University of Miami	Missouri S&T	Penn State	Owens Corning
Core #	Test				
WV_C1_B1	Fiber Content- burn				
Size: #3	Tg- MDSC			1 x 0.5"	
Length: 2.5"	SEM/EDS				
Used: 2.5"	Interlaminar Shear				
	Moisture Content				
	Water Absorption			2 x 1"	
WV_C1_B2	Fiber Content				
Size: #4	Tg- DSC				
Length: .875"	SEM/EDS	2 x .375"			
Used: .75"	Interlaminar Shear				
	Moisture Content				
	Water Absorption				
WV_C1_B3	Fiber Content- burn				
Note: #3	Tg				
Length: 2.375	SEM/EDS	1 x .375"			
Used: 2.375"	Interlaminar Shear	1 x 2"			
	Moisture Content				
	Water Absorption				
WV_C3_B1	Fiber Content- burn off	3 x 1"			
Note: #4	Tg- DSC				
Length: 3.125"	SEM/EDS				
Used: 3"	Interlaminar Shear				
	Moisture Content				
	Water Absorption				
WV_C3_B2	Fiber Content				
Note: #3	Tg- MDSC			2 x .25"	
Length: 3.5"	SEM/EDS				
Used: 3.5"	Interlaminar Shear	1 x 2"			
	Moisture Content				
	Water Absorption			1 x 1"	
WV_C3_B3	Fiber Content- burn				
Size: #3	Tg				
Length: 2.75"	SEM/EDS	2 x .375"			
Used: 2.75"	Interlaminar Shear	1 x 2"			
	Moisture Content				
	Water Absorption				
WV_C4_B1	Fiber Content- burn off			1 x .5"	
Size: #5	Tg- DSC				
Length: 1.875"	SEM/EDS				
Used: 1.5"	Interlaminar Shear				
	Moisture Content				
	Water Absorption			1 x 1"	
WV_C4_B2	Fiber Content- acid				1 x .5"
Size: #5	Tg				1 x .25"
Length: 2.875"	SEM/EDS				1 x .5"
Used: 2.5"	Interlaminar Shear				
	Moisture Content				
	Water Absorption				
WV_C5_B1	Fiber Content- burn off			2 x .5"	
Size: #5	Tg				
Length: 3.375"	SEM/EDS				
Used: 3"	Interlaminar Shear				
	Moisture Content				
	Water Absorption			2 x 1"	
WV_C5_B2	Fiber Content- acid				2 x .5"
Size: #5	Tg- DSC				2 x .25"
Length: 3.375"	SEM/EDS				2 x .5"
Used: 2.5"	Interlaminar Shear				
	Moisture Content				
	Water Absorption				

APPENDIX II: EXTENDED TEST PROCEDURES

This appendix presents extended test procedures for the procedures described in Section 4. The information presented herein aims to clarify each test performed in this study and to identify the different methods used by different collaborators while performing the same test.

NOMENCLATURE

VA and GI =	Gills Creek Bridge
CO and OF =	O'Fallon Park Bridge
OH1 and SA =	Salem Ave. Bridge
IA and BE =	Bettendorf Bridge
OH2 and CU =	Cuyahoga County Bridge
WV =	McKinleyville Bridge
IN =	Thayer Road Bridge
KY =	Roger's Creek Bridge
TX and SI =	Sierrita de la Cruz Creek Bridge
MO1 and WA =	Walker Box Culvert Bridge
MO2 and SO =	Southview Bridge

Table of Contents

List of Figures

List of Tables

1. Fiber Content

1.1 Penn State

Burn-off samples were 0.5 in. (13 mm) long. The samples were preconditioned in a non-convection oven for 48 h. at 104°F (40°C). Ceramic crucibles were preheated to 932°F (500°C) for ten minutes to burn-off any residuals from previous tests. The crucibles were then cooled and cleaned with soap and water. Next, the specimens were weighed. Once the crucibles were dry, the specimens were placed in the crucibles and the combined weights were measured. Then, the lids were put onto the crucibles and the covered crucibles were placed in the oven. The burn-off procedure was then performed using the temperature profile shown in Fig 1**Error! Reference source not found.**. The ramp rates between holds for the temperature profile are not shown because the ramp rate was not programmable.

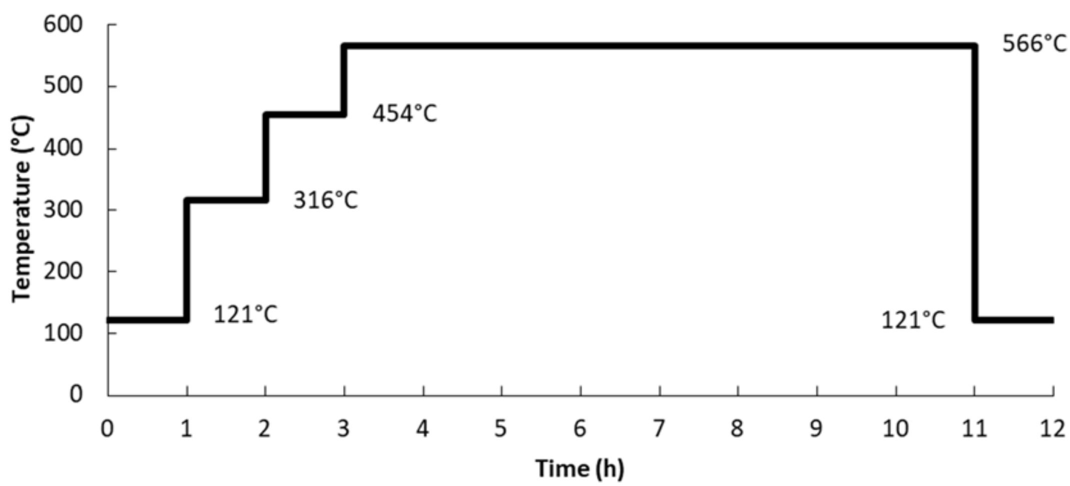

Fig 1. Burn-off temperature profile

Once the burn-off was complete, the crucibles were removed from the furnace and placed in a desiccator. The crucibles were allowed to cool for two hours in the desiccator. After cooling, the crucibles were removed from the desiccator, the lids were removed, and the combined weights of the crucible and contents were immediately weighed. The main axis fibers were then removed, leaving behind only the helical wrap (if present), sand particles, and filler inside the crucibles. The crucibles were then weighed again.

1.2 University of Miami

Fiber content specimens were 1 in. (25.4 mm) long. Specimens were pre-conditioned at 104°F (40°C) for 48 hours. Crucibles were cleaned and then placed in muffled furnace at 932°F (500°C) for 10 minutes to burn off any residue from previous tests. Crucibles were then cooled to room temperature in a desiccator. Once cooled, each specimen was placed in a crucible and weighed.

Specimens and crucibles were then placed in the muffle furnace. The furnace temperature was set at 330°C for 50 minutes, 450°C for 50 minutes, and then 590°C for 1.5 hours (not including time required for temperature to increase). The specimens and crucibles were removed from furnace and cooled to room temperature in a desiccator for two hours. Once cool, specimen and crucible were removed from desiccator and immediately weighed. Longitudinal fibers were then removed from crucibles and crucible, sand, and helical wrap were weighed.

1.3 Missouri S&T

Specimens used for the horizontal shear test were cut into pieces about 0.011 lb. (5g) each and then conditioned in an oven at 104º F (40º C) for 48 hours. The specimens were weighed and then placed in a muffle furnace at a temperature of 1067º F (575º C) until all the resin was gone. Specimens were then removed from the furnace and weighed after cooling.

1.4 Owens Corning

The mesh basket used for testing was weighed. A specimen was placed in the basket and weighed. The basket and specimen were placed in furnace at 1050°F (565º C) for two hours. The basket was removed and allowed to cool. The specimen and basket were weighed to get loss of ignition (LOI) percentage. The basket was placed in a 3 to 1 water-acid mixture to remove remnant filler. Once all filler was removed, the specimen was rinsed under water. The basket was then placed back into the furnace for 30 minutes to dry. The basket and specimen were then weighed for the glass content.

2. Moisture Absorption

2.1 Penn State

Weighing Procedure for O'Fallon and Cuyahoga Bars

For the first week, the specimens were weighed every day. During this time period, the weighing procedure was as follows:

- Remove specimens from water
- Dry specimens with lint-free tissue paper
- Set specimens on wood dowels to cool in air for 15 minutes
- Blow dry nitrogen gas over the bars
- Set specimens back on wood dowels to equilibrate 15 minutes
- Weigh specimens on digital scale with 1 mg resolution
- Put specimens back in water and return container to oven

After the first week, the weighing interval was changed to one week and after a running total of five weeks the interval was changed to two weeks. In order to standardize the cool/dry procedure among the project team members, the cool/dry procedure was changed after the third week as follows:

- Remove specimens from water
- Dry specimens with lint-free tissue paper
- Place specimens in desiccator for 30 minutes
- Weigh specimens on digital scale with 1 mg resolution
- Put specimens back in water and return container to oven

The stopping criterion for the moisture uptake test was when the average weight change for three consecutive measurements (i.e. over six weeks) is less than 5 mg.

Weighing Procedure for Thayer and McKinleyville Bars

For the first week, weights were obtained every day. The next weight was obtained after one more week. After the first two weeks, the weighing interval was two weeks. The cool/dry procedure and stopping criterion were the same as the final procedures adopted for the O'Fallon and Cuyahoga bars.

2.2 University of Miami

After 24 hours of immersion, specimens were removed from water, dried with a lint free towel until surface dry, and then immediately weighed. Specimens were then returned to water and placed in oven. After 1 week, this process was repeated. The weighing interval was then changed to two weeks. The weighing was stopped once the increase in weight per two-week period averaged less than 1 % of the total increase in weight for three consecutive weightings.

2.3 Missouri S&T

This test was conducted following ASTM D570 (ASTM-D570-98, 2018). The specimens were cut into little pieces about 5 g each and then were placed in an oven at 104^o F (40^o C) for 48 hours for conditioning. After that, the specimens were weighed and recorded as an initial weight. Next, specimens were put inside plastic containers had distilled water and heated to 122^o F (50^o C) inside an oven. The weights of the specimens were first taken every day for the first week and then were taken once every two weeks until the difference in weight was less than 0.01% for consecutive two weeks' readings. The recording procedure was done by first removing the specimens from the distilled water and followed by drying them using a lint-free tissue paper. Next, they were left to cool for 30 min. inside a desiccator and were then weighed with 1 mg resolution. After weighing is over, the specimens were returned to their containers inside the ovens. A sample image of the specimens are shown in *Fig 2*.

Fig 2. Moisture Absorption Specimens

3. Horizontal Shear

3.1 Missouri S&T

This test was conducted to find the interlaminar shear capacity of the GFRP bars. ASTM D4475 (ASTM-D4475-02, 2016) was followed to determine the shear capacity. Three-point setup was used in this test where the span between supports was three times the diameter of the bar. Even though ASTM D4475 (ASTM-D4475-02, 2016) recommends testing at least five specimens, only one specimen was tested from each core (C4, C5, and C6) due to a limited number of GFRP samples extracted from the field. Specimens were conditioned at 104^{o} F (40^{o} C) for 48 hours and tested under a temperature of 73.4^{o} F (23^{o} C) and humidity of 50%. The load rate used was 0.05 in./min. (1.27 mm/min.) and the time of the test did not exceed the allowable ASTM D4475 time limit of 20 min. The load was applied to the specimen until an interlaminar shear failure took place. That being said, even if the specimen deflected substantially, the test did not stop as long as there were no sings for interlaminar shear failure. The shear capacity was calculated based on the following equation:

Eq.(3) Shear capacity

$$S = 0.849\, P/d^2 \; (lb;in)$$

$$S = 547.8P/d^2 \; (N;\, mm)$$

Where S is the interlaminar shear stress (psi or MPa), P is the breaking load (lb. or N), and d is the diameter of the specimen (in. or mm). An image of the setup used is shown in *Fig 3* below.

Fig 3. Short Bar Shear – Three Point Load Setup

4. DSC

4.1 Missouri S&T

This test was conducted following ASTM E1640 (ASTM-E1640-13, 2018). The test was conducted using differential scanning calorimetry (DSC) technique. In this technique, the heat flow into petite pieces of GFRP bar in a sealed aluminum pan was measured relative to an empty pan using a constant temperature rate. Before conducting the test, specimens were conditioned for 48 hours at 104^o F (40^o C). The procedure started by cutting little pieces of the GFRP bar about 10 mg total. Next, the tiny pieces were put inside an aluminum pan and were then sealed and placed inside the TA Instrument. Inside the TA Instrument, the specimen was placed next to an empty aluminum pan. The test setup was set on the following:

- Temperature used was up to 392^o F (200^o C)
- Ramp rate used was 33.8^o F/min (5 ^{o} C/min.).
- Specimen was heated from the room temperature up to 392^o F (200^o C) and then cooled down the room temperature.

Based on ASTM-E1356 (ASTM-E1356-08, 2014), T_g is represented by the midpoint temperature (T_m) that is the point on the heat flow - thermal curve corresponding to 0.5 the heat flow change between the extrapolated onset and extrapolated end. TA Instrument used in the tests is shown in *Fig 4*.

Fig 4. TA Instruments

4.2 Owens Corning

Samples were cut into 0.2 x 0.2 x 0.11 in. (5 x 5 x 3 mm) specimens. They were then subjected to a 50^{o} F/min (10 °C/min) heating ramp from 14 to 392^{o}F (-10 to 200 °C) and then cooled at 50^{o} F/min (10 °C/min). Each specimen underwent two heating cycles.

4.3 Penn State- Modulated DSC

The Penn State DSC technique used a small, sinusoidal temperature modulation superposed on the linear-temperature ramp, such that the reversible and non-reversible heat flows can be analyzed separately from the total heat flow. This technique, known as the modulated DSC technique (MDSC), can provide separate T_g values from the total-heat-flow curve (like a regular DSC) and the reversible-heat-flow curve. Theoretically, the reversible-heat-flow curve eliminates the effects of non-reversible phenomena such as post-cure and volatile-matter evolution (including water).

Particles for DSC testing were extracted by slicing a thin (~0.5 mm) wafer from the bar with a water-cooled diamond saw and then using a single-edged razor blade to slice the wafer into small pieces of 0.5–2 mg each. The particles were put into separate paper envelopes for each bar and pre-conditioned for 48 h. at 118^{o} F (48°C). After preconditioning, the envelopes were put into a thick sealable plastic bag, which in turn was placed into another thick sealable plastic bag containing desiccant. This double bag arrangement was used to store the DSC specimens until four days after the end of preconditioning when testing was performed.

A TA Q2000 differential scanning calorimeter (TA Instruments, New Castle, DE) was used to perform the MDSC tests. Particles weighing approximately 14–20 mg were put into “standard aluminum” TA pans with non-hermitically-sealed lids. The lids were pressed into the pans using a cup-shaped die. **Error! Reference source not found.** displays the MDSC test parameters. The mid-point T_g was identified in the data using the TA Universal Analysis software (Version 4.5A, Build 4.5.0.5).

Table 1. MDSC test parameters

Temperature Ramp Rate	10°C/min	50°F/min
Modulation Amplitude	±1°C	±1°C
Modulation Period	10 s	10 s
Temperature Range	45°C–145°C	113°F–293°f
N_2 Purge Rate	50 mL/min	50 mL/min
Data Sampling Rate	5 Hz	5 Hz

5. SEM/EDS

5.1 Missouri S&T

Helios NanoLab 600 was used to conduct the test. Several levels of magnifications were used in the tests. In this test, the specimens were cut into smaller pieces using an electrical saw. Next, these small samples were mechanically paper-sanded using different grades including: 400, 600, 800, and 1200, as part of sample preparation for the SEM test. After each sanding step, sonic bath was used to remove suspended particles. Sample conditioning was then taken place by putting specimens into an oven for 48 hours under 104º F (40º C) (ASTM - C1723, 2016). Once the conditioning was completed, specimens were coated using either gold or gold-palladium and then were ready for SEM testing.

EDS was conducted to categorize the chemical elemental changes of the GFRP. A 10 to 20 KeV electron beam was applied at the surface of the GFRP specimen. The results were shown in terms of graphs that has the elements found when the X-ray was applied.

6. Moisture Content

6.1 Missouri S&T

The test followed ASTM D5229 – Procedure D (ASTM-D5229/D5229M-92, 2010) to determine the moisture content (ASTM-D5229/D5229M-92, 2010). The test was performed by drying the bars as they were without any type of conditioning to equilibrium in a forced-air oven set to 176º F (80º C). In this test, the specimens were cut to a length of approximately 1-in. (25.4 mm) using a water-cooled diamond saw and then were dried instantly to avoid any excess moisture. Next, the specimens were weighed on a digital scale with 1 mg resolution and placed in the oven. In the first week, the specimens were weighed every day, but after that, the weights were taken every two weeks. Regarding weight measurements during the test process, the hot specimens were left to cool down to room temperature in a desiccator for 30 min. before weighing. After that, the specimens were immediately returned to the oven. The test was considered complete when the change in specimens' weights was less than 0.02% for two consecutive 14-day periods.

6.2 Penn State

Moisture content of the bars was measured by drying the as received bars (no pre-conditioning) to equilibrium in a forced-air oven set to 176°F (80°C), according to ASTM D5229 (2014), Procedure D. The specimens were cut to a length of 13 mm using a water cooled diamond saw and were dried following cutting. This drying process involved blow drying the samples with compressed nitrogen, then hand drying with a lint-free tissue paper. After drying, the specimens were weighed on a digital scale with 1 mg resolution and placed in a corrugated aluminum pan with labels for each specimen position, as shown in **Error! Reference source not found.**. The corrugated pan was chosen because it would allow convection underneath the specimen so that both faces were exposed to circulating air in the oven. Once the dry-out test was underway, specimens were weighed every day for 10 days and every week thereafter. For weight measurement during the dry-out process, the hot specimens were allowed to cool to room temperature in a desiccator for 30 minutes prior to weighing. Following weighing, the specimens were promptly returned to the oven. The dry-out test was terminated when the weight changes of all of the specimens were less than 0.02% for two consecutive 7-day periods.

7. Modified Tensile Strength Test

A modified tensile strength test was developed due to the size of the GFRP rebar specimen. The 22 in rebars, both extracted from the bridges and virgin (unused) bars were cut into coupons of approximately 0.45 x 10 x 0.1in (11 x 254 x 3 mm) using a precision saw at Owens Corning. Tabs were attached to the end of the coupons, providing a gauge length of approximately 5.4 in (137 mm). The coupons were tested to determine a coupon ultimate tensile strength. Part of the same virgin rebars were used for a full-sized tensile strength test according to ASTM D7205 (ASTM-D7205/D7205-06, 2016). Using the results for the virgin rebars, a correlation factor was calculated between the coupon ultimate tensile strength and the full-sized ultimate tensile strength. This correlation factor was then applied to the results of the extracted tensile coupons to estimate the full-sized tensile strength of the extracted rebars.

8. Chloride Penetration

Chloride penetration depth was evaluated using a 0.1M Silver Nitrate solution to evaluate the presence of chlorides at the depth of the GFRP rebar. Silver nitrate colorimetric method uses the principle that a white deposit is formed through the reaction of silver ion (Ag+) and chloride ion. Concrete cores were split to expose a fresh surface, and compressed air was used to remove dust particles from this surface. The Silver Nitrate solution was sprayed onto the surface and allowed to dry. The dry surface results in a specimen with a color-changer border, in which the lighter color indicates the area of chloride penetration, and a darker color indicates areas not affected by chlorides. The difference in color however, may be very small and hard to distinct.

9. Carbonation Depth

9.1 Missouri S&T

Carbon dioxide that penetrates the surface of concrete can react with alkaline components in the cement paste, primarily $Ca(OH)_2$. As a result, the pH value of the pore solution will drop to less than 9. The depth that is affected by the carbon dioxide-alkaline reaction is called carbonation depth. The test was conducted following RILEM Recommendations – CPC 18 (Rilem and Matt, 1988).This test was carried out by spraying a solution over a fresh-cut concrete surface and then monitoring the change in surface's color. The indicator used in the solution is phenolphthalein. The solution mixture has 1% phenolphthalein, 70% ethyl-alcohol and 29% distilled water – volume ratio.

10. pH

10.1 Missouri S&T

Grubb's procedure was used to conduct the test where 1 g of concrete powder was extracted from each core and then placed inside a mixing pan (Grubb, J et al., 2007). Next, a 1 g of distilled water was added and mixed with concrete powder. After that, the pH was determined using measuring strips.

Appendix III: GFRP Test Results

This appendix presents the test results of the extracted GFRP rebars from eleven bridges. The tests included in this appendix are: fiber content, water absorption, horizontal shear, DSC, moisture content and modified tensile strength test. These tests were performed according to Section 4. The results are shown per test and its respective bridge.

NOMENCLATURE

VA and GI =	Gills Creek Bridge
CO and OF =	O'Fallon Park Bridge
OH1 and SA =	Salem Ave. Bridge
IA and BE =	Bettendorf Bridge
OH2 and CU =	Cuyahoga County Bridge
WV =	McKinleyville Bridge
IN =	Thayer Road Bridge
KY =	Roger's Creek Bridge
TX and SI =	Sierrita de la Cruz Creek Bridge
MO1 and WA =	Walker Box Culvert Bridge
MO2 and SO =	Southview Bridge

Table of Contents

List of Figures

List of Tables

1. Fiber Content

1.1 Gills Creek

Fiber content tests for the *Gills Creek Bridge* were performed at the University of Miami using the burn off technique described in Section 4.1.1.1 and at Owens Corning using the acid wash technique described in Section 4.1.1.2. The percent fiber for the tests performed at the University of Miami, Penn State University, and Missouri S&T includes the weight of the filler and the glass fiber (filler is not removed). The tests performed at Owens Corning used an acid wash, which allowed for the removal of the filler and a true measurement of the percent fiber can be seen in Table 1.

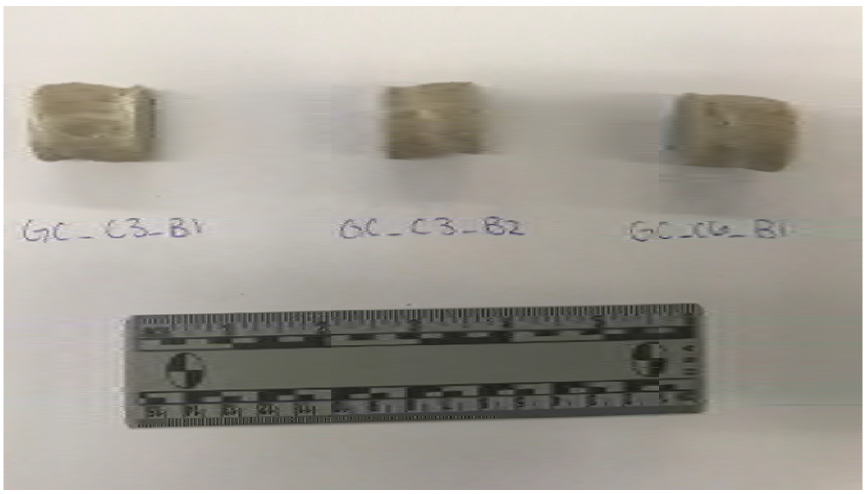

Fig. 1. Photograph of Gills Creek fiber content specimens – UM

Table 1. Gills Creek fiber content results – UM

Sample	%WT Fiber + Filler
VA_C3_B1	71.2
VA_C3_B2	70.3
VA_C6_B1	70.1
Average	70.5
Std dev	0.58

Table 2. Gills Creek fiber content results – OC

Sample	%WT Fiber+ Filler	%WT Fiber
VA_C1_B1	73.7	63.6
VA_C2_B2	73.9	59.5

VA_C4_B2	73.5	62.5
Average	73.7	61.9
Std dev	0.20	2.12

1.2 O’Fallon Park

Fiber content tests for *O’Fallon Park Bridge* were conducted at the University of Miami and Penn State University according to ASTM D2584 (ASTM-D2584-18, 2018). The specimens tested at UM are shown in Fig. 2 and their test results are in

Table 3. The results of the specimen tests at PSU are shown in Table 4.

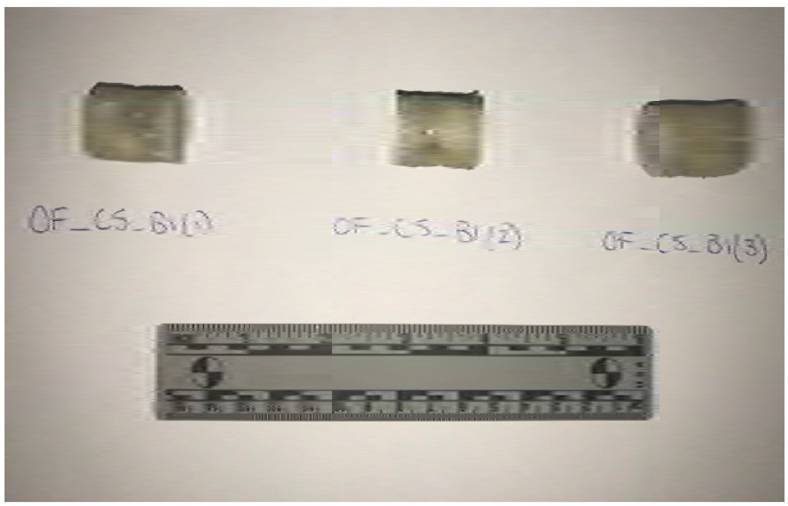

Fig. 2. Photograph of O'Fallon fiber content specimens – UM

Table 3. O'Fallon Park fiber content results – UM

Sample	%WT Fiber + Filler
CO_C5_B1(1)	71.2
CO_C5_B1(2)	71.1
CO_C5_B1(3)	71.1
Average	71.1
Std dev	0.058

Table 4. O'Fallon Park fiber content results – PSU

Sample	%WT Fiber + Filler

CO_C2_B2	74.3
CO_C3_B2	75.0
CO_C5_B2	74.6
Average	74.6
Std dev	0.35

1.3 Salem Ave

Fiber content tests for the *Salem Ave. Bridge* were performed at the University of Miami using the burn off technique described in Section 4.1.1.1. The samples tested are shown in Fig. 3 and the results are shown in Table 5.

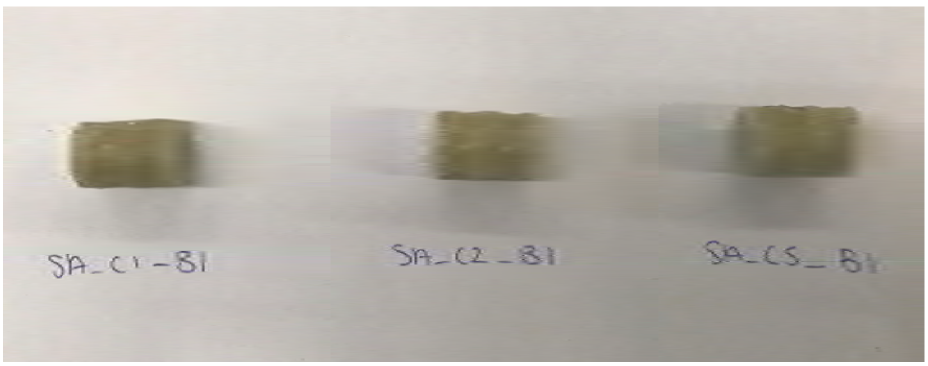

Fig. 3. Photograph of Salem Ave. fiber content specimens – UM

Table 5. Salem Ave. fiber content results – UM

Specimen	%WT Fiber + Filler
OH1_C1_B1	72.5
OH1_C2_B1	72.5
OH1_C5_B1	72.4
Average	72.5
Std dev	0.058

1.4 Bettendorf

Fiber content tests for the *Bettendorf Bridge* were performed at the University of Miami following the procedure explained in Section 4.1.1.1. The samples tested are shown in Fig. 4 and the results are shown in Table 6 .

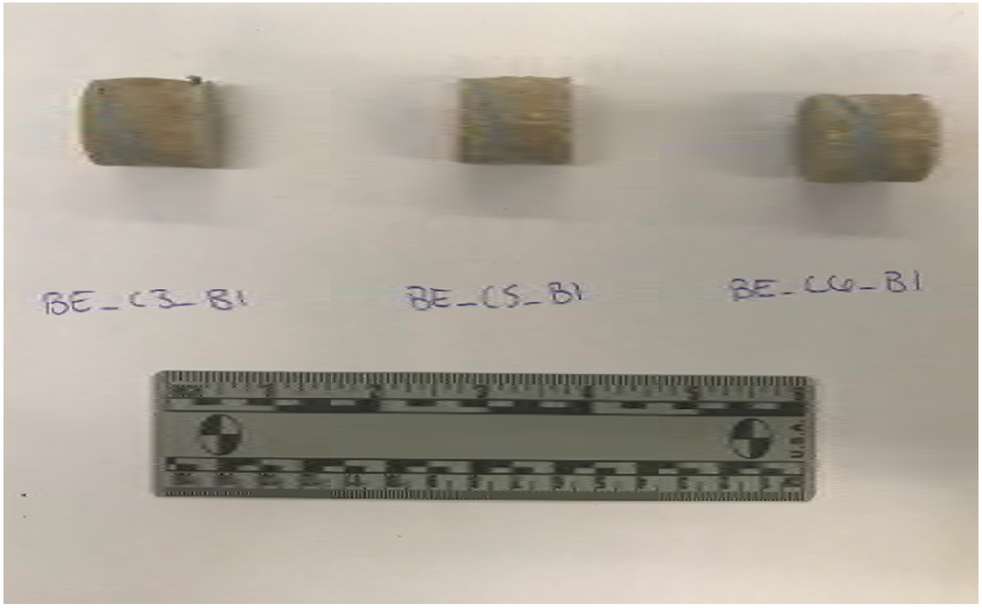

Fig. 4. Photograph of Bettendorf fiber content specimens – UM

Table 6. Bettendorf fiber content results – UM

Sample	%WT Fiber + Filler
IA_C3_B1	72.4
IA_C5_B1	74.8
IA_C6_B1	72.8
Average	73.3
Std dev	1.29

1.5 Cuyahoga

Fiber content tests for the *Cuyahoga County Bridge* were performed at Missouri S&T and Penn State following the burnoff procedure outlined in Section 4.1.1.1. Owens Corning performed fiber content tests for the *Cuyahoga County Bridge* using burnoff followed by an acid wash to remove remnant filler from the fiber, as described in Section 4.1.1.2. The Owens Corning measurements of fiber weight before the acid wash should be comparable to the burnoff test results done by Missouri S&T and Penn State. These fiber contents which include remnant filler are referred to as "%WT fiber + Filler in Table 7 through Table 9.

Table 7. Cuyahoga County fiber content results – MST

Sample	%WT Fiber + Filler	Sample	%WT Fiber + Filler	Sample	%WT Fiber + Filler
OH2_C4_B1(1)	75.1	CU_C5_B1(1)	75.6	CU_C6_B1(1)	81.0
OH2_C4_B1(2)	75.6	CU_C5_B1(2)	76.0	CU_C6_B1(2)	81.0

OH2_C4_B1(3)	75.1	OH2_C5_B1(3)	76.4	OH2_C6_B1(3)	80.6
Average	75.3	Average	76.0	Average	80.9
Std dev	0.26	Std dev	0.35	Std dev	0.17

Table 8. Cuyahoga County fiber content results – PSU

Sample	%WT Fiber + Filler
OH2_C2_B1	75.2
OH2_C3_B1	75.9
OH2_C4_B2	74.6
Average	75.2
Std dev	0.53

For some samples, it was difficult to remove the main longitudinal fibers without crushing the fiber bunch with the tongs. If the fibers were crushed, it was difficult to remove some of the fibers because they would have to be picked one by one without picking up the other particles. For the most part, the fiber bunches stuck together even without the presence of the polymer matrix. Notwithstanding these complicating factors, the longitudinal fiber weight fraction of the bars obtained by the described modification of ASTM D2584(ASTM-D2584-18, 2018) ranges from 74.1% to 81.0%—well above the 70% minimum required in ASTM D7957(ASTM D7957, 2017) for quality control and certification.

The results of fiber content tests performed at Owens Corning using the acid wash technique are listed as "%WT Fiber" in Table 9. It can be seen that removal of remnant filler from the fibers after burnoff reduces the fiber weight percent by approximately 13 percentage points.

Table 9. Cuyahoga County fiber content results – OC

Sample	%WT Fiber+ Filler	%WT Fiber
OH2_C1_B1	75.5	62.9
OH2_C5_B2	74.1	60.8
OH2_C8_B1	74.1	61.1
Average	74.5	61.6
Std dev	0.81	1.14

1.6 McKinleyville Bridge

Fiber content tests for the *McKinleyville Bridge* were performed at the University of Miami and Penn State using the burn off technique described in Section 4.1.1.1. Results are shown in Table 10.

Table 10. McKinleyville fiber content results – UM and PSU

UM		PSU	
Sample	%WT Fiber + Filler	Sample	%WT Fiber + Filler
WV _C3_B1	76.20	WV_C4_B1	71.02
WV_C4_B1	76.31	WV_C5_B1-1	70.70
WV_B1(3)	75.79	WV_C5_B1-2	71.15
Average	76.10	Average	70.96
Std dev	0.27	Std dev	0.23

1.7 Roger’s Creek Bridge

Fiber content tests for the *Roger’s Creek Bridge* were performed at Missouri S&T using the burn off technique described in Section 4.1.1.1. Results are shown in Table 11.

Table 11. Roger’s creek fiber content results - MST

Sample	%WT Fiber + Filler
KY_C1_B1	70.14
KY_C1_B1	70.56
KY_C1_B2	68.74
KY_C1_B2	68.69
KY_C6_B1	67.98
Average	69.22
Std dev	1.08

1.8 Thayer Road Bridge

Fiber content tests for *Thayer Road Bridge* were performed at the University of Miami using the burn off technique described in Section 4.1.1.1. Results are shown in Table 12.

.

Table 12. Thayer Road fiber content results – UM

Sample	%WT Fiber + Filler
IN_B1 (1)	76.46
IN_B1(2)	76.36
IN_B1(3)	76.55
Average	76.46
Std dev	0.078

1.9 Sierrita de la Cruz Creek

Fiber content tests for the *Sierrita de la Cruz Creek Bridge* were performed at the University of Miami using the burn off technique described in Section 4.1.1.1. Tests were performed in 2015 and 2018. The results of the test performed in 2015 were compared with the same test performed in 2000 prior to construction. Table 13 shows the summary of the result where α_c and α_s respectively correspond to fiber content ratio of control and extracted samples. The samples tested in 2018 are shown in Fig. 5. Photograph of Sierrita de la Cruz Creek fiber content specimens tested in 2018 are shown in Table 14.

Table 13. Sierrita de la Cruz Creek fiber content results (fiber + filler) of tests performed in 2015 – UM

Rebar Size	α_c			α_s			Ratio (α_s/α_c)
	No. of Samples	Average (%)	CoV (%)	No. of Samples	Average (%)	CoV (%)	
#5	4	75.7	1.2	3	77.9	1.8	1.03
#6	2	80.5	2.2	3	79.5	0.2	0.99

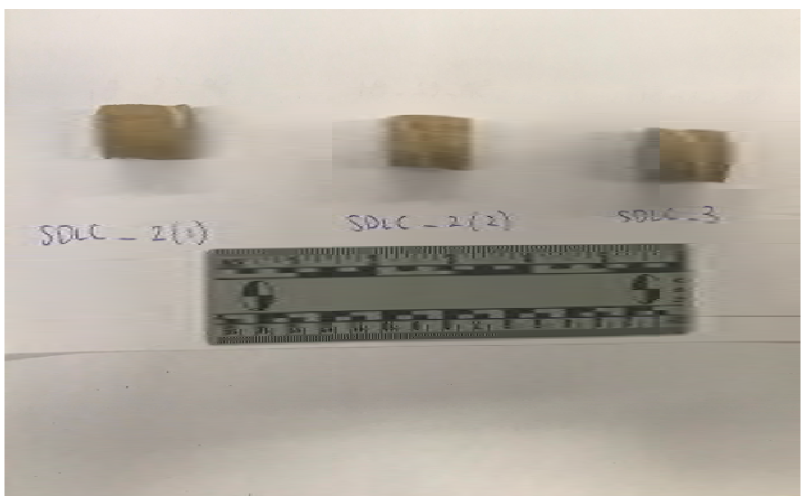

Fig. 5. Photograph of Sierrita de la Cruz Creek fiber content specimens used in 2018 – UM

Table 14. Sierrita de la Cruz Creek fiber content results of tests performed in 2018 – UM

Sample	%WT Fiber + Filler
TX_B2(1)	73.6
TX_B2(2)	73.4
TX_B3	72.3
Average	73.1

Std dev	0.70

1.10 Walker Box Culvert Bridge

Samples of *Walker Box Culvert Bridge* were tested at the University of Miami and compared with the same test performed in the GFRP rebars prior to construction.

Table 15 shows the summary of the result where α_c and α_s respectively correspond to fiber ratio of control and extracted samples The measured fiber content after 17 years of field exposure was consistent with the expected values and well above the minimum fiber content requirement of 70% by mass (Alkhrdaji and Nanni, 2001).

Table 15. Walker Box Culvert fiber content results (fiber + filler) – UM

Bridge	α_c			α_s		
	No. of Samples	Average (%)	CoV (%)	No. of Samples	Average (%)	CoV (%)
Walker	4	75.7	1.2	4	82.38	4.0

1.11 Southview

Samples of *Southview Bridge* were tested at the University of Miami and compared with the same test performed in the GFRP rebars prior to construction. Table 16 shows the summary of the result where α_c and α_s respectively correspond to fiber ratio of control and extracted samples. The measured fiber content after 11 years of field exposure was consistent with the expected values and well above the minimum fiber content requirement of 70% by mass (ICC, 2015).

Table 16. Southview fiber content results (fiber + filler) – UM

Bridge	α_c			α_s		
	No. of Samples	Average (%)	CoV (%)	No. of Samples	Average (%)	CoV (%)
Southview	4	75.7	1.2	4	73.4	2.0

2. Water Absorption

2.1 Gills Creek

Water absorption tests for the *Gills Creek Bridge* were performed at the University of Miami, according to the procedure depicted in Section 4.1.2. Drying and measurement procedures are described in Appendix II. The results for 24-hour moisture absorption and long-term immersion (as of September 17, 2018) indicated a weight gain of more than 1%, as shown in Table 17.

Table 17. Gills Creek water absorption results – UM

Sample	24-hour Immersion Weight Change (%)	Long-term Immersion Weight Change (%)	Length of Saturation (days)
VA_C2_B1	0.59	1.61	179
VA_C4_B1	0.54	1.57	179
VA_C6_B1	0.60	1.52	179

2.2 O’Fallon Park

Water absorption tests for the *O’Fallon Park Bridge* were performed at Penn State University, according to the procedure depicted in Section 4.1.2. Drying and measurement procedures are described in Appendix II. The results for 24-hour water absorption and long-term immersion (as of September 17, 2018) are shown in Table 18.

Table 18. O'Fallon Park moisture absorption results – PSU

Sample	24-hour Immersion Weight Change (%)	Long-term Immersion Weight Change (%)	Length of Saturation (days)
CO_C2_B2	0.02	0.34	133
CO_C3_B2	0.05	0.40	133
CO_C5_B2	-0.03	0.24	133

During uptake testing, one specimen lost weight between some of the measurements. Fig. 6 displays the causes for the loss in weight. CO_C5_B2 lost many small sand particles over the first two weeks.

Fig. 6. Sand particles at the bottom of the immersion chamber of CO_C5_B2

Weight losses as a result of pre-conditioning at 104°F (40°C) for 48 h in non-circulating oven air are shown in Table 19. The CO_C2B_B2 bar had considerably less pre-conditioning weight change than the other bars from *O'Fallon Bridge*.

Table 19. Weight of O'Fallon Park specimens (g) for uptake testing, before and after pre-conditioning at 104°F (40°C) for 48 h in non-circulating oven air – PSU

Elapsed Time (days)	CO_C2B_B2	CO_C3_B2	CO_C5_B2
0.000	13.050	13.239	13.444
1.982	13.049	13.235	13.44
Change	-0.008%	-0.030%	-0.030%

Percent weight changes for the *O'Fallon* and *Cuyahoga* bars up to Dec. 15, 2018 (271 days) are shown on a log time scale in Fig. 7. The acronym used for *O'Fallon* here is OF and the acronym used for *Cuyahoga* is CU. By 259 days, all bars had met the ASTM D570 (ASTM-D570–98, 2018) equilibrium condition of less than 5 mg average weight gain per two-week period over the last three bi-weekly measurement intervals.

Table 20 lists the weight gains at 24 hours, at equilibrium, and at the most recent measurement (271 days). The average weight gain for the *O'Fallon* bars at saturation is 0.30%, which is much less than the 1% qualification limit established in ASTM D7957 (ASTM D7957, 2017) for the same test conditions.

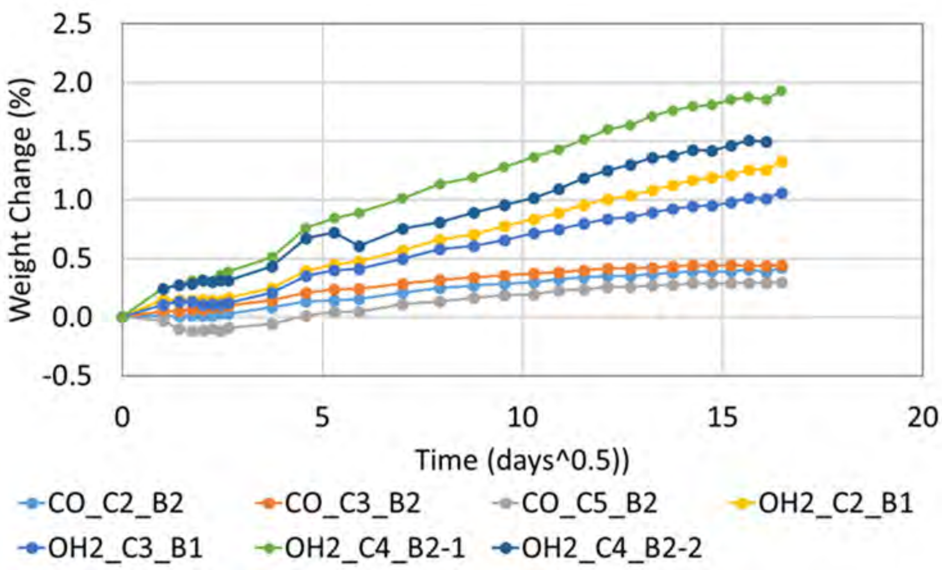

Fig. 7. Moisture uptake vs. square root of time for O'Fallon and Cuyahoga bars – PSU

Table 20. O'Fallon water absorption results – PSU

Specimen ID	% Weight Change at 24 hours	% Weight Change at D570 Equilibrium / days	% Weight Change at 271 Days
CO_C2B_B2	0.015	0.322 / 119	0.421
CO_C3_B2	0.053	0.355 / 91	0.446
CO_C5_B2	-0.030	0.223 / 119	0.298

Congruently with the weight loss observed in dry-out tests, the average weight gain of the *O'Fallon* bars is about 0.388%. The CO_C5_B2 specimen has less weight gain than the other *O'Fallon* specimens due to the loss of many sand particles as mentioned earlier.

2.3 Salem Ave

Water absorption tests for the *Salem Ave Bridge* were performed at the University of Miami, according to the procedure depicted in Section 4.1.2. Drying and measurement procedures are described in Appendix II. The results for 24-hour water absorption and long-term immersion (as of September 17, 2018) are shown in Table 21.

Table 21. Salem water absorption results - UM

Sample	24-hour Immersion Weight Change (%)	Long-term Immersion Weight Change (%)	Length of Saturation (days)
OH1_C1_B2	0.08	0.30	85
OH1_C2_B2	0.17	0.53	85

OH1_C3_B1(1)	0.07	0.22	85
OH1_C3_B1(2)	0.09	0.25	85
OH1_C4_B1	0.07	0.21	85

2.4 Bettendorf

Water absorption tests for the *Bettendorf Bridge* were performed at the University of Miami, according to the procedure depicted in Section 4.1.2. Drying and measurement procedures are described in Appendix II. The results for 24-hour water absorption and long-term immersion (as of September 17, 2018) are shown in Table 22.

Table 22. Bettendorf water absorption results - UM

Sample	24-hour Immersion Weight Change (%)	Long-term Immersion Weight Change (%)	Length of Saturation (days)
IA_C7_B1(1)	0.48	2.30	179
IA_C7_B1(2)	0.60	2.18	179
IA_C7_B1(3)	0.55	2.01	179

2.5 Cuyahoga

Water absorption tests for the *Cuyahoga County Bridge* were performed at Penn State University and Missouri S & T, according to the procedure depicted in Section 4.1.2. Drying and measurement procedures are described in Appendix II.

Tests at Penn State University:

During moisture absorption testing, OH2_C4_B2(2) lost weight between some of the measurements. Between 28 and 35 days into uptake testing, lost a large piece of helical wrap. Fig. 8 displays the cause for this loss in weight.

Fig. 8. Part of the helical wrap fell off of OH2_C4_B2-2

Weight losses as a result of pre-conditioning at 104 °F (40°C) for 48 h in non-circulating oven air are shown in Table 23. The two OH2_C4_B2 specimens had consistently higher pre-conditioning weight loss than any other bar. Such a faster change in percent weight can be expected for the OH2_C4_B2 bar because of its smaller diameter versus the other bars.

Table 23. Weight of Cuyahoga specimens (g) for uptake testing before and after preconditioning at 104°F (40°C) for 48 h in non-circulating oven air – PSU

Elapsed Time (days)	OH2_C2_B1	OH2_C3_B1	OH2_C4_B2-1	OH2_C4_B2-2
0.000	14.037	14.283	10.570	10.239
1.982	14.033	14.278	10.565	10.234
Change	-0.028%	-0.035%	-0.047%	-0.049%

Percent weight changes for the *O'Fallon* and *Cuyahoga* bars up to Dec. 15, 2018 (271 days) are shown on a log time scale in Fig. 7. By 259 days, all bars had met the ASTM D570 (ASTM-D570−98, 2018) equilibrium condition of less than 5 mg average weight gain per two-week period over the last three bi-weekly measurement intervals. Table 24 lists the weight gains at 24 hours, at equilibrium, and at the most recent measurement (271 days) for the *Cuyahoga* bars. The average weight gain for the *Cuyahoga* bars at saturation is 1.37%, which is more than the 1% qualification limit in ASTM D7957 (ASTM D7957, 2017).

Table 24. Cuyahoga water absorption results – PSU

Specimen ID	% Weight Change at 24 hours	% Weight Change at D570 Equilibrium / days	% Weight Change at 271 Days
OH2_C2_B1	0.150	1.254 / 259	1.325
OH2_C3_B1	0.105	0.946 / 203	1.058
OH2_C4_B2-1	0.246	1.874 / 245	1.931
OH2_C4_B2-2	0.244	1.417 / 217	1.563

The average weight gain for *Cuyahoga* is 1.469%. The weight gains in the smaller-diameter OH2_C4_B2 specimens differ substantially from each other due to the dislodged spiral wrap on one of them as mentioned earlier. Once again, the outlier behavior of OH2_C4_B2 can be attributed to its smaller diameter versus the other bars.

Tests at Missouri S&T:

Other bars from the same bridge were tested at Missouri S&T. The bars were CU_C4_B1, CU_C5_B1, and CU_C6_B1. ASTM D570 requires a change of no more than 0.01% for two successive readings before the test can be terminated, or a consequential change in weight of two consecutive times to total weight change of less than 1%. CU_C4_B1 and CU_C5_B1 reached equilibrium after 219 days, while CU_C6_B1 after 233 days. The weight change compared to time (days$^{0.5}$) is shown in the Fig 9. Cuyahoga moisture uptake vs. square root of time and Table 25. Cuyohoga water absorption results – MST It can be seen that the results fluctuated (i.e. spiked) during the first week of testing and then have been changing steadily. This abrupt spike in trend is not known for certain, but the following reasons are being investigated:

- The humidity level inside the room.
- Even though the desiccator was used to keep the specimen in a controlled temperature, opening and closing desiccator by other users of the same equipment could possibly affect the temperature inside the desiccator and expose the specimen to unstable range of temperature.
- Despite using the same scale to read the specimens' weights, scales' errors cannot be totally avoided. There will be some noise and/or calibration issues.
- Even though these bars were pre-conditioned in order to prepare them for the same test parameters, regardless of their original condition, their field locations were different from each other which means their environmental conditions were different since the day they were embedded in the bridge. Thus, they could have influenced these changes in weight of specimens.
- The way these bars were stored could have also influenced these changes in weight.

According to ASTM D570, any observation as to warping, cracking or change in appearance of the specimens should be reported. Between 30 and 44 days into uptake testing, CU_C4_B1and CU_C6_B1, lost a little piece of helical wrap around 7 mg and 5 mg respectively. In addition to losing a piece of helical wrap, some residue was noticed in all of the specimens' containers after 6 weeks of testing.

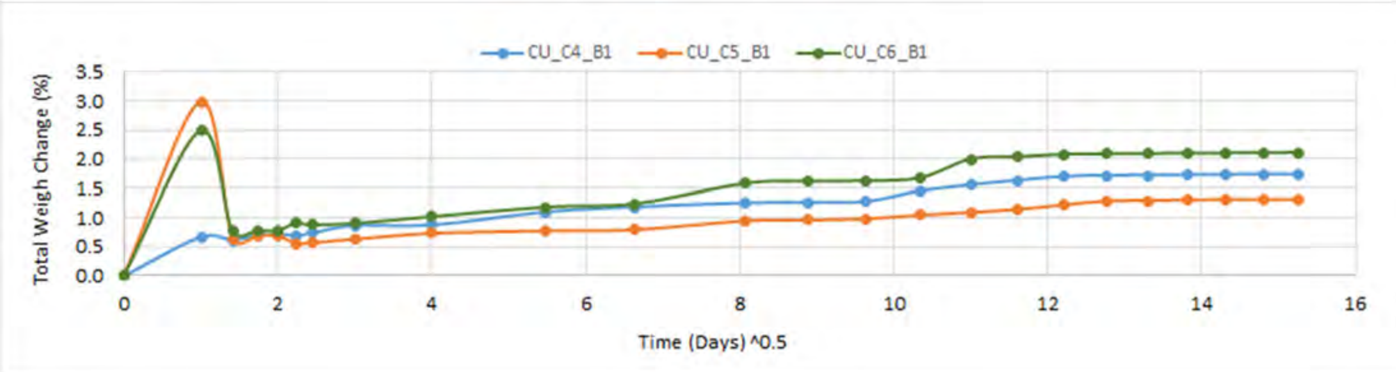

Fig 9. Cuyahoga moisture uptake vs. square root of time – MST

Table 25. Cuyohoga water absorption results – MST

Specimen ID	% Weight Change at D570 Equilibrium / days
CU_C4_B1	1.732/219
CU_C5_B1	1.307/219
CU_C6_B1	2.1/233

2.6 McKinleyville

Water absorption tests for the *McKinleyville Bridge* were performed at the Penn State University, according to the procedure depicted in Section 4.1.2. Drying and measurement procedures are described in Appendix II. Percent weight changes for the *McKinleyville and Thayer* bars up to Mar. 9, 2019 (162 days) are shown on a square root of time scale in Fig. 10.

Table 26 lists the weight gains of the WV bars at 24 hours, at equilibrium, and at the last measurement (162 days). Equilibrium was reached in 56 days for the WV bars.

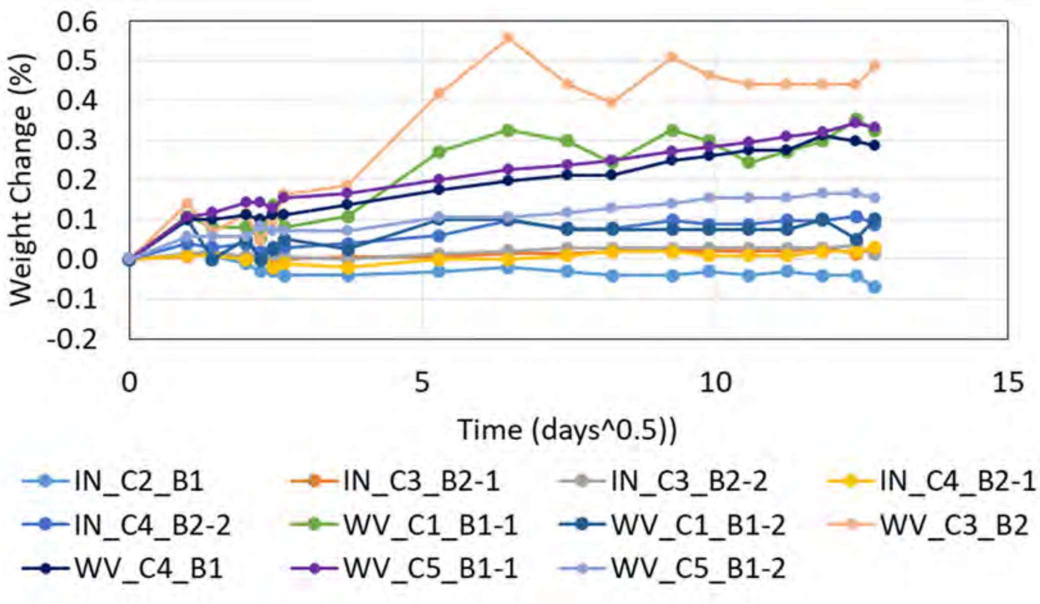

Fig. 10. Moisture uptake vs. square root of time for McKinleyville and Thayer bars – PSU

Table 26. McKinleyville water absorption results – PSU

Specimen ID	% Weight Change at 24 hours	% Weight Change at D570 Equilibrium / days	% Weight Change at 162 Days
WV_C1_B1-1	0.109	0.299 / 56	0.326
WV_C1_B1-2	0.101	0.076 / 56	0.101
WV_C3_B2	0.139	0.441 / 56	0.487
WV_C4_B1	0.100	0.212 / 56	0.286
WV_C5_B1-1	0.107	0.237 / 56	0.332
WV_C5_B1-2	0.059	0.118 / 56	0.154

2.7 Thayer Road

Water absorption tests for the *Thayer Road Bridge* were performed at the Penn State University, according to the procedure depicted in Section 4.1.2. Drying and measurement procedures are described in Appendix II. Percent weight changes for the *Thayer* bars up to Mar. 9, 2019 (162 days) are shown on a square root of time scale in Fig. 10. Table 27 lists the weight gains of the IN bars at 24 hours, at equilibrium, and at the last measurement (162 days). Equilibrium was reached in 56 days for the IN bars.

Table 27. Thayer water absorption results – PSU

Specimen ID	% Weight Change at 24 hours	% Weight Change at D570 Equilibrium / days	% Weight Change at 162 Days
IN_C2_B1	0.010	-0.030 / 56	-0.070
IN_C3_B2-1	0.007	0.015 / 56	0.029

IN_C3_B2-2	0.014	0.029 / 56	0.014
IN_C4_B2-1	0.010	0.010 / 56	0.030
IN_C4_B2-2	0.039	0.079 / 56	0.089

2.8 Roger’s Creek

Three bars from Roger’s Creek (KY) were tested for Moisture Absorption following the ASTM D570. The bars are: KY_C1_B1_S1, KY_C6_B1_S1, and KY_C6_B1_S2. They reached moisture equilibrium at 77 days with a total change in weight of 0.16%, as seen in Fig. 11 and Table 28. There were no signs of delamination of wrapping or shedding some parts of the bar.

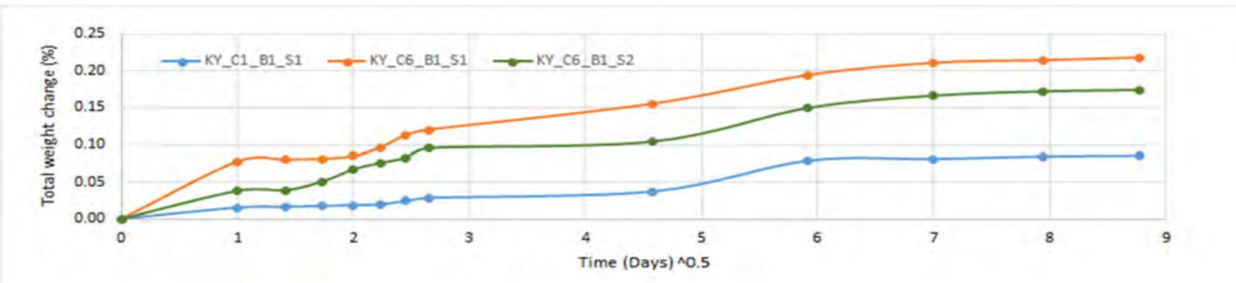

Fig. 11. Roger’s Creek moisture uptake vs. square root of time – MST

Table 28. Rogers Creek water absorption results – MST

Specimen ID	% Weight Change at D570 Equilibrium / days
KY_C1_B1_S1	0.085/77
KY_C6_B1_S1	0.218/77
KY_C6_B1_S2	0.174/77

3. Horizontal shear

3.1 O’Fallon Park

Specimens from the *O’Fallon Park Bridge* were tested for apparent horizontal shear strength at the University of Miami. Because of the limited number of samples, only two specimens were tested from apparent horizontal shear strength. The procedure for the tests is described in Section 4.1.3. The results are shown in Table 29 (calculated according to ASTM D4475 (ASTM-D4475, 2016).

Table 29. O'Fallon Park horizontal shear results – UM

Sample	Diameter, in.(mm)	Span Length, in. (mm)	Peak Load , lb (N)	Apparent Shear Strength, psi (MPa)
CO_C3_B1	0.8965 (23)	2.6265 (57)	5744 (25550)	6068 (42)
CO_C4_B1	0.9013 (23)	2.6265 (57)	5896 (26227)	6162 (42)
			Average (psi)	6115 (42)

3.2 Salem Ave

Specimens from *Salem Ave. Bridge* were tested for apparent horizontal shear strength at the University of Miami. The procedure for the tests is described in Section 4.1.3. The results are shown in Table 30 (calculated according to ASTM D4475 (ASTM-D4475, 2016)

Table 30. Salem Ave horizontal shear results — UM

Sample	Diameter, in. (mm)	Span Length, in. (mm)	Peak Load (lb.)	Apparent Shear Strength, psi (MPa)
OH1_C1_B1	0.7875 (20)	2.2465 (57)	4872 (21672)	6670 (46)
OH1_C2_B1	0.7987 (20)	2.2465 (57)	4871 (21667)	6483 (45)
OH1_C5_B1	0.8017 (20)	2.2465 (57)	4711 (20956)	6223 (43)
			Average (psi)	6459 (45)

3.3 Cuyahoga

The *Cuyahoga County Bridge* specimens were tested for apparent horizontal shear strength at Missouri S&T. The procedure for these tests is described in Section 4.1.3. Due to the size of the bars, the test was not performed according to ASTM standards. The bars tested were #6 and presented an apparent shear strength lower than the values from pristine bars at the time of construction. Pristine bars apparent shear strength was recorded to average 6,500 psi while the apparent shear strength result in *Cuyahoga Bridge*, after 16 years in service, averaged 4,316 psi, a decrease of approximately 33%. Results are shown in Table 31.

Table 31. Cuyahoga horizontal shear results – MS&T

Sample	Diameter ,in. (mm)	Span Length, in. (mm)	Peak Load (lb.)	Apparent Shear Strength, psi (MPa)
OH2_C4_B1	0.75 (19)	2.25 (57)	2678 (11912)	4042 (28)
OH2_C5_B1	0.75 (19)	2.25 (57)	3285 (14612)	4958 (34)
OH2_C6_B1	0.75 (19)	2.25 (57)	2616 (11636)	3948 (27)
			Average (psi)	4316 (30)

3.4 McKinleyville Bridge

Specimens from the *McKinleyville Bridge* were tested for apparent horizontal shear strength at the University of Miami. The procedure for the tests is described in Section 4.1.3. The results are shown in Table 32 (calculated according to ASTM D4475 (ASTM-D4475, 2016).

Table 32. McKinleyville horizontal shear results – UM

Sample	Diameter, in. (mm)	Span Length, in. (mm)	Peak Load (lb.)	Apparent Shear Strength (psi)
WV_C3_B2	0.40 (10)	1.5 (38)	769 (3421)	4100 (28)
WV_C3_B3	0.45 (11)	1.25 (32)	1170 (5204)	4905 (34)
WV_C1_B3	0.414 (11)	1.25 (32)	1340 (5960)	6638 (46)
			Average (psi)	5214 (39)

3.5 Thayer Road Bridge

Specimens from *Thayer Road Bridge* were tested for apparent horizontal shear strength at the University of Miami. The procedure for the tests is described in Section 4.1.3. The results are shown in Table 33 (calculated according to ASTM D4475 (ASTM-D4475, 2016).

Table 33. Thayer Road Bridge horizontal shear results – UM

Sample	Diameter, in (mm)	Span Length, in. (mm)	Peak Load (lb.)	Apparent Shear Strength (psi)
IN_C1_B1	0.653 (17)	2 (51)	3380 (15035)	6730 (46)
IN_C4_B1	0.664 (17)	2 (51)	3551 (15796)	6838 (47)
IN_C1_B3	0.666 (17)	2 (51)	3584 (15942)	6860 (47)
			Average (psi)	6809 (47)

3.6 Sierrita de la Cruz Creek

Specimens from the *Sierrita de la Cruz Bridge* were tested for apparent horizontal shear strength at the University of Miami in 2015 and 2018. The procedure for the tests is described in Section 4.1.3. The results of the test performed in 2015 were compared with the same test performed in 2000 prior to construction. Table 34 shows the summary of the result where P_c and P_s correspond to the peak load of control and extracted samples, respectively. Likewise, S_c and S_s correspond to the peak apparent horizontal shear strength control and extracted samples, respectively. The bars tested in 2018 were #5 and presented an apparent shear strength higher than the values from pristine bars at the time of construction. The pristine bars average apparent shear strength was 5,157 psi and the extracted bars from *Sierrita de la Cruz Creek* averaged 6,014 psi (41 MPa). Therefore, indicating an increase in shear strength of approximately 16%. Because horizontal shear is greatly affected by the property of the resin, the increase may be a result of resin crosslinking over time. The results are shown in Table 35 (calculated according to ASTM D4475 (ASTM-D4475, 2016).

Table 34. Sierrita de la Cruz Creek horizontal shear results of 2015 – UM

		P_c			P_s				
Rebar Size, imperial (metric)	Span Length, in (mm)	No. of Samples	Ave. , lbs (N)	CoV (%)	No. of Samples	Value lbs (N)	S_c psi (MPa)	S_s psi (MPa)	Ratio (S_s/S_c)
#5 (#16)	1.87 (47)	10	3.01 (14)	2	1	3.14 (14)	6540 (45)	6833 (47)	1.04
#6 (#19)	2.25 (57)	10	4.66 (21)	3.7	1	3.55 (16)	7404 (51)	5361 (37)	0.76

Table 35. Sierrita de la Cruz Creek horizontal shear results of 2018 – UM

Sample	Diameter, in. (mm)	Span Length, in. (mm)	Peak Load, lb. (N)	Apparent Shear Strength, psi (MPa)
TX_ B1	0.6552 (17)	1.8925 (48)	2870 (12766)	5677 (39)
TX_ B2	0.6615 (17)	1.8925 (48)	3059 (13607)	5935 (41)
TX_ B3	0.6583 (17)	1.8925 (48)	3282 (14600)	6429 (4432)
			Average (psi)	6014 (41)

3.7 Southview Bridge

Specimens from the *Southview Bridge* were tested for apparent horizontal shear strength at the University of Miami. The test was performed on three GFRP coupons: i) one #4 GFRP bar with the total length of 2.3 in (58 mm), and ii) two #6 GFRP bars with the total length of 3 in. (76 mm) and 2.9 in (74 mm). Since no historic data was available at the time of construction, the results were compared to the test performed on pristine bars produced by the same manufacturer in 2015 as a benchmark. Specimens were tested with the span-to-diameter ratio equal to three, according to standard and compared with pristine samples.

All three specimens presented the horizontal shear mode of failure. The results of the individual tests is shown in Table 36 and a summary of the results is shown in Table 37, where S_c and S_s, refer to the shear strength of control samples tested in 2015 and extracted samples, respectively. The same notation is employed for the failure load. The extracted GFRP bars showed about 5%

increase in horizontal shear strength compared to the samples produced in 2015. Since the horizontal shear is greatly affected by the property of the resin, the increase may be a result of resin crosslinking over time.

Table 36. Southview horizontal shear results – UM

Sample	Diameter, in. (mm)	Span Length, in. (mm)	Peak Load, lb. (N)	Apparent Shear Strength (psi)
MO2_C1_B1	0.550 (14)	1.5 (38)	2098 (9332)	5888 (41)
MO2_C1_B2	0.794 (20)	2.25 (57)	4937 (21961)	6649 (46)
MO2_C2_B3	0.794 (20)	2.25 (57)	4812 (21404)	6480 (47)
			Average (psi)	6340 (44)

Table 37 Southview horizontal shear results – UM

		P_c			P_s				
Rebar Size	Span Length, in. (mm)	No. of Samples	Ave. lbs. (N)	CoV (%)	No. of Samples	Value, lbs. (N)	S_c, psi (MPa)	S_s psi (MPa)	Ratio (S_s/S_c)
#4 (#13)	1.5 (38)	5	1.97 (9)	2.4	1	2.1 (9)	6817 (47)	7106 (49)	1.05
#6 (#19)	2.25 (57)	5	4.66 (21)	3.6	2	4.9 (22)	6962 (48)	7397 (51)	1.06

4. DSC

4.1 Bettendorf

DSC analysis for *Bettendorf Bridge* was performed at Missouri S&T using the procedure described in Section 4.1.4. The results are summarized in Table 38 and the results for each bar are shown in Fig. 12 through Fig. 19.

Table 38. Bettendorf DSC results – MST

Sample	Net Weight (mg)	T_g, °F (°C)
IA_C3_B1(1)	13.237	230 (110)
IA_C3_B1(2)	16.6	221 (105)
IA_C3_B1(3)	15.56	226 (108)
IA_C6_B1(1)	14.2	230 (110)
IA_C6_B1(2)	11.22	230 (110)
IA_C6_B1(3)	19.017	230 (110)
IA_C7_B1(1)	19.567	230 (110)
IA_C7_B1(2)	17.908	230 (110)
IA_C7_B1(3)	12.723	230 (110)

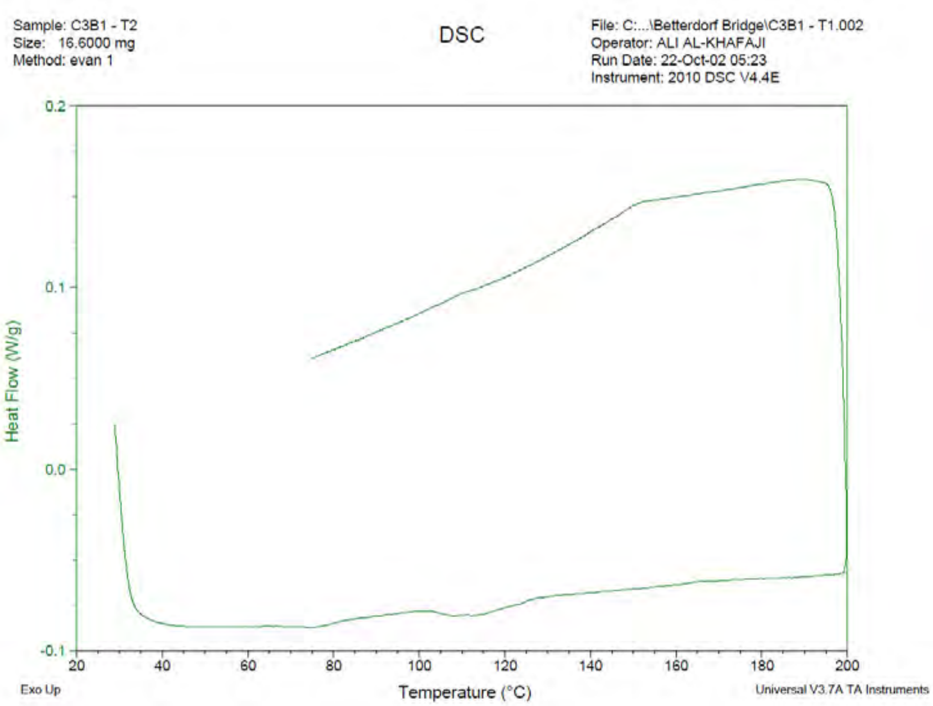

Fig. 12. Bettendorf core#3 bar#1 sample 2 DSC curve – MST

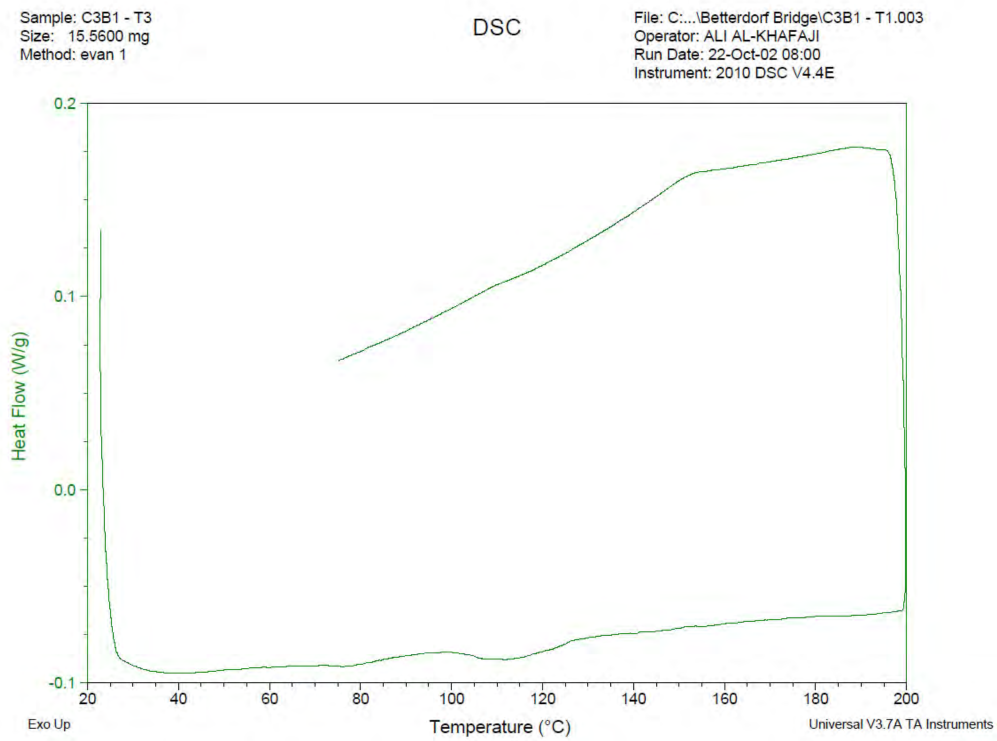

Fig. 13. Bettendorf core#3 bar#1 sample 3 DSC curve – MST

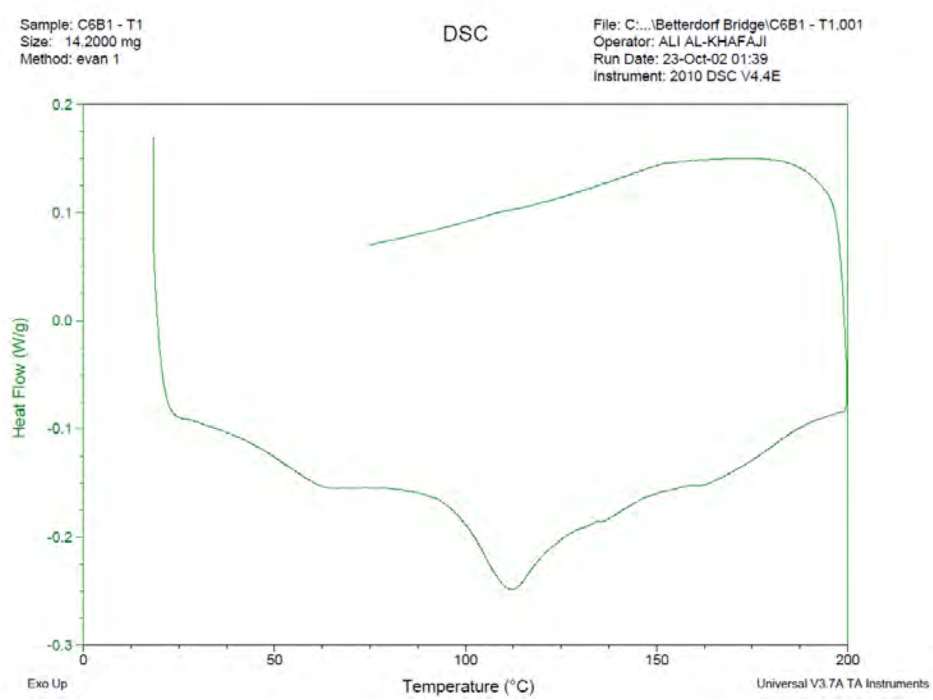

Fig. 14. Bettendorf core#6 bar#1 sample 1 DSC curve – MST

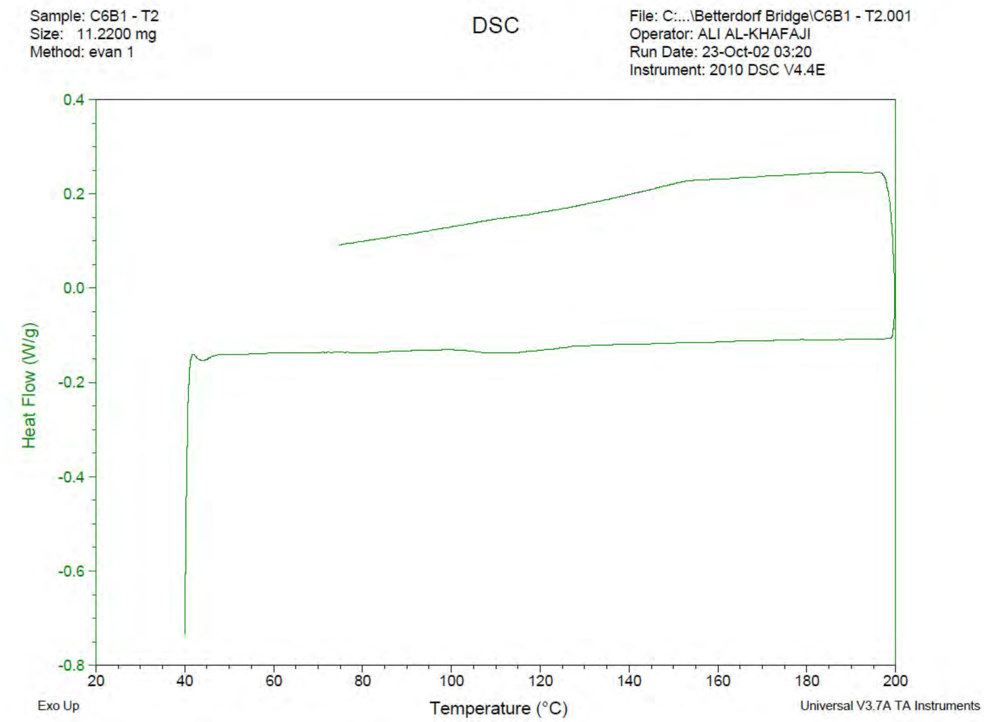

Fig. 15. Bettendorf core#6 bar#1 sample 2 DSC curve –MST

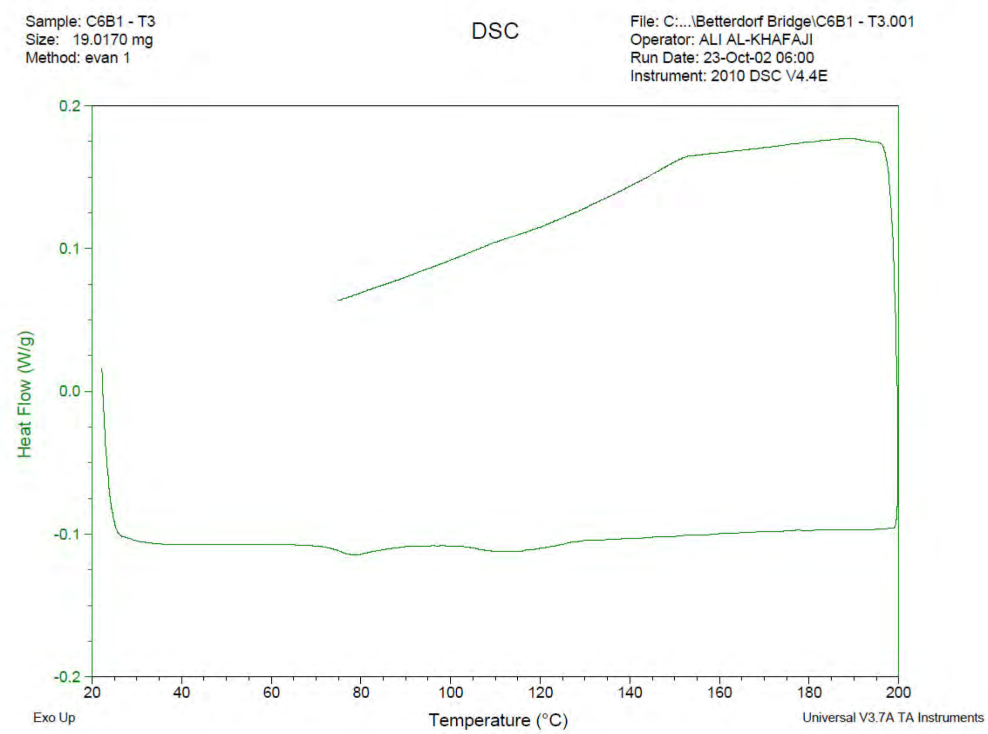

Fig. 16. Bettendorf core#6 bar#1 sample 3 DSC curve – MST

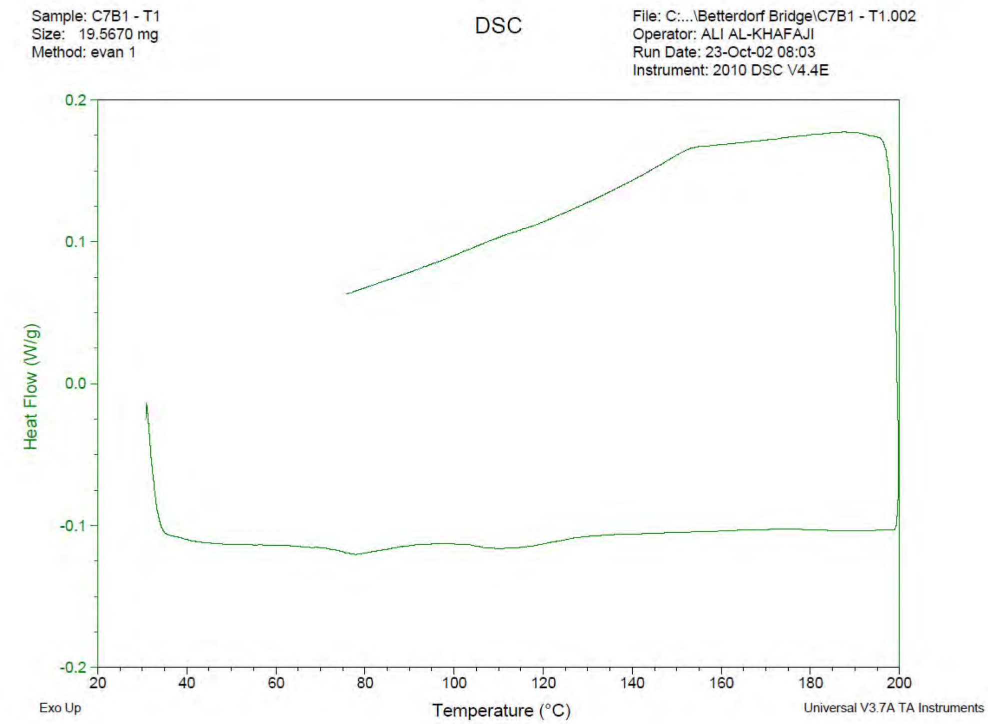

Fig. 17. Bettendorf core#7 bar#1 sample 1 DSC curve – MST

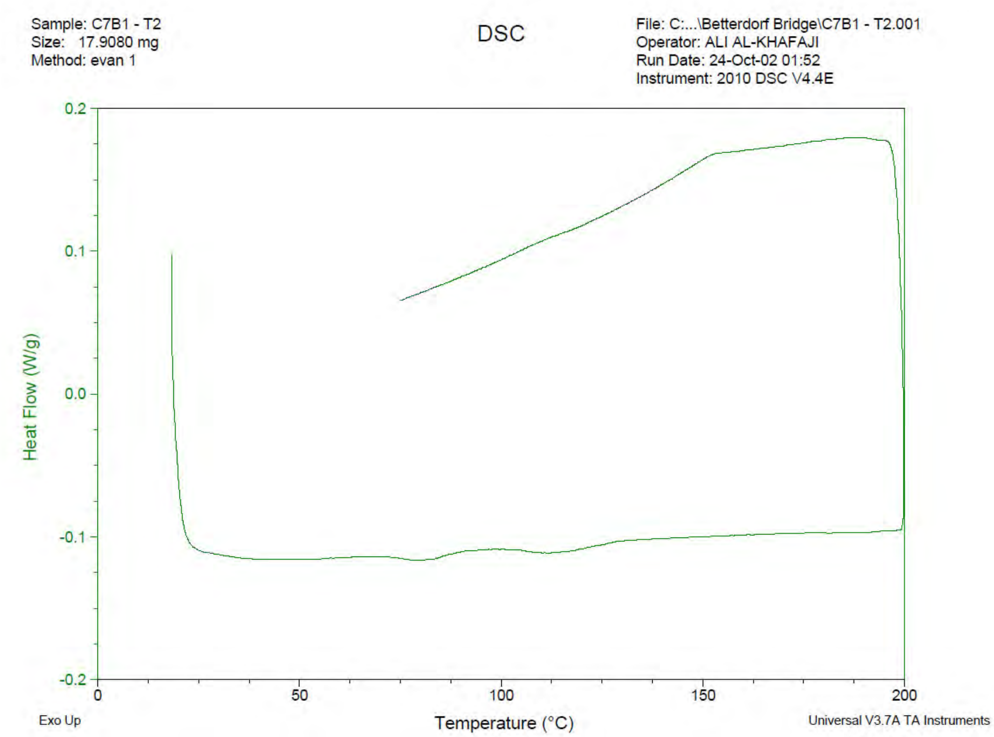

Fig. 18. Bettendorf core#7 bar#1 sample 2 DSC curve – MST

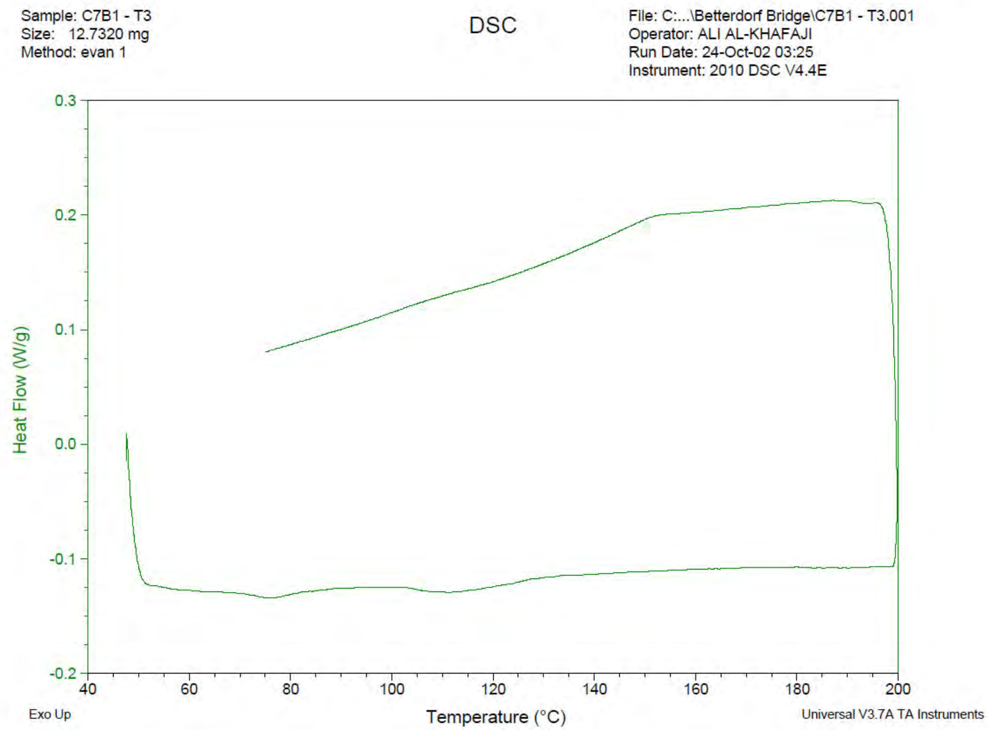

Fig. 19. Bettendorf core#7 bar#1 sample 3 DSC curve – MST

4.2 Cuyahoga

DSC analysis for Cuyahoga Bridge was performed at Missouri S&T, Owens Corning, and Penn State using the procedure described in Section 4.1.4. The tabulated results are provided in Table 39 through Table 41 and full DSC graphs for the Cuyahoga bars tested at Penn State are shown in Fig. 20 through Fig. 23.

Table 39. Cuyahoga DSC results – MST

Sample	Net Weight (mg)	T_g, °F (°C)
OH2_C4_B1(1)	9.303	221 (105)
OH2_C4_B1(2)	5.57	216 (102)
OH2_C4_B1(3)	9.911	203 (95)
OH2_C5_B1(1)	16.304	212 (100)
OH2_C5_B1(2)	7.595	194 (90)
OH2_C5_B1(3)	12.006	203 (95)
OH2_C6_B1(1)	7.511	221 (105)
OH2_C6_B1(2)	19.086	194 (90)
OH2_C6_B1(3)	9.89	203 (95)

Table 40. Cuyahoga DSC Results – OC

Sample	T_g 1st Heat ,°F (°C)	SD T_g 1st ,°F (°C)	T_g 2nd Heat ,°F (°C)	SD T_g 2nd ,°F (°C)
OH2_C1_B1	180 (82.0)	32 (0.2)	175(79.4)	33 (0.3)
OH2_C5_B2	181 (82.7)	34 (1.2)	175(79.4)	32 (0.2)
OH2_C8_B1	180 (82.5	32 (0.1)	175 (79.4)	34 (1.3)

Table 41. Cuyahoga MDSC results – PSU

Sample	Net weight (mg)	Total T_g,°F (°C)	Reversible T_g,°F (°C)
OH2_C2_B1	17.3	192 (89)	199 (93)
OH2_C3_B1(1)	14.5	196 (91)	190 (88)
OH2_C3_B1(2)	15.2	194 (90)	217 (103)
OH2_C4_B2	16.1	185 (85)	180 (82)

The heat flow curves for MDSC, shown in Fig. 20 to Fig. 23, show generally weak undulations associated with T_g, possibly due to the thermal influence of glass and filler materials mixed in with the matrix material. Evidence of exothermic processes can be seen in the non-reversible heat flow data for all bars. The exotherms appear between 50–70°C and again above 105–110°C. The onset or end of these ranges are believed to be close to the T_g of the materials, which can deviate the total heat flow curve up or down depending on whether the exotherm is starting or ending. Therefore, the influence of exotherms on the total heat flow curves should be considered when attempting to assign a T_g from the total heat flow.

The T_g from the reversible heat flow curves is believed to be a better representation of the T_g of the material in the majority of cases where it could be observed because it was not affected by the onset or end of an exothermic process in the material. For the OH2_C3_B1(1) and CU_C3_B1(2), the T_g results from total heat flow show 1°C variation, which is likely within graphical error, while the T_g results from reversible heat flow show 15°C variation.

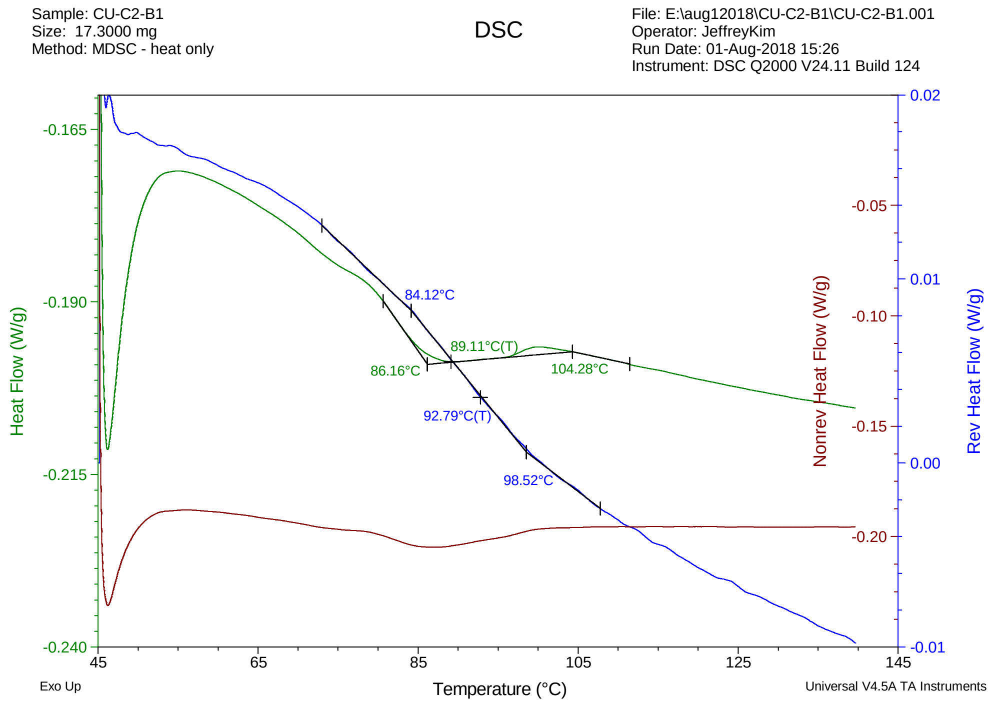

Fig. 20. Cuyahoga core#2 bar#1 MDSC curve – PSU

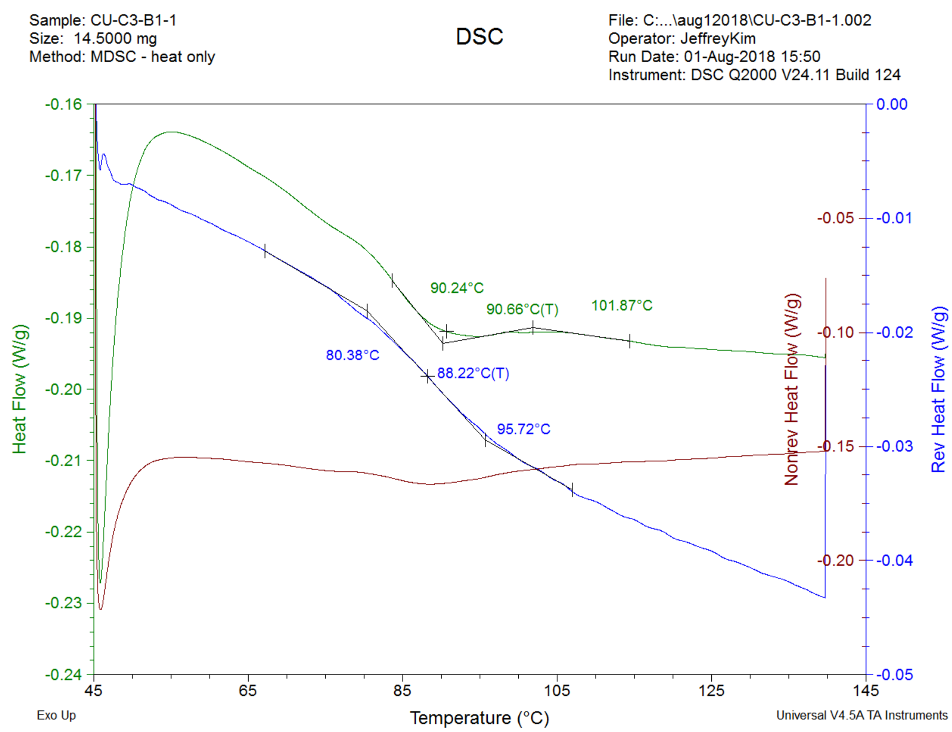

Fig. 21. Cuyahoga core#3 bar#1A MDSC curve – PSU

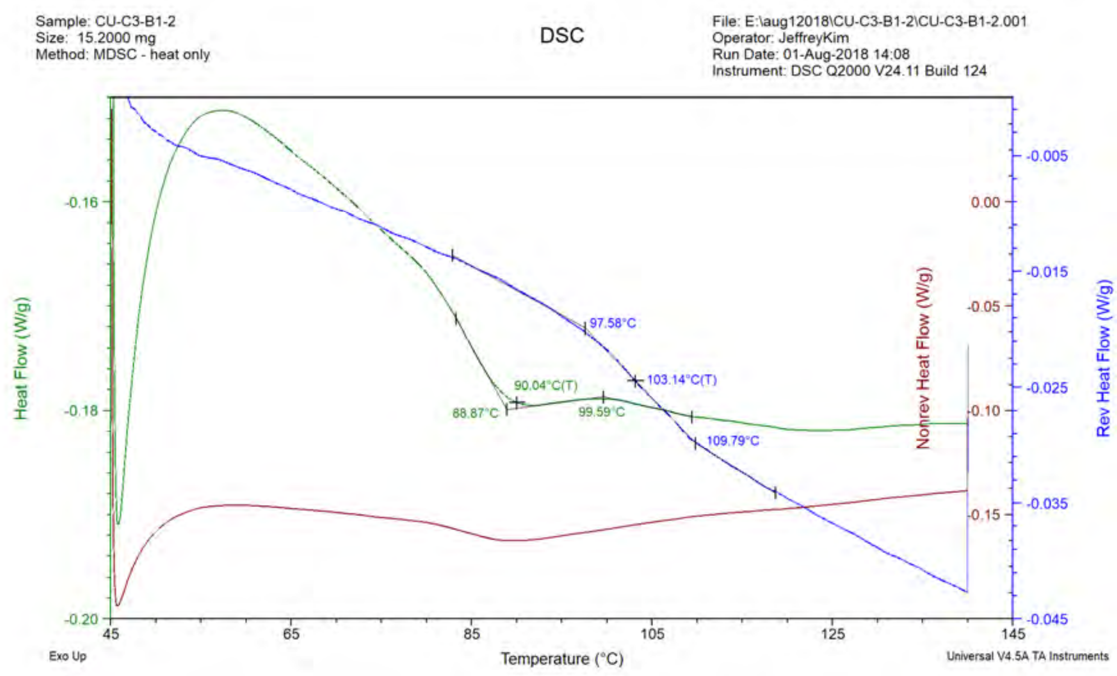

Fig. 22. Cuyahoga core#3 bar#1B MDSC curve – PSU

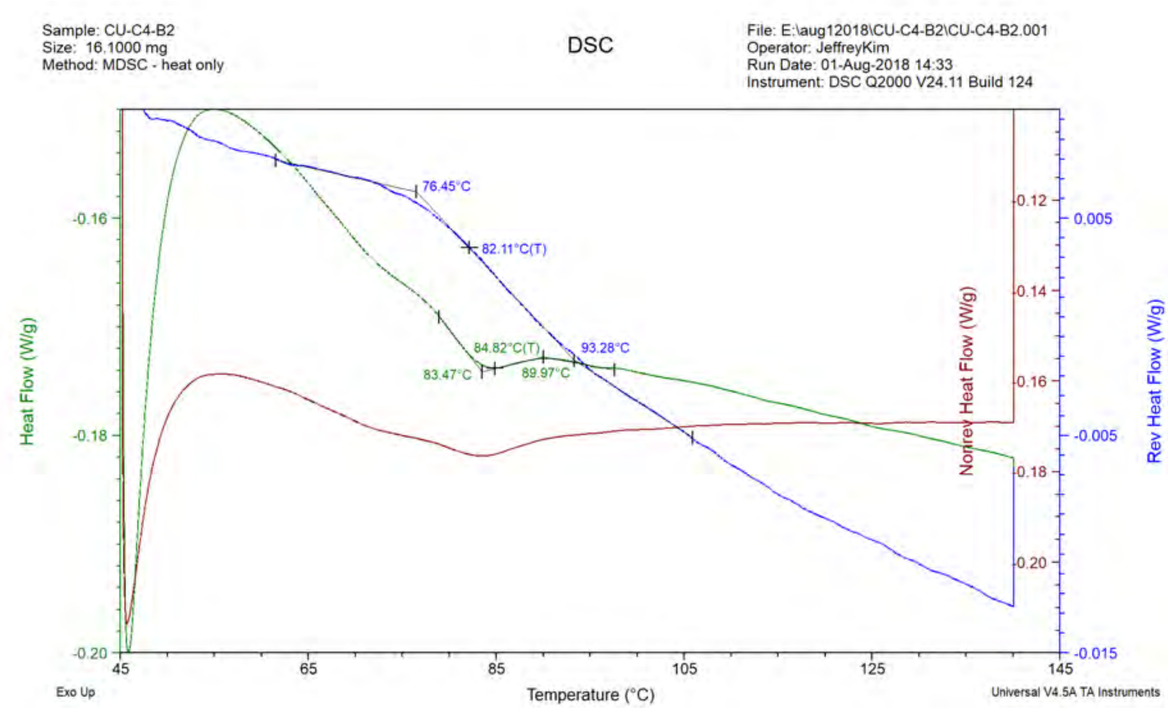

Fig. 23. Cuyahoga core#4 bar#2 MDSC curve – PSU

4.3 O'Fallon Park

MDSC analysis for *O'Fallon Park Bridge* was performed at Penn State University using the procedure described in Section 4.1.4. The results are summarized in

Table 42 and the results for each bar are shown in Fig. 24 through Fig. 26.

Table 42. O'Fallon Park MDSC results – PSU

Sample	Net weight (mg)	Total T_g,°F (°C)	Reversible T_g,°F (°C)
CO_C2_B2	14.2	180 (82)	--
CO_C3_B2	19.6	172 (78)	181 (83)
CO_C5_B2	17.2	176 (80)	--

The T_g from the reversible heat flow curves is believed to be a better representation of the T_g of the material in the majority of cases where it could be observed because it was not affected by the onset or end of an exothermic process in the material. For reasons that remain unknown at this time, the T_g from the reversible heat flow was difficult to observe in the *O'Fallon* bars. Thus, no entry is given in the above table for two of the three *O'Fallon* bars and the value given for the third bar is considered questionable.

It appears that the total heat flow provides a clearer and more consistent T_g than the reversible heat flow. However, the total heat flow is believed to be influenced by the proximity of non-reversible heat flow related to exothermic processes. Aside from these concerns, the T_g values measured using the method prescribed in ASTM D7957(ASTM D7957, 2017) (i.e., ASTM D1356, total heat flow, mid-point T_g) appear to fall in the approximate range of 78°C to 83°C, which is below the mean value of at least 100°C required in ASTM D7957 (ASTM D7957, 2017) for qualification and the minimum value of 100°C required in ASTM D7957 (ASTM D7957, 2017) for quality control and certification.

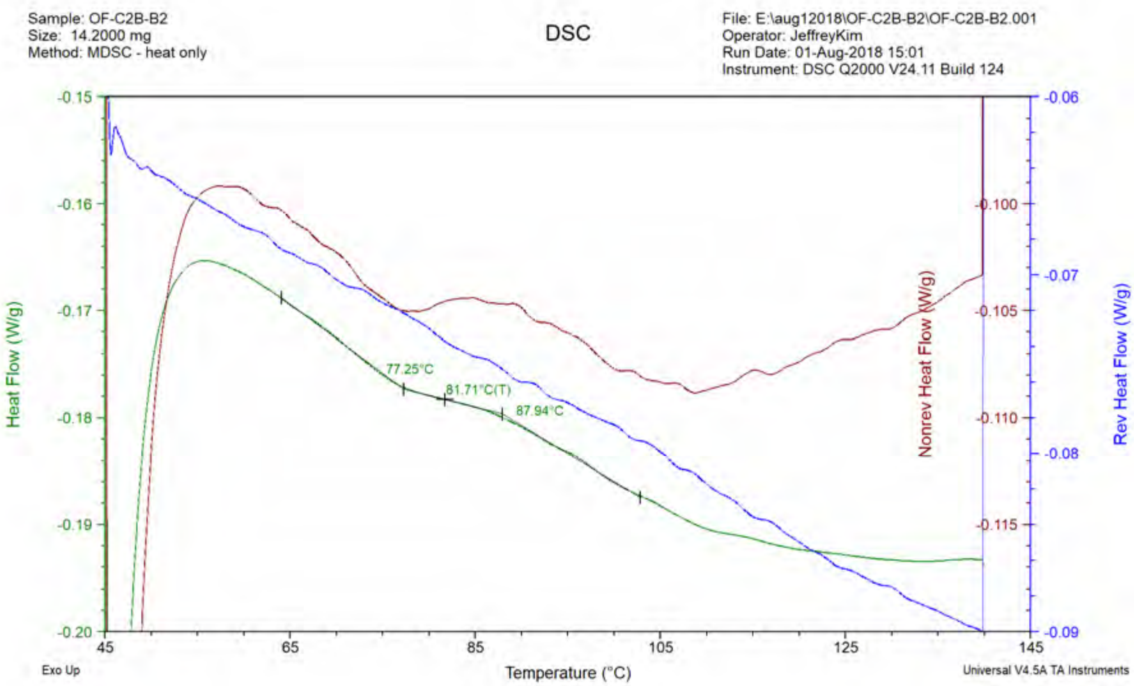

Fig. 24. O'Fallon core#2 bar#2 MDSC curve – PSU

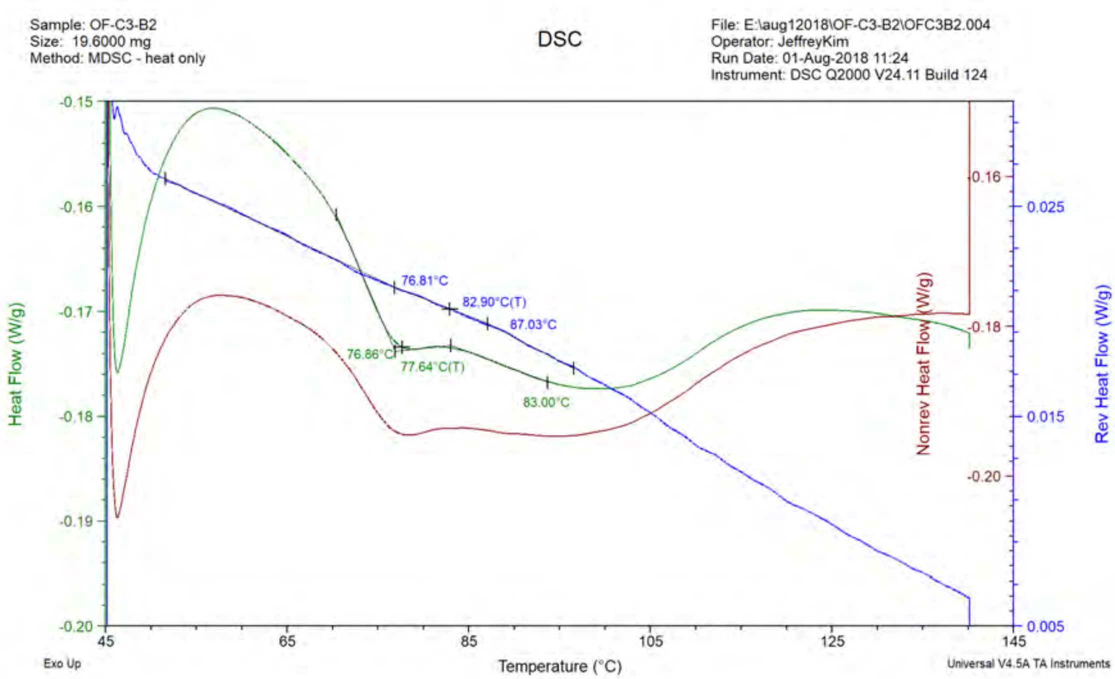

Fig. 25. O'Fallon core#3 bar#2 MDSC curve – PSU

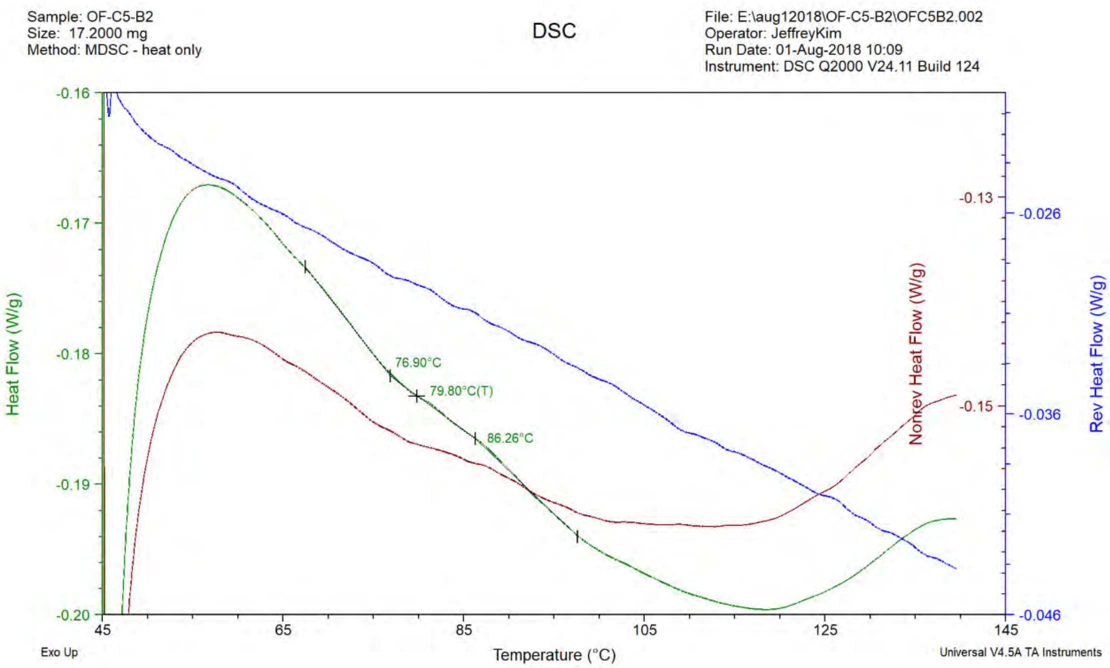

Fig. 26. O'Fallon core#5 bar#2 MDSC curve – PSU

4.4 Salem Ave

DSC analysis for *Salem Ave. Bridge* was performed at Missouri S&T using the procedure described in Section 4.1.4. The results are summarized in Table 43 and the results for each bar are shown in Fig. 27 through Fig. 31.

Table 43. Salem Ave DSC results – MST

Sample	Net Weight (mg)	T_g, °F (°C)
OH1_C1_B2(1)	15.305	x*
OH1_C1_B2(2)	16.081	221 (105)
OH1_C1_B2(3)	13.797	x*
OH1_C3_B1(1)	16.742	230 (110)
OH1_C3_B1(2)	15.445	221 (105)
OH1_C3_B1(3)	15.808	230 (110)

x* test is neglected due to its atypical curve

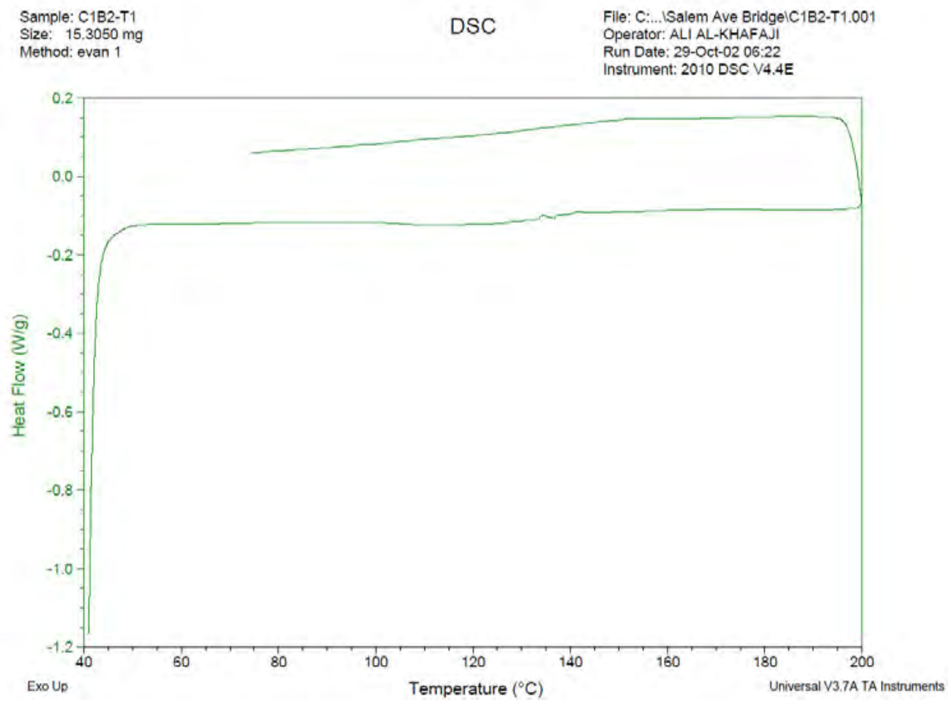

Fig. 27. Salem Ave core#1 bar#2 sample 1 DSC curve – MST

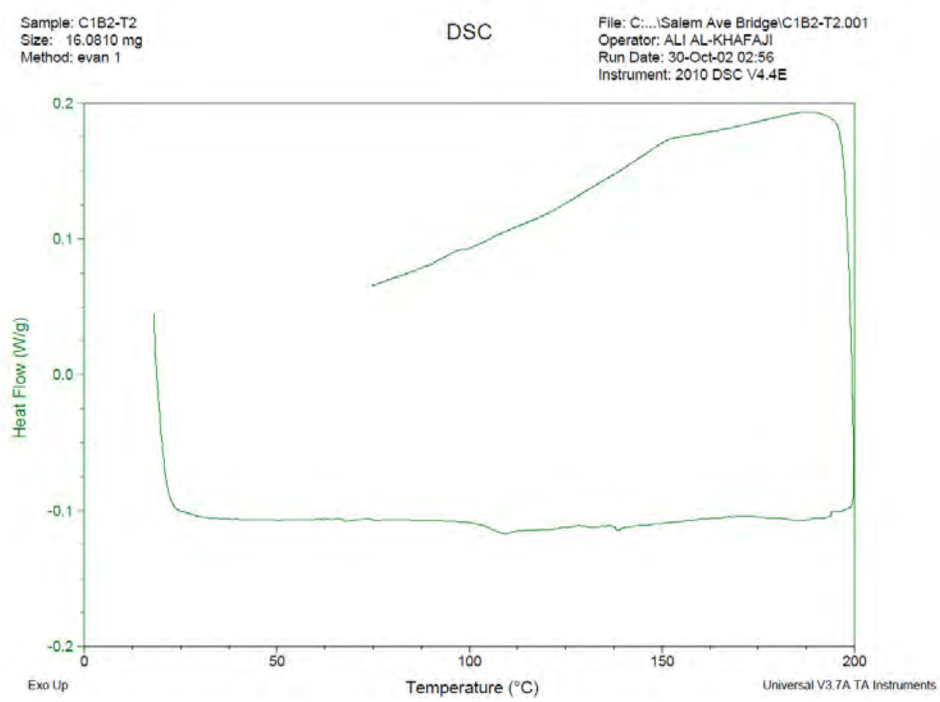

Fig. 28. Salem Ave core#1 bar#2 sample 2 DSC curve – MST

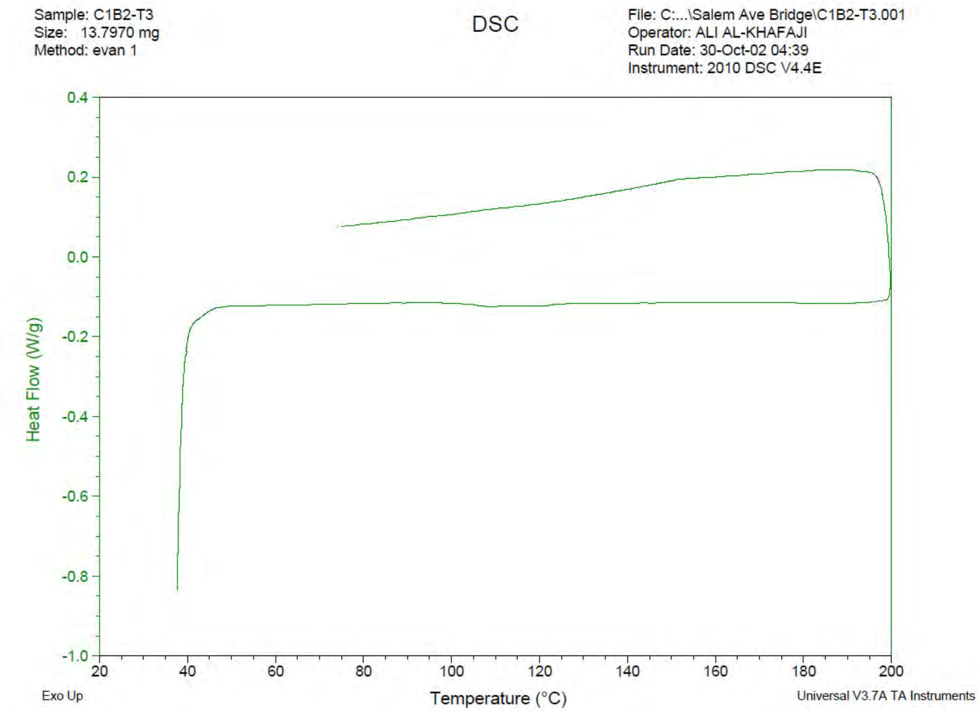

Fig. 29.Salem Ave core#1 bar#2 sample 3 DSC curve – MST

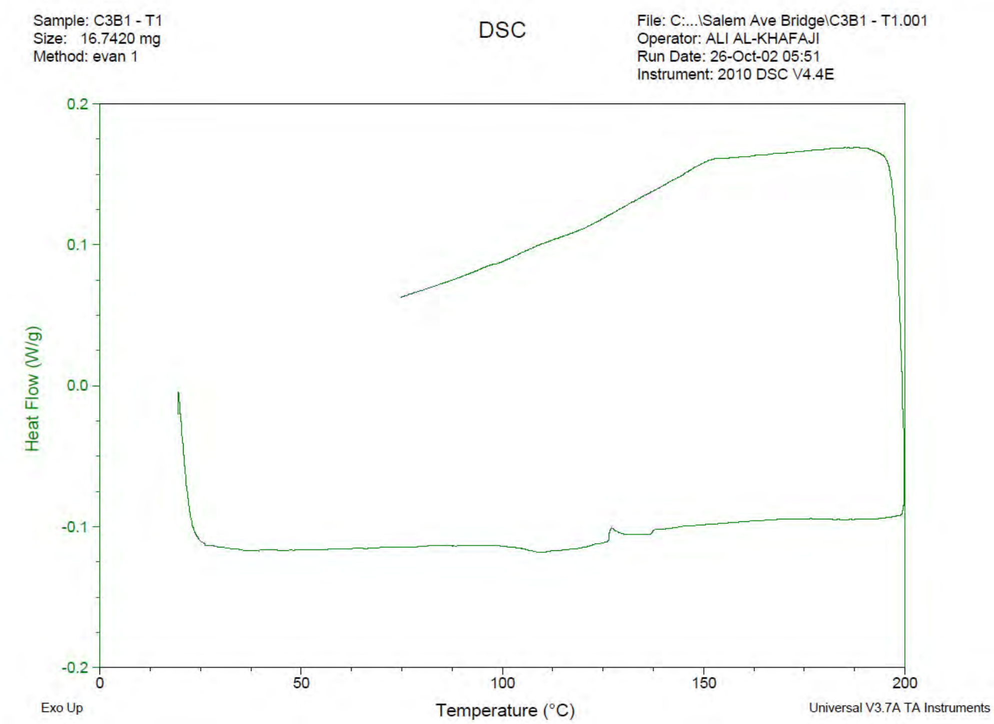

Fig. 30. Salem Ave core#3 bar#1 sample 1 DSC curve – MST

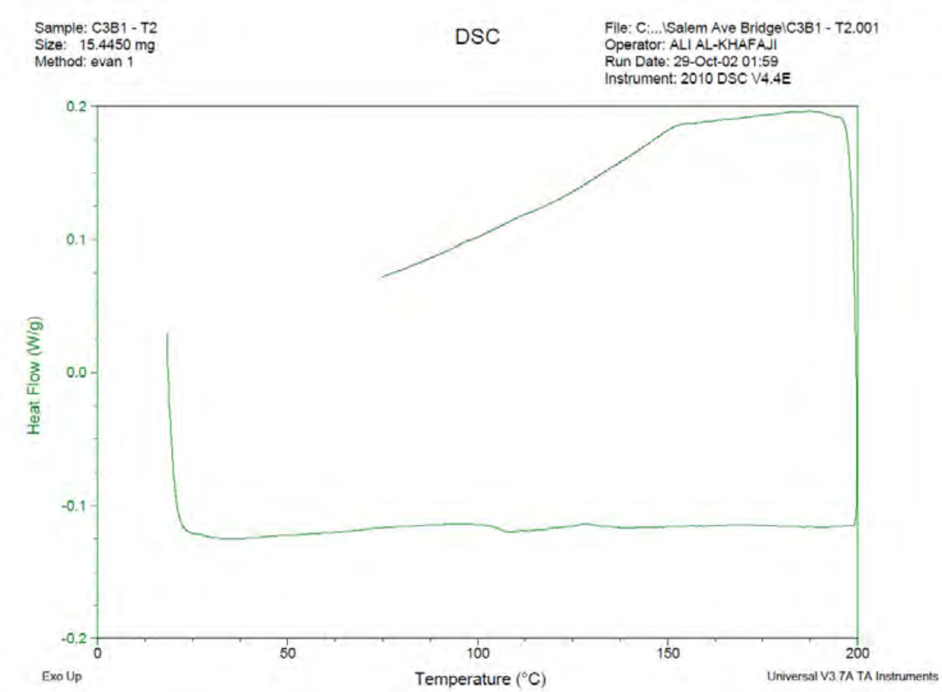

Fig. 31. Salem Ave core#3 bar#1 sample 2 DSC curve – MST

4.5 Gills Creek

DSC analysis for *Gills Creek Bridge* was performed at Missouri S&T and Owens Corning using the procedure described in Section 4.1.4. The results are summarized in Table 44 and

Table 45 and the results for each bar are shown in Fig. 32 through Fig. 37.

Table 44. Gills Creek DSC results – MST

Sample	Net Weight (mg)	T_g,°F (°C)
VA_C2_B1(1)	20.442	221 (105)
VA_C2_B1(2)	19.418	x*
VA_C2_B1(3)	18.206	230 (110)
VA_C4_B1(1)	17.189	x*
VA_C4_B1(2)	22.909	x*
VA_C4_B1(3)	21.424	221 (105)

x* test is neglected due to its atypical curve

Table 45. Gills Creek DSC results – OC

Sample	T_g 1st Heat,°F (°C)	SD T_g 1st,°F (°C)	T_g 2nd Heat,°F (°C)	SD T_g 1st,°F (°C)
VA_C1_B1	179 (81.9)	33 (0.3)	176 (80)	33 (0.3)
VA_C2_B2	182 (83.4)	32 (0.0)	179 (81.5)	36 (2.3)
VA_C4_B2	181 (82.9)	33 (0.5)	179 (81.6)	36 (2.1)

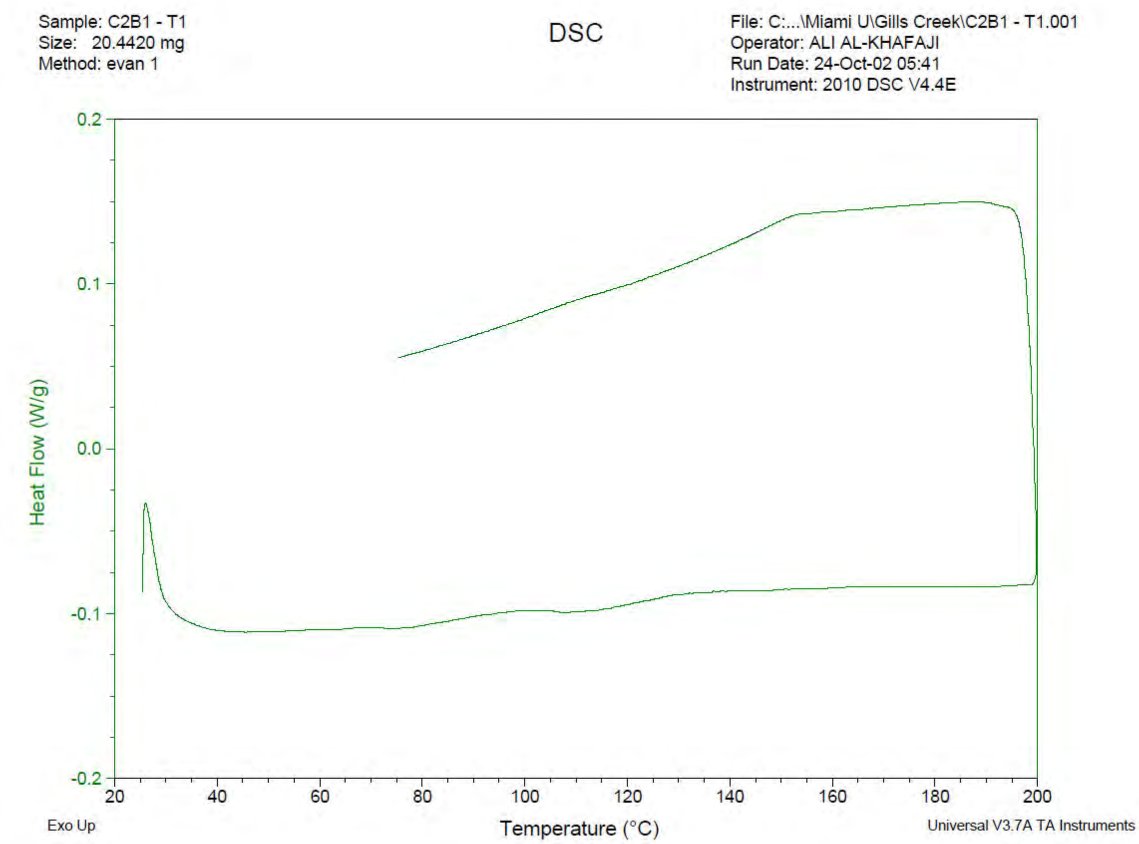

Fig. 32. Gills Creek core#2 bar#1 sample 1 DSC curve – MST

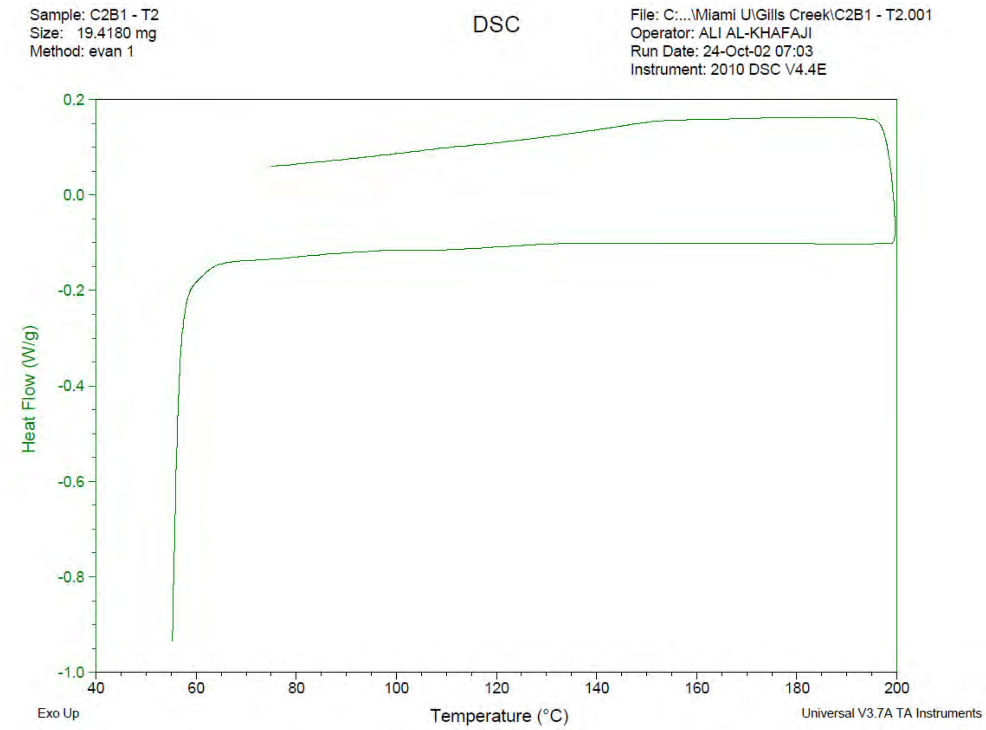

Fig. 33. Gills Creek core#2 bar#1 sample 2 DSC curve – MST

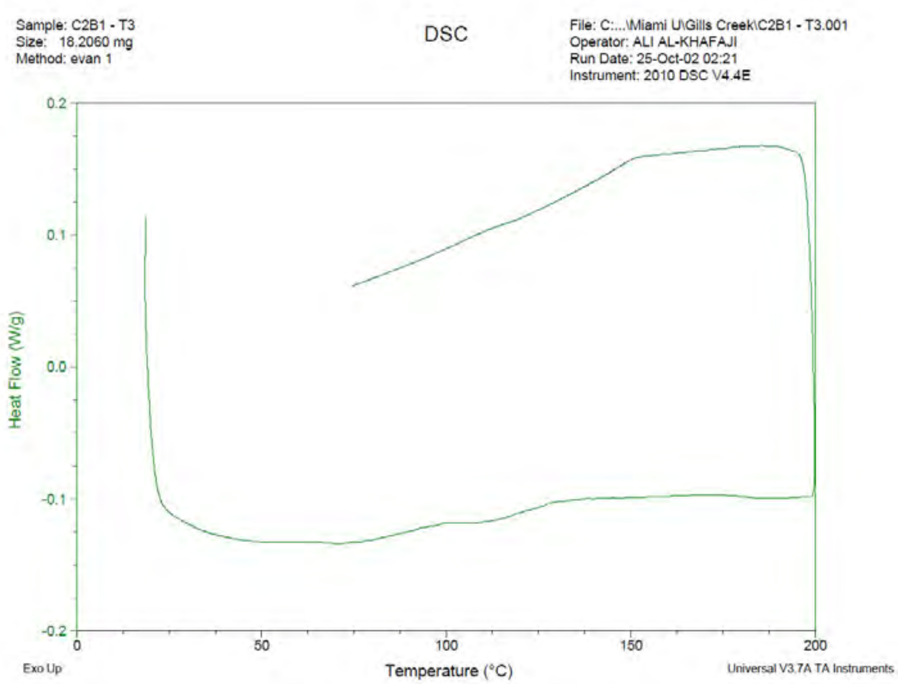

Fig. 34. Gills Creek core#2 bar#1 sample 3 DSC curve – MST

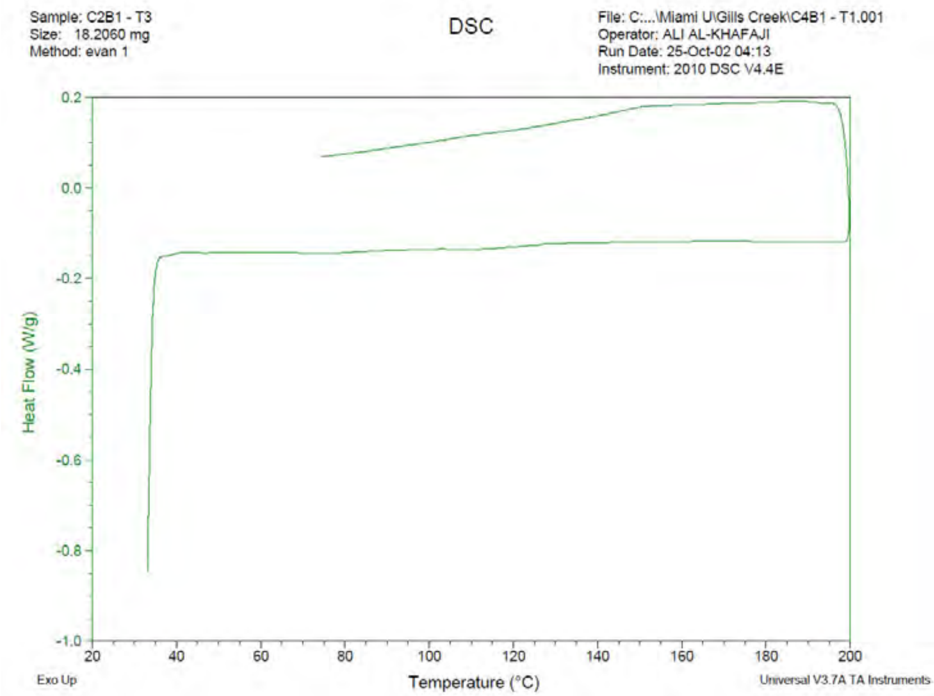

Fig. 35. Gills creek core#4 bar#1 sample 1 DSC curve – MST

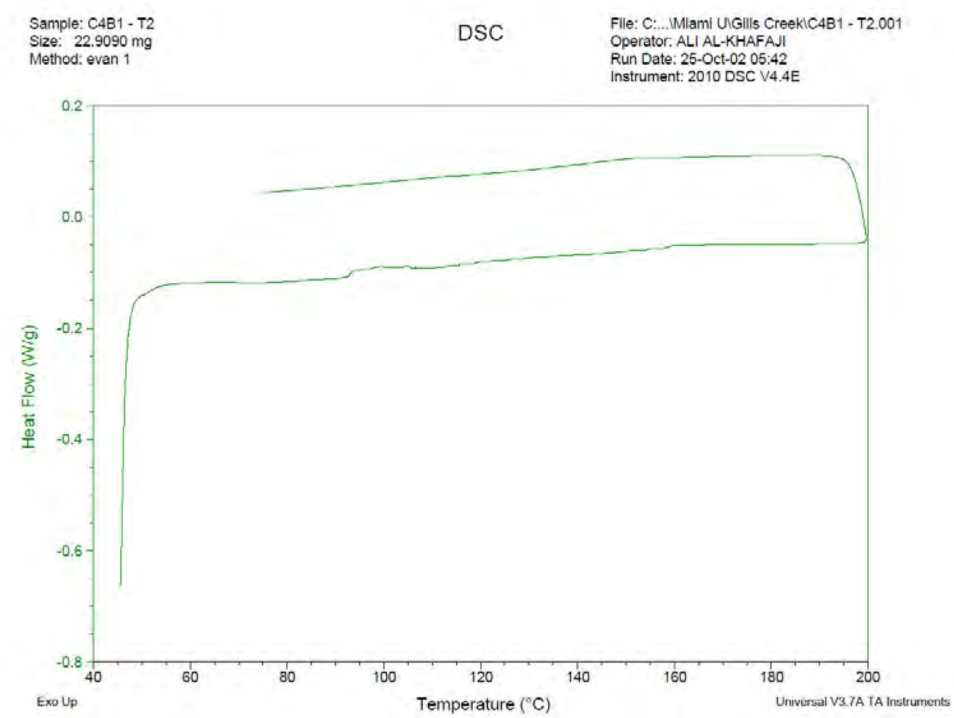

Fig. 36. Gills creek core#4 bar#1 sample 2 DSC curve – MST

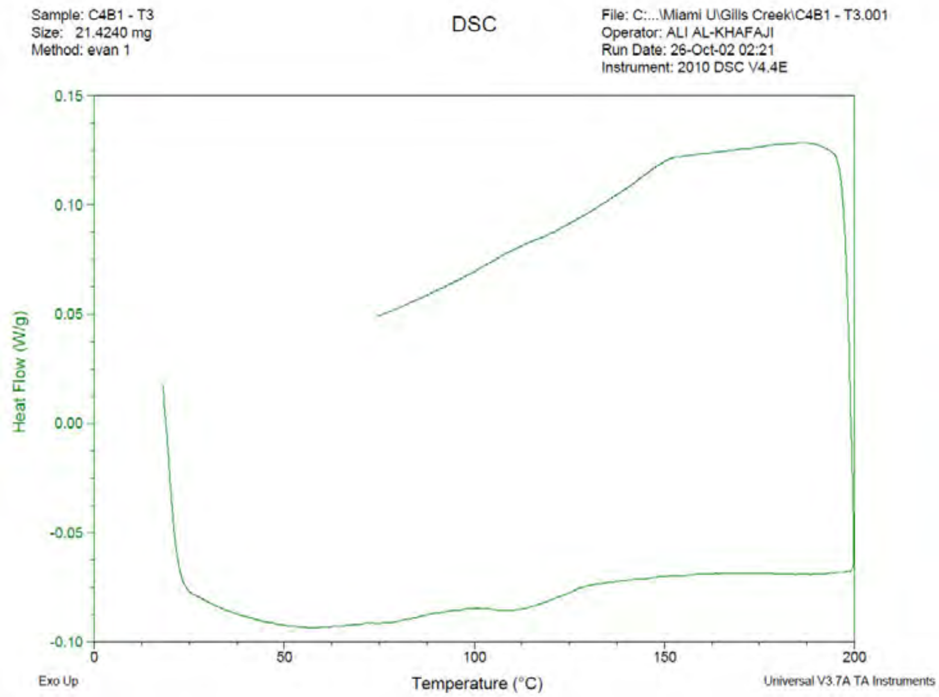

Fig. 37. Gills Creek core#4 bar#1 sample 3 DSC curve – MST

4.6 Roger's Creek

DSC analysis for *Roger's Creek Bridge* was performed at Missouri S&T using the procedure described in Section 4.1.4. The DSC results for each bar are shown in Fig. 38 through Fig. 43 and the numerical results are tabulated in Table 46.

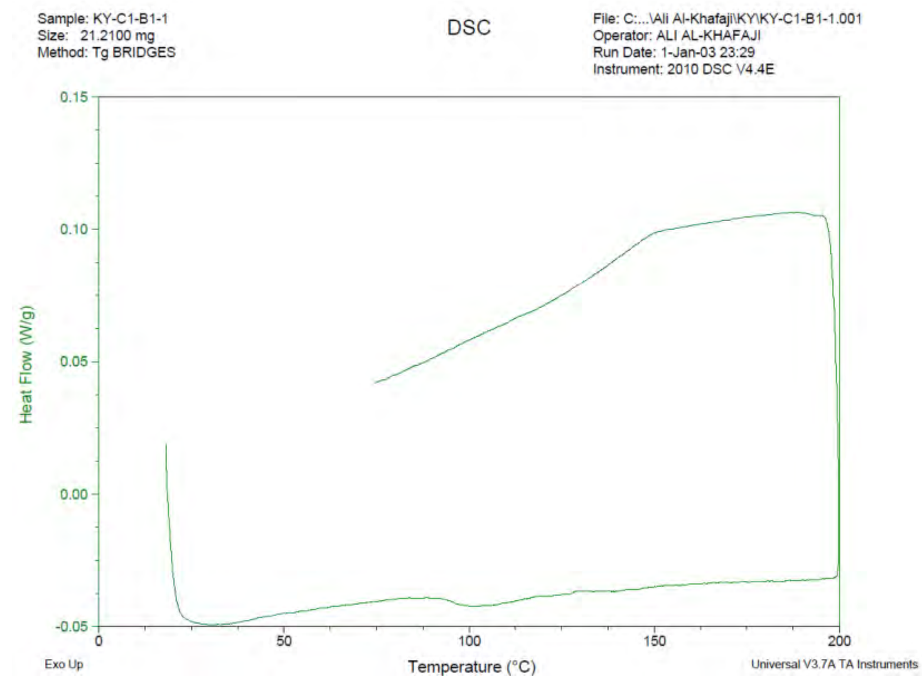

Fig. 38. Roger's Creek core#1 bar#1 sample 1 DSC curve – MST

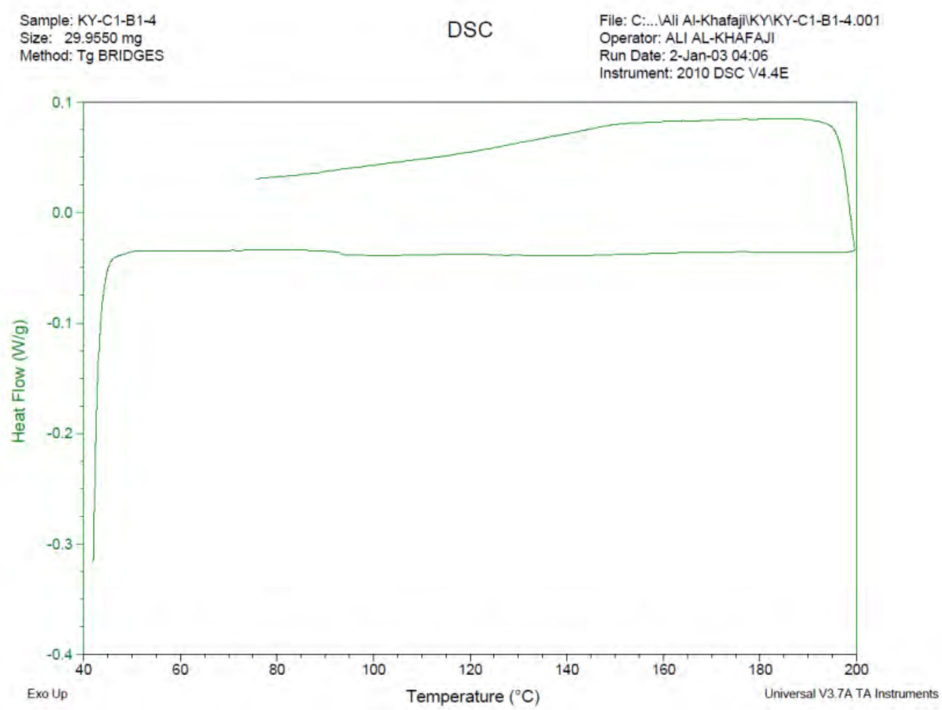

Fig. 39. Roger's Creek core#1 bar#1 sample 2 DSC curve

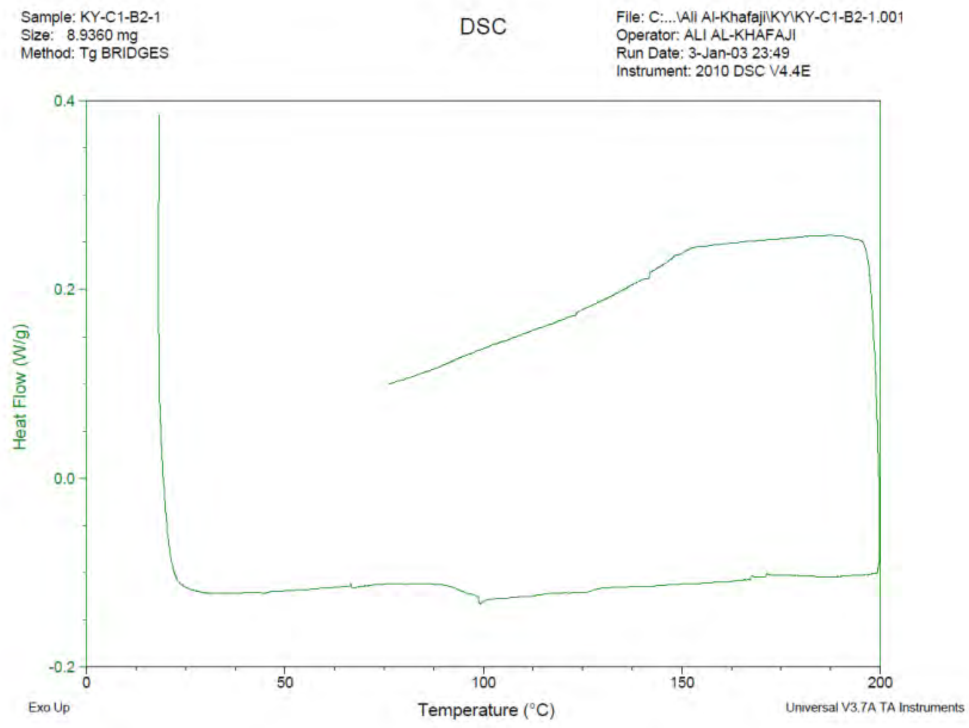

Fig. 40. Roger's Creek core#1 bar#2 sample 1 DSC curve

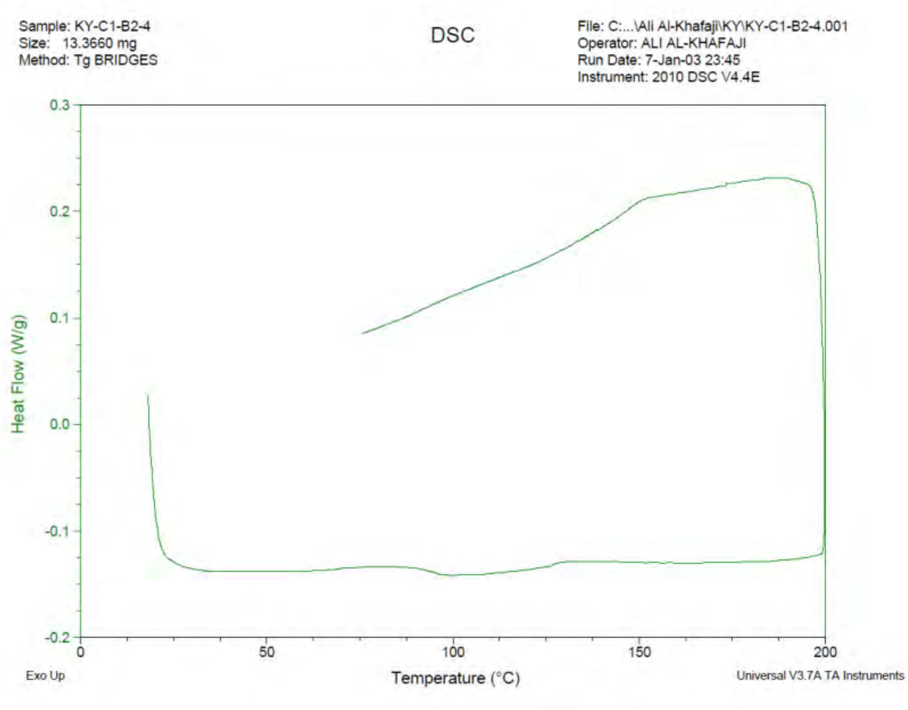

Fig. 41. Roger's Creek core#1 bar#2 sample 2 DSC curve

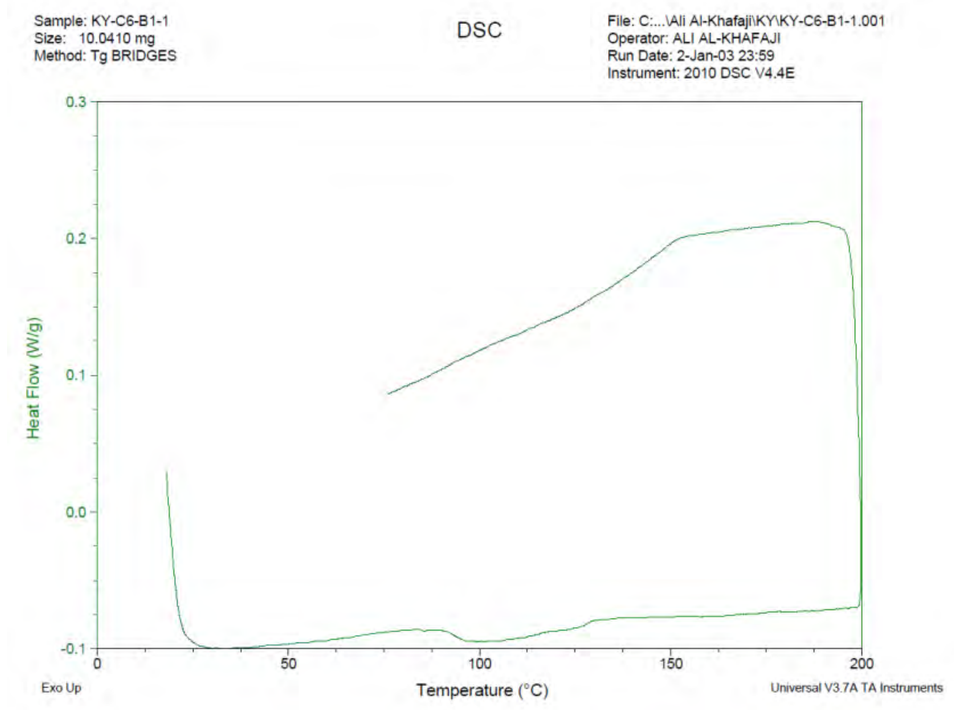

Fig. 42. Roger's Creek core#6 bar#1 sample 1 DSC curve

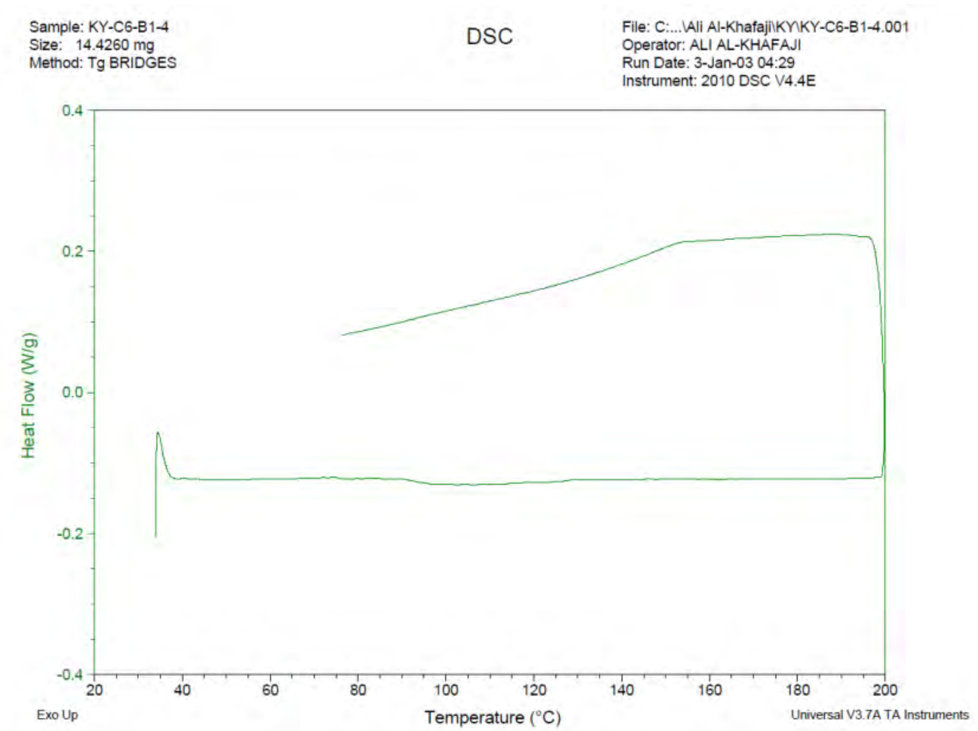

Fig. 43. Roger's Creek core#6 bar#1-4 sample 2 DSC curve

Table 46. Roger's Creek DSC results – MST

Sample	Net Weight (mg)	T_g,°F (°C)
KY_C1_B1(1)	21.210	203 (95)
KY_C1_B1(2)	29.950	x*
KY_C1_B2(1)	8.936	203 (95)
KY_C1_B2(2)	13.366	203 (95)
KY_C6_B1(1)	10.041	203 (95)
KY_C6_B1(2)	14.426	x*

x* test is neglected due to its atypical curve

4.7 Sierrita de la Cruz Creek

Glass transition temperature for *Sierrita de la Cruz Creek Bridge* was analyzed at the University of Miami using dynamic mechanical analysis (DMA) rather than DSC as in the other laboratories. The T_g is generally desired to be higher than 100˚C (212˚F) as a critical parameter in load transfer capability of the resin (ACI-440.6, 2008). Three rectangular specimens of $0.04 \times 0.2 \times 2.0$ in. ($1 \times 5 \times 50$ mm) were extracted from the outer core of the extracted bars according to ASTM E1640 (ASTM-E1640-18, 2018). The DMA test was performed with a three-point-bending fixture for a temperature ranging from 35 to 150 ˚C (95 to 302 ˚F), and a heating rate of 1 ˚C/min (1.8 ˚F/min). Due to lack of T_g test data on GFRP bars prior to construction, T_g tests were performed on samples from pristine bars produced in 2015 from the same manufacturer, to serve as a benchmark for comparison. Table 47 provides a summary of the results for the control bars, T_g^c, and the bars extracted from the bridge, T_g^s.

Table 47. Sierrita de la Cruz T_g results by dynamic mechanical analysis on extracted bars and control bars produced in 2015 - UM

Control T_g^c			Extracted T_g^s			Ratio (T_g^s/ T_g^c)
No. of Specimens	Average, °F (˚C)	CoV (%)	No. of Specimens	Average, °F (˚C)	CoV (%)	
3	178 (81)	16.9	3	239 (115)	7.1	1.4

The T_g of the extracted bars is 61°F (34°C) higher than the control samples pultruded in 2015. Due to changes in glass fibers, resin formulation, additive, and catalysts of the bars manufactured in 2015 compared to the ones produced in 2000, a direct comparison is not possible. In general, T_g is expected to increase over time due to continued cross-linking of the resin if it is not 100% cured at the time of manufacture.

4.8 Walker Box Culvert

Analysis of T_g for *Walker Box Culvert Bridge* bars was performed at the University of Miami using the DMA procedure described in the Sierrita de la Cruz Section of this Appendix. Due to lack of T_g test data on GFRP bars prior to construction, T_g tests were performed on samples from pristine bars produced in 2015 from the same manufacturer, to serve as a benchmark for comparison. Table 48 provides a summary of the results for the control bars, T_g^c, and the bars extracted from the bridge, T_g^s.

Table 48. Walker Box Culvert T_g results by dynamic mechanical analysis on extracted bars and control bars produced in 2015 – UM

Control T_g^c			Extracted T_g^s		
No. of Specimens	Average, °F (°C)	CoV (%)	No. of Specimens	Average, °F (°C)	CoV (%)
3	178 (81)	16.9	3	233 (112)	2.5

The T_g of the extracted bars is 55°F (31°C) higher than the control samples pultruded in 2015. While due to the changes in glass fibers and resin formulation of the bars manufactured in 2015 compared to the ones produced in 1999, a direct comparison is not possible. In general, T_g is expected to increase over time due to cross-linking of the resin if it is not 100% cured at the time of manufacture.

4.9 Southview

Analysis of T_g of *Southview Bridge* bars was performed at the University of Miami using the DMA procedure described in the Sierrita de la Cruz Section of this Appendix. Due to lack of T_g test data on GFRP bars prior to construction, T_g tests were performed on samples from pristine bars produced in 2015 from the same manufacturer, to serve as a benchmark for comparison. Table 49 provides a summary of the results for the control bars, T_g^c, and the bars extracted from the bridge, T_g^s.

Table 49. Southview T_g results by dynamic mechanical analysis on extracted bars and control bars produced in 2015 – UM

Control T_g^c			Extracted T_g^s		
No. of Specimens	Average,°F (˚C)	CoV (%)	No. of Specimens	Average, °F (˚C)	CoV (%)
3	178 (81)	16.9	3	213 (101)	2

The T_g of the extracted bars is 35°F (20°C) higher than the control samples pultruded in 2015. While due to the changes in glass fibers and resin formulation of the bars manufactured in 2015 compared to the ones produced in 2004, a direct comparison is not possible. In general, T_g is expected to increase over time due to cross-linking of the resin if it is not 100% cured at the time of production.

4.10 McKinleyville

MDSC analysis of bars from the *McKinleyville Bridge* was performed at Penn State University using the procedure described in Section 4.1.4. The results are summarized in Table 50 and the graphical results for each bar are shown in Fig. 44 through Fig. 46. The *McKinleyville* bars displayed no discernable inflection point in the reversible heat flow curves, although nearly all of the total heat flow curves for these bars had two separate T_g values. The lower and upper T_g values are both reported for the bars in Table 50. Only the lower T_g average is reported in the main body of this report, as it is considered the more relevant one for bar performance. The lower T_g values to not satisfy the contemporary GFRP bar specification (ASTM-D7957-17, 2017) of 212°F (100°C), but the upper ones do.

Table 50. McKinleyville MDSC results – PSU

Specimen ID	Sample Mass (mg)	T_g, °F (°C)	
		Lower	Upper
WV_C1_B1	15.0	197 (92)	x*
WV_C3_B2-1	15.2	207 (97)	239 (115)
WV_C3_B2-2	14.9	203 (95)	234 (112)

Notes: x* – value not discernable

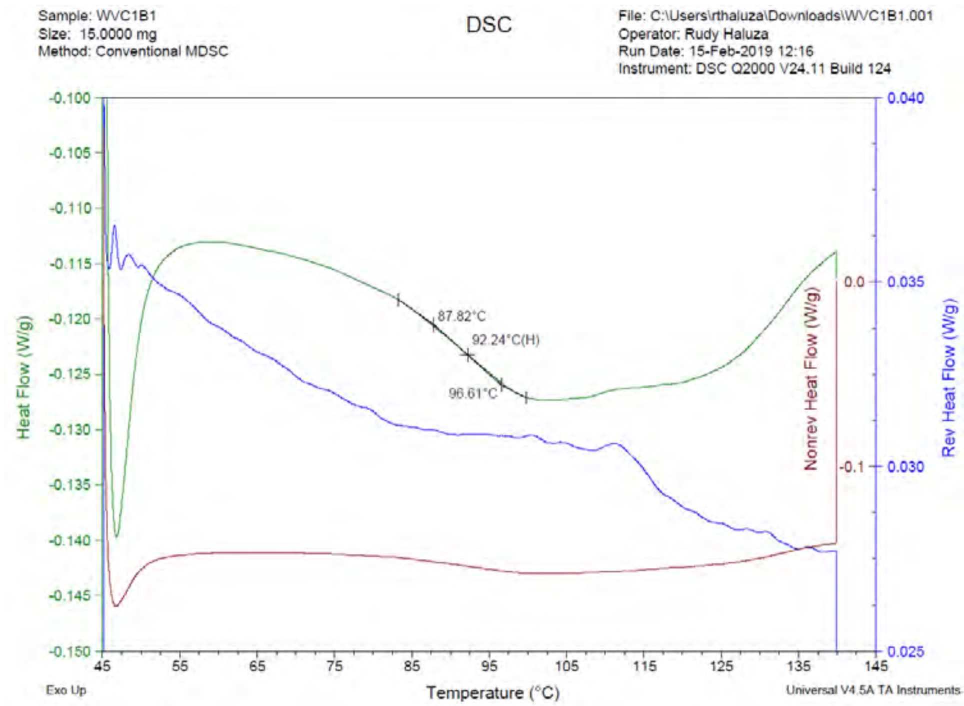

Fig. 44. McKinleyville core#1 bar#1 MDSC curves – PSU

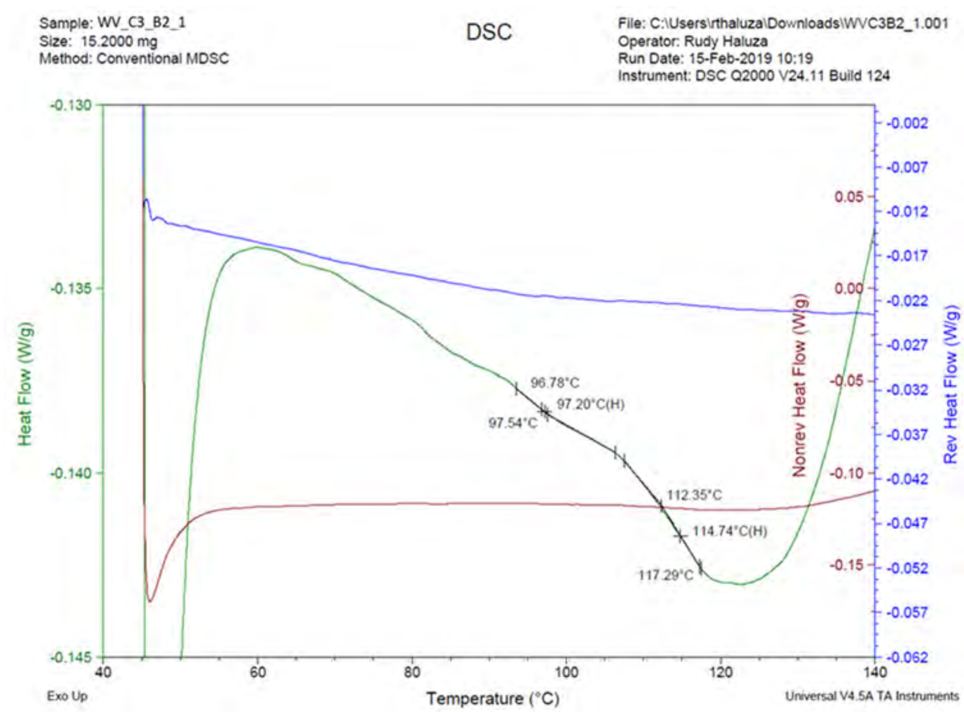

Fig. 45. McKinleyville core#3 bar#2 sample 1 MDSC curves – PSU

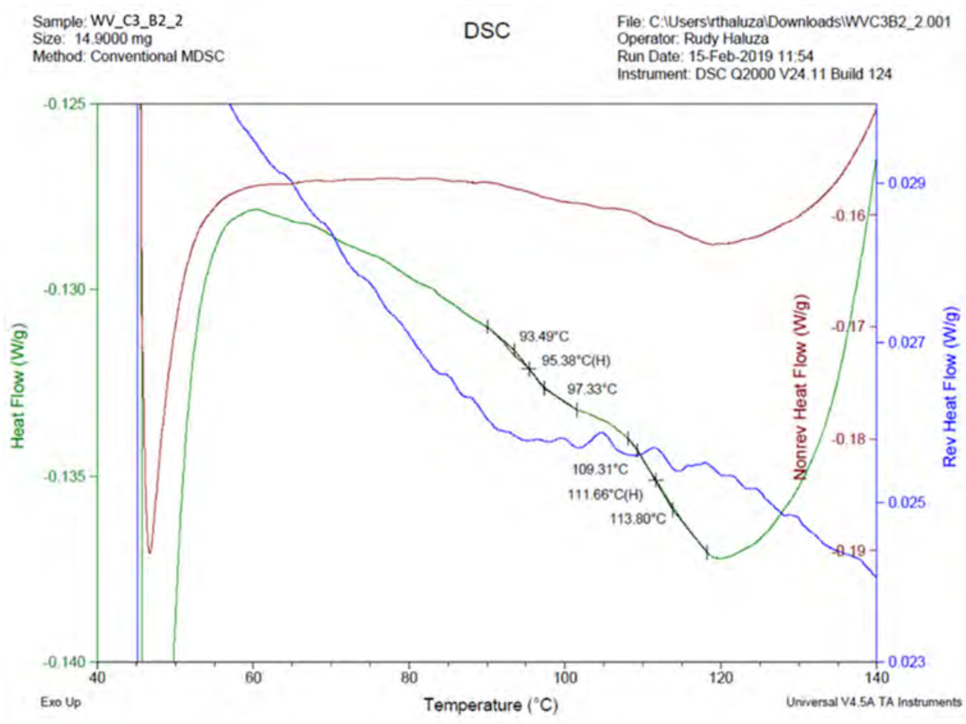

Fig. 46. McKinleyville core#3 bar#2 sample 2 MDSC curves – PSU

4.11 Thayer Road

MDSC analysis of bars from the *Thayer Road Bridge* was performed at Penn State University using the procedure described in Section 4.1.4. The results are summarized in Table 51 and the graphical results for each bar are shown in Fig. 47 through Fig. 50. The *Thayer Road* bars displayed no discernable inflection point in the reversible heat flow curves, although all of the total heat flow curves for these bars had two separate T_g values. The lower and upper T_g values are both reported for the bars in Table 51. Only the lower T_g average is reported in the main body of this report, as it is considered the more relevant one for bar performance. The lower T_g values to not satisfy the contemporary GFRP bar specification (ASTM-D7957-17, 2017) of 212°F (100°C), but the upper ones do.

Table 51. Thayer MDSC results – PSU

Specimen ID	Sample Mass (mg)	T_g, °F (°C)	
		Lower	Upper
IN_C2_B1	15.2	185 (85)	219 (104)
IN_C3_B2	15.4	187 (86)	235 (113)
IN_C4_B2-1	15.0	190 (88)	223 (106)
IN_C4_B2-2	15.0	194 (90)	225 (107)

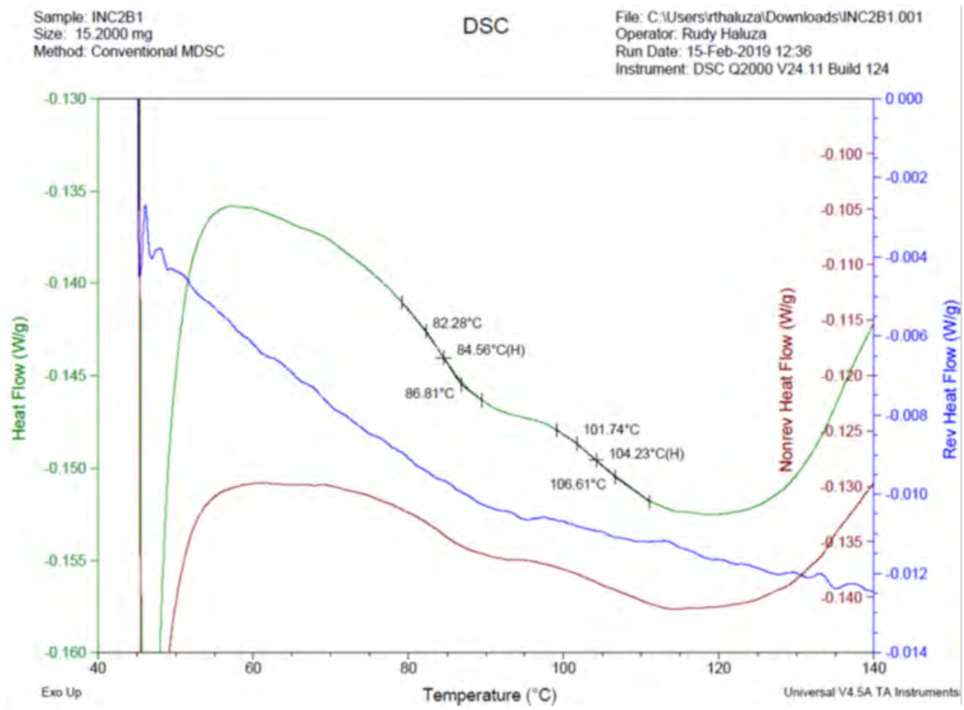

Fig. 47. Thayer Road core#2 bar#1 MDSC curves – PSU

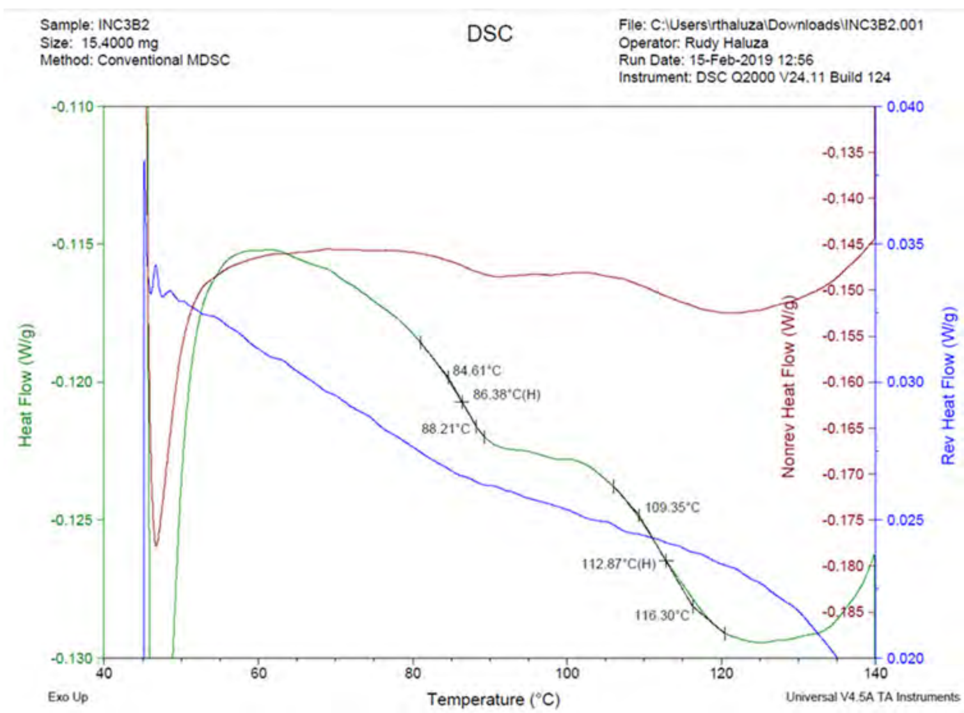

Fig. 48. Thayer Road core#3 bar#2 MDSC curves – PSU

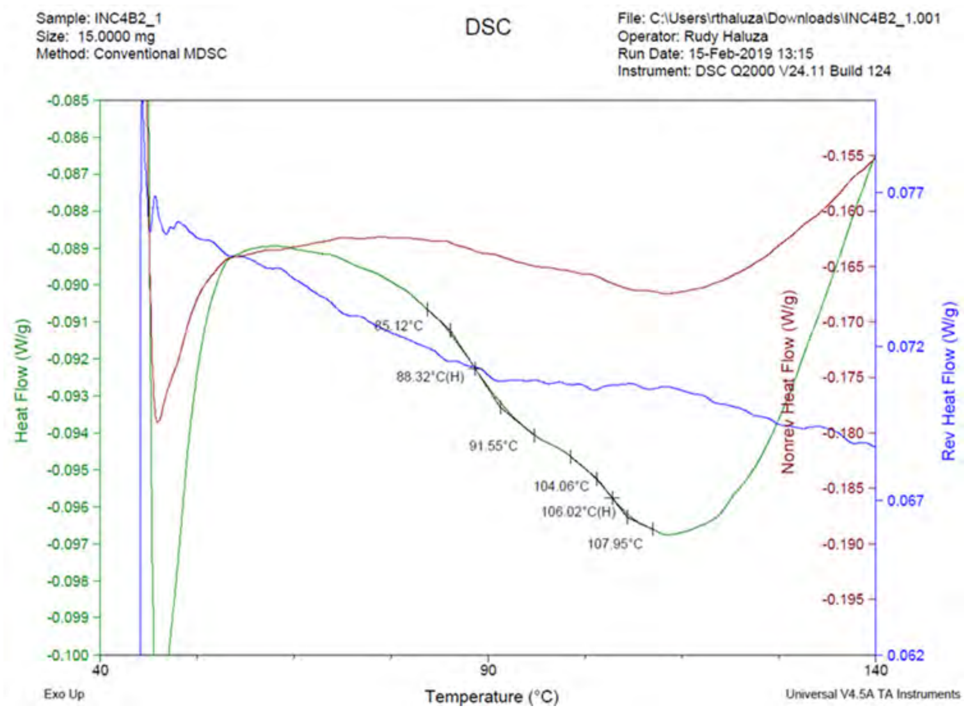

Fig. 49. Thayer Road core#4 bar#2 sample 1 MDSC curves – PSU

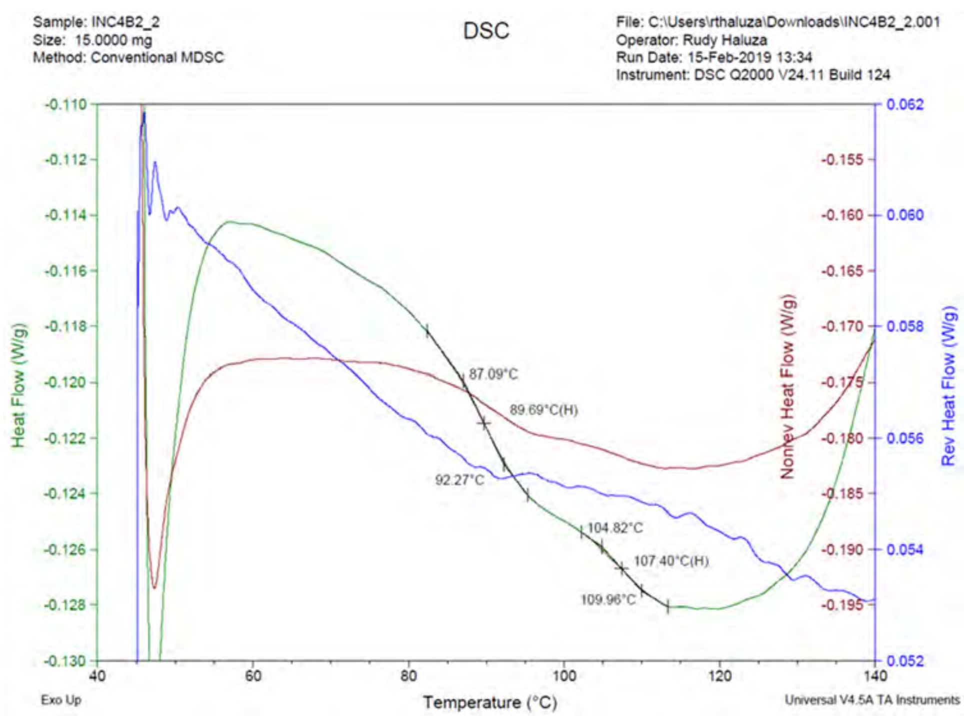

Fig. 50. Thayer Road core#4 bar#2 sample 2 MDSC curves – PSU

5. Moisture Content

5.1 O’Fallon Park

Moisture content for *O’Fallon Park Bridge* was performed at Penn State University according to the method described in Section 4.1.6. All dry-out specimens reached equilibrium after 56 days at 176°F (80°C). A plot of percent weight loss versus the square root of time (in days) is shown in Fig. 51. The acronym used for the *O’Fallon Park Bridge* here is OF instead of CO. It can be seen that the weight loss is not monotonic. It is suspected that the deviations from monotonic weight loss are due to abnormal humidity conditions in the laboratory, although this possibility cannot be verified.

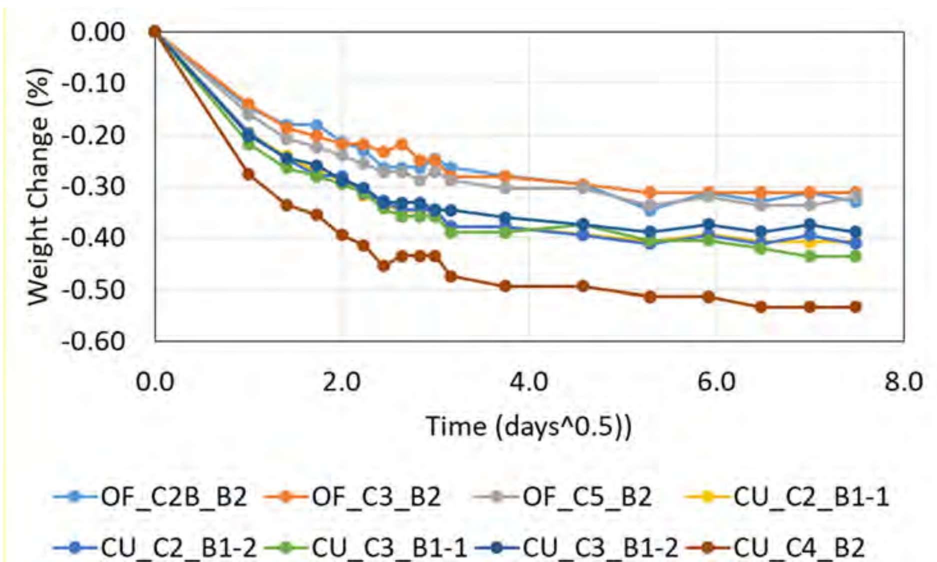

Fig. 51.O’Fallon (OF) weight change versus the square root of drying time, in 176°F (80°C) circulating oven air – PSU

The weight changes at equilibrium, as a percent of weight before the drying procedure, are listed in Table 52. Overall, the weight losses from the dry-out procedure ranged from 0.31% to 0.32%. Upon conversion of these results to weight gains from a substantially dry initial state, the as-received moisture content of these bars due to field exposure likewise ranged from 0.31% to 0.32%. It should be kept in mind that the moisture content of the bars between the several months’ time between when the bars were extracted from the bridges and when they were tested could be affected by the environment in which they were stored.

Table 52. O’Fallon percent weight change at equilibrium for specimens dried in 176°F (80°C) circulating oven air – PSU

Specimen ID	% Weight Change
CO_C2B_B2	-0.329
CO_C3_B2	-0.312
CO_C5_B2	-0.320

The *O'Fallon Bridge* bars had generally less as-received moisture (0.320%, on average) than the *Cuyahoga Bridge* bars (0.436%, on average). As a point of reference, ASTM D7957 (ASTM D7957, 2017) requires that GFRP bars absorb no more than 1% moisture at saturation at a temperature of 122°F (50°C).

5.2 Salem Ave.

Moisture content for *Salem Ave. Bridge* are still ongoing at Missouri S&T.

5.3 Cuyahoga

Moisture content for *Cuyahoga Bridge* was performed at Penn State University according to the method described in Section 4.1.6. All dry-out specimens reached equilibrium after 56 days at 176°F (80°C). A plot of percent weight loss versus the square root of time (in days) is shown in Fig. 52. The acronym used for *Cuyahoga Bridge* here is CU instead of OH2. It can be seen that the weight loss is not monotonic. It is suspected that the deviations from monotonic weight loss are due to abnormal humidity conditions in the laboratory, although this possibility cannot be verified.

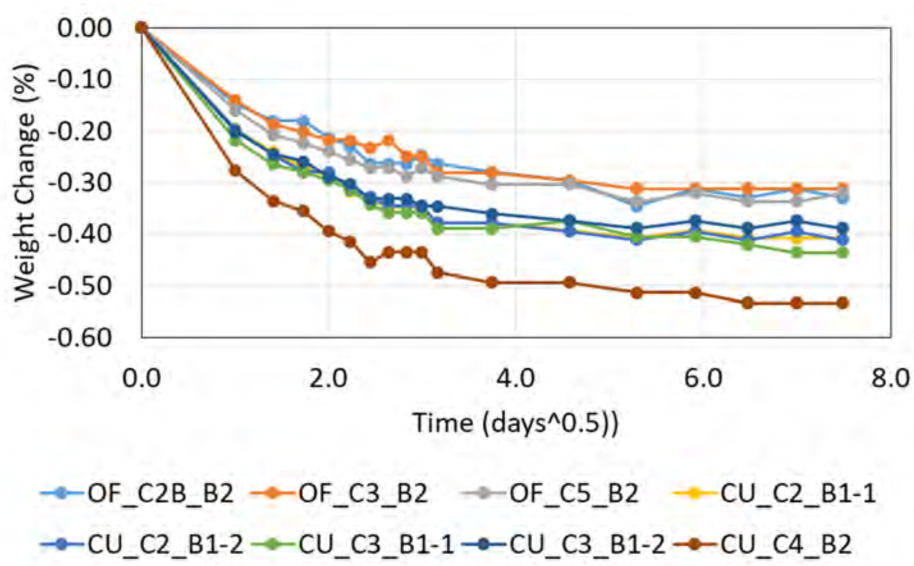

Fig. 52. Cuyahoga weight change versus the square root of drying time, in 176°F (80°C) circulating oven air – PSU

The weight changes at equilibrium, as a percent of weight before the drying procedure, are listed in Table 53. Overall, the weight losses from the dry-out procedure ranged from 0.38% to 0.53%. Upon conversion of these results to weight gains from a substantially dry initial state, the as-received moisture content of these bars due to field exposure likewise ranged from 0.38% to 0.53%. It should be kept in mind that the moisture content of the bars between the several months' time between when the bars were extracted from the bridges and when they were tested could be affected by the environment in which they were stored.

Table 53. Cuyahoga percent weight change at equilibrium for specimens dried in 80°C circulating oven air – PSU

Specimen ID	% Weight Change
OH2_C2_B1-1	-0.408
OH2_C2_B1-2	-0.411
OH2_C3_B1-1	-0.436
OH2_C3_B1-2	-0.389
OH2_C4_B2	-0.533

It is noteworthy that the OH2_C4_B2 bar with the highest as-received moisture content of all tested bars is also the only smaller diameter (5/8 in. [16 mm]) bar of all bars tested. The other bars have a larger (3/4 in. [19 mm]) diameter, which according to theory leads to less weight gain/loss for a given immersion/dry-out time because of a larger moisture permeation path in the material.

Cuyahoga Bridge was also tested at Missouri S&T. Three bars were used in this test. Results from the moisture content test are shown in Fig. 53. The graph was drawn according to ASTM D5229 requirements, which were to draw the results in term of weight change and days$^{0.5}$. All specimens reached equilibrium after 68 days at 176º F (80º C). However, the test was continued for a total of 96 days to monitor any abnormal changes in weights. It may be noted in Fig. 53. Cuyahoga weight change versus the square root of drying time, in in 176°F (80°C) circulating oven air that there was no significant change in weight after 68 days (X-axis – at point 8.2), as the curve trend levels off pass that point. However, a slight change in weight can be noticed from core 4 (CU_C4_B1), and it could be due to balance instability. The final weight change percentages respectively were 0.8% for CU_C4_B1, 0.7% for CU_C5_B1 and 2.1% for CU_C6_B1. The higher percentage of moisture content for the larger diameter bar could be related to larger surface area. Moisture content test was not conducted on control bars to benchmark these results. Additional tests are required to improve the dataset and validate these results. In addition, if test methods exist to measure moisture levels throughout the cross section on thin slices (i.e. relative to distance from the core to the outer surface of the bar) for different bar diameters, this may be examined to better understand moisture content relative to bar surface area and depth.

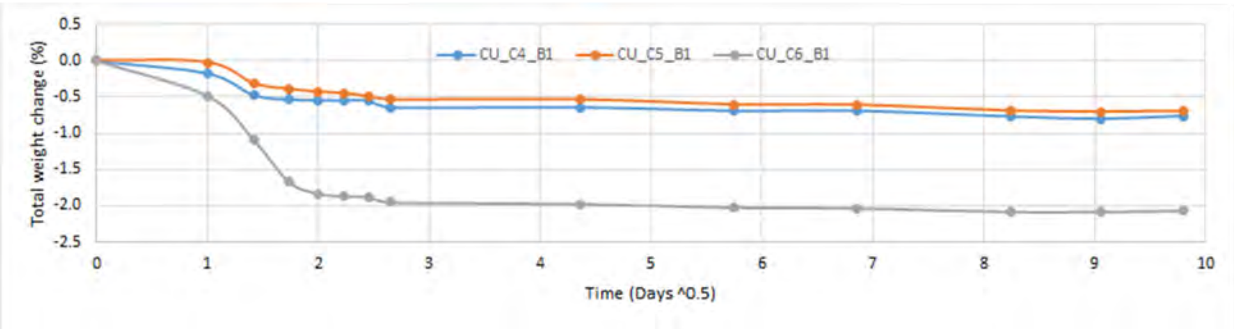

Fig. 53. Cuyahoga weight change versus the square root of drying time, in in 176°F (80°C) circulating oven air

6. Constituent Volume Contents by Image Analysis

For the three *O'Fallon* bars analyzed by image analysis at Penn State, the fiber, matrix, and void volume percents (V_v, V_m, and V_v, respectively) for each image are listed in Table 54 through

Table 56.

Table 54. Image analysis results for CO_C2_B2 – PSU

Image	V_f (%)	V_m (%)	V_v (%)
1	58.24	39.93	1.83
2	71.27	27.63	1.10
3	56.75	43.24	0.02
4	53.60	44.66	1.75
5	44.07	55.92	0.01
6	52.97	46.98	0.05
7	52.25	47.70	0.06
8	53.97	45.94	0.09
9	54.19	45.48	0.33
10	62.11	37.72	0.16
11	44.55	55.20	0.25
12	49.38	49.03	1.59
13	49.40	50.32	0.27
14	59.33	40.58	0.09
15	54.41	45.05	0.53
16	54.28	45.66	0.06
17	51.85	47.31	0.84
18	49.71	50.25	0.03
19	56.38	43.60	0.02
20	50.29	49.17	0.54
21	51.38	45.25	3.37
22	51.73	48.18	0.09
23	54.35	45.63	0.01
24	62.60	36.31	1.09
25	55.90	43.63	0.47
26	59.64	39.23	1.13
27	53.47	46.45	0.08
28	51.31	48.57	0.12
29	34.08	65.88	0.04
30	46.81	53.17	0.02
Mean	53.34	46.12	0.54
Stdev	6.59	6.79	0.77

Table 55. Image analysis results for CO_C3_B3 – PSU

Image	V_f (%)	V_m (%)	V_v (%)
1	46.09	53.11	0.79
2	58.11	41.57	0.31
3	59.11	40.83	0.06

4	50.34	49.19	0.47
5	55.97	43.66	0.37
6	55.52	42.17	2.32
7	53.31	46.50	0.20
8	54.49	45.37	0.15
9	57.49	42.50	0.01
10	53.42	45.47	1.10
11	52.94	46.08	0.98
12	58.93	40.29	0.79
13	49.87	49.90	0.23
14	53.41	45.24	1.35
15	57.11	42.72	0.17
16	45.41	53.94	0.65
17	55.63	43.35	1.01
18	51.89	48.05	0.06
19	47.80	51.07	1.12
20	56.48	43.48	0.05
21	52.06	46.70	1.24
22	41.98	55.79	2.23
23	49.23	49.56	1.21
24	50.06	49.15	0.79
25	56.74	42.76	0.50
26	56.17	43.00	0.83
27	57.39	42.27	0.34
28	40.08	58.34	1.59
29	40.71	59.21	0.08
30	50.46	49.51	0.03
Mean	52.27	47.03	0.70
Stdev	5.32	5.14	0.63

Table 56. Image analysis results for CO_C5_B2 – PSU

Image	V_f (%)	V_m (%)	V_v (%)
1	53.26	46.62	0.12
2	55.04	44.76	0.20
3	59.65	40.28	0.07
4	56.93	42.99	0.08
5	50.56	49.43	0.01
6	60.45	39.55	0.00
7	62.01	37.99	0.00
8	72.19	27.81	0.00
9	70.13	29.87	0.00
10	71.54	26.65	1.80
11	60.49	36.68	2.83
12	53.34	44.49	2.17
13	55.83	42.65	1.52
14	55.80	42.21	1.99
15	43.11	56.47	0.43
16	43.77	54.64	1.59
17	45.05	54.56	0.39
18	53.05	46.94	0.01
19	38.93	60.99	0.08
20	49.83	50.04	0.13
21	43.01	56.90	0.09
22	50.83	48.63	0.54
23	45.54	54.45	0.01
24	42.68	57.31	0.01
25	47.78	52.19	0.03
26	37.91	60.59	1.50
27	49.74	50.22	0.04
28	64.79	35.11	0.10
29	66.43	31.16	2.41
30	44.01	54.81	1.17
Mean	53.46	45.90	0.64
Stdev	9.59	9.74	0.88

Appendix IV Concrete Tests Results

This appendix presents the results of tests performed on extracted concrete cores from eleven bridges with 15 to 20 years in service. The tests included here are: chloride penetration, carbonation depth and pH. The results are shown per test method and subdivided by bridge.

Nomenclature

VA and GI =	Gills Creek Bridge
CO and OF =	O’Fallon Park Bridge
OH1 and SA =	Salem Ave. Bridge
IA and BE =	Bettendorf Bridge
OH2 and CU =	Cuyahoga County Bridge
WV =	McKinleyville Bridge
IN =	Thayer Road Bridge
KY =	Roger’s Creek Bridge
TX and SI =	Sierrita de la Cruz Creek Bridge
MO1 and WA =	Walker Box Culvert Bridge
MO2 and SO =	Southview Bridge

Table of Contents

List of Figures

List of Tables

1. Chloride Penetration

1.1 Bettendorf

Chloride penetration depth was determined for three concrete samples from the *Bettendorf Bridge*. The chloride penetration appears to be approximately 1-in. from the exposed face of the concrete, as shown in Fig. 1.

Fig. 1. Bettendorf chloride penetration samples

1.2 Cuyahoga

Chloride penetration depth was determined for three concrete samples from the *Cuyahoga Bridge*. The chloride penetration varied from approximately 1-in to 2.5-in from the exposed face of the concrete, as shown in Fig. 2.

Fig. 2. Cuyahoga chloride penetration samples

1.3 Gills Creek

Chloride penetration depth was determined for three concrete samples from the *Gills Creek Bridge*. The chloride penetration for Gills Creek was small, less than 0.5-in from the exposed face of the concrete, as shown in Fig. 3.

Fig. 3. Gills Creek chloride penetration samples

1.4 O’Fallon Park

Chloride penetration depth was determined for three concrete samples from the *O’Fallon Park Bridge*. The chloride penetration depth for *O’Fallon Park Bridge* appears to be less than 1-in from the exposed face of the concrete, as shown in *Fig. 4*.

Fig. 4. O'Fallon Park chloride penetration samples

1.5 Salem Ave

Chloride penetration depth was determined for one concrete sample from the *Salem Ave Bridge*. The chloride penetration was approximately 1.5-in. from the exposed face of the concrete, as shown in *Fig. 5*.

Fig. 5. Salem Ave chloride penetration sample

1.6 McKinleyville Bridge

Chloride penetration depth was determined for one concrete sample from the *McKinleyville Bridge*. Chloride penetration was observed on the very close to the exposed face of the concrete, approximately less than 1-in., as shown in the Fig. 6.

Fig. 6. McKinleyville chloride penetration sample

1.7 Thayer Road Bridge

Chloride penetration depth was determined for one concrete sample from the *Thayer Road Bridge*. Minor chloride penetration appeared near the face of the exposed concrete face, as shown in the *Fig. 7*.

Fig. 7. Thayer Road chloride penetration sample

1.8 Roger's Creek Bridge

No evidence of chloride diffusion was observed in the tested specimens of *Roger's Creek Bridge*. The results are shown in the *Fig. 8*.

Fig. 8. Roger's Creek chloride penetration sample

1.9 Walker Box Culvert

No clear evidence of chloride diffusion was observed in all the tested specimens using this method. It was noticed that the surface became darker, to a color similar to brown, while there was no visible gray area (*Fig. 9*).

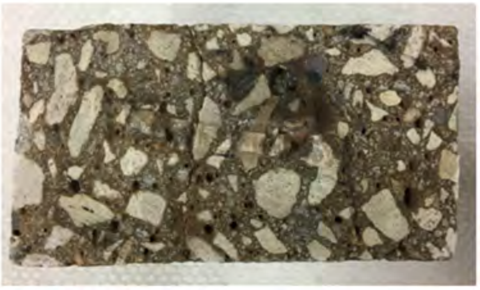

Fig. 9. Walker Box Culvert chloride penetration sample

1.10 Southview

No clear evidence of chloride diffusion was observed in all the tested specimens of both bridges using this method. It was noticed that the surface became darker, to a color similar to brown, while there was no visible gray area (*Fig. 10*).

Fig. 10. Southview chloride penetration sample

2. Carbonation Depth

2.1 Bettendorf

Carbonation depth was determined for three concrete samples from the *Bettendorf Bridge*. The results are shown in *Fig. 11*. Pictured samples are oriented such that the exposed surface (typically bridge deck) of the core is at the top of the image.

Fig. 11. Bettendorf carbonation depth results

2.2 Cuyahoga

Carbonation depth was determined for three concrete samples from the *Cuyahoga Bridge*. The results are shown in *Fig. 12*. Pictured samples are oriented such that the exposed surface (typically bridge deck) of the core is at the top of the image.

Fig. 12. Cuyahoga carbonation depth results -UM

Carbonation depth tests were also performed at Missouri S&T for the *Cuyahoga Bridge*. The results are shown in *Fig. 13*.

Fig. 13. Cuyahoga carbonation depth results -S&T

2.3 Gills Creek

Carbonation depth was determined for three concrete samples from the *Gills Creek Bridge*. The results are shown in *Fig. 14*. Pictured samples are oriented such that the exposed surface (typically bridge deck) of the core is at the top of the image.

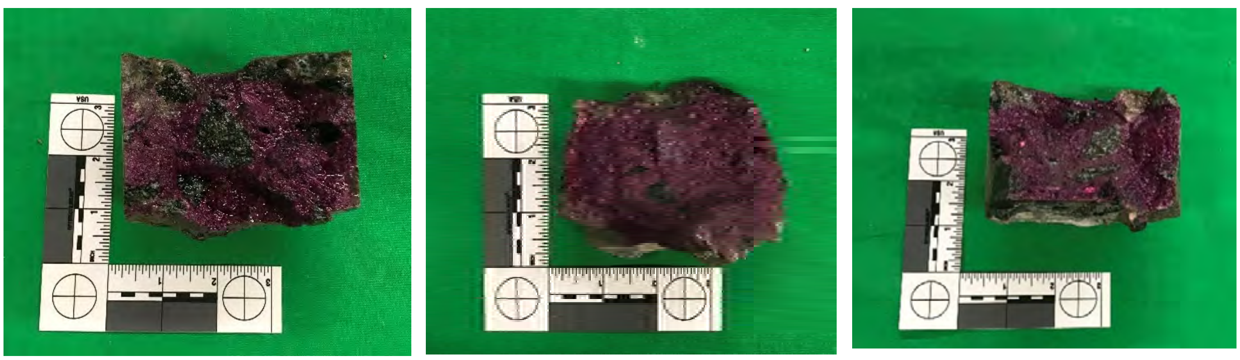

Fig. 14. Gills Creek carbonation depth results

2.4 O'Fallon Park

Carbonation depth was determined for three concrete samples from the *O'Fallon Park Bridge*. The results are shown in *Fig. 15*.

Fig. 15. O'Fallon Park carbonation depth results

2.5 Salem Ave

Carbonation depth was determined for two concrete samples from the *Salem Ave Bridge*. The results are shown in *Fig. 16*. Pictured samples are oriented such that the exposed surface (typically bridge deck) of the core is at the top of the image.

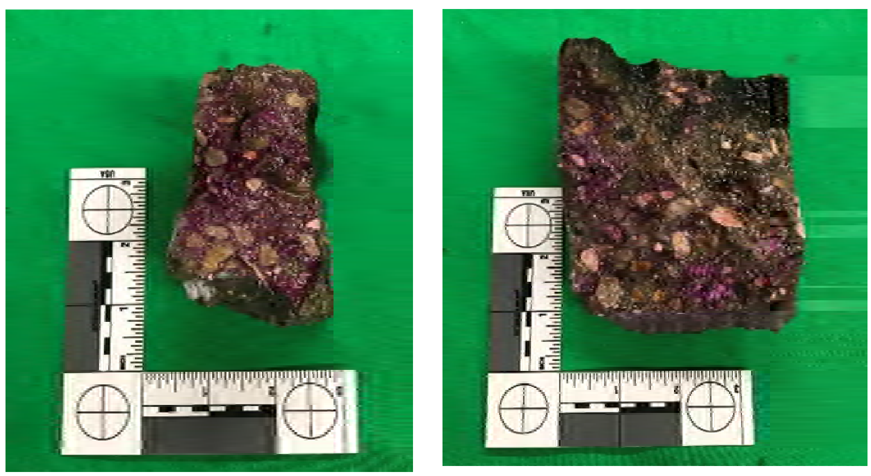

Fig. 16. Salem Ave carbonation depth results

2.6 Walker Box Culvert

No indication of concrete carbonation was observed in samples extracted from this bridge (*Fig. 17*). While no carbonation of concrete can be considered beneficial to steel rebars because the pH remains at high values, the opposite is true for GFRP reinforcement that is more sensitive to high alkalinity. Thus, the GFRP bars extracted from these cores were subject to an alkaline environment over the 17 years of service in *Walker Box Culvert Bridge*.

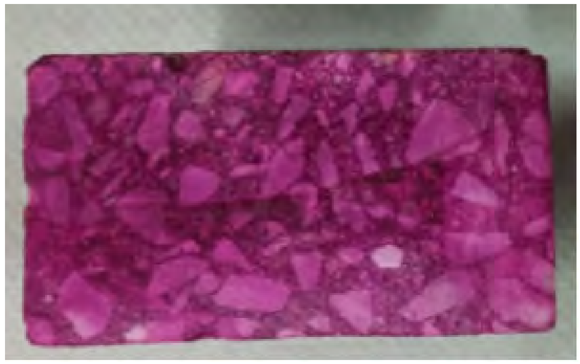

Fig. 17. Walker carbonation depth results

2.7 Southview Bridge

No indication of concrete carbonation was observed in samples extracted from Southview Bridge (*Fig. 18*). While no carbonation of concrete can be considered beneficial to steel rebars because the pH remains at high values, the opposite is true for GFRP reinforcement that is more sensitive to high alkalinity. Thus, the GFRP bars extracted from these cores were subject to an alkaline environment over the 11 years of service.

Fig. 18. Southview carbonation depth results

3. pH

3.1 Bettendorf

The pH tests for the *Bettendorf Bridge* were conducted at the University of Miami according to the procedure outlined in Section **Error! Reference source not found.**. The results are shown in Table 1 below. Pictured samples are oriented such that the exposed surface (typically bridge deck) of the core is at the top of the image.

Table 1. pH of concrete samples results

Sample	Depth (in.)	pH
IA_C1	0.5	11.9
	1.5	12
	2	12
Average		12.0
IA_C3	1	12.1
	1.5	12.1
	2	12.1
Average		12.1

Fig. 19. Bettendorf core 1 pH test

Fig. 20. Bettendorf core 3 pH test

3.2 Cuyahoga

The pH tests for the *Cuyahoga Bridge* were conducted at the University of Miami and Missouri S & T according to the procedure outlined in Section **Error! Reference source not found.**. The results are shown in

Table 2 and

Table 3. Pictured samples are oriented such that the exposed surface (typically bridge deck) of the core is at the top of the image.

Table 2. pH concrete sample results - UM

Sample	Depth (in.)	pH
OH2_C2	0.5	12.1
	2	12.2
	3	12.2
Average		12.2
OH2_C4	0.5	12.1
	1	12.2
	1.5	12.3
Average		12.2

Sample	pH
OH2_C4	12
OH2_C5	11.5
OH2_C6	12

Sample	Depth (in.)	pH
OH2_C2	0.5	12.1
	2	12.2
	3	12.2
Average		12.2
OH2_C4	0.5	12.1
	1	12.2
	1.5	12.3
Average		12.2

Fig. 21. Cuyahoga core 2 pH test

Fig. 22. Cuyahoga core 4 pH test

Table 3. pH of concrete sample results - S&T

Sample	pH
OH2_C4	12
OH2_C5	11.5
OH2_C6	12

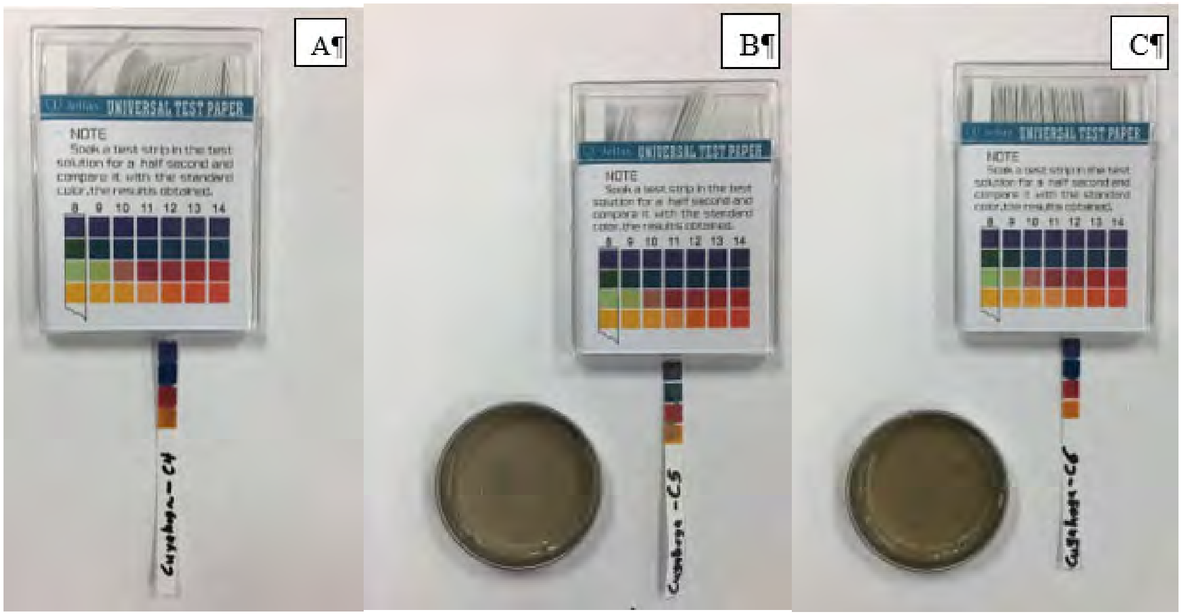

Fig. 23. pH color range

3.3 Gills Creek

The pH tests for the *Gills Creek Bridge* were conducted at the University of Miami according to the procedure outlined in Section **Error! Reference source not found.**. The results are shown in

Table 4. Pictured samples are oriented such that the exposed surface (typically bridge deck) of the core is at the top of the image.

Table 4. pH of concrete sample results

Sample	Depth (in)	pH
VA_C4	0.5	11.9
	1.5	12.1
	2	12.2
Average		12.1
VA_C5	0.5	12.2
	1.5	12.2
Average		12.2

Fig. 24. Gills Creek core 4 pH test

Fig. 25. Gills Creek core 5 pH test

3.4 O’Fallon Park

The pH tests for the *O’Fallon Park Bridge* were conducted at the University of Miami according to the procedure outlined in Section **Error! Reference source not found.**. The results are shown in Table 5.

Table 5. pH of concrete sample results

Sample	Depth (in)	pH
CO_C4	1	12
	1.5	12.1
Average		12.1

Fig. 26. O'Fallon Park core 4 pH test

3.5 Salem Ave

The pH tests for the *Salem Ave Bridge* were conducted at the University of Miami according to the procedure outlined in Section **Error! Reference source not found.**. The results are shown in

Table 6 below. Pictured samples are oriented such that the exposed surface (typically bridge deck) of the core is at the top of the image.

Table 6. pH of concrete sample results

Sample	Depth (in)	pH
OH1_C2	0.5	11.4
	1.5	11.5
	2.5	11.6
Average		11.5
OH1_C4	1	11.5
	2	11.7
	3	11.7
Average		11.6

Fig. 27. Salem Ave core 2 pH test

Fig. 28. Salem Ave core 4 pH test

3.6 McKinleyville Bridge

The method utilized to measure the pH for the last three bridges was different than the previous one. A rainbow indicator was used to observe the pH of the concrete samples. The color observed was matched to the color pallet, as seen in Fig. 29, to obtain the pH.

Fig. 29. Rainbow indicator color palette

All the core samples were tested with the rainbow indicator and the value varied between samples and location of where the indicator was applied. *McKinleyville Bridge* samples indicated a pH of 13 in the inside of the concrete sample and a pH between 7 and 13 on the outside face of the concrete core, as seen in Fig. 30.

Fig. 30. McKinleyville pH test

3.7 Thayer Road Bridge

A rainbow indicator was used to observe the pH of the concrete samples. The color observed was matched to the color pallet to obtain the pH.

The pH obtained for *Thayer Road Bridge* concrete samples only varied between 11 and 13, as shown in *Fig. 31*.

Fig. 31. Thayer Road pH test

3.8 Roger's Creek Bridge

A rainbow indicator was used to observe the pH of the concrete samples. The pH varied between 7 and 13, as shown in *Fig. 32*.

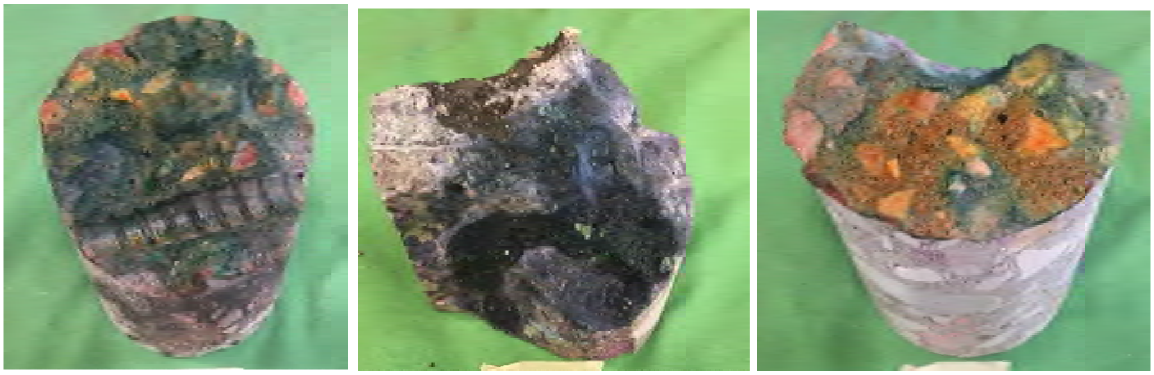

Fig. 32. Roger's Creek pH test

3.9 Sierrita de la Cruz Creek Bridge

The measured pH values range between 11 and 12 (*Fig. 33*) which is considered acceptable for that type of concrete and age (Grubb et al., 2007). The procedure was performed in three different locations and the results are consistent results for all locations.

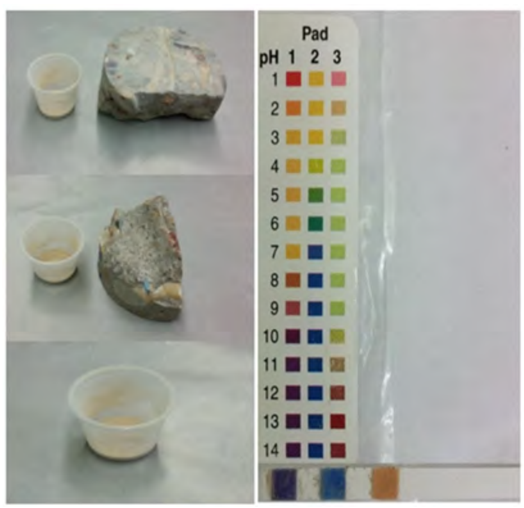

Fig. 33. Concrete pH measurement: ground concrete from extracted cores (left) and pH evaluation using the pH strip (right)

3.10 Walker Bridge

The pH measurement was performed in three different locations. The values of the measured pH range between 11 and 12, which is deemed acceptable for the type and age of concrete (Kakade et al., 2007).

3.11 Southview Bridge

The pH values measured in samples extracted from *Southview Bridge* range between 11 and 12, which is deemed acceptable for the type and age of concrete (Kakade et al., 2007)

APPENDIX V: SEM AND EDS RESULTS

This appendix presents the results of SEM and EDS test performed on the extracted GFRP rebars from eleven bridges. These tests were performed according to Section 4. The results are shown per test method and subdivided by bridge.

NOMENCLATURE

VA and GI =	Gills Creek Bridge
CO and OF =	O’Fallon Park Bridge
OH1 and SA =	Salem Ave. Bridge
IA and BE =	Bettendorf Bridge
OH2 and CU =	Cuyahoga County Bridge
WV =	McKinleyville Bridge
IN =	Thayer Road Bridge
KY =	Roger’s Creek Bridge
TX and SI =	Sierrita de la Cruz Creek Bridge
MO1 and WA =	Walker Box Culvert Bridge
MO2 and SO =	Southview Bridge

Table of Contents

List of Figures

List of Tables

1. SEM Images

1.1 Bettendorf

SEM imaging for *Bettendorf Bridge* was performed at the University of Miami. The results of each bar is shown in Fig. 1 through Fig. 9.

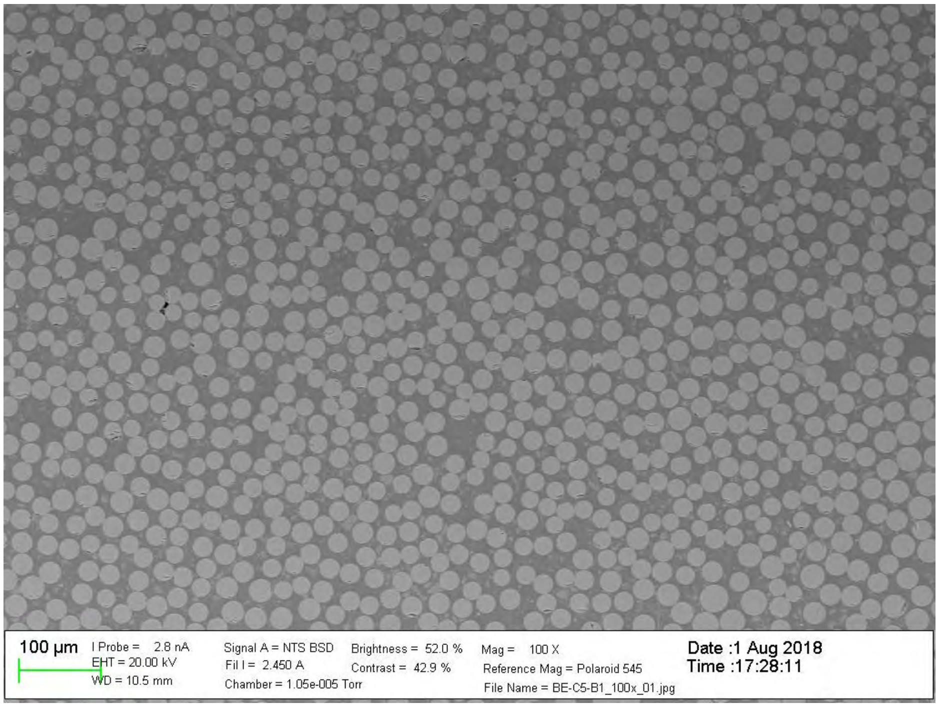

Fig. 1: IA_C5_B1(1) at 100x magnification SEM

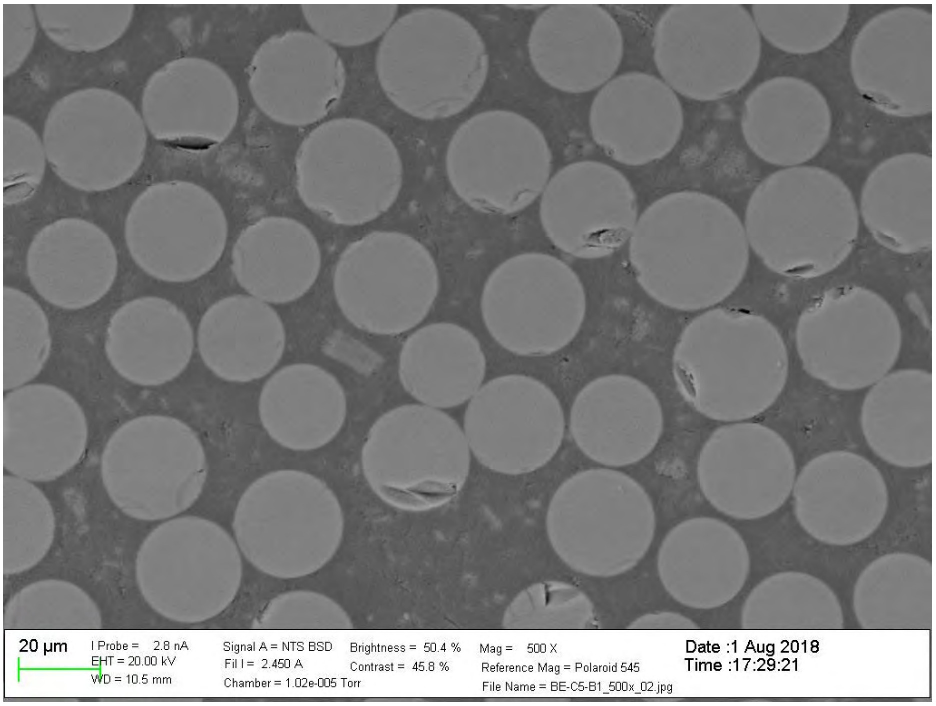

Fig. 2: IA_C5_B1(1) at 500 x magnification SEM

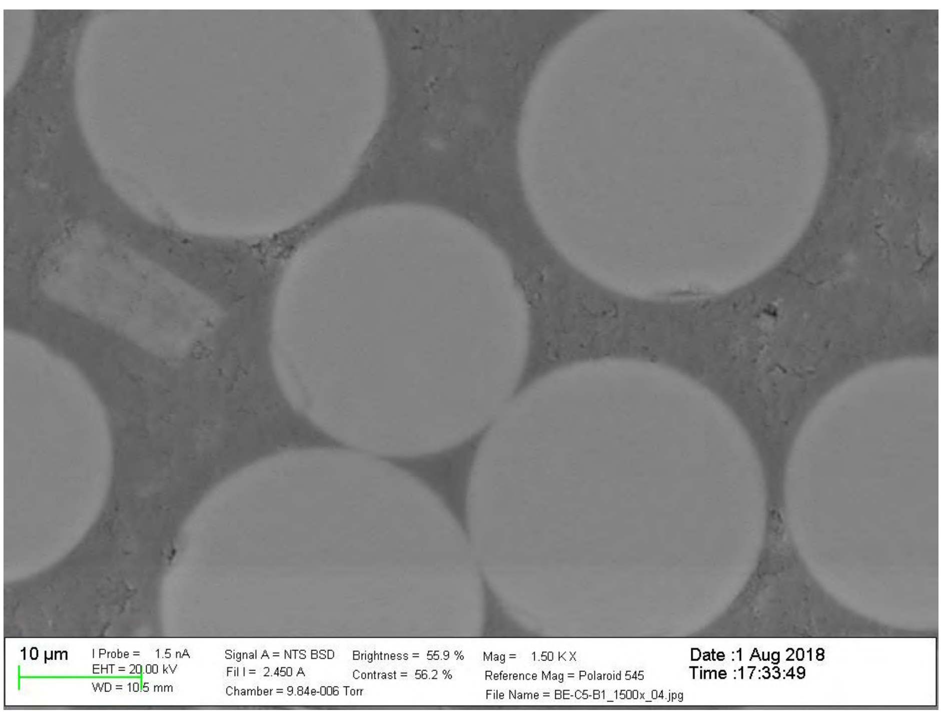

Fig. 3: IA_C5_B1(1) at 1500x magnification SEM

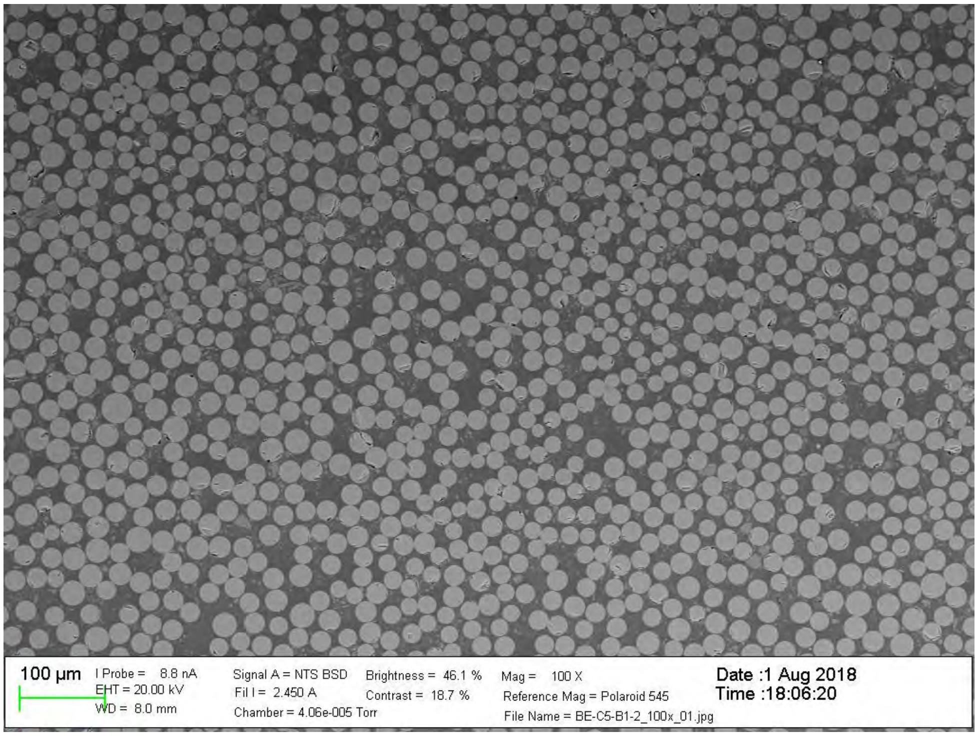

Fig. 4: IA_C5_B1(2) at 100x magnification SEM

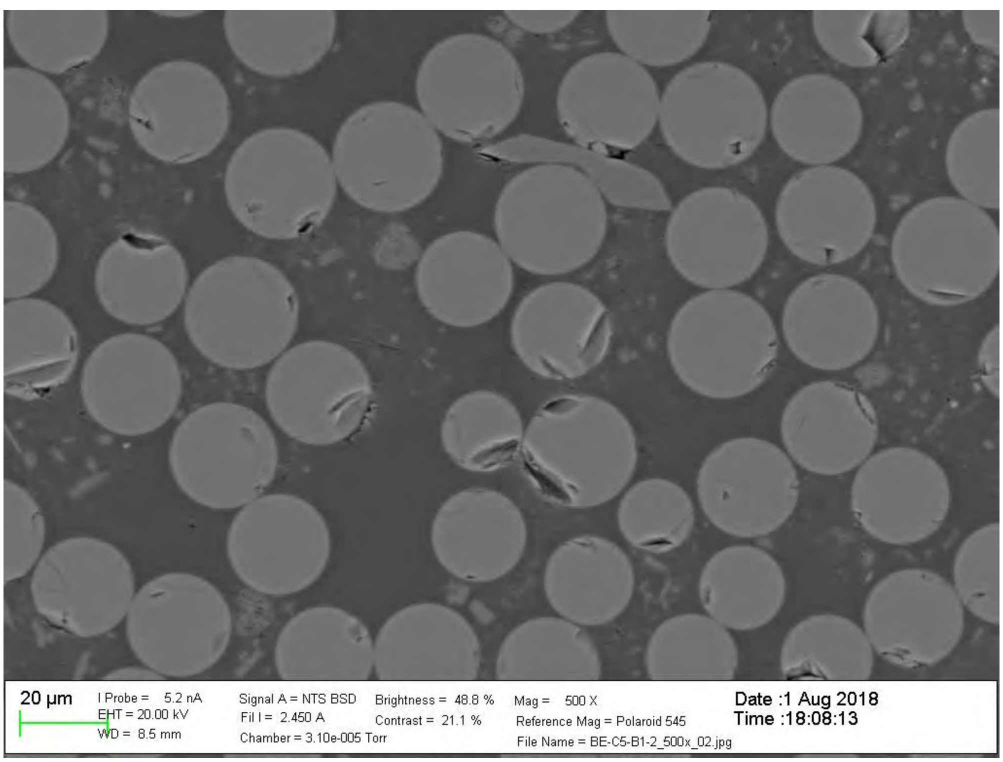

Fig. 5: IA_C5_B1(2) at 500x magnification SEM

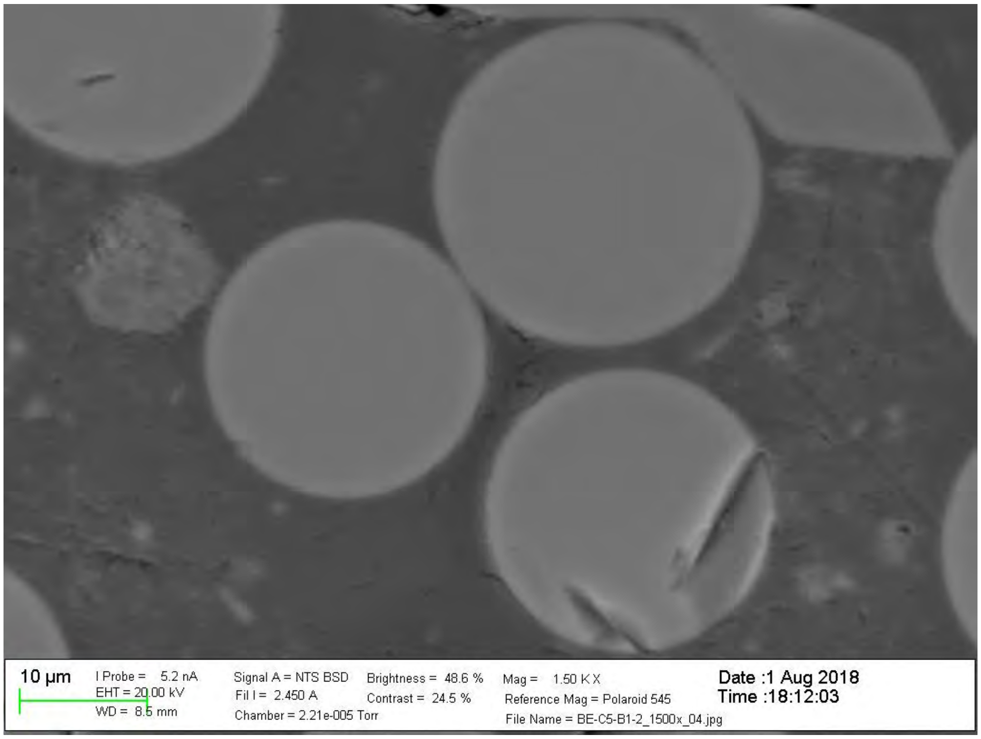

Fig. 6: IA_C5_B1(2) at 1500x magnification SEM

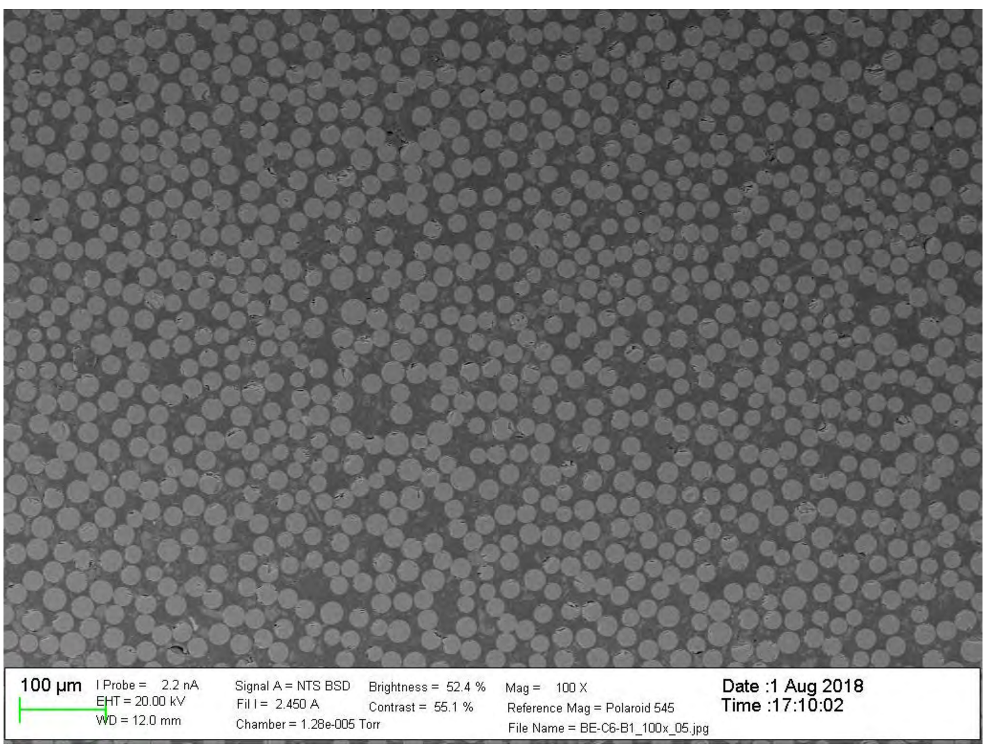

Fig. 7: IA_C6_B1 at 100x magnification SEM

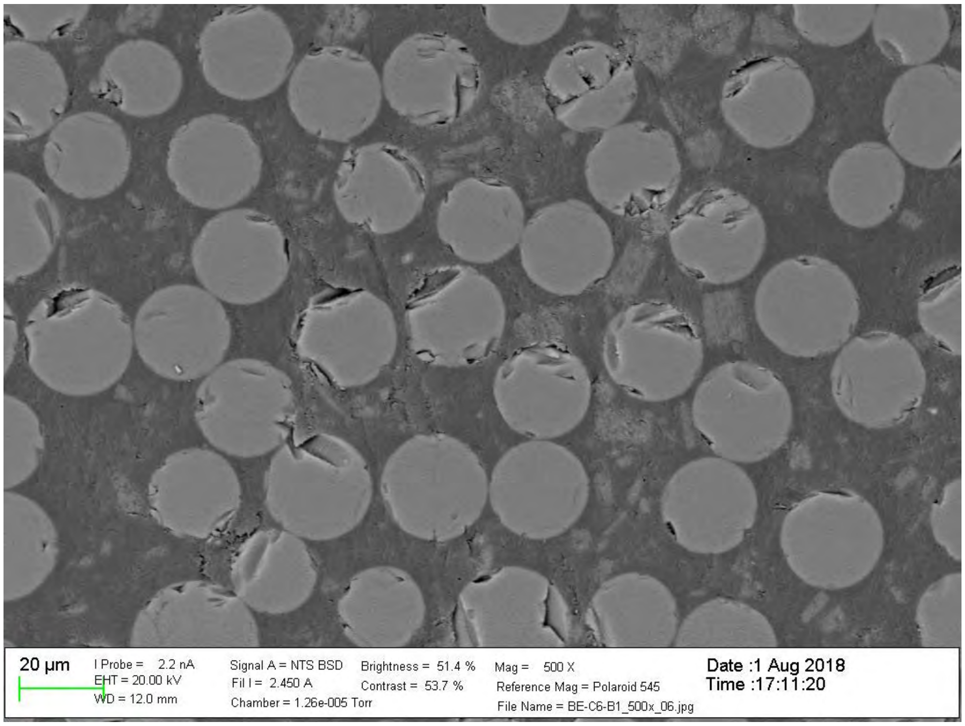

Fig. 8: IA_C6_B1 at 500x magnification SEM

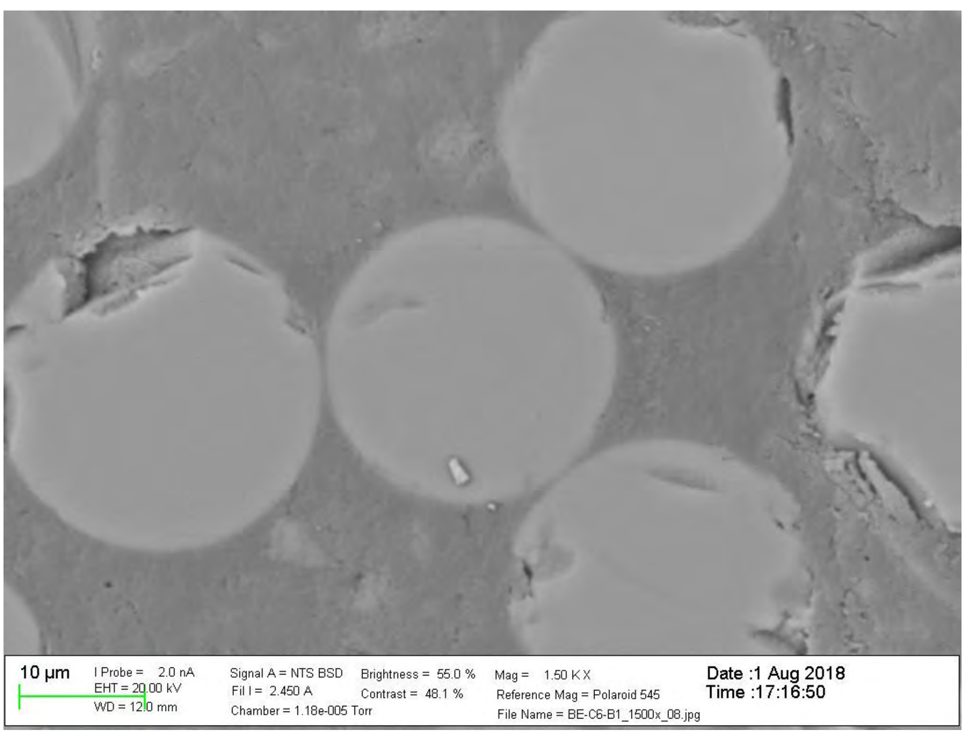

Fig. 9: IA_C6_B1 at 1500x magnification SEM

1.2 O’Fallon Park

SEM imaging for *O’Fallon Park Bridge* was performed at the University of Miami. The results of each bar is shown in Fig. 10 through Fig. 18.

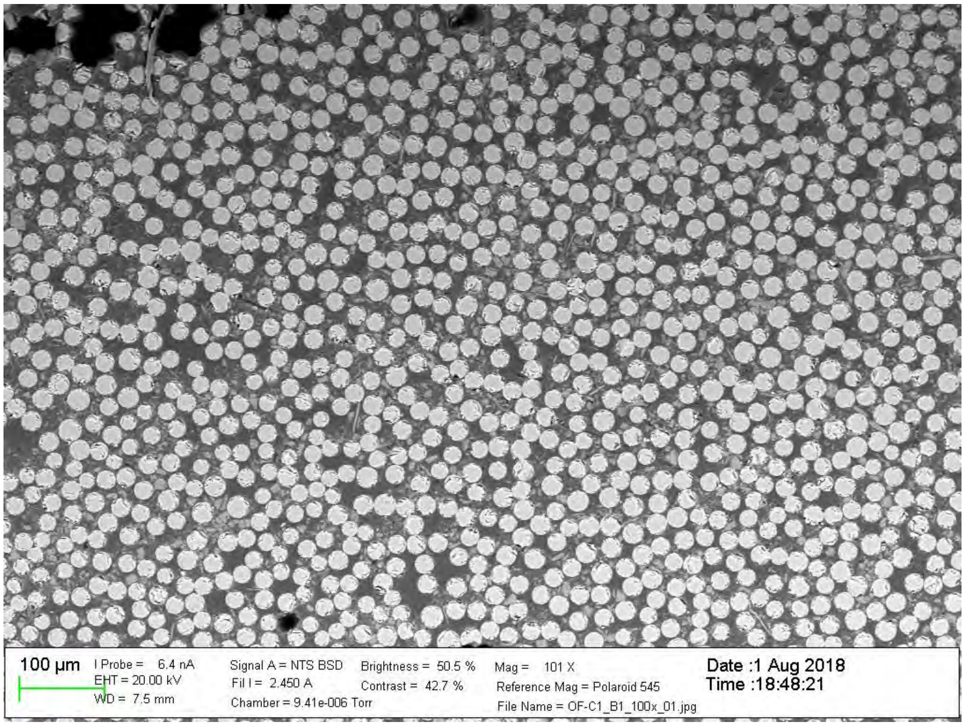

Fig. 10: CO_C1_B1 at 100x magnification

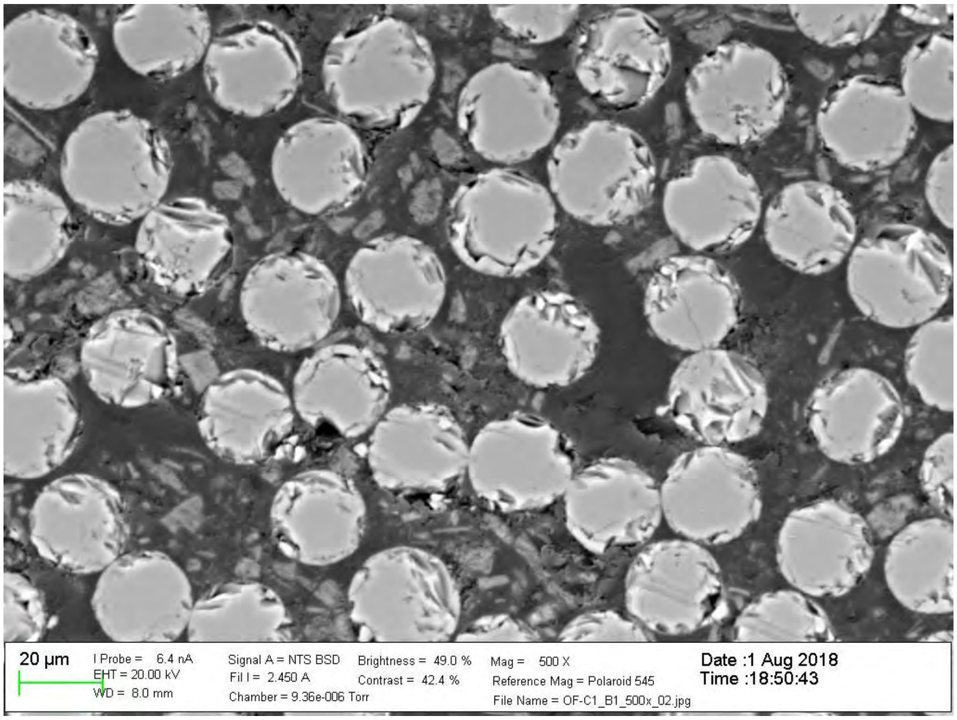

Fig. 11: CO_C1_B1 at 500x magnification

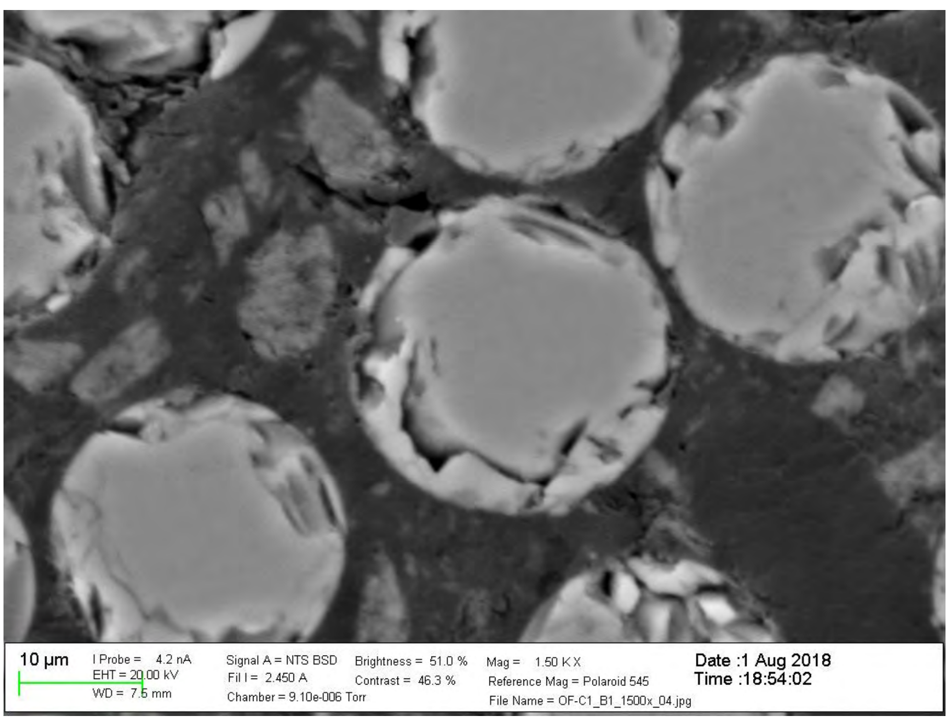

Fig. 12: CO_C1_B1 at 1500x magnification

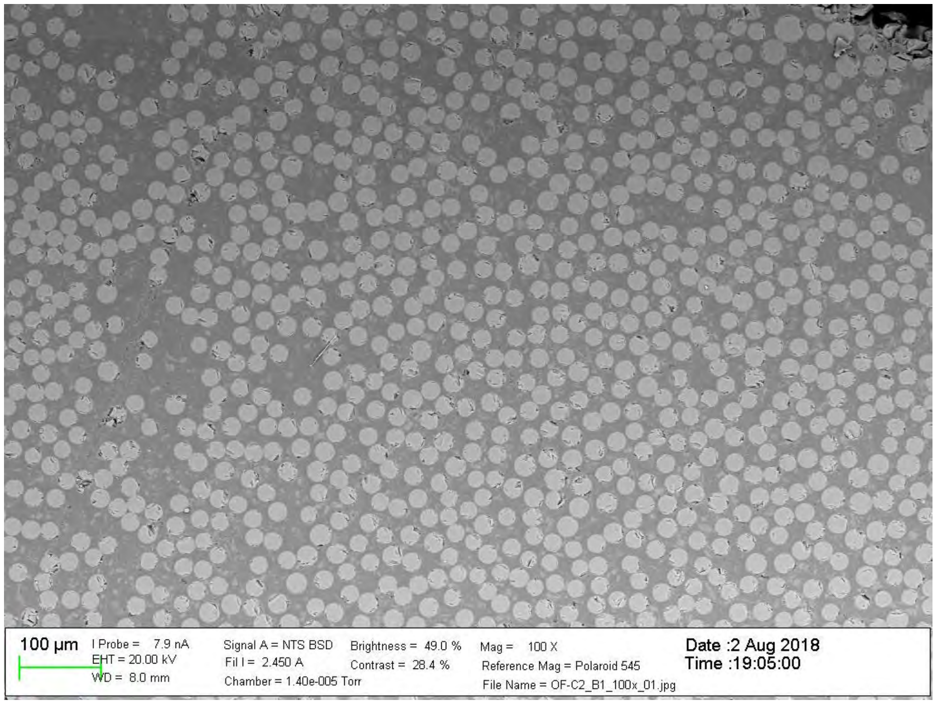

Fig. 13: CO_C2_B1 at 100x magnification

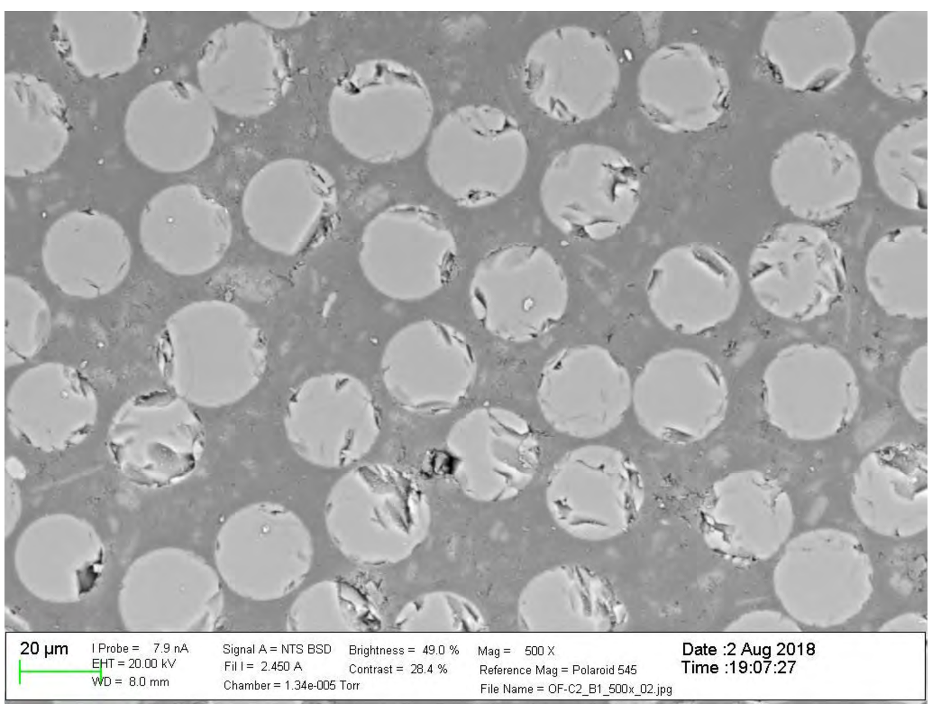

Fig. 14: CO_C2_B1 at 500x magnification

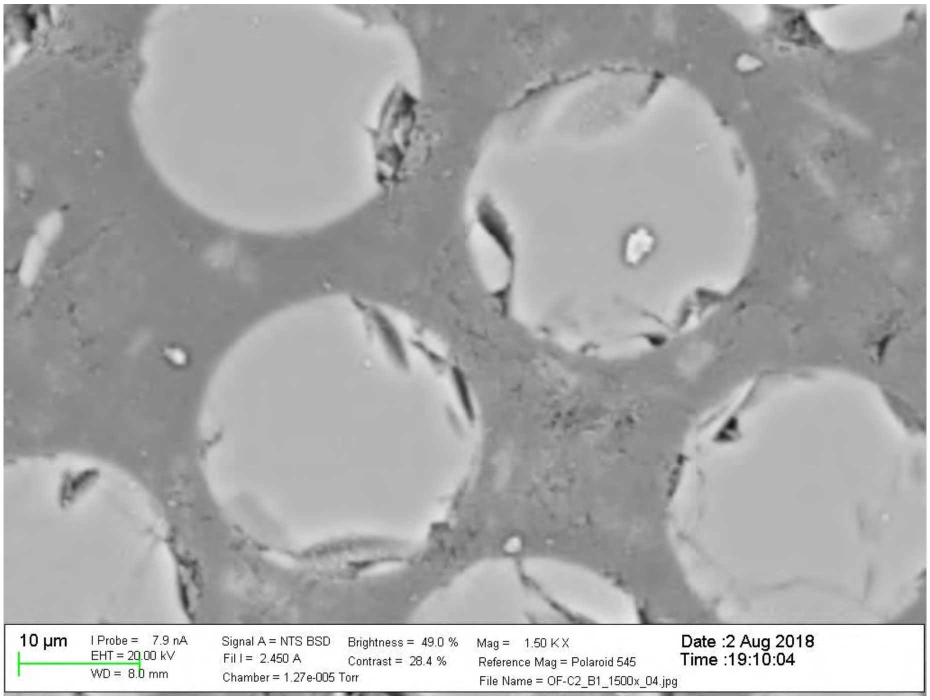

Fig. 15: CO_C2_B1 at 1500x magnification

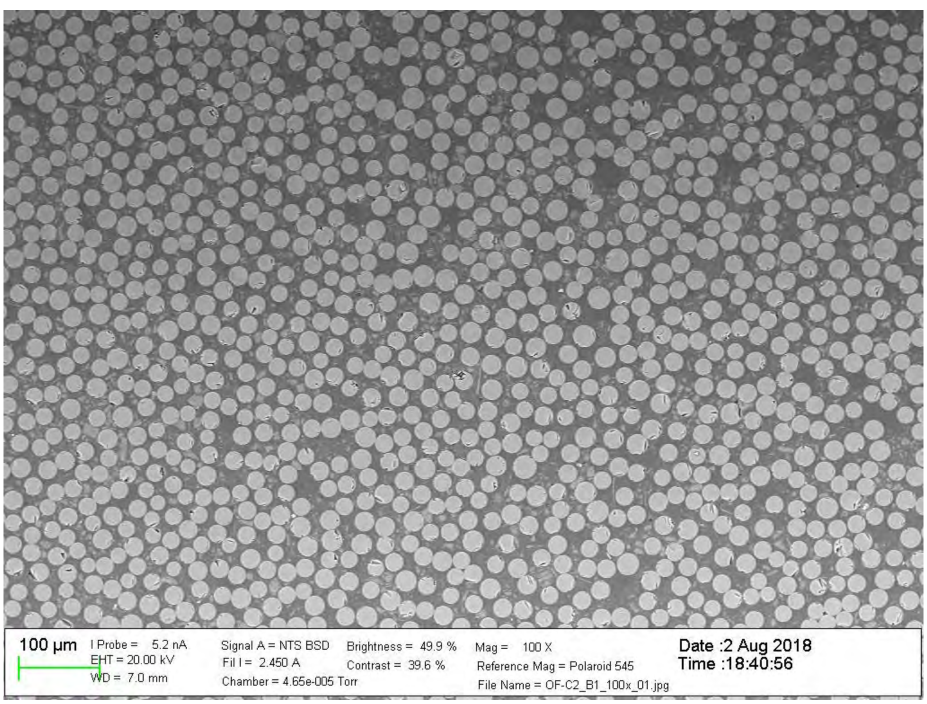

Fig. 16: CO_C5_B1 at 100x magnification

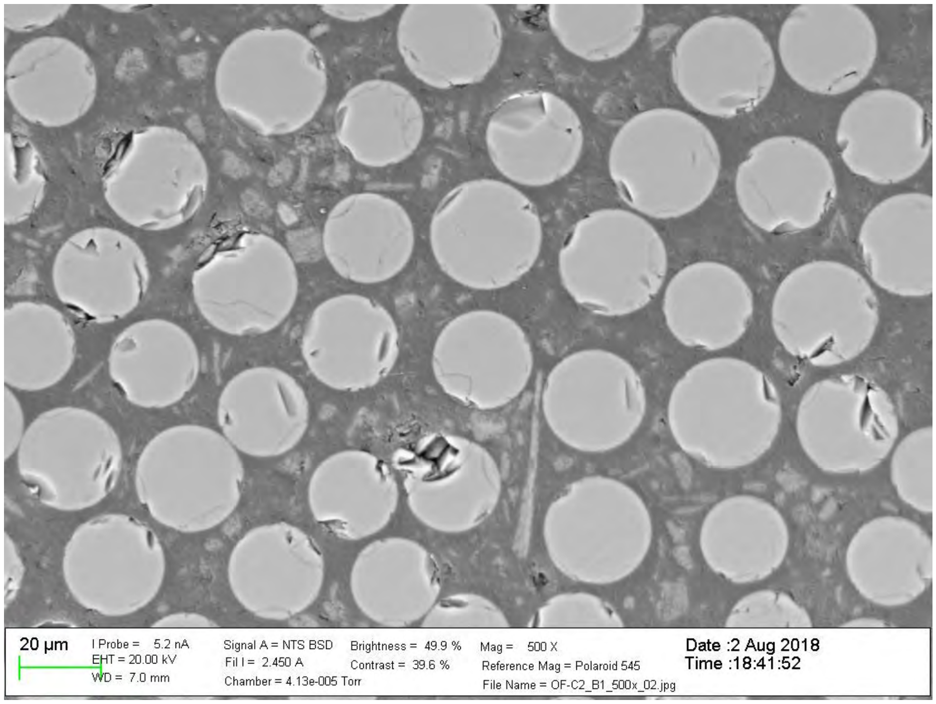

Fig. 17: CO_C5_B1 at 500x magnification

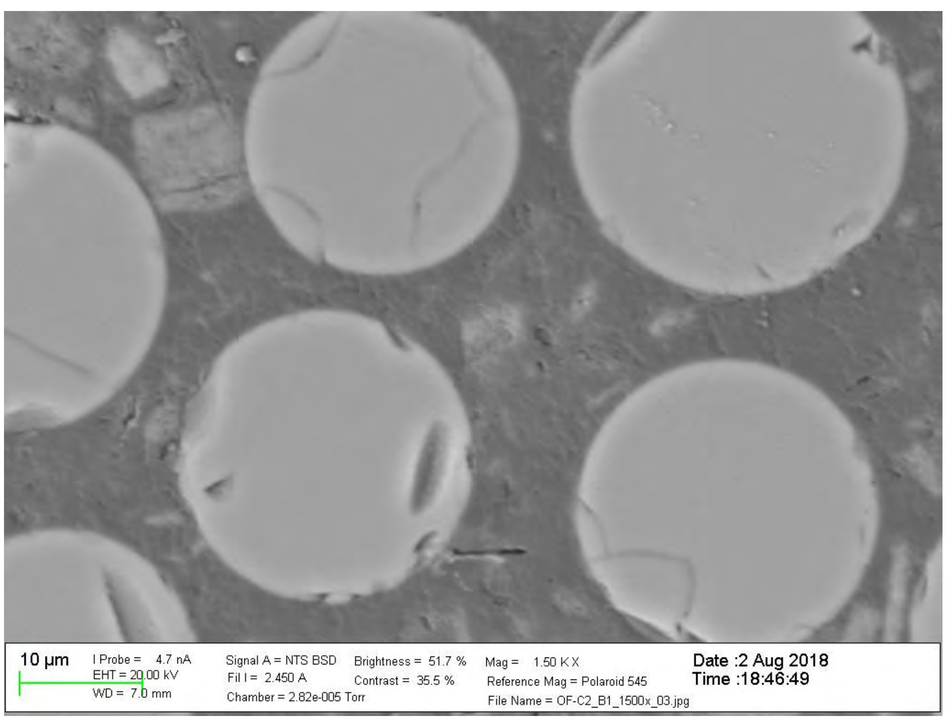

Fig. 18: CO_C5_B1 at 1500x magnification

1.3 Salem Ave

SEM imaging for *Salem Ave. Bridge* was performed at the University of Miami. The results of each bar is shown in Fig. 19 through Fig. 27.

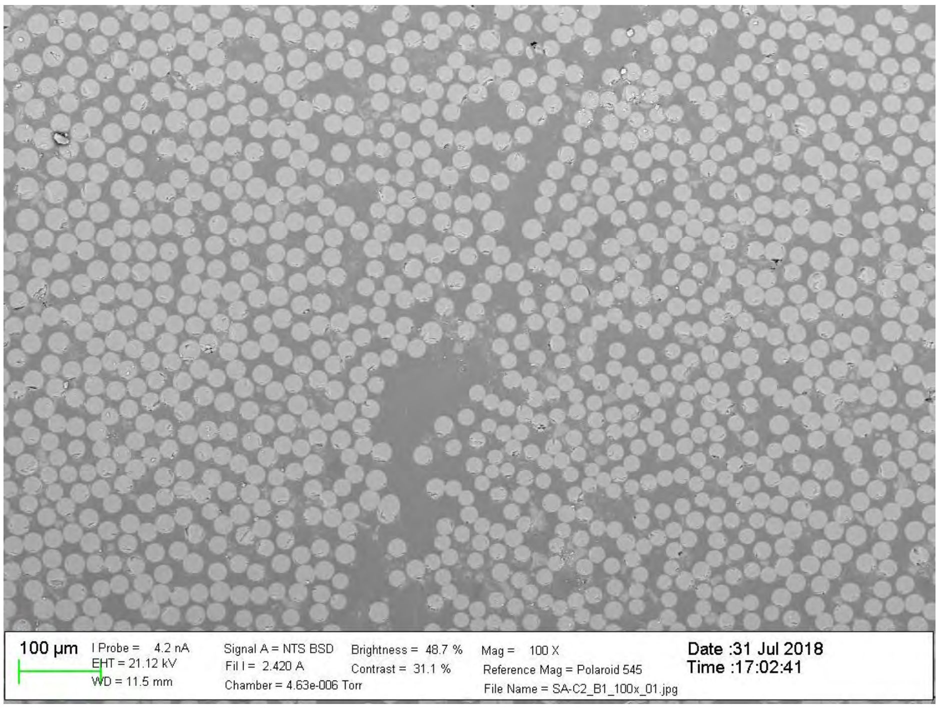

Fig. 19: OH1_C2_B1 at 100x magnification

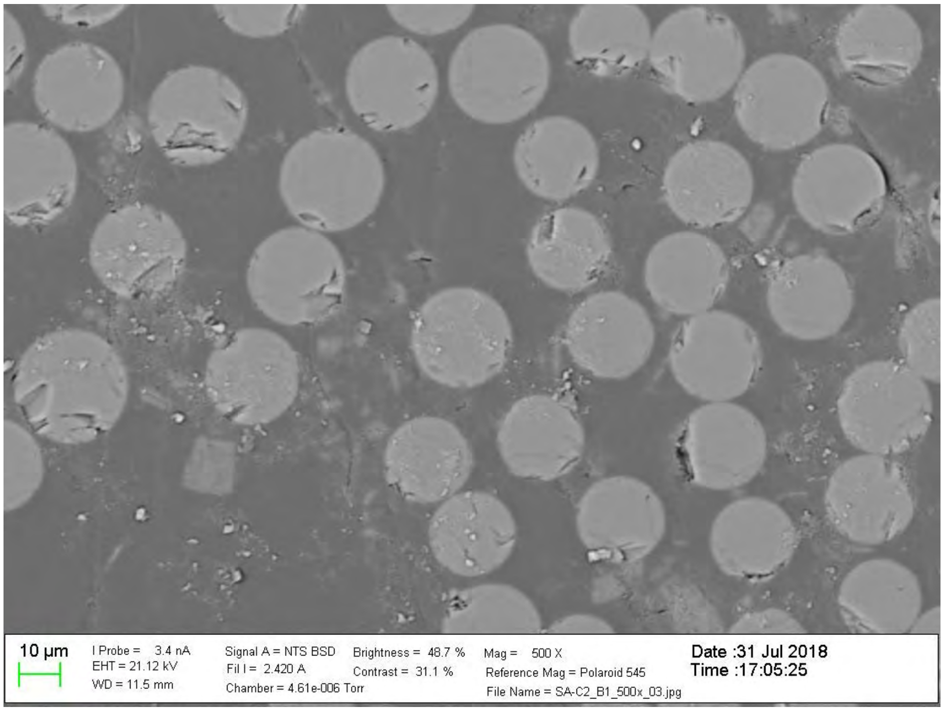

Fig. 20: OH1_C2_B1 at 500x magnification

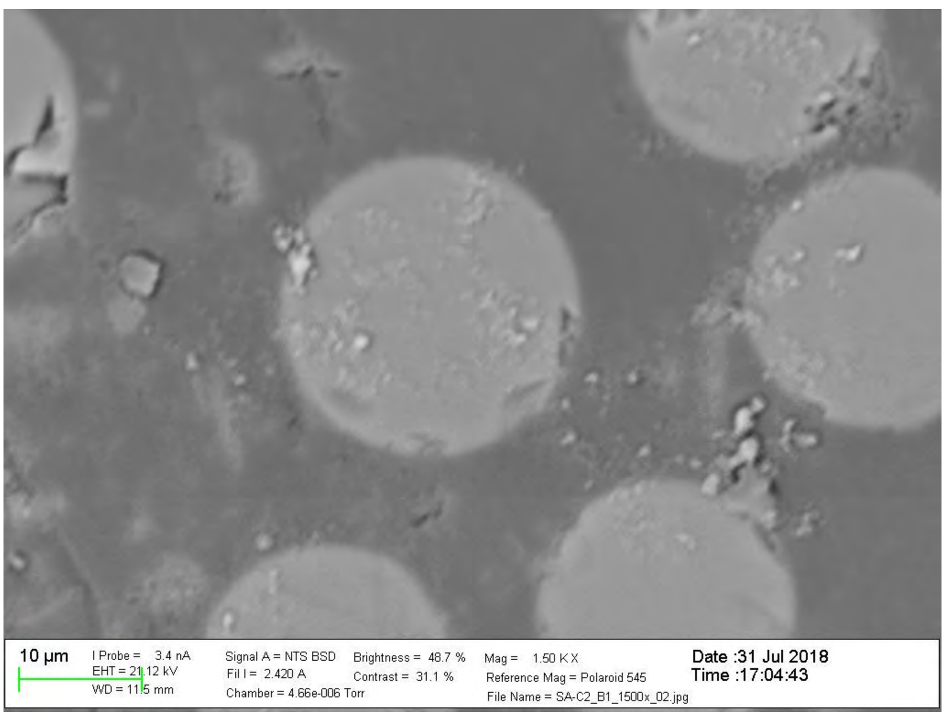

Fig. 21: OH1_C2_B1 at 1500x magnification

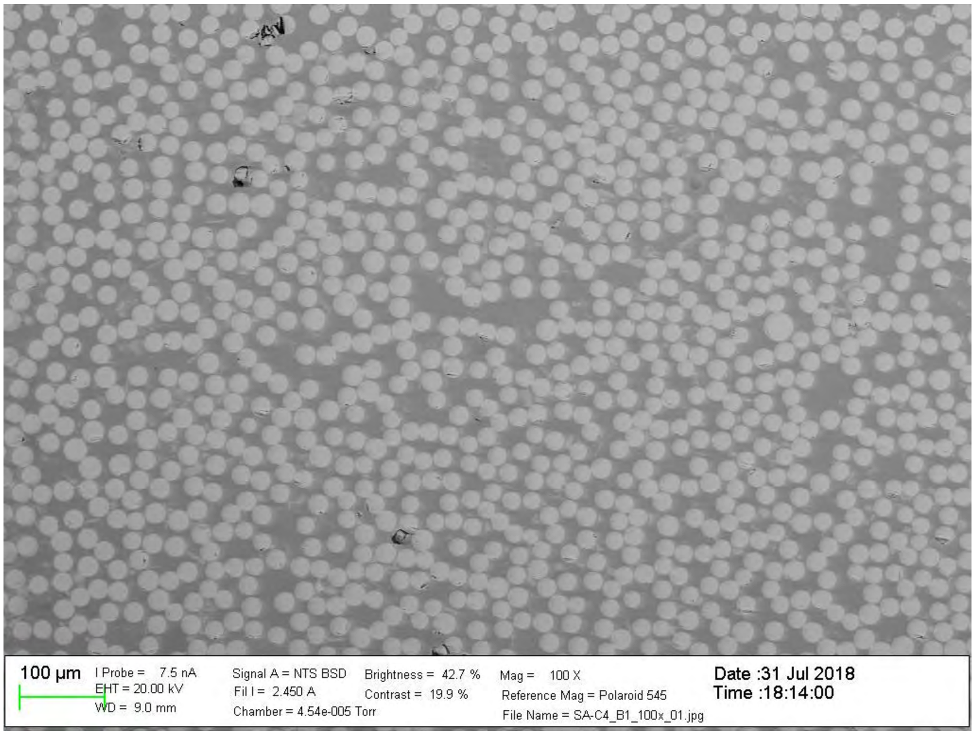

Fig. 22: OH1_C4_B1 at 100x magnification

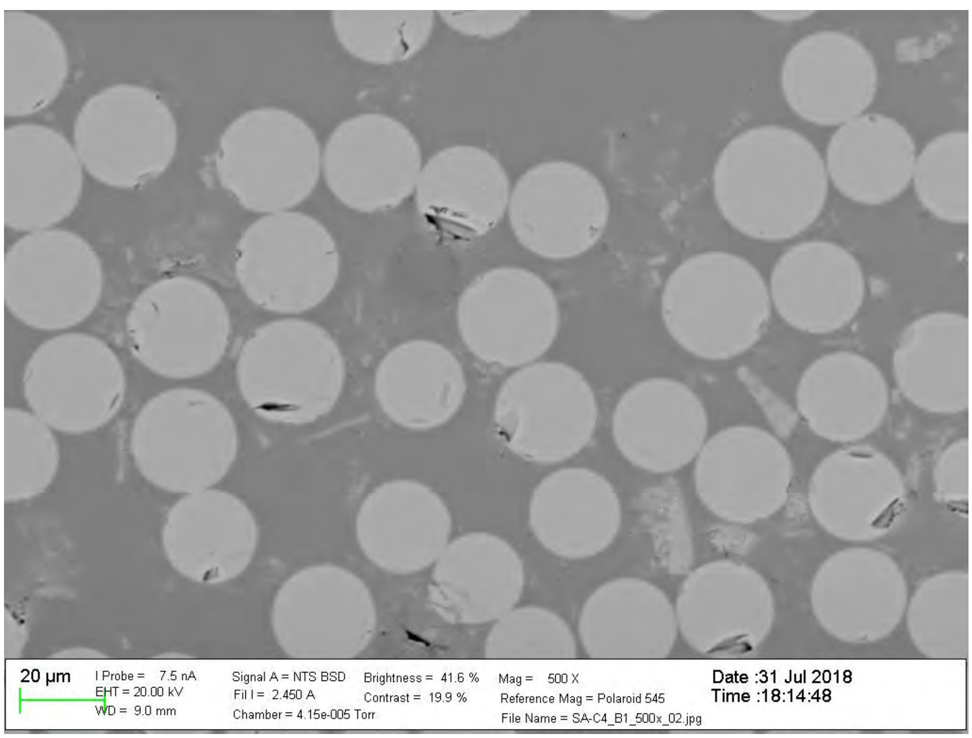

Fig. 23: OH1_C4_B1 at 500x magnification

Fig. 24: OH1_C4_B1 at 1500x magnification

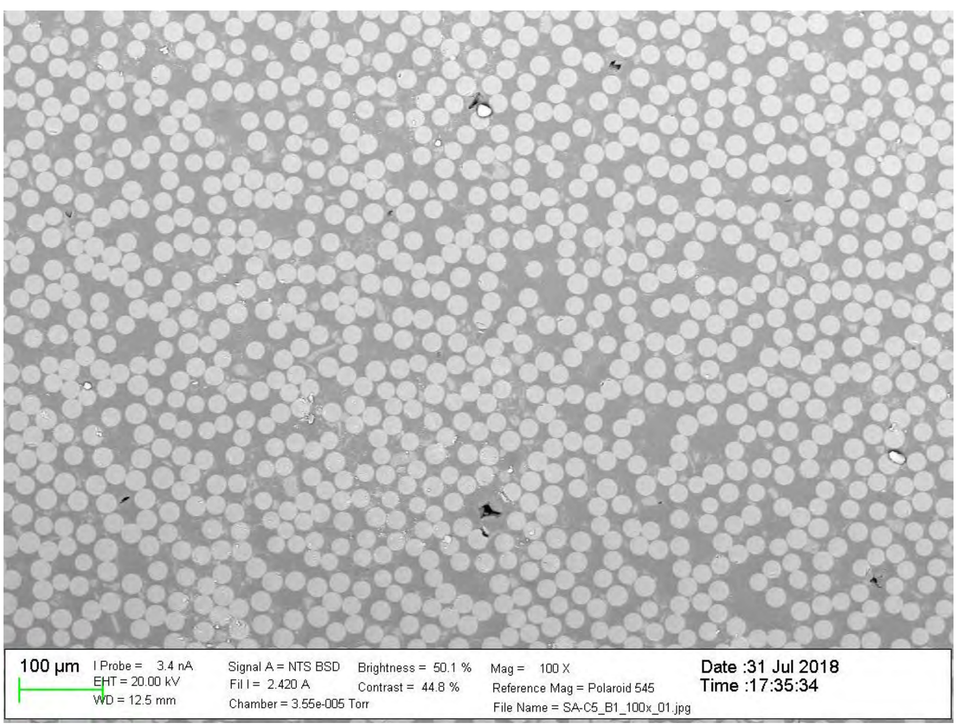

Fig. 25: OH1_C5_B1 at 100x magnification

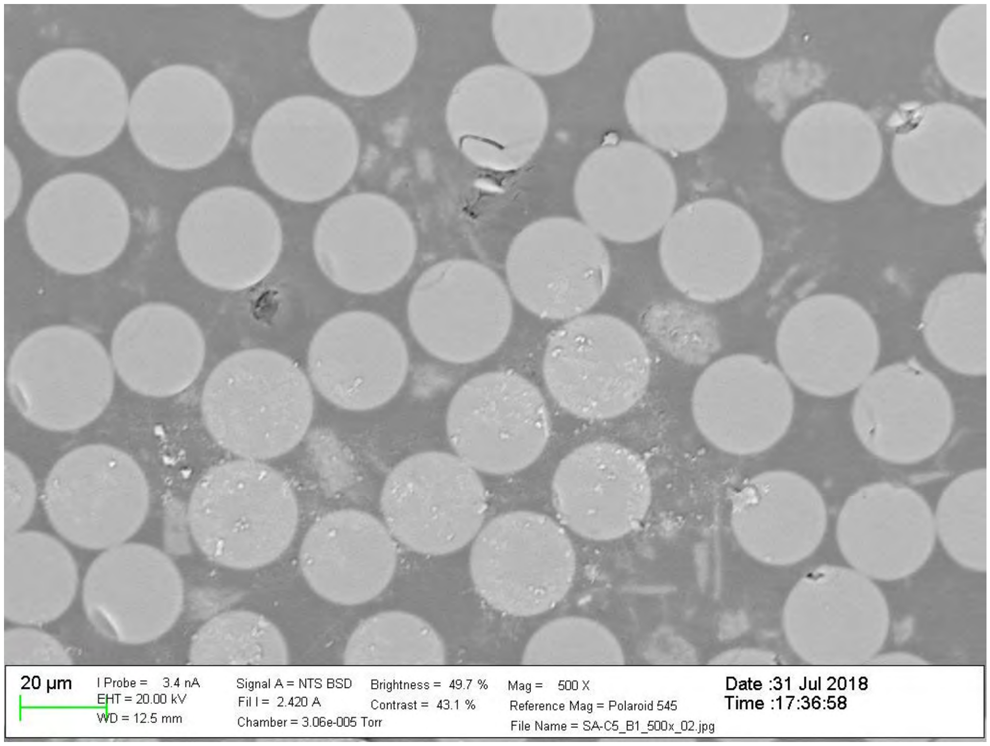

Fig. 26: OH1_C5_B1 at 500x magnification

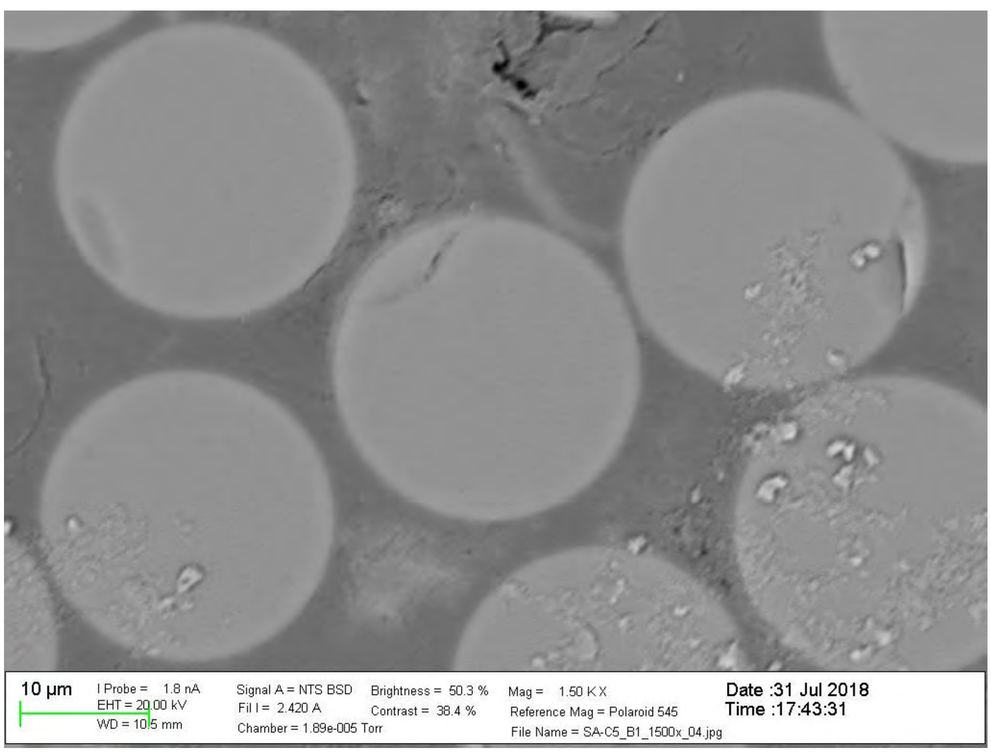

Fig. 27: OH1_C5_B1 at 1500x magnification

1.4 Gills Creek

SEM imaging for *Gills Creek Bridge* was performed at Owens Corning. Only between 0.05% to 0.12% of total fibers showed evidence of being negatively affected by concrete environment after 15 years in service. The affected fibers are typically on the outer edge of the rebar and have negligible impact on mechanical properties.

The fibers evidently affected (192 out of 352,000 fibers) were estimated from counting fibers with obvious signs of damage in 1 quadrant, multiplied by 4. The extrapolation for affected fibers (412 out of 352,000 fibers) was estimated from counting fibers with obvious signs of damage and fibers with polishing artifacts in 1 quadrant, multiplied by 4. This quantity is much less than expected or predicted by accelerated test methods, The results of each bar is shown in Fig. 28 through Fig. 31.

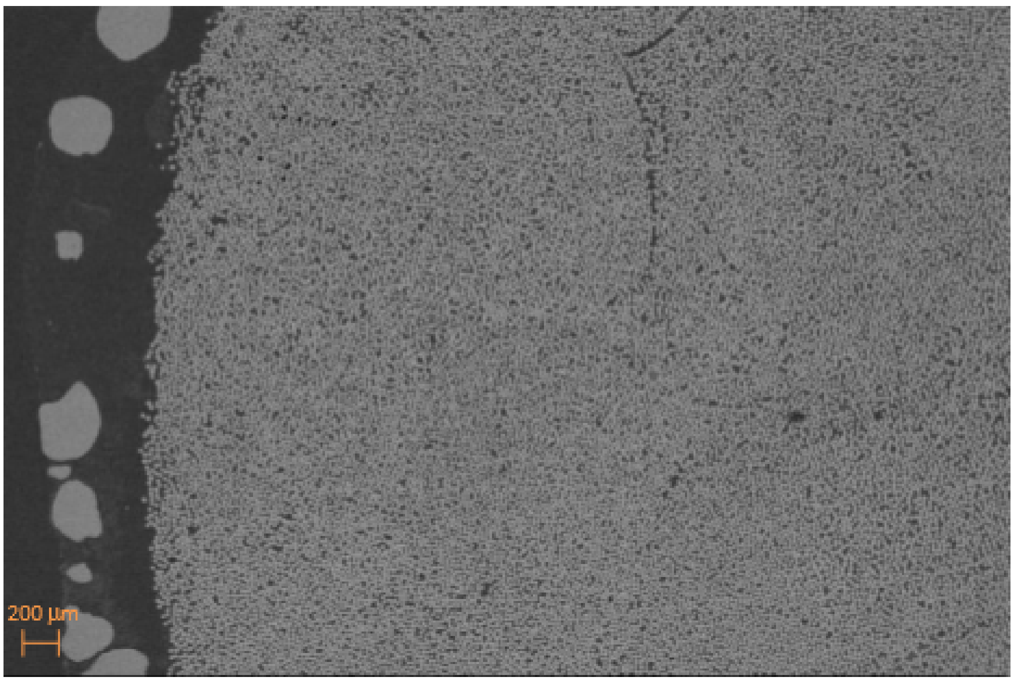

Fig. 28: VA_C4_B2

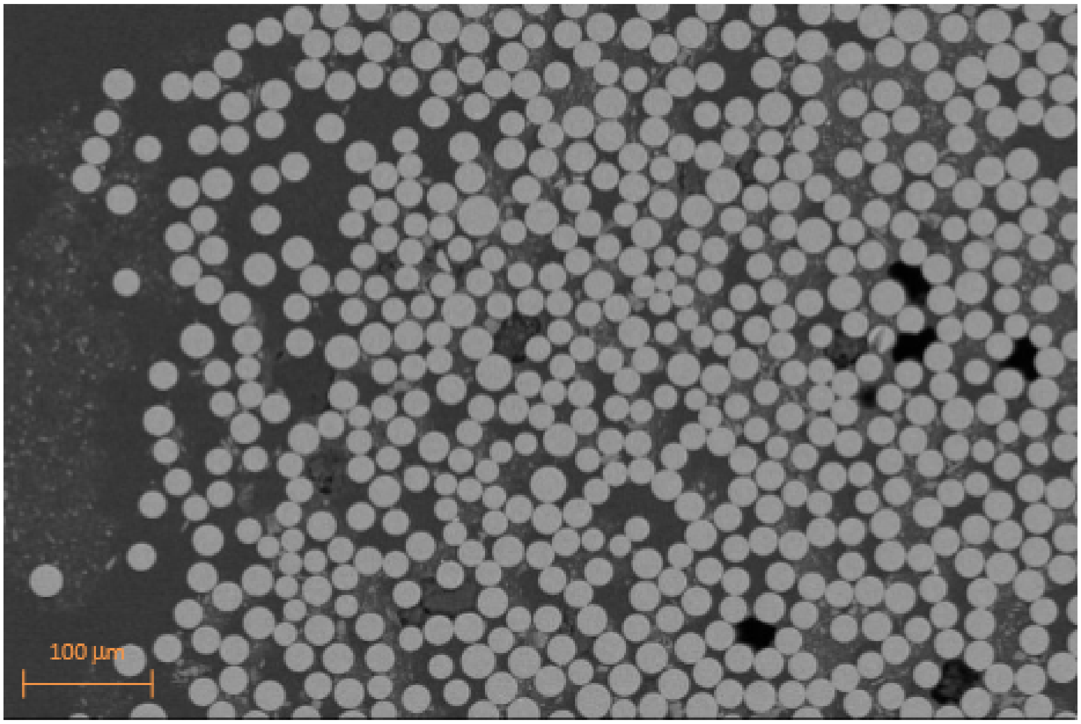

Fig. 29: VA_C4_B2

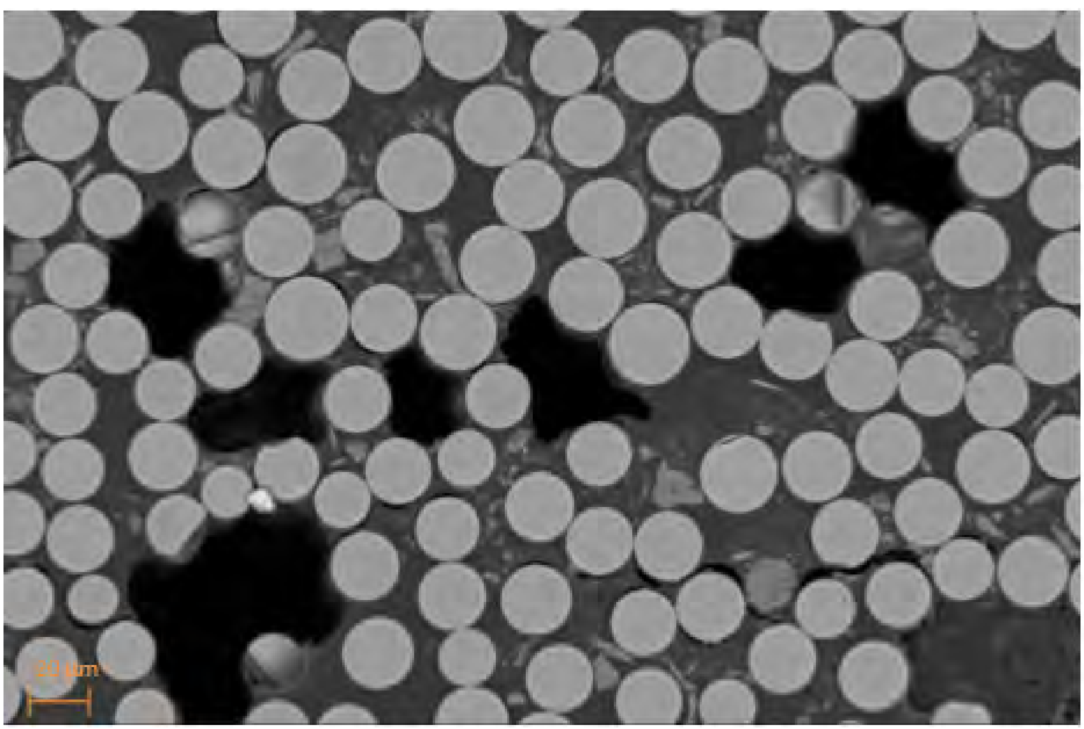

Fig. 30: VA_C4_B2

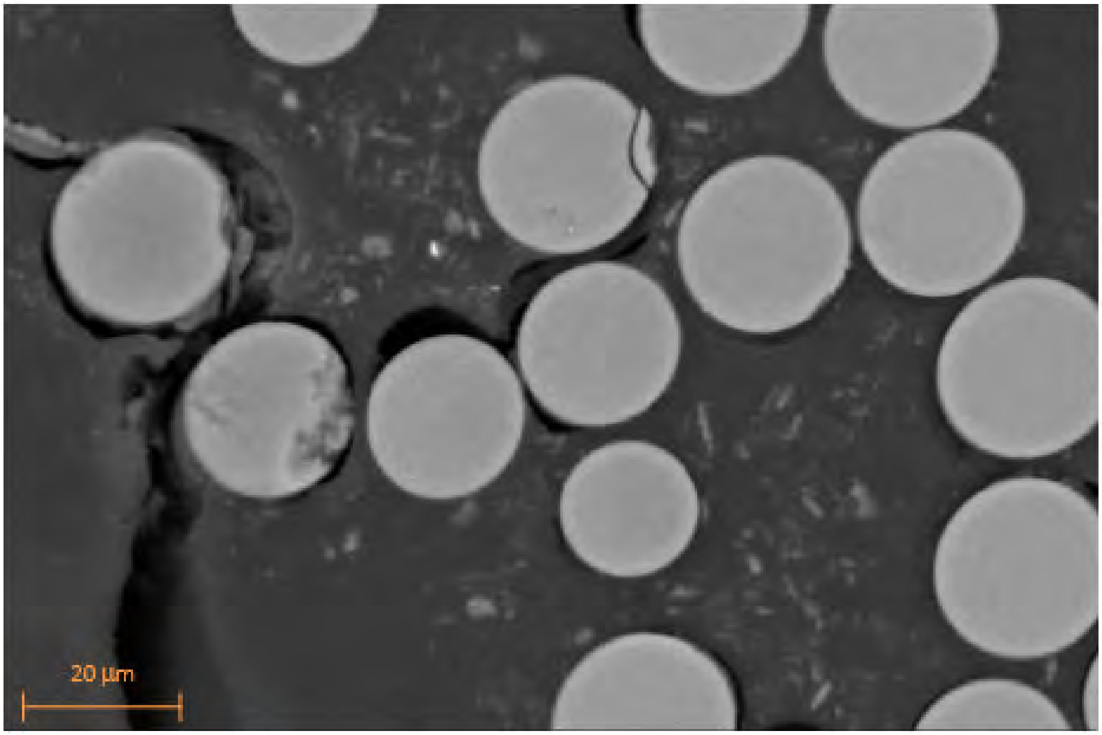

Fig. 31: VA_C4_B2

1.5 Cuyahoga

SEM imaging for *Cuyahoga Bridge* was performed at Owens Corning. GFRP rebar extracted from Cuyahoga bridges show some damage on 0.05 to 0.12 % of the glass fibers. This is much less than expected or predicted by accelerated test methods, and has a negligible impact on mechanical properties. The affected fibers were typically on the outer edge of the rebar. The results of each bar is shown in Fig. 32 through Fig. 35.

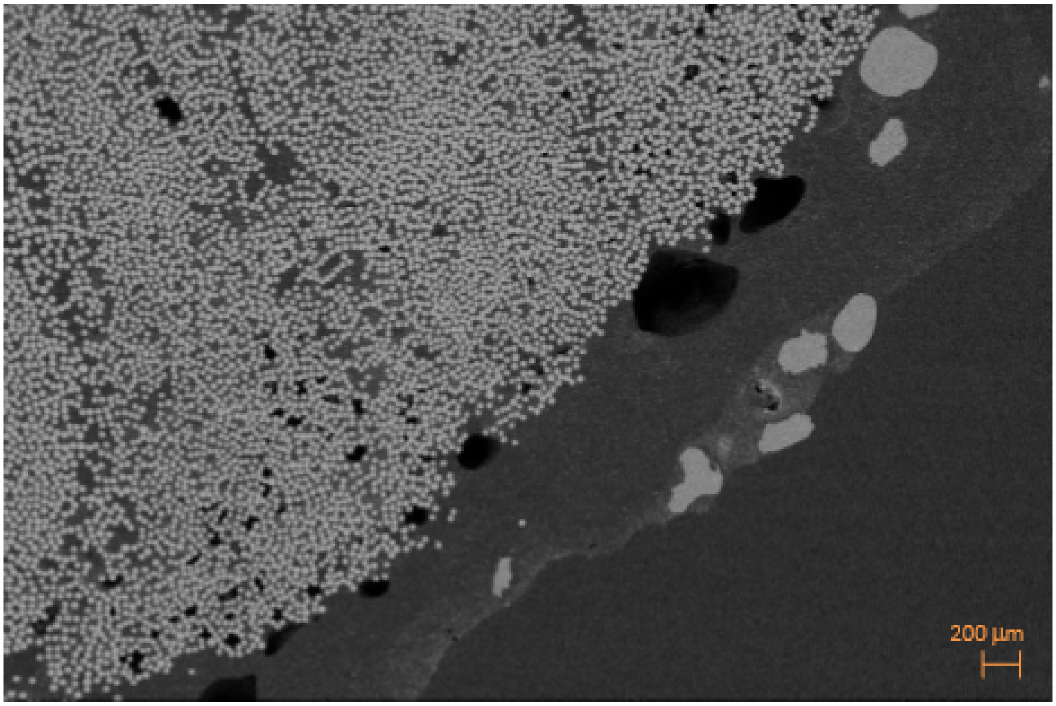

Fig. 32: OH2_C5_B2

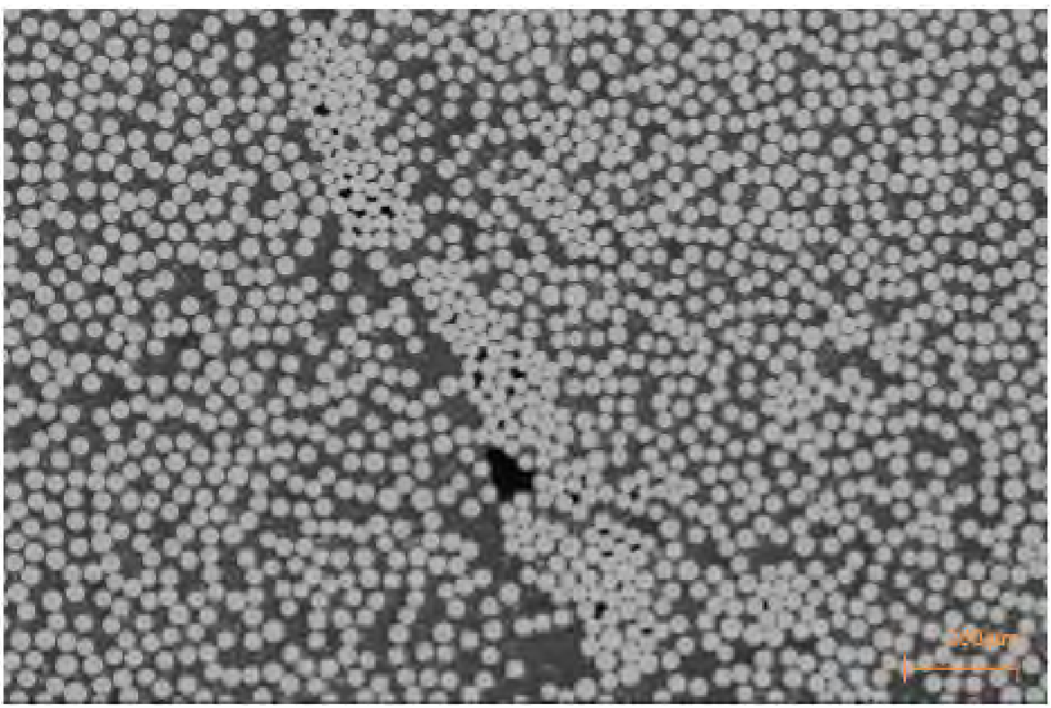

Fig. 33: OH2_C5_B2

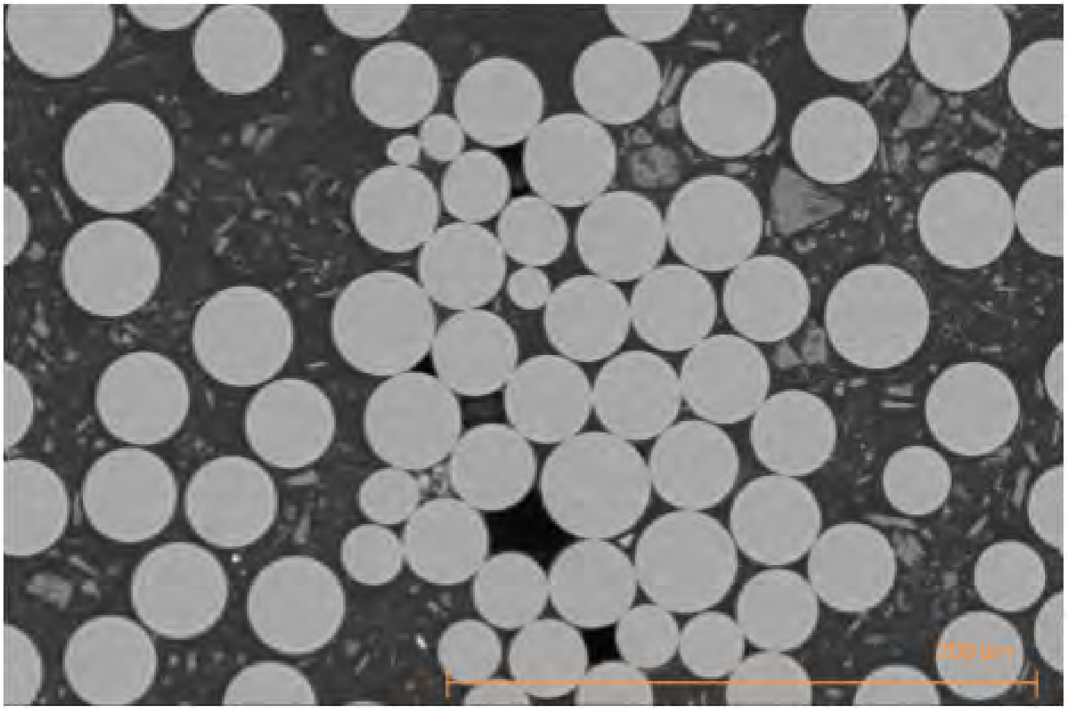

Fig. 34: OH2_C5_B2

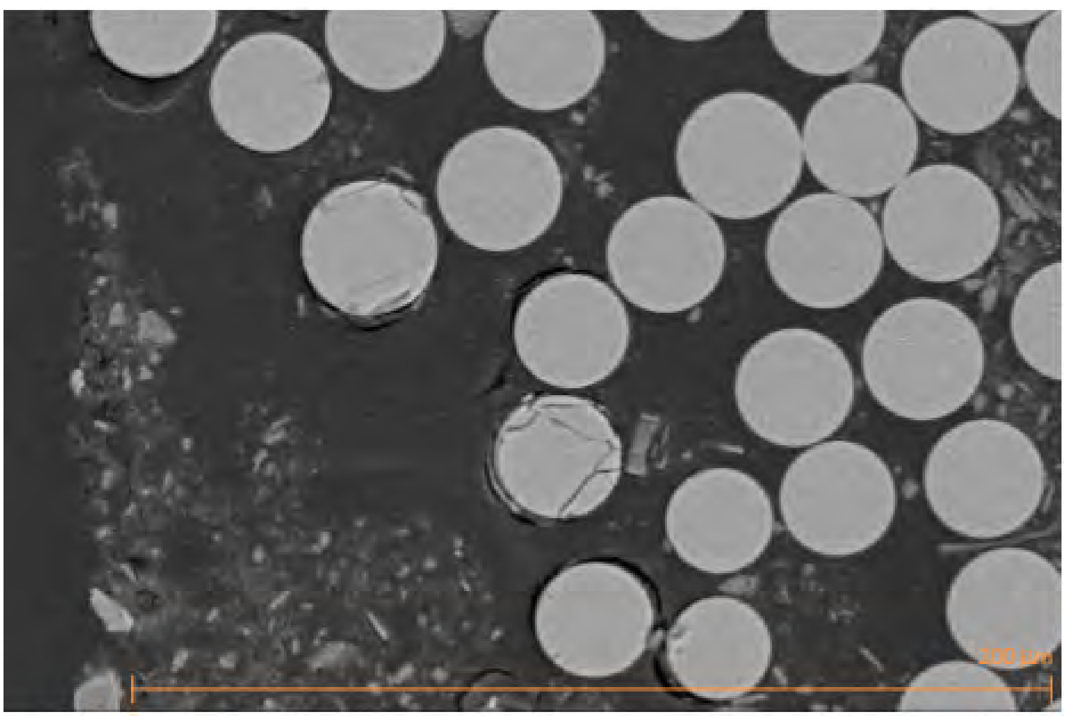

Fig. 35: OH2_C5_B2

1.6 McKinleyville

SEM imaging for *McKinleyville Bridge* was performed at Owens Corning. Nearly no negatively affected fibers were observed on the interior or exterior of in-service rebar. The few negatively affected fibers appear to have physical damage from specimen preparation as they are near resin voids. The SEM images of each bar is shown in Fig. 36 through Fig. 80.

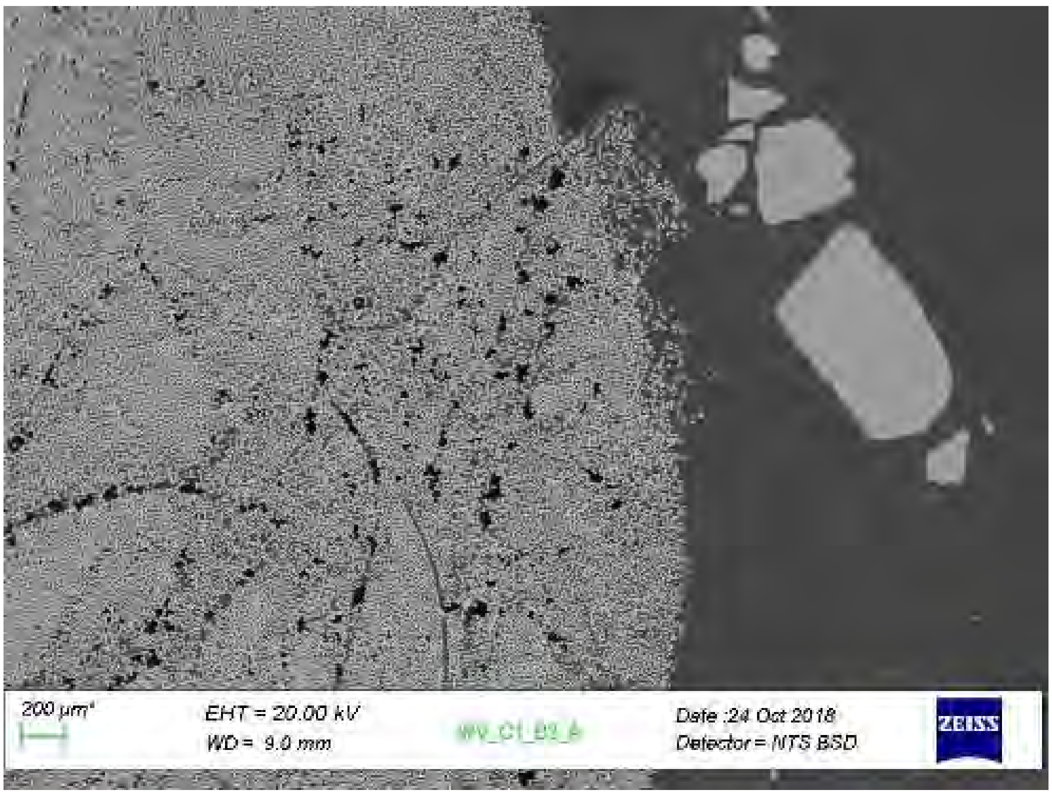

Fig. 36. WV_C1_B2A

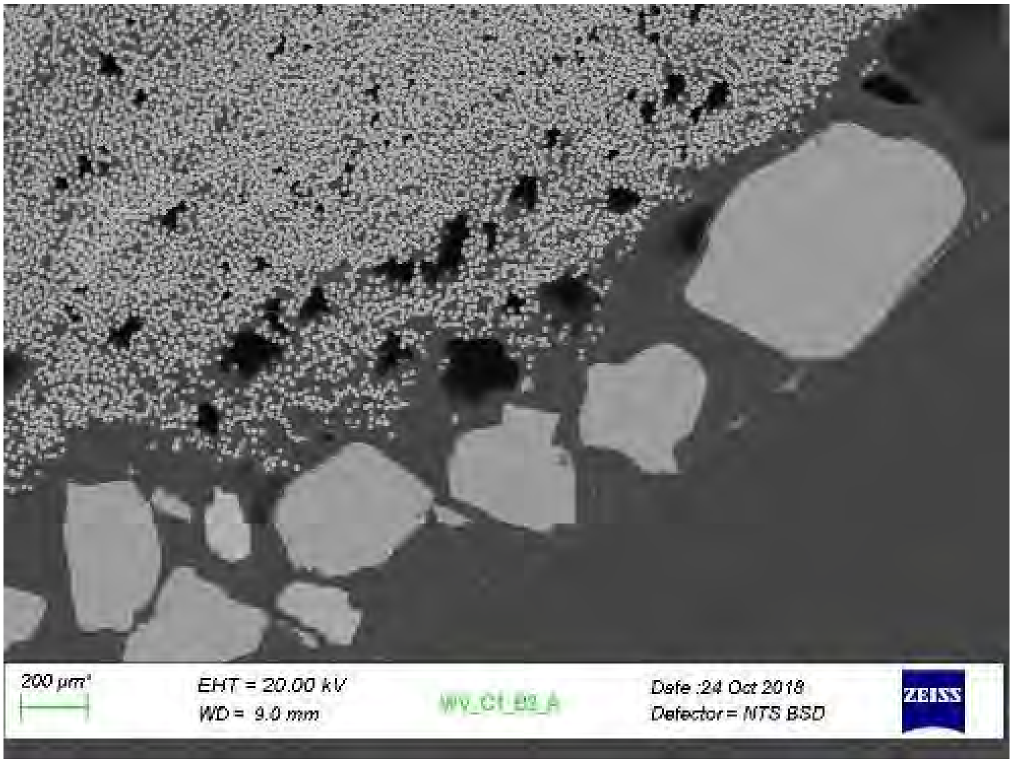

Fig. 37. WV_C1_B2A

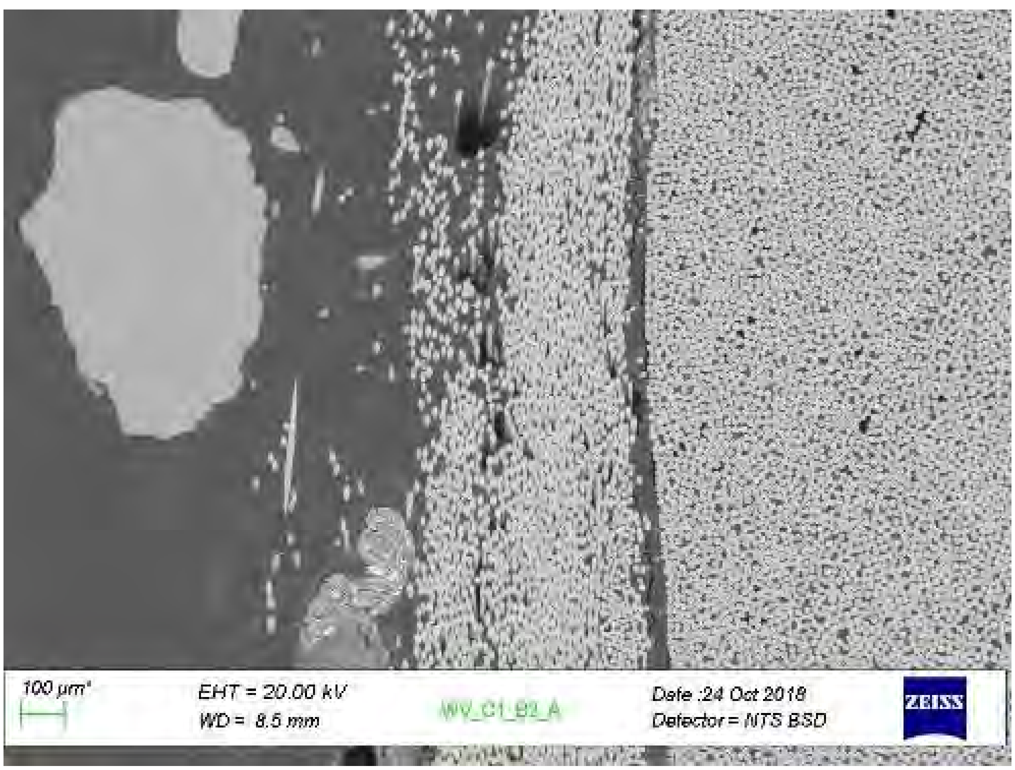

Fig. 38. WV_C1_B2A

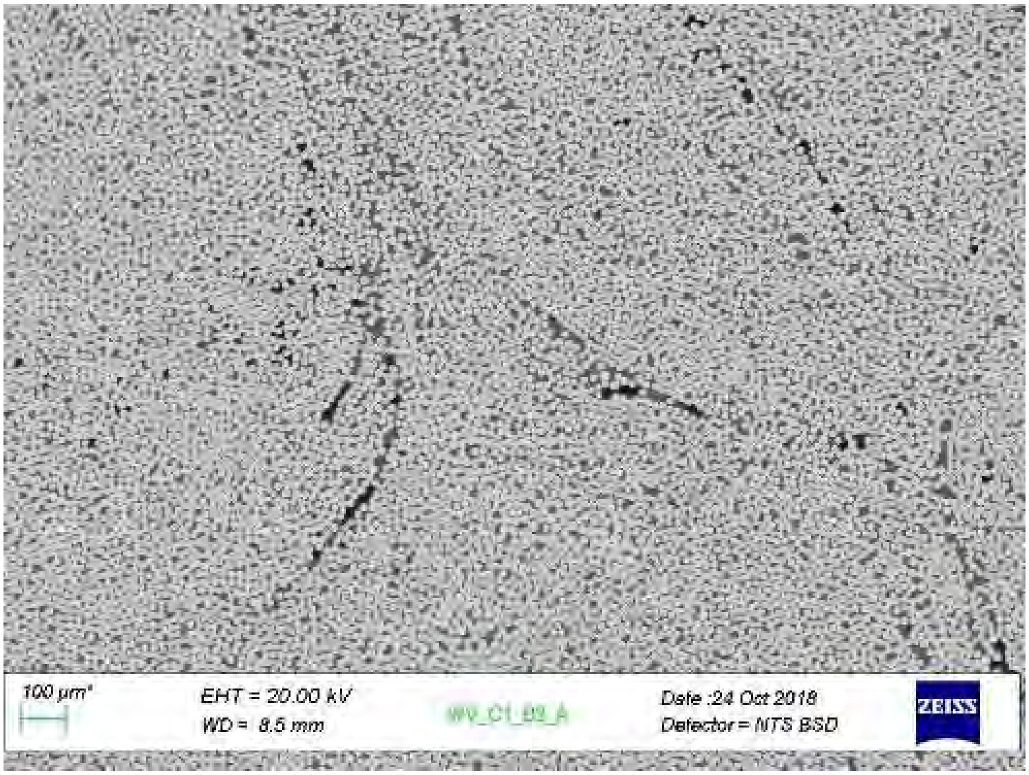

Fig. 39. WV_C1_B2A

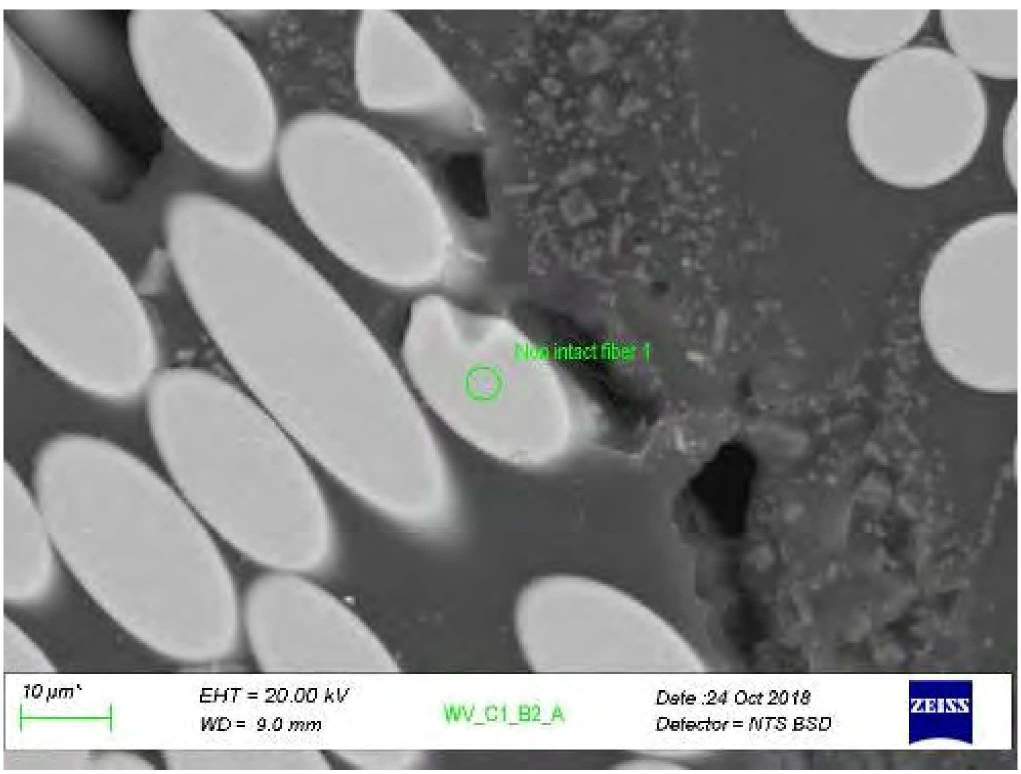

Fig. 40. WV_C1_B2A

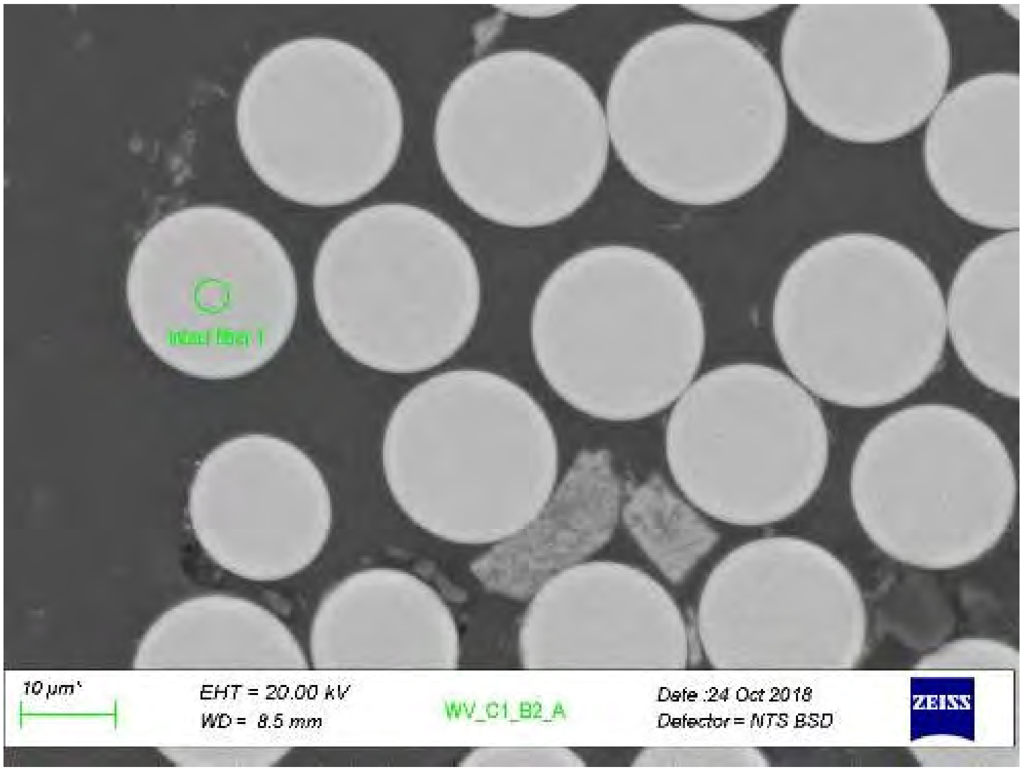

Fig. 41. WV_C1_B2A

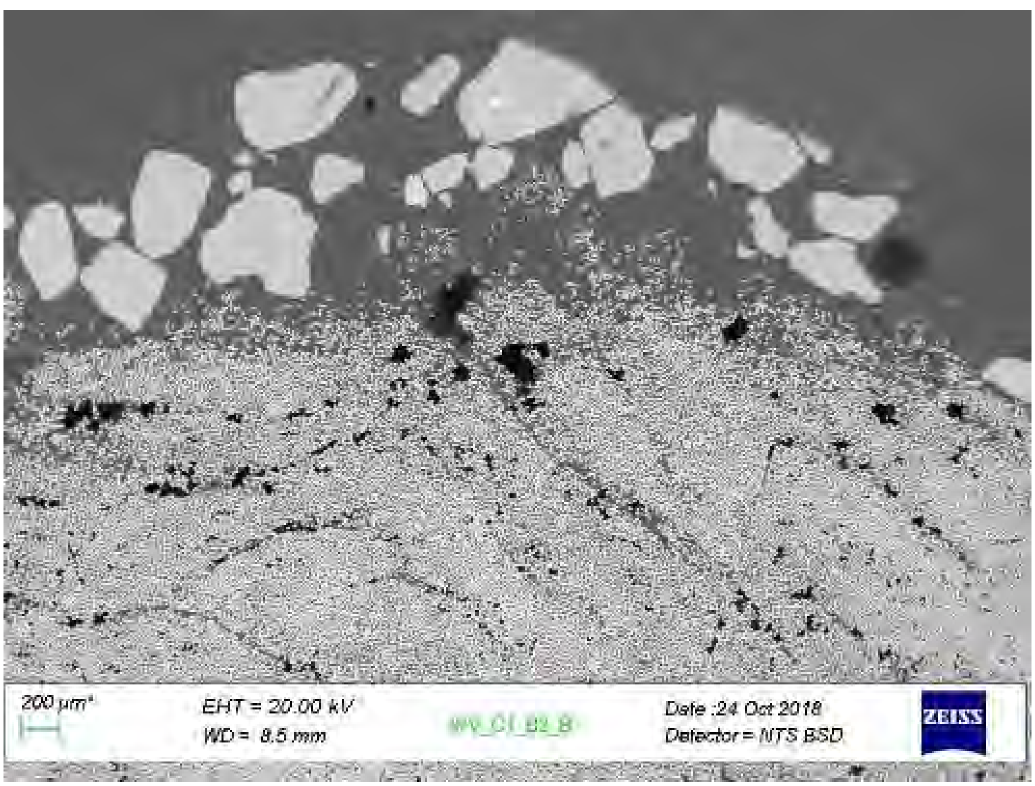

Figure 42. WV_C1_B2B

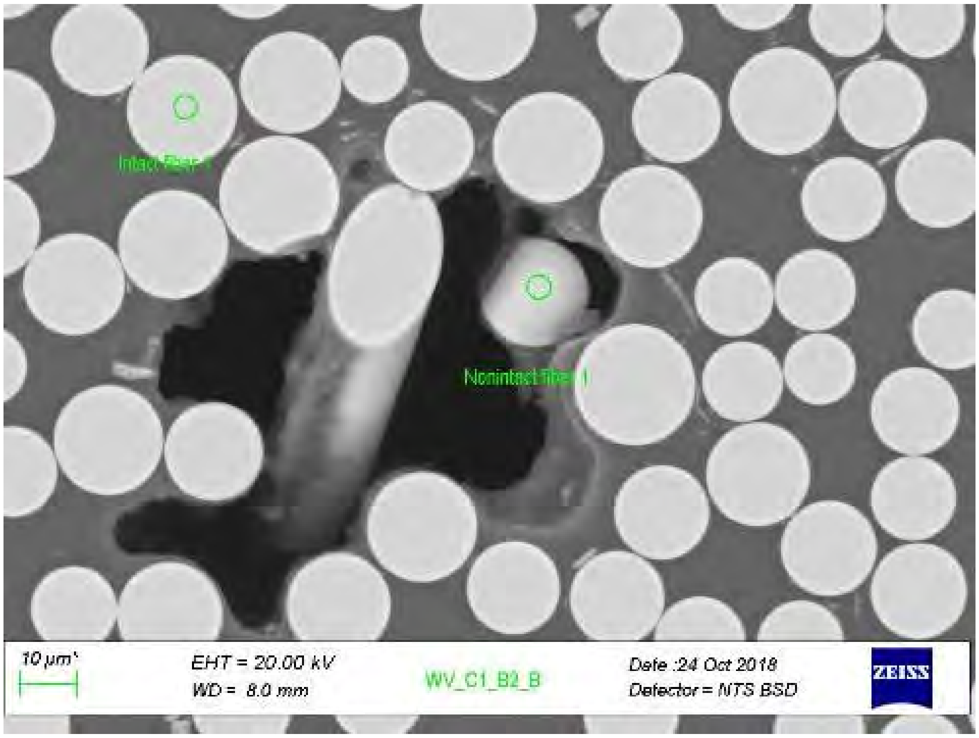

Figure 43. WV_C1_B2B

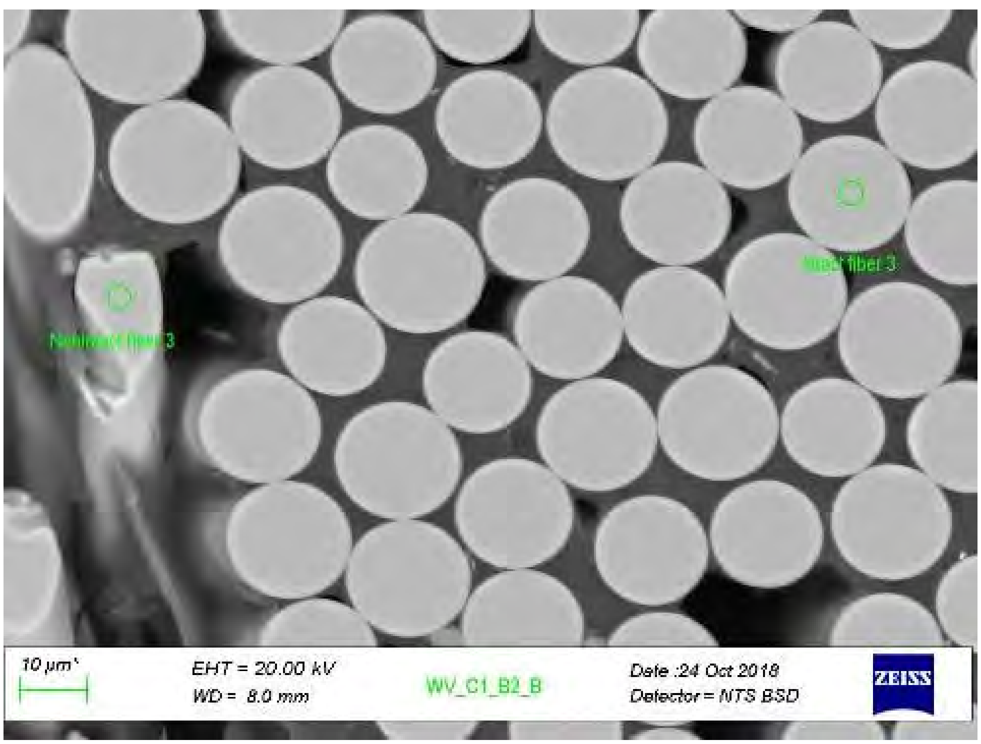

Figure 44.WV_C1_B2B

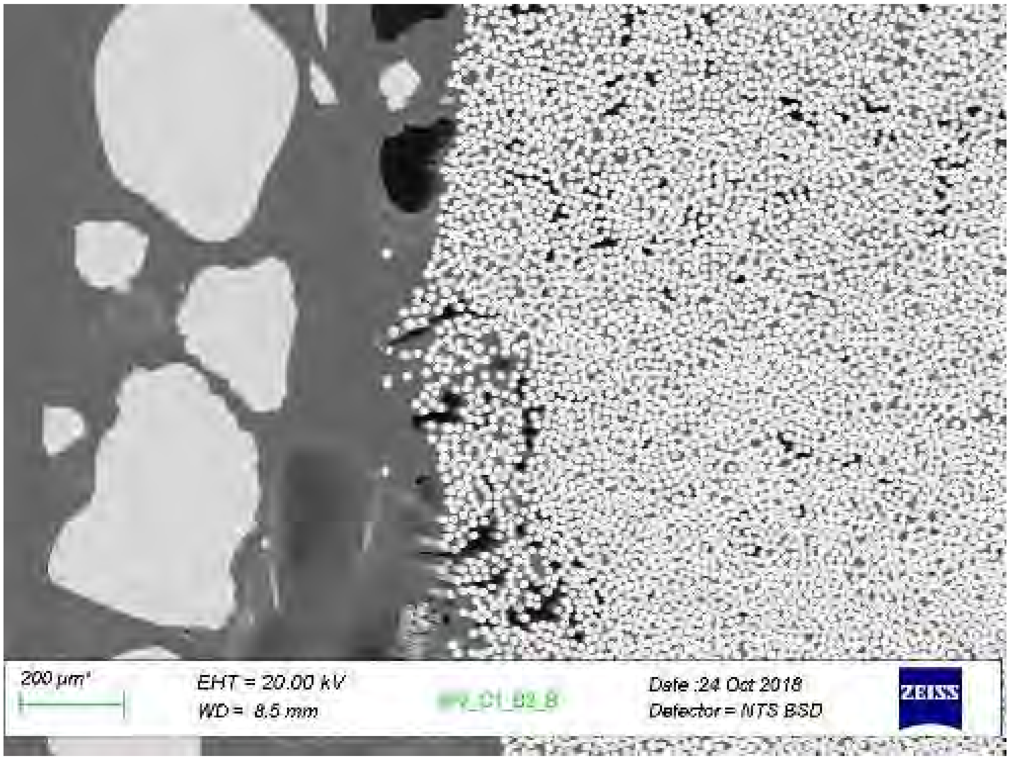

Figure 45. WV_C1_B2B

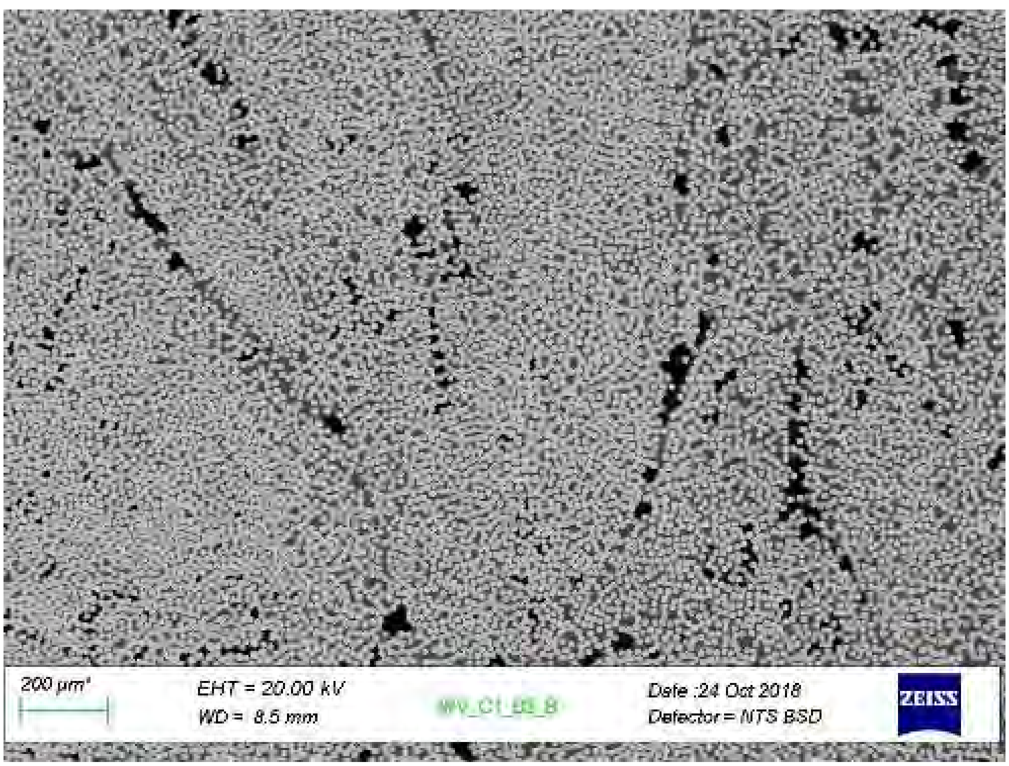

Fig. 46. WV_C1_B2B

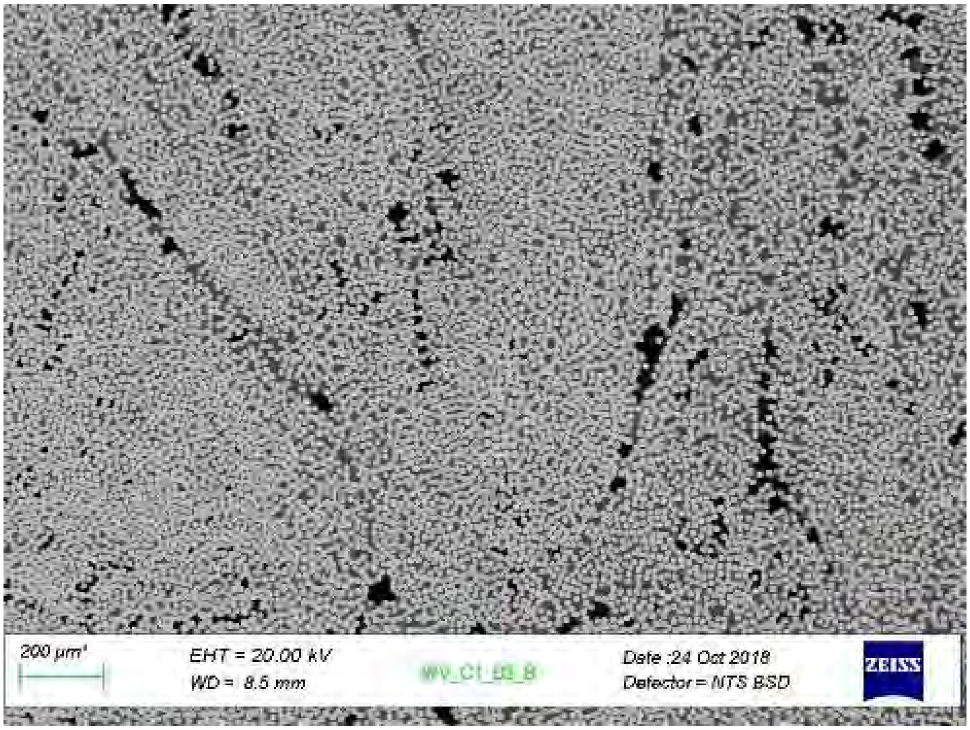

Fig. 47. WV_C1_B2B

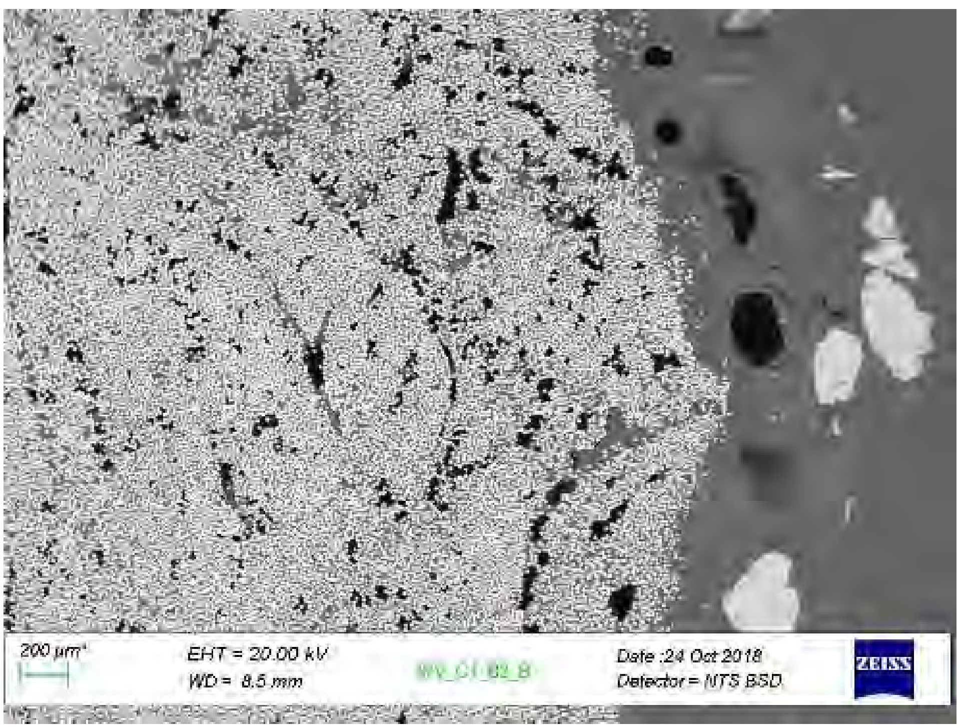

Figure 48. WV_C1_B2B

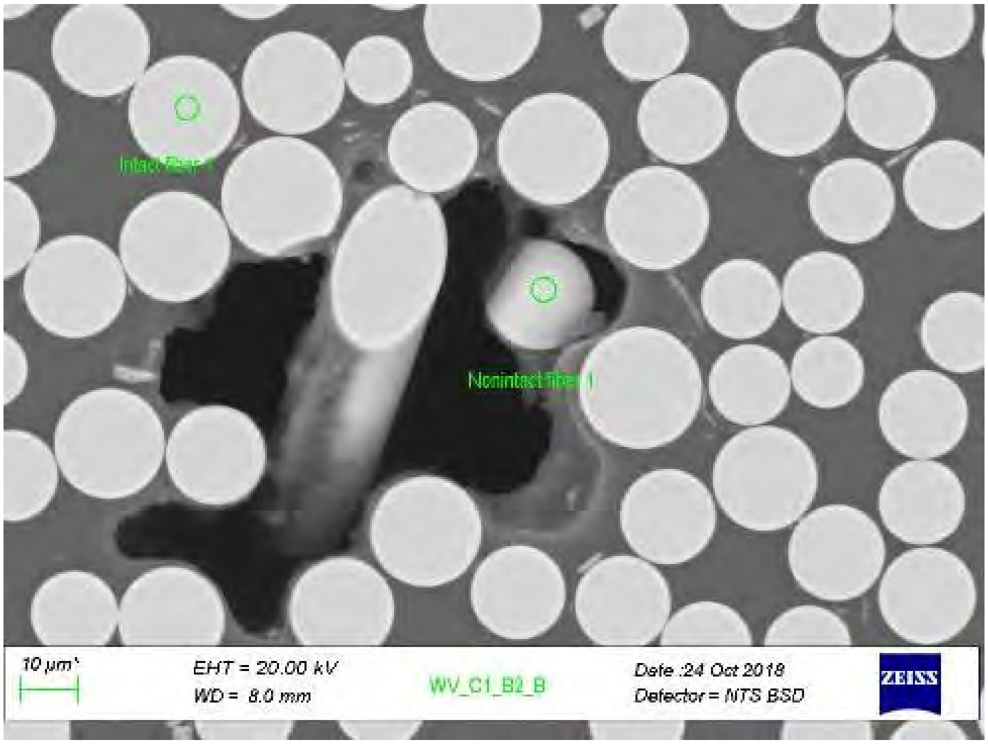

Fig. 49. WV_C1_B2B

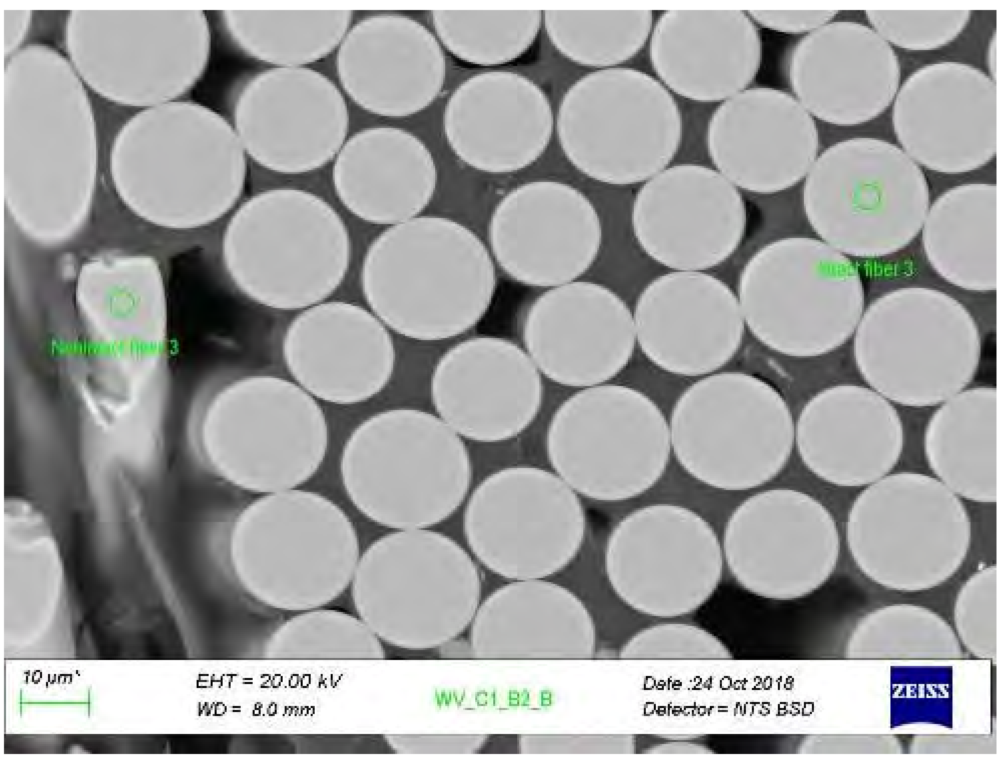

Fig. 50. WV_C1_B2B

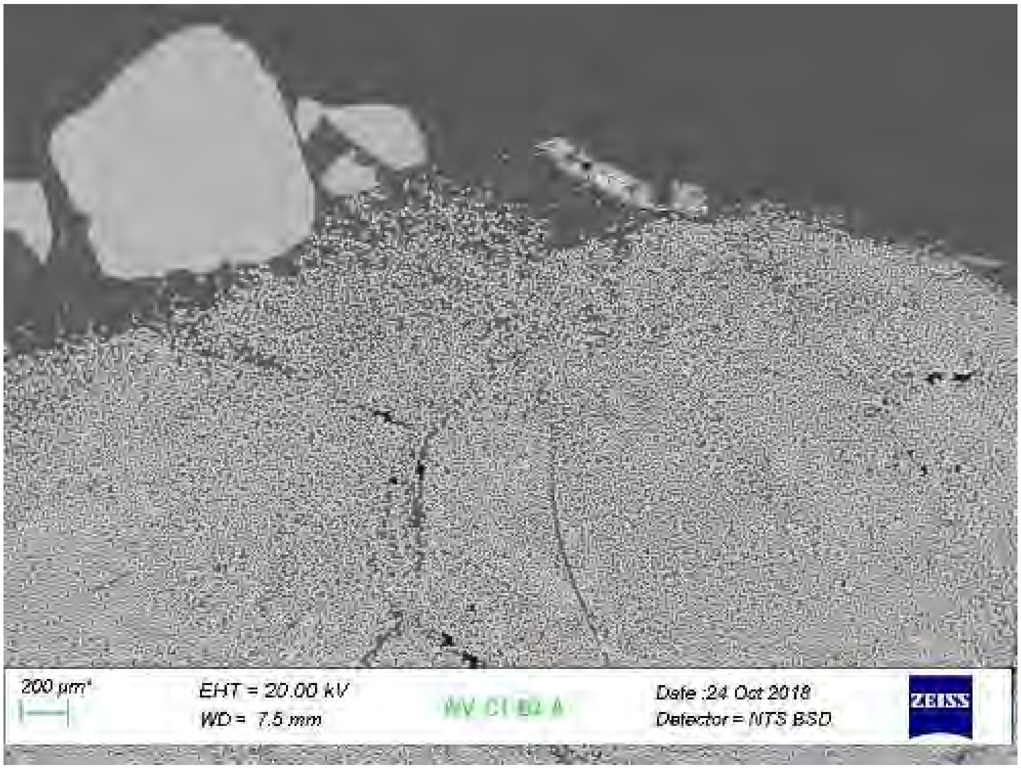

Fig. 51. WV_C1_B3A

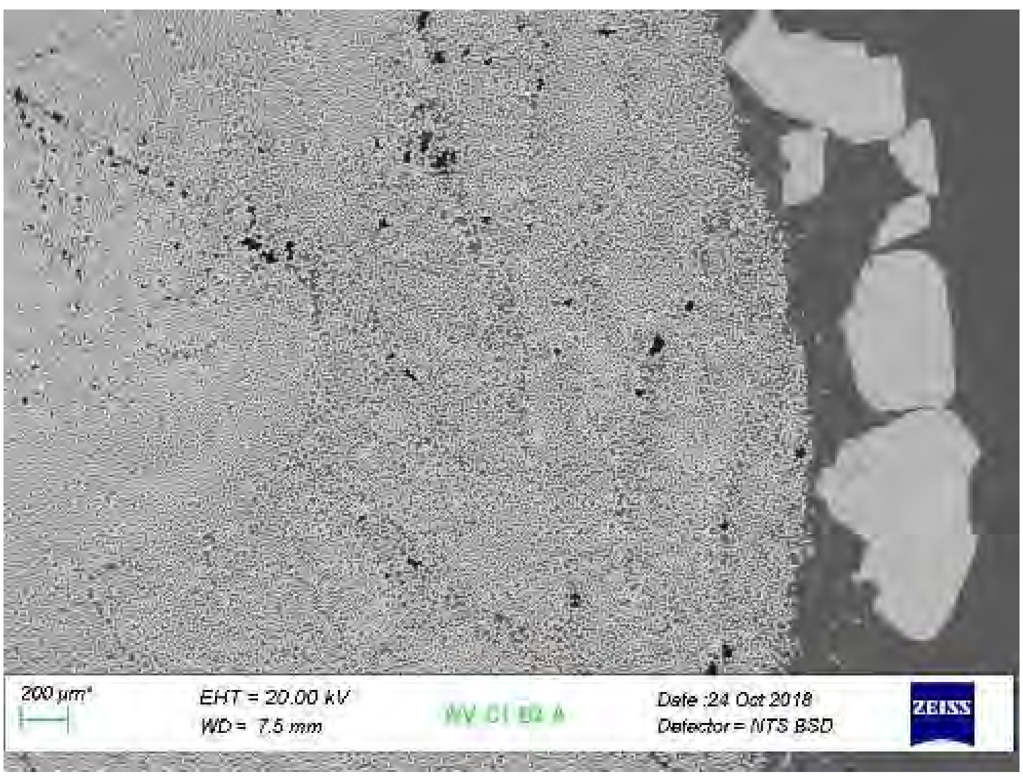

Fig. 52. WV_C1_B3A

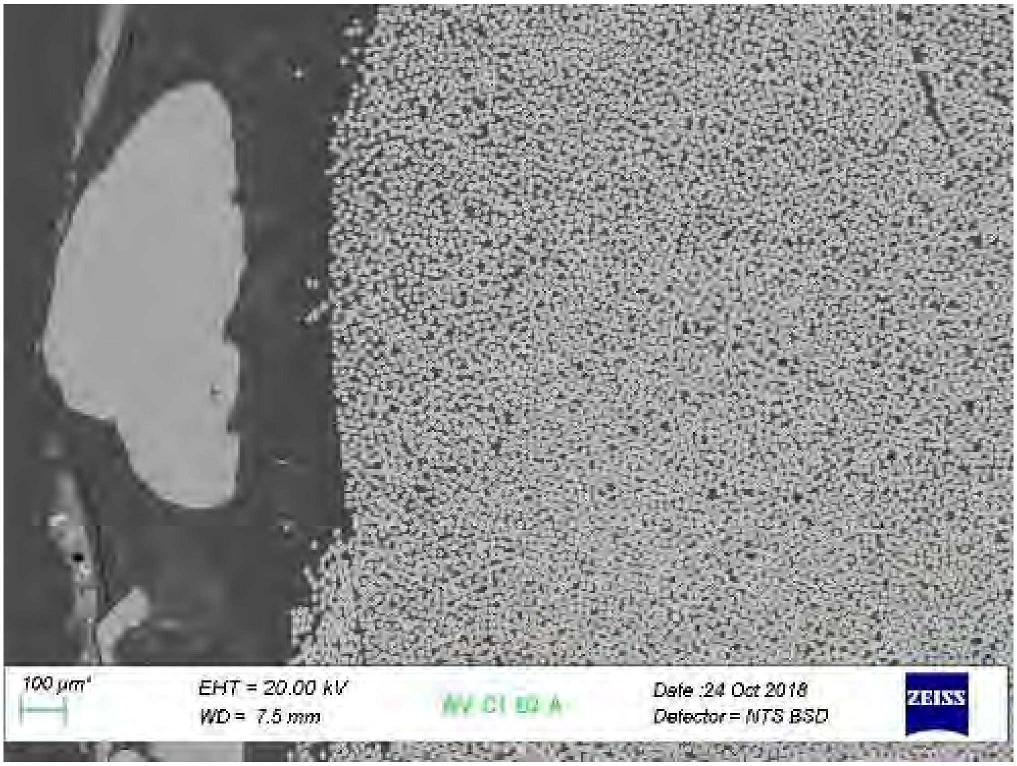

Fig. 53. WV_C1_B3A

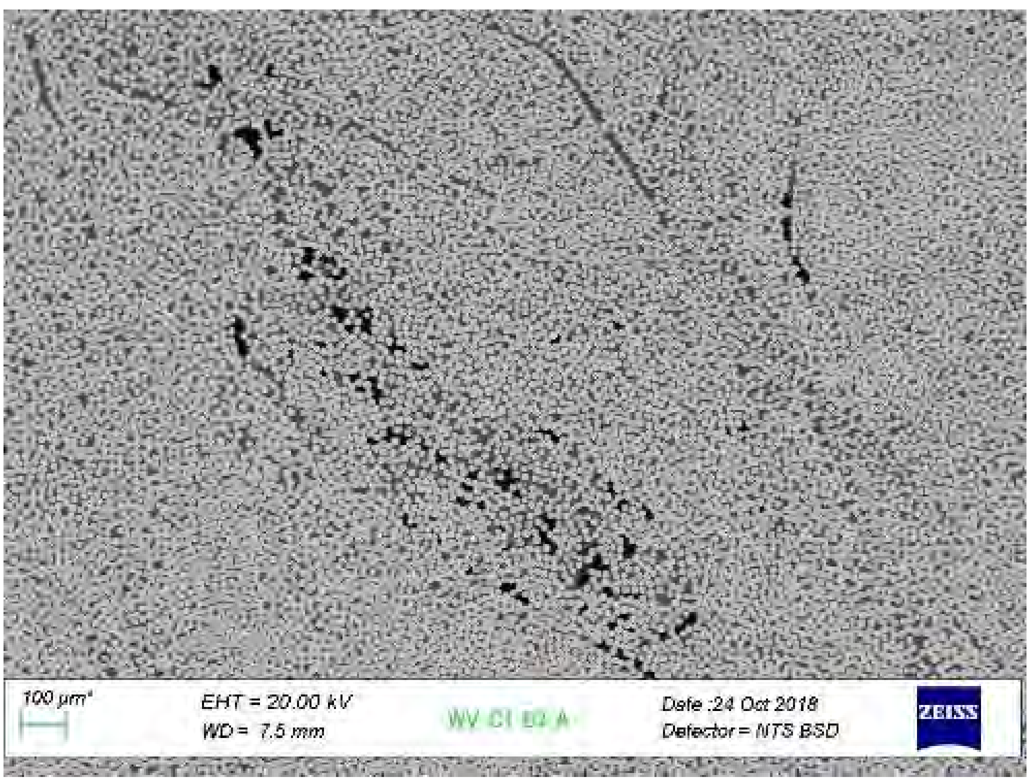

Fig. 54. WV_C1_B2A

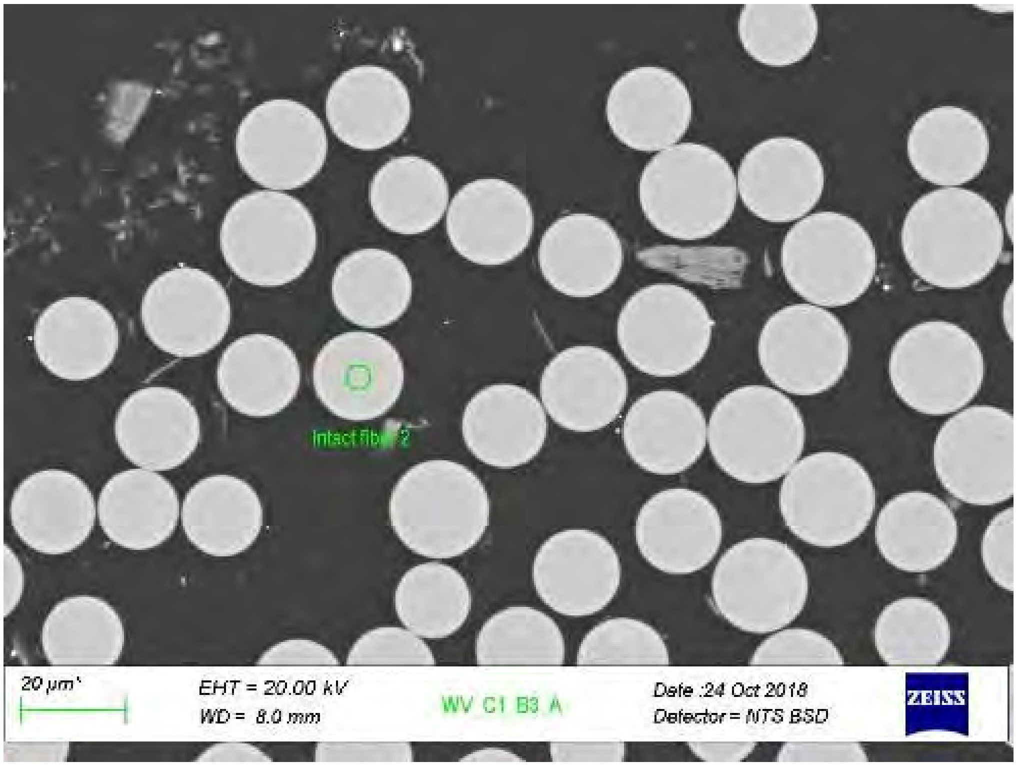

Fig. 55. WV_C1_B3A

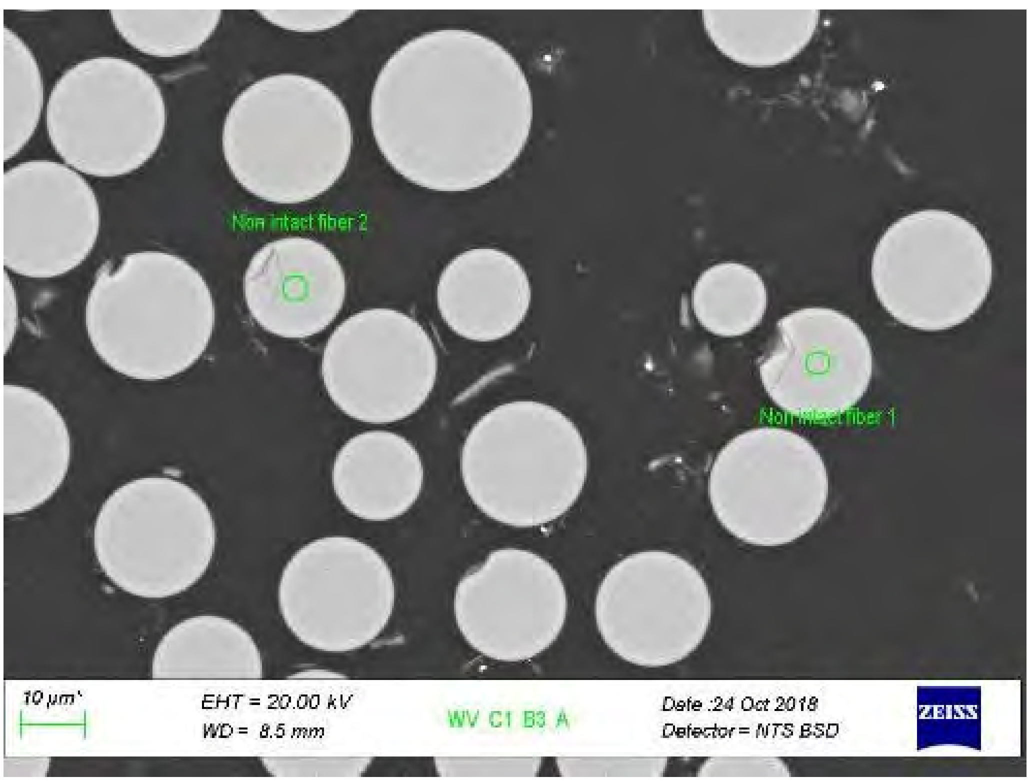

Fig. 56. WV_C1_B3A

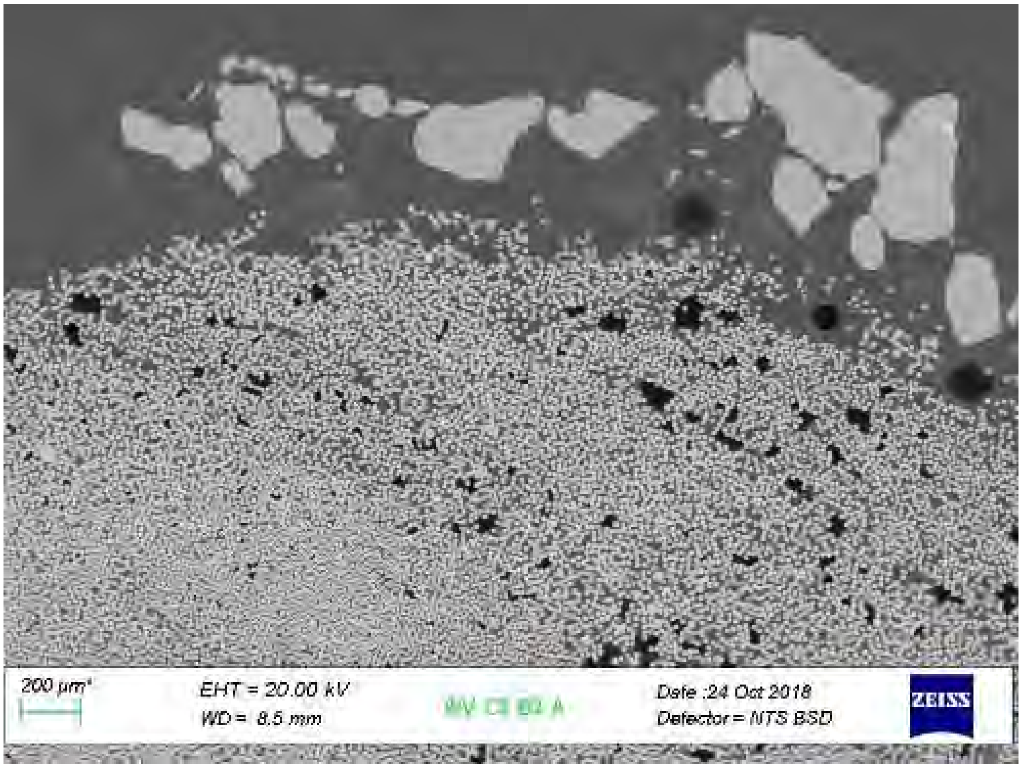

Fig. 57. WV_C3_B3A

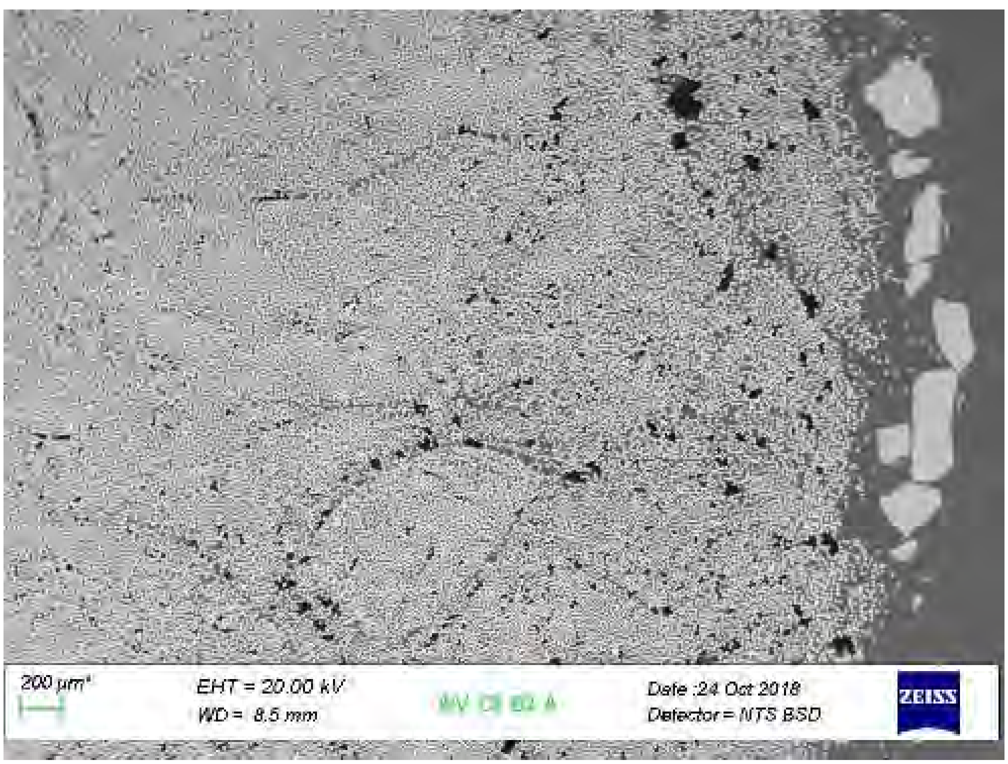

Fig. 58. WV_C3_B3A

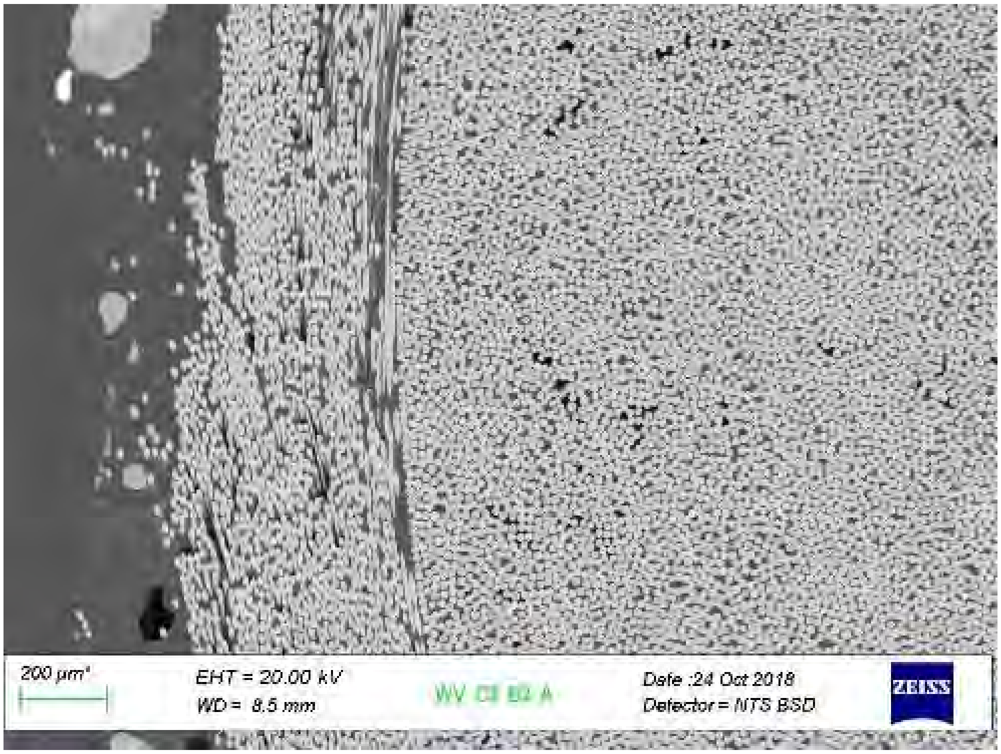

Fig. 59. WV_C3_B3A

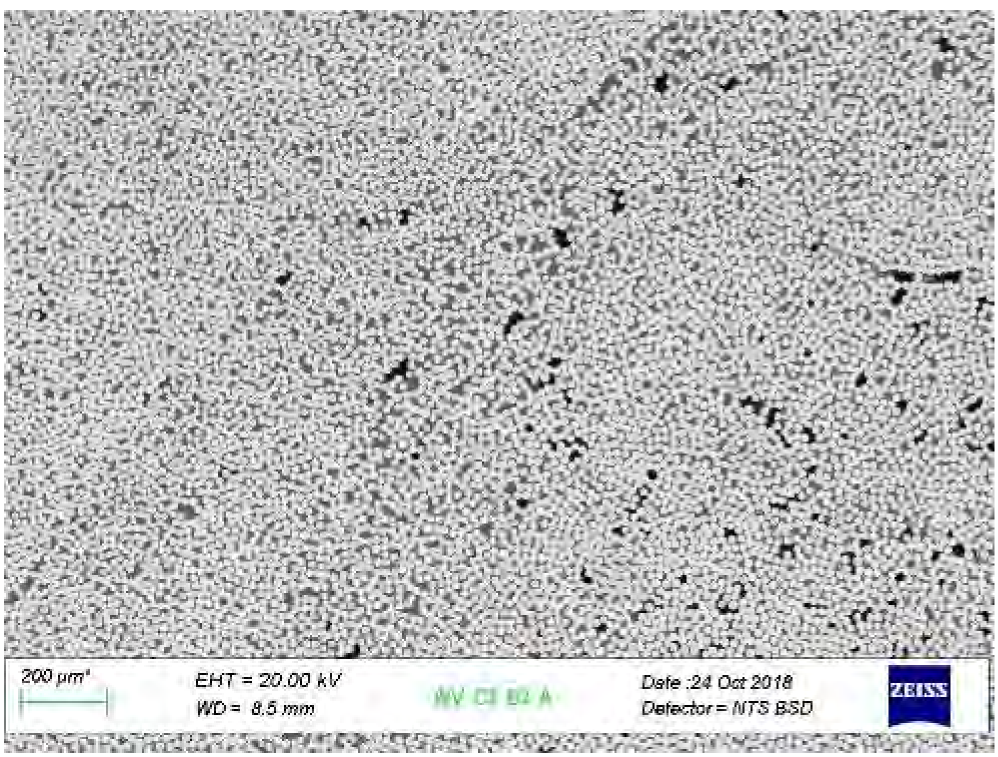

Fig. 60. WV_C3_B3A

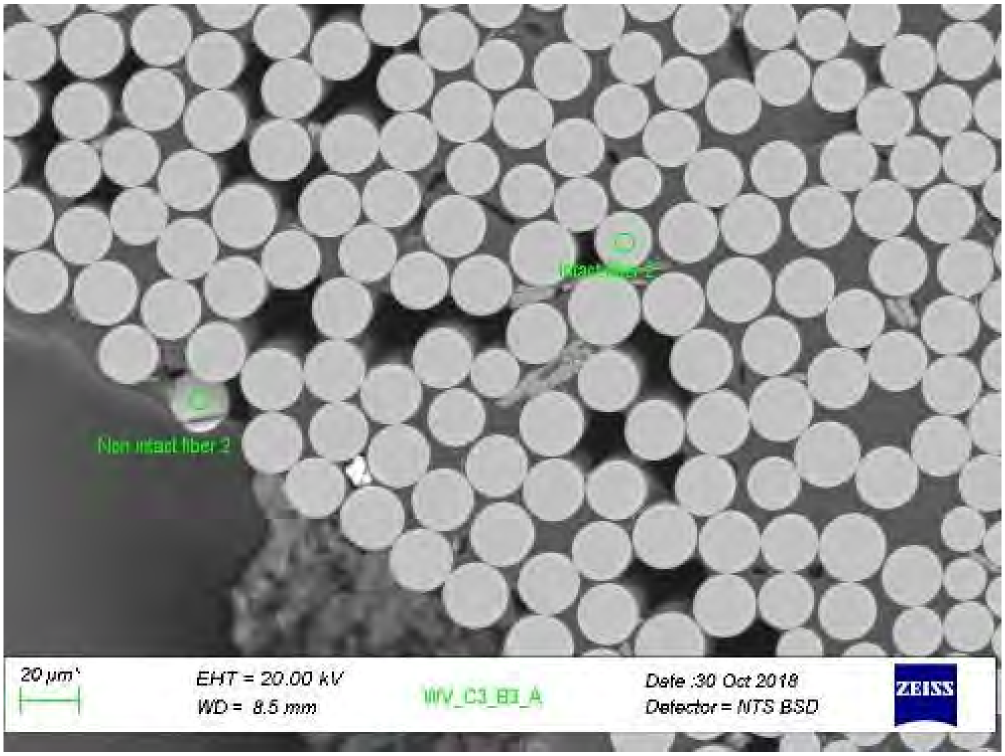

Fig. 61. WV_C3_B3A

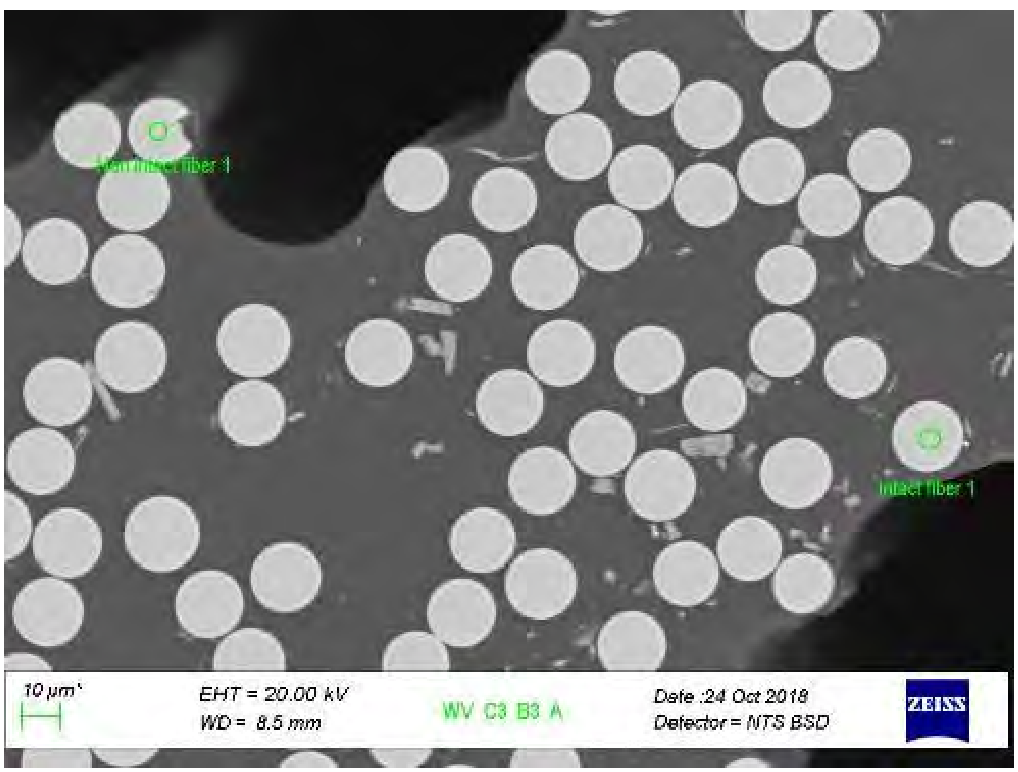

Fig. 62. WV_C3_B3A

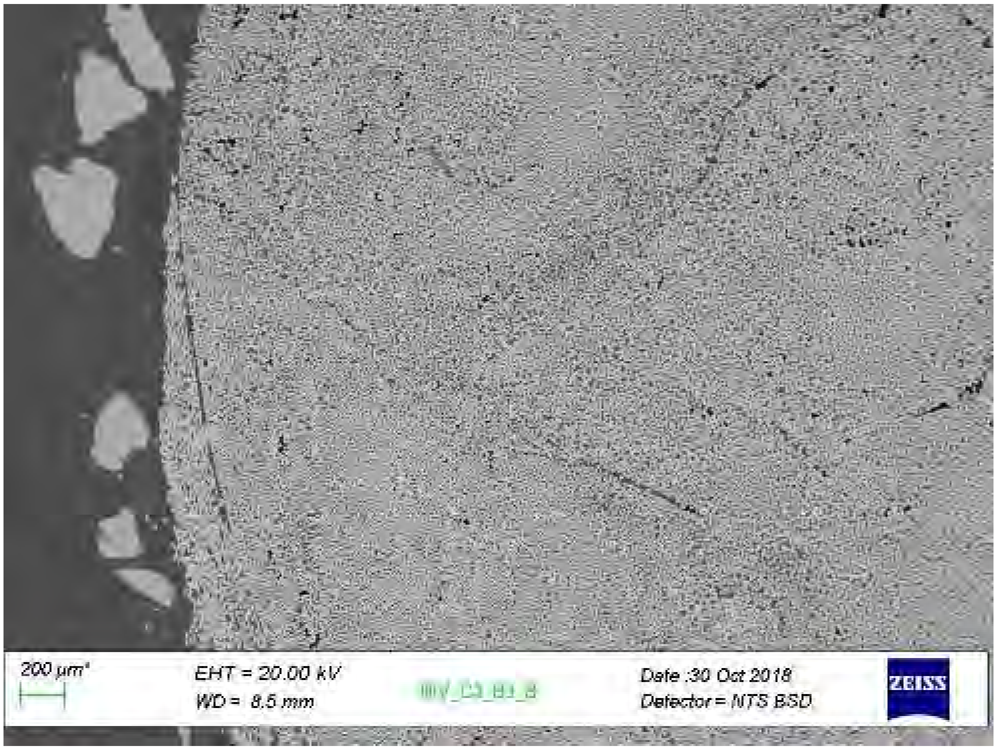

Fig. 63. WV_C3_B3B

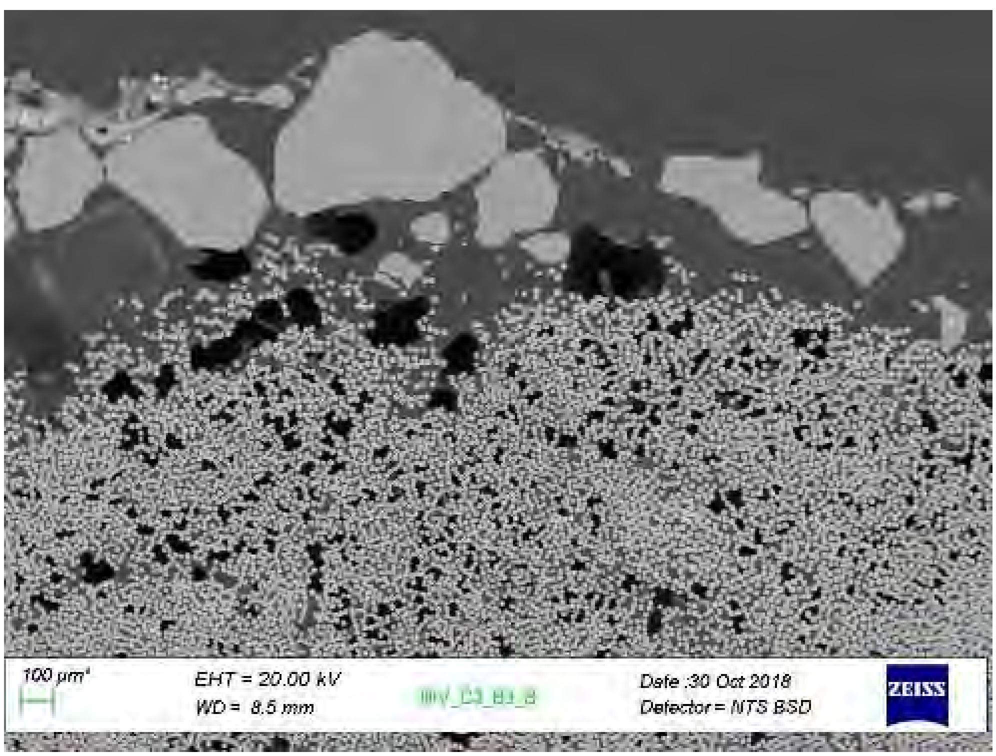

Fig. 64. WV_C3_B3B

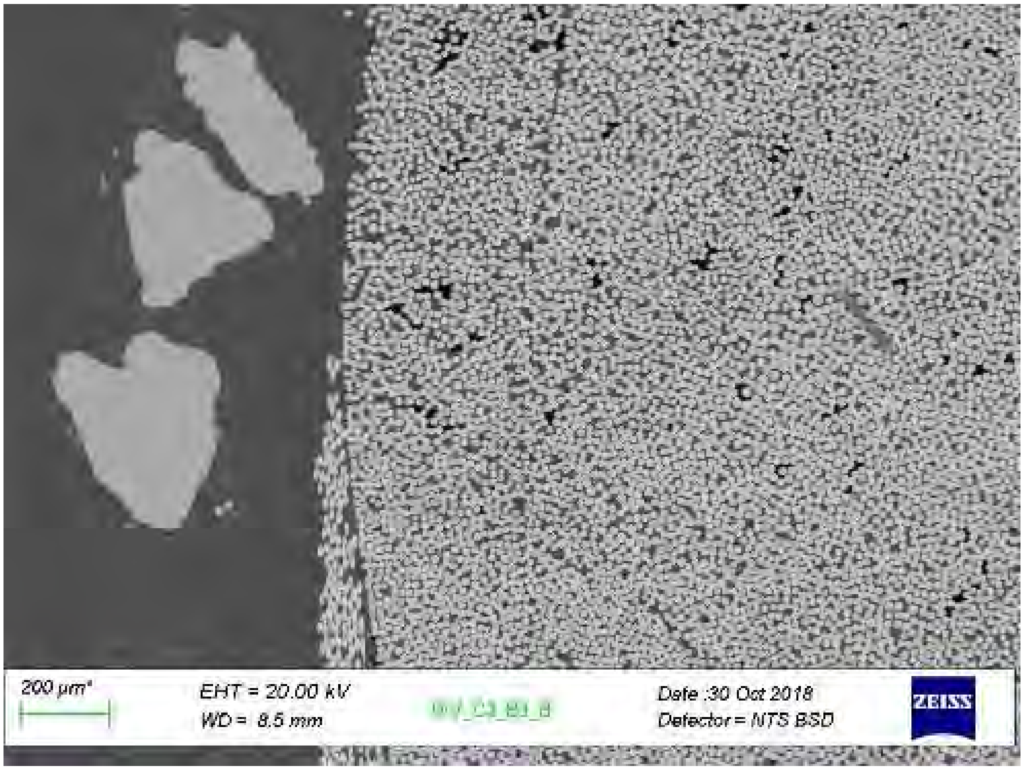

Fig. 65. WV_C3_B3

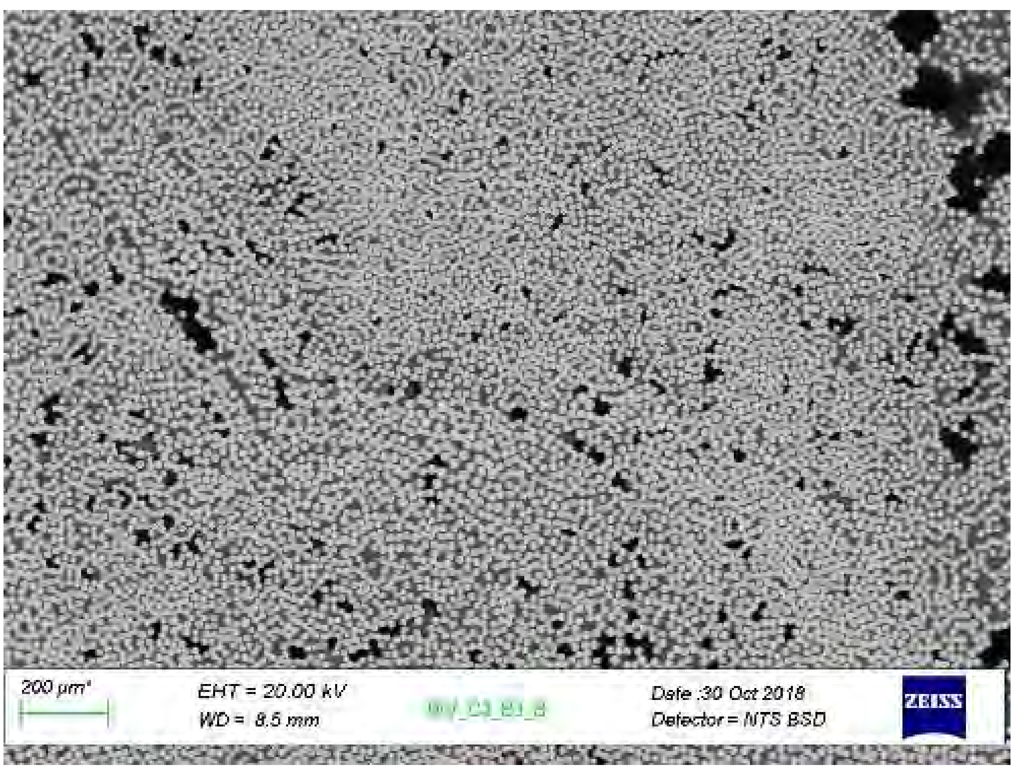

Fig. 66. WV_C3_B3B

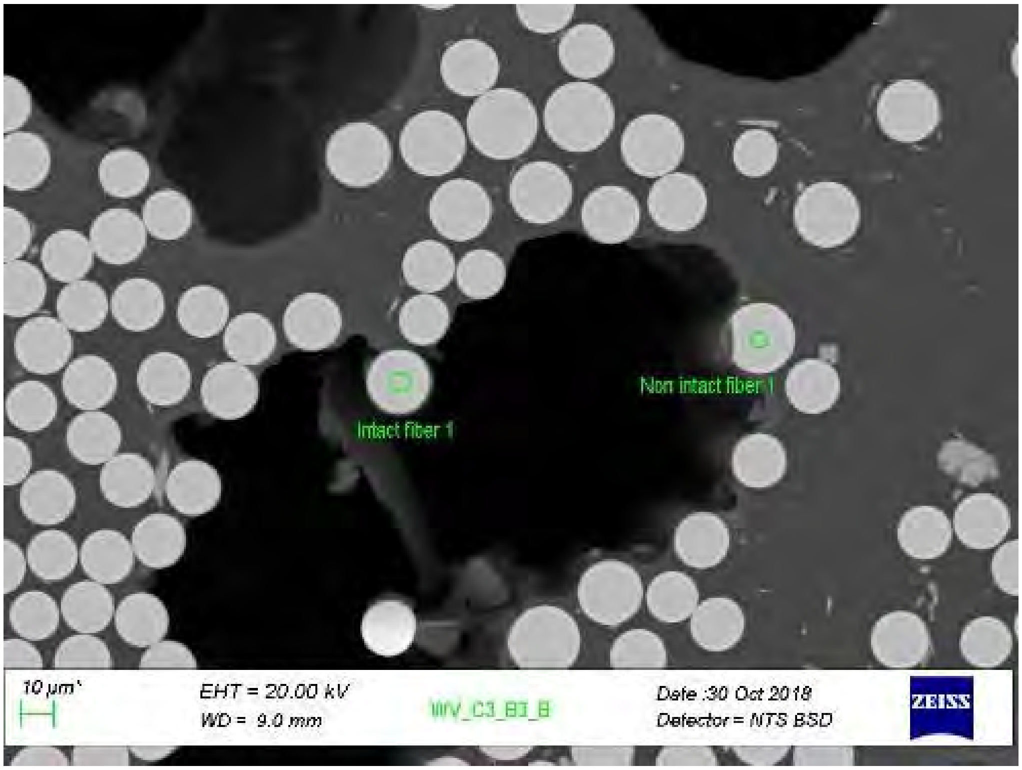

Fig. 67. WV_C3_B3B

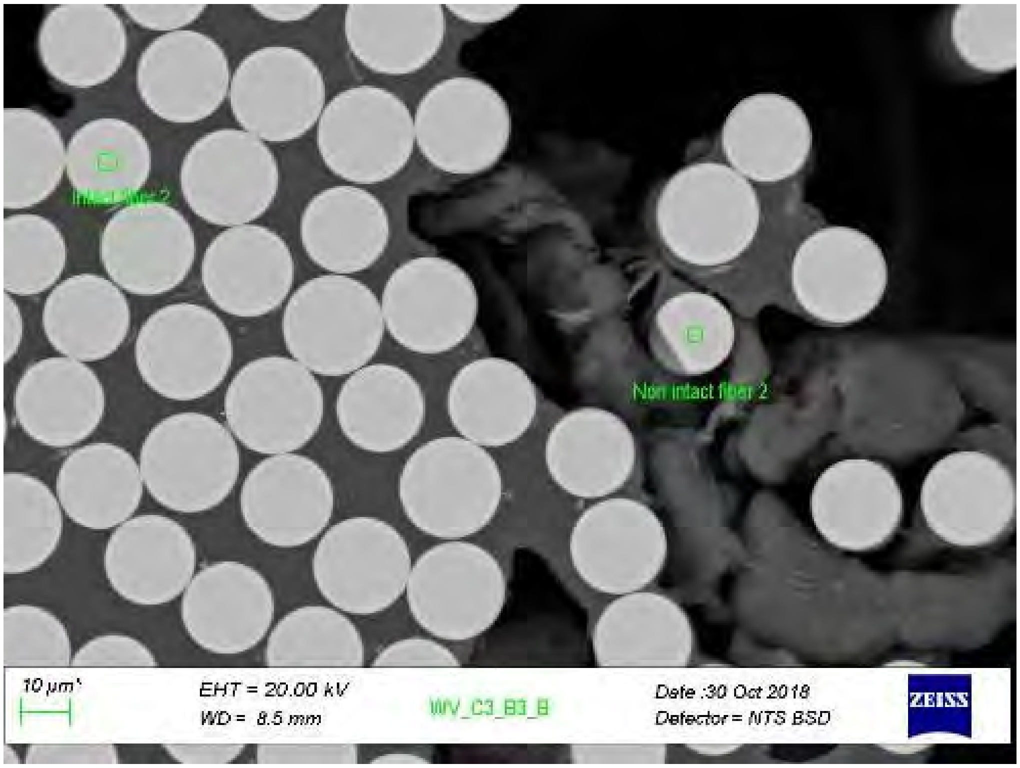

Fig. 68. WV_C3_B3B

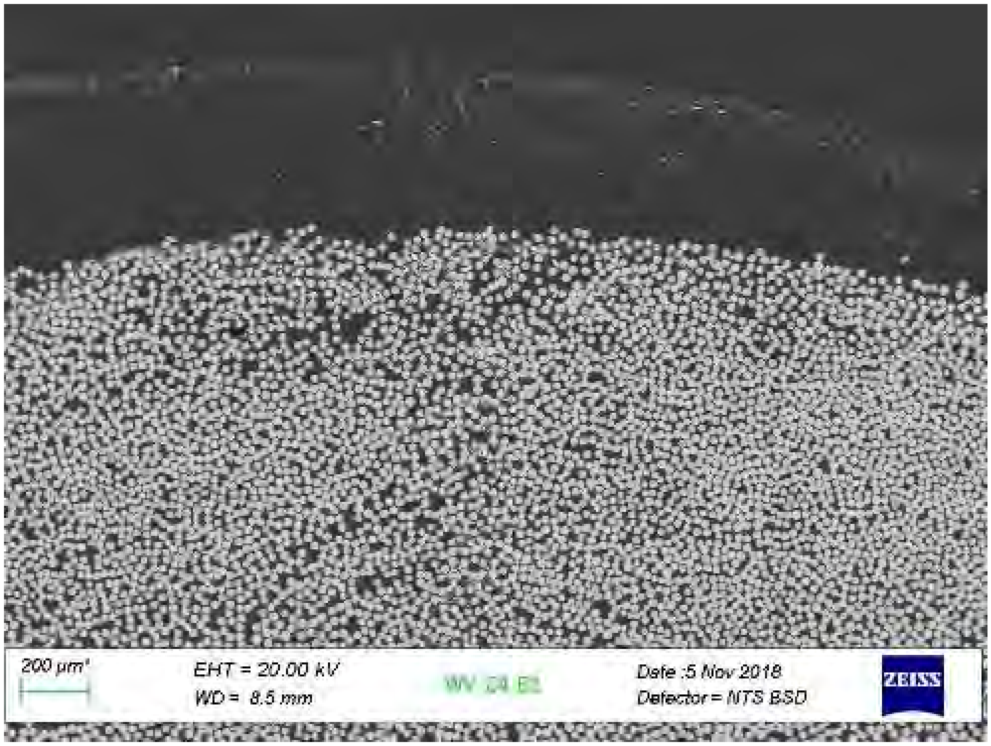

Fig. 69. WV_C4_B2

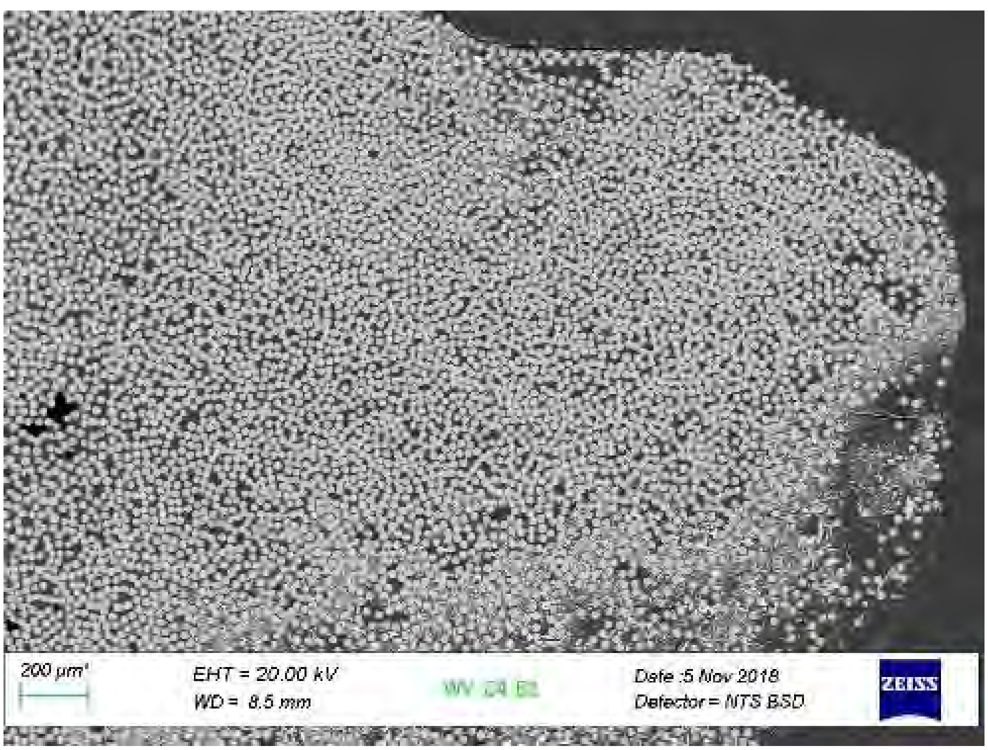

Fig. 70. WV_C4_B2

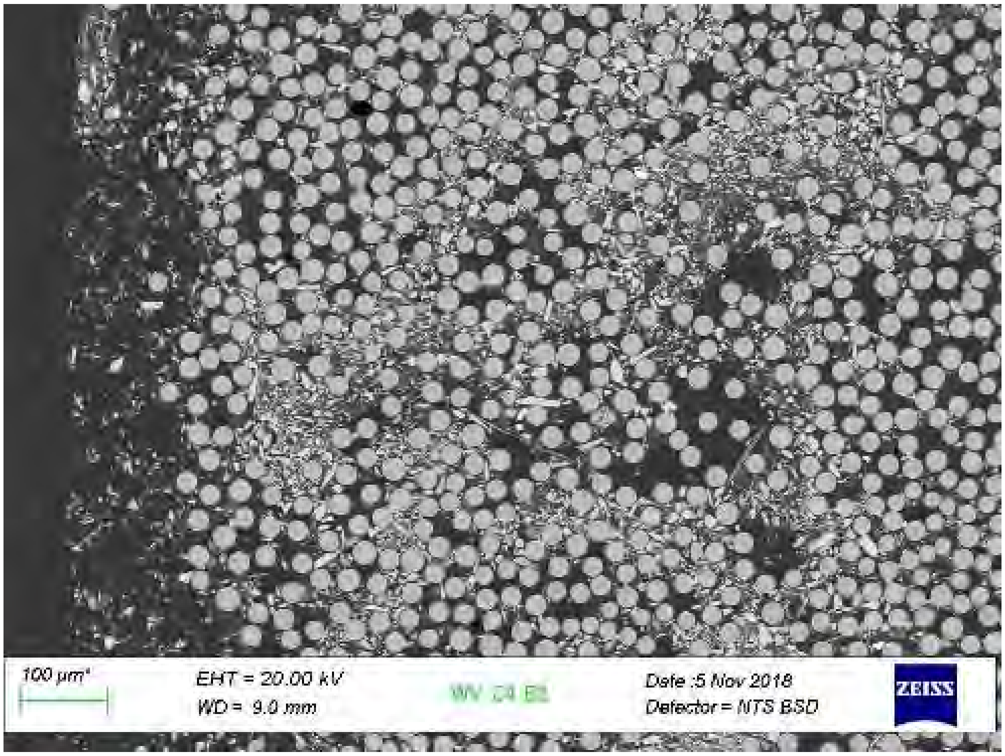

Fig. 71. WV_C4_B2

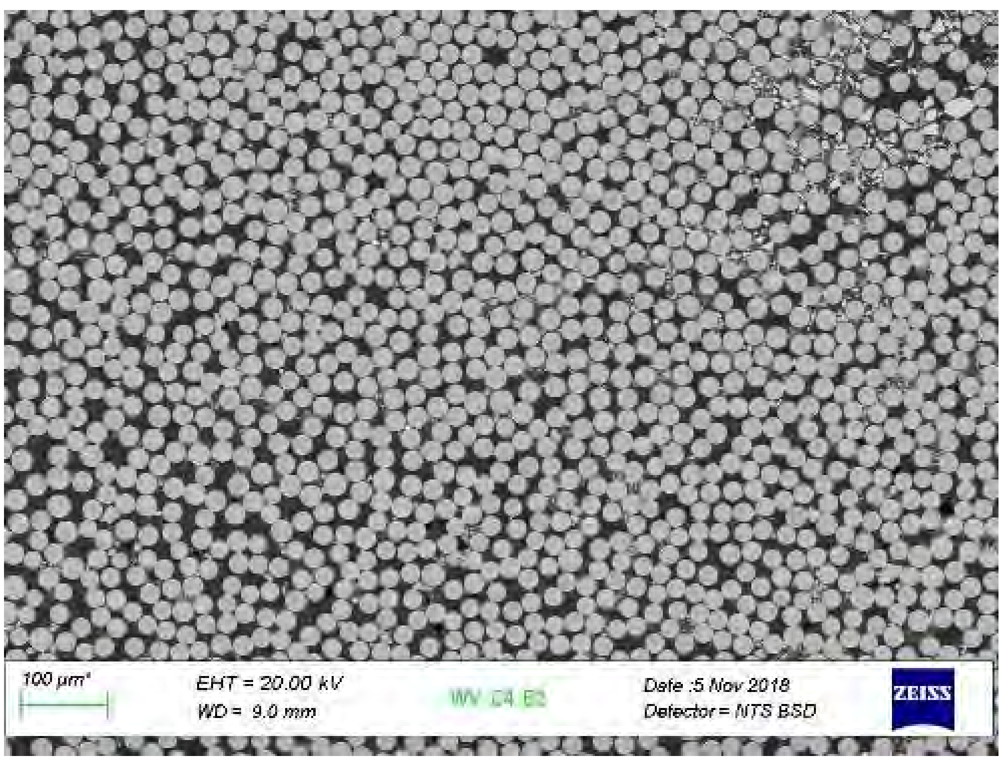

Fig. 72.WV_C4_B2

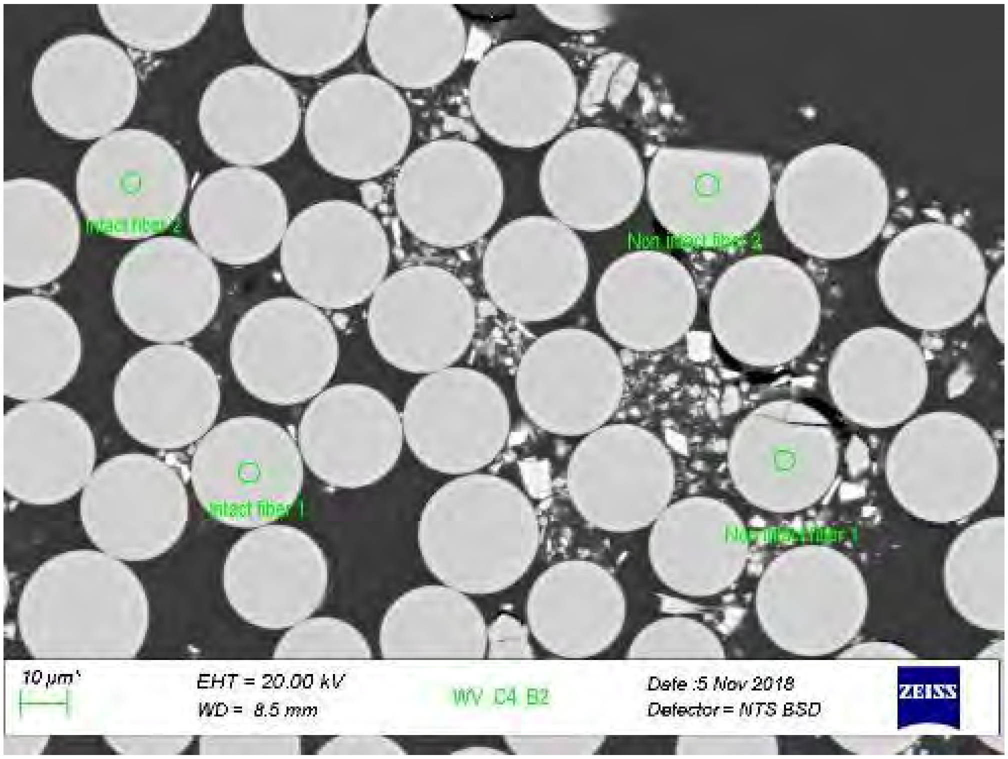

Fig. 73. WV_C4_B2

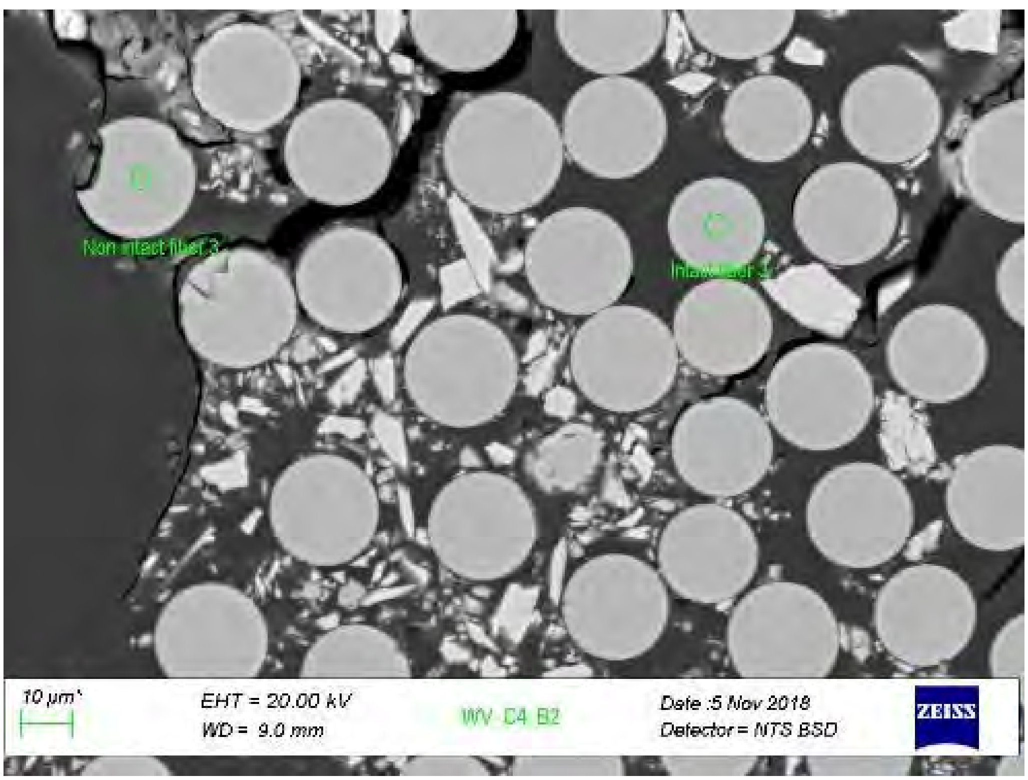

Fig. 74. WV_C4_B2

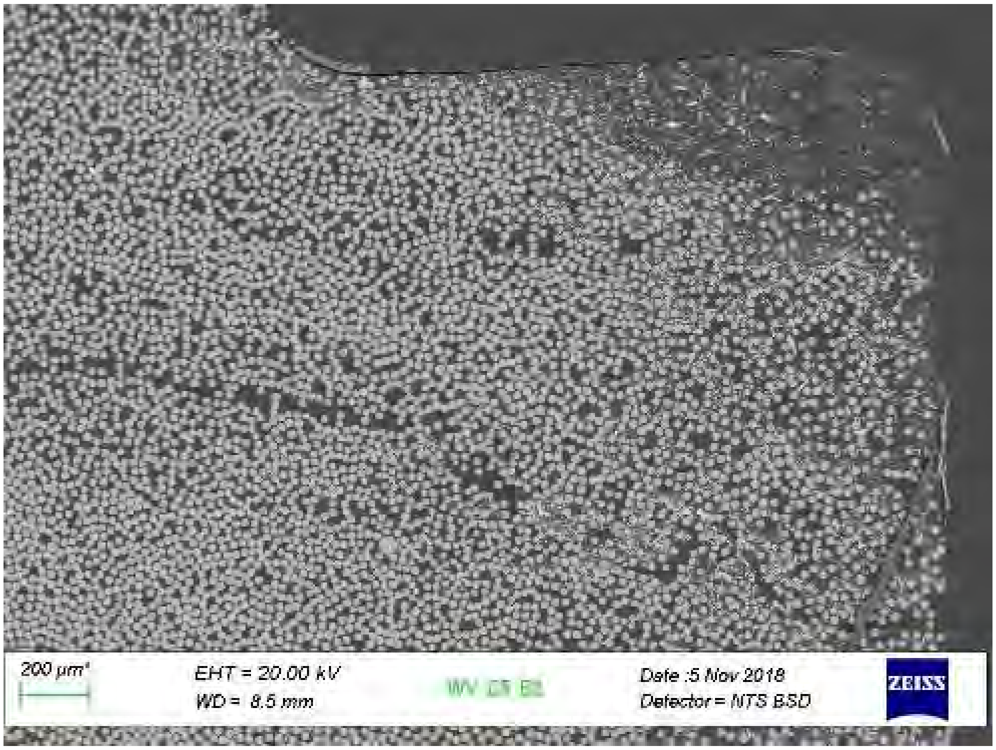

Fig. 75. WV_C5_B2

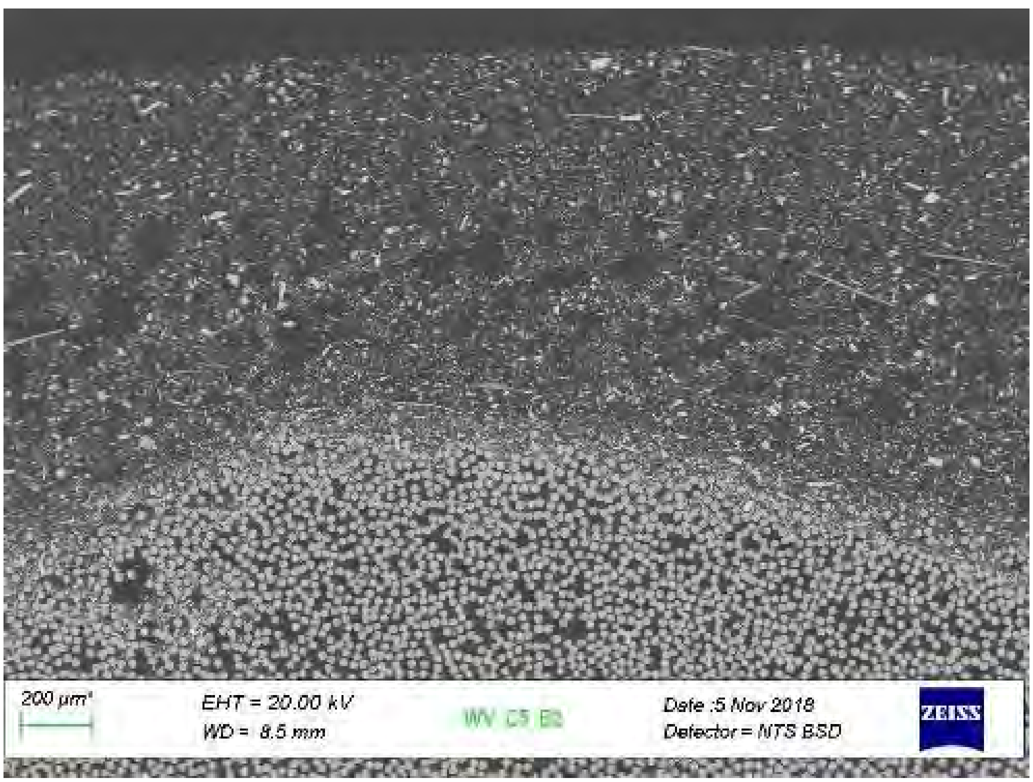

Fig. 76. WV_C5_B2

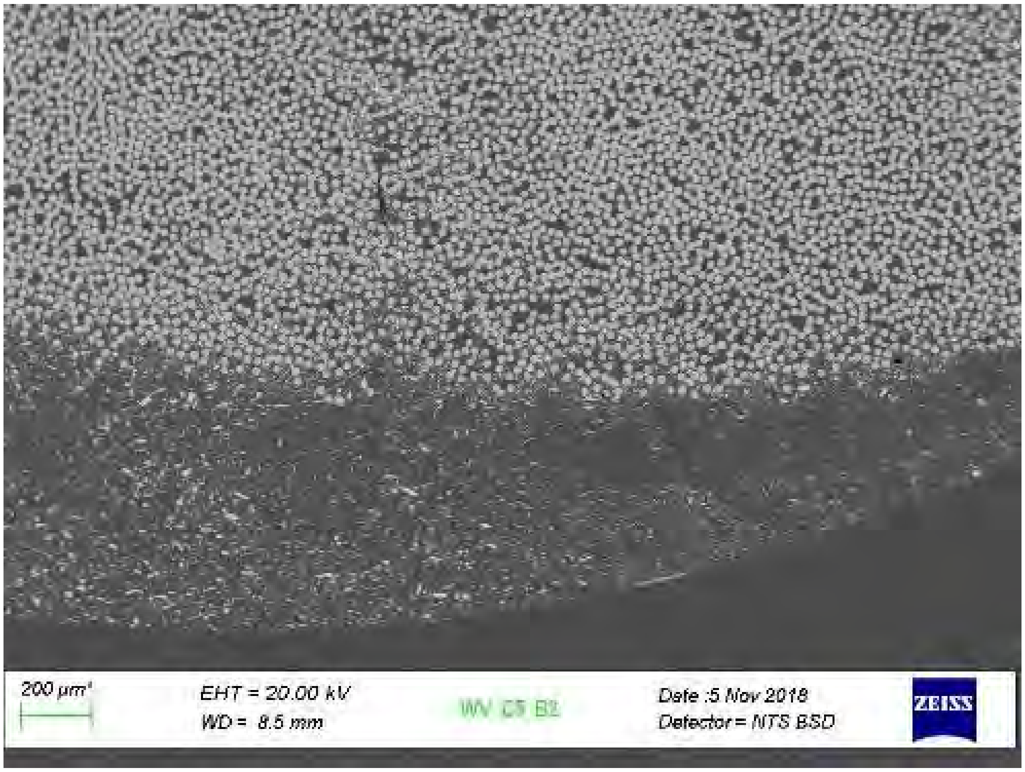

Fig. 77. WV_C5_B2

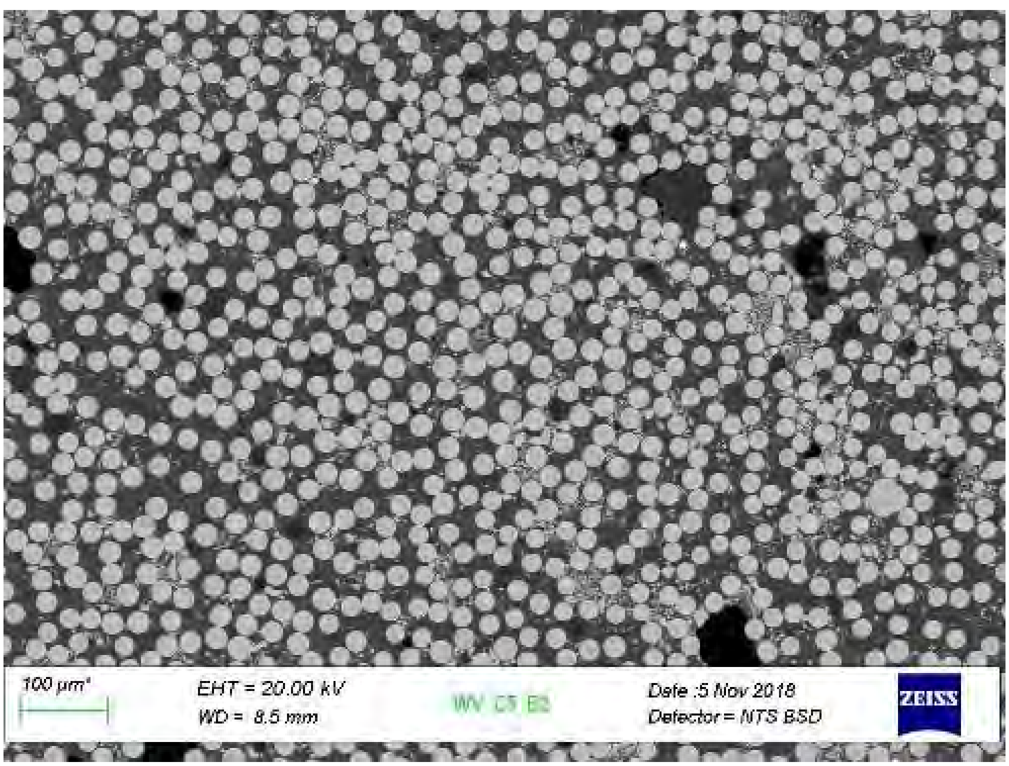

Fig. 78. WV_C5_B2

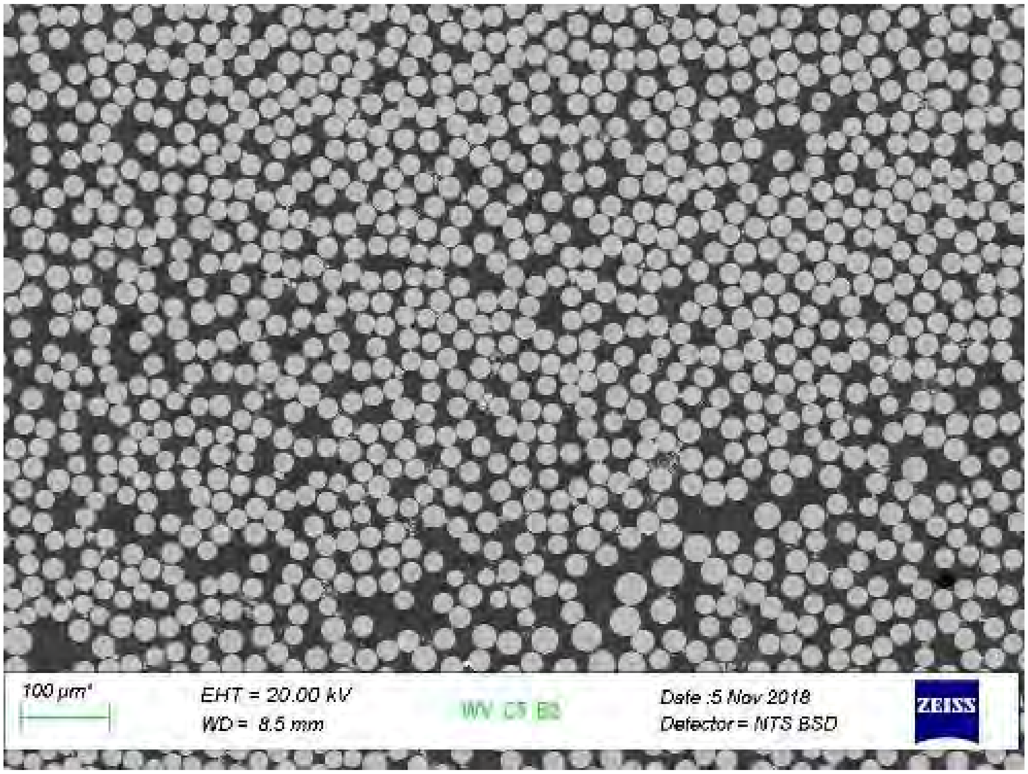

Fig. 79. WV_C5_B2

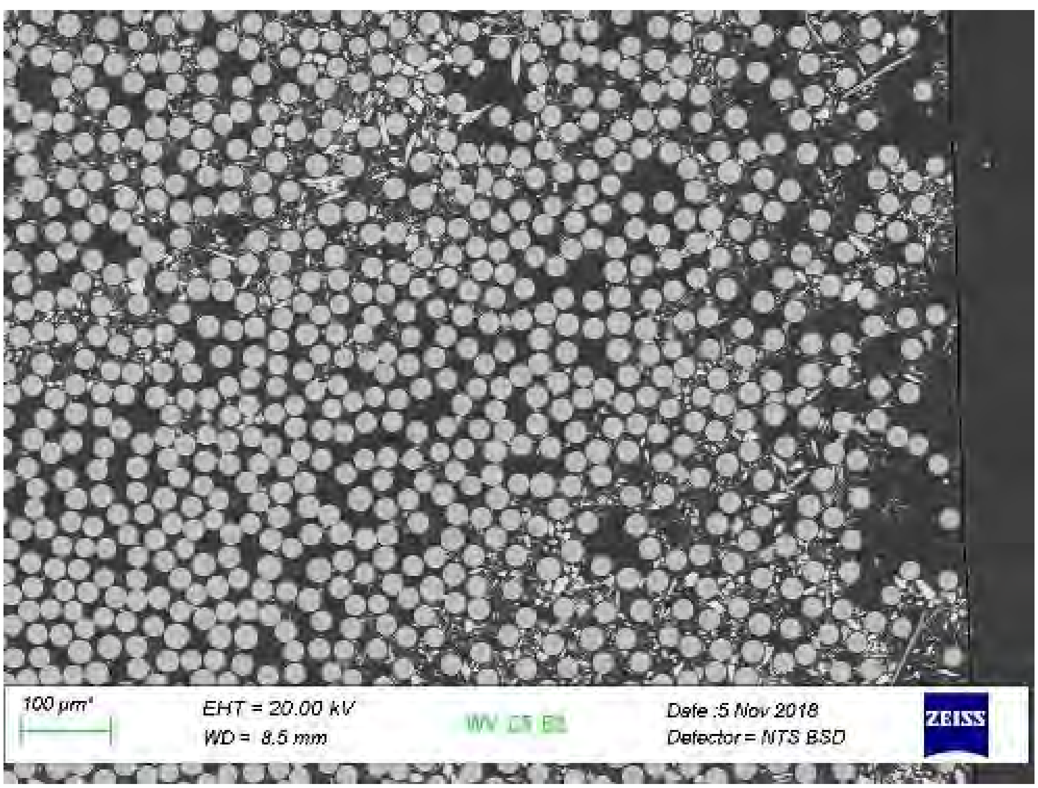

Fig. 80. WV_C5_B2

1.7 Thayer Road

SEM imaging for *Thayer Road Bridge* was performed at Owens Corning. A few negatively affected fibers were observed but appeared to be isolated on the outer perimeter of in-service rebar. The affected fibers only indicated physical damage, likely from manufacturing process. Extrapolated damage was not visible in this sample. Swirls observed in optical microscopy can be seen in low magnification images and are related to resin rich areas. The SEM imaging of each bar is shown in Fig. 81 through Fig. 98.

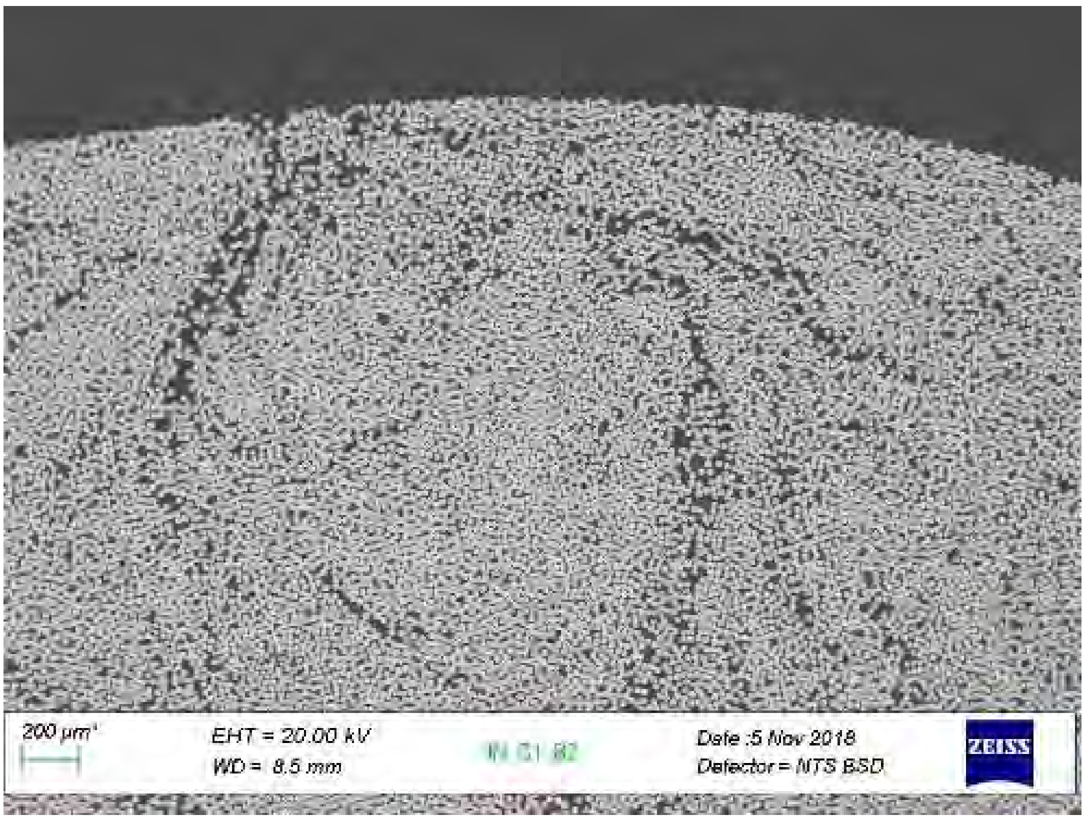

Fig. 81. IN_C1_B2

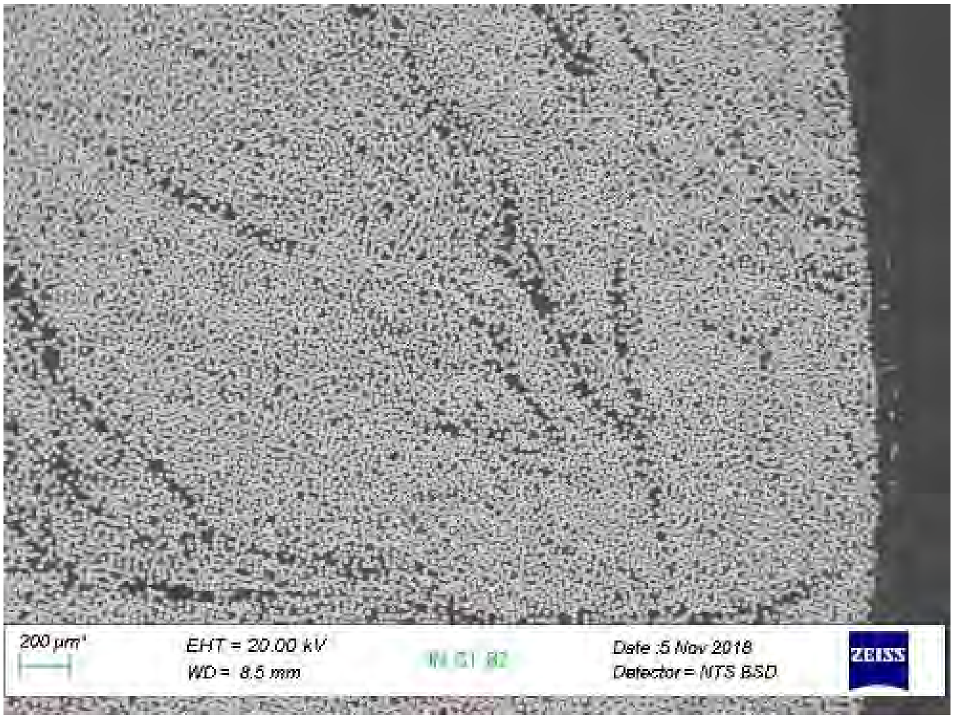

Fig. 82. IN_C1_B2

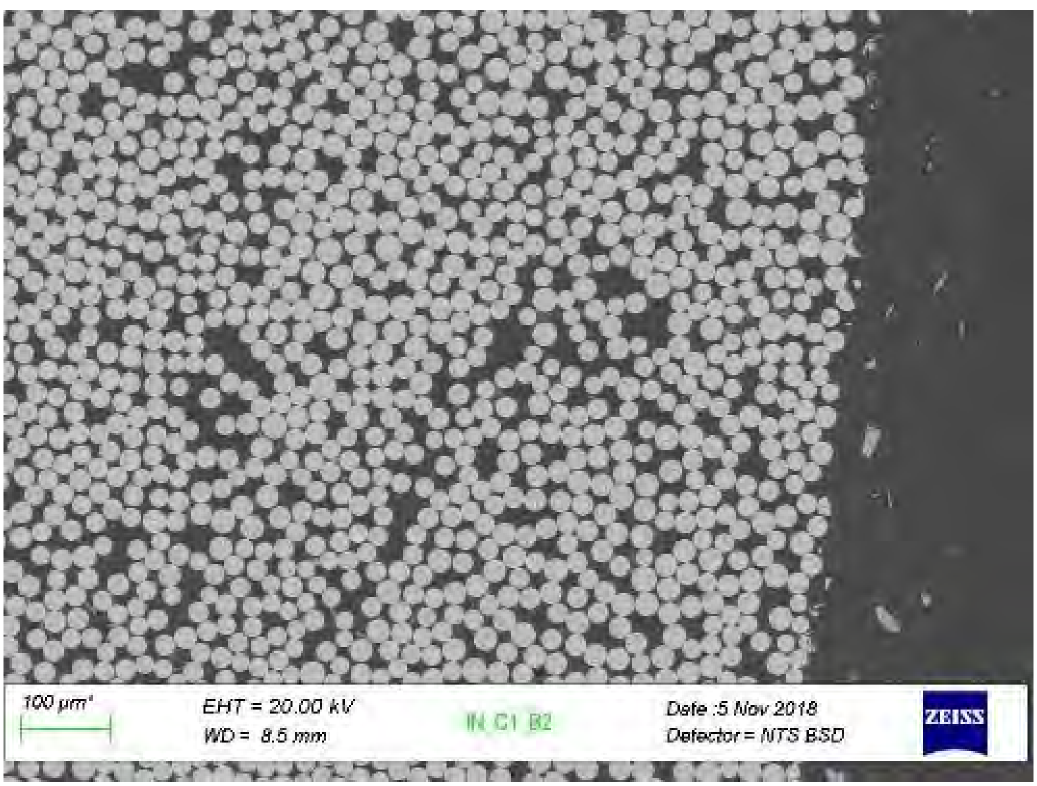

Fig. 83. IN_C1_B2

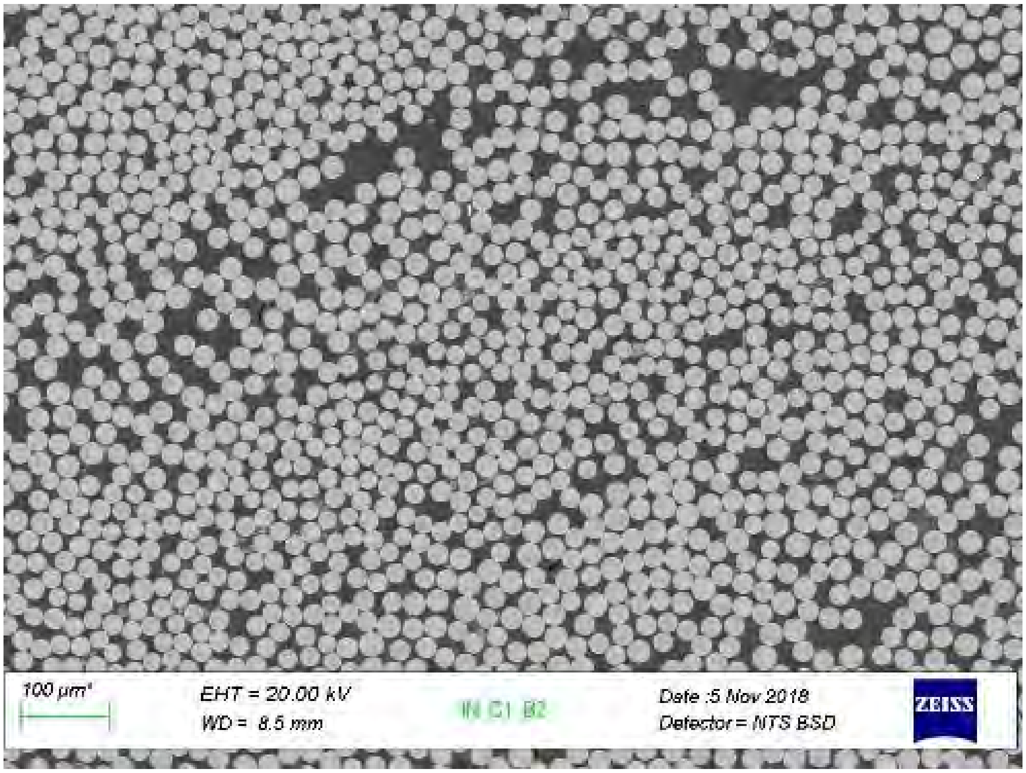

Fig. 84. IN_C1_B2

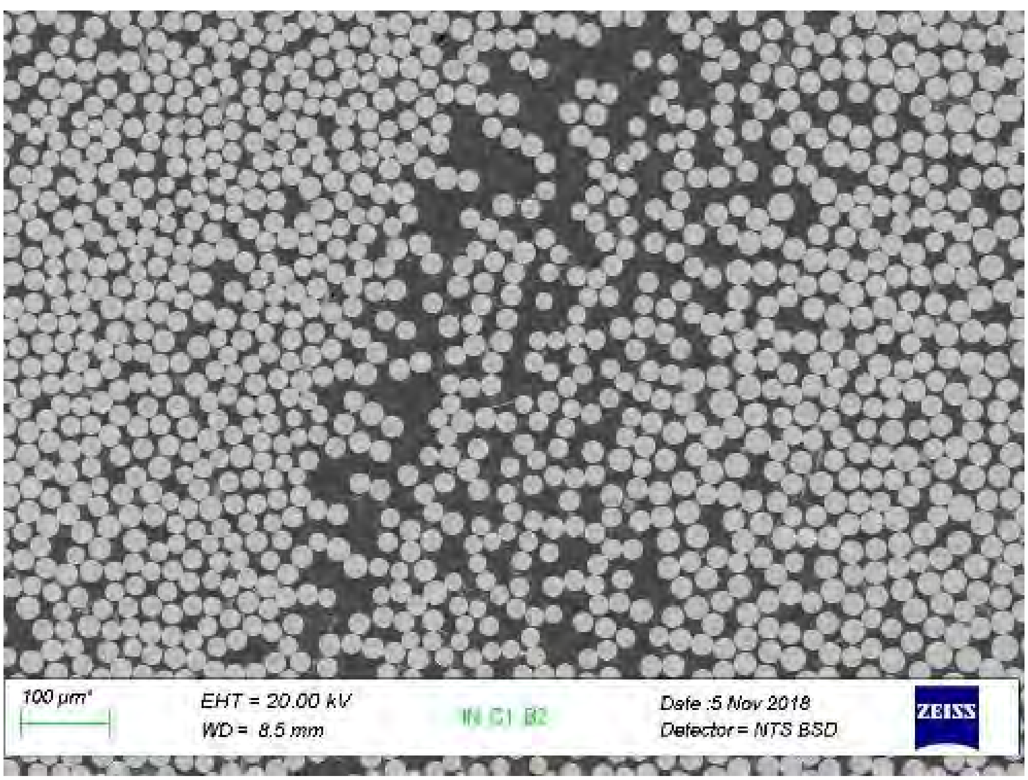

Fig. 85. IN_C1_B2

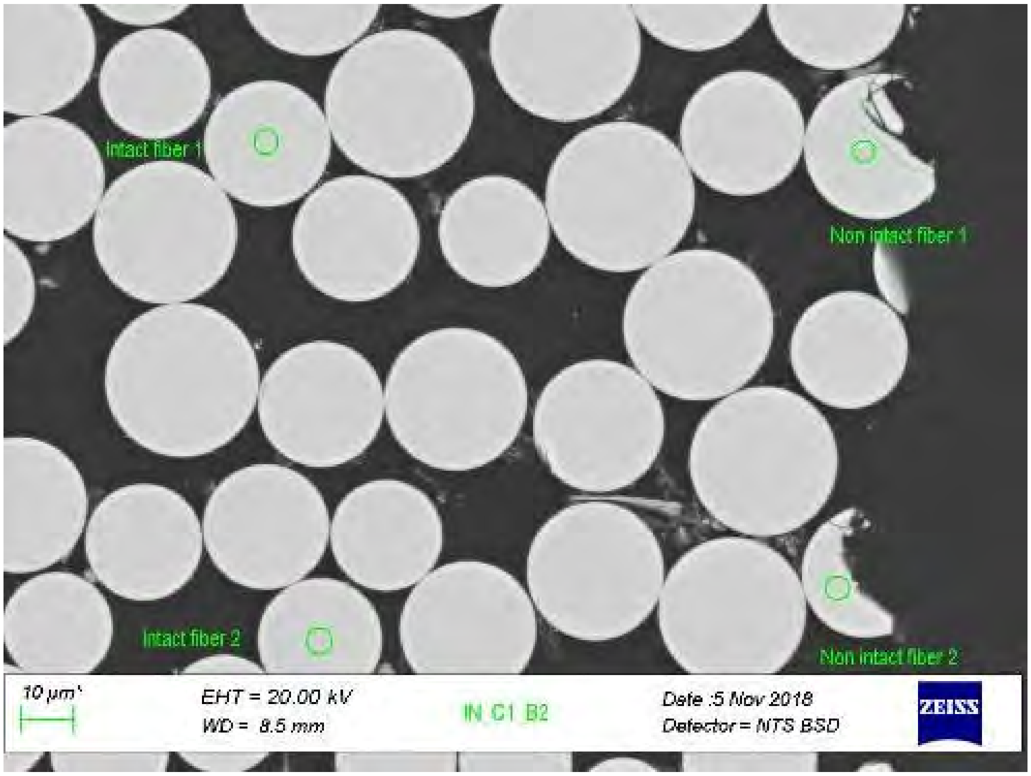

Fig. 86. IN_C1_B2

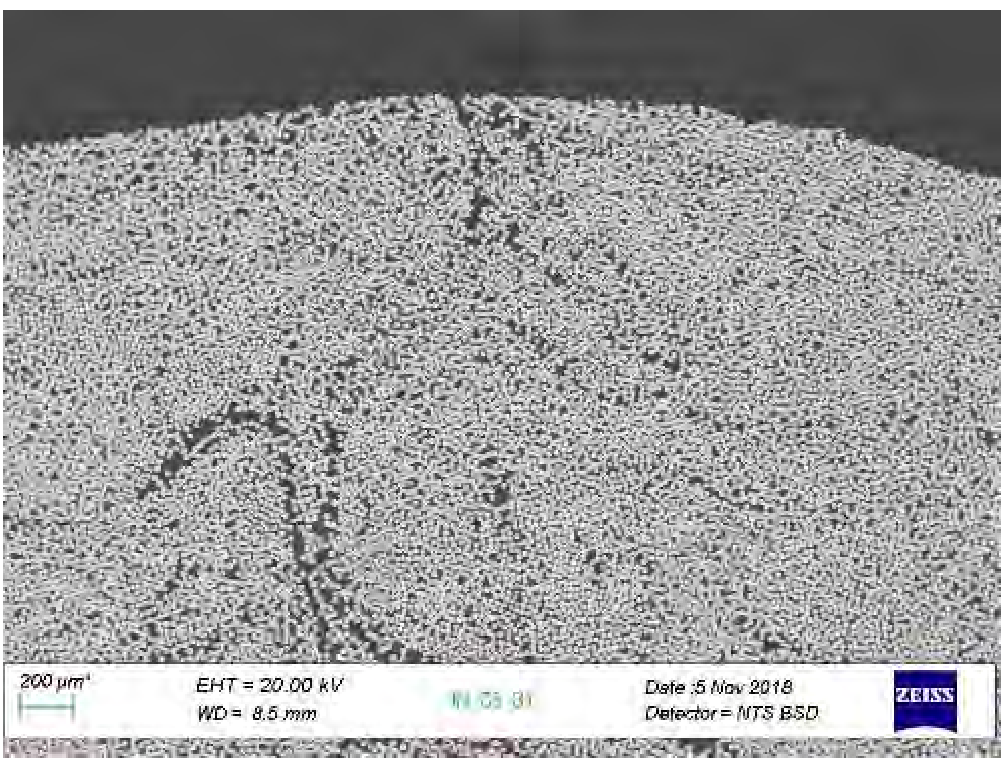

Fig. 87. IN_C5_B1

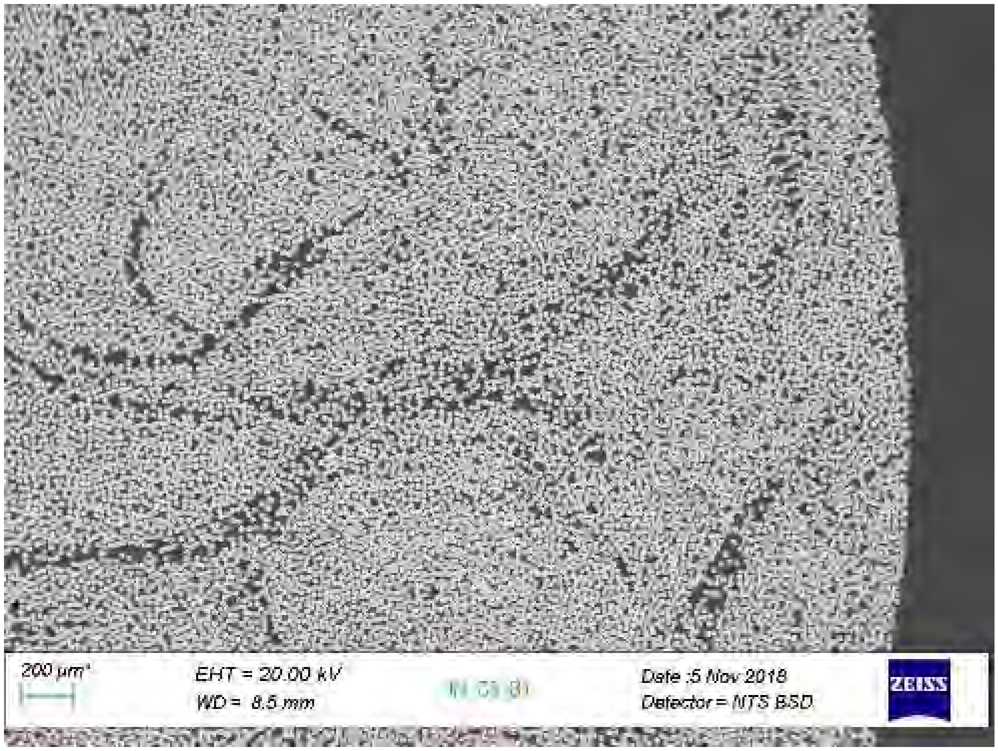

Fig. 88. IN_C5_B1

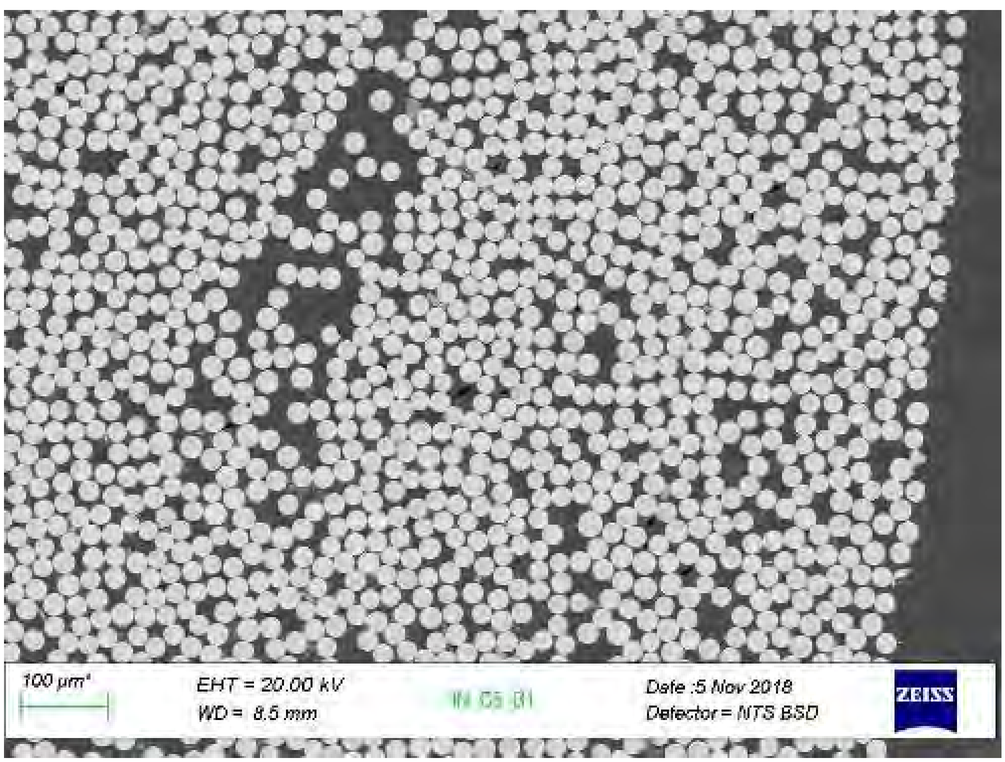

Fig. 89. IN_C5_B1

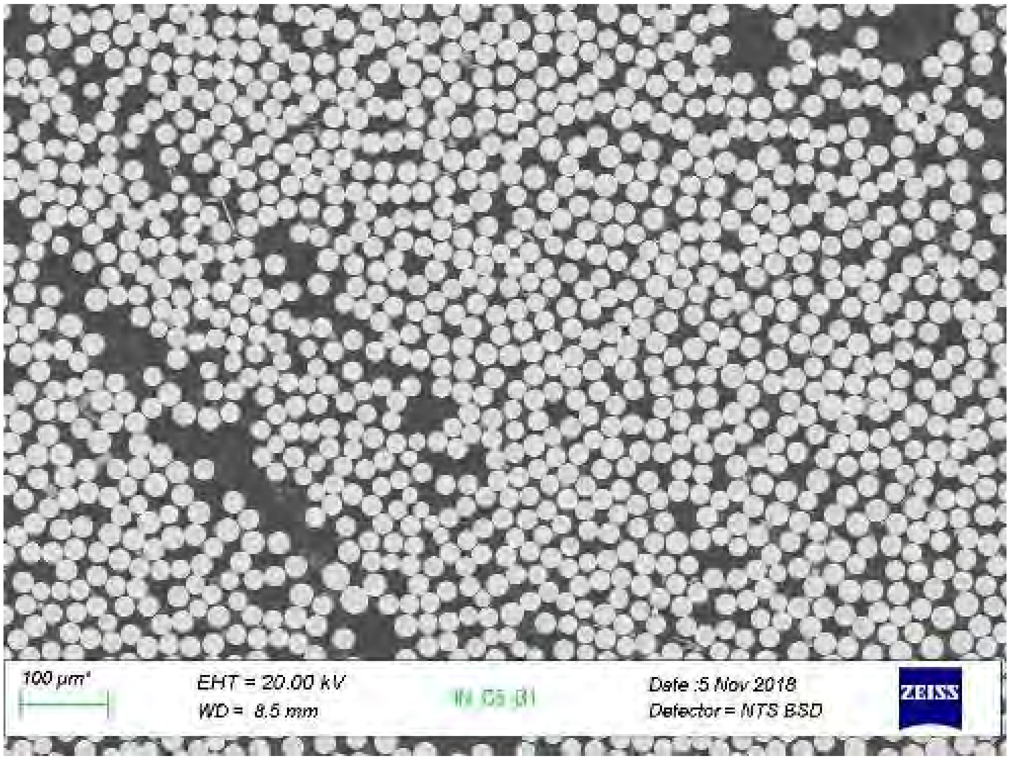

Fig. 90. IN_C5_B1

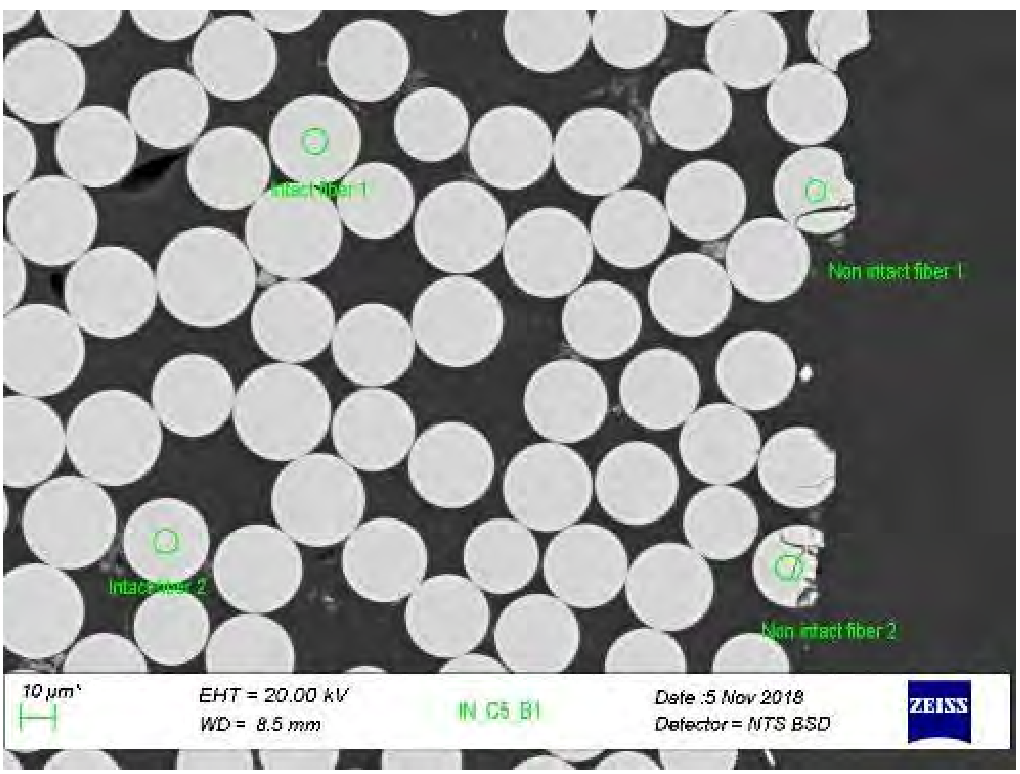

Fig. 91. IN_C5_B1

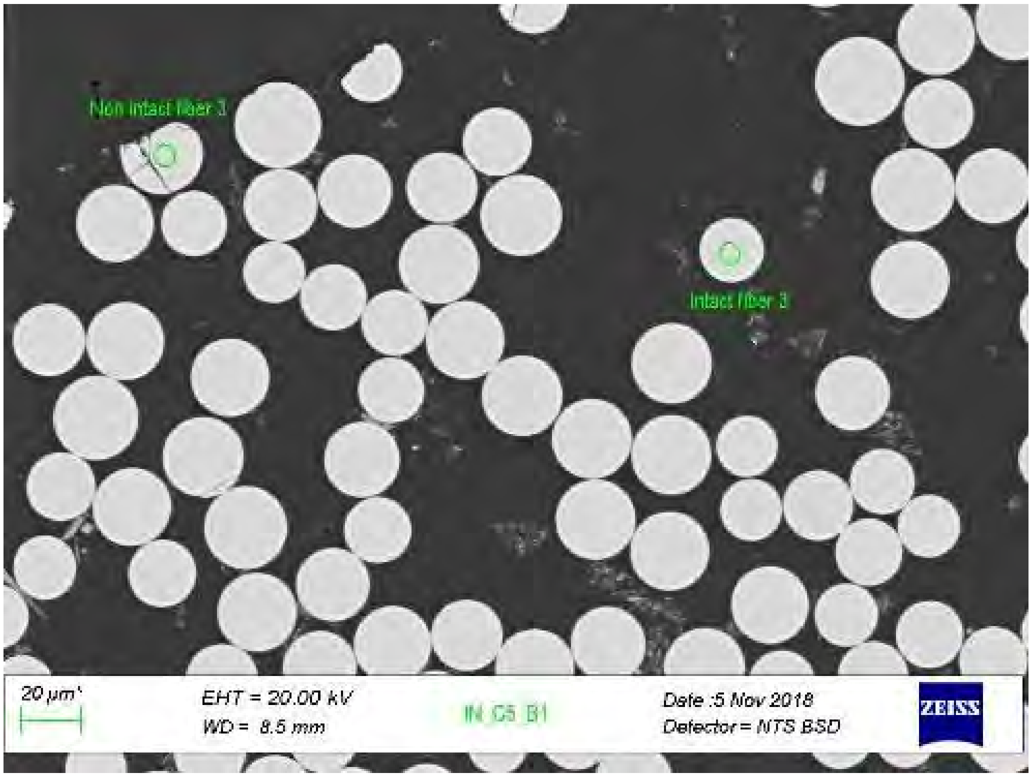

Fig. 92. IN_C5_B1

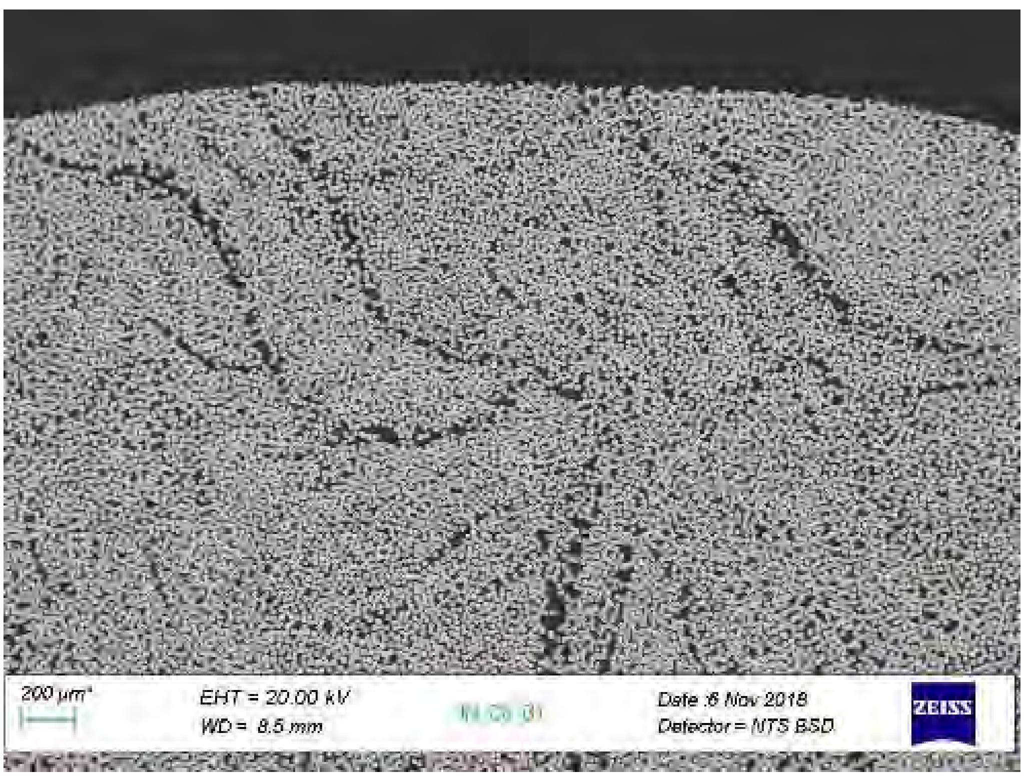

Fig. 93. IN_C6_B1

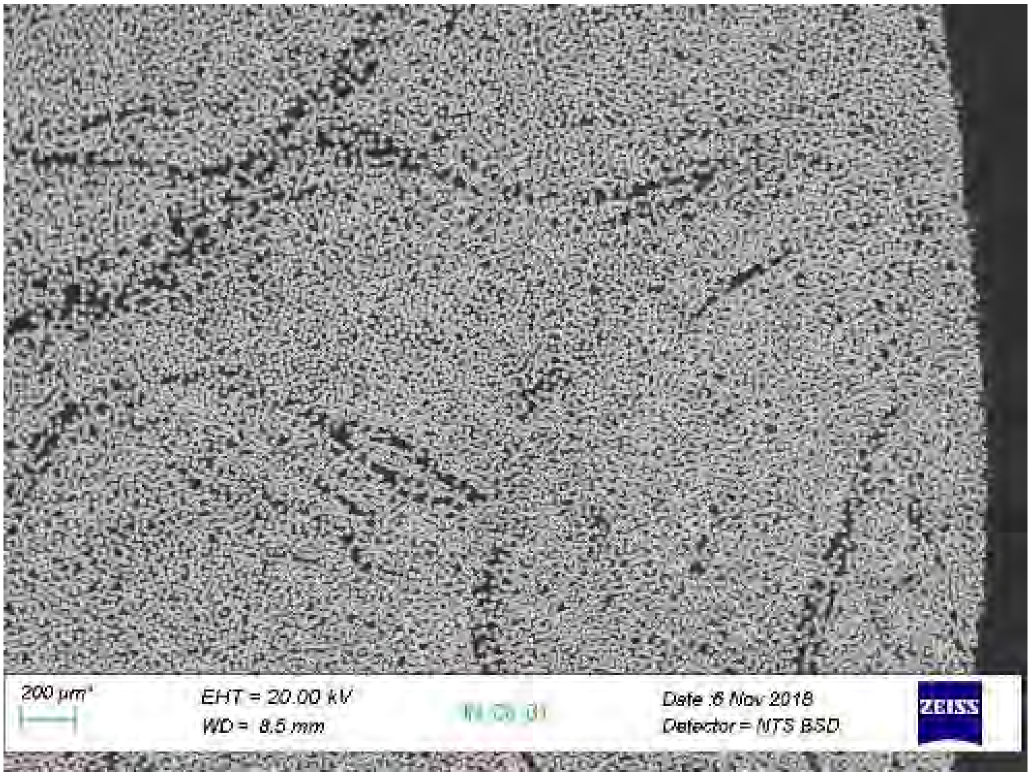

Fig. 94. IN_C6_B1

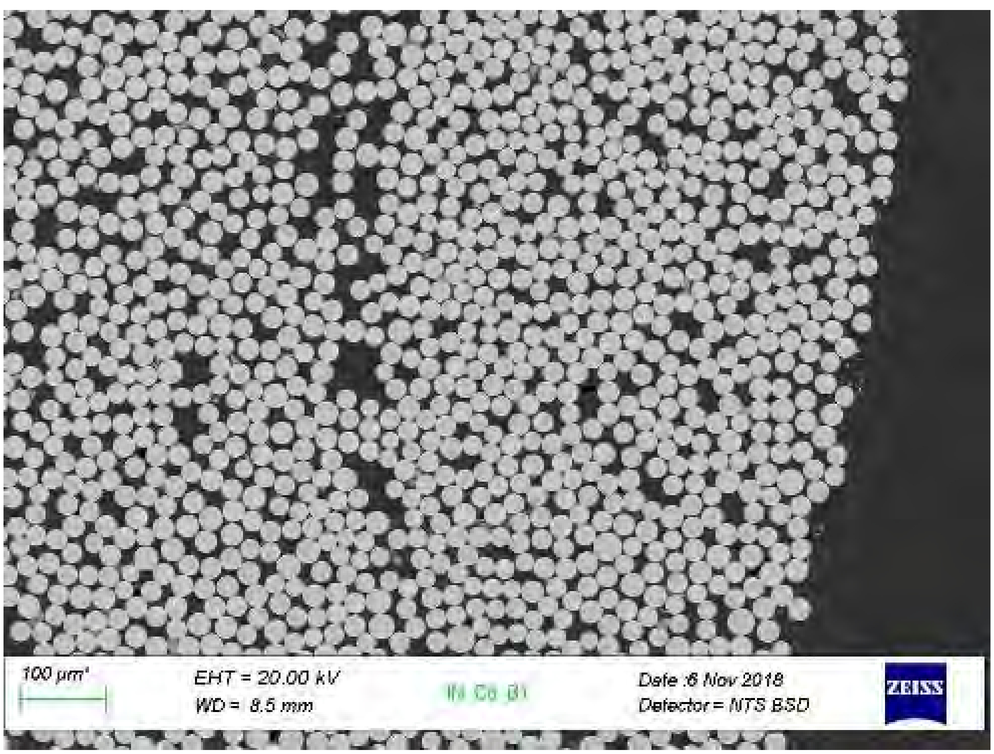

Fig. 95. IN_C6_B1

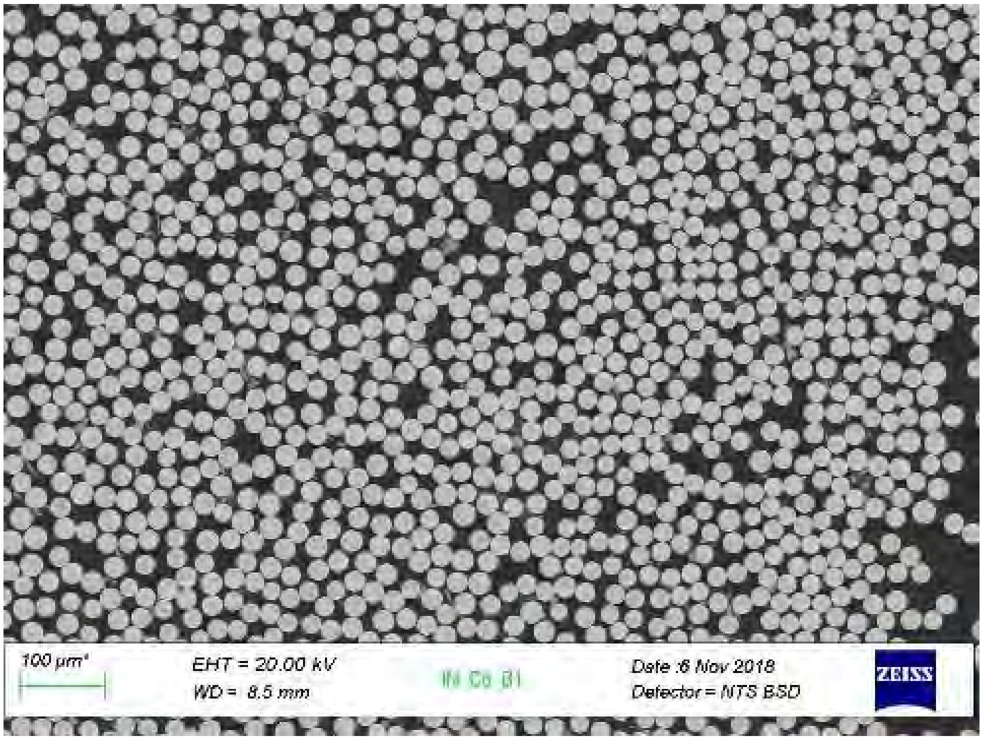

Fig. 96. IN_C6_B1

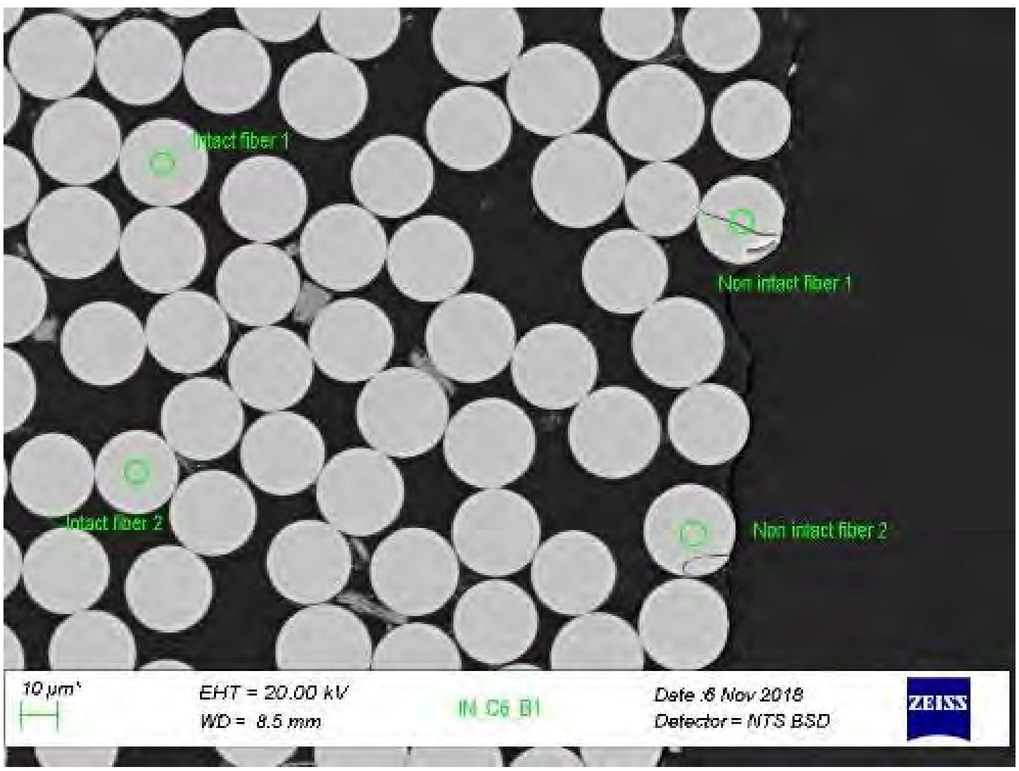

Fig. 97. IN_C6_B1

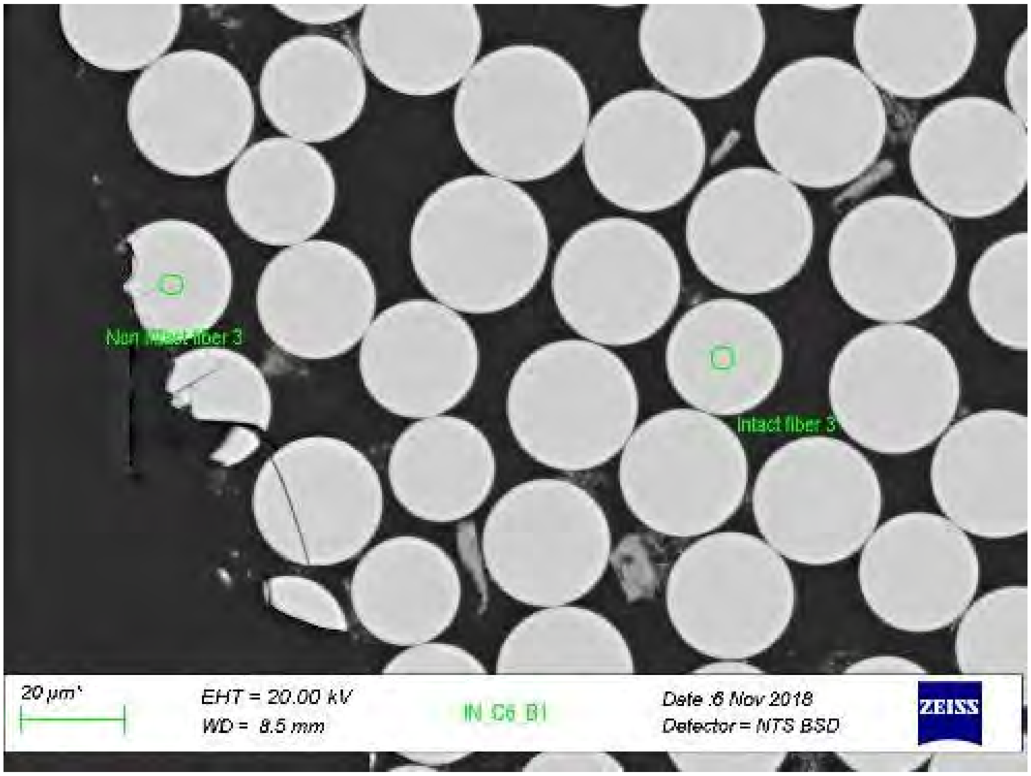

Fig. 98. IN_C6_B1

1.8 Roger’s Creek

SEM imaging for *Roger’s Creek Bridge* was performed at Owens Corning. The fibers from *Roger’s Creek Bridge* showed some evidence of being negatively affected by concrete exposure. Of the few negatively affected, they were located on the exterior or near large cracks. The number of affected fibers is expected to be similar or less than the Cuyahoga or Gills Creek samples. The SEM imaging of each bar is shown in Fig. 99 through Fig. 109.

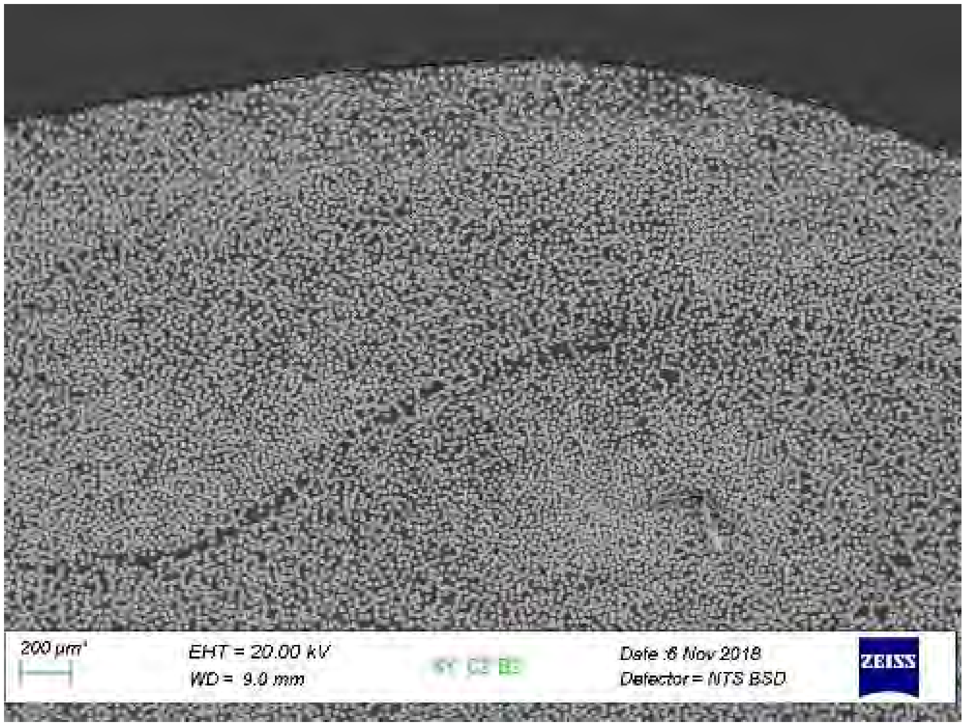

Fig. 99. KY_C2_B2

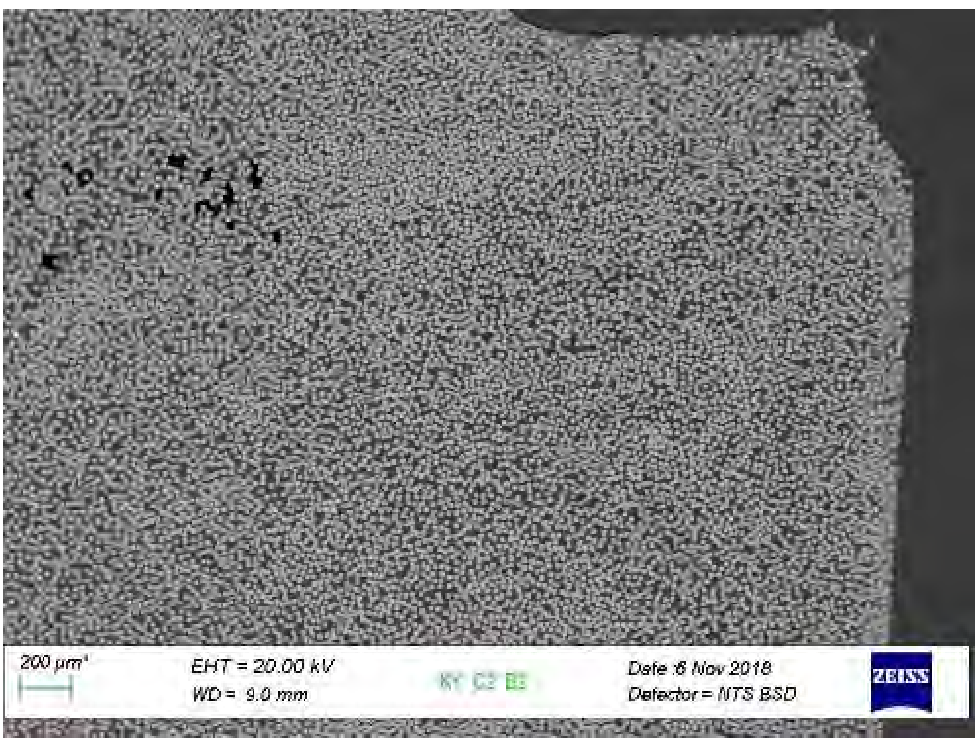

Fig. 100. KY_C2_B2

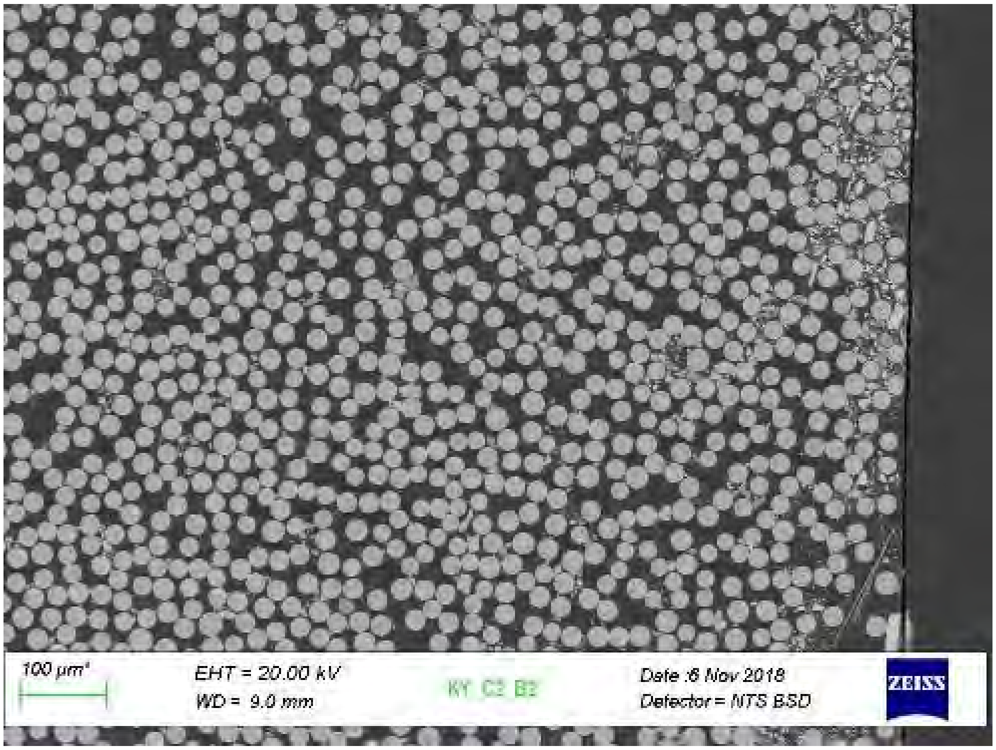

Fig. 101. KY_C2_B2

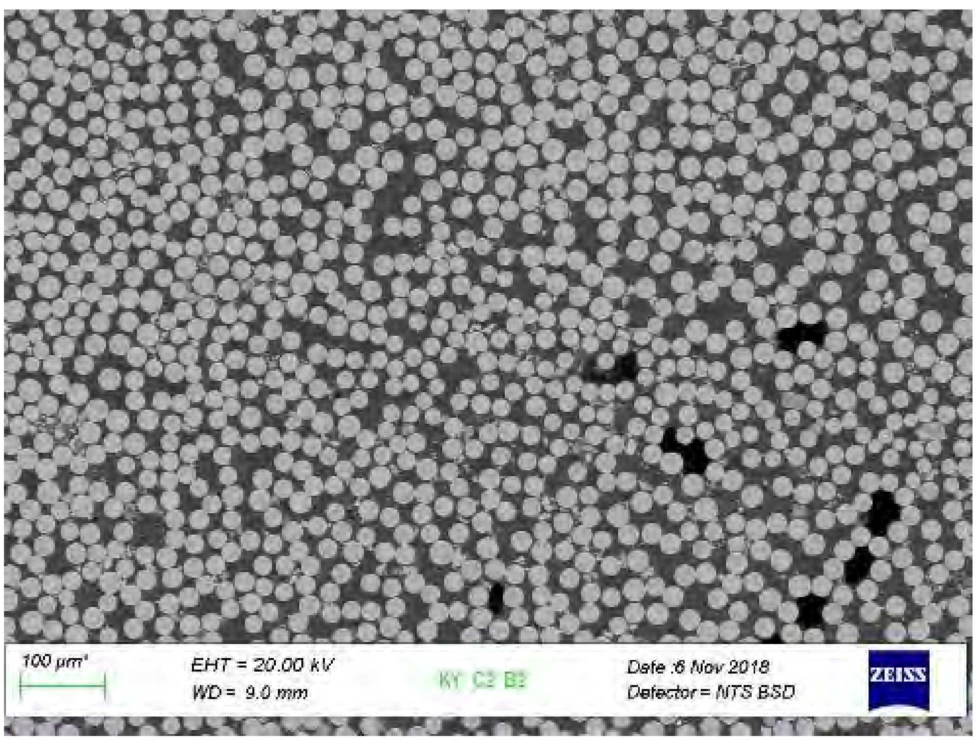

Fig. 102. KY_C2_B2

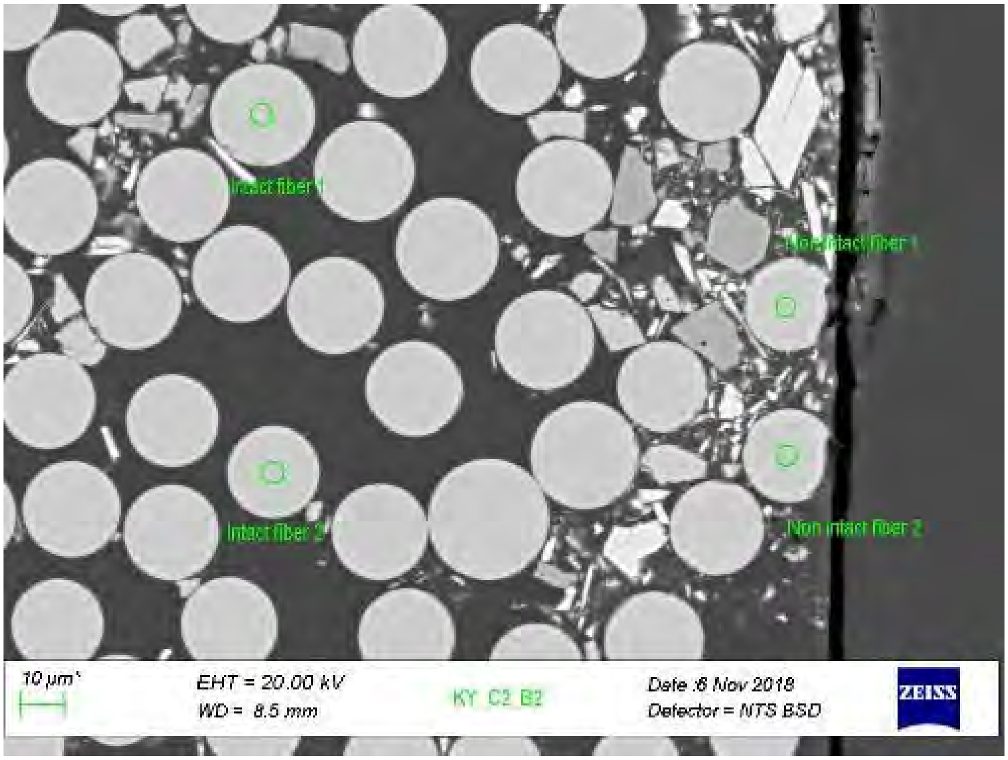

Fig. 103. KY_C2_B2

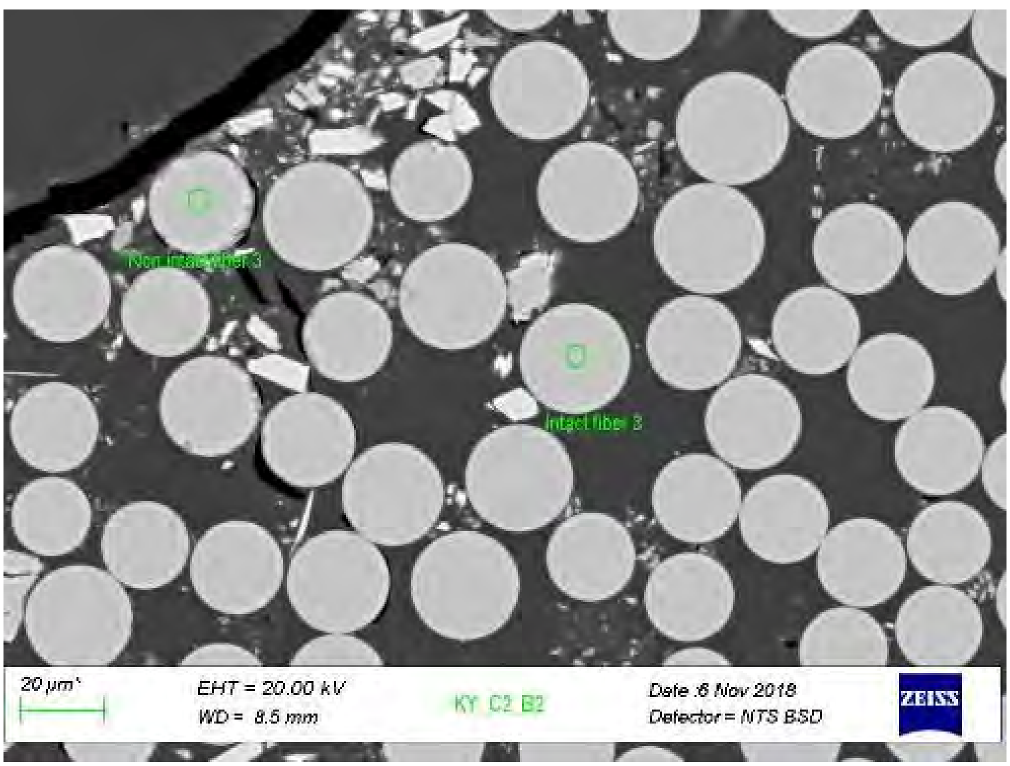

Fig. 104. KY_C2_B2

Fig. 105. KY_C4_B1

Fig. 106. KY_C4_B1

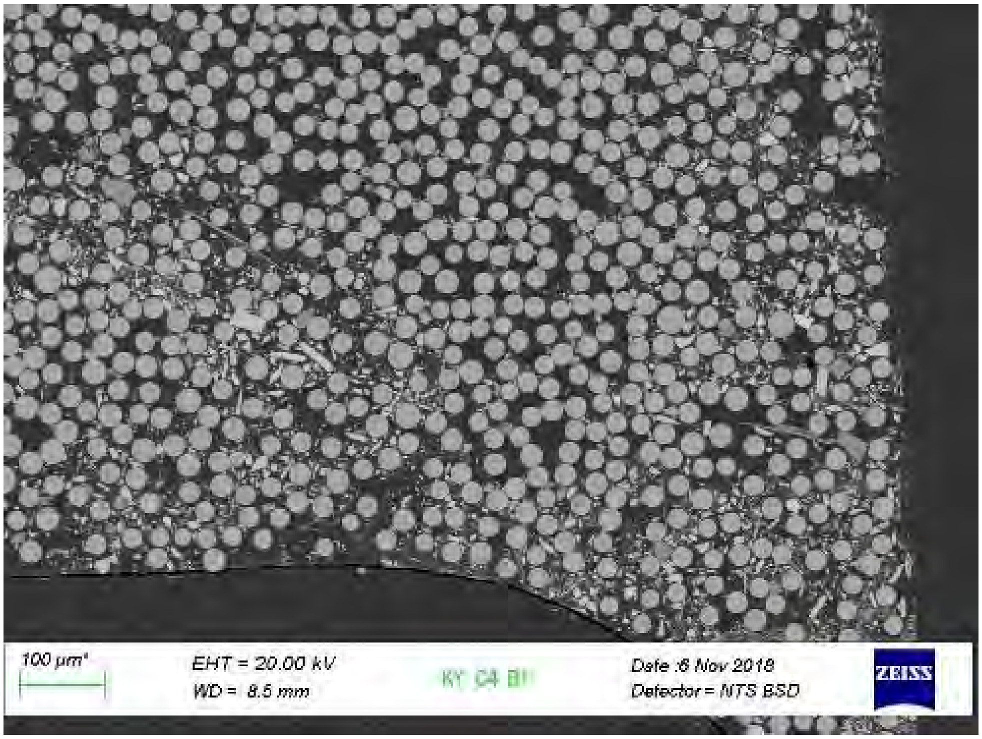

Fig. 107. KY_C4_B1

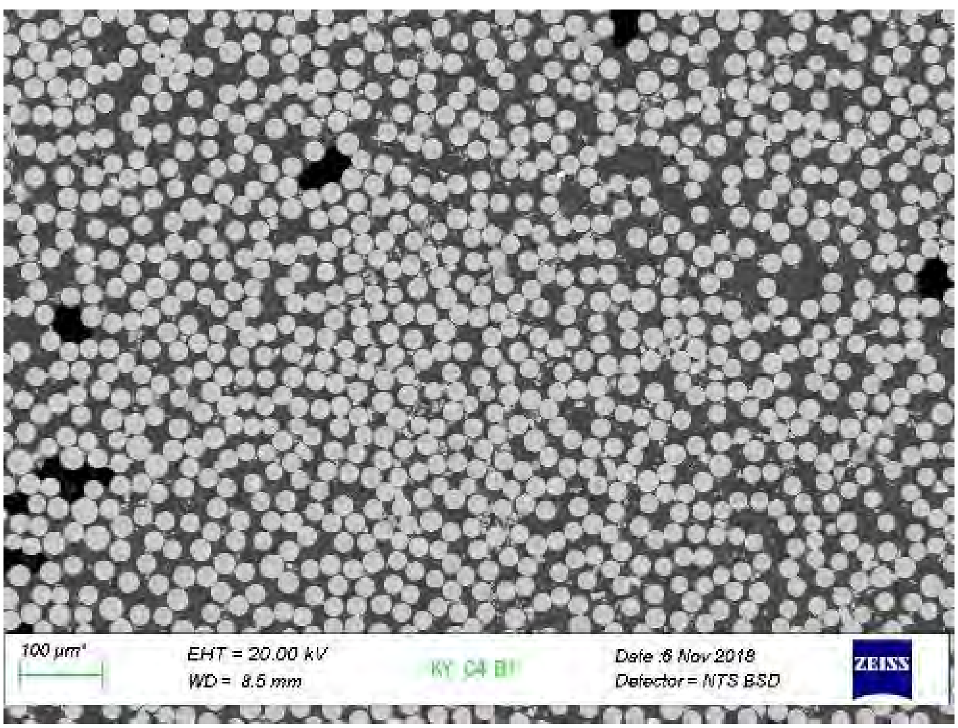

Fig. 108. KY_C4_B1

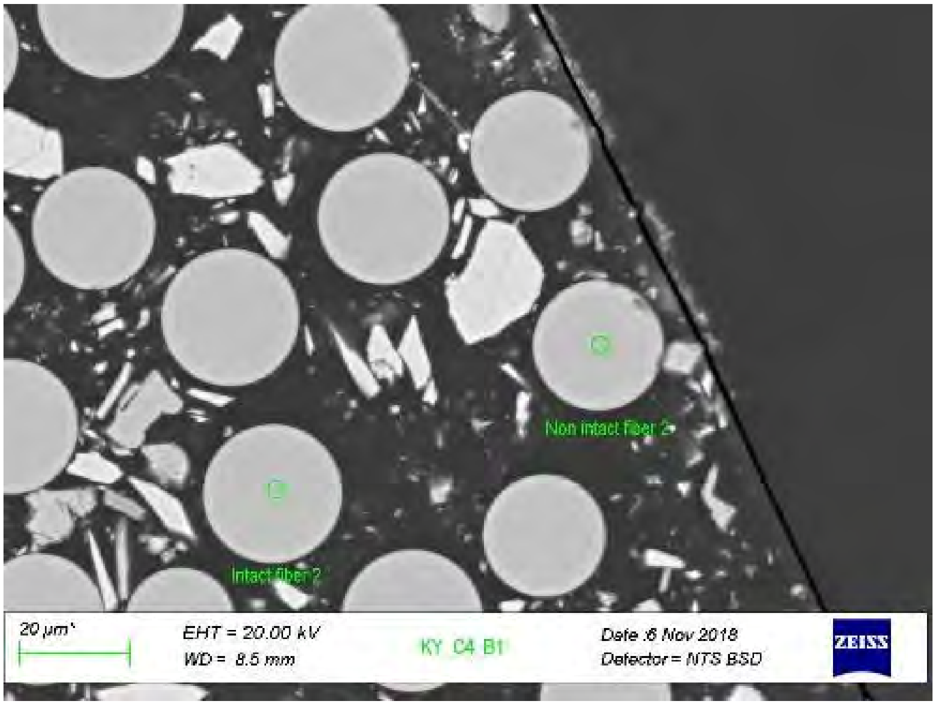

Fig. 109. KY_C4_B1

1.9 Sierrita de la Cruz Creek

SEM imaging for *Sierrita de la Cruz Creek Bridge* was performed at the University of Miami. The results of each bar is shown in Fig. 110 through Fig. 112.

The full cross-sections of three slices of No.5 GFRP bars were scanned at different levels of magnification and images were taken at random locations. A representative image is shown in Fig. 110. The image of a single fiber is shown in Fig. 111.

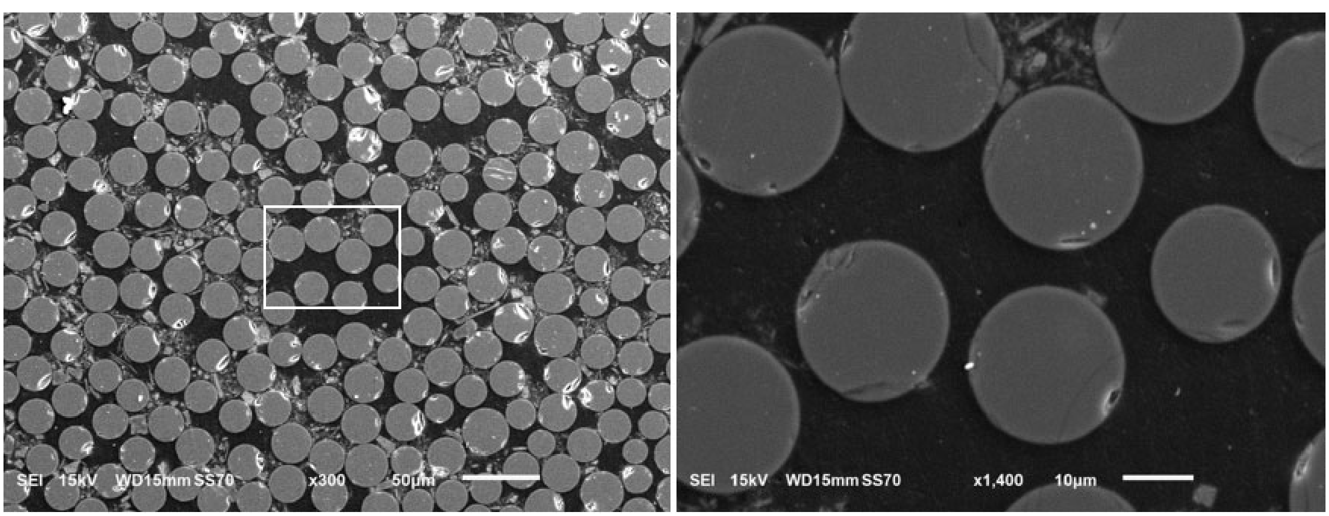

Fig. 110. SEM images of fibers at magnifications of 300X (left) and 1400X (right))

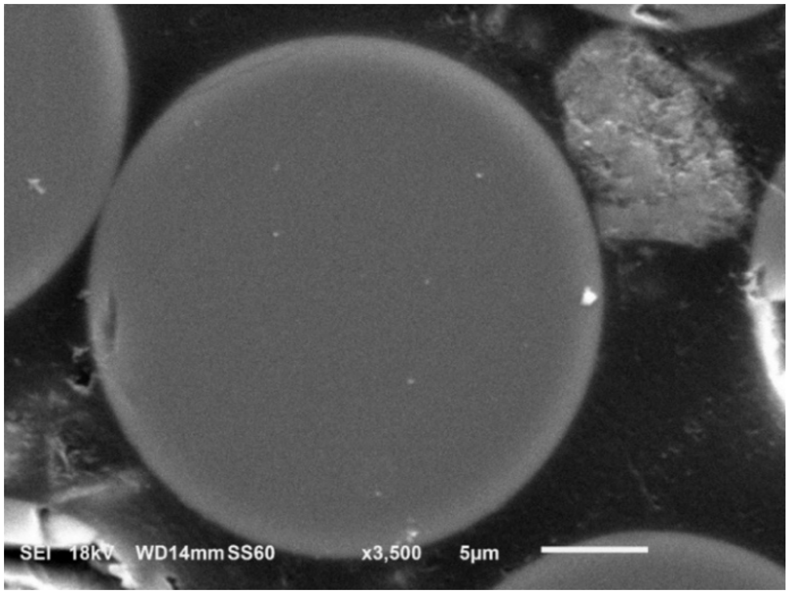

Fig. 111. SEM image of a single fiber at magnification of 3500X

SEM analysis confirmed that there was no sign of deterioration in the GFRP coupons. Glass fibers were intact without a loss of cross-sectional area. Similarly, fibers were surrounded by the resin matrix and no sign of loss of bond between matrix and fiber was observed.

GFRP-to-concrete interfacial bond appeared to be maintained properly and no sign of bond degradation nor loss of contact was observed as presented in Fig. 112. As documented by others (Aftab A. Mufti et al., 2007), the visible interfacial damage was the result of sample preparation and drying in the SEM chamber.

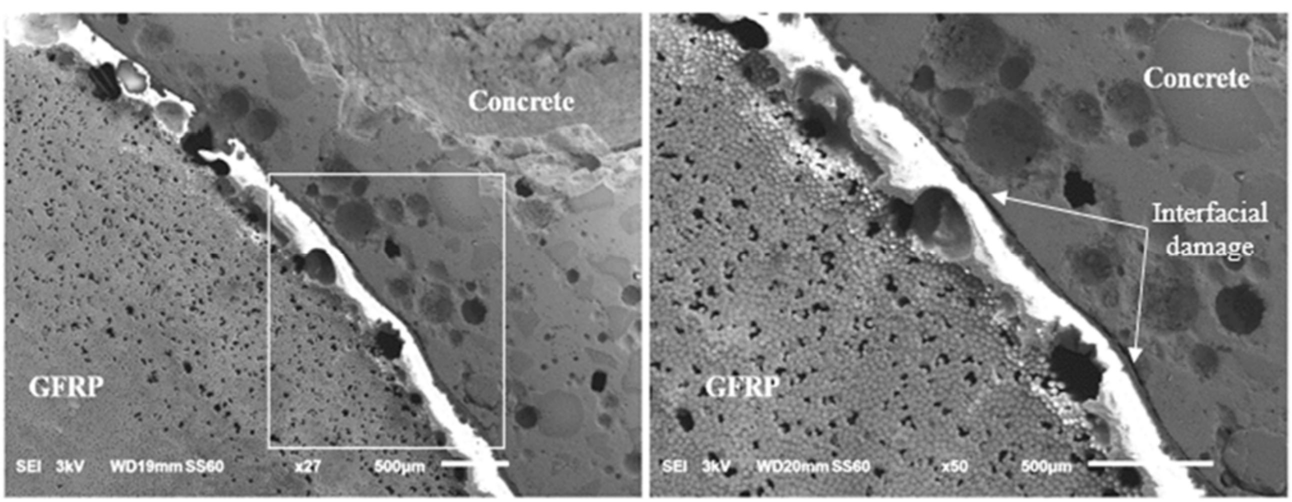

Fig. 112. SEM images of concrete-GFRP interface at magnifications of 27x (left) 50x (right)

1.10 Walker Box Culvert Bridge

SEM imaging for *Walker Box Culvert Bridge* was performed at the University of Miami. The results of each bar is shown in Fig. 110 through Fig. 112.

SEM analysis suggests that there was no apparent sign of deterioration in the GFRP coupons. No damage was observed in the matrix and at the matrix-fiber interface. Glass fibers appeared to be intact without no loss of cross-sectional area.

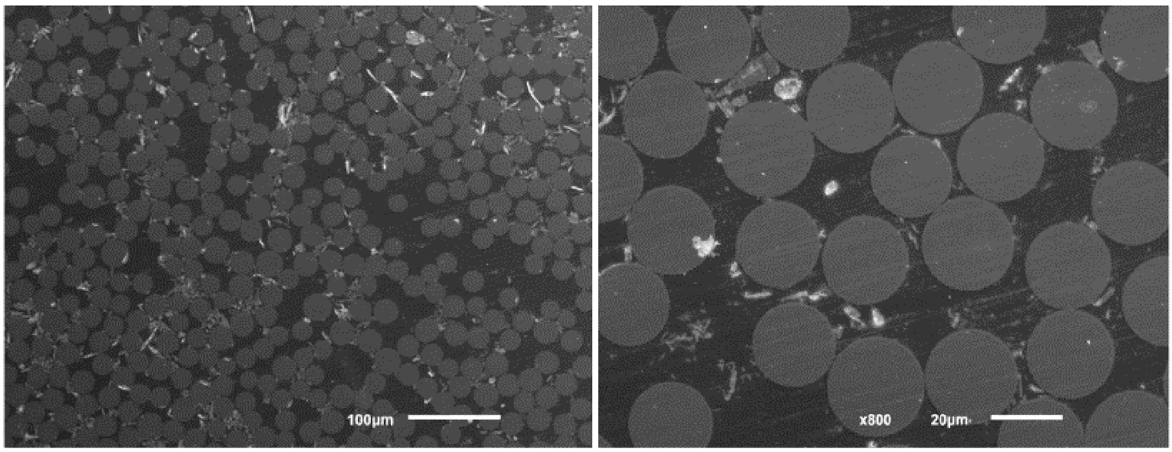

Fig. 113. SEM image of GFRP bar after 16 years of service in Walker Bridge at magnifications of 200x (left) and 800x (right)

1.11 Southview

SEM imaging for *Southview Bridge* was performed at the University of Miami. The results of each bar is shown in Fig. 114 through Fig. 110. SEM analysis suggests that there was no apparent sign of deterioration in the GFRP coupons. No damage was observed in the matrix and at the matrix-fiber interface. Glass fibers appeared to be intact without no loss of cross-sectional area.

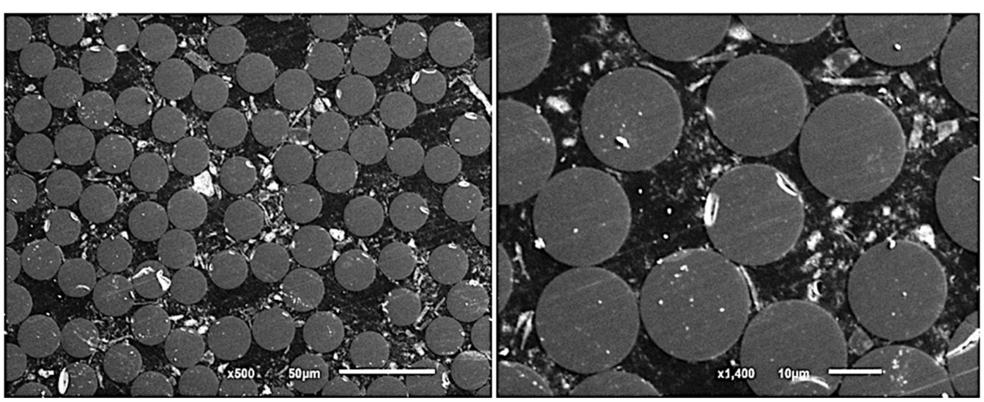

Fig. 114. SEM images of GFRP bar after 11 years if service in Southview Bridge at magnifications of 500x (left) and 1400x (right)

2. EDS

2.1 Bettendorf

EDS for *Sierrita de la Cruz Creek Bridge* was performed at the University of Miami using the method described in Section 4.1.5. Results are shown in Fig. 115 through Fig. 124.

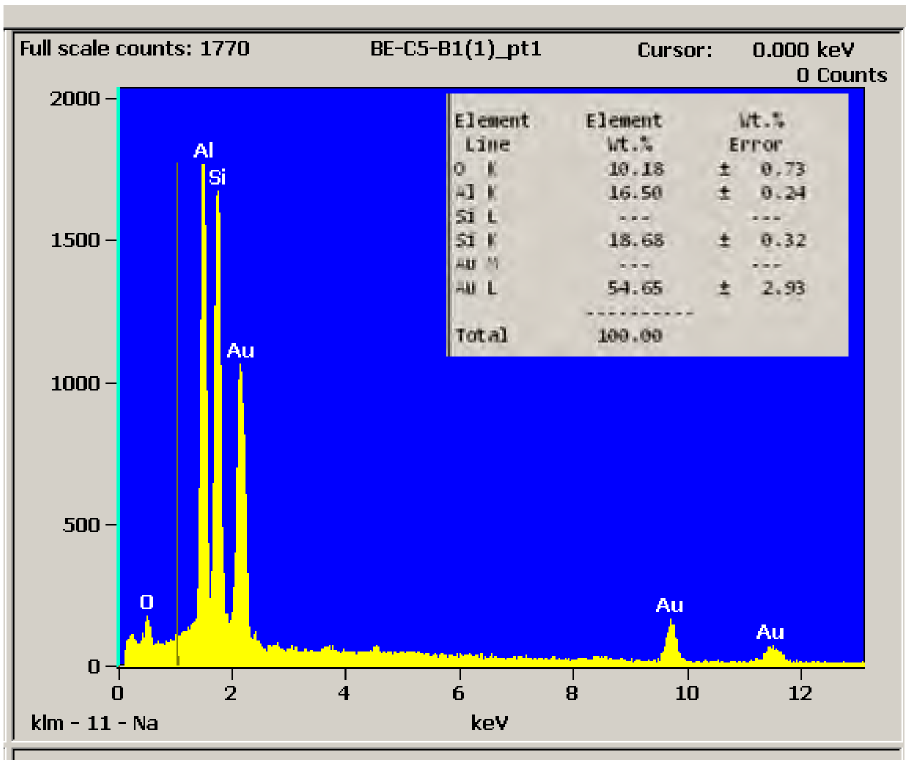

Fig. 115. BE_C5_B1-1 pt. 1

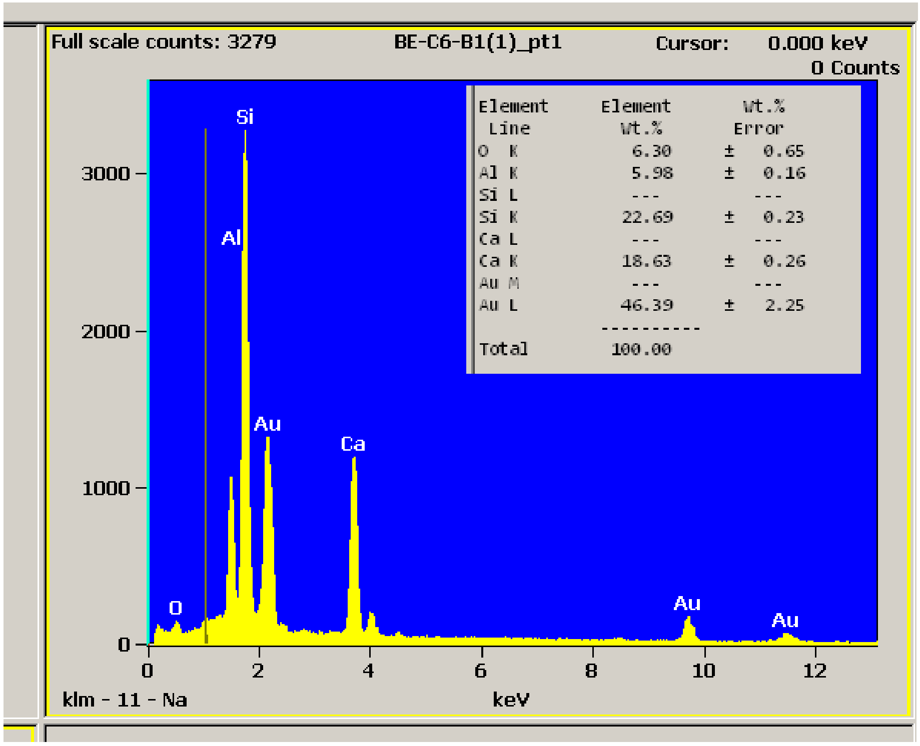

Fig. 116. BE_C6_B1-1 pt. 1

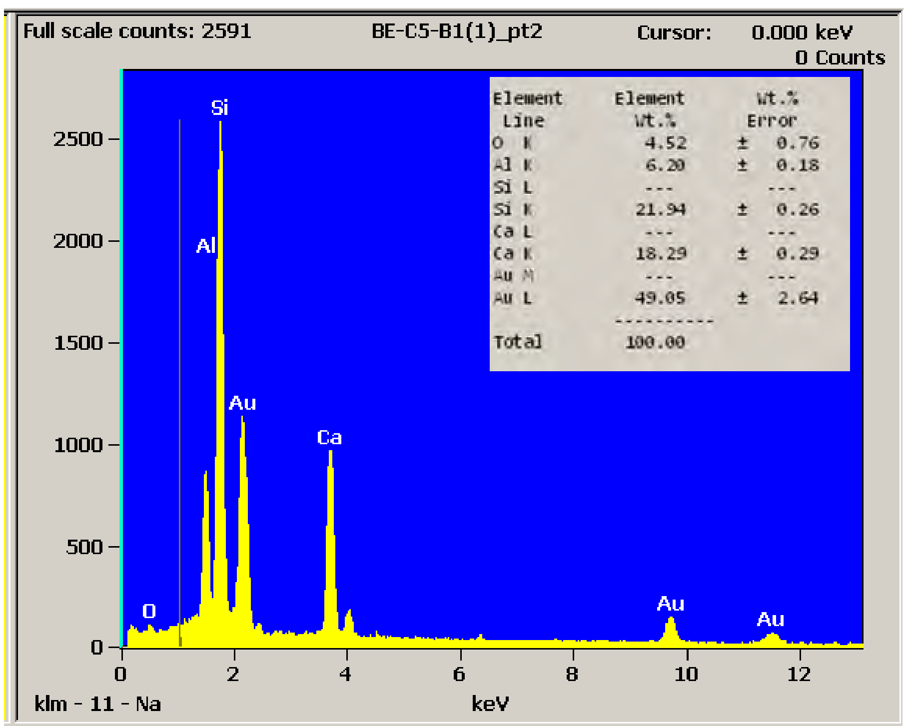

Fig. 117. BE_C5_B1-1 pt. 2

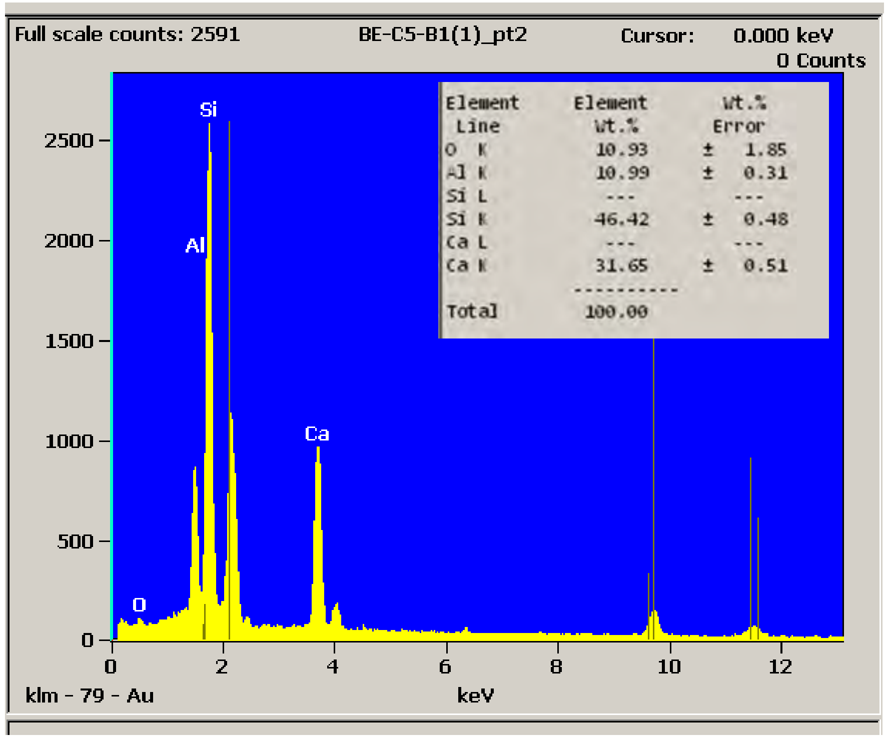

Fig. 118. BE_C5_B1-1 pt. 2 gold not included

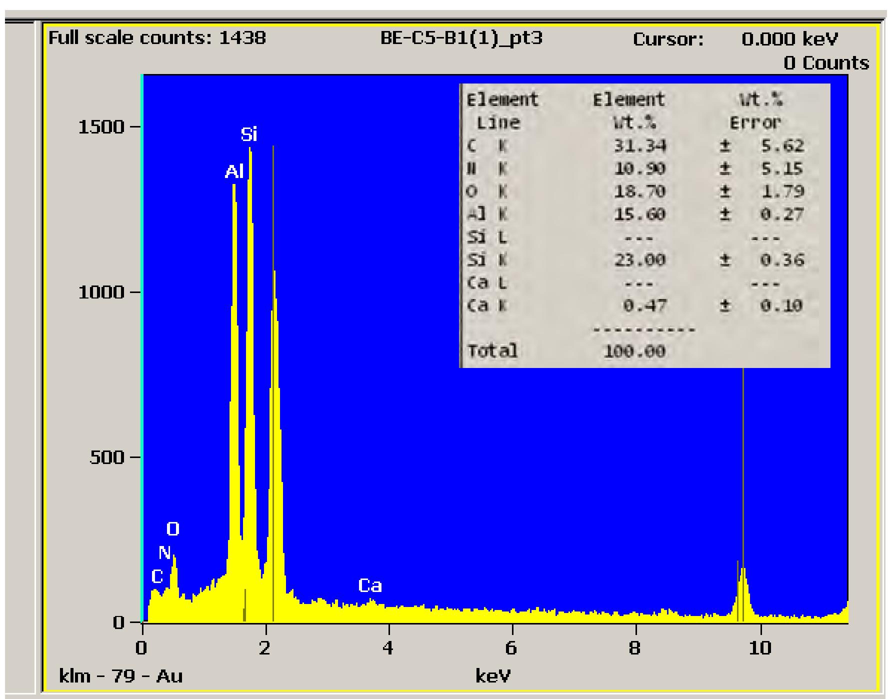

Fig. 119. BE_C5_B1-1 pt.3 gold not included. Presence of C, O and N and yielded high aluminum.

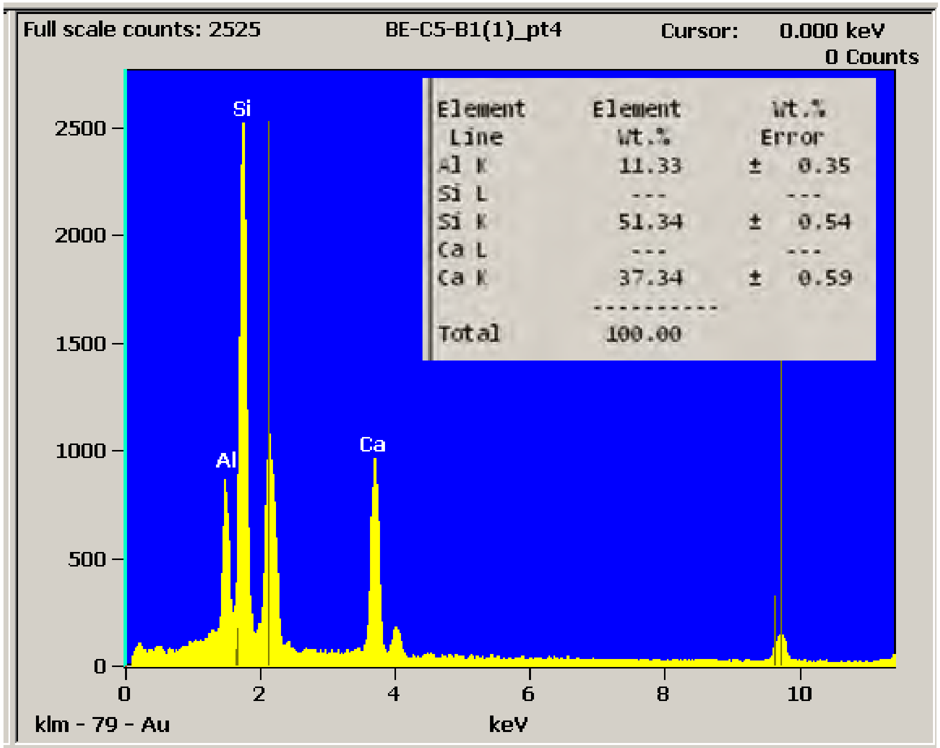

Fig. 120. BE_CE_B1-1 pt. 4 gold not included. Yielded Al, Si and Ca.

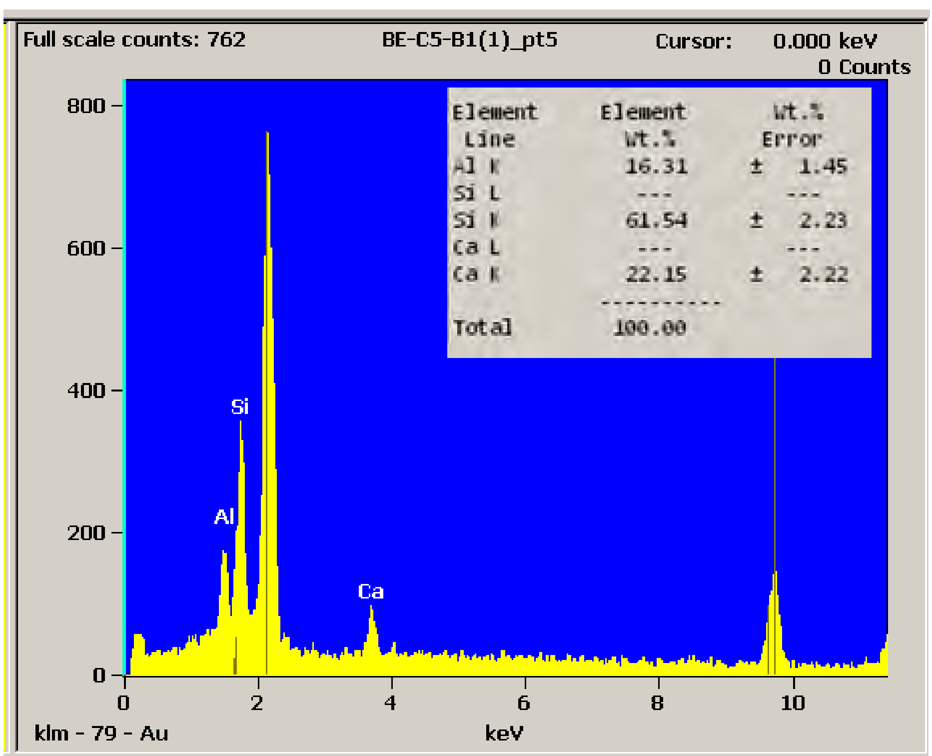

Fig. 121. BE_C5_C1-1 pt 5 no gold included. Yielded less Al, Si and Ca.

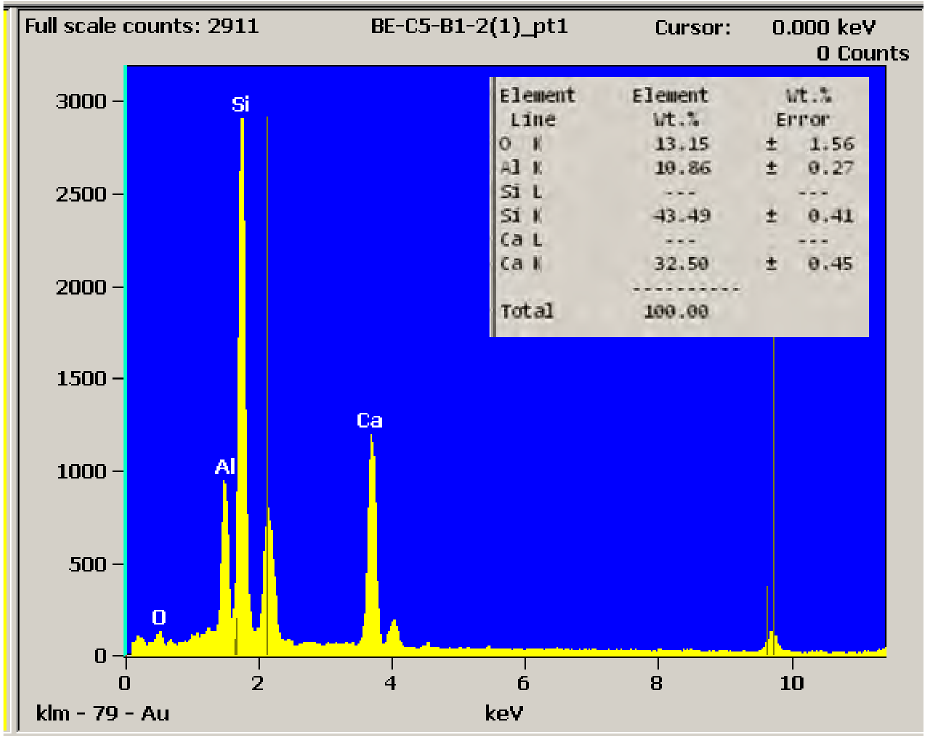

Fig. 122. BE_C5_B1-2 pt. 1 EDS result

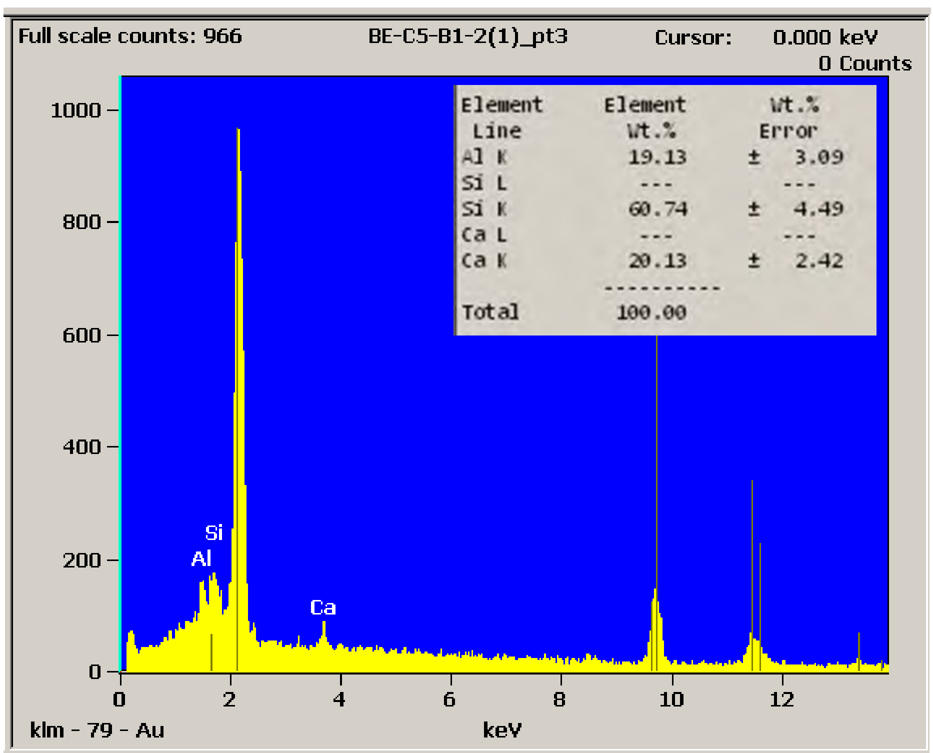

Fig. 123. BE_C5_B1-2 pt. 2.

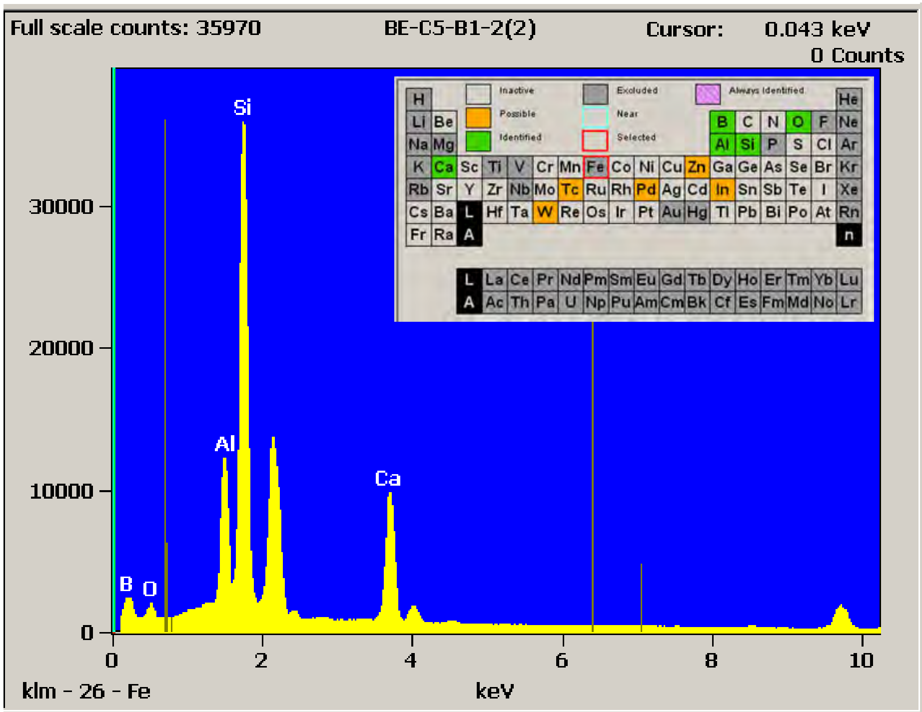

Fig. 124. BE_C5_B1-2

2.2 O'Fallon

EDS O'Fallon *Park Bridge* was performed at the University of Miami using the method described in Section 4.1.5. Results are shown in Fig. 115

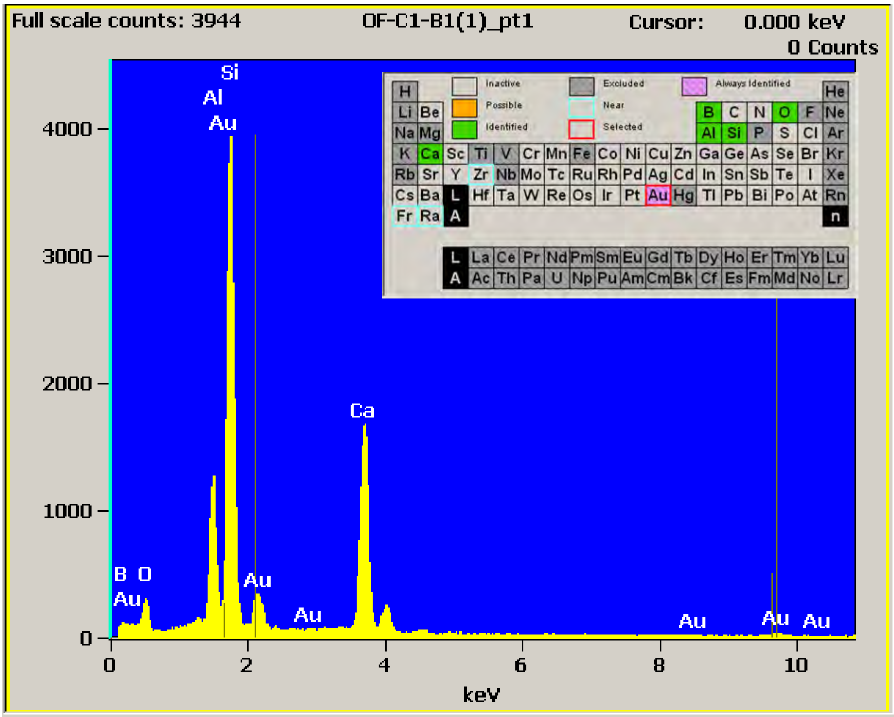

Fig. 125. OF_C1_B1-1 part 1

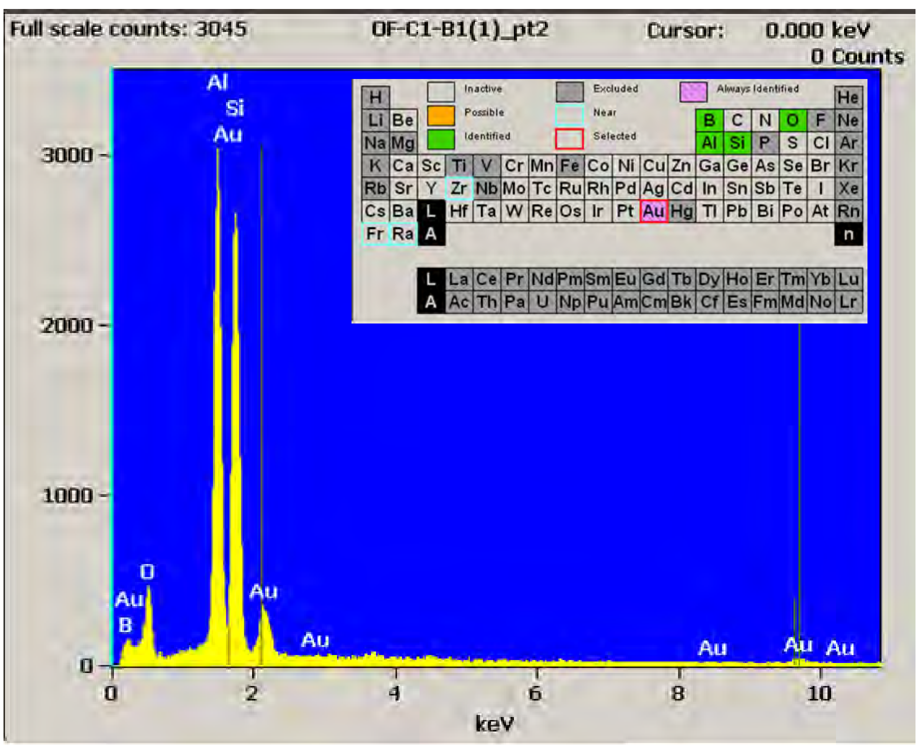

Fig. 126. OF_C1_B1-1 part 2

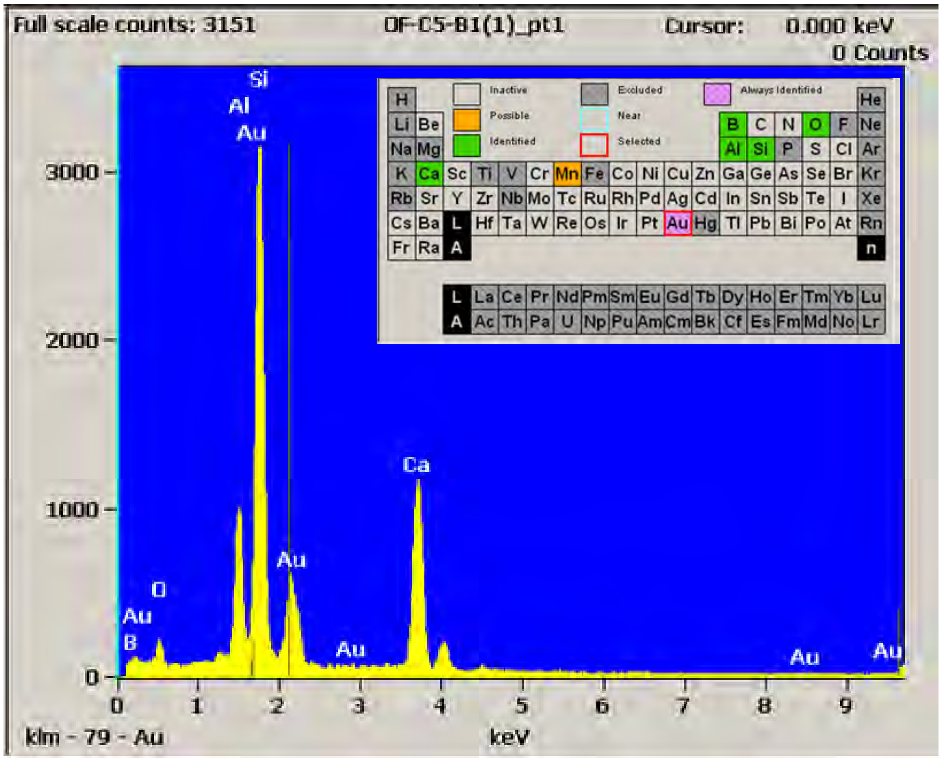

Fig. 127. OF_C5_B1-1 part 1

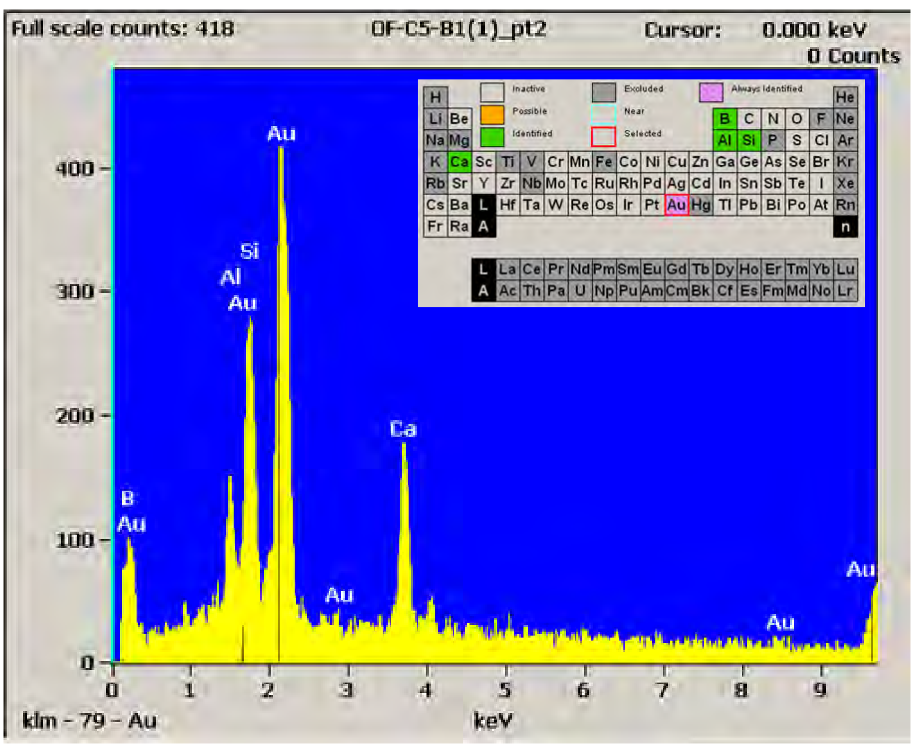

Fig. 128. OF_C5_B1-1 part 2

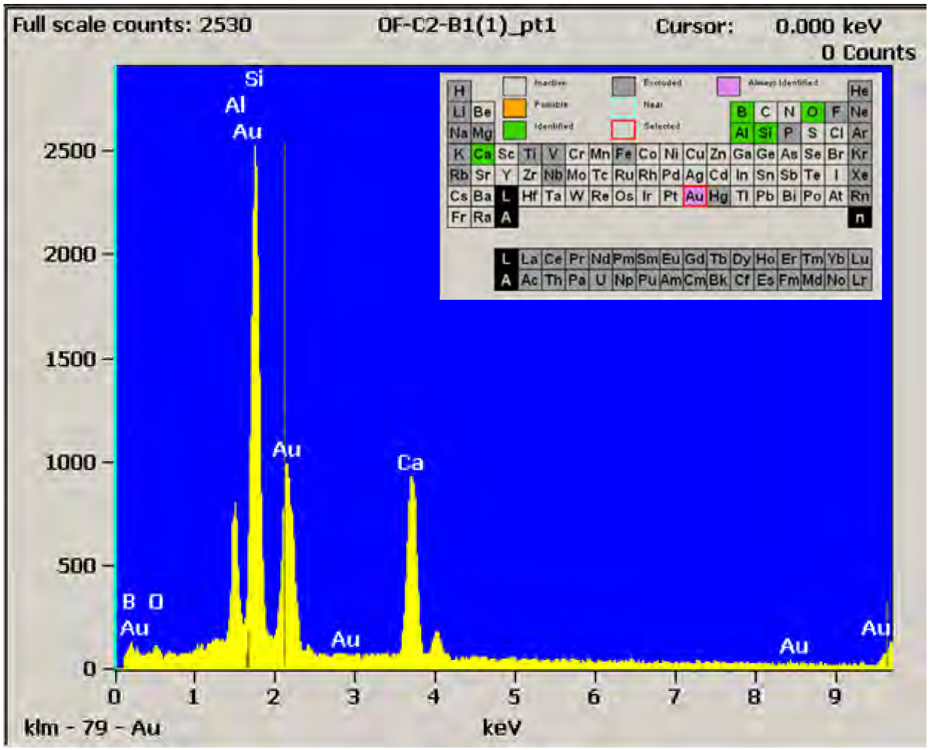

Fig. 129. OF_C2_B1-1 part 1

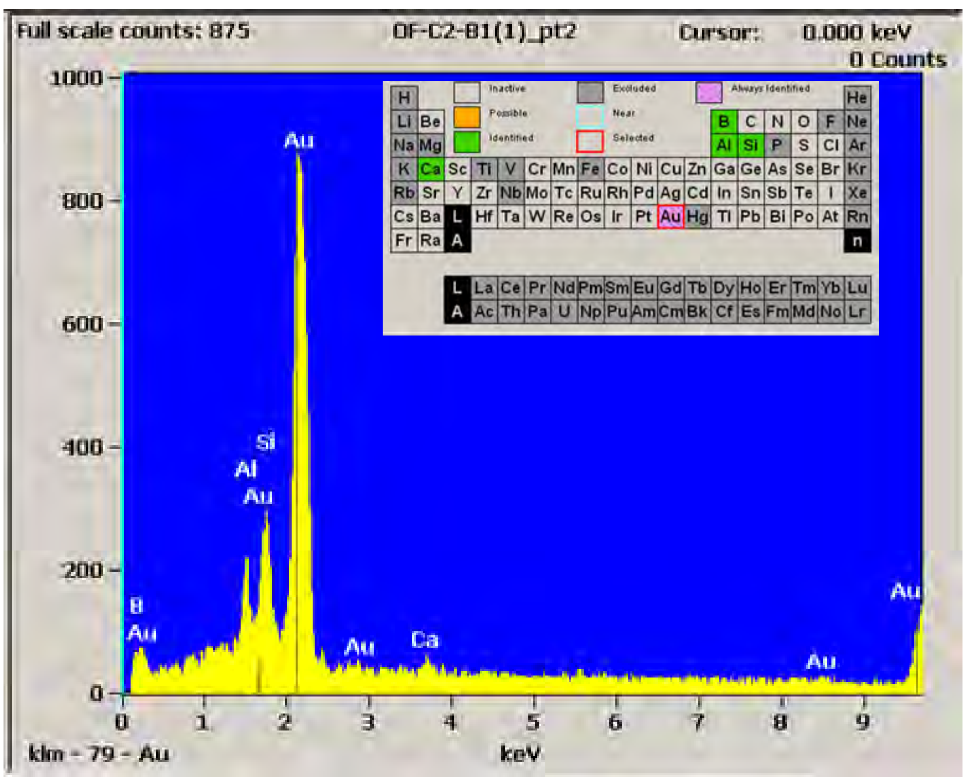

Fig. 130. OF_C2_B1-1 part 2

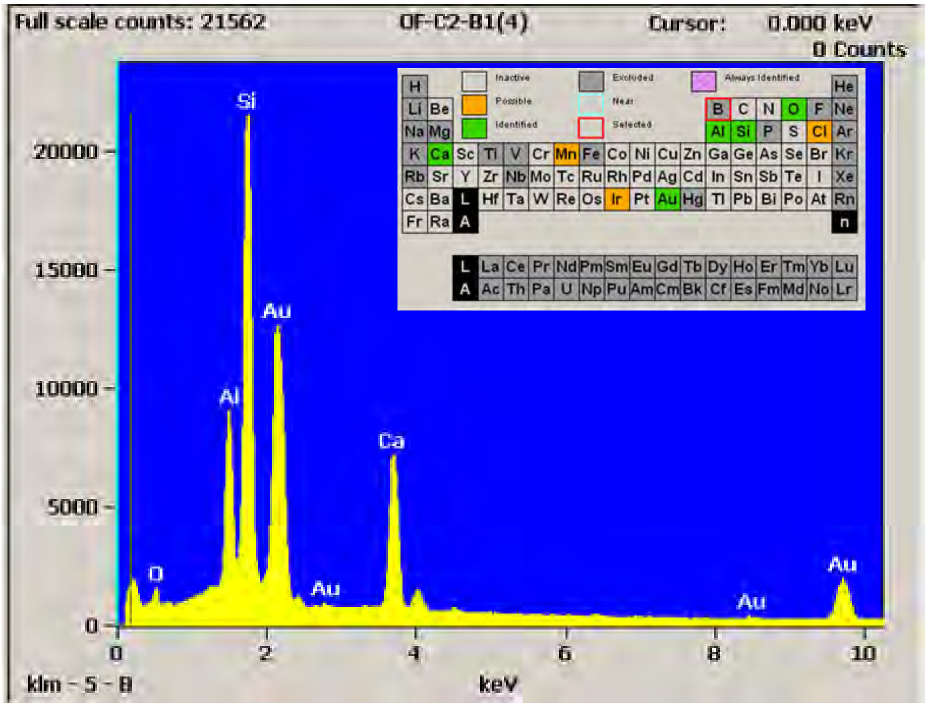

Fig. 131.OF_C2_B1-4

2.3 Salem Ave.

EDS for *Salem Ave. Bridge* was performed at the University of Miami using the method described in Section 4.1.5. Results are shown Fig. 132 through Fig. 143.

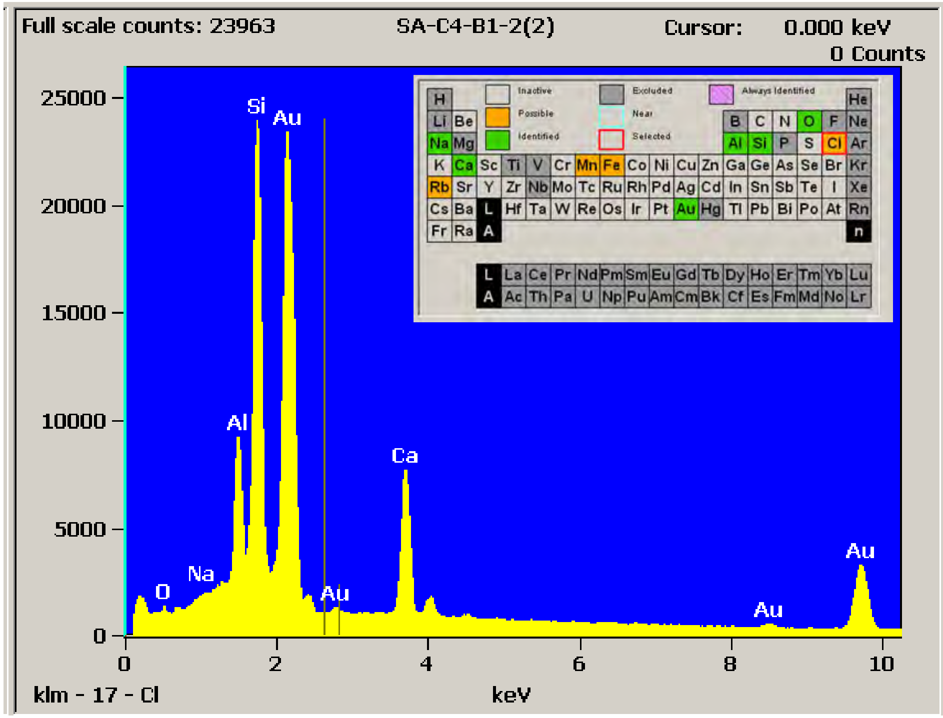

Fig. 132. SA_C4_B1-2

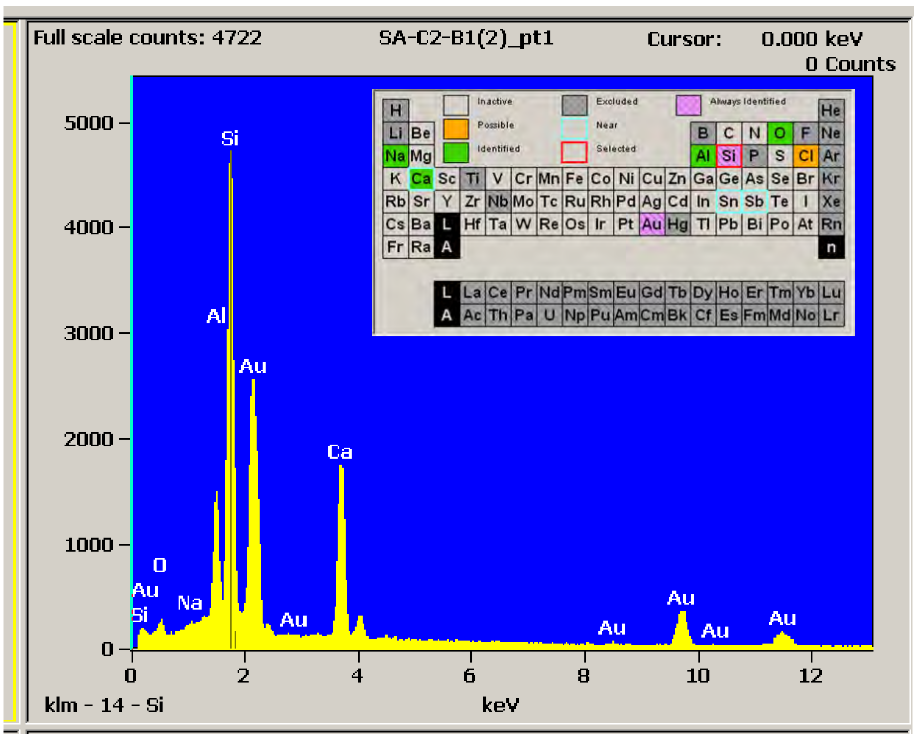

Fig. 133. SA_C2_B1-2 pt. 1

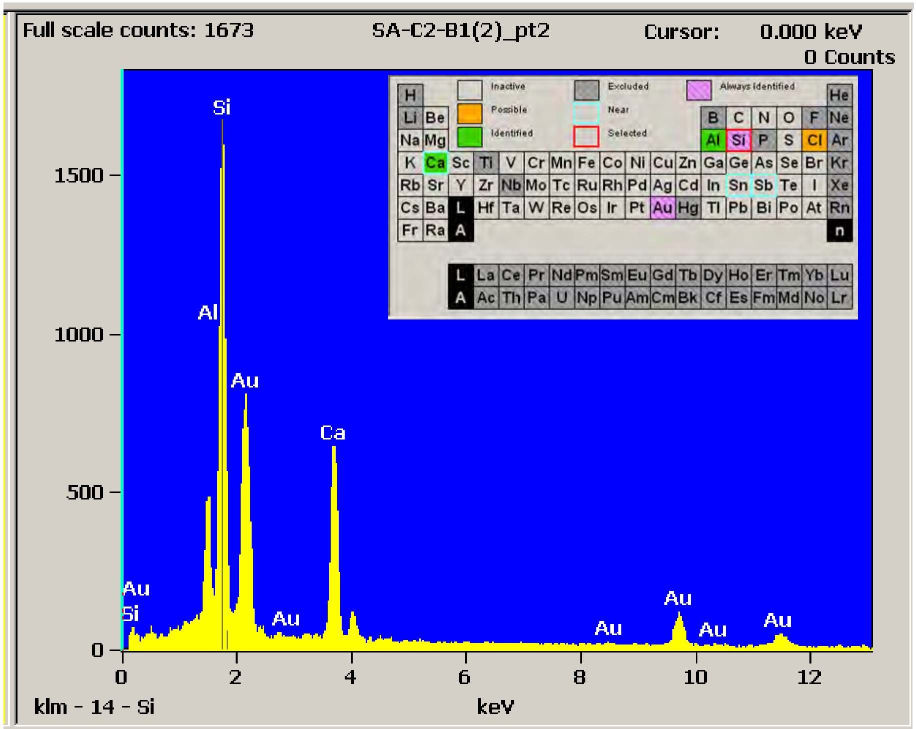

Fig. 134. SA_C2_B1-2 pt.2

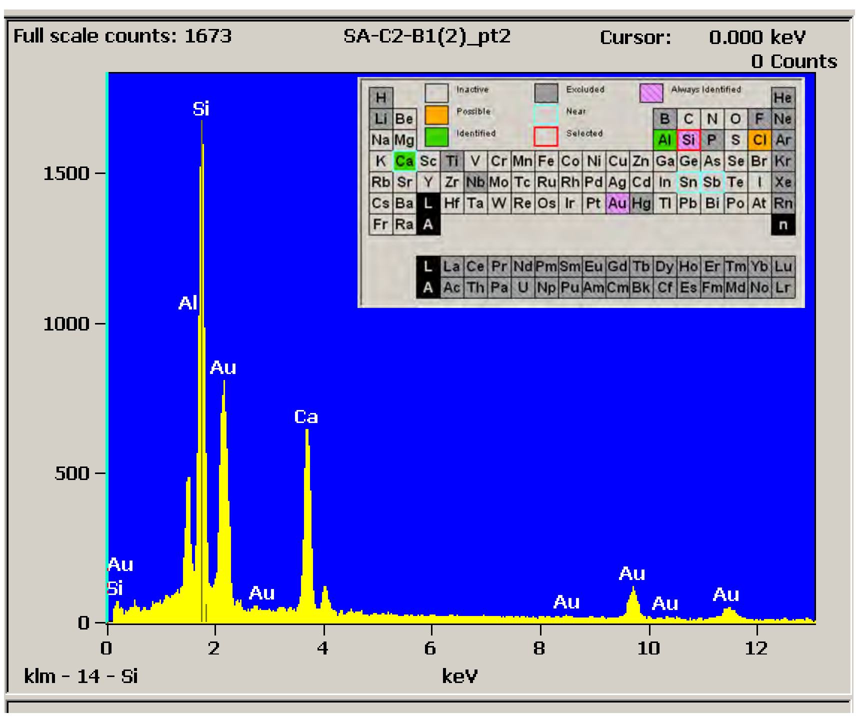

Fig. 135. SA_C2_B1-2 pt. 2

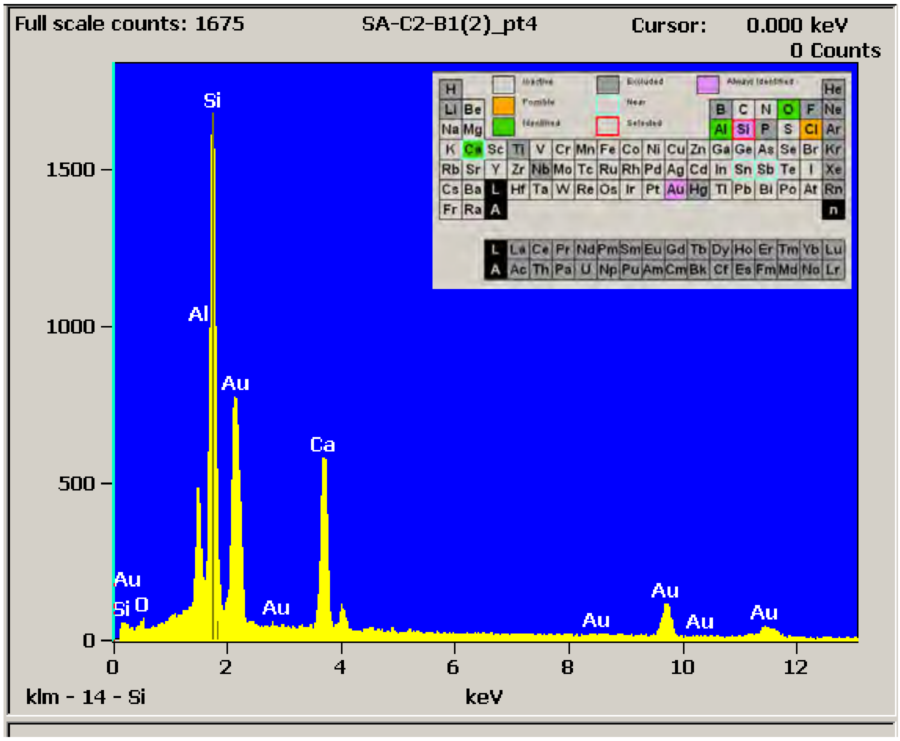

Fig. 136. SA_C2_B1-1 pt.4

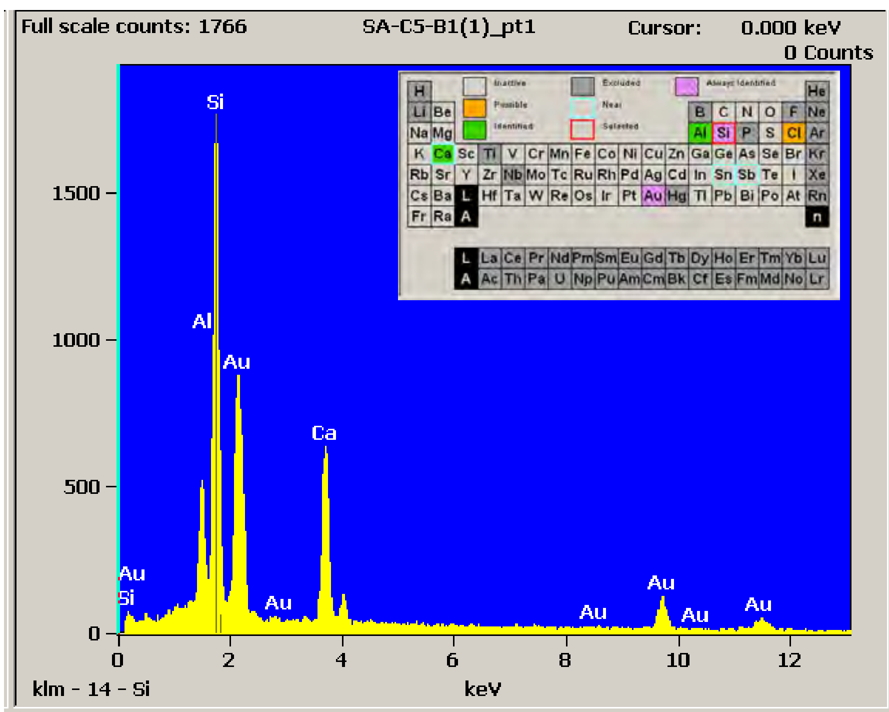

Fig. 137. SA_C5_B1-1 pt.1

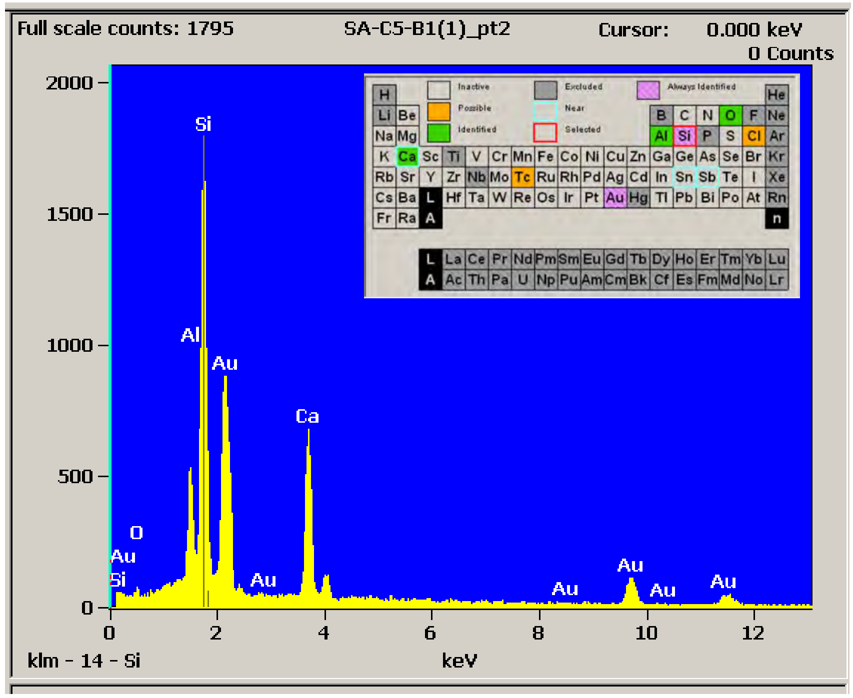

Fig. 138. SA_C5_B1-1 pt.2

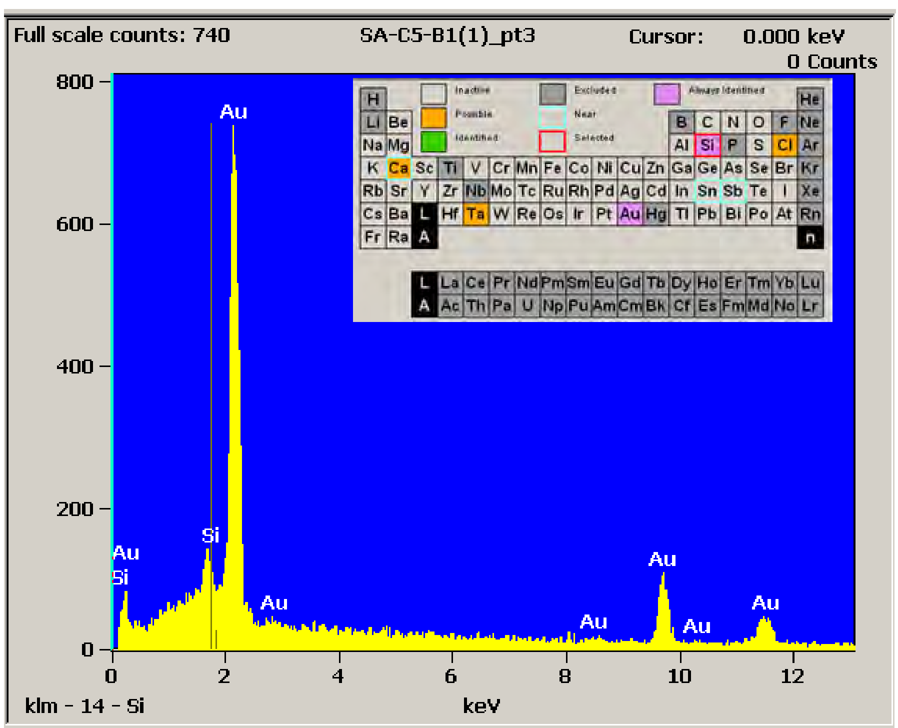

Fig. 139. SA_C5_B1-1 pt.3

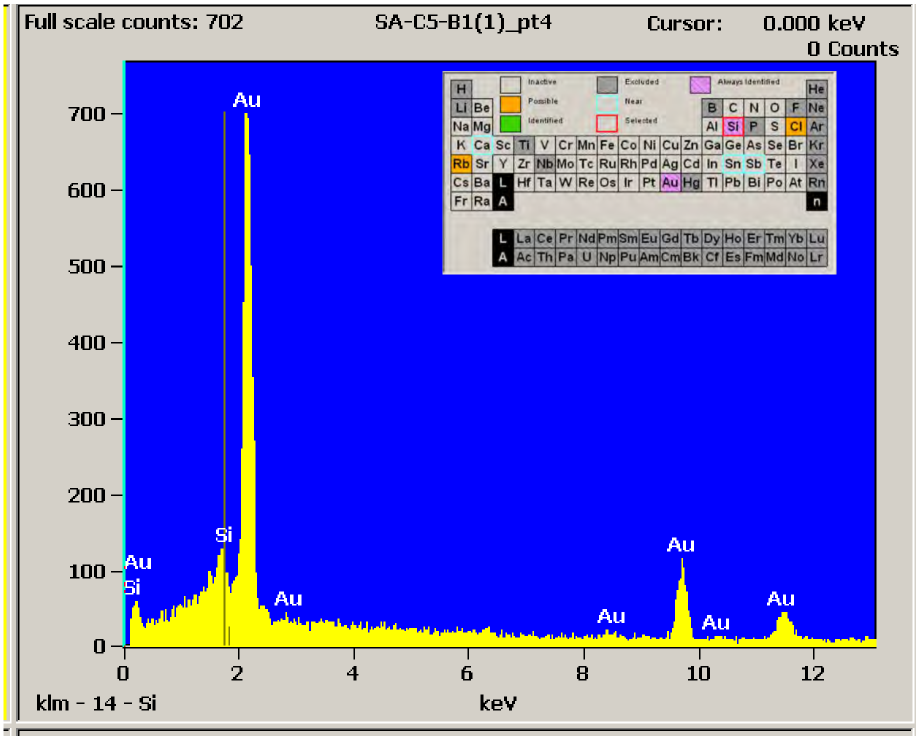

Fig. 140. SA_C5_B1-1 pt.4

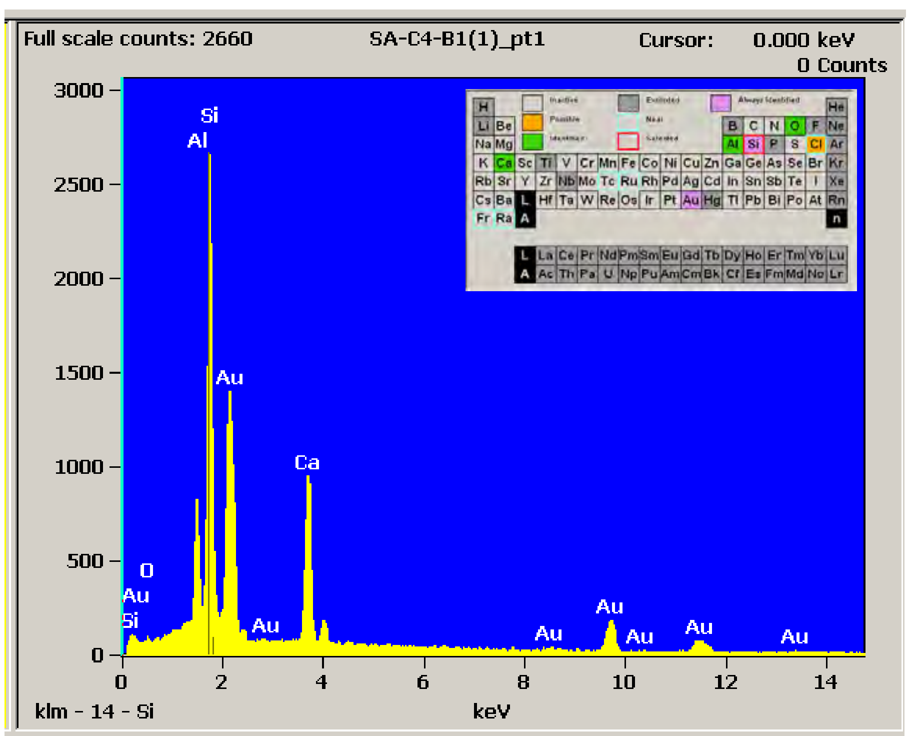

Fig. 141. SA_C4_B1-1 pt.1

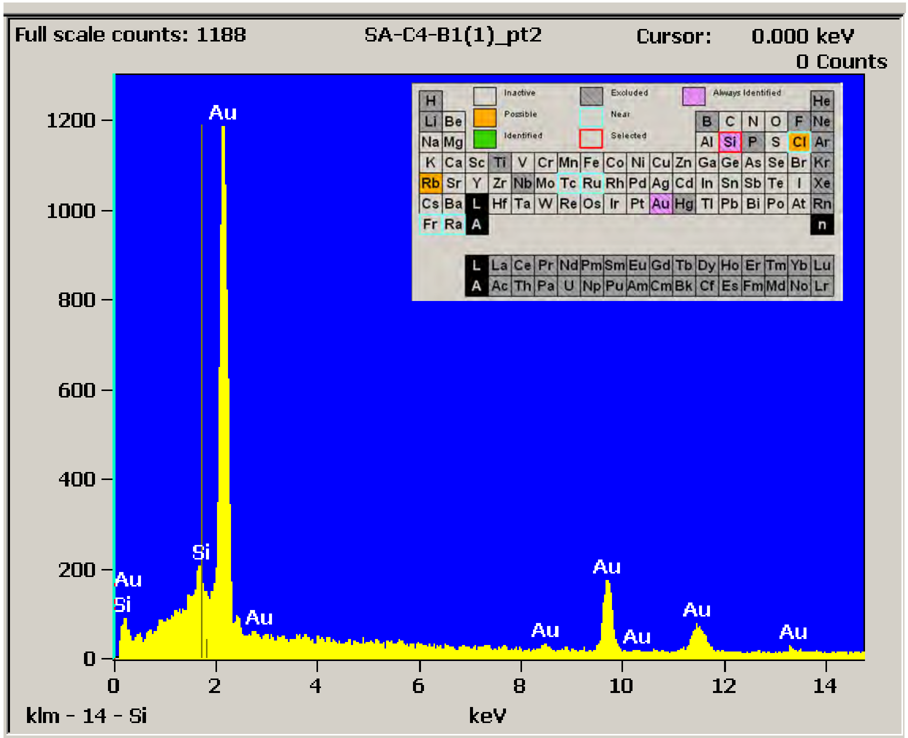

Fig. 142. SA_C4_B1-1 pt. 2

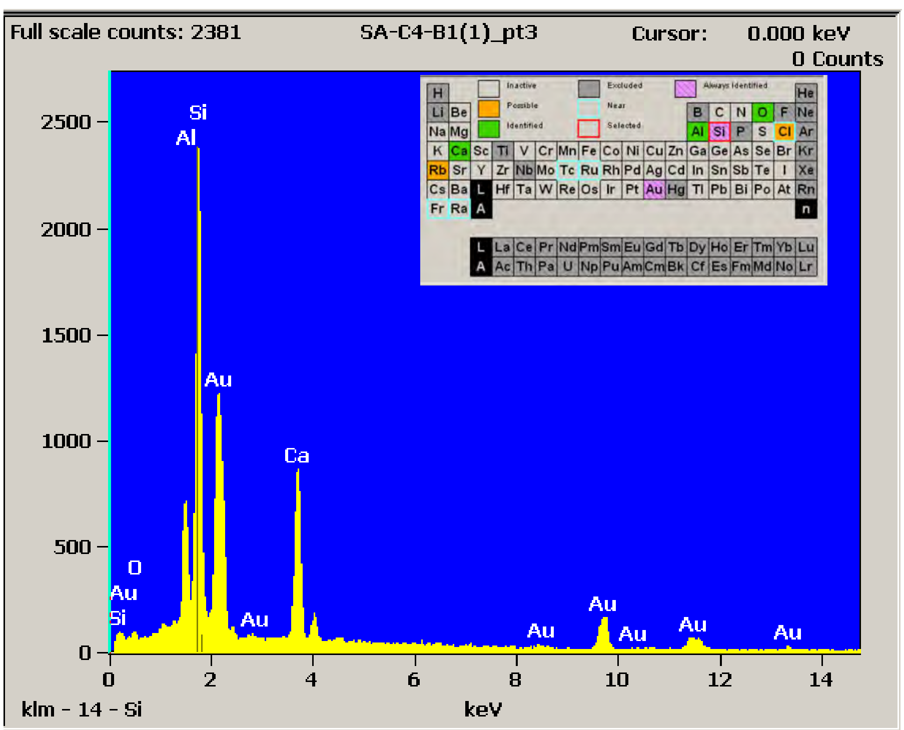

Fig. 143. SA_C4_B1-1 pt.3

2.4 McKinleyville

EDS for *McKinleyville Bridge* was performed at the Owens Corning using the method described in Section 4.1.5. The result is shown in Table 1

Table 1. McKinleyville EDS results

Sample Name		Na	Mg	Al	Si	Ca	Ti	Fe	Total
WV_C1_B2A	Central Fiber (avg)	1.30	2.60	14.20	6.80	20.70	0.50	0.00	100.00
WV_C1_B2B	Central Fiber (avg)	13.00	2.70	14.80	61.20	19.50	0.50	0.00	100.00
WV_C1_B3A	Central Fiber (avg)	1.10	2.70	14.30	60.30	21.10	0.50	0.10	100.10
WV_C3_B3A	Central Fiber (avg)	1.10	2.80	14.40	60.50	20.60	0.50	0.00	100.00
WV_C3_B3B	Central Fiber (avg)	1.20	2.60	14.20	60.20	21.30	0.60	0.00	100.00
WV_C4_B2	Central Fiber (avg)	1.60	0.60	14.80	60.50	21.80	0.60	0.20	100.10
WV_C5_B2	Central Fiber (avg)	1.50	0.70	14.80	60.10	22.30	0.60	0.10	100.10
WV_C1_B2A	Non-intact fiber (avg)	1.00	1.30	14.50	60.70	22.00	0.40	0.10	100.10
WV_C1_B2B	Non-intact fiber (avg)	1.30	2.90	14.70	61.20	19.40	0.50	0.10	100.00
WV_C1_B3A	Non-intact fiber (avg)	1.10	2.80	14.20	60.10	21.10	0.50	0.20	100.00
WV_C3_B3A	Non-intact fiber (avg)	1.30	2.90	14.70	61.10	19.50	0.50	0.00	100.00
WV_C3_B3B	Non-intact fiber (avg)	1.20	2.60	14.20	60.10	21.30	0.60	0.00	100.10
WV_C4_B2	Non-intact fiber (avg)	1.60	0.70	14.70	60.50	21.70	0.60	0.30	100.00
WV_C5_B2	Non-intact fiber (avg)	1.50	0.70	14.60	59.80	22.30	0.70	0.40	100.00

2.5 Thayer Road

EDS for *Thayer Road Bridge* was performed at the Owens Corning using the method described in Section 4.1.5. The result is shown in Table 2.

Table 2. Thayer Road EDS results

Sample Name		Na	Mg	Al	Si	Ca	Ti	Fe	Total
IN_C1_B2	Central Fiber (avg)	0.90	0.20	14.40	59.70	24.10	0.60	0.20	100.00
IN_C5_B1	Central Fiber (avg)	1.00	0.30	14.20	59.80	24.10	0.60	0.00	100.00
IN_C6_B1	Central Fiber (avg)	0.80	0.40	14.40	59.80	23.70	0.60	0.20	100.00
IN_C1_B2	Non-intact fiber (avg)	0.90	0.40	14.30	59.50	24.30	0.60	0.10	100.00
IN_C5_B1	Non-intact fiber (avg)	0.80	0.20	14.30	59.40	24.60	0.70	0.10	100.10
IN_C6_B1	Non-intact fiber (avg)	0.90	0.40	14.40	60.00	23.80	0.50	0.10	100.10

2.6 Roger’s Creek

EDS for *Roger’s Creek Bridge* was performed at the Owens Corning using the method described in Section 4.1.5. The result is shown in Table 3.

Table 3. Roger’s Creek EDS results

Sample Name		Na	Mg	Al	Si	Ca	Ti	Fe	Total
KY_C2_B2	Central Fiber (avg)	1.50	0.70	14.50	60.40	22.20	0.50	0.20	100.10
KY_C4_B1	Central Fiber (avg)	1.40	0.70	14.40	60.10	22.40	0.60	0.30	100.00
KY_C2_B2	Non-intact fiber (avg)	1.50	0.70	14.50	60.30	22.30	0.60	0.20	100.00
KY_C4_B1	Non-intact fiber (avg)	1.50	0.70	14.30	60.00	22.50	0.60	0.30	99.90

2.7 Sierrita de la Cruz Creek

EDS for *Sierrita de la Cruz Creek Bridge* was performed at the University of Miami using the method described in Section 4.1.5. EDS was performed at seven selected locations of the No.5 GFRP slices with a focus on the edge of the bar to identify existing chemical elements in GFRP bars. The results were compared with pristine samples produced in 2015 from the same manufacturer. The results are shown in Fig. 144 and Fig. 145, where the vertical axis corresponds to the counts (number of X-rays received and processed by the detector) and the horizontal axis presents the energy level of those counts.

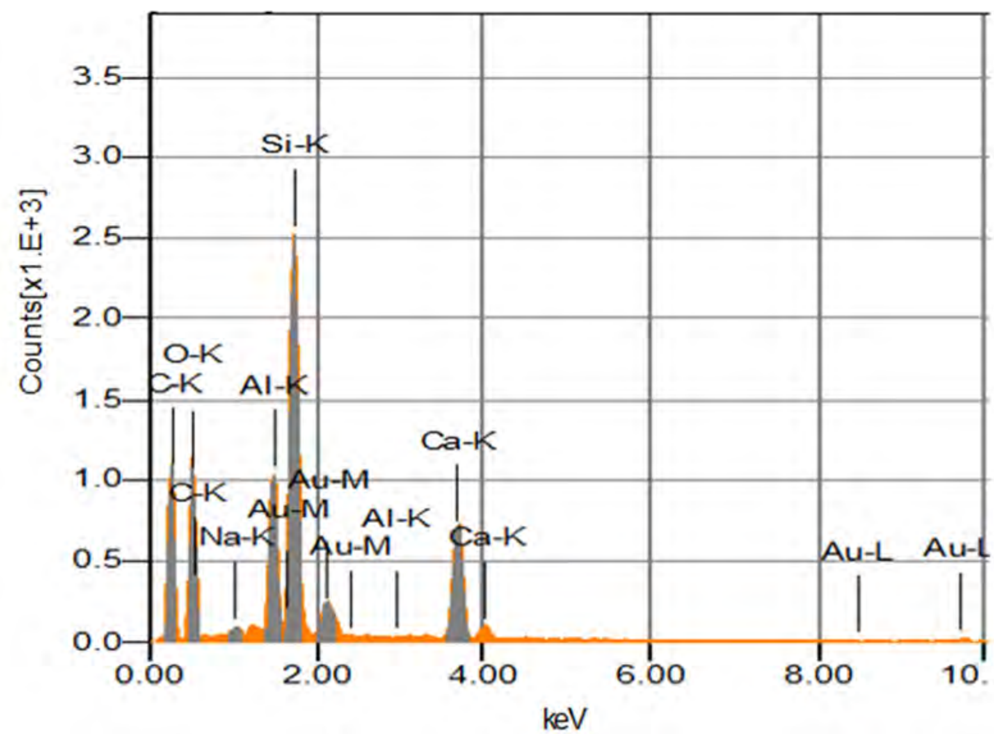

Fig. 144. Sierrita de la Cruz Creek result of the EDS analysis performed on GFRP bars after 15 years of servce

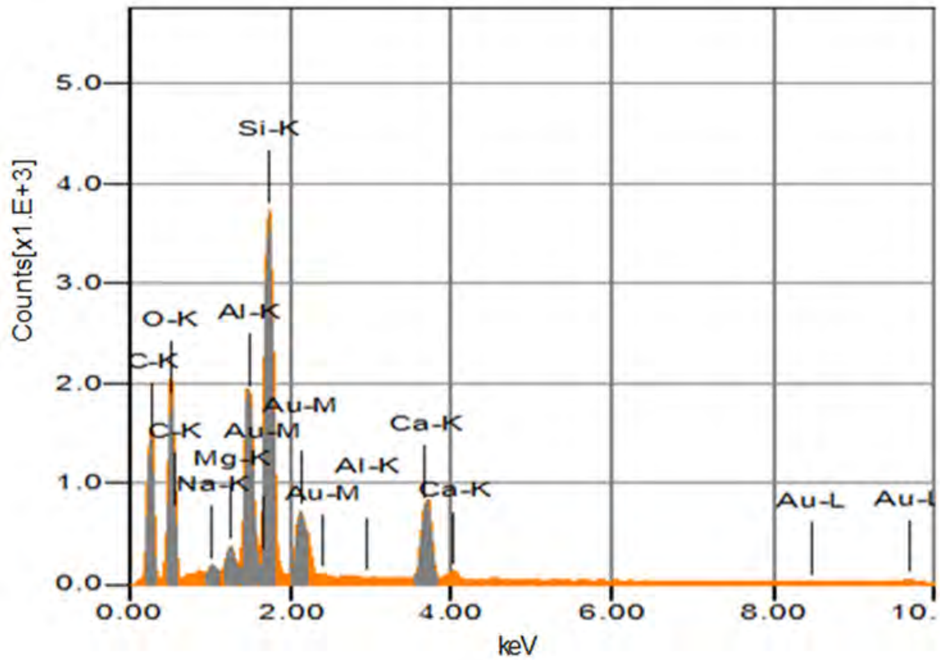

Fig. 145. Sierrita de la Cruz Creke results of the EDS analysis performed on control GFRP samples produced in 2015

Si, Al, Ca (from glass fibers) and C (from the matrix) were the predominant chemical elements in the extracted samples, which were also identical to the control samples. Although, there is a variation in fiber/resin constituents for GFRP bars produced in 2015 compared to the ones manufactured in 2000, the only difference in detected elements between the two, was the presence of Mg in the control samples, which was not found in extracted bars. Additionally, the presence of Na was observed in both control and extracted samples and may be due to contamination during sample preparation. Comparing the result of EDS analysis performed on the extracted and control samples confirmed that no change in chemical composition of fiber and matrix occurred after 15 years of service.

2.8 Walker Box Culvert

EDS for *Walker Box Culvert Bridge* was performed at the University of Miami using the method described in Section 4.1.5. The result of EDS analysis is shown in Fig. 146. Si, Al, Ca (from glass fibers) and C (from the matrix) were the predominant chemical elements in the extracted samples. No apparent sign of any chemical attack was observed in the bars.

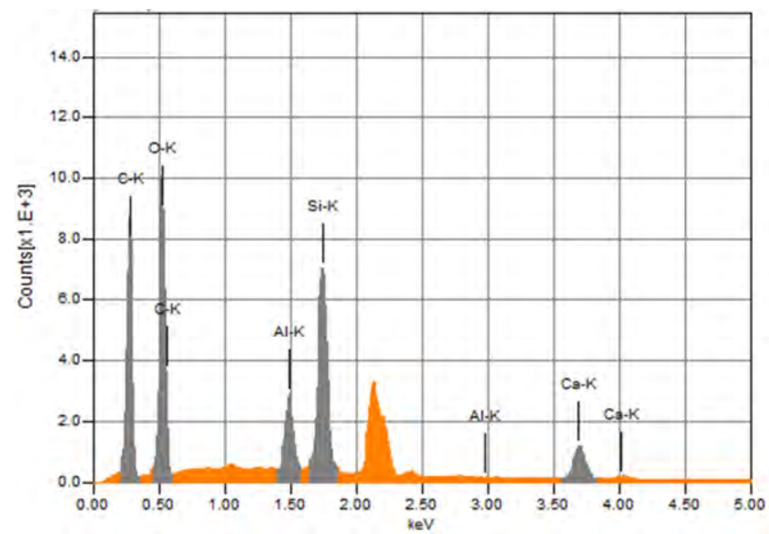

Fig. 146. Result of the EDS analysis performed on GFRP samples extracted from Walker Bridge

2.9 Southview

EDS for *Southview Bridge* was performed at the University of Miami using the method described in Section 4.1.5.

The result of EDS analysis is shown in Fig. 147. Si, Al, Ca (from glass fibers) and C (from the matrix) were the predominant chemical elements in the extracted samples. No apparent sign of any chemical attack was observed in the bars.

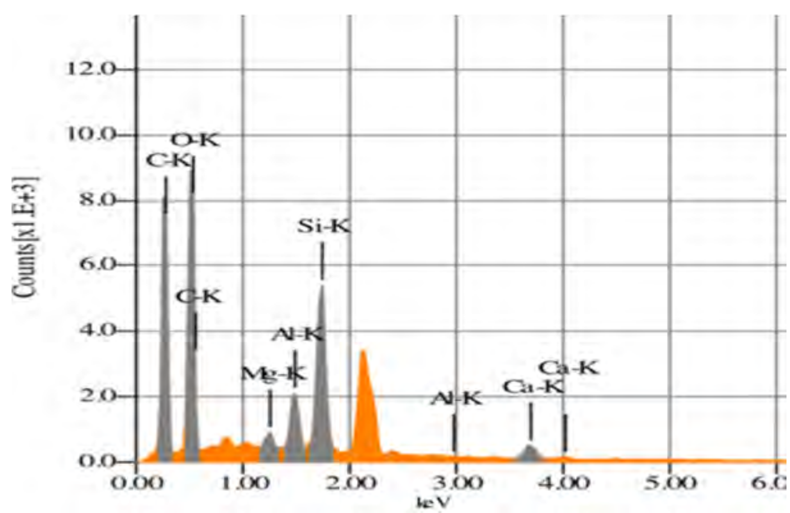

Fig. 147. Result of the EDS analysis performed on GFRP samples extracted from Southview Bridge

APPENDIX VI: TENSILE TEST RESULTS

This appendix presents the results of a regular tensile test and a modified tensile test. The regular tensile test analyzed 10 full #5 GFRP rebars. While the modified tensile test consisted of testing GFRP coupons from Sierrita de la Cruz Creek Bridge and from pristine bars (produced by the same manufacturer in 2018) in tension, as described in Section 4.1.8. The coupons consisted of slices of a full bar, resulting in three slices per rebar: left side of rebar, center of rebar and right side of rebar that measured approximately 0.45 x 10 x 0.1 in. (11 x 254 x 3 mm) (width x length x dia.).

The extracted rebars from Sierrita de la Cruz Creek Bridge were labeled E_XL, with E for extracted, X with the corresponding rebar number and L in this case for left. The pristine bars, however, were not identified as center, left or right.

NOMENCLATURE

VA and GI =	Gills Creek Bridge
CO and OF =	O’Fallon Park Bridge
OH1 and SA =	Salem Ave. Bridge
IA and BE =	Bettendorf Bridge
OH2 and CU =	Cuyahoga County Bridge
WV =	McKinleyville Bridge
IN =	Thayer Road Bridge
KY =	Roger’s Creek Bridge
TX and SI =	Sierrita de la Cruz Creek Bridge
MO1 and WA =	Walker Box Culvert Bridge
MO2 and SO =	Southview Bridge

Table of Contents

Table of Figures

List of Tables

1. Modified Coupon Tensile Test

1.1 Sierrita de la Cruz Creek Bridge extracted coupons

A total of nine coupons from Sierrita de la Cruz Creek were tested. Fig. 1 shows the extracted coupons.

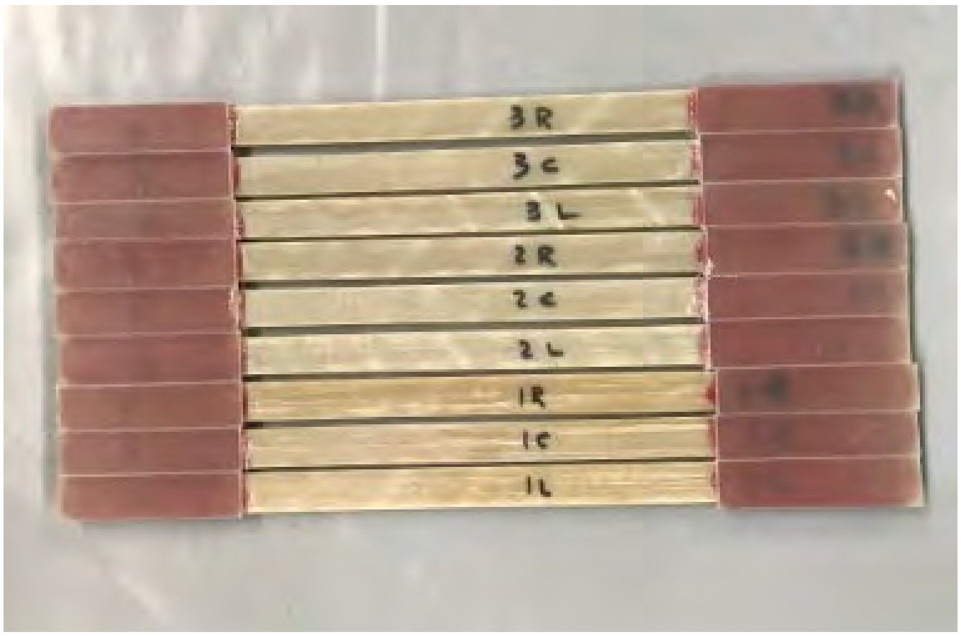

Fig. 1. Sierrita de la Cruz Creek Bridge coupons

1.1.1. Bar E_1L

Sierrita de la Cruz Creek coupon 1 from the left side of the rebar failed at the lateral grip on the top at a peak load of 2,732 lbs. (12 kN) and a peak strain of $10{,}000 \times 10^{-6}$. The coupon before testing and test set up are shown in Fig. 2 and Fig. 3, respectively. The failed coupon and the stress strain curve are shown in Fig. 4 and Fig. 5, respectively. The strain values were recorded with both strain gauges and extensometer; however, the extensometer was removed at 2,500 lbs. Therefore, the stress strain curve uses the values obtained from the strain gauge. A summary of the tensile test results is shown in Table 1.

Since the failure of this coupon happened at the location of the tab, the test is rejected.

Fig. 2. Coupon E_1L before testing

Fig. 3. Test set up

Fig. 4. E_1L after failure

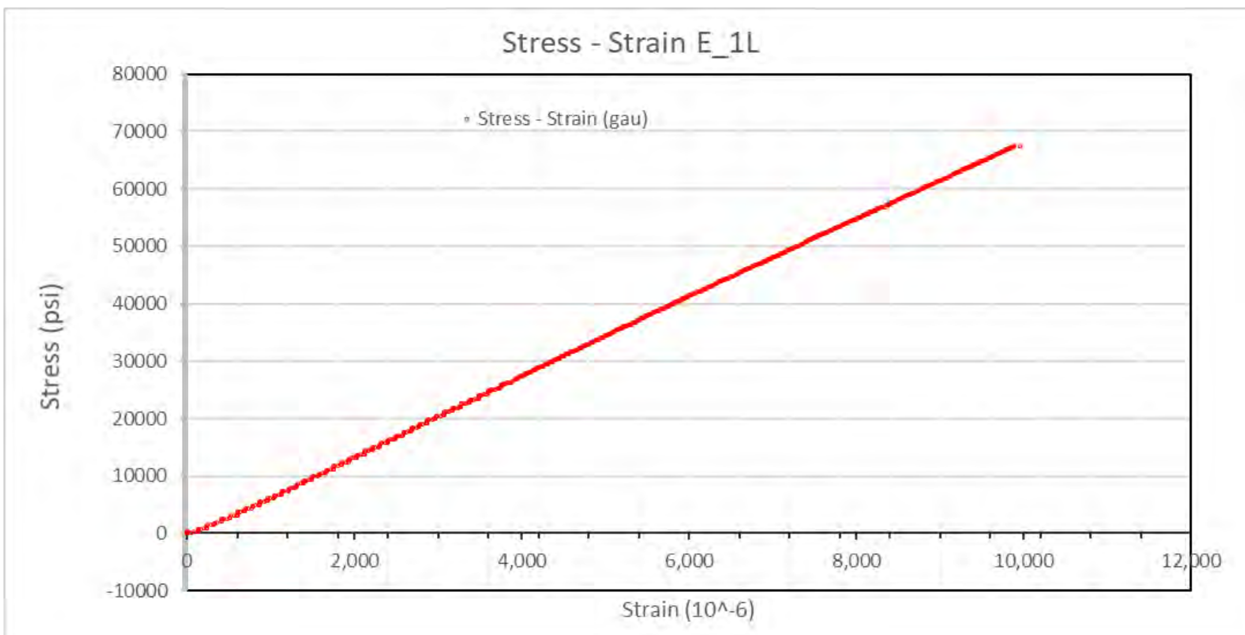

Fig. 5. Stress strain curve for E_1L

Table 1. 1L properties

Sample #	**Area, sq. in (sq. mm)**	**Peak Load, lbs (kN)**	**Max Stress, psi (MPa)**	**Peak Strain (10^-6)**
1L	0.0405 (26)	2,732 (12)	67,442 (465)	10,000

1.1.2. Bar E_1C

Sierrita de la Cruz Creek coupon 1 from the center of the rebar failed with the splitting of gage at various points at a peak load of 4,140 lbs. (18 kN) and a peak strain of 12,300x10^{-6}. The coupon before testing and after failure are shown in Fig. 6 and Fig. 7, respectively. The strain values were recorded with both strain gauges and extensometer; however, the extensometer was removed at 3,500 lbs. Therefore, the stress strain curve uses the values obtained from the strain gauge. The strain gauge recorded inaccurate values at stresses higher than about 77,000 psi. The stress strain curve for this bar is shown in Fig. 8. A summary of the tensile test results is shown in Table 2.

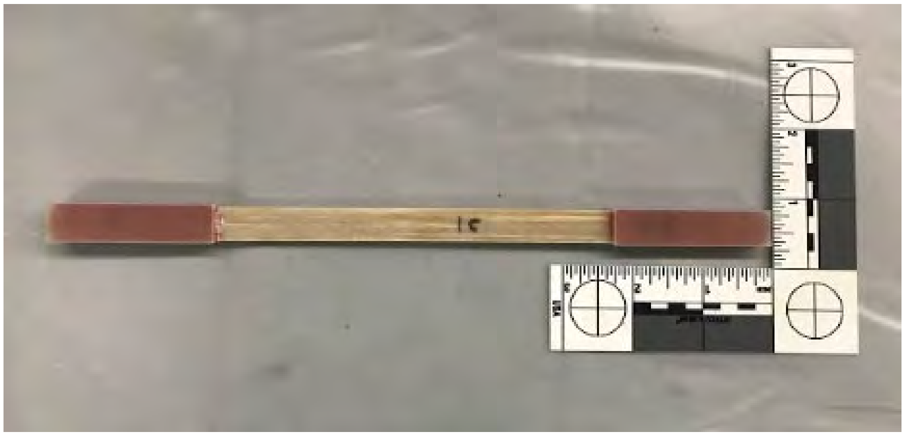

Fig. 6. Coupon E_1C before testing

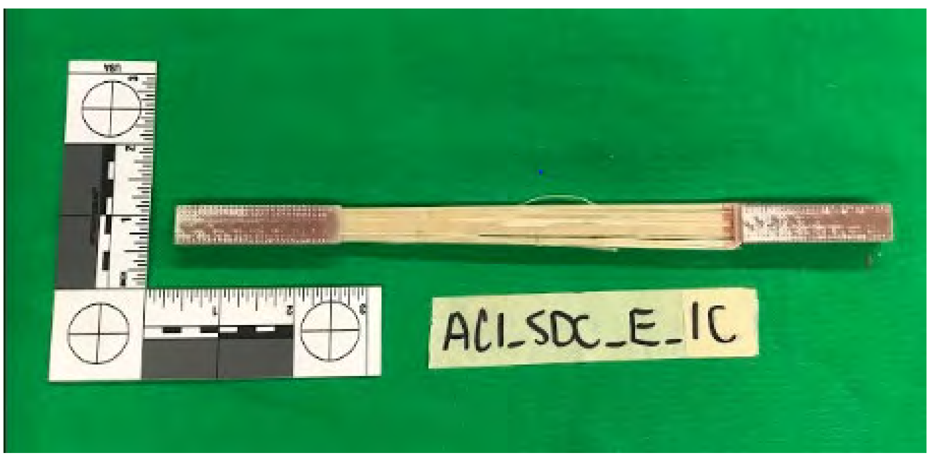

Fig. 7. Coupon E_1C after failure

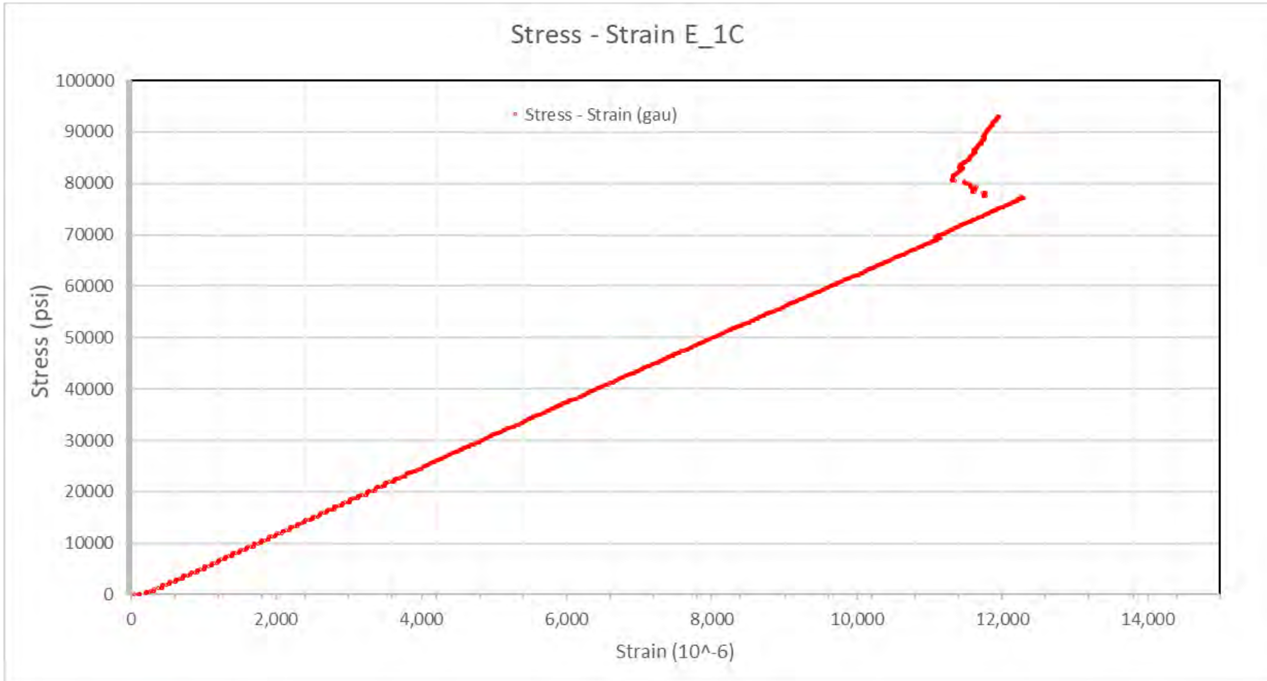

Fig. 8. Stress strain curve for E_1C

Table 2. 1C properties

Sample #	Area, sq. in (sq. mm)	Peak Load, lbs (kN)	Max Stress, psi (MPa)	Peak Strain (10^-6)
1C	0.0445 (26.7)	4,140 (18)	93,118 (642)	12,300

1.1.3. Bar E_1R

Sierrita de la Cruz Creek coupon 1 from the of the right side of the rebar failed with the splitting of gage at various points at a peak load of 5,038 lbs. (22kN) and a peak strain of 12,000x10^{-6}. The coupon before testing and after failure are shown in Fig. 9 and Fig. 10, respectively. The strain values were recorded with both strain gauges and extensometer; however, the extensometer was removed at 2,250 lbs. Therefore, the stress strain curve uses the values obtained from the strain gauge. The strain gauge recorded inaccurate values at stresses higher than about 90,000 psi. The stress strain curve for this bar is shown in Fig. 11. A summary of the tensile test results is shown in Table 3.

Fig. 9. Coupon E_1R before testing

Fig. 10. Coupon E_1R after failure

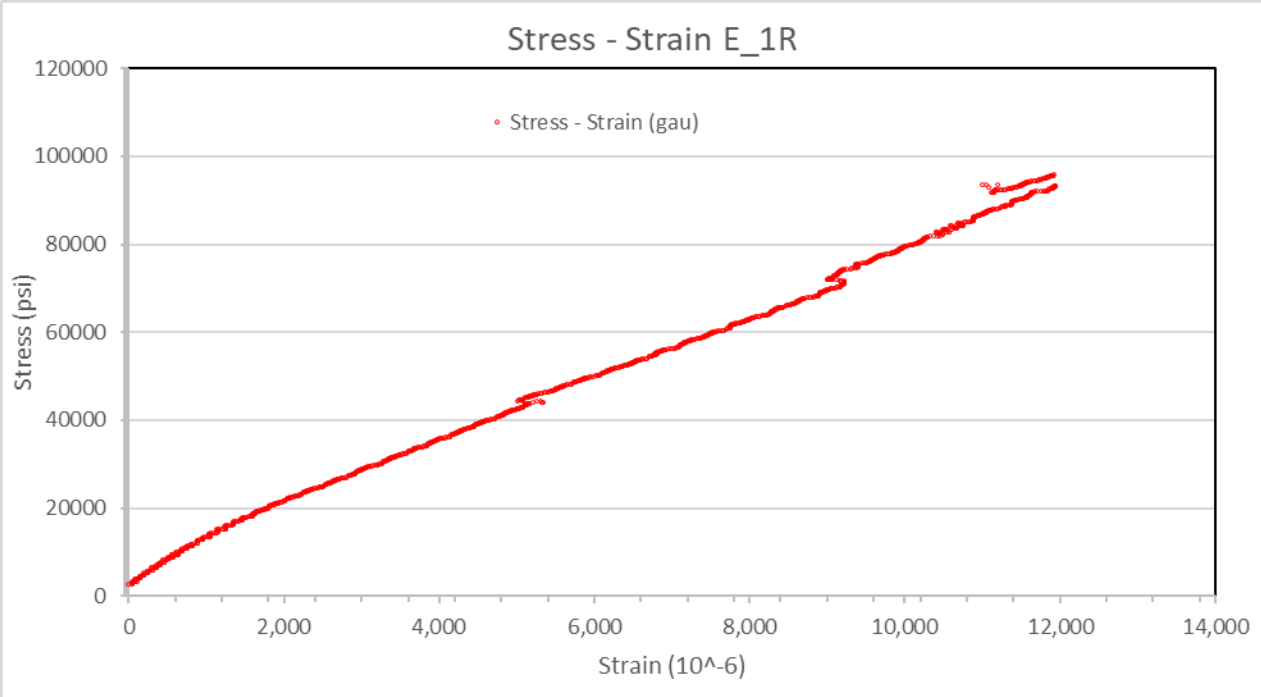

Fig. 11. Stress strain for E_1R

Table 3. 1R properties

Sample #	Area, sq. in (sq. mm)	Peak Load, lbs (kN)	Max Stress, psi (MPa)	Peak Strain (10^-6)
1R	0.0526 (34)	5,038 (22)	95,747 (660)	12,000

1.1.4. Bar E_2L

Sierrita de la Cruz Creek coupon 2 from the left side of the rebar failed with the splitting of gage at various points at a peak load of 3,649 lbs. (16 kN) and a peak strain of 16,200x10^{-6}. The coupon before testing and after failure are shown in Fig. 12 and Fig. 13, respectively. The strain values were recorded with both strain gauges and extensometer; however, the extensometer was removed at 3,500 lbs. Therefore, the stress strain curve uses the values obtained from the strain gauge. The stress strain curve for this bar is shown in Fig. 14. A summary of the tensile test results is shown in Table 4.

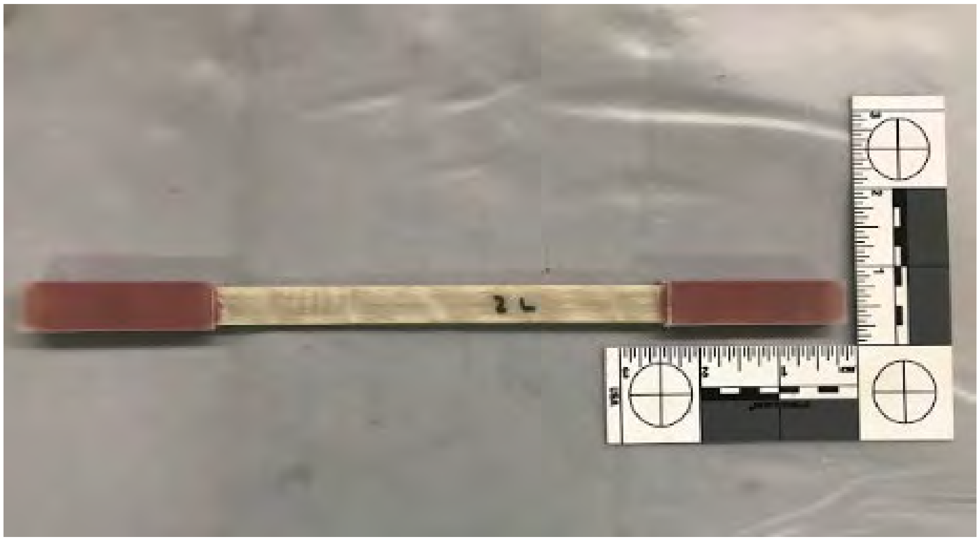

Fig. 12. Coupon E_2L before testing

Fig. 13. Coupon E_2L after failure

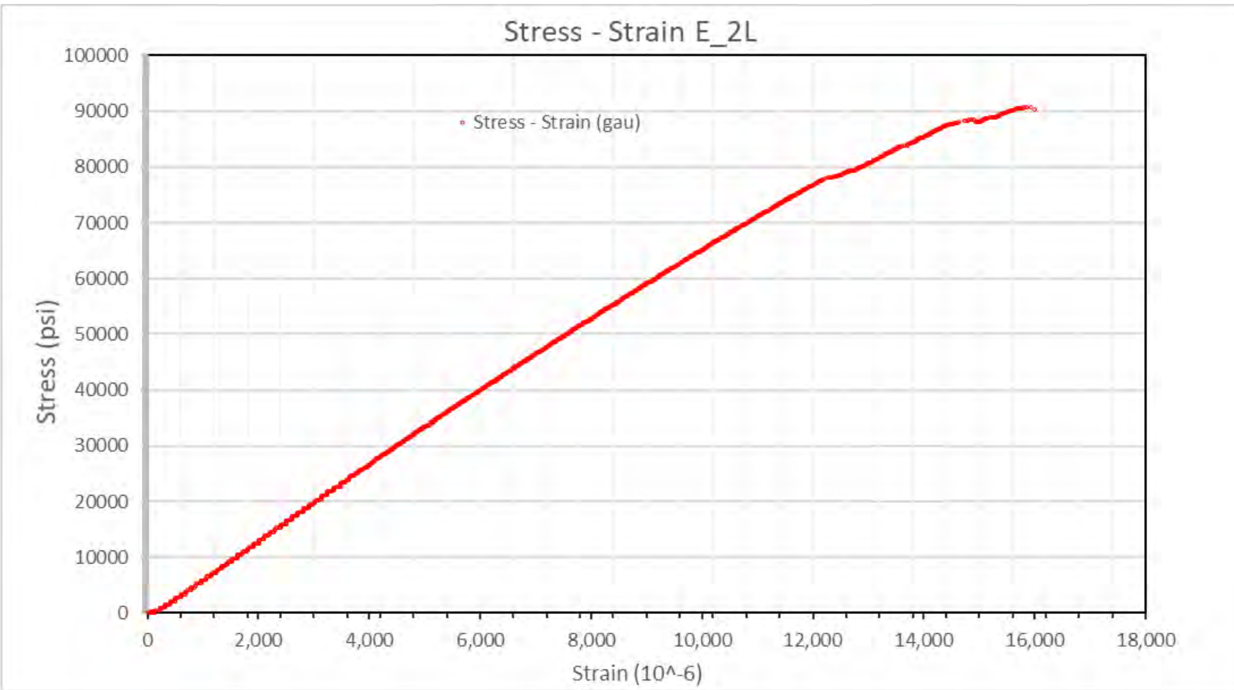

Fig. 14. Stress strain curve for E_2L

Table 4. 2L properties

Sample #	Area, sq. in (sq. mm)	Peak Load, lbs (kN)	Max Stress, psi (MPa)	Peak Strain (10^-6)
2L	0.0402 (26.0)	3,649 (16)	90,689 (625)	16,200

1.1.5. Bar E_2C

Sierrita de la Cruz Creek coupon 2 from the center of the rebar failed at the lateral grip on the top at a peak load of 4,475 lbs. (20 kN) and a peak strain of 15,300x10^{-6}. The strain values were recorded with both strain gauges and extensometer; however, the extensometer was removed at 3,500 lbs. Therefore, the stress strain curve uses the values obtained from the strain gauge. The stress strain curve for this bar is shown in Fig. 17. A summary of the tensile test results is shown in Table 5.

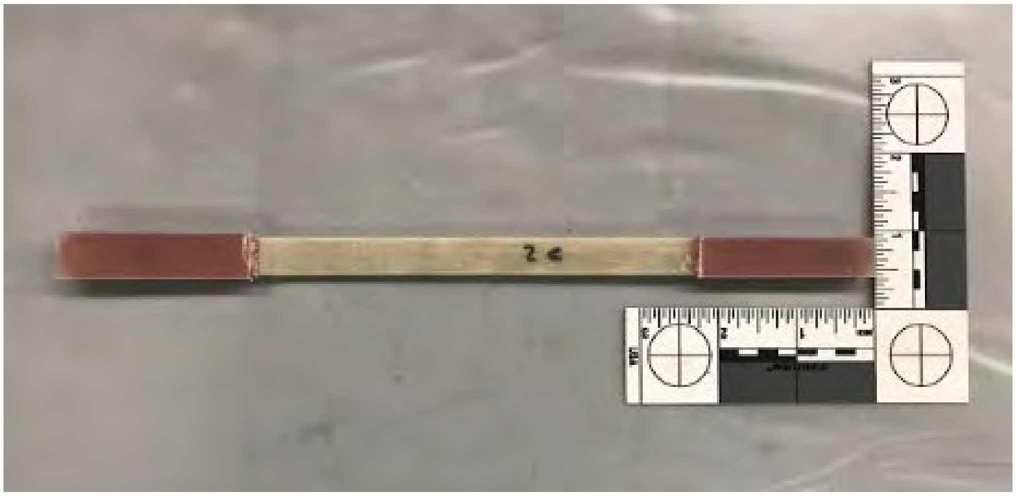

Fig. 15. Coupon E_2C before testing

Fig. 16. Coupon E_2C after failure

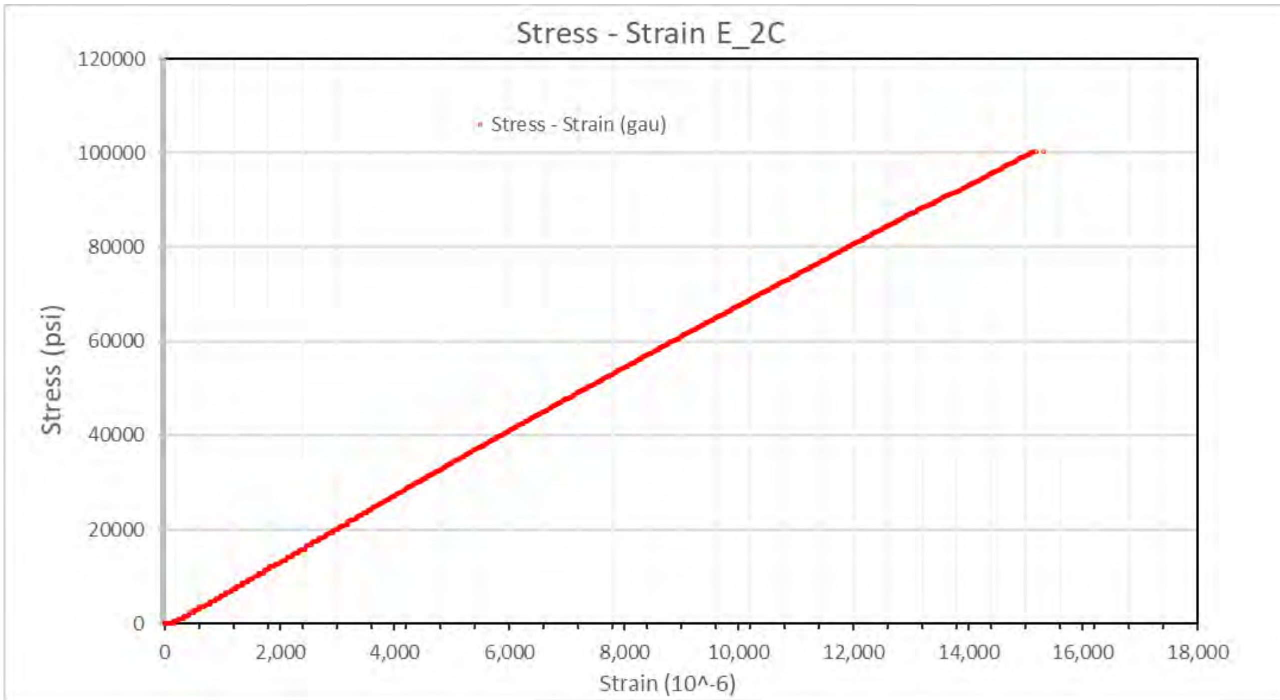

Fig. 17. Stress strain curve for E_2C

Table 5. 2C properties

Sample #	Area, sq. in (sq. mm)	Peak Load, lbs (kN)	Max Stress, psi (MPa)	Peak Strain (10^-6)
2L	0.0446 (29)	4,475 (20)	100,215 (691)	15,300

1.1.6. Bar E_2R

Sierrita de la Cruz Creek coupon 2 from the right side of the rebar failed with the splitting of gage at various points at a peak load of 4,597 lbs. (20 kN) and a peak strain of $13{,}000 \times 10^{-6}$. The coupon before testing and after failure are shown in Fig. 18 and Fig. 19, respectively. The strain values were recorded with both strain gauges and extensometer; however, the extensometer was removed at 3,500 lbs. Therefore, the stress strain curve uses the values obtained from the strain gauge. The stress strain curve for this bar is shown in Fig. 20. A summary of the tensile test results is shown in Table 6.

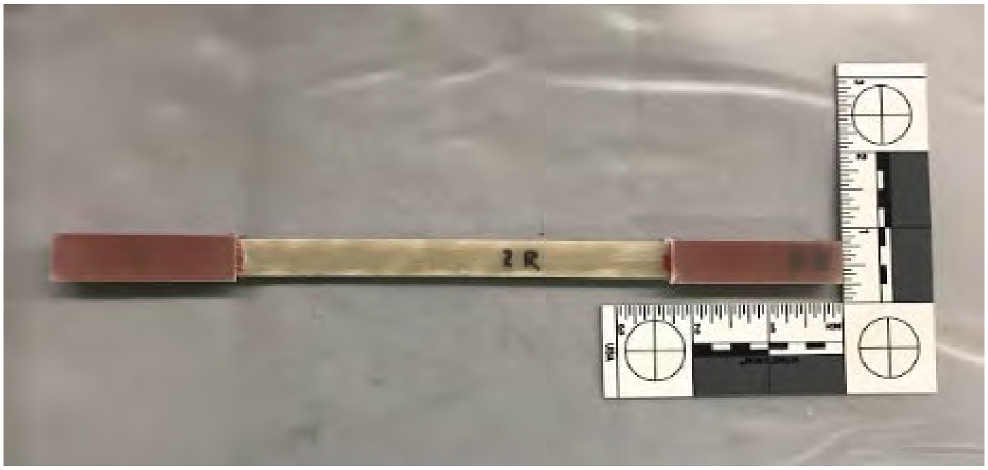

Fig. 18. Coupon E_2R before testing

Fig. 19. Coupon E_2R after failure

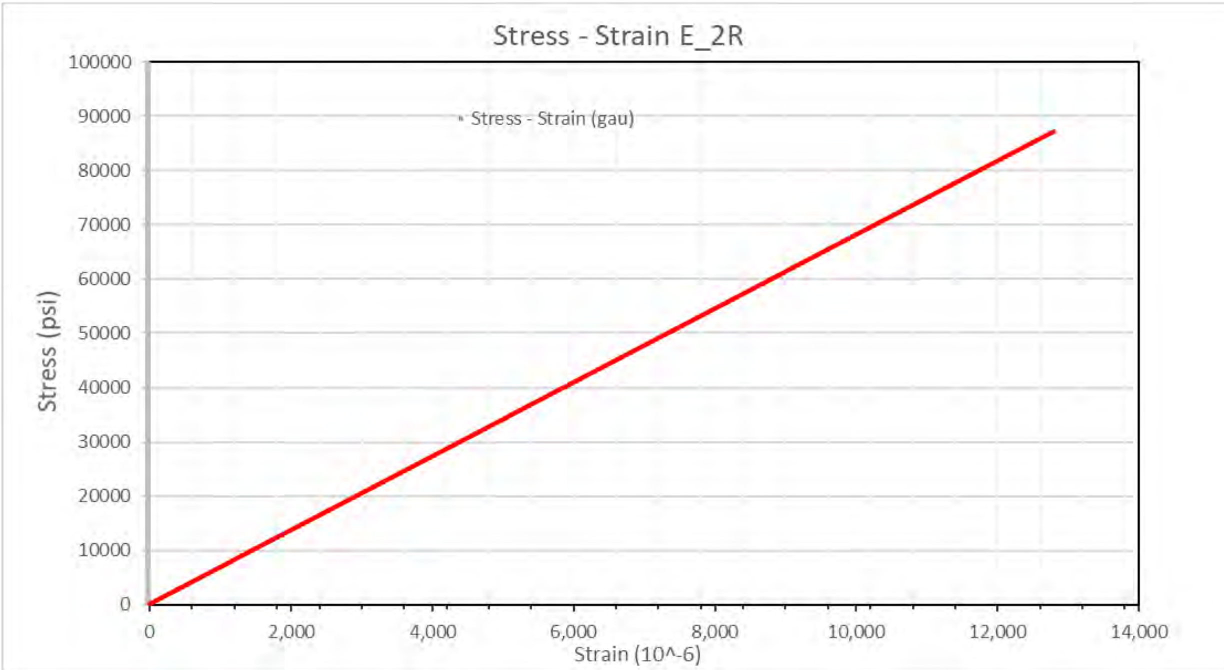

Fig. 20. Stress strain curve for E_2R

Sample #	Area, sq. in (sq. mm)	Peak Load, lbs (kN)	Max Stress, psi (MPa)	Peak Strain (10^-6)
2R	0.0528 (34.0)	4,597 (20)	87,131 (601)	13,000

Table 6. 2R properties

1.1.7. Bar E_3L

Sierrita de la Cruz Creek coupon 3 from the left side of the rebar failed with the splitting of gage at various points at a peak load of 2,992 lbs. (13 kN) The coupon before testing and after failure are shown in Fig. 21 and Fig. 22, respectively. Due to test issues, the strain for this bar could not be recorded, however, a stress curve is shown in Fig. 23. A summary of the tensile test results is shown in Table 7.

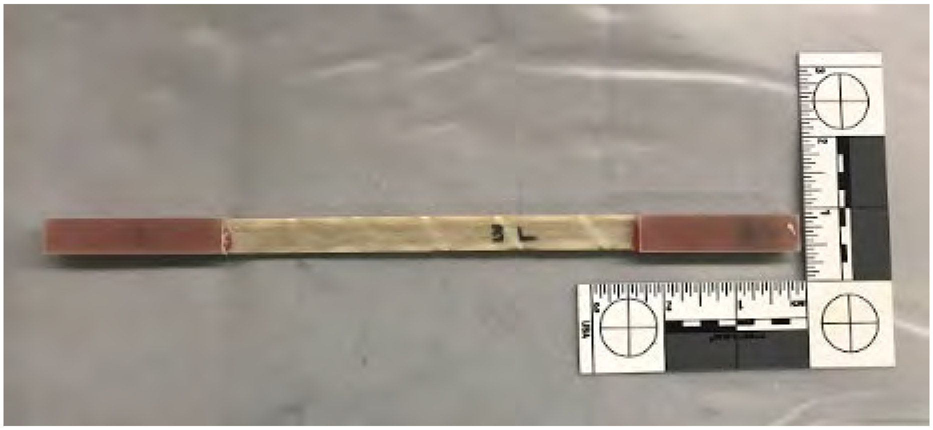

Fig. 21. Coupon E_3L before testing

Fig. 22. Coupon E_3L after failure

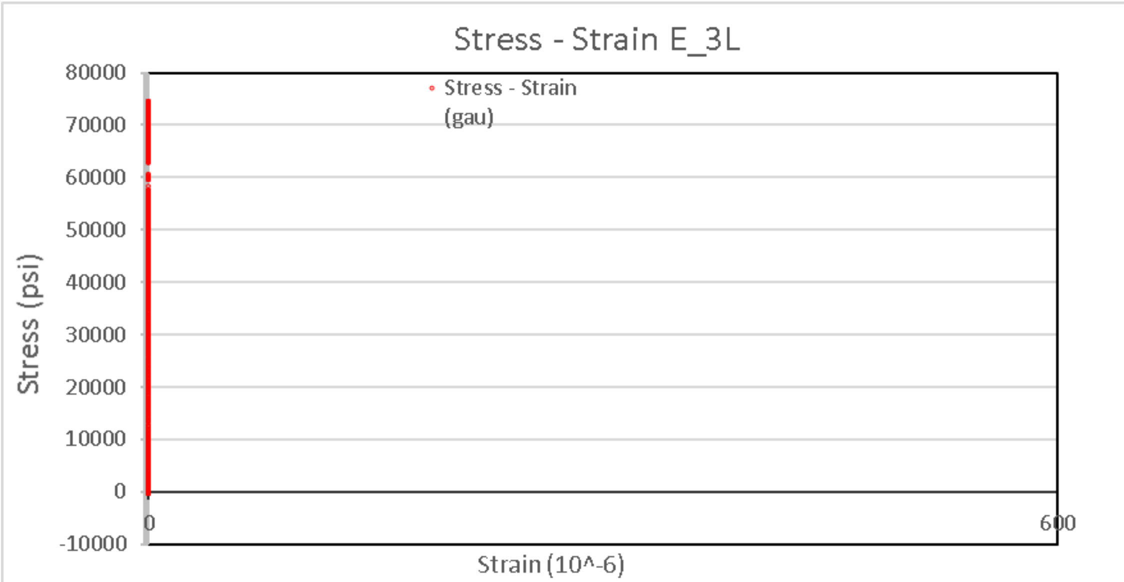

Fig. 23. Stress curve for E_3L. Strain was not recorded.

Table 7. 3L properties

Sample #	Area, sq. in (sq. mm)	Peak Load, lbs (kN)	Max Stress, psi (MPa)
3L	0.0402 (25.9)	2,989 (13)	74,386 (513)

1.1.8. Bar E_3C

Sierrita de la Cruz Creek coupon 3 from the center of the rebar failed with the splitting of gage at various points at a peak load of 4,621 lbs. (21 kN). The coupon before testing and after failure are shown in Fig. 24 and Fig. 25, respectively. Due to test issues, the strain for this bar could not be recorded, however, a stress curve is shown in Fig. 26. A summary of the tensile test results is shown in Table 8.

Fig. 24. Coupon E_3C before testing

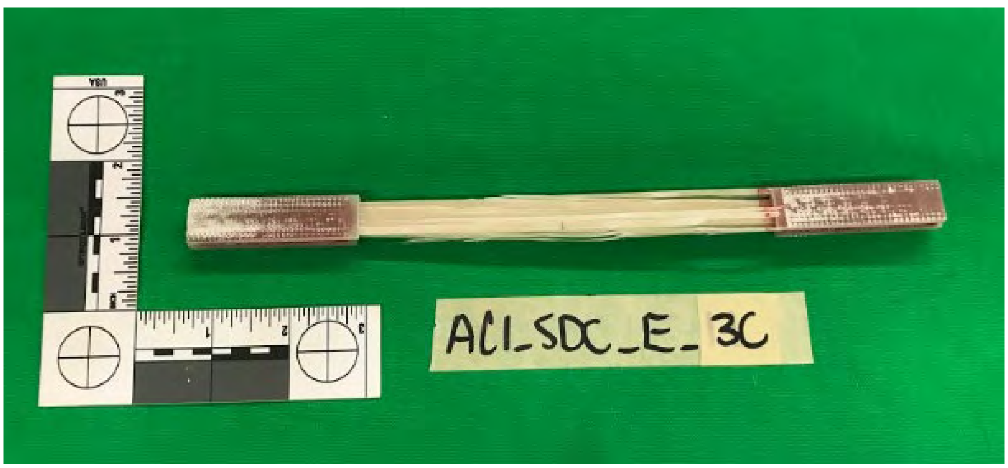

Fig. 25. Coupon E_3C after failure

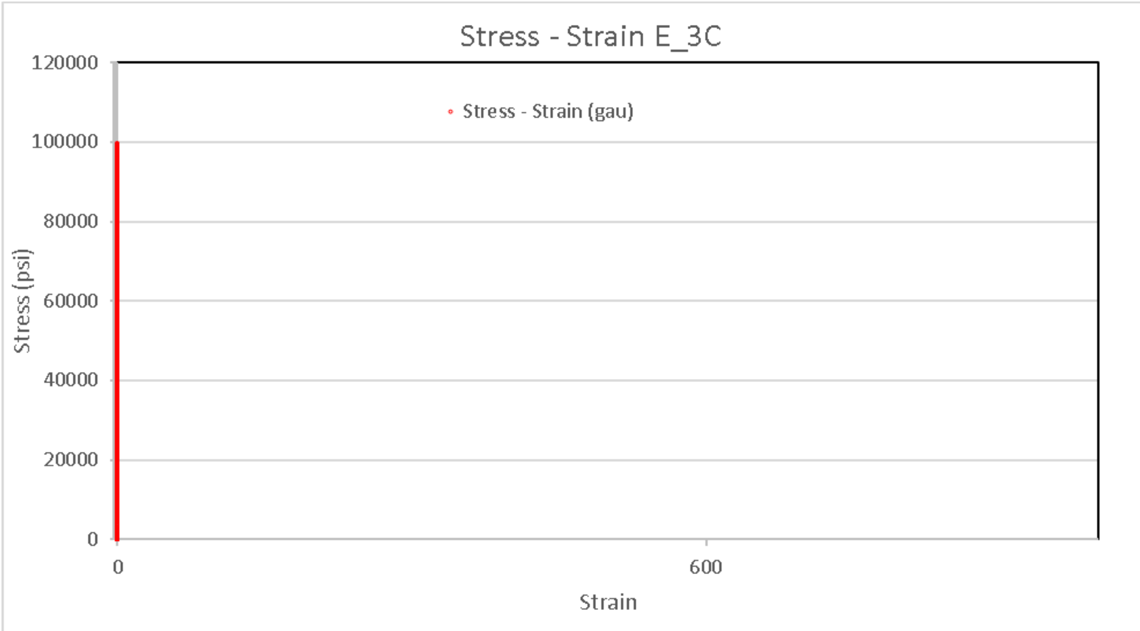

Fig. 26. Stress strain curve for E_3C. Strain was not recorded

Table 8. 3C properties

Sample #	Area, sq. in (sq. mm)	Peak Load, lbs (kN)	Max Stress, psi (MPa)
3C	0.0464 (29.9)	4,621 (21)	99,434 (686)

1.1.9. Bar E_3R

Sierrita de la Cruz Creek coupon 3 from the right side of the rebar failed with the splitting of gage at various points at a peak load of 4,330 lbs. (19 kN) and a peak strain of 13,112x10^{-6}. The coupon before testing and after failure are shown in Fig. 27 and Fig. 28, respectively. The strain values were recorded with both strain gauges and extensometer; however, the extensometer was removed at 3,500 lbs. Therefore, the stress strain curve uses the values obtained from the strain gauge. The stress strain curve for this bar is shown in Fig. 29. A summary of the tensile test results is shown in Table 9.

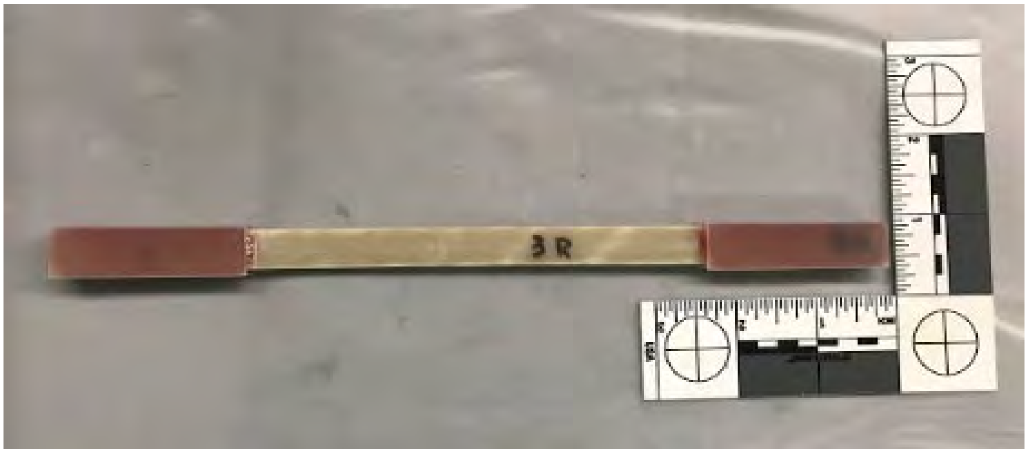

Fig. 27. Coupon E_3R

Fig. 28. Coupon E_3R after failure

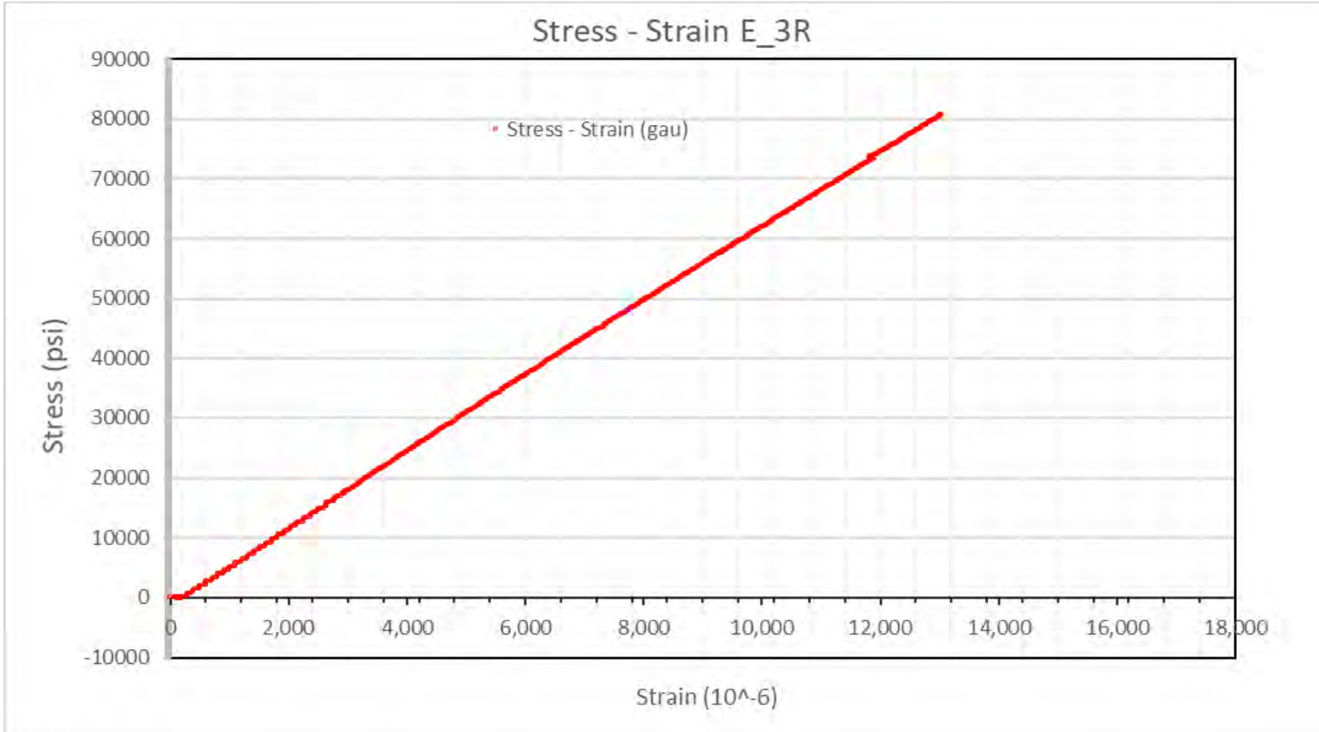

Fig. 29. Stress strain for E_3R

Table 9. 3R properties

Sample #	Area, sq. in (sq. mm)	Peak Load, lbs (kN)	Max Stress, psi (MPa)	Peak Strain (10^-6)
3R	0.0533 (34.4)	4,330 (19)	81,188 (560)	13,112

1.2 Pristine coupons

A total of 10 coupons from pristine bars were tested. Fig. 30 shows the pristine coupons.

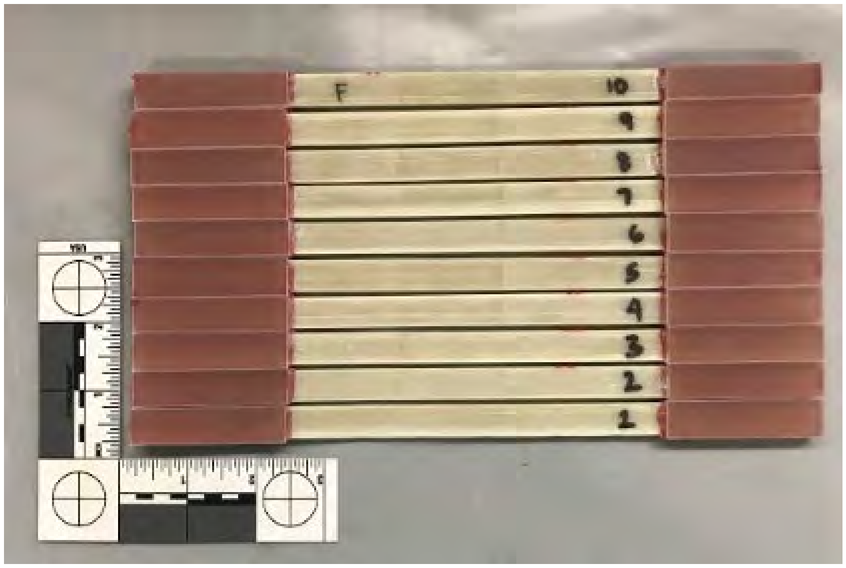

Fig. 30. Pristine coupons

1.2.1 Bar F_1

Pristine coupon 1 failed with the splitting of gage at various points at a peak load of 4,929 lbs (22kN) and a peak strain of 17,900x10^{-6}. The coupon after failure is shown in Fig. 31. The strain values were recorded with both strain gauges and extensometer; however, the extensometer was removed at 4,000 lbs. Therefore, the stress strain curve uses the values obtained from the strain gauge. The stress strain curve for this bar is shown in Fig. 32. A summary of the tensile test results is shown in Table 10.

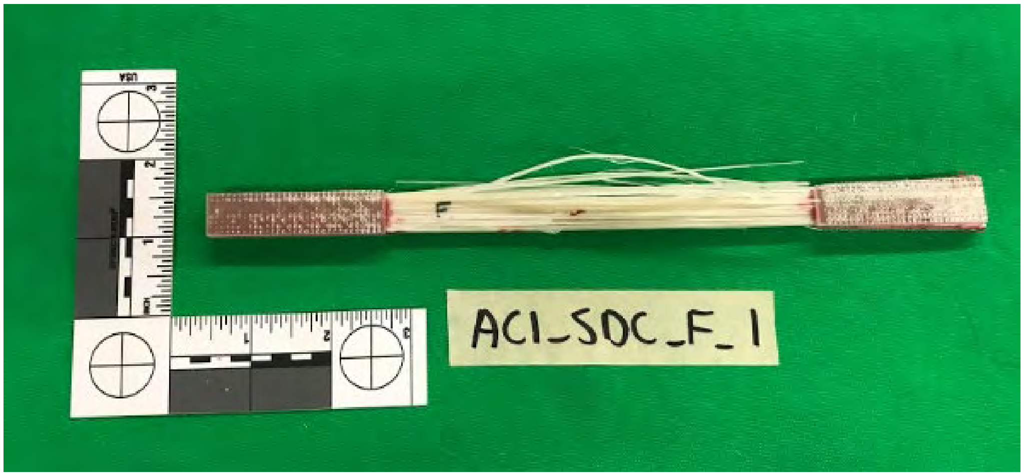

Fig. 31. Coupon F_1 after failure

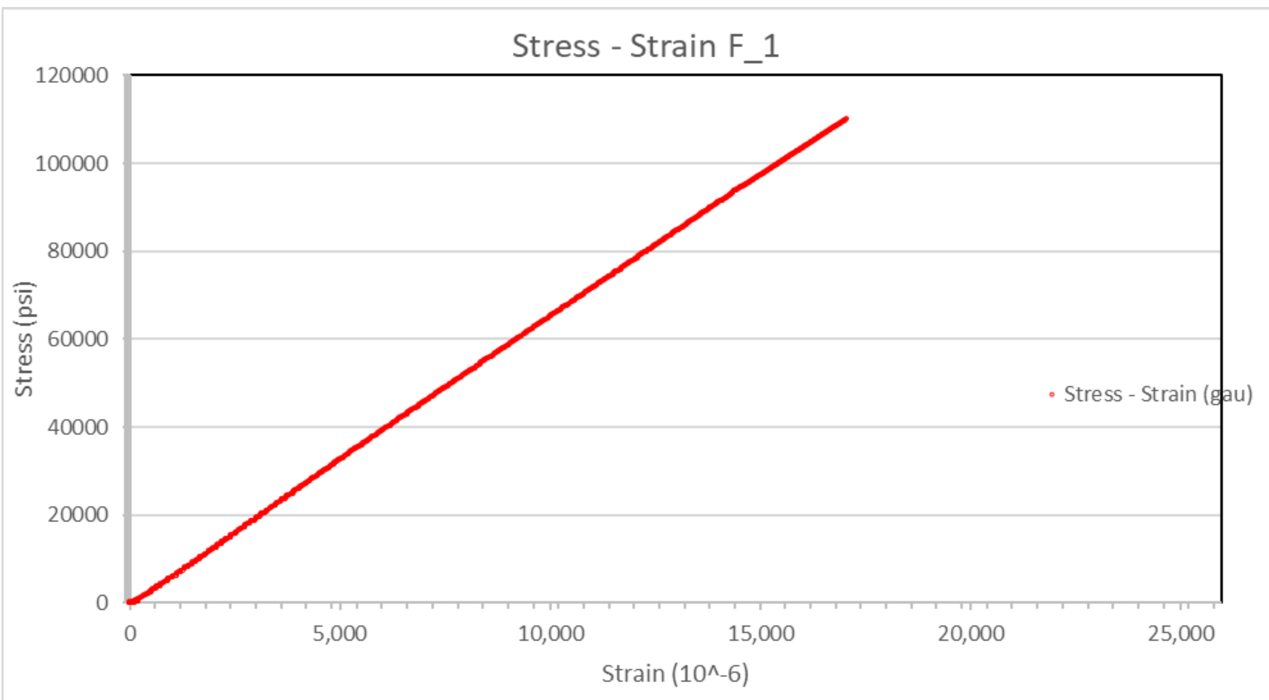

Fig. 32. Stress strain curve for F_1

Table 10. F_1 properties

Sample #	Area, sq. in (sq. mm)	Peak Load, lbs (kN)	Max Stress, psi (MPa)	Peak Strain (10^-6)
F_1	0.0518 (33.4)	5,696 (25)	110,014 (759)	17,900

1.2.2 Bar F_2

Pristine coupon 2 failed with the splitting of gage at various points at a peak load of 4,609 lbs. (20 kN). The coupon after failure is shown in Fig. 33. Due to test issues, the strain for this bar could not be recorded, however, a stress curve is shown in Fig. 34. A summary of the tensile test results is shown in Table 11.

Fig. 33. Coupon F_2 after failure

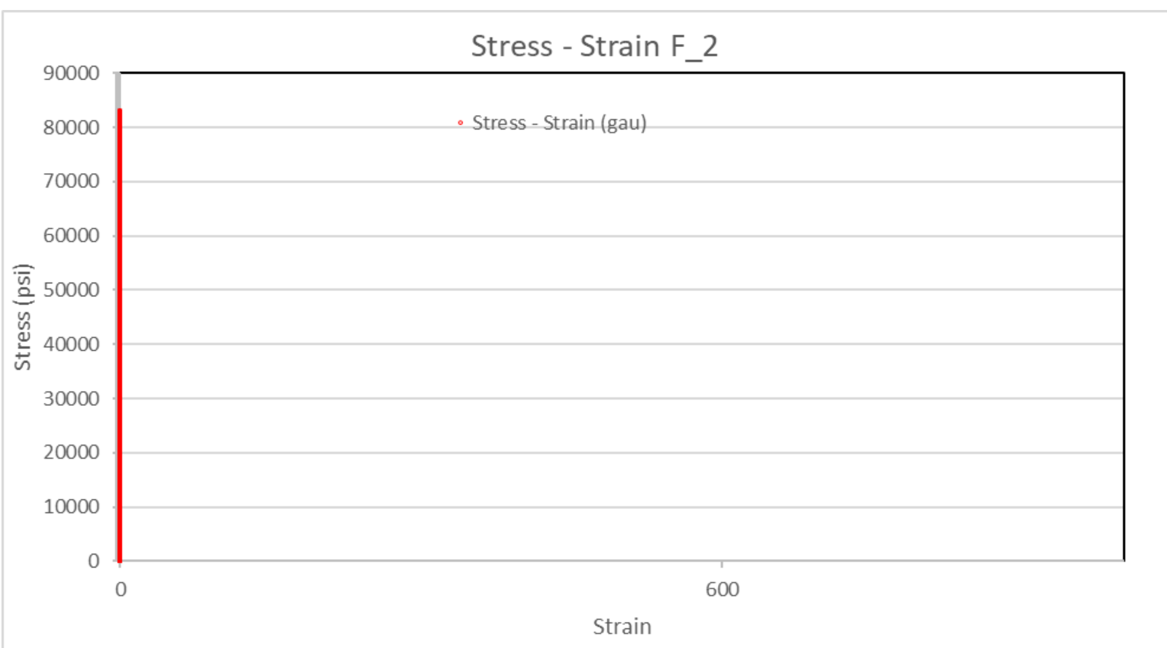

Fig. 34. Stress strain for F_2. Strain was not recorded.

Table 11. F_2 properties

Sample #	Area, sq. in (sq. mm)	Peak Load, lbs (kN)	Max Stress, psi (MPa)
F_2	0.0555 (35.8)	4,609 (20)	83,094 (573)

1.2.3 Bar F_3

Pristine coupon 3 failed with the splitting of gage at various points at a peak load of 4,894 lbs. (12 kN) and peak strain of 15,000x10^{-6}. The coupon after failure is shown in Fig. 35. The strain values were recorded with both strain gauges and extensometer; however, the extensometer was removed at 4,000 lbs. Therefore, the stress strain curve uses the values obtained from the strain gauge. The stress strain curve for this bar is shown in Fig. 36. A summary of the tensile test results is shown in Table 12.

Fig. 35. Coupon F_3 after failure

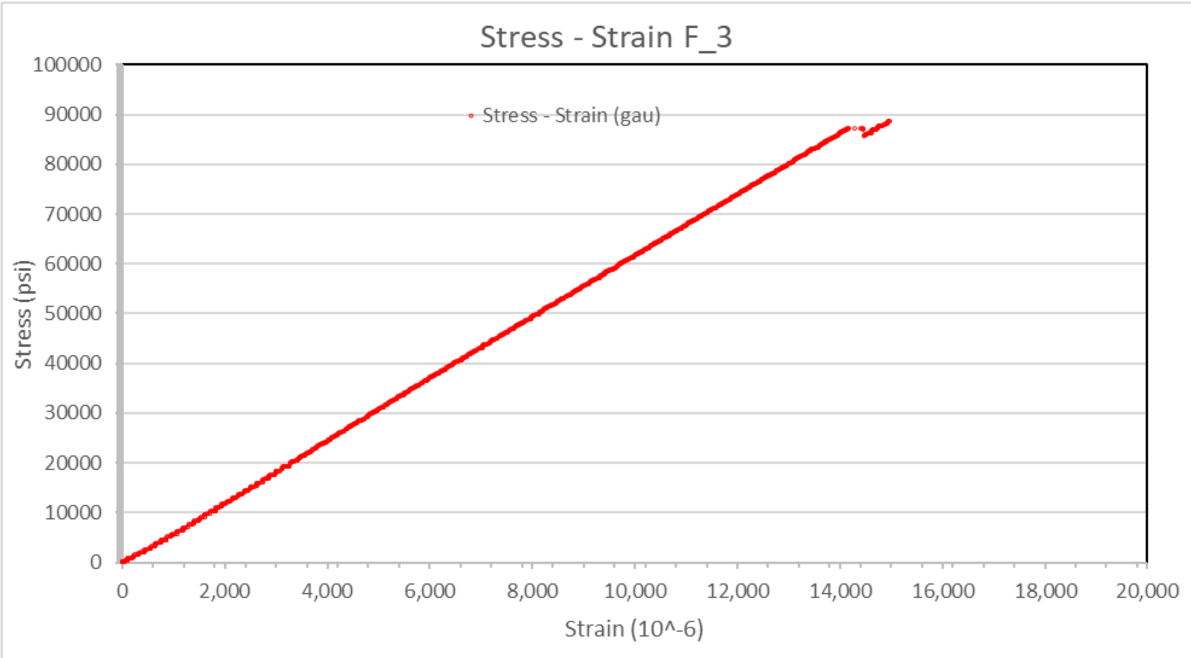

Fig. 36. Stress strain curve for F_3

Table 12. F_3 properties

Sample #	Area, sq. in (sq. mm)	Peak Load, lbs (kN)	Max Stress, psi (MPa)	Peak Strain (10^-6)
F_3	0.0553 (37)	4,894 (22)	88,488 (610)	15,000

1.2.4 Bar F_4

Pristine coupon 4 failed with the splitting of gage at various points at a peak load of 4,538 lbs. (20 kN) and a maximum strain of 15,500x10^{-6}. The coupon after failure is shown in Fig. 37. The strain values were recorded with both strain gauges and extensometer; however, the extensometer was removed at 4,000 lbs. Therefore, the stress strain curve uses the values obtained from the strain gauge. The strain gauge recorded inaccurate values at stresses higher than about 98,000 psi. The stress strain curve for this bar is shown in Fig. 38. A summary of the tensile test results is shown in Table 13.

Fig. 37. Coupon F_4 after failure

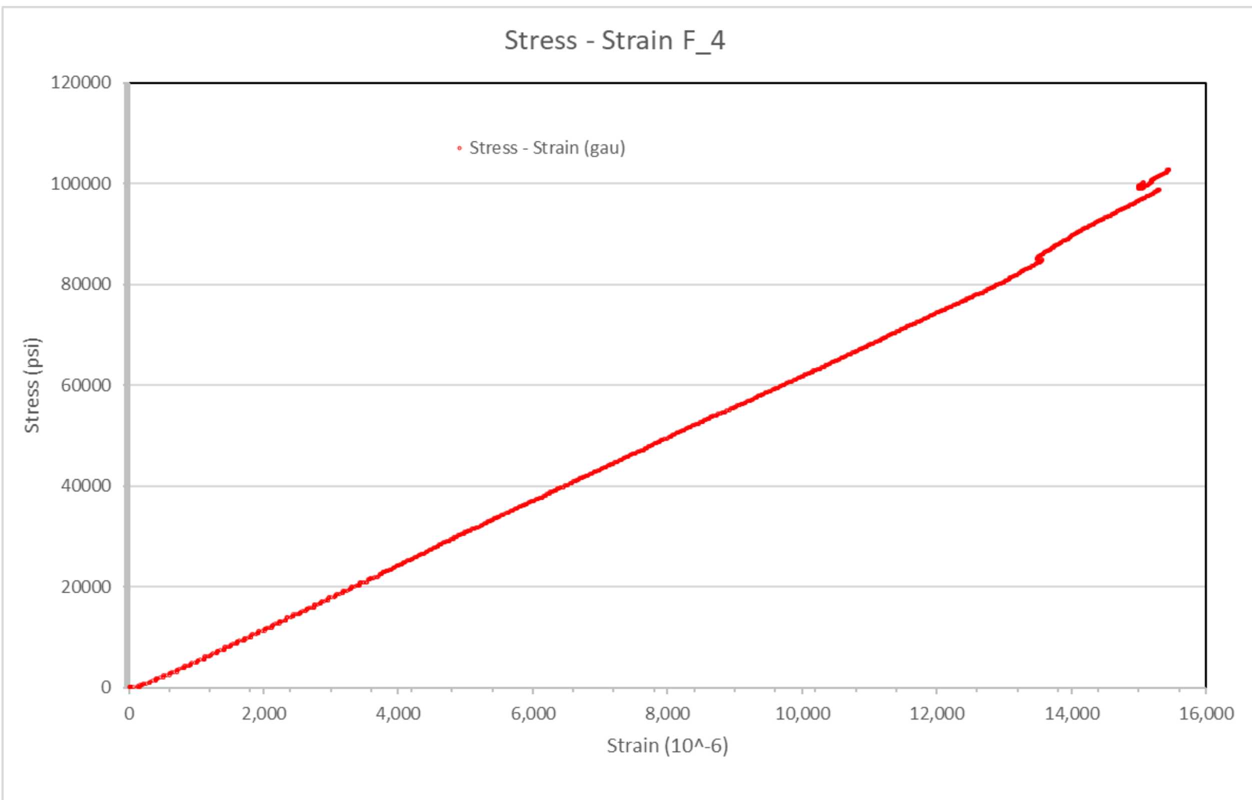

Fig. 38. Stress strain curve for F_4

Table 13. F_4 properties

Sample #	**Area, sq. in (sq. mm)**	**Peak Load, lbs (kN)**	**Max Stress, psi (MPa)**	**Peak Strain (10^-6)**
F_4	0.0442 (28.5)	4,538 (20)	102,772 (709)	15,500

1.2.5 Bar F_5

Pristine coupon 5 failed with the splitting of gage at various points at a peak load of 5,321 lbs. (24 kN) and a maximum strain of 19,400x10^{-6}. The coupon after failure is shown in Fig. 39. The strain values were recorded with both strain gauges and extensometer; however, the extensometer was removed at 4,000 lbs. Therefore, the stress strain curve uses the values obtained from the strain gauge. The stress strain curve for this bar is shown in Fig. 40. A summary of the tensile test results is shown in Table 14.

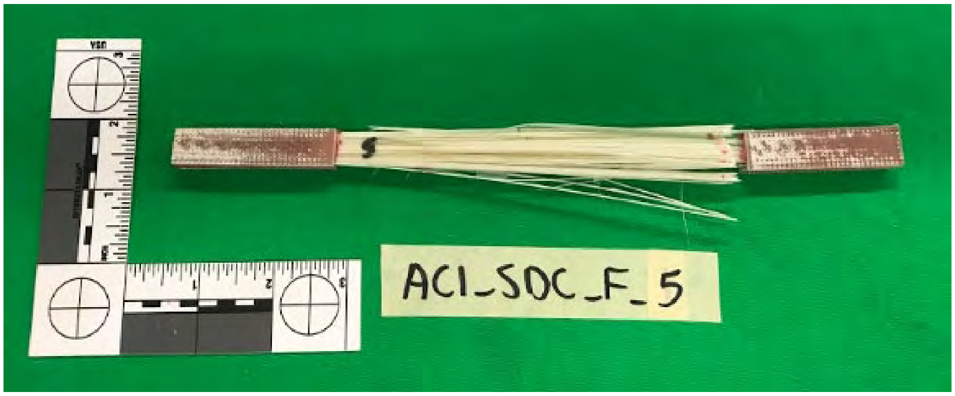

Fig. 39. Coupon F_5 after failure

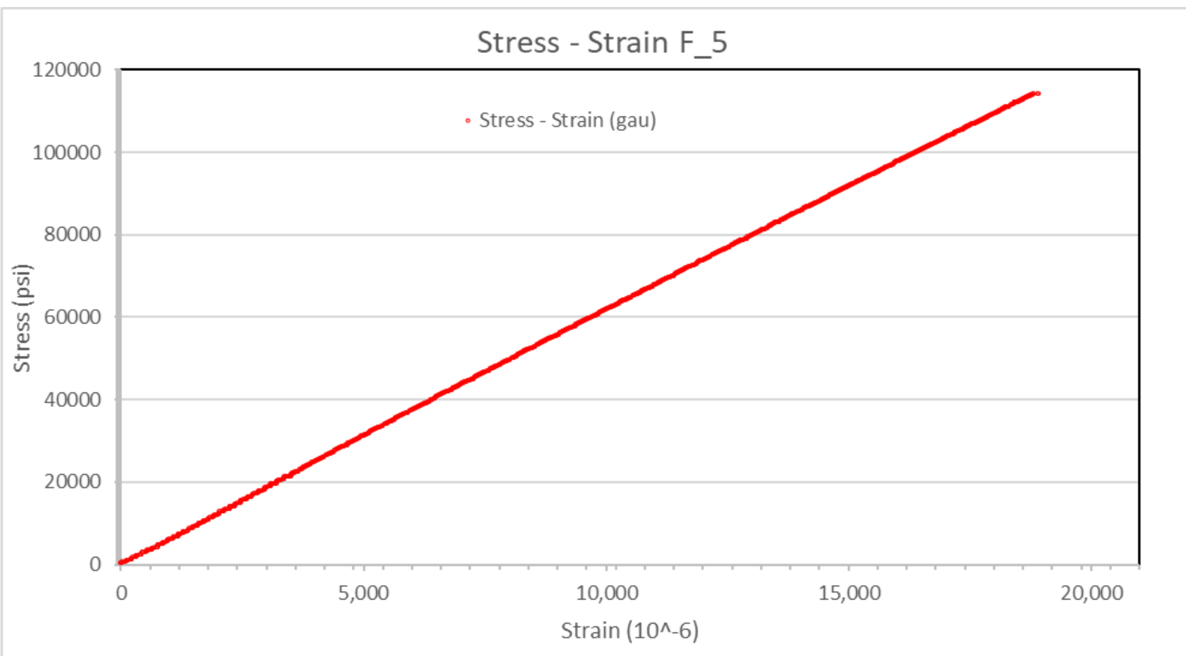

Fig. 40. Stress strain curve for F_5

Table 14. F_5 properties

Sample #	Area, sq. in (sq. mm)	Peak Load, lbs (kN)	Max Stress, psi (MPa)	Peak Strain (10^-6)
F_5	0.0466 (30.1)	5,321 (24)	114,108 (787)	19,400

1.2.6 Bar F_6

Pristine coupon 6 failed with the splitting of gage at various points at a peak load of 4,065 lbs. and a maximum strain of $14{,}077 \times 10^{-6}$. The coupon after failure is shown in Fig. 41. The strain values were recorded with both strain gauges and extensometer; however, the extensometer was removed at 4,000 lbs. Therefore, the stress strain curve uses the values obtained from the strain gauge. The stress strain curve for this bar is shown in Fig. 42. A summary of the tensile test results is shown in Table 15.

Fig. 41. Coupon F_6 after failure

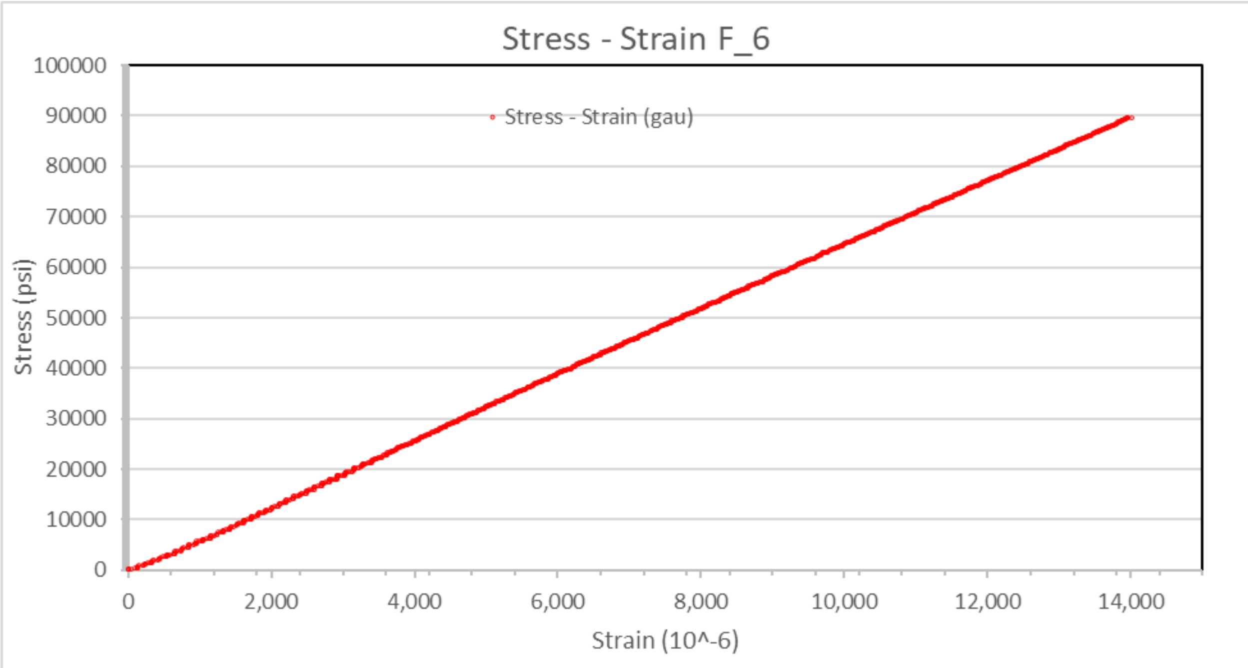

Fig. 42. Stress strain curve for F_6

Table 15. F_6 properties

Sample #	Area, sq. in (sq. mm)	Peak Load, lbs (kN)	Max Stress, psi (MPa)	Peak Strain (10^-6)
F_6	0.0454 (30)	4,065 (18)	89,583 (618)	14,077

1.2.7 Bar F_7

Pristine coupon 7 failed with the splitting of gage at various points at a peak load of 4,110 lbs. (18 kN) and strain of 15,300x10^{-6}. The coupon after failure is shown in Fig. 43. The stress strain curve for this bar is shown in Fig. 44. The strain values were recorded with both strain gauges and extensometer; however, the extensometer was removed at 4,000 lbs. Therefore, the stress strain curve uses the values obtained from the strain gauge. A summary of the tensile test results is shown in Table 16.

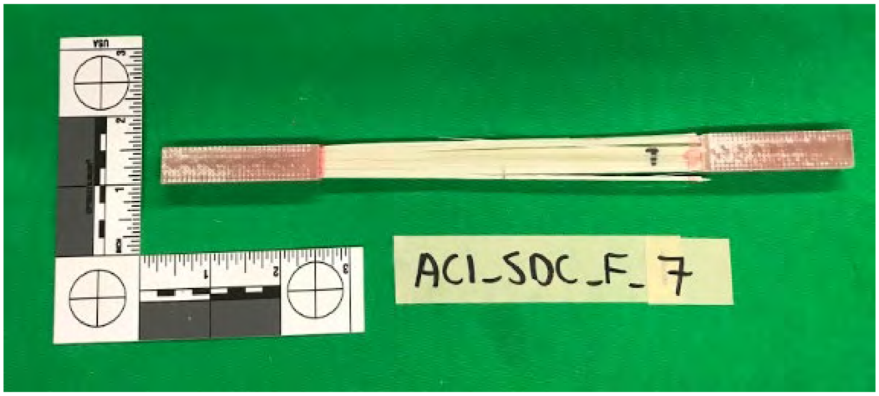

Fig. 43. Coupon F_7 after failure

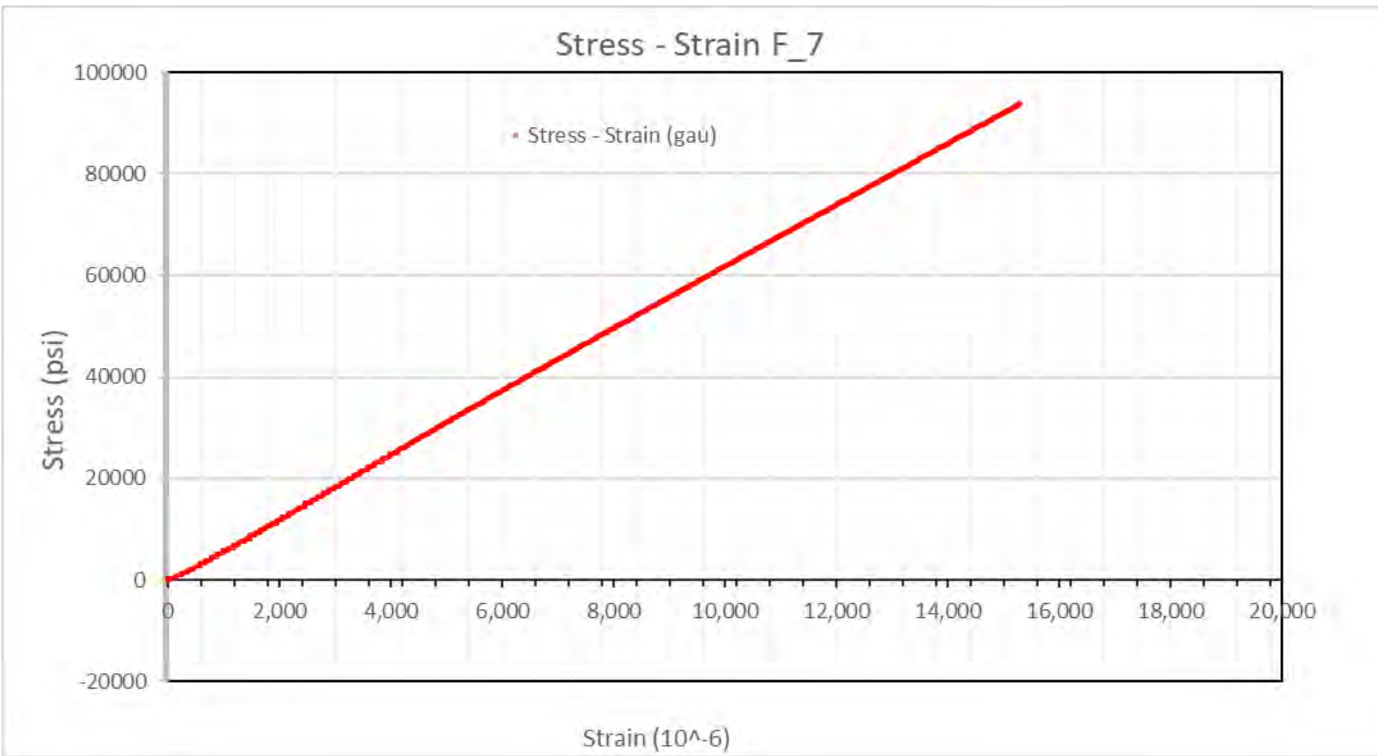

Fig. 44. Stress strain curve for F_7

Table 16. F_7 properties

Sample #	**Area, sq. in (sq. mm)**	**Peak Load, lbs (kN)**	**Max Stress, psi (MPa)**	**Peak Strain (10^-6)**
F_7	0.0439 (28)	4,110 (18)	93,740 (646)	15,300

1.2.8 Bar F_8

Pristine coupon 8 failed with the splitting of gage at various points at a peak load of 4,609 lbs. (20 kN) and a maximum strain of 15,900x10^{-6}. The coupon after failure is shown in Fig. 45. The stress strain curve for this bar is shown in Fig. 46. The strain values were recorded with both strain gauges and extensometer; however, the extensometer was removed at 4,000 lbs. Therefore, the stress strain curve uses the values obtained from the strain gauge. A summary of the tensile test results is shown in Table 17.

Fig. 45. Coupon F_8 after failure

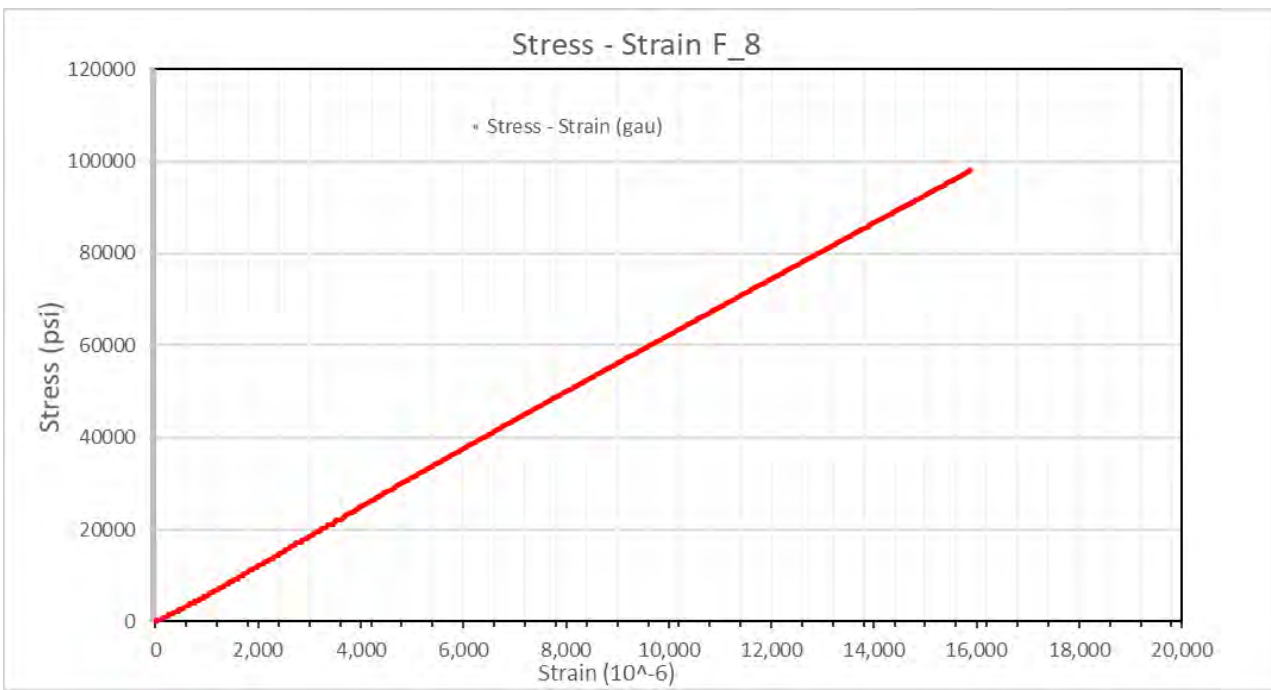

Fig. 46. Stress strain for F_8

Table 17. F_8 properties

Sample #	Area, sq. in (sq. mm)	Peak Load, lbs (kN)	Max Stress, psi (MPa)	Peak Strain (10^-6)
F_8	0.0471 (30.4)	4,609 (20)	97,934 (675)	15,900

1.2.9 Bar F_9

Pristine coupon 9 failed with the splitting of gage at various points at a peak load of 5,207 lbs. (23 kN) and a maximum strain of 15,600x10^{-6}. The coupon after failure is shown in Fig. 47. The stress strain curve for this bar is shown in Fig. 48. The coupon before testing and test set up are shown in Fig. 2 and Fig. 3, respectively. The failed coupon and the stress strain curve shown in Fig. 4 and Fig. 5, respectively. The strain values were recorded with both strain gauges and extensometer; however, the extensometer was removed at 4,000 lbs. Therefore, the stress strain curve uses the values obtained from the strain gauge. A summary of the tensile test results is shown in Table 18.

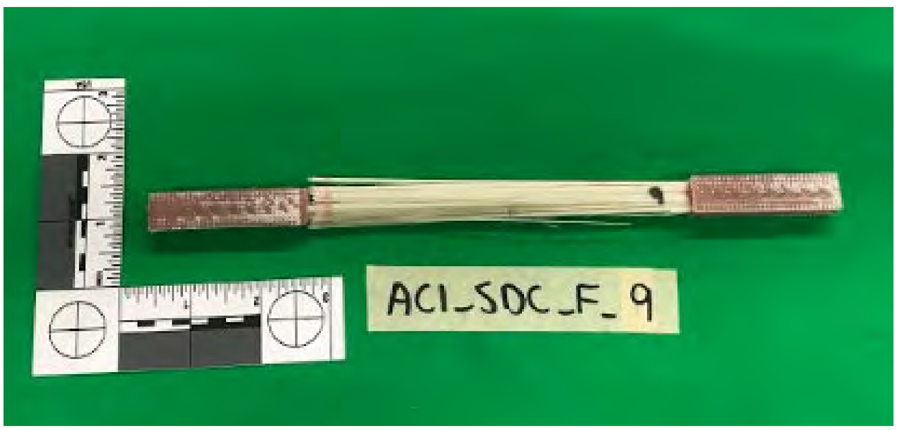

Fig. 47. Coupon F_9 after failure

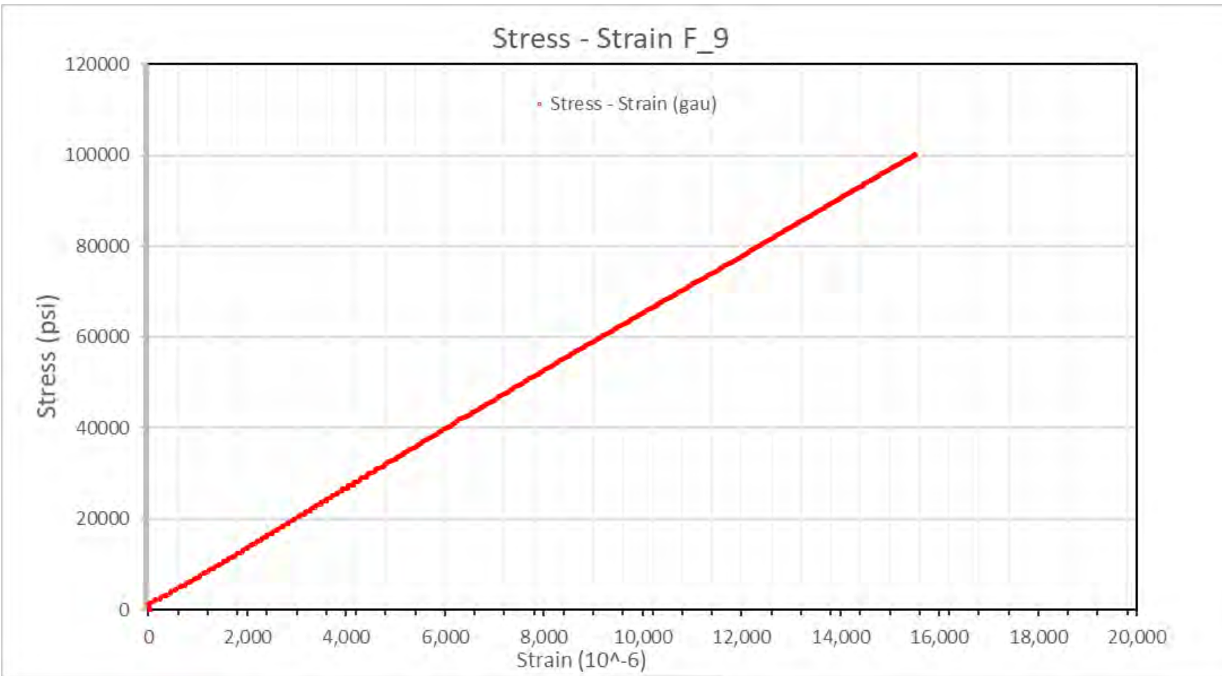

Fig. 48. Stress strain curve for F_9

Table 18. F_9 properties

Sample #	Area, sq. in (sq. mm)	Peak Load, lbs (kN)	Max Stress, psi (MPa)	Peak Strain (10^-6)
F_9	0.0521 (33.6)	5,207 (23)	99,929 (689)	15,600

1.2.10 Bar F_10

Pristine coupon 10 failed with the splitting of gage at various points at a peak load of 4,618 lbs. (21 kN) and a maximum strain of 16,500x10^{-6}. The coupon after failure is shown in Fig. 49. The stress strain curve for this bar is shown in Fig. 50. The strain values were recorded with both strain gauges and extensometer; however, the extensometer was removed at 4,000 lbs. Therefore, the stress strain curve uses the values obtained from the strain gauge. A summary of the tensile test results is shown in Table 19.

Fig. 49. Coupon F_10 after failure

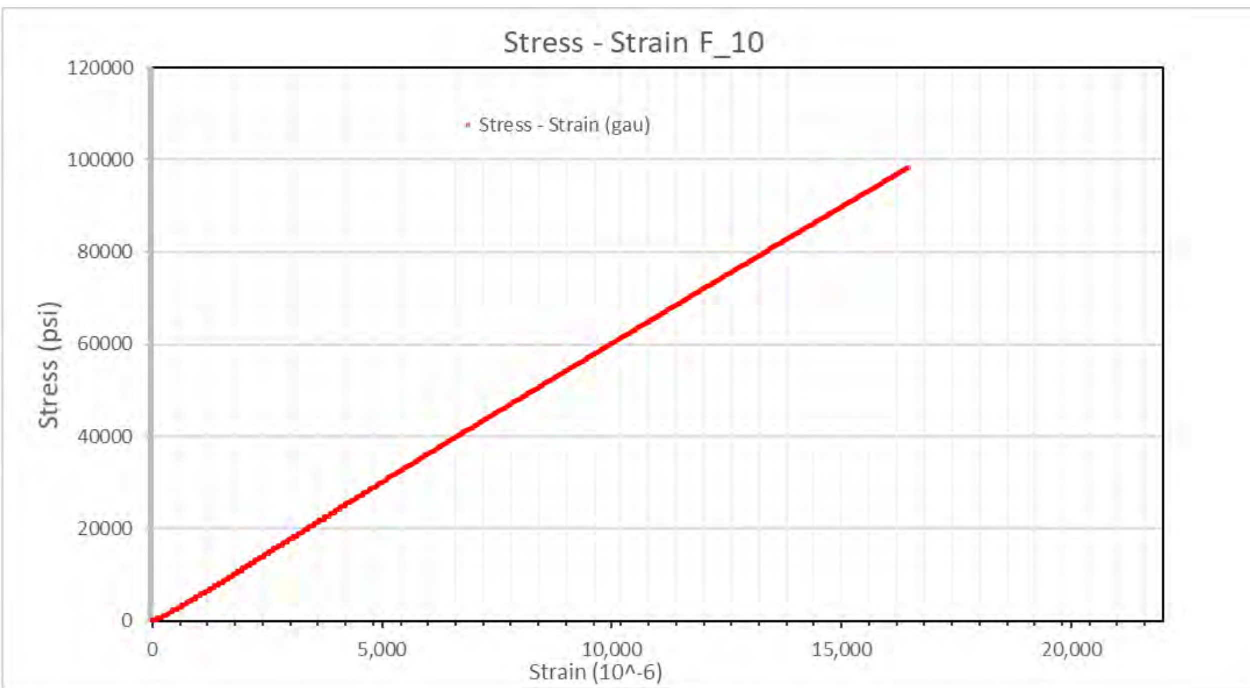

Fig. 50. Stress strain for F_10

Table 19. F_10 properties

Sample #	**Area, sq. in (sq. mm)**	**Peak Load, lbs (kN)**	**Max Stress, psi (MPa)**	**Peak Strain (10^-6)**
F_10	0.0470 (30.3)	4,618 (21)	98,265 (678)	16,500

2. Full size bar tension test

Ten full size virgin GFRP rebars were tested in tension at the University of Miami. The procedure is described in Section 4.1.8.2. The results of the pristine bar tensile tests are summarized in Table 20. All bars failed in tension.

The strain was measured with an extensometer, which was removed prior to the rebar failure. Therefore, the stress strain curves shown in this section do not include the values after the removal of the extensometer.

Table 20. Pristine GFRP bars tension test results

Sample #	Rebar Size (metric rebar size)	Peak Load, lbs (kN)	Stress, psi (MPa)
1	#5 (#16)	37312 (166)	120,360 (830)
2	#5 (#16)	38008 (169)	122,608 (845)
3	#5 (#16)	35608 (158)	114,866 (792)
4	#5 (#16)	37259 (166)	120,190 (829)
5	#5 (#16)	38186 (170)	123,180 (849)
6	#5 (#16)	35264 (157)	113,756 (784)
7	#5 (#16)	37488 (167)	120,928 (834)
8	#5 (#16)	37212 (166)	120,040 (828)
9	#5 (#16)	36756 (164)	117,986 (813)
10	#5 (#16)	36972 (165)	119,264 (822)
	Average	36988 (165)	119,318 (823)
	Std. Deviation	9335 (4.16)	3041 (21)

2.1 Bar 001

Pristine bar 001 failed at a peak load of 37,312 lbs. (166 kN). The test set up is shown in Fig. 51 and the bar after failure is shown in Fig. 52. The extensometer was removed at a load of 11,620 lbs., and therefore, the maximum strain could not be determined. The stress strain curve for this bar is shown in Fig. 53. A summary of the tensile test results is shown in Table 21.

Fig. 51. Full size virgin bar test set up

Fig. 52. Bar 001 after failure

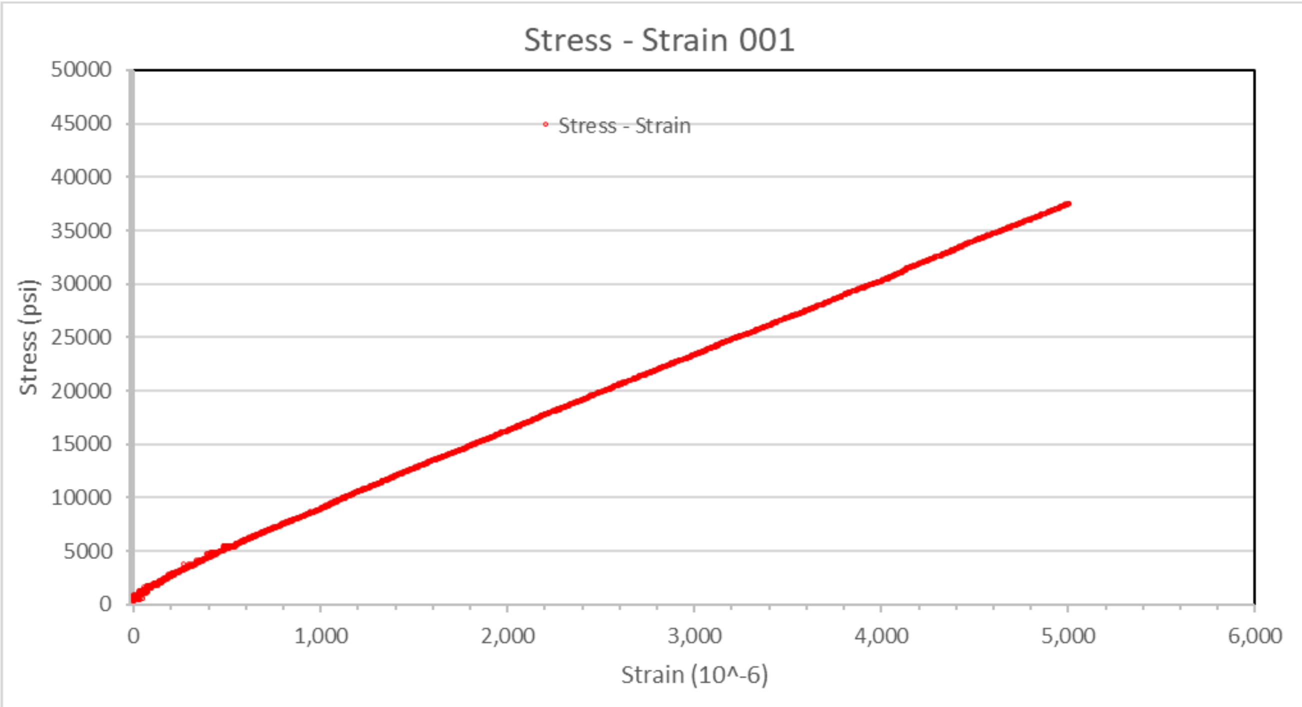

Fig. 53. Stress strain curve for bar 001

Table 21. Bar 001 properties

Sample #	Area, sq. in (sq. mm)	Peak Load, lbs (kN)	Max Stress, psi (MPa)
1	0.3100 (200)	37,312 (166)	120,360 (830)

2.2. Bar 002

Pristine bar 002 failed at a peak load of 38,008 lbs. (169 kN). The extensometer was removed at a load of 12,360 lbs., and therefore, the maximum strain could not be determined. The stress strain curve for this bar is shown in Fig. 54. A summary of the tensile test results is shown in Table 22.

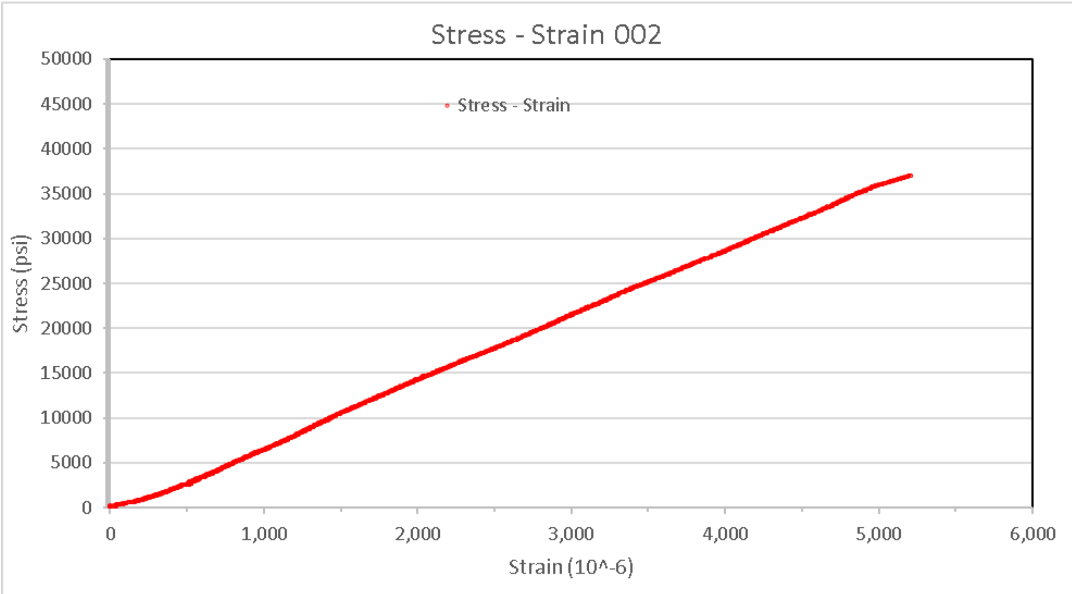

Fig. 54. Stress strain curve for bar 002

Table 22. Bar 002 properties

Sample #	Area, sq. in (sq. mm)	Peak Load, lbs (kN)	Max Stress, psi (MPa)
2	0.3100 (200)	38,008 (169)	122,608 (845)

2.3 Bar 003

Pristine bar 003 failed at a peak load of 35,608 lbs. (159 kN). A photograph of the bar after failure is shown in Fig. 55. The extensometer was removed at a load of 11,690 lbs., and therefore, the maximum strain could not be determined. The stress strain curve for this bar is shown in Fig. 56. Due to initial manipulation of the extensometer, initial conditions show initial deflection at load zero. This curve has A summary of the tensile test results is shown in Table 23.

Fig. 55. Bar 003 after failure

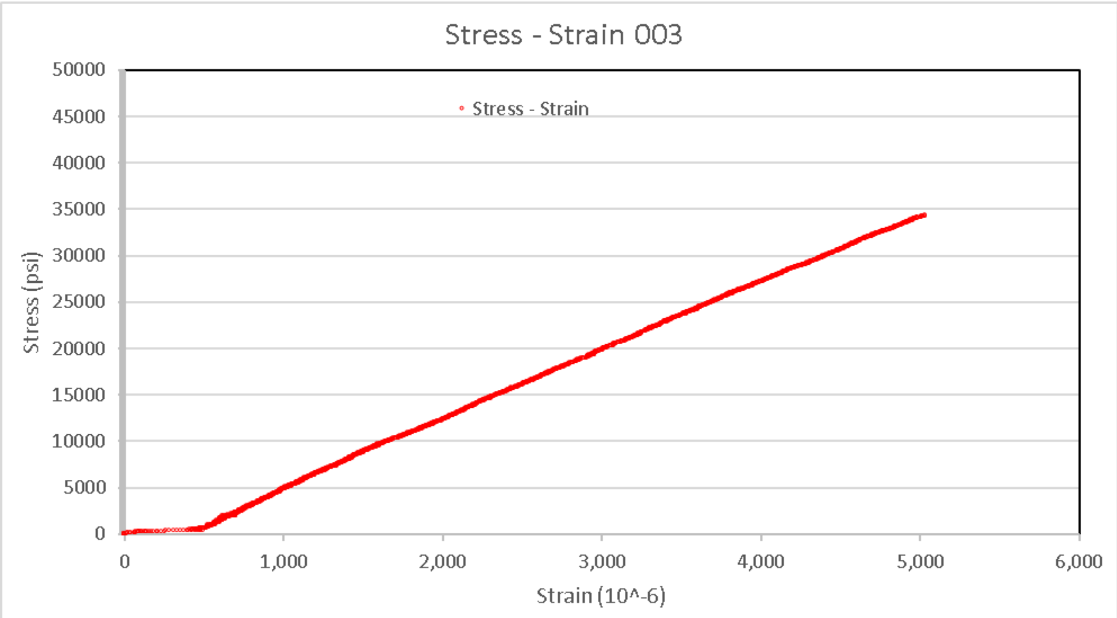

Fig. 56. Stress strain curve for bar 003

Table 23. Bar 003 properties

Sample #	Area, sq. in (sq. mm)	Peak Load, lbs (kN)	Max Stress, psi (MPa)
3	0.3100 (200)	35,608 (159 kN)	114,866 (792)

2.4 Bar 004

Pristine bar 004 failed at a peak load of 37,259 lbs. (166 kN). The extensometer was removed at a load of 12,770 lbs., and therefore, the maximum strain could not be determined. The stress strain curve for this bar is shown in Fig. 57. A summary of the tensile test results is shown in Table 24.

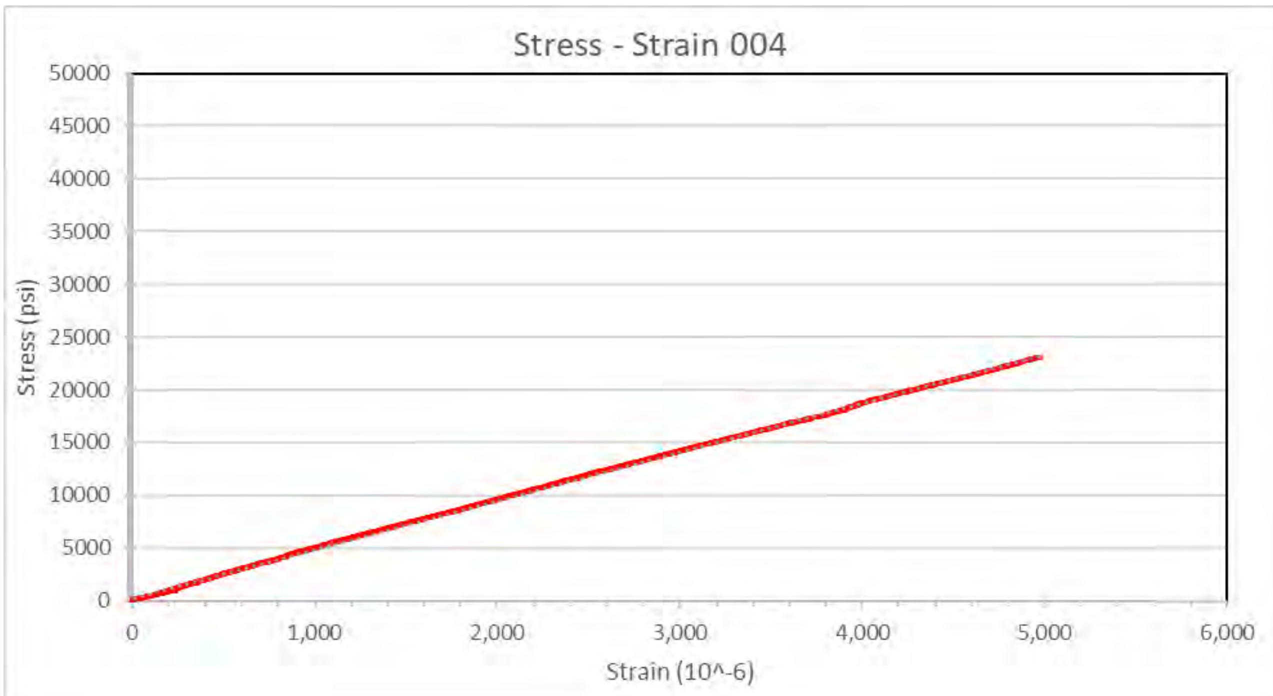

Fig. 57. Stress strain curve for bar 004

Table 24. Bar 004 properties

Sample #	Area, sq. in (sq. mm)	Peak Load, lbs (kN)	Max Stress, psi (MPa)
4	0.31 (200)	37,259 (166)	120,190 (829)

2.5 Bar 005

Pristine bar 005 failed at a peak load of 38,186 lbs. (170 kN). A photograph of the bar after failure is shown in Fig. 58. The extensometer was removed at a load of 12,150 lbs., and therefore, the maximum strain could not be determined. The stress strain curve for this bar is shown in Fig. 59. A summary of the tensile test results is shown in Table 25.

Fig. 58. Bar 005 after failure

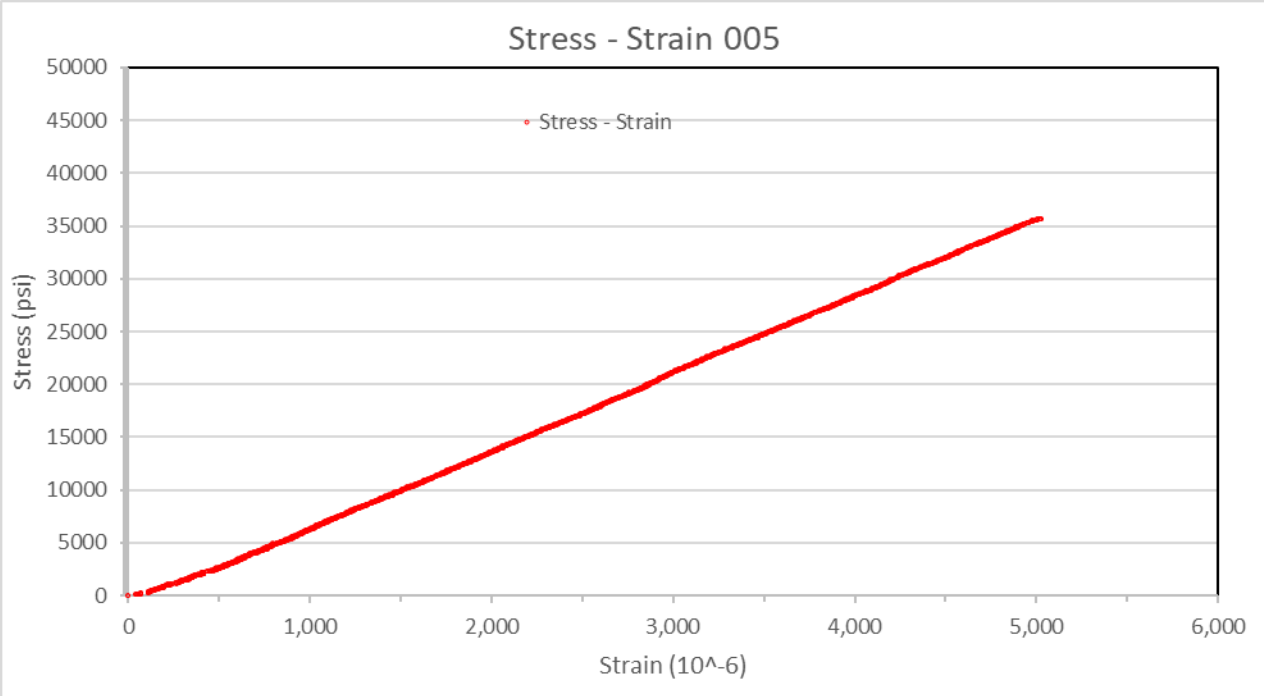

Fig. 59. Stress strain curve for bar 005

Table 25. Bar 005 properties

Sample #	Area, sq. in (sq. mm)	Peak Load, lbs (kN)	Max Stress, psi (MPa)
5	0.31 (200)	38,186 (170)	123,180 (849)

2.6 Bar 006

Pristine bar 006 failed at a peak load of 35,264 lbs. (157 kN). A photograph of the bar after failure is shown in Fig. 60. The extensometer was removed at a load of 13,360 lbs., and therefore, the maximum strain could not be determined. The stress strain curve for this bar is shown in Fig. 61. A summary of the tensile test results is shown in Table 26.

Fig. 60. Bar 006 after failure

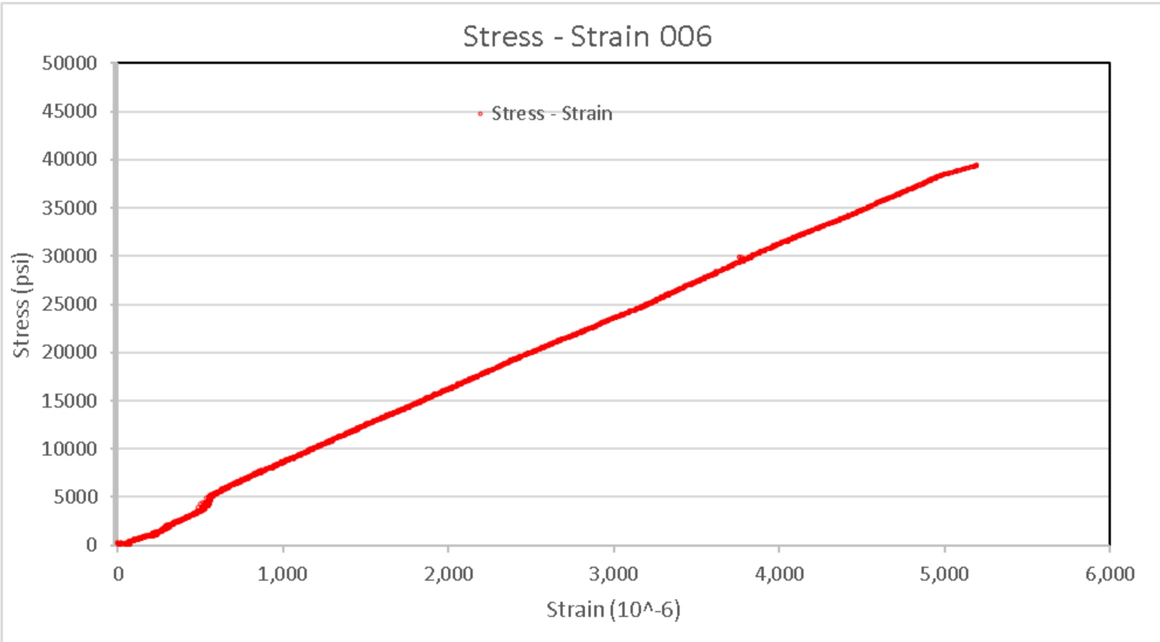

Fig. 61. Stress strain curve for bar 006

Table 26. Bar 006 properties

Sample #	Area, sq. in (sq. mm)	Peak Load, lbs (kN)	Max Stress, psi (MPa)
6	0.31 (200)	35,264 (157)	113,756 (784)

2.7 Bar 007

Pristine bar 007 failed at a peak load of 37,488 lbs. (167 kN). The extensometer was removed at a load of 14,130 lbs., and therefore, the maximum strain could not be determined. The stress strain curve for this bar is shown in Fig. 62. However, the recorded strain values are considered invalid due to the high magnitude, which is outside the range of strain for a #5 GFRP rebar. The A summary of the tensile test results is shown in Table 27.

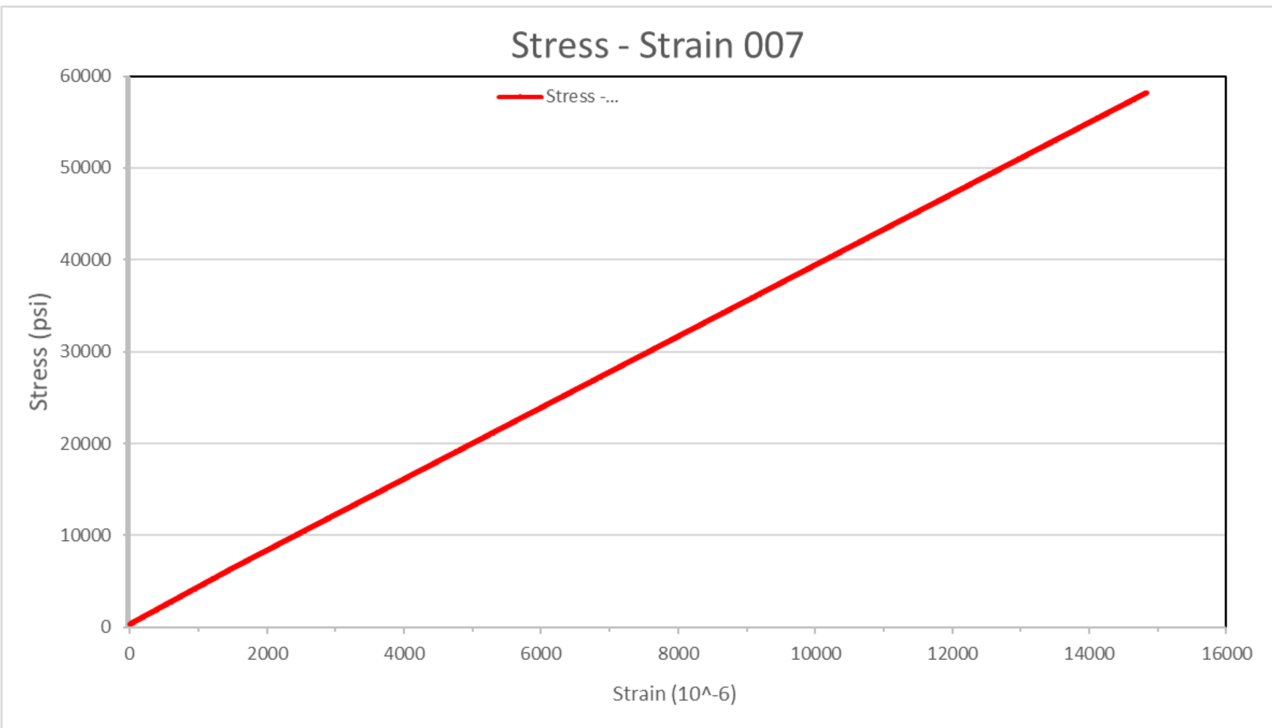

Fig. 62. Stress strain curve for bar 007

Table 27. Bar 007 properties

Sample #	Area, sq. in (sq. mm)	Peak Load, lbs (kN)	Max Stress, psi (MPa)
7	0.31(200)	37,488 (167)	120,928 (834)

2.8 Bar 008

Pristine bar 008 failed at a peak load of 37,212 lbs. (166 kN). The extensometer was removed at a load of 11,880 lbs., and therefore, the maximum strain could not be determined The bar after failure is shown in Fig. 63 and the stress strain curve for this bar is shown in Fig. 64. A summary of the tensile test results is shown in Table 28.

Fig. 63. Bar 008 after failure

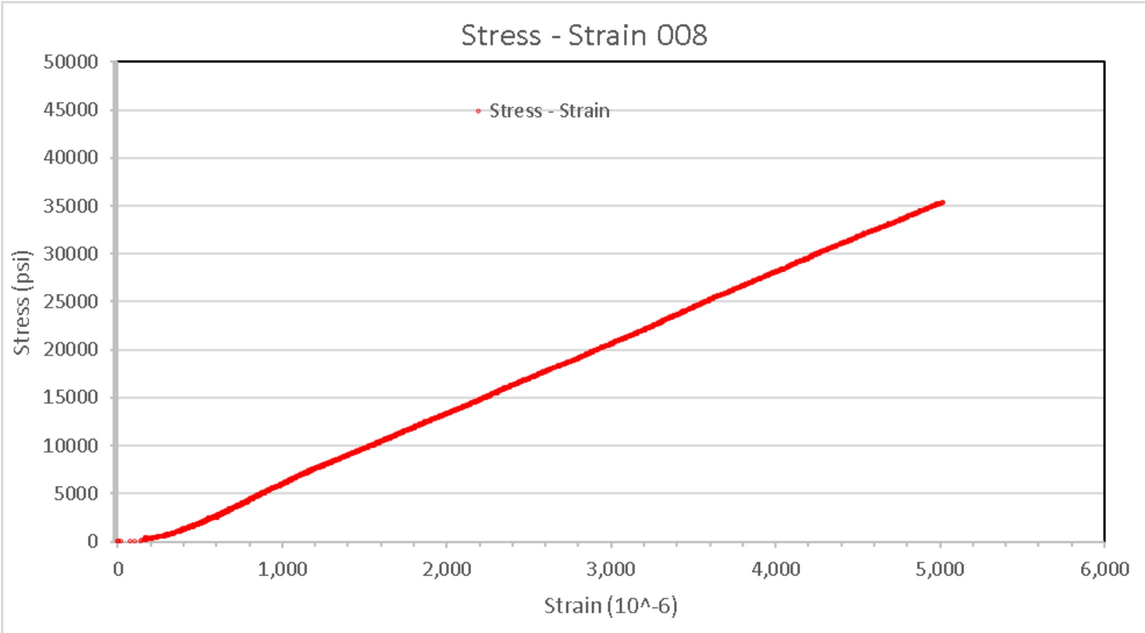

Fig. 64. Stress strain curve for bar 008

Table 28. Bar 008 properties

Sample #	Area, sq. in (sq. mm)	Peak Load, lbs (kN)	Max Stress, psi (MPa)
8	0.31 (200)	37,212 (166)	120,040 (828)

2.9 Bar 009

Pristine bar 009 failed at a peak load of 36,576 lbs. (164 kN). The extensometer was removed at a load of 12,250 lbs., and therefore, the maximum strain could not be determined. The stress strain curve for this bar is shown in Fig. 65. A summary of the tensile test results is shown in Table 29.

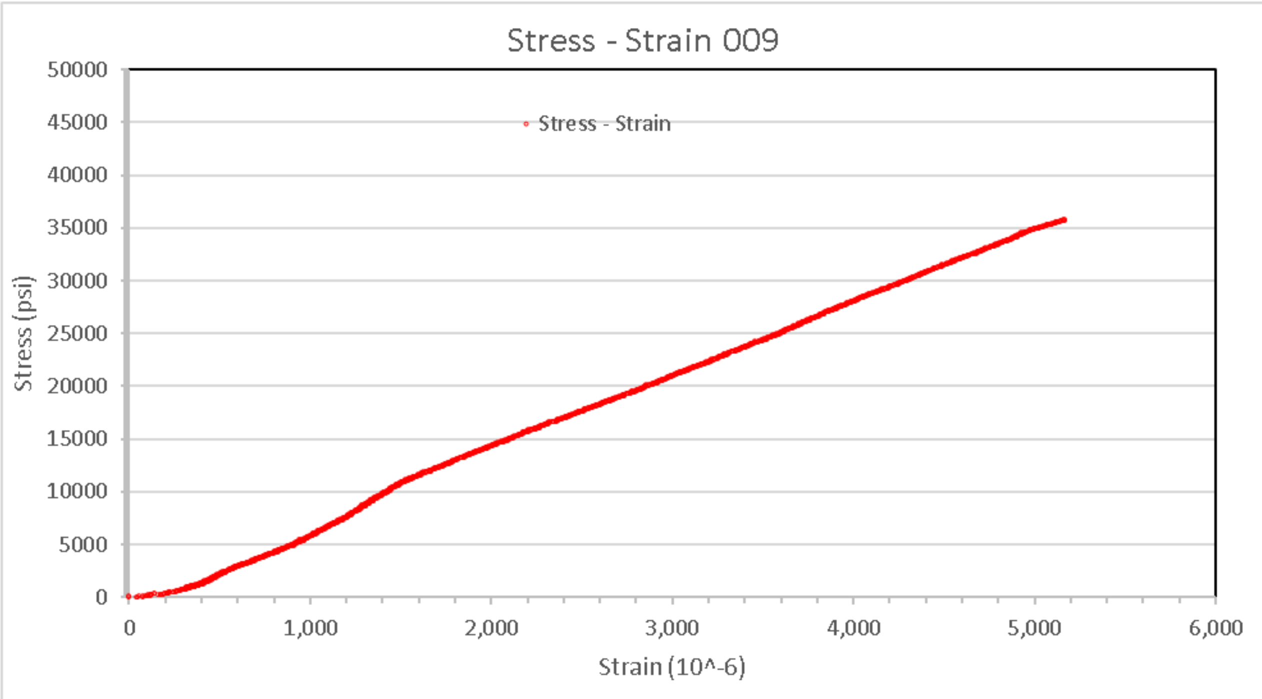

Fig. 65. Stress strain for bar 009

Table 29. Bar 009 properties

Sample #	Area, sq. in (sq. mm)	Peak Load, lbs (kN)	Max Stress, psi (MPa)
9	0.31 (200)	36,576 (163)	117,987 (813)

2.10 Bar 010

Pristine bar 009 failed at a peak load of 36,972 lbs. (165 kN). The extensometer was removed at a load of 12,100 lbs., and therefore, the maximum strain could not be determined. The bar after failure is shown in Fig. 66 and the stress strain curve for this bar is shown in Fig. 67. Due to initial manipulation of the extensometer, initial conditions show initial deflection at load zero. A summary of the tensile test results is shown in Table 30.

Fig. 66. Bar 010 after failure

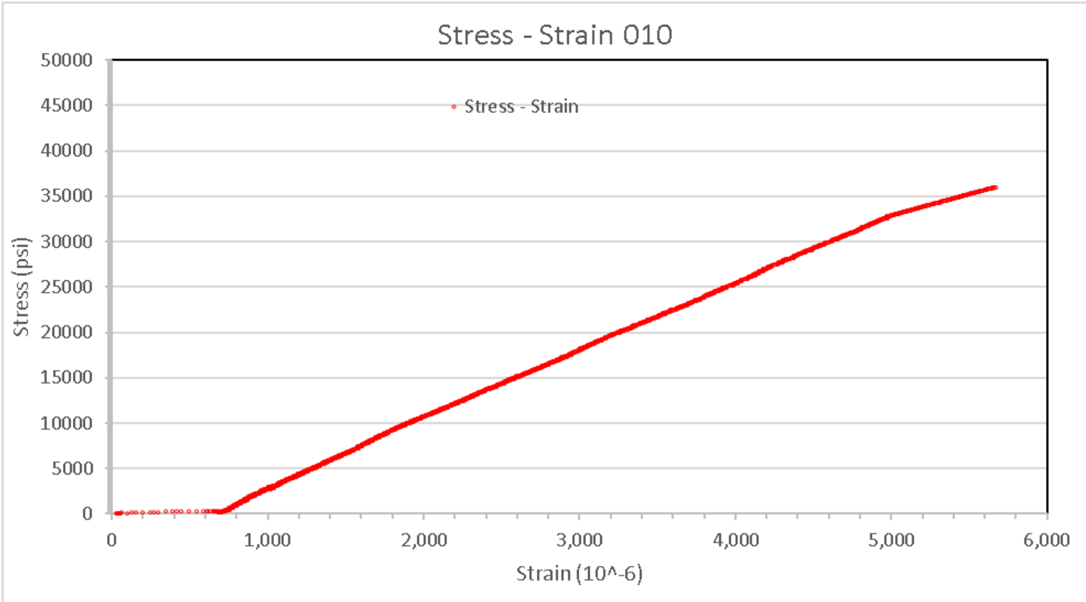

Fig. 67. Stress strain curve for bar 010

Table 30. Bar 010 properties

Sample #	Area, sq. in (sq. mm)	Peak Load, lbs (kN)	Max Stress, psi (MPa)
10	0.31 (200)	36,972 (165)	119,265 (822)

ADDENDUM I: DRY DOCK #4 AT PEARL HARBOR

This addendum presents an extension of the work presented in *Durability of GFRP Bars Extracted from Bridges with 15 to 20 Years of Service Life.* In it, the results of concrete and GFRP tests performed on extracted concrete and GFRP bars from Dry Dock #4 at Pearl Harbor, Hawaii after 18 years of service, are reported. The concrete tests included in this addendum are ultrasonic pulse velocity (UPV), bulk resistivity, rebound hammer, density, compressive strength, and chloride and carbonation penetration. The GFRP tests performed are fiber content, water absorption, horizontal shear, differential scanning calorimetry (DSC), scanning electron microscope (SEM) imaging and energy dispersive spectroscopy (EDS). Most tests were performed according to Section 4 of the cited report or as specified herein. The results are reported for each test and conclusions are drawn by comparing these results to data collected at the time of installation, or to current standards when data on pristine bars is not available.

Table of Contents

1. Structure

1.1. Dry Dock #4 at Pearl Harbor (HI)

The Dry Dock #4 at Pearl Harbor in Oahu, Hawaii was built in 1942. The original structure was built with concrete walls approximately 25 to 30 ft (7.6 to 9.1 m) thick. Repairs to the fascia were performed in the 1990's with the use of steel reinforcement with 2 in. (50 mm) of concrete cover. The steel reinforcement corroded and caused concrete spalling and delamination, which generated the need to repair the structure with non-corrosive reinforcement (Nanni, 2001).

In 2001, repairs to the Dry Dock #4 at Pearl Harbor were performed with the use of GFRP bars. The rehabilitation of the Dry Dock #4 is shown in Figure 1, and its overall view is shown in Figure 2. A grid of GFRP bars was doweled and epoxied in place as shown in Figure 3. The straight bars consisted of #3 and #4 (M10 and M13) bars and the bent bars were #3, #4 and #5 (M10, M13 and M16) bars. The use of non-corrosive reinforcement also allowed an emergency use of the dock during construction, when it was flooded to receive a damaged submarine (Nanni, 2001).

Fig. 1 –Overview of the Dry Dock #4 at Pearl Harbor.

Fig. 2 –Rehabilitation of Dry Dock #4.

Fig. 3 –GFRP grid at fascia during rehabilitation.

In April 2019, nineteen 4 in. (102 mm) diameter concrete cores from the Dry Dock #4 at Pearl Harbor were extracted from the fascia. The approximate location of the extracted cores is shown in Figure 4 with core numbers superimposed over an old picture. Given the extraction challenges and the inability to detect the position of the GFRP bars, several cores (13 out of 19) had no reinforcement in them.

Fig. 4 –Location of extracted cores.

2. Specimen inventory

Table 1 provides a summary of specimen inventory for Dry Dock #4 at Pearl Harbor. The core specimens are identified using a two-part identification scheme NN_Cx, where NN is the abbreviation of the state name or state and Cx indicates the x-th core number in reference to its location in Fig. 4. When more than one core was taken from the same location, the second part identification included an extra digit Cx-x. All GFRP bars were #5 (M16) of the same kind. Pictures and dimensions from each extracted core are included in Addendum II.

The received cores were double sealed with zip lock bags immediately after coring and placed in a sealed plastic bucket for shipment. A typical extracted concrete core is shown in Figure 5.

Table 1. Dry Dock #4 at Pearl Harbor specimen inventory.

Core Label	# of GFRP bars	Rebar Length, in. (mm)	Core Depth, in. (mm)
HI_C1	0		5 (127)
HI_C2	2	0.5 & 3 (13 & 76)	4 (102)
HI_C3-1	2	3.5 & 3 (89 & 76)	6 (152)
HI_C3-2	0		6 (152)
HI_C4	1	3.5 (89)	8 (203)
HI_C5	0	-	5 (127)
HI_C6	0	-	6 (152)
HI_C7	0	-	6 (152)
HI_C8	2	3 & 2.5 (76 & 64)	6 (152)
HI_C9-1	0	-	4 (102)
HI_C9-2	0	-	7 (178)
HI_C10	0	-	10 (254)
HI_C11	0	-	5 (127)
HI_C12	0	-	4 (102)
HI_C13-1	3	3.5, 3.3 & 3.4 (89, 84 & 86)	4 (102)
HI_C13-2	0	-	3.5 (89)
HI_C14	0	-	5 (127)
HI_C15	2	1.1 & 3 (28 & 76)	8 (203)
HI_C16	0	-	5 (127)

Fig. 5 –Typical extracted core HI_C8.

3. Concrete tests

All concrete tests were performed at the University of Miami. The cores, when received, were not of "standard" or uniform length. Several cores were short and had uneven end surfaces. The uneven surface would not allow for measurement of ultrasonic pulse velocity (UPV), bulk resistivity, and compressive strength. Therefore, these cores were cut with a wet saw to make the end surfaces smooth enough to carry out the aforementioned tests. Some examples are shown in Figures 6 through 8.

(a) (b)

Fig. 6 –Core HI_C11 (a) Before saw cutting. (b) After saw cutting.

(a) (b)

Fig. 7 – Core HI_C13-1 (a) Before saw cutting. (b) After saw cutting.

(a) (b)

Fig. 8 –Core HI_C14 a) Before saw cutting. (b) After saw cutting.

Some of the cores were also in poor condition—they had a significant amount of visible voids, or had extremely irregular end surfaces. These cores were split to obtain carbonation depth and chloride penetration using phenolphtalein and silver nitrate, respectively. An example of a core prior to splitting is shown in Figure 9.

Fig. 9–. Core specimen with irregular ends and voids.

Some of the cores still had steel reinforcement embedded in them. Carbonation and chloride depth were tested on these cores. Evident steel corrosion was observed in these specimens as shown in Figure 10.

Fig. 10–. Core #15 with corrosion from embedded steel bar.

3.1. Density

The as-is density was calculated from the measured mass and volume of concrete. The density values and the respective mass, length, diameter and volume used to calculate the density are shown in Table 2.

Table 2. Density results

Core ID	Mass oz. (g)	Length ft (m)	Volume (x10^{-4}) ft^3 (m^3)	Density pcf (kg/m^3)
HI_C1	50.30 (1425.88)	0.315 (0.096)	235 (7)	133.6 (2140.3)
HI_C3-1	22.86 (648.12)	0.136 (0.0415)	102 (3)	140.5 (2250.4)
HI_C3-2	68.53 (1942.71)	0.358 (0.109)	267 (8)	160.3 (2568.2)
HI_C4	31.59 (895.62)	0.213 (0.065)	159 (5)	123.9(1985.5)
HI_C6	65.88 (1867.54)	0.426 (0.130)	319 (9)	129.2 (2070.1)
HI_C7	70.28 (1992.33)	0.451 (0.138)	337 (9)	130.3 (2087.9)
HI_C9	87.08 (2468.68)	0.456 (0.139)	341 (10)	159.8 (2559.2)
HI_C9-1	49.87 (1413.92)	0.269 (0.082)	201 (6)	155.1 (2484.7)
HI_C10	54.23 (1537.32)	0.287 (0.087)	214 (6)	158.0 (2531.7)
HI_C10*	46.97 (1331.66)	0.262 (0.080)	196 (6)	149.9 (2401.6)
HI_C11	58.55 (1659.88)	0.236 (0.100)	244 (7)	150.1 (2403.9)
HI_C12	43.75 (1240.36)	0.238 (0.073)	178 (5)	153.9 (2465.3)
HI_C13	36.68 (1039.96)	0.231 (0.071)	173 (5)	132.7(2125.6)
HI_C14	60.29 (1709.10)	0.328 (0.100)	245 (7)	153.75 (2462.8)
HI_C15	37.48 (1062.45)	0.236 (0.072)	176 (5)	132.7 (2126.3)
HI_C15	19.97 (566.01)	0.131 (0.040)	98 (3)	127.3 (2039.0)
HI_C16	57.49 (1629.76)	0.310 (0.095)	232 (7)	155.2 (2485.1)
Average				143.9 (2305.1)
Std. Dev.				12.9 (207.5)
COV %				9.0

*cores that were split into two during testing

3.2. Rebound hammer

A rebound hammer is a device used to estimate the strength of concrete in terms of surface hardness. The test hammer hits the concrete at a defined energy and measures the rebound, which is dependent on the hardness of the concrete. Typically, a greater value of the rebound hammer measurement indicates a greater concrete strength, however, several factors, such as aggregate type, surface condition, carbonation, etc., affect this relationship. The correlation between compressive strength of concrete and UPV is discussed in section 3.5.

The typical rebound hammer measurements are on a linear scale ranging from 10 to 100. Twenty-three specimens were tested and the values obtained were very low (ranging from 13 to 25), which suggests the concrete is of poor quality (Liu et al. 2009). The results are shown in Table 3.

Table 3. Rebound hammer test results

Core ID	Rebound hammer	Core ID	Rebound hammer
HI_C1	19	HI_C9	22
HI_C2	13	HI_C9-1	17
HI_C3	17	HI_C10	19
HI_C3-1	20	HI_C10*	18
HI_C4	19	HI_C11	18
HI_C4*	16	HI_C12	19
HI_C3*	25	HI_C13	16
HI_C5	15	HI_C13	19
HI_C6	20	HI_C14	23
HI_C7	18	HI_C15	18
HI_C8	16	HI_C15	19
HI_C8 *	16	HI_C16	21
		Average	18.34
		Std. Dev.	2.57
		Coefficient of Variant (COV) %	14.01

*Specimens that were split into two.

3.3. Ultrasonic pulse velocity

Ultrasonic pulse velocity (UPV) is a non-destructive test (NDT) to determine the quality of concrete. The test consists of passing an ultrasonic pulse through a concrete specimen or structure and measuring the time it takes for the pulse to get through it using two transducers. Higher velocities indicate good quality and continuity of the material, while lower velocities may indicate lower quality concrete or concrete with cracks or voids.

The UPV test was performed using Pundit lab+, Proceq instrument. Since the surfaces of the cores were wet due to the usage of wet saw cutting for surface preparation, the samples were gently dried using dry cloth to remove any moisture before carrying out the test in the direct mode according to ASTM C597-16. A water-soluble gel was used as a coupling agent to ensure that there were no air gaps while carrying out measurements. The UPV values of specimens with a length/diameter ratio of less than 1.0 are not reported as these values are likely not reliable.

Eight specimens were tested, and the results were rather high, considering common values for normal strength lab concretes are between 3000 – 5000 m/s (Solis-Carcaño & Moreno 2008). The results are shown in Table 4. It is known that concrete compressive strength and modulus increase with age, and as this is significantly old concrete (18 years old), the higher UPV values may be expected. These high values could suggest that the concrete quality is "excellent", based on UPV classifications (Malhotra 1976), however, without knowing the mixture design, it is difficult to evaluate the true quality of the concrete. Apart from the aged concrete, the high values could also be due to the use of granitic aggregates (Limbachiya et al. 2008). Typical coefficient of variation (COV) values for lab concretes are 5% or below (Nepomuceno & Lopes2017), and the COV value measured here is much higher (14.67%) which suggests significant variation in the concrete quality. This, however, may be simply because higher variability may be expected in field mixtures subjected to complicated environmental conditions.

The modulus of elasticity of the concrete was calculated in accordance with the study of Chavhan and Vyawahare (2015). To use the UPV values to obtain the dynamic and static modulus of elasticity, formulas 1 and 2 were used. As the concrete mix is unknown, a n=0.15 for the poisson's ratio was assumed. The results of the elastic modulus obtained are shown in Table 5. The modulus of elasticity also present high coefficient of variation (34%).

$$Ed = v^2 Q * (1+n) * (1-2n)/(1-n) \tag{1}$$

$$Ec = 1.05Ed \tag{2}$$

Where, v = velocity in km/s
Q = Concrete density in kg / m^3
n =Poisson's ratio (for high strength concrete n = 0.15, for low strength concrete n = 0.30)
Ed = Dynamic elastic modulus.
Ec = Static modulus of elasticity

Table 4. UPV test results

Core	UPV ft/s (m/s)
HI_C1	16,070 (4,898)
HI_C3	20,436 (6,229)
HI_C6	14,557 (4,437)
HI_C7	13,497(4,114)
HI_C9	19,740 (6,017)
HI_C11	18,045 (5,500)
HI_C14	18,228 (5,556)
HI_C16	19,770 (6,026)
Average	17,543 (5,347)
Std. Dev.	2,572 (784)
COV (%)	14.67

Table 5. Calculated modulus of Elasticity

Core	E_d MPa (Ksi)		E_c, MPa (Ksi)	
HI_C1	48,627	(7,053)	46,312	(6,717)
HI_C3	88,314	(12,809)	84,109	(12,199)
HI_C6	38,596	(5,598)	36,758	(5,331)
HI_C7	33,467	(4,854)	31,873	(4,623)
HI_C9	87,749	(12,727)	83,570	(12,121)
HI_C11	68,867	(9,988)	65,587	(9,513)
HI_C14	71,998	(10,443)	68,570	(9,945)
HI_C16	85,464	(12,395)	81,394	(11,805)
Average	65,385	(9,483)	62,272	(9,032)
Std. Dev.	22,368	3,244	21,302	3,090
COV (%)	34	(34)	34	(34)

3.4. Bulk resistivity

Bulk resistivity is a non-destructive test for measuring the electrical resistivity of concrete specimens in the laboratory without any additional specimen preparation requirements. It is noted that the degree of saturation has a complex effect on the bulk resistivity (Layssi et al. 2015); therefore, interpretation of values is not trivial in specimens with an unknown saturation state.

Since the specimens were cut using a wet saw, the specimens were dried and wiped gently using a cotton cloth and were left in lab conditions to dry. After this, bulk resistivity was measured using a Giatec RCON (Giatec Scientific Inc., Ottawa, Canada) bulk resistivity meter at a frequency of

10 kHz. Seventeen specimens were tested, and the results were somewhat low (ASTM C1202 2019). For dense aggregate concretes that are older than 10 years, the resistivity values are 300-1000 Ω-m for concrete containing SCMs and in the splash/submerged zone. For concrete exposed to atmosphere for more than 10 years, the resistivity values are reported to be 500-2000 Ω-m (Polder 2001). Considering the concrete age, these results may imply that the concrete quality is somewhat poor, but this is difficult to evaluate without knowing the concrete mixture and the degree of saturation. The COV is also high, which suggests significant variance between the specimens. The results are shown in Table 6.

Table 6. Bulk resistivity results.

Core ID	Bulk resistivity (Ω-m)	Core ID	Bulk resistivity (Ω-m)
HI_C1	119.1	HI_C10*	169.2
HI_C3-1	120.8	HI_C11	144.8
HI_C4	153.14	HI_C12	88.3
HI_C6	106.0	HI_C13	83.4
HI_C7	68.1	HI_C14	180.1
HI_C9	113.4	HI_C15	99.1
HI_C9-1	88.1	HI_C15	74.0
HI_C10	104.0	HI_C16	180.6
		Average	118.3
		Std. Dev.	37.1
		COV (%)	31.32

*Specimens that were split into two.

The bulk resistivity tests on the eight specimens for which UPV results are available show a significantly higher average (131.9 Ω-m) and a COV close to the value of the entire population (27.8%). The values between UPV and bulk resistivity can generally be empirically correlated (Sertçelik et al. 2018). However, in this case, because the specimens were tested in their "as received" condition, the values only have a moderate correlation as shown in Figure 11.

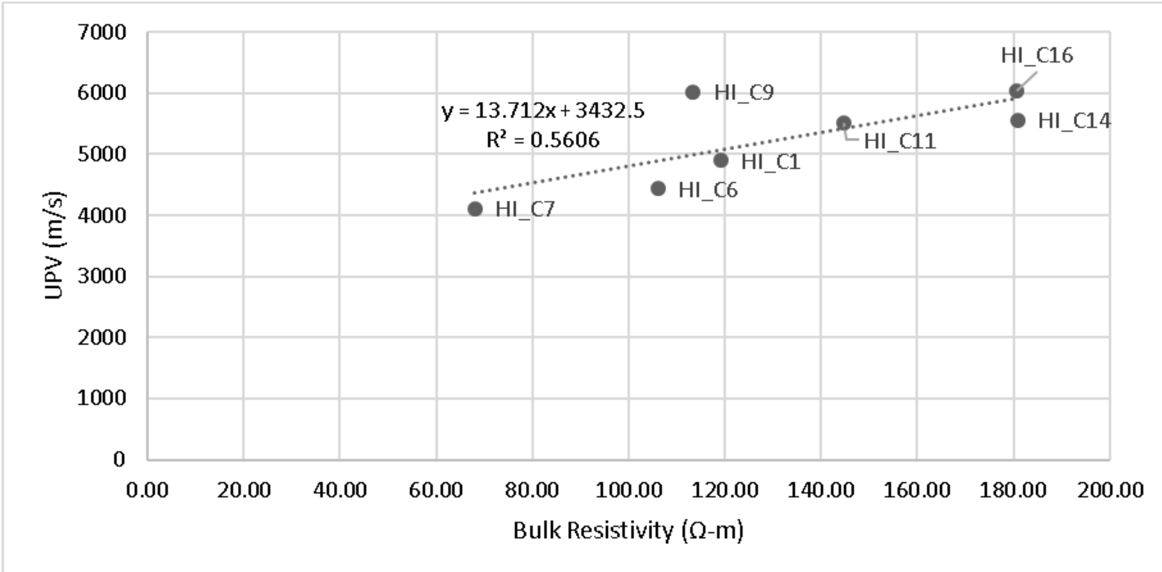

Fig. 12 –UPV vs. Bulk resistivity.

3.5. Compressive strength

After carrying out the non-destructive concrete tests, cores were tested for their compressive strength using a mechanical testing device (SATEC Instruments, MkIII-C 400 PT, University of Miami, Coral Gables, FL, good condition, Fig. 13) according to ASTM C39/C39M-18. The concrete cylinders were capped with a sulfur mortar (in accordance with ASTM C617/ C617M) and subjected to a stress rate of 0.25 ± 0.05 MPa/s (35 ± 7 psi/s) in load control. Five specimens were tested in compression, a correlation strength factor was used for specimens with an L/D less than 1.75, in accordance with ASTM C42/C42M.The results obtained are shown in Table 7. The compressive strength varied significantly, which is consistent with the results from the other tests. These values suggest a concrete of average quality, although this is hard to assess without knowing initial mixture designs.

Table 7. Compressive strength test results

Core ID	Compressive strength psi (MPa)
HI_C3	6,965 (48)
HI_C6	3,572 (25)
HI_C7	4,381 (30)
HI_C9	7,415 (51)
HI_C11	5,957 (41)
Average	5,658 (39)
Std. Dev.	1648 (11)
COV (%)	30.76

The values of UPV (from Section 3.3) and compressive strength are correlated as shown in Figure 12 (though the number of data points is limited).

On the whole, it is not possible to accurately assess the concrete quality based on the results of the testing because UPV suggests higher quality concrete, strength testing suggests average quality concrete, and bulk resistivity and rebound hammer suggest lower quality concrete. A more accurate assessment of the concrete quality can be made if further testing is done and if the concrete mixture design is known. At any rate, all tests suggest that the concrete is highly variable, which is possibly because of damage (due to seawater and steel corrosion).

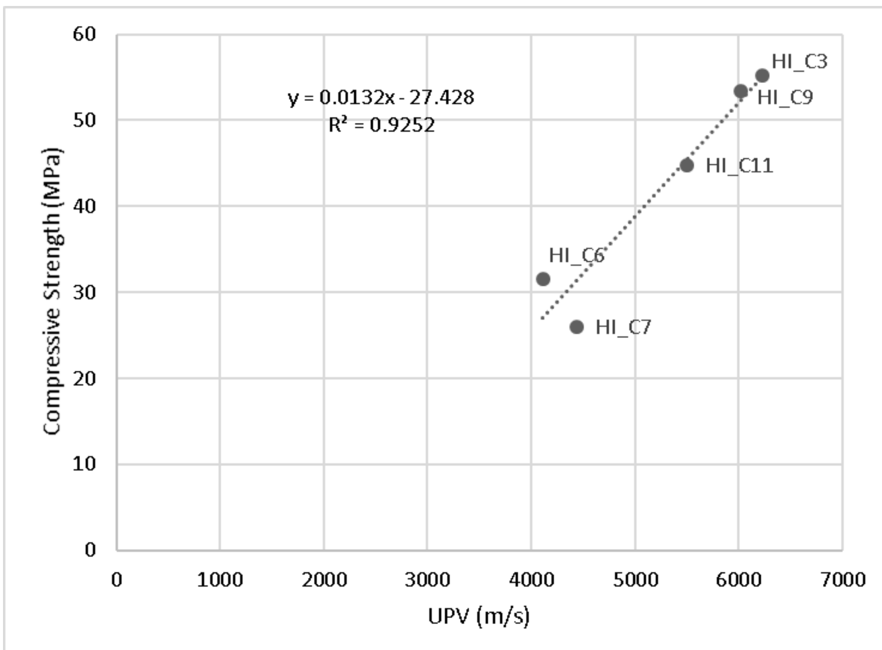

Fig. 32 – Compressive strength vs. UPV.

3.6. Splitting tensile strength

The remaining cores after carrying out NDT and compressive strength were tested for splitting tensile strength according to ASTM C496/C496M-17 using a mechanical testing device shown in Figure 13 (SATEC Instruments, MkIII-C 400 PT). Six specimens were tested, and the results are shown in Table 8. The coefficient of variance is high (32%), which indicates significant variations in concrete quality. The splitting tensile strength values obtained were high, which could be due to the increase in strength with aging of concrete (Munitz and Cotler 2000). According to Munitz and Cotler, the ultimate tensile strength increases with the initial aging of concrete, reaches a maximum, and then decreases with further aging of concrete.

According to ACI 363R-92 (1997), the relationship between splitting tensile strength and compressive strength of concrete is shown by equations 3 and 4, where fsp' is the split tensile strength and fsp' is the compressive strength at 28 days. Because there is no information on the 28-day compressive strength, these equations were used to back calculate f_c', which was found to be 7,409 psi (55.36 MPa). These values are significantly higher than the compressive strength found in Section 3.5, which would indicate a decrease in compressive strength. However, several authors disagree with the relationship developed by ACI and have developed different relationships between split tensile strength and compressive strength for different concrete mixes and/or concrete ages. Arıoglu et al. (2006) state that the ACI model should be re-evaluated for high-strength concrete, and Yao et al. (2017) suggest a relationship between splitting tensile strength and compressive strength through equation 3 for aged concrete exposed to a marine environment, where $fcu$is the aged compressive strength. By using equation 3, the relationship between splitting tensile strength and compressive strength is found to be closer but perhaps not accurate for this case.

$$fsp' = 7.4\sqrt{fc'} \text{ psi for 3,000 psi < fc' < 12,000 psi} \quad (3)$$

$$fsp' = 0.59\sqrt{fc'} \text{ MPa for 21 MPa < fc' < 83 MPa} \quad (4)$$

$$fsp' = 1.02\, fcu^{0.36} \quad (5)$$

Fig. 43 –Mechanical testing machine used for compressive and split tensile strength.

Table 8. Split tensile test results.

Core ID	Split tensile strength psi (MPa)
HI_C3-1	687.5 (4.7)
HI_C10	500.4 (3.4)
HI_C13	485.9 (3.4)
HI_C14	635.3 (4.4)
HI_C15	603.4 (4.2)
HI_C16	909.9 (6.3)
Average	637.0 (4.4)
Std. Dev.	205.1 (1.1)
COV (%)	32.2 (24.3)

3.7. Chloride penetration and carbonation depth

Chloride penetration test was performed following the procedure explained in Section 4.2.1 and 4.2.3 of the cited report.

Representative images for chloride and carbonation depths measured (by spraying silver nitrate on one half of the core and phenolphthalein on the other half) are shown in Figure 6. Since some cores tested were partially broken (or not full in length), an exact depth from the surface cannot be calculated without further details. However, the values were measured for the respective cores using a Vernier caliper, and the results are shown in Table 9. Chloride ingress was observed in all specimens and carbonation was observed in eight out of the twelve tested specimens. When no carbonation was observed, N/A was recorded in Table 9.

Table 9. Chloride penetration depth

Core Number	Chloride depth in. (mm)	Carbonation depth in. (mm)
#3-1	1.77 (45)	0.16 (4)
#3-2	0.83 (21)	N/A
#4*	1.85 (47)	0.31 (8)
#6	1.54 (39)	0.51 (13)
#8 XX	2.08 (53)	0.28 (7)
#9	0.51 (13)	N/A
#11	1.81 (46)	0.16 (4)
#13	1.02 (26)	N/A
#13	1.77 (45)	0.12 (3)
#14	1.89 (48)	0.16 (3)
#15	1.57 (40)	N/A
#16	1.93 (49)	0.16 (3)

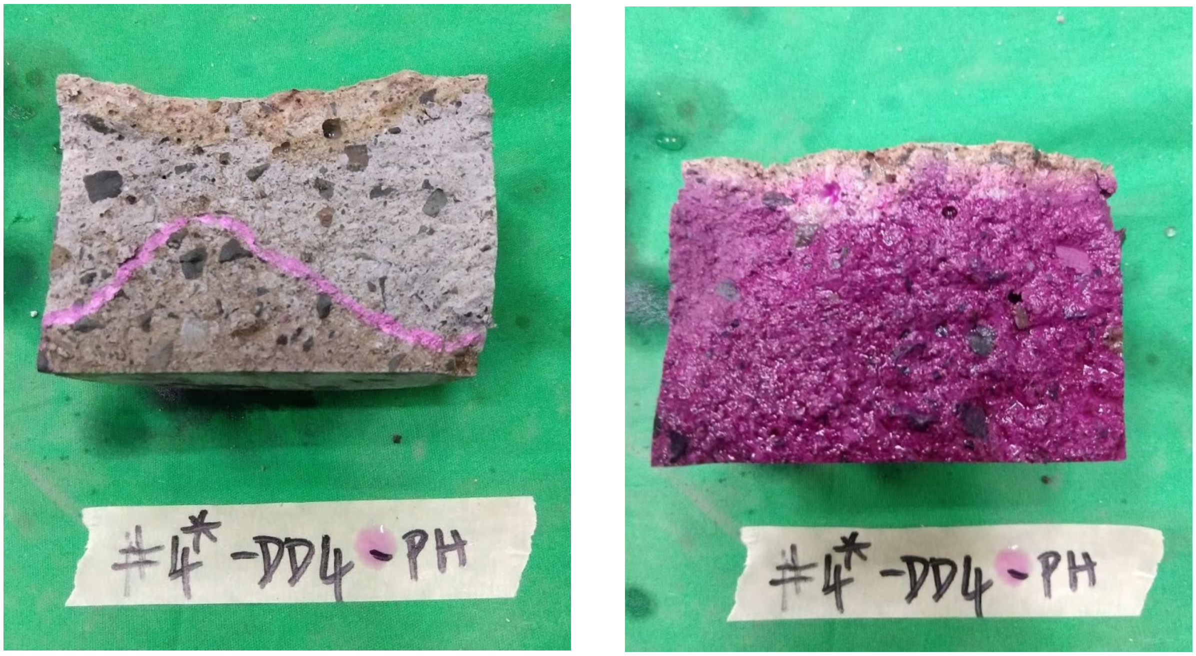

Fig. 54 –Core #4 – Representative image for chloride and carbonation depths.*

In the tested core specimens, some of the cores had full depth for chloride penetration and no carbonation. Representative images are shown below.

Fig. 65 –Core #15– Representative image for full chloride and zero carbonation depths.

The specimen HI_C8 was observed to have discolorations and layers. This core split in half while performing rebound hammer test on the core specimen. The depth of chloride and carbonation depths are shown in Figure 8. Carbonation was confirmed in the cores based on thermogravimetric analysis performed on the mortar.

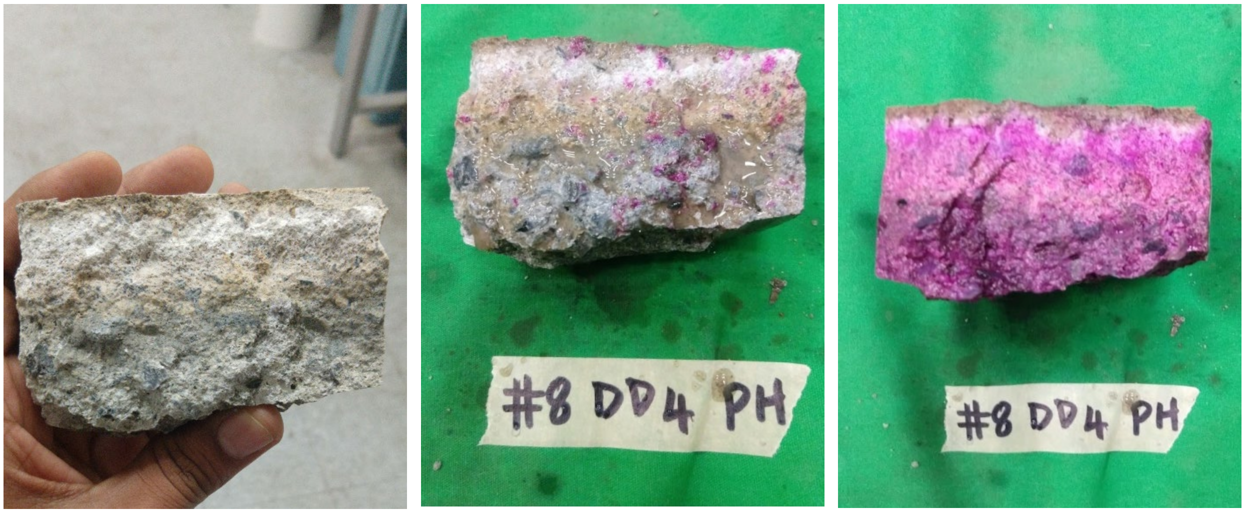

Fig. 76 –Core #8 – Discoloration and layers observed in core specimen.

3.8. Concrete tests observations and conclusions

The concrete specimens were tested to observe their current conditions by calculating a) density, b) rebound hammer, c) UPV, d) bulk resistivity, e) compressive strength, f) splitting tensile strength and g) chloride penetration and carbonation depth. No information on the concrete mix design was available, which makes the analysis challenging. The outcomes of the tests are briefly summarized as follows:

- The majority of tests presented high COV, which indicates the quality of concrete varies significantly among the specimens.
- The rebound hammer results were low, which suggests poor quality concrete.
- The UPV results were high, which suggests the concrete quality is “excellent” (Malhotra 1976). However, without knowing the mixture design, it is difficult to evaluate the true quality of the concrete as the high values could be due to the granitic aggregates or the age of concrete (Limbachiya et al. 2008).
- Given the age of the concrete, the bulk resistivity and compressive strength results were somewhat low. This indicates the concrete quality is somewhat poor.
- Carbonation was observed in most specimens and was found to be moderate. Chloride penetration was observed in all specimens, and it was found to be high.
- The overall concrete quality was found to be somewhat poor and highly variable. Seawater ingress has likely affected the concrete strength; however, this cannot be confirmed without knowing the original concrete.

4. GFRP Tests

4.1. Fiber content

Fiber content testing was performed following the procedure explained in Section 4.1.1.1 of the main report. The recorded weight percentage of the longitudinal fibers included the weight of possible filler used in the resin. No effort was made to remove any remnant filler in the resin or bar coats (such as sand and wraps).

Nine specimens from four different extracted bars (#5) from Dry Dock #4 were tested. Figure 17 and 18 show the specimens before and after the test. The results of the fiber weight of the bars were consistently above 70% in weight, which is the minimum required percentage by ASTM D7957 for quality control and certification. The result of the average fiber content was 75.4 %, which is slightly higher than the original bars data sheets, which had an average fiber content of 73.6%. This slight increase (1.8%) may be due to the inclusion of concrete residues, which were not present in the pristine bars. The results of the average percentage of fiber content and standard deviation for Dry Dock #4 can be seen in Table 10.

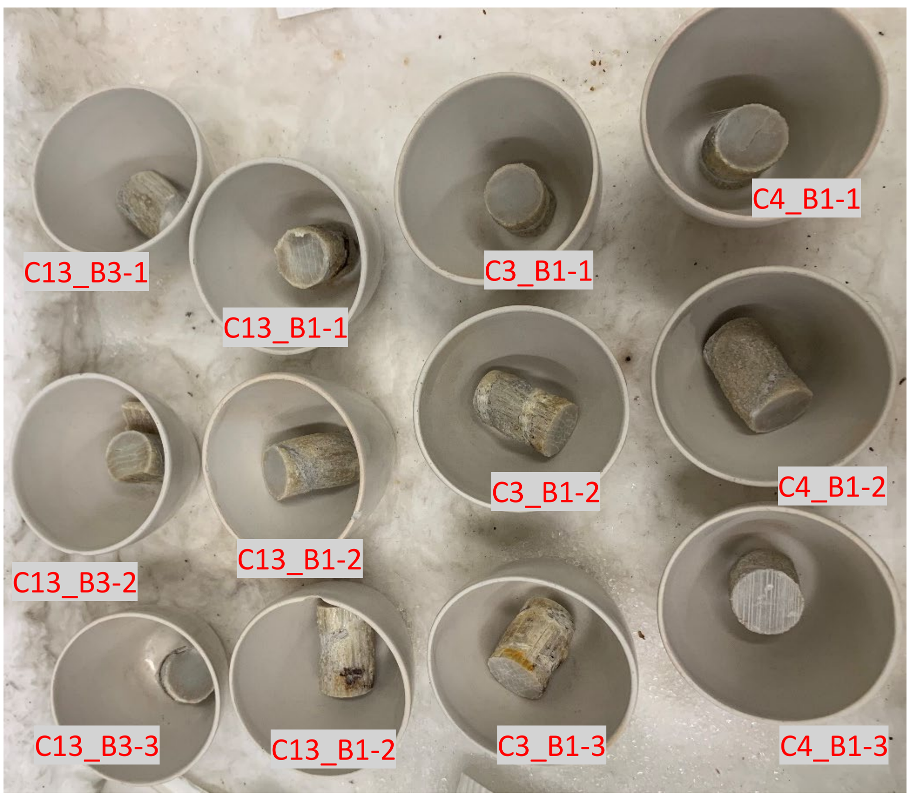

Fig. 87 – Fiber content specimens before test.

Fig. 98 –. Fiber content specimens after test.

Table 10. Dry Dock #4 fiber content results

Specimen	Fiber Content + filler
HI_C13_B3-1	75.65%
HI_C13_B3-2	74.59%
HI_C13_B3-3	74.93%
HI_C13_B1-1	75.30%
HI_C13_B1-2	75.16%
HI_C13_B1-3	75.12%
HI_C3_B1-1	75.50%
HI_C3_B1-2	75.71%
HI_C3_B1-3	75.27%
HI_C4_B1-1	75.82%
HI_C4_B1-2	76.06%
HI_C4_B1-3	75.69%
Average	75.40%
Std. Dev.	0.0042

4.2. Horizontal shear

The horizontal shear testing was performed following the procedure described in Section 4.1.3 of the cited report. The test set up is shown in Figure 19.

Horizontal shear tests were performed on four coupons from Dry Dock #4. Only one specimen, C14_B1, presented a clear horizontal shear failure, where a crack on the cross section could be observed. The other specimens presented horizontal cracks on the outside surface, near where the load was being applied as shown in Figures 20 and 21. When specimens C3_B1 and C13_B3 were cut to perform fiber content, visual horizontal shear cracks and matrix crack between fiber and resin could be observed at the cross section as shown in Figure 22. This delamination between resin and fiber was later confirmed with SEM images, which can be found in Section 4.5. This could be due to cyclic swelling and shrinking with water and/or temperature exposure, facilitated by a weak interface between fiber and resin.

The results of shear strength from the original bars tested in 2001 are shown in Table 11 for bars after cure at ambient temperature (AP) and in Table 12 for bars post-cured at 210 ºF (100 ºC) for 12 hours (PC). The average results of the shear strength of the in-service bars were much lower than recorded in the original data sheets. The original bars had an average apparent shear strength of 7,467 psi (51 MPa) for AP bars while the tested bars had an average apparent shear strength of 4,874 psi (33.6 MPa), which indicates a reduction of 39%. This reduction in strength could be due to the presence of voids in fiber-resin interface, as these play a significant role in controlling the degradation due to exposure conditions (Benmokrane et al., 2017). The results of the horizontal shear test for each bar is shown in Table 13.

The obtained results for horizontal shear were in accordance with values predicted by accelerated aging tests in the literature. For instance, in the study of Khatibmasjedi et al. (2017), GFRP bars of the same kind, made of E-glass fibers and vinyl-ester, had a reduction of 16% in transverse shear after being exposed to a 60 ºC alkaline solution over a period of 1 year, which would be representative of approximately 9 years under normal conditions. If a linear degradation is expected, a GFRP bar in service for 18 years is expected to have a transverse shear reduction of 32%.

Fig. 109– Horizontal shear test set up.

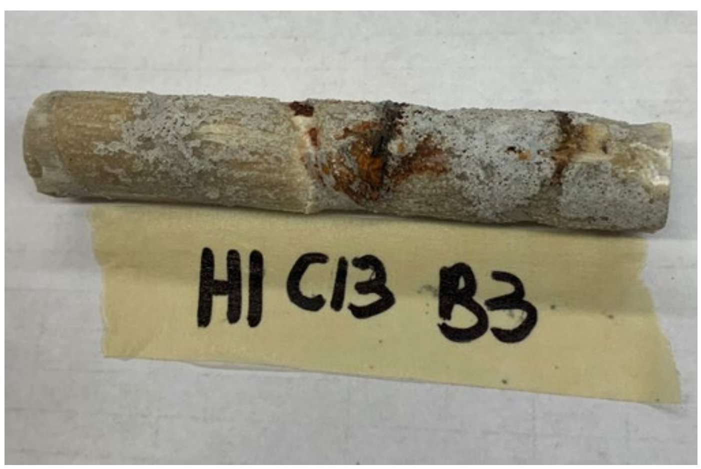

Fig. 20 –Bar #3 from core #13 after horizontal shear test.

Fig. 211 –Bar #1 from core #3 with horizontal cracks after horizontal shear test.

Fig. 22 –Bar #1 from core #3 cross section at midspan with matrix cracking.

Table 11. Horizontal shear results of original bars at ambient cure.

Specimen No.	Load at Failure lbs. (N)	Deflection in. (mm)	Mode of Failure	Apparent Shear Strength psi (MPa)
1	3,420 (15,213)	0.098 (2.489)	Side Shear	7,433 (51)
2	3,200 (14,234)	0.093 (2.362)	Side Shear	6,955 (48)
3	3,340 (14,857)	0.113 (2.870)	Side Shear	7,259 (50)
4	3,910 (17,392)	0.132 (3.352)	Side Shear	8,498 (59)
5	3,310 (14,724)	0.108 (2.743)	Side Shear	7,194 (50)
			Average	7,467 (52)
			Std. Dev.	600 (4)

Table 12. Horizontal shear results of original bars after post-cured.

Specimen No.:	Load at Failure lbs. (N)	Deflection in. (mm)	Mode of Failure	Apparent Shear Strength psi (MPa)
1	3,700 (16458)	0.130 (3.302)	Side Shear	8,041 (55)
2	4,010 (17837)	0.100 (2.540)	Side Shear	8,715 (60)
3	4,000 (17793)	0.102 (2.591)	Side Shear	8,694 (60)
4	3,980 (17704)	0.101 (2.565)	Side Shear	8,650 (60)
5	3,890 (17303)	0.099 (2.515)	Side Shear	8,455 (58)
			Average	8,511 (59)
			Std. Dev.	282 (2)

Table 13. Dry Dock #4 at Pearl Harbor horizontal shear results.

Specimen	Diameter, in (mm)	Span Length, in. (mm)	Peak Load, lbs. (N)	Apparent Shear Strength, psi (MPa)
HI_C3_B1	0.6585 (16.7259)	2.0 (50.8)	2,723 (12,112)	5,331 (37)
HI_C4_B1	0.6465 (16.4211)	3.0 (76.2)	1,838 (8,176)	3,733 (26)
HI_C13_B1	0.6565 (16.6751)	2.0 (50.8)	2,617 (11,640)	5,155 (35)
HI_C13_B3	0.6792 (17.2517)	2.0 (50.8)	2,866 (12,748)	5,275 (36)
			Average (psi)	4,874 (34)
			Std. Dev.	764 (5)

4.3. Differential scanning calorimetry (DSC)

DSC was performed on ten samples from four different bars. The samples were tested according to the procedure described in Section 4.1.4. The T_g was determined from the change in slope on the DSC curve, as shown in Figure 23 through Figure 32. The results of the T_g for each sample are shown in Table 14.

Currently, the T_g is required to be higher than 212 °F (100 °C) as a critical parameter in load transfer capability of the resin (ACI 440.6) and as specified in ASTM D7957 for quality control and certification. The average T_g for the tested samples was 194 °F (90 °C), which is lower than currently required threshold. No information on the bars at the time of installation was available to compare the T_g. However, values below the current standards are expected given the age of the bars, and the changes in the manufacturing process.

The high standard deviation indicates high variation in T_g between the samples. The higher T_gs can be expected due to cross-linking of the resin when the bars are not fully cured at the time of manufacturing. Similar values of T_g were obtained from in service bars extracted from bridges across the United States (Benzecry et al. 2019).

Table 14. Dry Dock #4 T_g results

Sample	Net Weight (mg)	T_g °F (°C)
HI_C8_B1-1	18.90	182 (83)
HI_C8_B1-2	32.14	183 (84)
HI_C8_B1-3	26.94	182 (83)
HI_C13_B2-1	26.30	171 (77)
HI_C13_B2-2	18.35	182 (83)
HI_C13_B2-3	34.94	176 (80)
HI_C2_B1-1	28.90	230 (110)
HI_C2_B1-2	19.10	230 (110)
HI_C2_B1-3	33.33	226 (108)
HI_C15_B1-1	41.52	189 (87)
	Average	194 (90)
	Std. Dev.	23 (13)

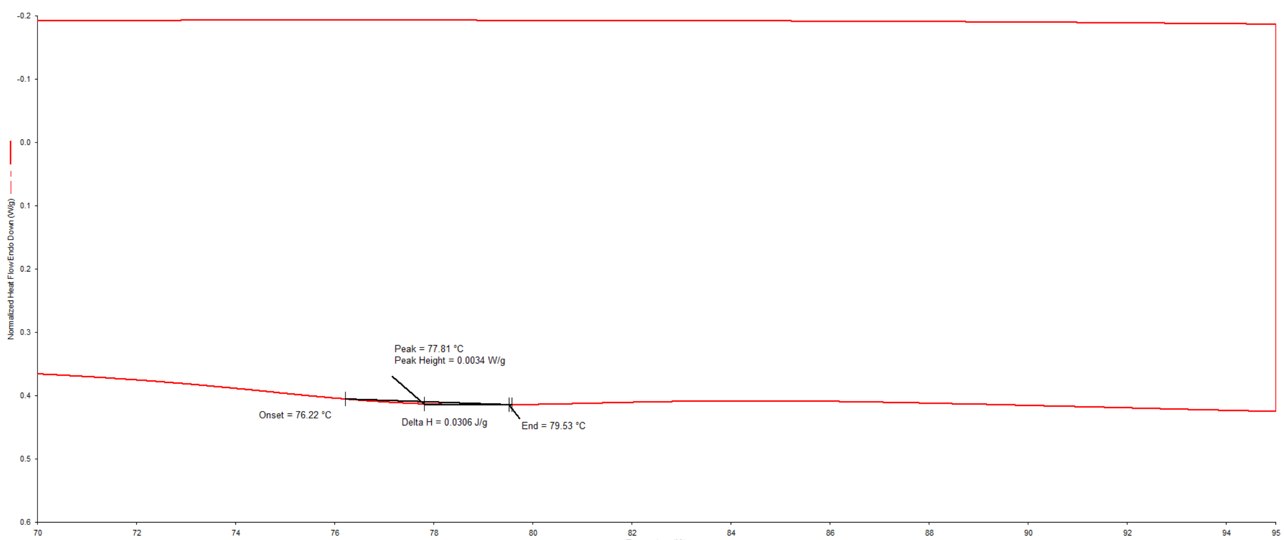

Fig. 23 –Dry Dock #4 core#13 bar #2A DSC curve.

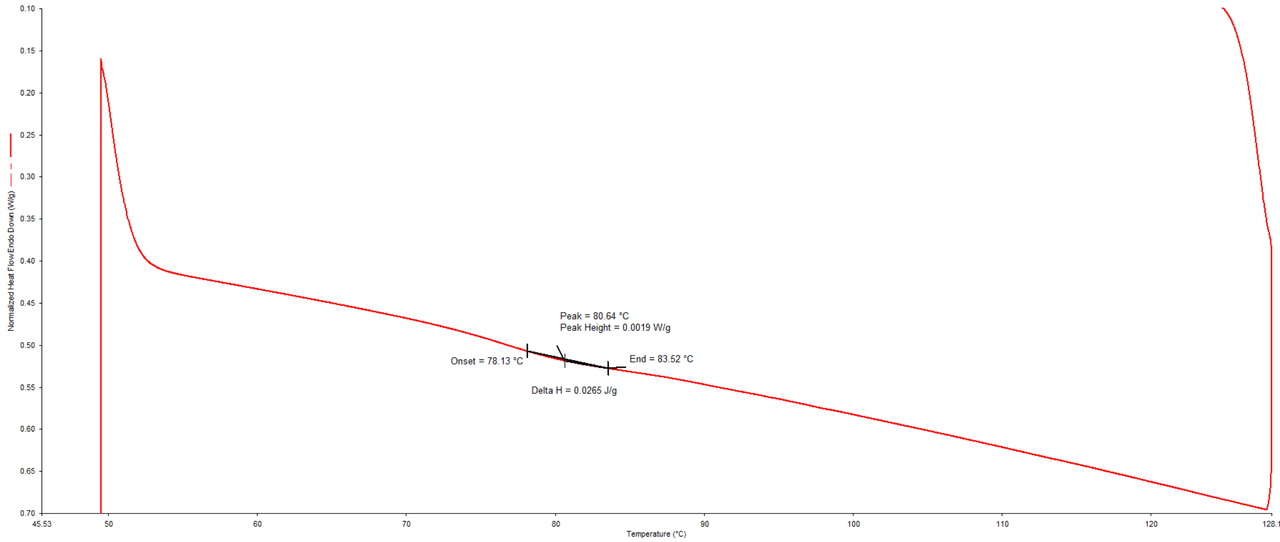

Fig. 24 –Dry Dock #4 core #13 bar #2B DSC curve.

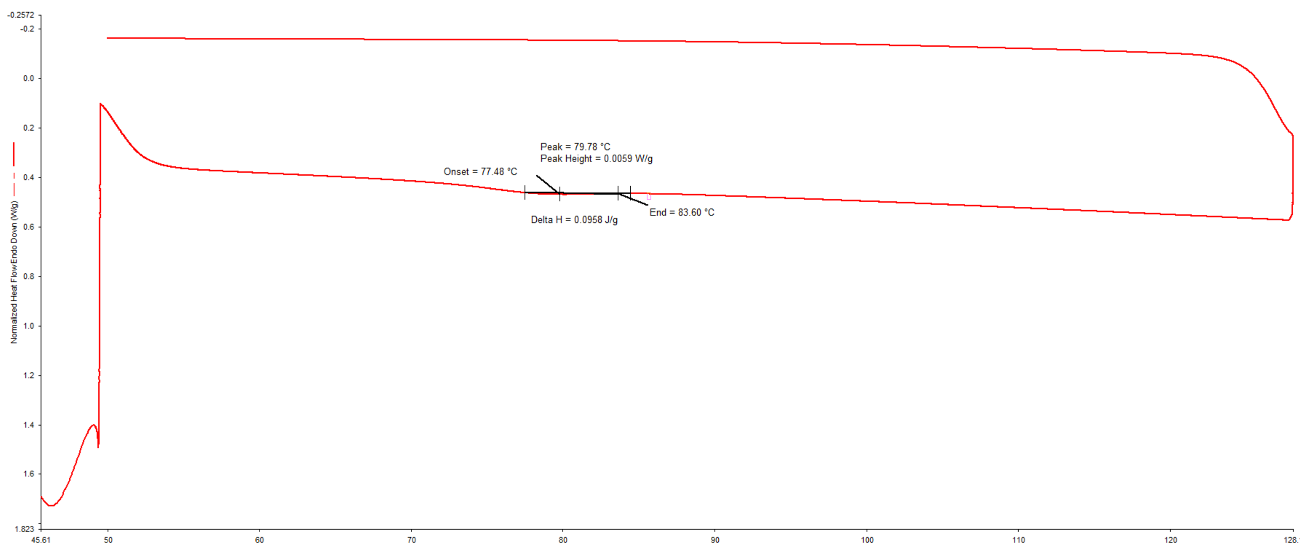

Fig. 25 –Dry Dock #4 core #13 bar #2C DSC curve.

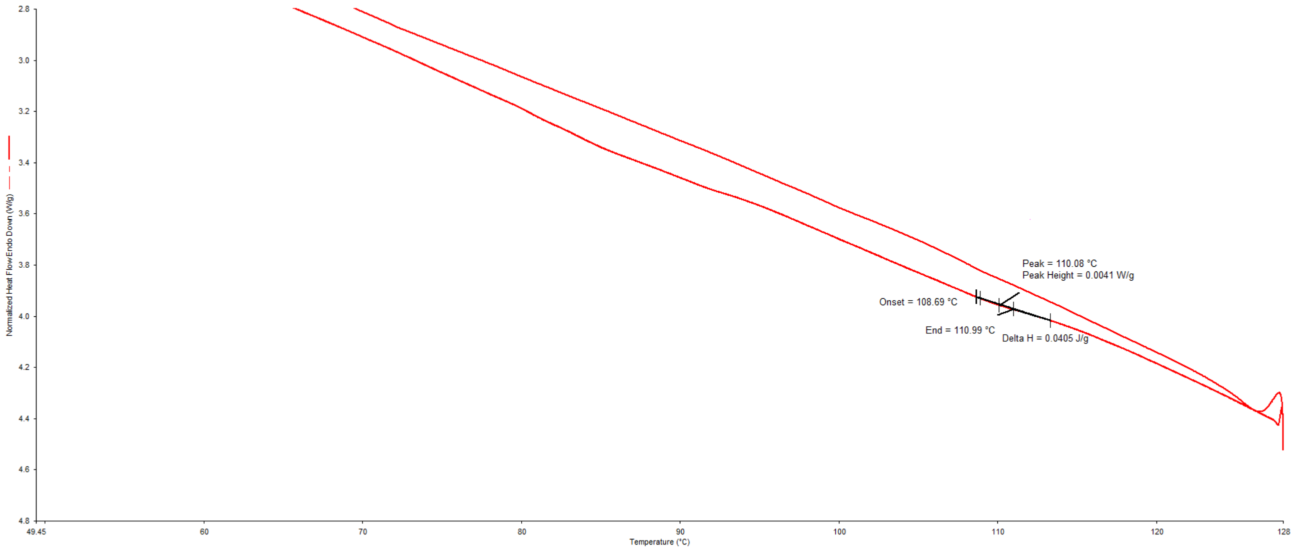

Fig. 26 –Dry Dock #4 core #2 bar #1A DSC curve.

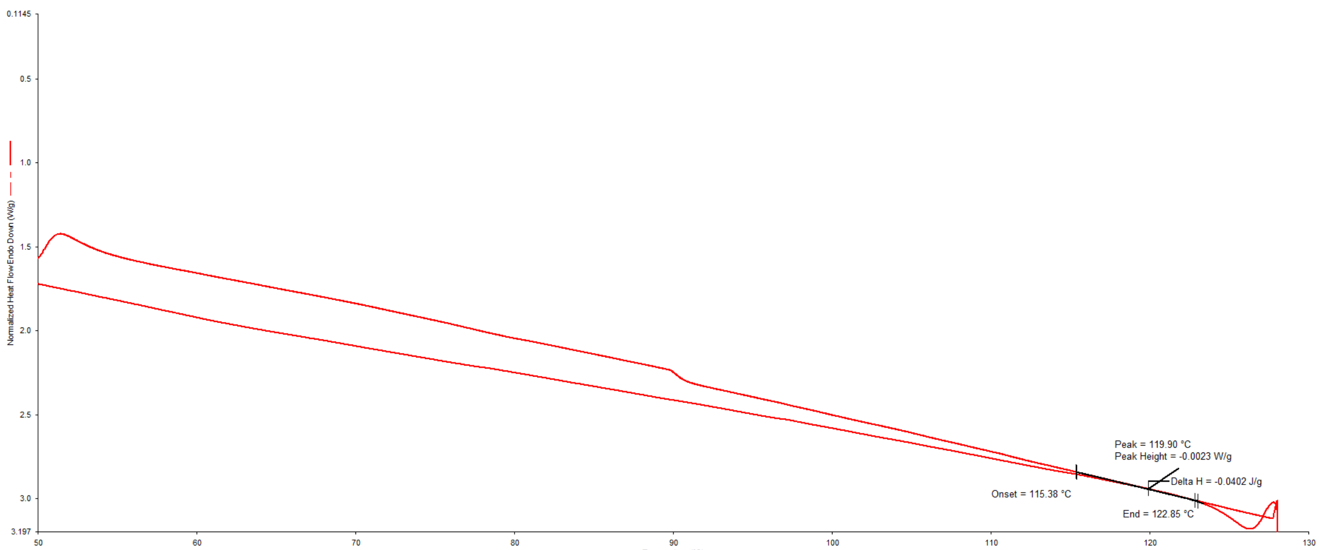

Fig. 27 – Dry Dock #4 core #2 bar #1B DSC curve.

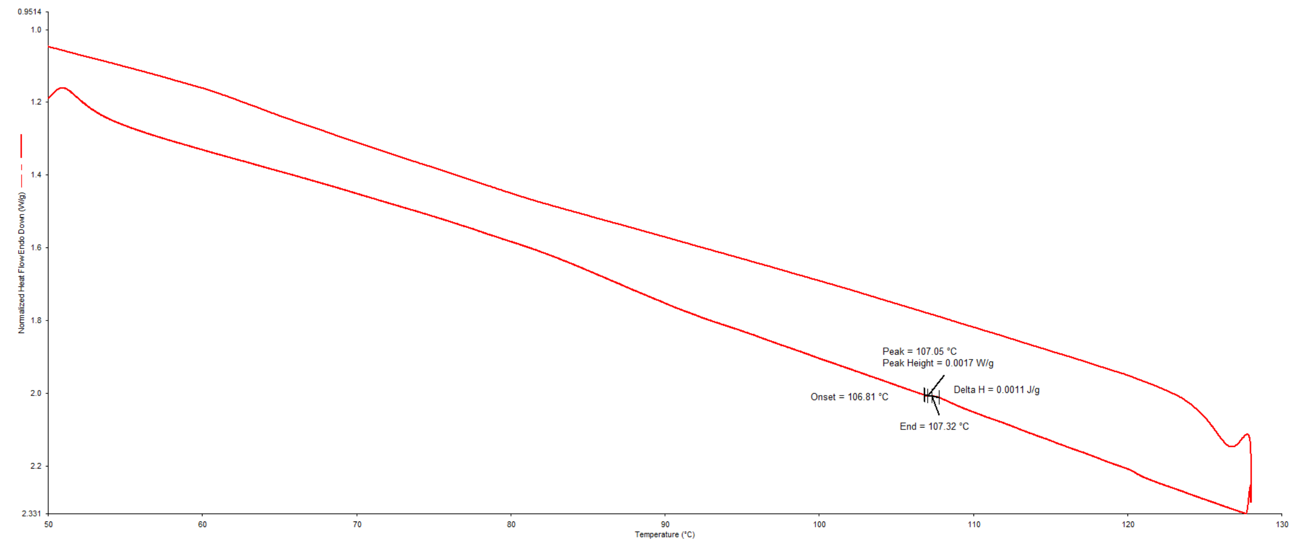

Fig. 28 –Dry Dock #4 core #2 bar #1C DSC curve.

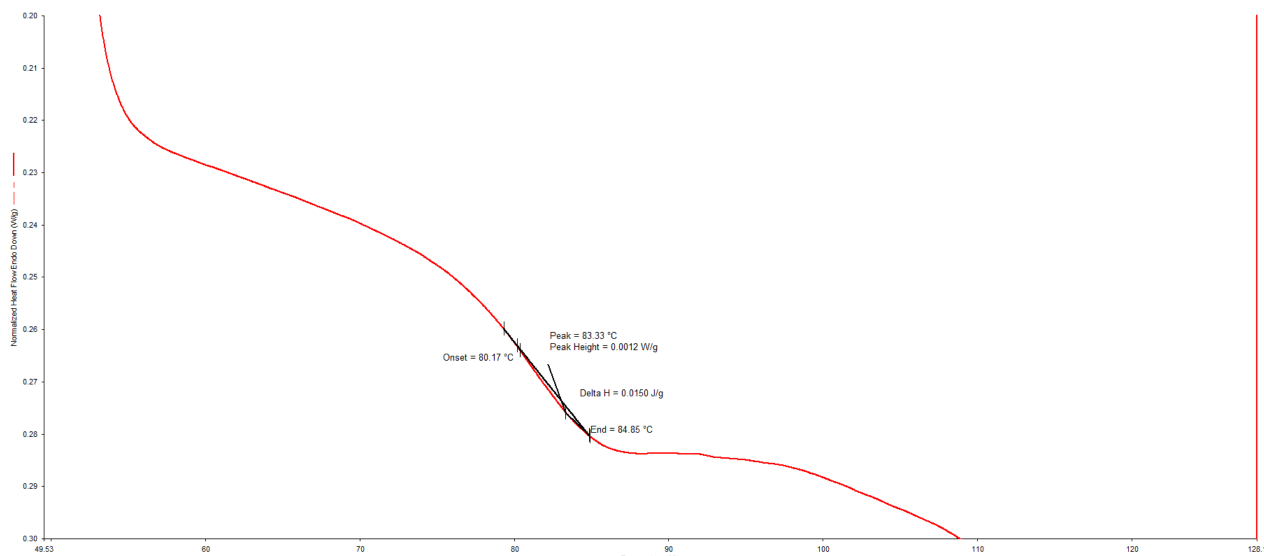

Fig. 29 –Dry Dock #4 core #8 bar #1A DSC curve.

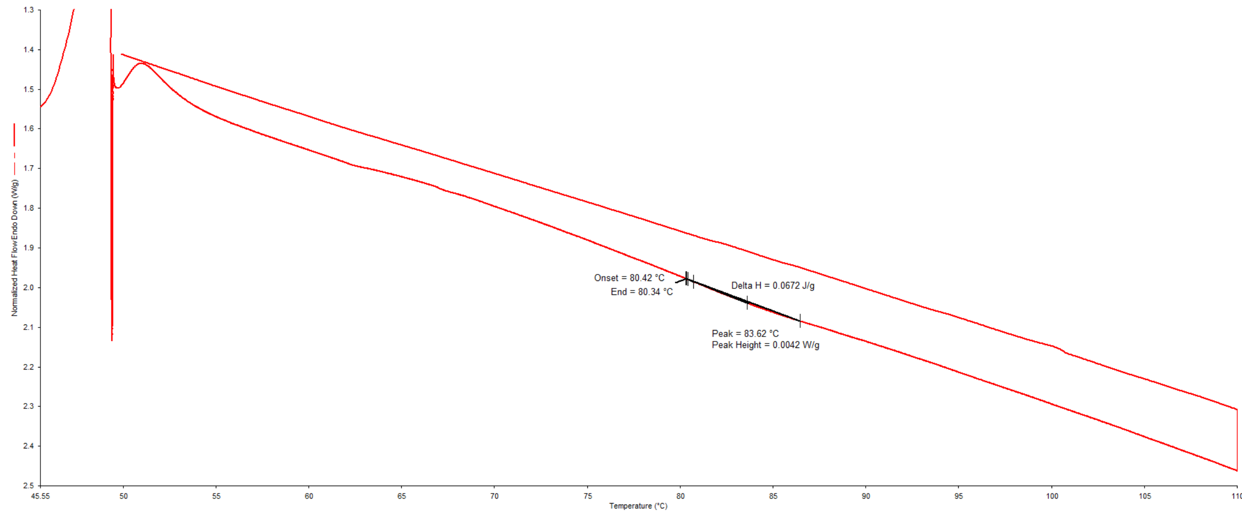

Fig. 30 –Dry Dock #8 core #2 bar #1B DSC curve.

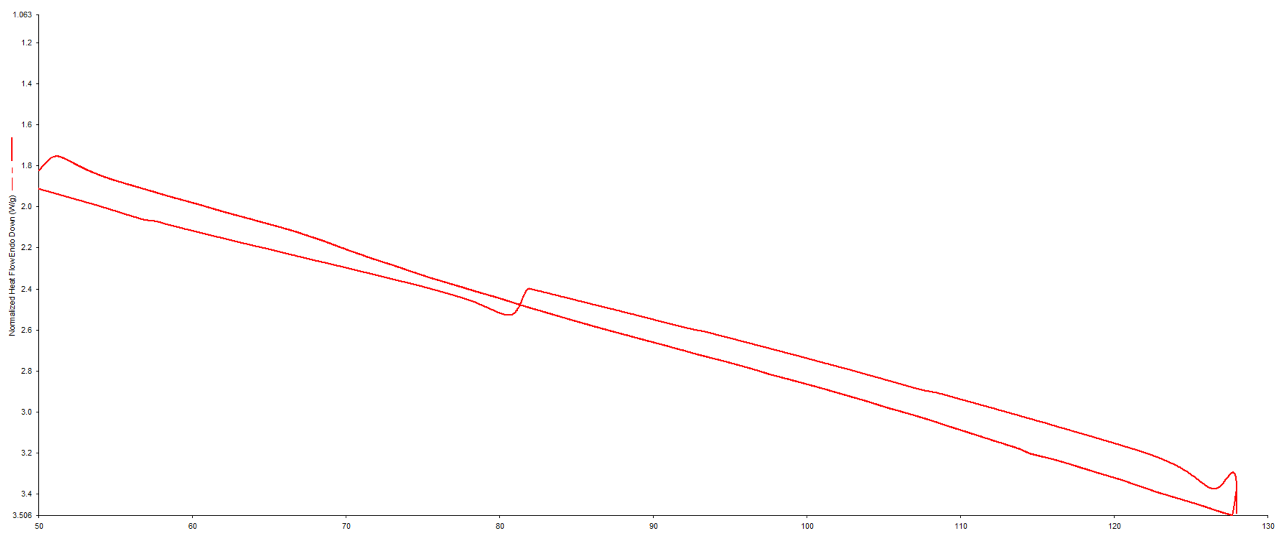

Fig. 31 –Dry Dock #4 core #2 bar #1C DSC curve.

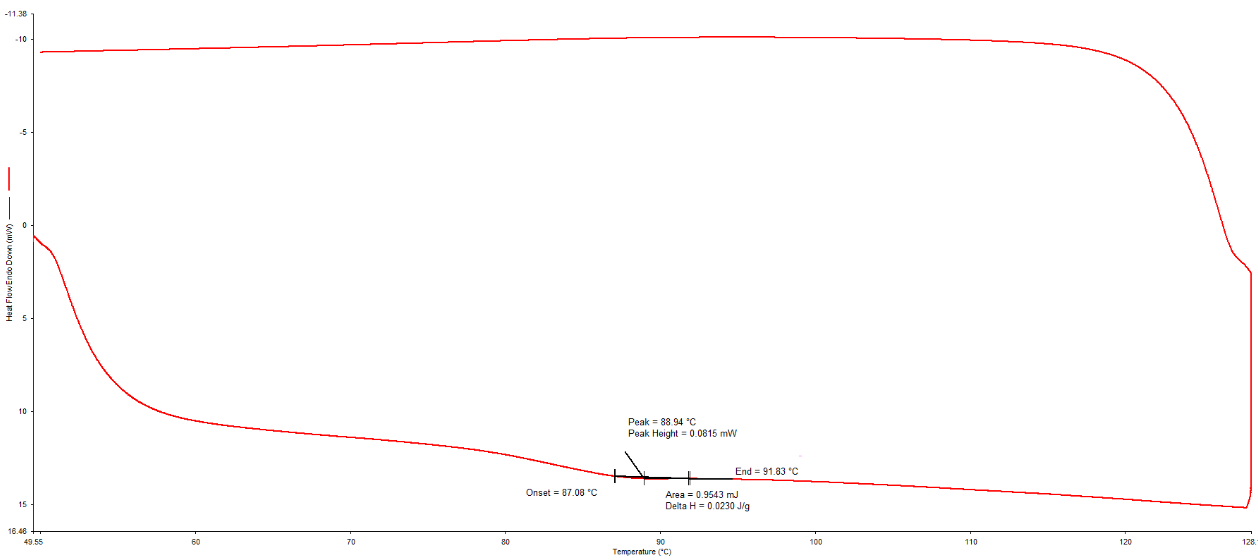

Fig. 32 –Dry Dock #4 core #15 bar #1 DSC curve.

4.4. Water absorption

Water absorption testing was performed according to the procedure depicted in Section 4.1.2 in the cited report. Drying and measurement procedures are described in Appendix II. Six specimens from two bars were tested for water absorption. All specimens presented less than 1% weight gain during the 24-hr immersion period. However, all specimens had weight gains higher than 1% at the equilibrium point, varying from 1.21% at the lowest to 1.52% at the highest. These values do not meet the current qualification limit (of 1%) established in ASTM D7957. The results of each bar are shown in Table 15 and a long-term water absorption graph is shown in Figure 33.

Table 15. Water absorption results

Specimen ID	% Weight Change at 24 hours	Weight Change at Equilibrium (%/ days)	Total Immersion Weight Change (%)
HI_C13_B2-1	0.60	1.21 / 63	1.32
HI_C13_B2-2	0.88	1.30 /119	1.30
HI_C13_B2-3	0.87	1.36 / 49	1.38
HI_C15_B2-1	0.97	1.50 / 63	1.59
HI_C15_B2-2	0.83	1.52 / 49	1.66
HI_C15_B2-3	0.84	1.40 / 91	1.47

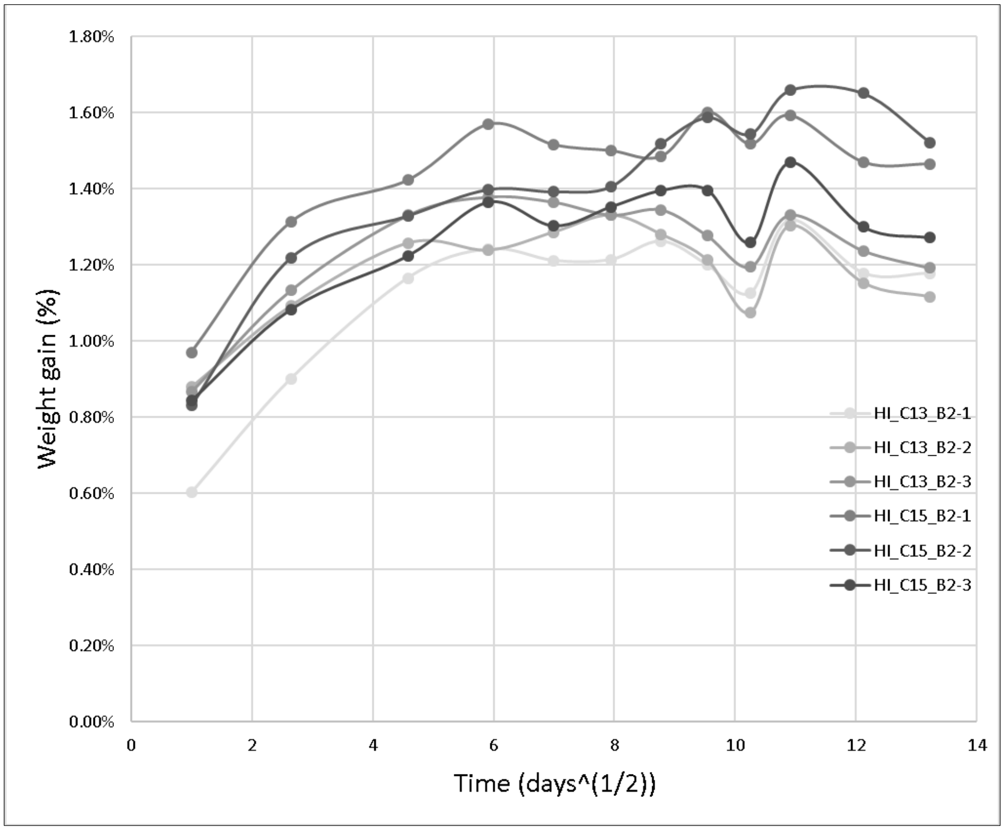

Fig. 33 –Long-term water absorption graph

4.5. Tensile strength

No tensile strength tests were performed on the extracted bars due to the size of the specimens. However, the original bars were tested at the time of installation. These bars were #4 bent bars and used PPG E-glass and vinyl ester matrix. The results of these bars are shown in Table 16.

Table 16. Tensile testing of original bars

Failure Mode	**Load at Failure lbs. (N)**	**Tensile Stress (psi) MPa**
Pulled Out	70,802 (15,917)	(81,085) 559
Grout Slip	85,819 (19,293)	(98,283) 678
Failure in Pipe	90,032 (20,240)	(103,107) 710
Failure in Pipe	86,268 (19,394)	(98,797) 681
Middle	90,058 (20,246)	(103,138) 711
Average	84,596 (19,018)	668 (98,877)
Std. Dev.	7968 (1,791)	9,125 (63)

4.6. SEM imaging and EDS

SEM imaging analysis and EDS were performed at the University of Miami and Owens Corning. The SEM imaging and EDS followed the procedure described in Section 4.1.5 in the main report. A total of five bars were tested and the results are reported below for each bar.

4.6.1. Bar C3_B2

A specimen from bar C2_B2, as shown in Figure 34, was used for SEM imaging. SEM images of the bar are shown in Figures 35 through 40. No negatively affected fibers were observed on the interior of the bar; however, some fibers near the outer edge were affected by concrete environment. Some voids in the resin between fibers were observed, in a few cases the voids appear to be from manufacturing, while, in most cases, they suggest degradation in the interface between fiber and resin.

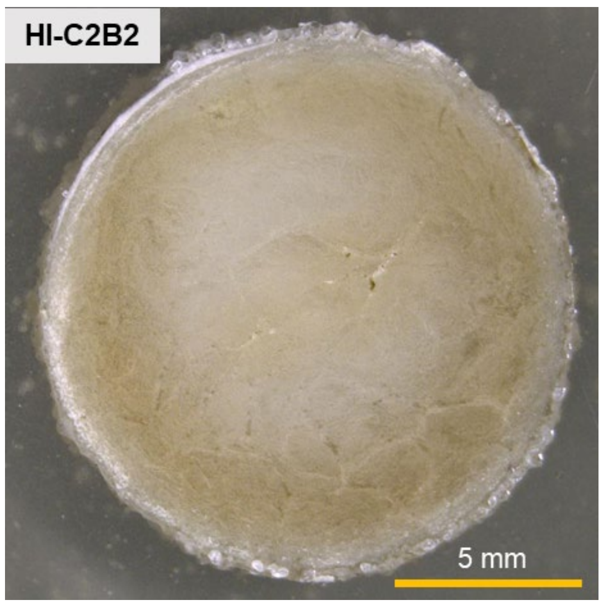

Fig. 34 –Specimen C2_B2 for SEM image

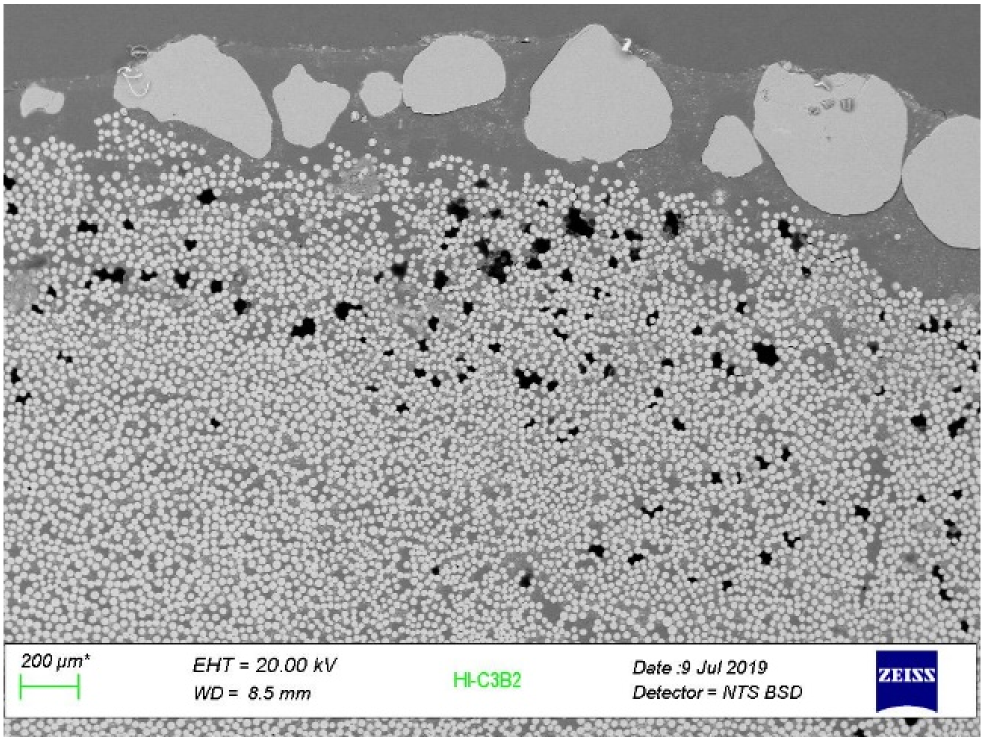

Fig. 35 –Core #3 Bar #2 at edge.

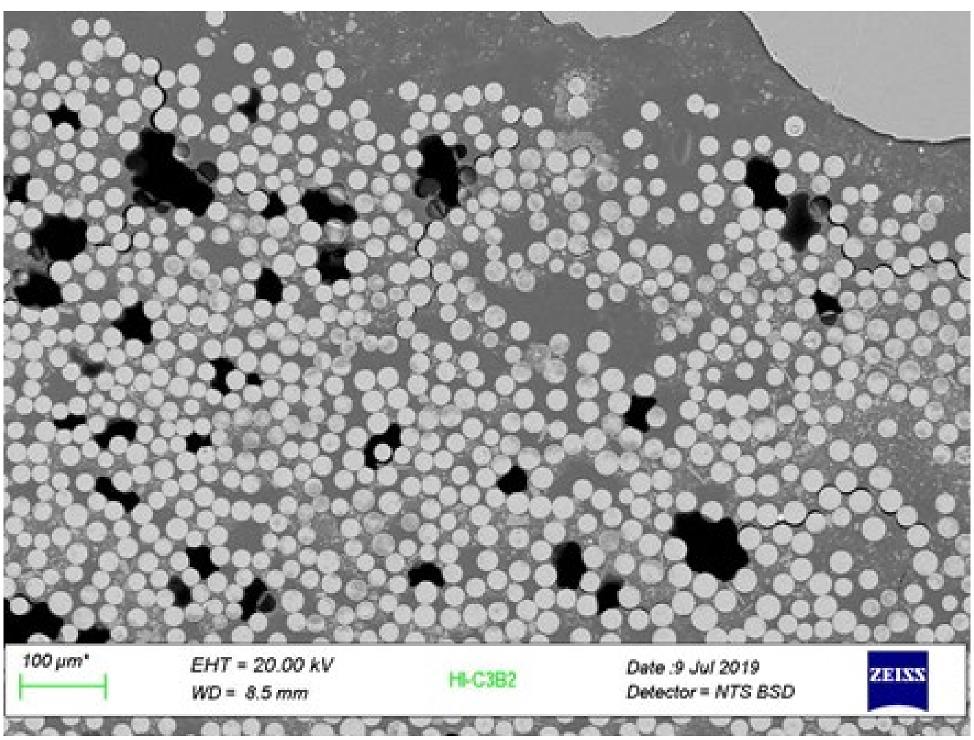

Fig. 36 –Core #3 Bar #2 at edge.

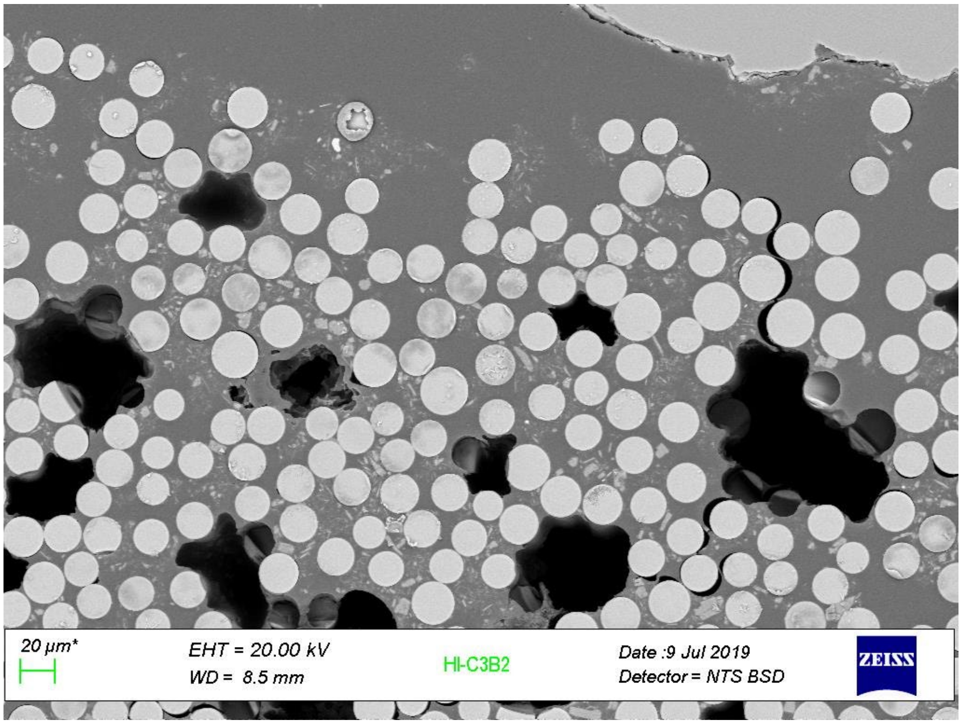

Fig. 37 –Core #3 Bar #2 at edge.

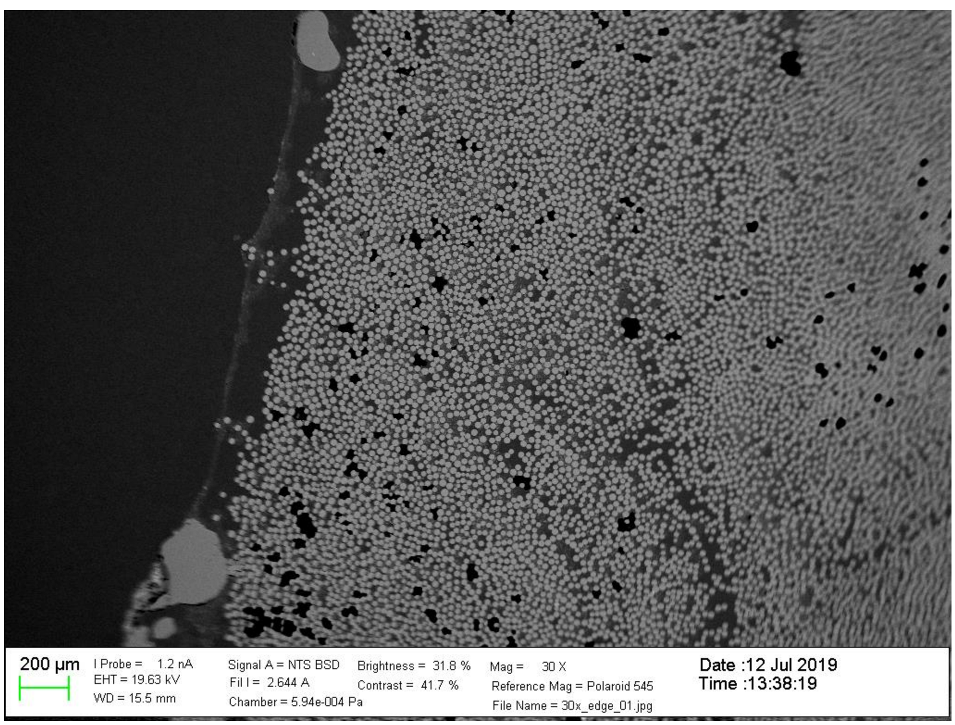

Fig. 38 –Core #3 Bar #2 Edge of bar.

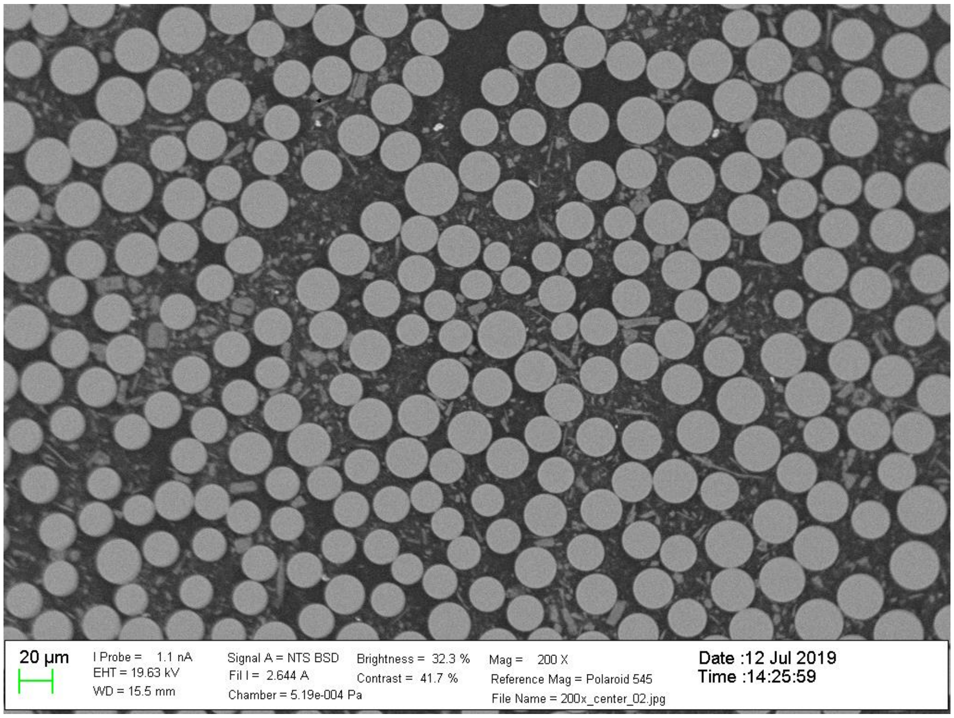

Fig. 39 –Core #3 Bar #2 center of bar.

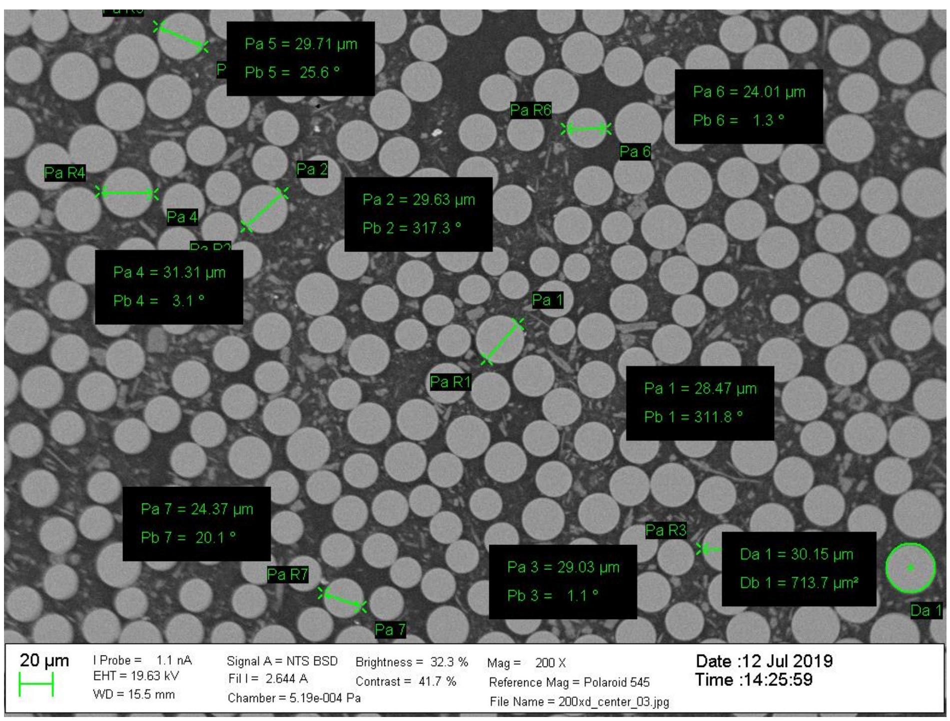

Fig. 40– Core #3 Bar #2 intact fibers of different diameters at the center of the bar.

4.6.2. Bar C2_B2

A specimen from bar C2_B2, as shown in Figure 41, was used for SEM image. SEM images, shown in Figures 42 through 48, suggest deterioration of fibers and resin near the edge of the bar. The fibers in the interior of the bar were intact and the damaged fibers were observed where the resin had heavy deterioration. The fibers negatively affected by the concrete environment were estimated by visual imagery to range between 0.05 to 0.12% of the total number. The damaged fibers were estimated from counting fibers with obvious signs of damage in 1 quadrant, multiplied by 4. Large voids causing delamination among the fibers were observed near the edge of the bar.

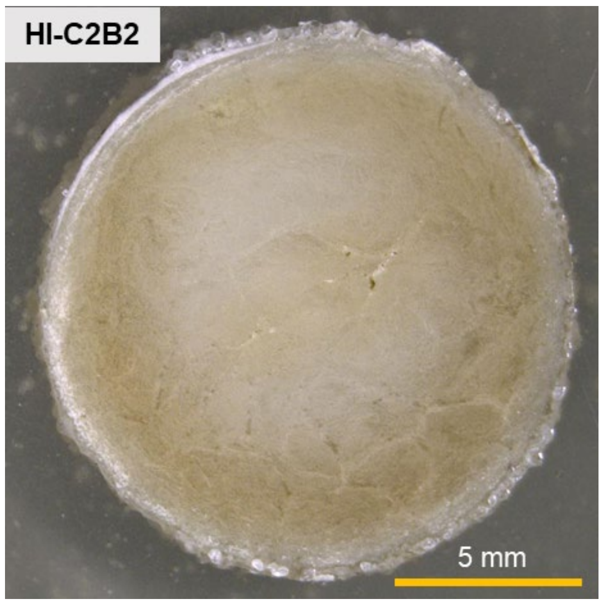

Fig. 41 –Specimen C2_B2 for SEM image

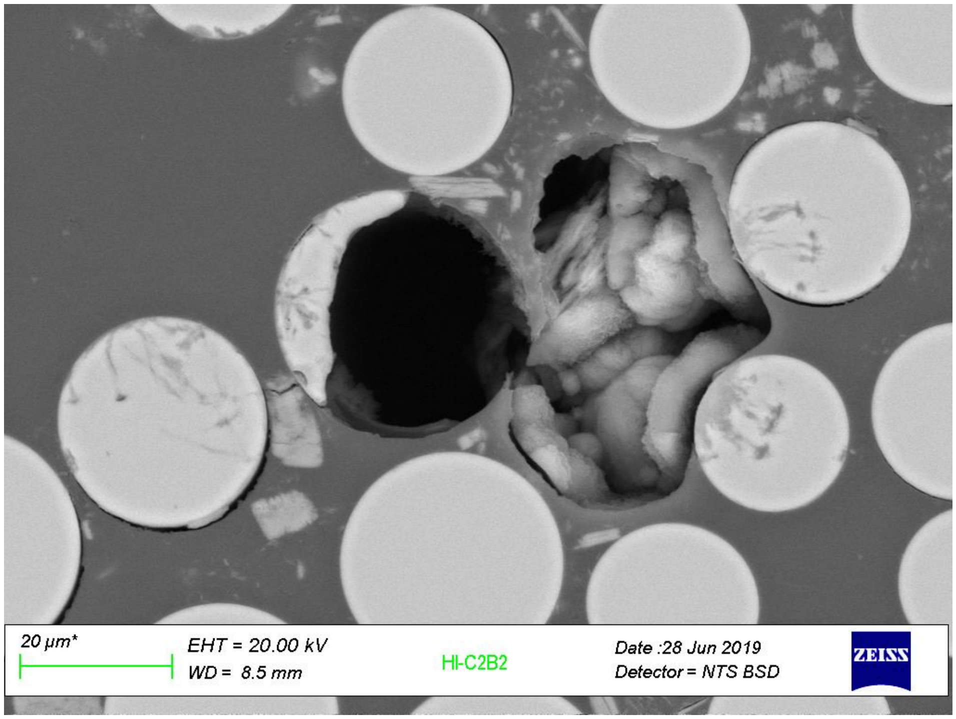

Fig. 42 –Core #2 Bar #2 damaged fibers at the outer edge of rebar.

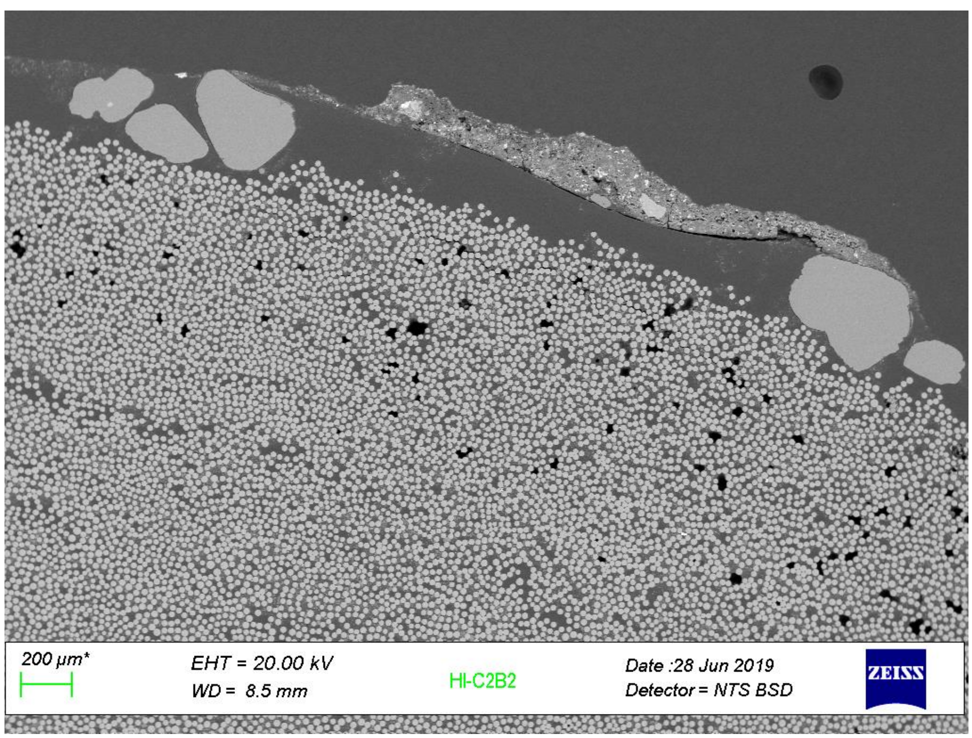

Fig. 43 –Core #2 Bar #2 at the edge. Some voids in the resin are observed.

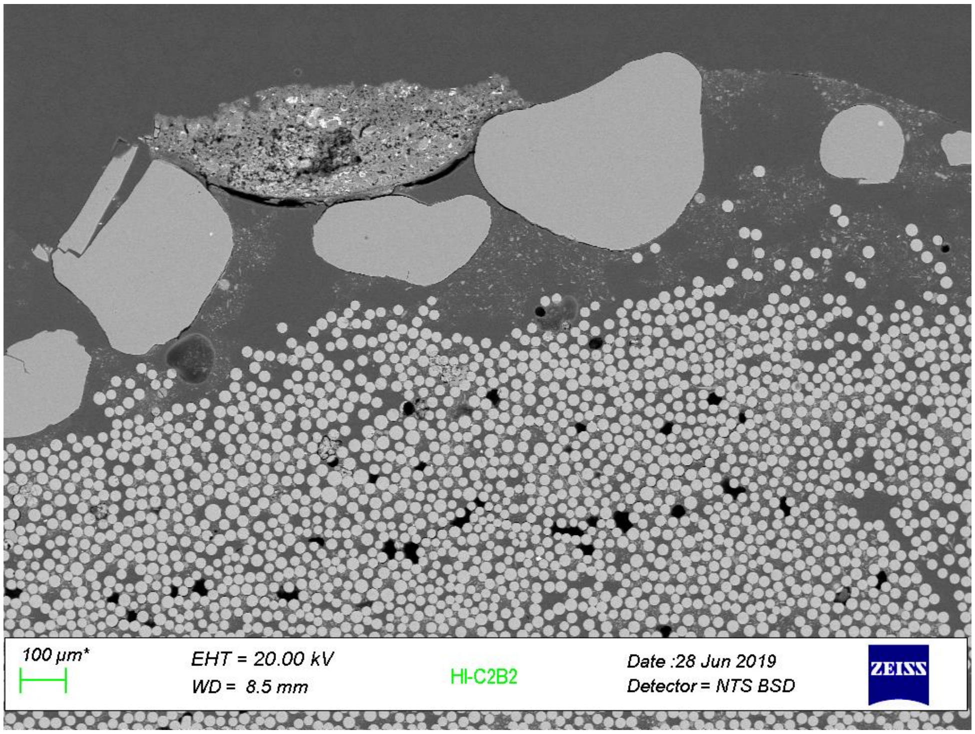

Fig. 44 –Core #2 Bar #2 at edge. Some voids in the resin are observed.

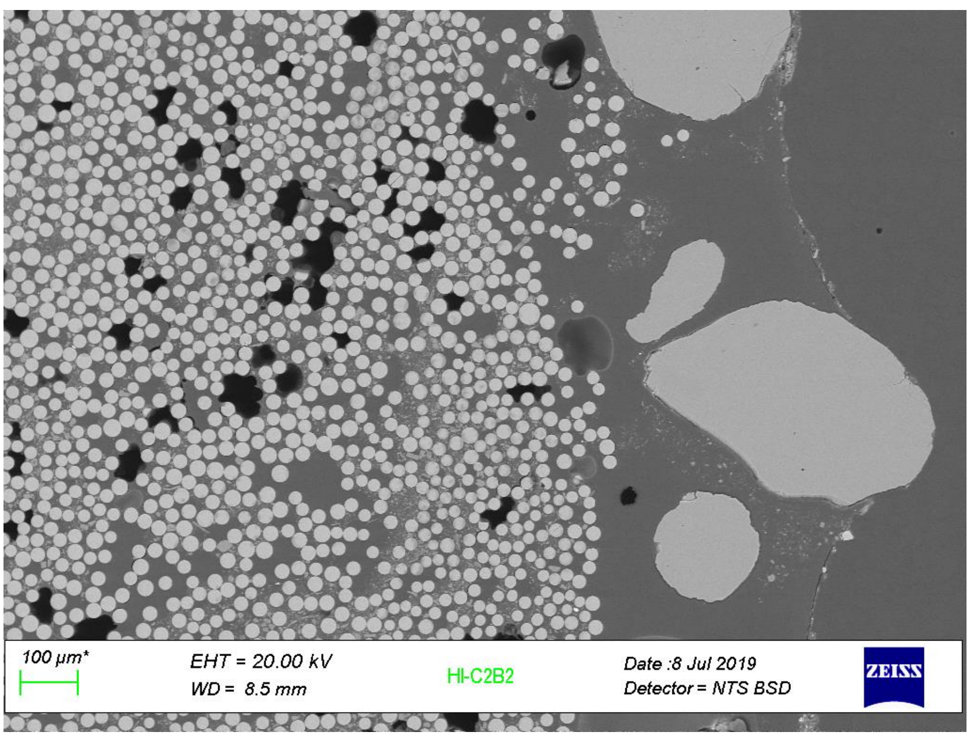

Fig. 45 –Core #2 Bar #2 at edge. Voids in the resin are observed.

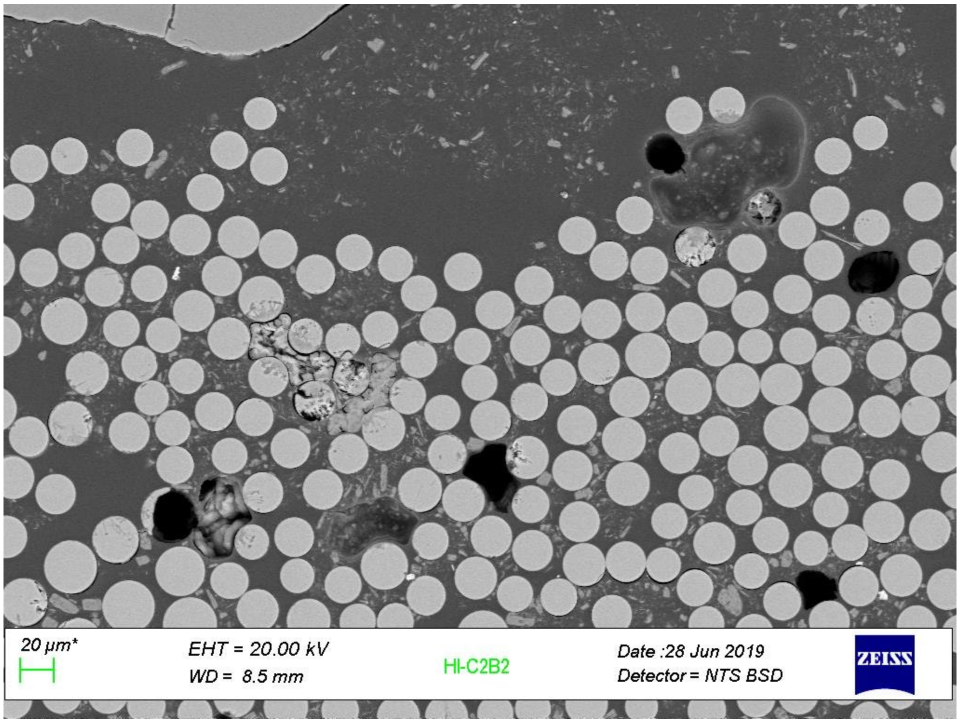

Fig. 46 –Core #2 Bar #2 at edge. Some voids and fiber damaged observed.

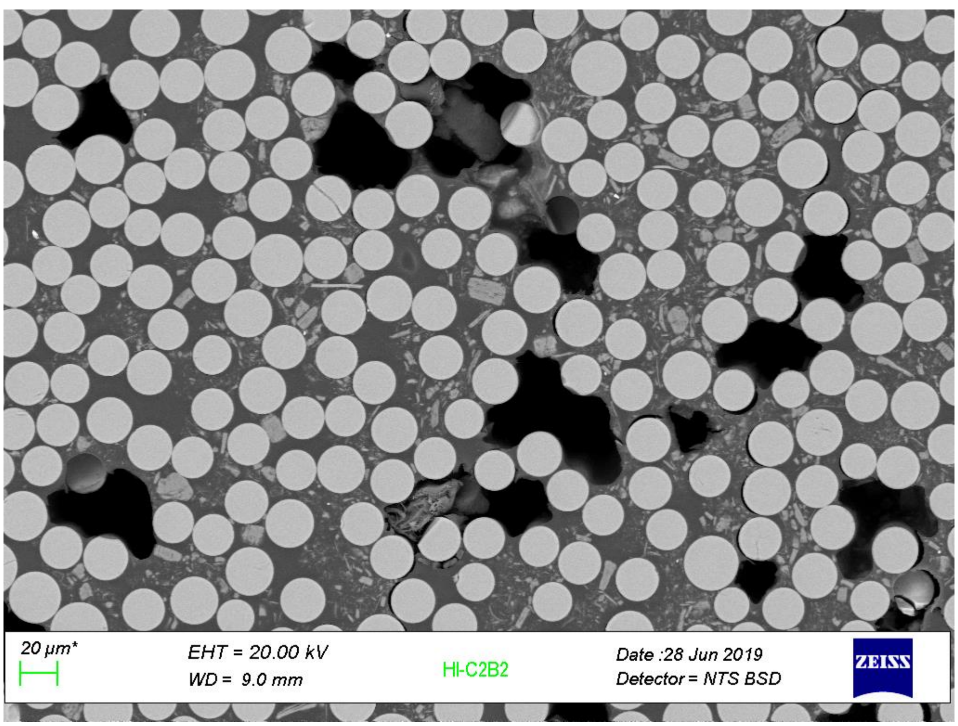

Fig. 47 – Core #2 Bar #2 at the inner edge. Some resin voids and minor fiber damage.

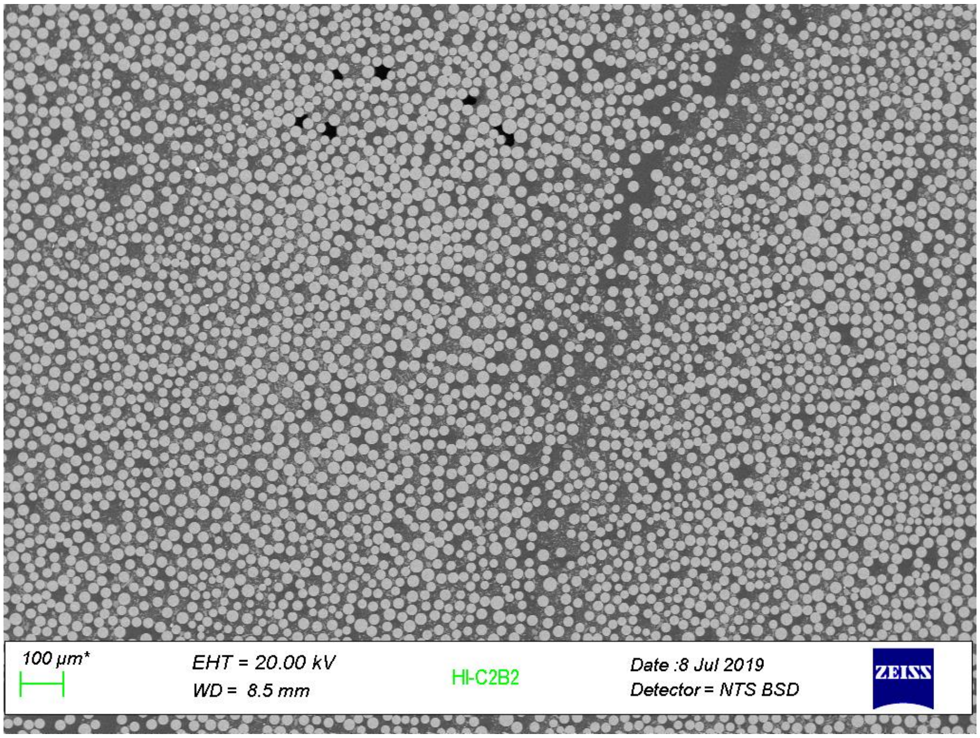

Fig. 48 –Core #2 Bar #2 center of rebar.

4.6.3. Bar C15_B1

A specimen from bar C2_B2, as shown in Figure 49, was used for SEM image. As shown in Figures 50 through 54, nearly no negatively affected fibers were observed on the interior or exterior of the bar. Large voids in the resin were observed near the edge of the bar where larger quantities of Na_2O and Cl where detected during EDS, however, it cannot be determined if the

voids were pre-existing or caused by these elements. Signs of fiber damage were only observed in locations corresponding to voids in the resin. Some voids appeared to be causing debonding among the fibers at different locations of the bar cross section.

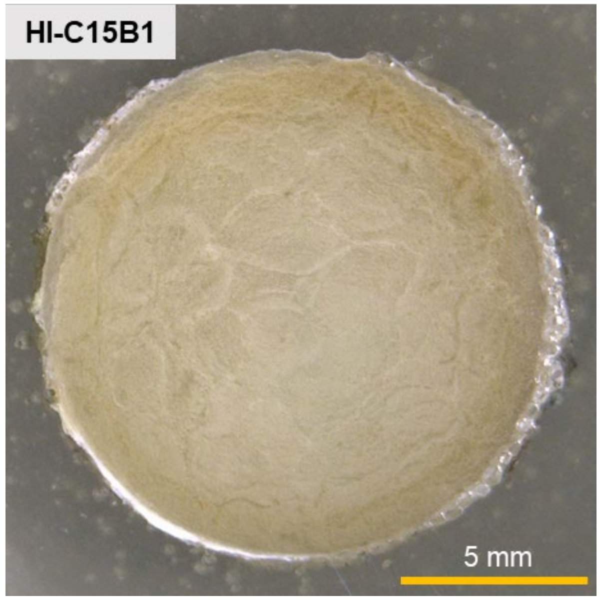

Fig. 49 –Specimen C15_B1 for SEM image

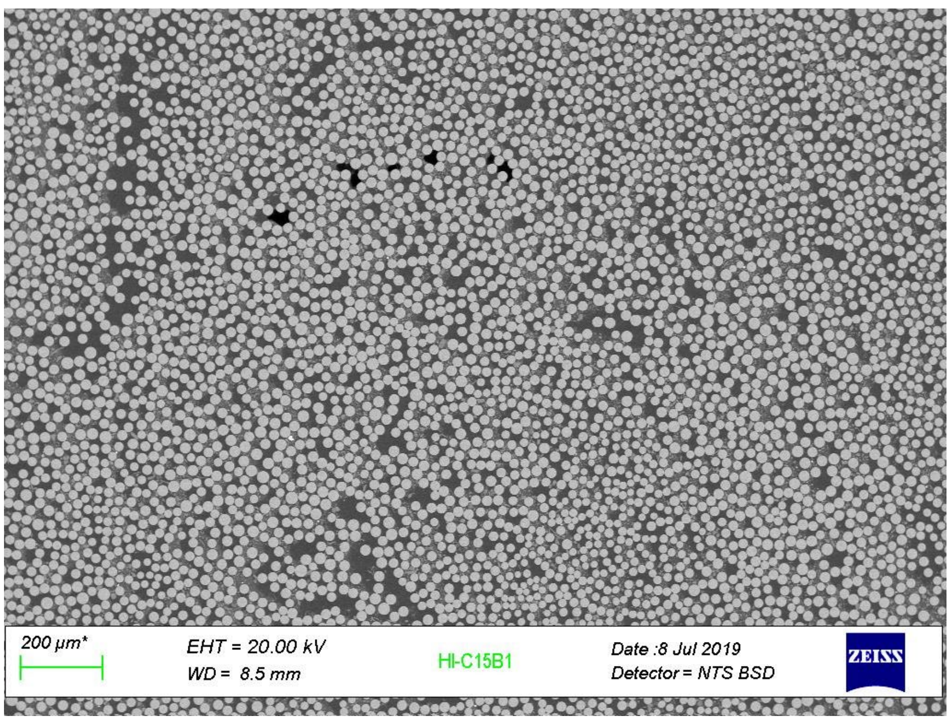

Fig. 50 –Core #15 Bar #1 at center

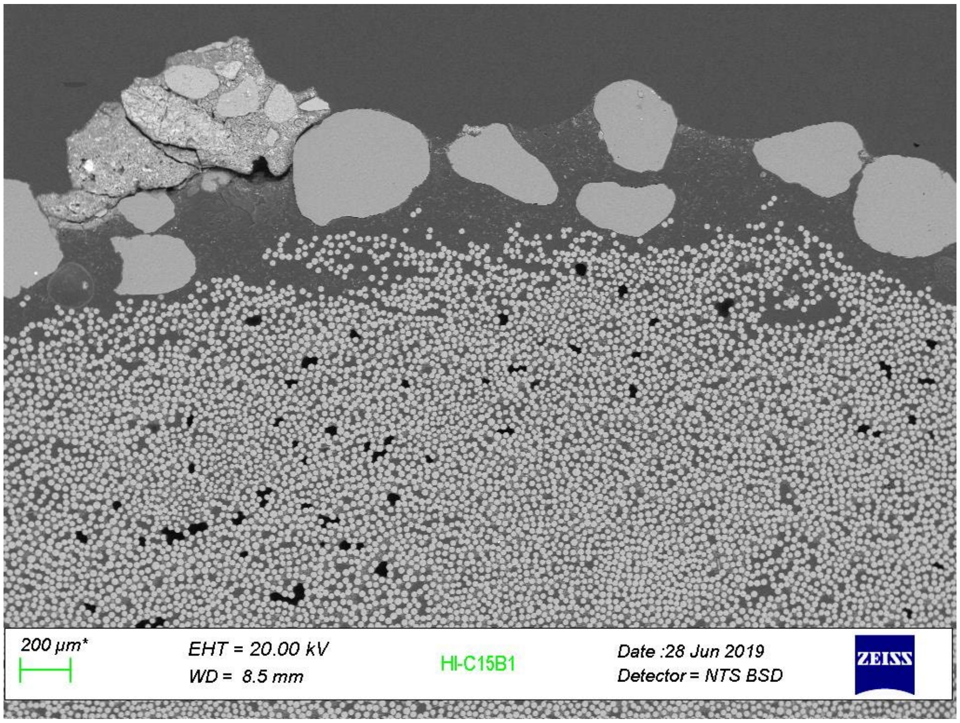

Fig. 51 –Core #15 Bar #1 at edge.

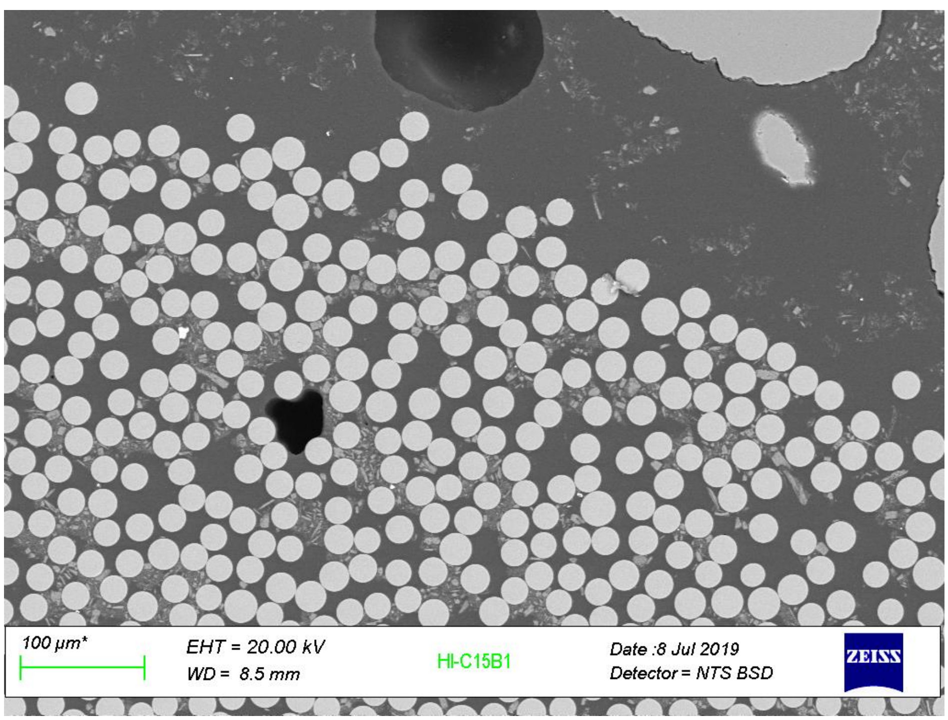

Fig. 52 –Core #15 Bar #1 at edge

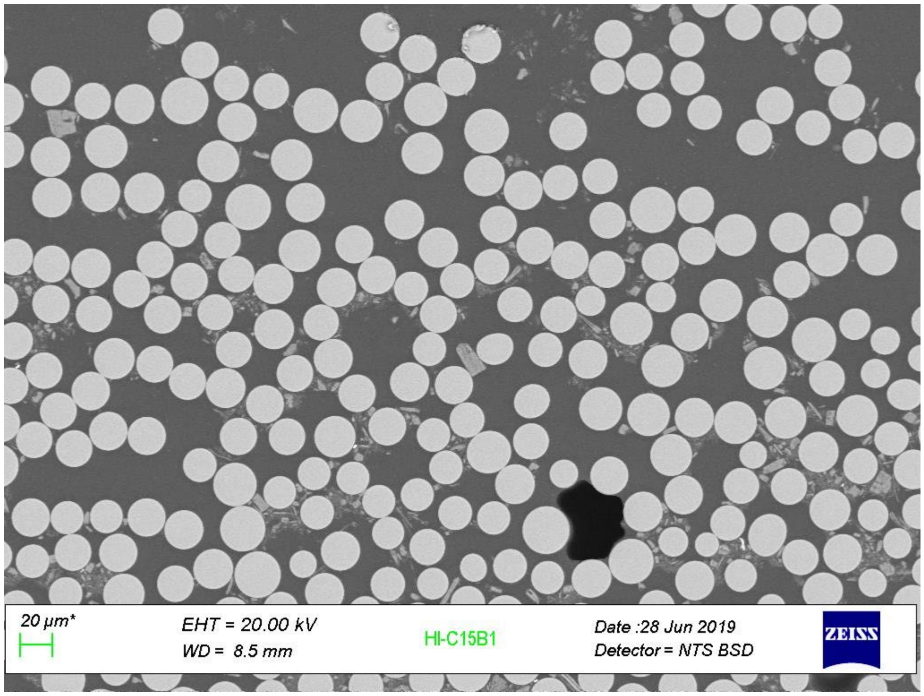

Fig. 53 –Core #15 Bar #1 at edge

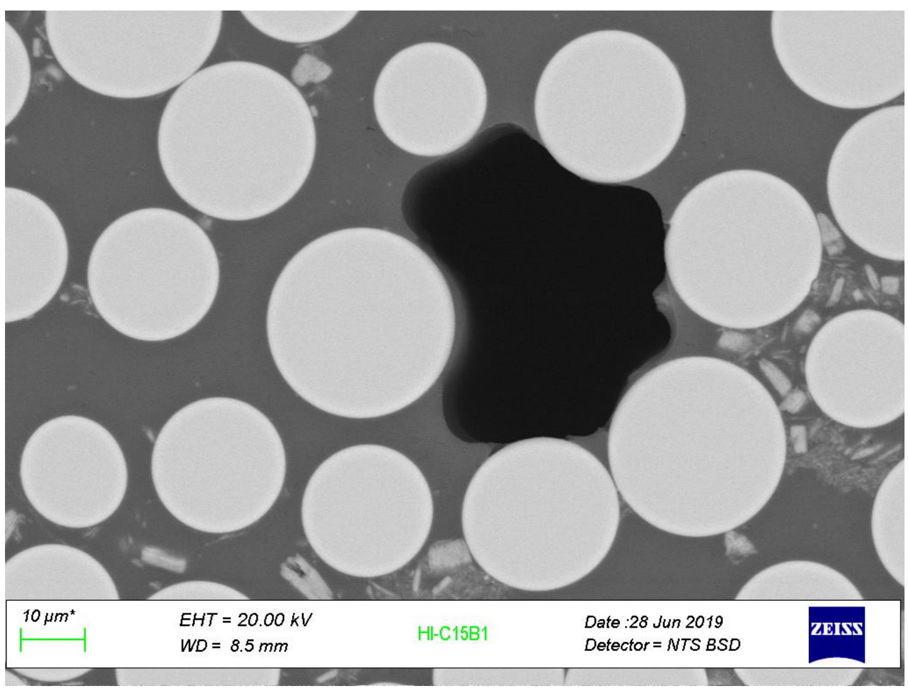

Fig. 54 –Core #15 Bar #1 at edge. Void in resin observed.

4.6.4. Bar C15_B3

A specimen from bar C2_B2 was used for SEM image. As shown in Figure 55, the specimen was not a full rebar cross section. As shown in Figures 56 through 60, some negatively affected fibers were observed, but appeared to be isolated on the outer perimeter. The damaged fibers were at locations where the resin is damaged. Some voids in the resin were also observed closer to the center of the bar, suggesting degradation in the interphase between fiber and resin.

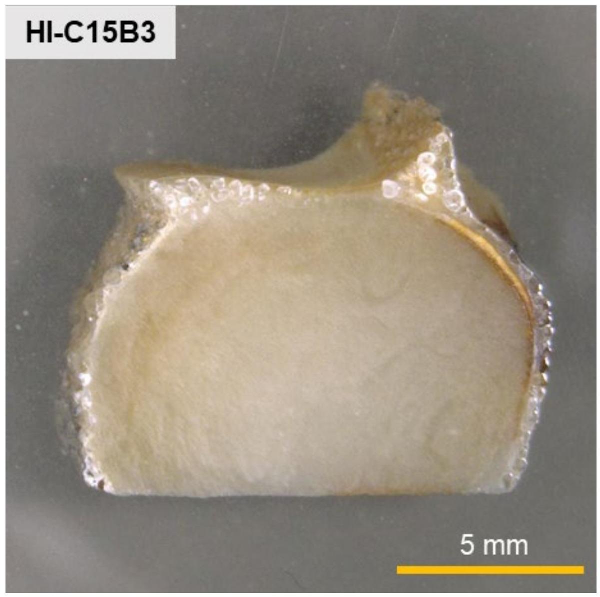

Fig. 55 – Specimen C15_B3 for SEM image

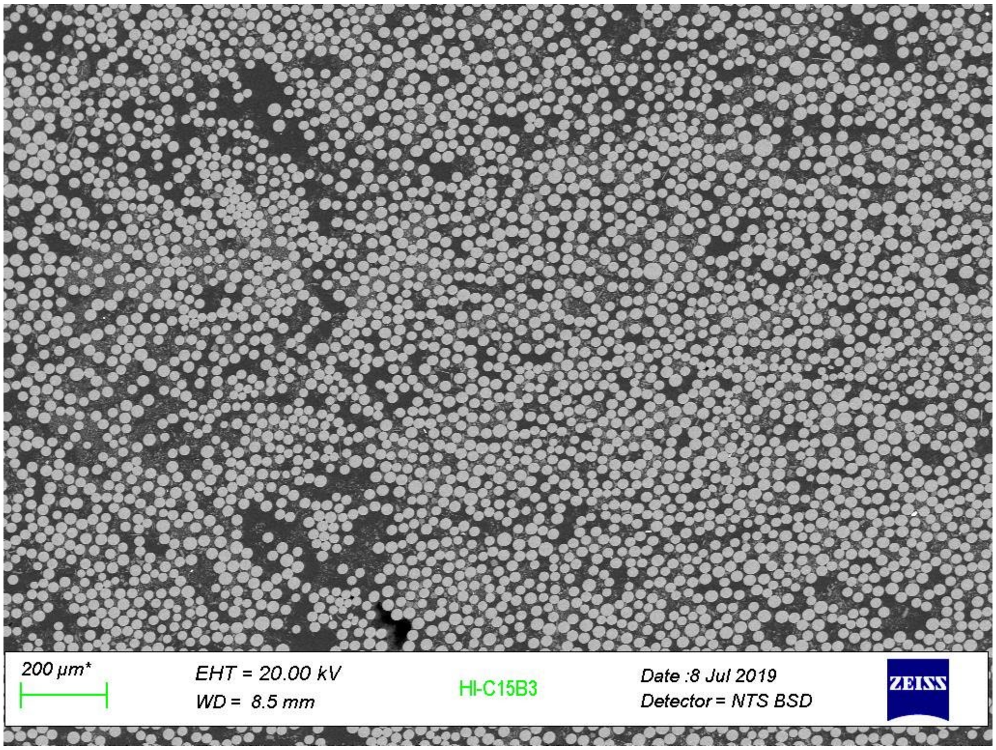

Fig. 56 –Core #15 Bar #3 at center

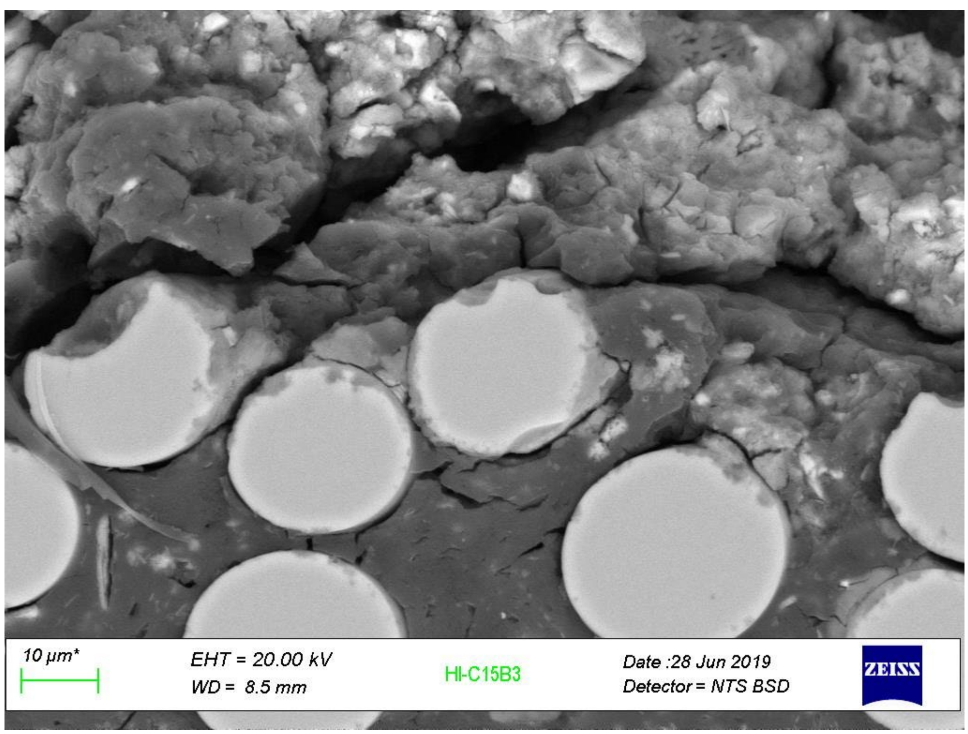

Fig. 57 –Core #15 Bar #3 at edge. Fibers negatively affected

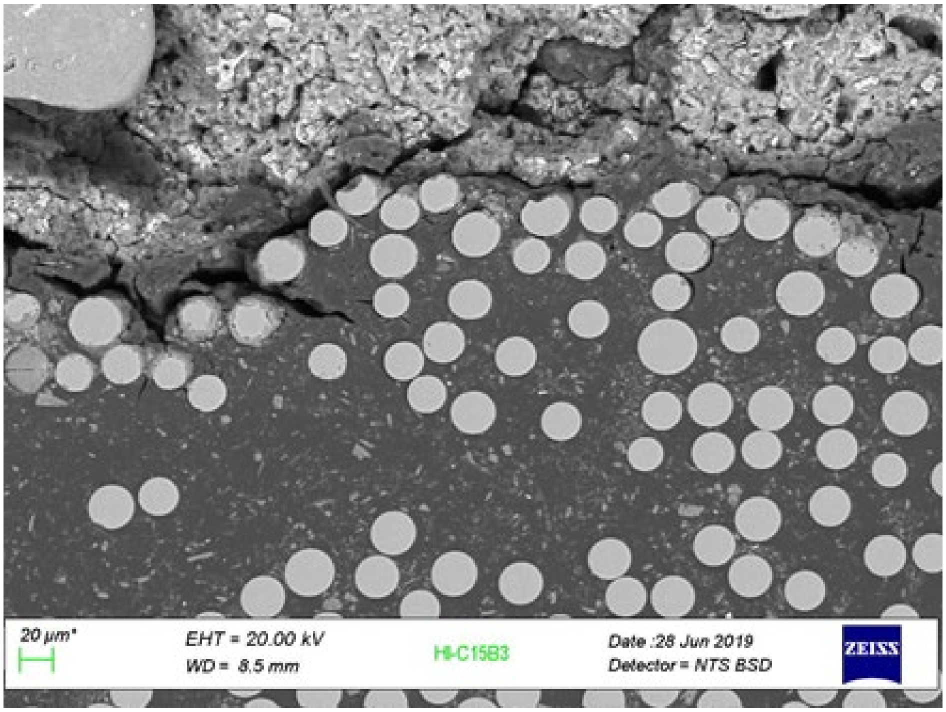

Fig. 58 –Core #15 Bar #3 at edge

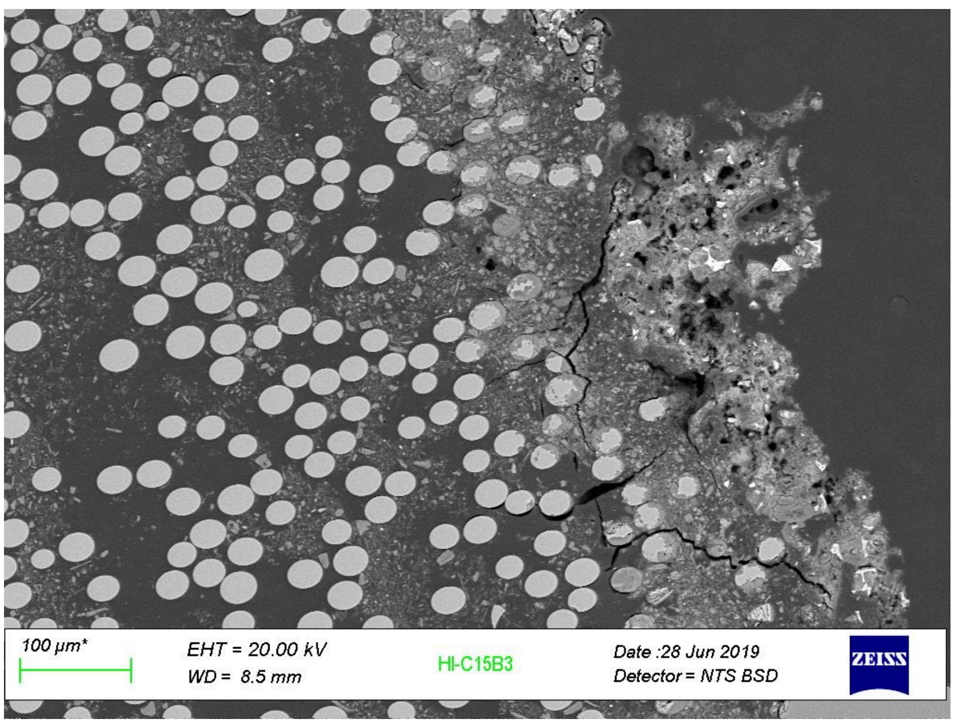

Fig. 59 –Core #15 Bar #3 at edge.

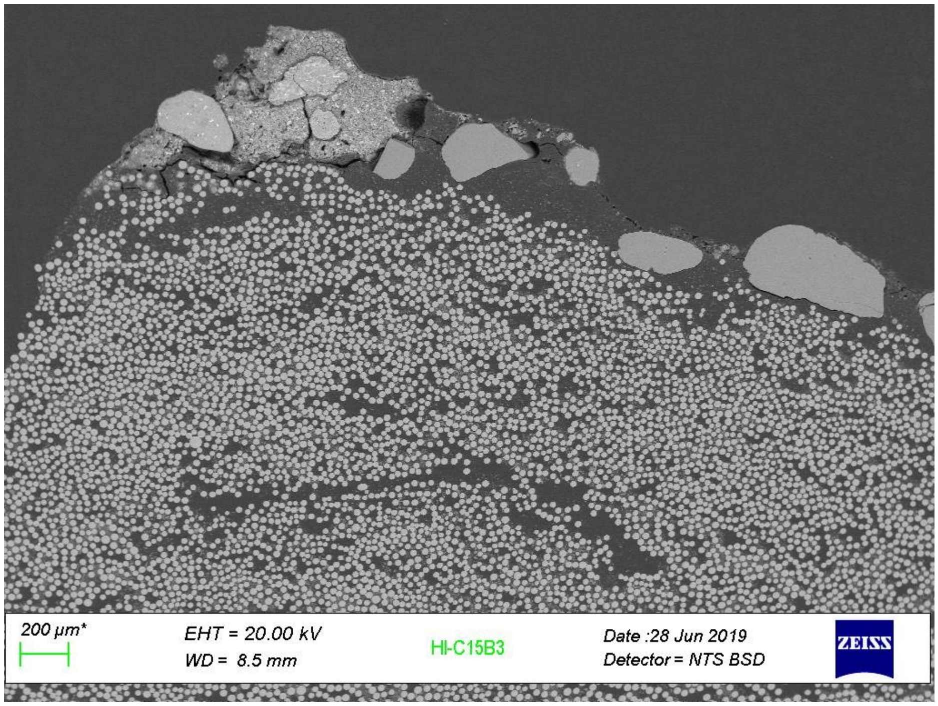

Fig. 60 –Core #15 Bar #3 at edge.

Overall, fiber damage was observed to be minor and generally near the edge of the bar. These results are comparable to those reported in literature such as the study from Benmokrane et al. (2017) that indicates that the GFRP bars made with vinyl-ester showed no significant changes but presented some delamination between fibers and vinyl-ester resin.

4.7. EDS test

EDS analysis was conducted to check for any chemical elemental changes. A voltage between 10 and 20 kV was applied to the specimens. The same specimens used for SEM testing were also used for EDS analysis. In all specimens, the main elements of fiber were detected including: O, Si, and Al. In addition, Mg was found too which confirms that the fibers used were E-glass and not E-CR, confirming the manufacturer's record. The main element of resin, carbon, was seen too. Even though, Na and Ca were observed in the analysis, they are not necessarily an indication of an alkali-hydrolysis attack, as they were seen in both resin and fibers with the same amount of concentration. Figure 61 through 65 show the results of four specimens, and Table 17 shows a summary of the chemical elements found in the specimen from C15_B1.

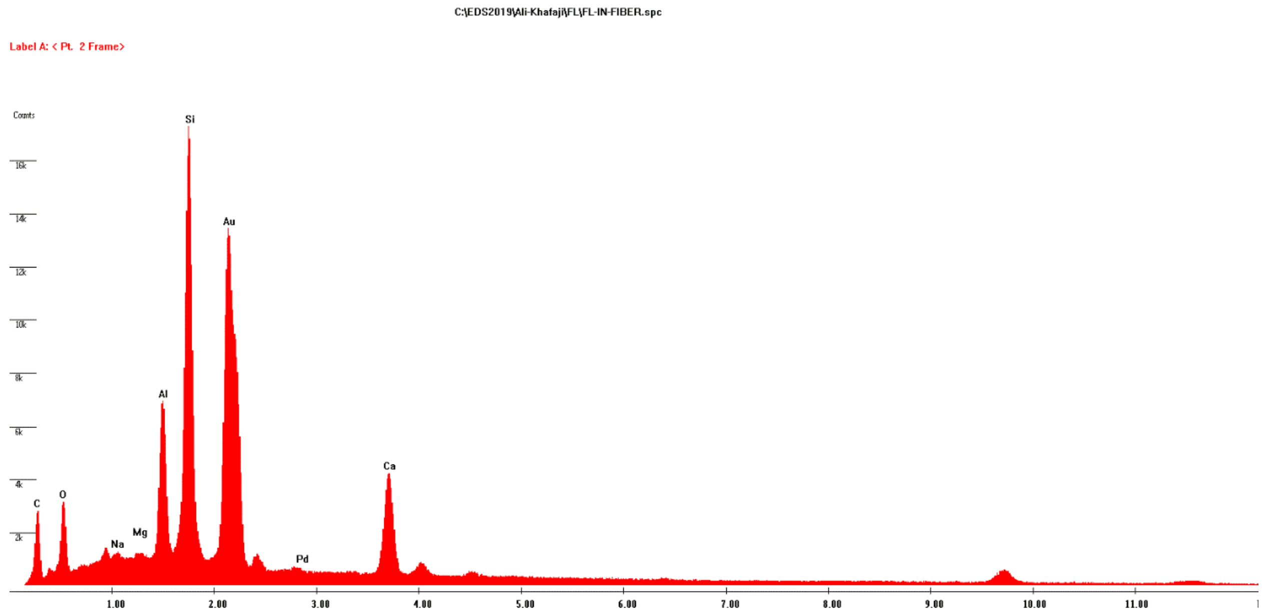

Fig. 61 –Core #2 Bar#2 Si, Al, Ca and small quantities of Na were detected on the center of the fiber

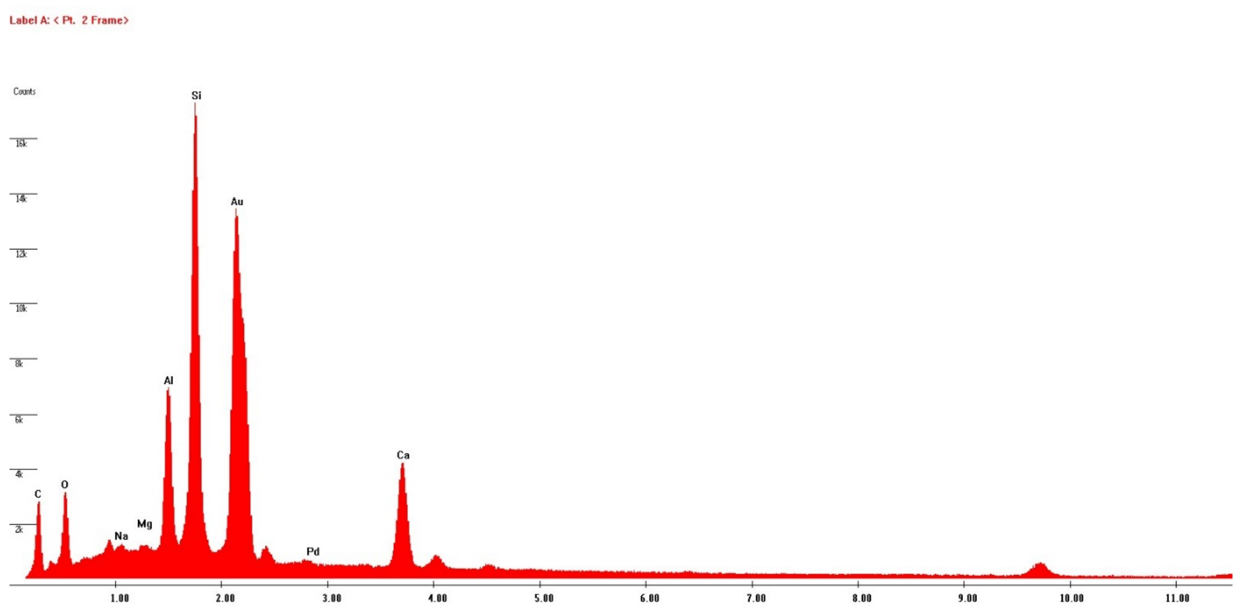

Fig. 62 –Core #3 Bar#2 Si, Al, Ca and small quantities of Na were detected on the center of the fiber

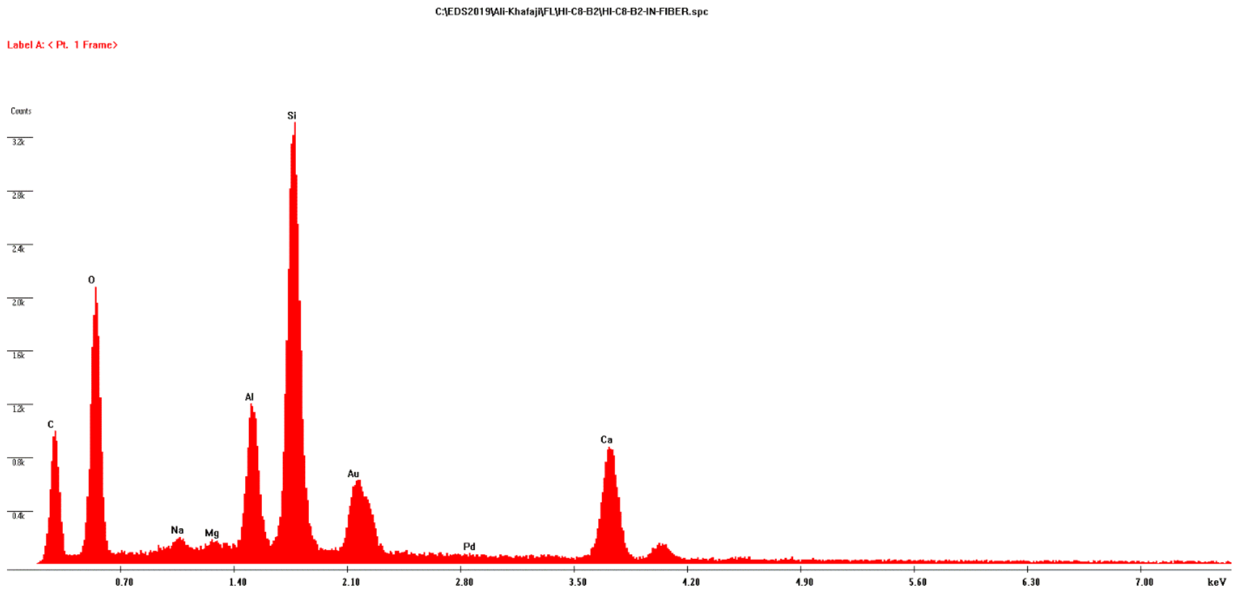

Fig. 63 –Core #8 Bar#2 Si, Al, Ca and small quantities of Na were detected on the center of the fiber

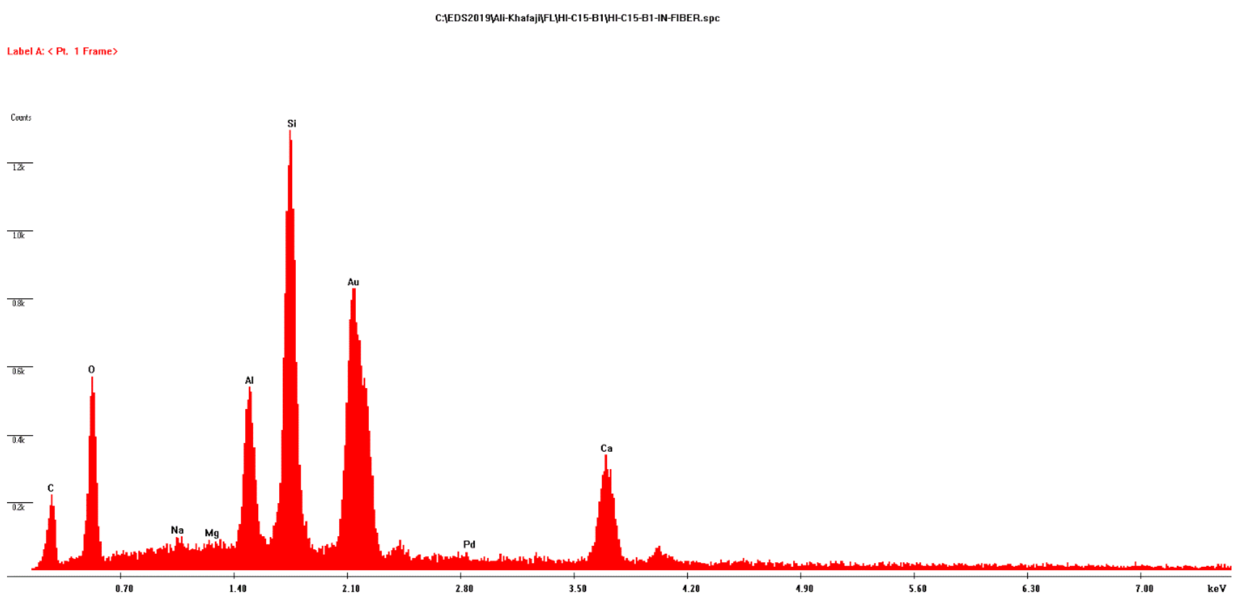

Fig. 64 –Core #15 Bar#1 Si, Al, Ca and small quantities of Na were detected on the center of the fiber

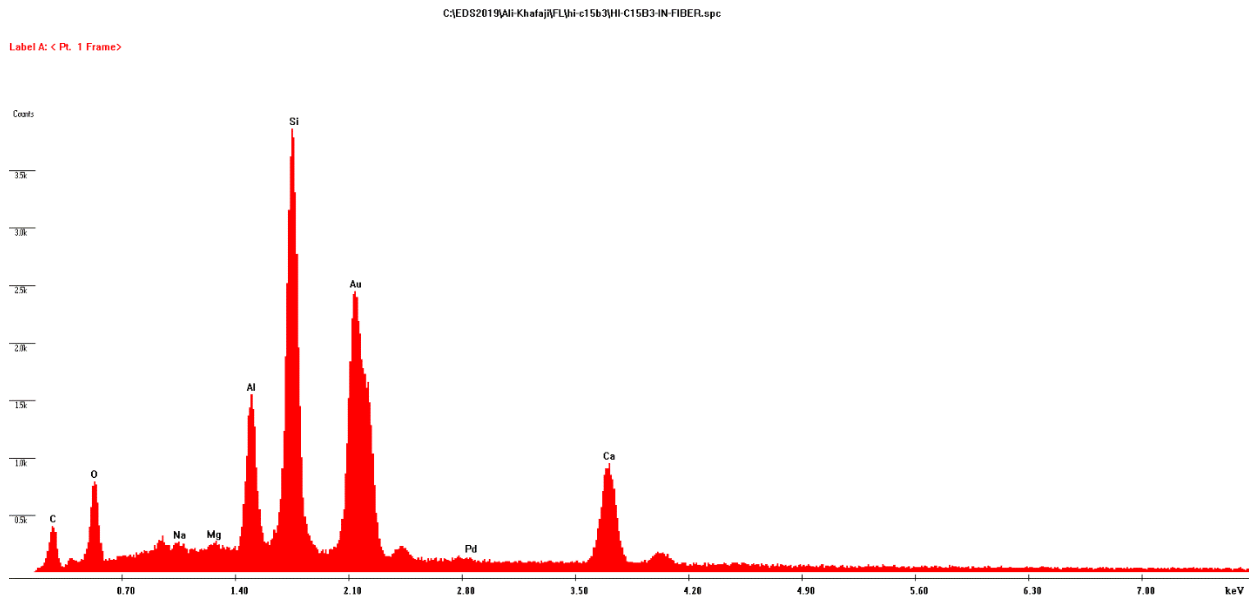

Fig. 65 –Core #15 Bar#3 Si, Al, Ca and small quantities of Na were detected on the center of the fiber

Table 17. EDS analysis of Core #15 Bar #1

	Average	Std. Dev.	Max	Min
Na_2O	1.73	1.03	4.41	0.5
MgO	1.45	1.42	5.34	0.1
Al_2O_3	16.95	3.64	23.82	6.59
SiO_2	64.01	7.39	85.09	53.97
Cl	0.45	0.27	1.48	0.13
CaO	15.26	3.95	23.98	7.05
K_2O	0.53	0.52	1.37	0.04

4.8. GFRP tests observations and conclusions

The GFRP bar specimens were tested to observe their current conditions by performing the following tests: a) fiber content, b) water absorption, c) horizontal shear, d) glass transition temperature (T_g), e) microscopic imaging and f) electron dispersive x-ray spectroscopy (EDS). Test results were compared to data collected from pristine bars at the time of construction of the Dry Dock or to current standards (ASTM D7957) when data was not available. The outcomes of the tests are briefly summarized as follows:

- The results from fiber content measurement by weight were above the 70% minimum required in ASTM D7957 for all specimens.

- The water absorption tests (ASTM D570) showed significant variability in weight gains after 24 hours and at saturation. Weight gains at 24 hours were less than 1% and varied between 0.60 and 0.97%. Weight gain at equilibrium were between 1.21 and 1.52%. These values are higher than the current qualification limit established in ASTM D7957, which is 1.0% at equilibrium.
- The glass transition temperature (T_g) measured by DSC varied from 171 °F (77 °C) to 230 °F (110 °C). No information on the original T_g was available; however, the T_g values obtained were similar to T_g from bars of the same age obtained from existing bridge installations. The limit currently established by ASTM D7957 requires a $T_g \geq$ 212°F (100°C), which was only achieved by certain bars. It should be noted that the current standards apply to test new generation (improved) GFRP bars.
- The results of horizontal shear were compared to data from pristine bars at the time of installation. The average apparent shear strength of in-service bars was 39% lower than the pristine bars. This reduction in strength could be due to the presence of voids at the fiber–resin interface, as these play a significant role in controlling the degradation due to exposure conditions (Benmokrane et al., 2017).
- The results of SEM showed voids in the resin between fibers, but these were most likely from manufacturing. Fibers negatively affected were observed at the edge of the bars but the overall quantity of negatively affected fibers was estimated by visual imagery to vary from 0.05 to 0.12%.
- The EDS test confirmed the fibers were E-glass by detecting the presence of O, Si, Al and Mg. Both Na and Ca were observed, however, because they were observed both in the resin and fiber, alkali-hydrolysis attack cannot be confirmed.

Acknowledgments

The authors would like to acknowledge ACI Strategic Development Council for their financial support. They would also like to give credit for permitting and extraction of cores by CPI Foundation staff: Scott L. Burghardt, Steven Aguilar, Tanya W. Komas, Ph.D.; CPI Foundation active duty military skillbridge team: SGT Morgan Kingston, SFC Corey Ray, LCPL Michael Acton, SGT Sebastian Angulo, SGT Dominic Barrera, PO2 Shawn Bartley, PO3 Jonathon Kammerer, SPC Michael Negron, CPL Kendrick Smith; U.S. Navy dry dock engineering team: Perry Schneck, Russell Risch, Daniel Baba.

References

American Society for Testing and Materials, Committee C-9 on Concrete and Concrete Aggregates, 2012, *Standard test method for electrical indication of concrete's ability to resist chloride ion penetration*, ASTM International.

Arıoglu, N., Girgin, Z.C. and Arıoglu, E., 2006, "Evaluation of ratio between splitting tensile strength and compressive strength for concretes up to 120 MPa and its application in strength criterion," *ACI Materials Journal*, *103*(1), pp.18-24.

ASTM International. C42/C42M-18a Standard Test Method for Obtaining and Testing Drilled Cores and Sawed Beams of Concrete. West Conshohocken, PA; ASTM International, 2018.

ASTM International. C39/C39M-18 Standard Test Method for Compressive Strength of Cylindrical Concrete Specimens. West Conshohocken, PA; ASTM International, 2018.

Benmokrane, B., Ali, A.H., Mohamed, H.M., ElSafty, A. and Manalo, A., 2017. "Laboratory assessment and durability performance of vinyl-ester, polyester, and epoxy glass-FRP bars for concrete structures," *Composites Part B: Engineering*, *114*, pp.163-174.

Benzecry, V., Brown, J., Al-Khafaji, Ali, Haluza, R., Koch, R, Nagarajan, M., Bakis, C.., Myers, J., Nanni, A., 2019. "Durability of GFRP Bars Extracted from Bridges with 15 to 20 years in service," *ACI CRC Research project.*

Chavhan, P. P., & Vyawahare, M. R. (2015). Correlation of static and dynamic modulus of elasticity for different SCC mixes. *International Journal on Recent and Innovation Trends in Computing and Communication*, *3*(7), 4914-4919.

Khatibmasjedi, M., Claure, G. and Nanni, A., 2017, "Durability of GFRP reinforcement in seawater concrete–Part I," *Proceedings of the 4th Annual Composites and Advanced Materials Expo, CAMX, Orlando, FL, USA*, pp.11-14.

Liu, J.C., Sue, M.L. and Kou, C.H., 2009. "Estimating the strength of concrete using surface rebound value and design parameters of concrete material," *Tamkang Journal of Science and Engineering*, *12*(1), pp.1-7.

Limbachiya, M.C. and Kew, H.Y., 2008, *Excellence in Concrete Construction through Innovation: Proceedings of the conference held at the Kingston University, United Kingdom, 9-10 September 2008*, CRC Press.

Malhotra V. Testing Hardened Concrete: Non-destructive Methods. Detroit. MI: ACI Monograph No. 9; 1976

Munitz, A., Cotler, C. and Talianker, M., 2000, "Aging impact on mechanical properties and microstructure of Al-6063," *Journal of materials science*, *35*(10), pp.2529-2538.

Nanni, A., 2001, October, "Relevant field applications of FRP composites in concrete structures," In *Proceedings of the international conference composites in construction–CCC2001, Portugal* (pp. 661-670).

Nepomuceno, M. C., & Lopes, S. M. (2017, October). Analysis of Within-Test Variability of Non-Destructive Test Methods to Evaluate Compressive Strength of Normal Vibrated and Self-Compacting Concretes. In *IOP Conference Series: Materials Science and Engineering* (Vol. 245, No. 3, p. 032025). IOP Publishing.

Polder, R. B. (2001). Test methods for onsite measurement of resistivity of concrete—a RILEM TC-154 technical recommendation. *Construction and building materials*, *15*(2-3), 125-131.

Sertçelik, İ., Kurtuluş, C., Sertçelik, F., Pekşen, E. and Aşçı, M., 2018, "Investigation into relations between physical and electrical properties of rocks and concretes," *Journal of Geophysics and Engineering*, *15*(1), pp.142-152.

Solis-Carcaño, R., & Moreno, E. I. (2008). Evaluation of concrete made with crushed limestone aggregate based on ultrasonic pulse velocity. *Construction and Building Materials*, *22*(6), 1225-1231.

Yao, W., Jiang, S., Fei, W. and Cai, T., 2017, "Correlation between the compressive, tensile strength of old concrete under marine environment and prediction of long-term strength," *Advances in Materials Science and Engineering*, *2017*.